IAEA TECDOC SERIES

IAEA-TECDOC-1797

Accident Tolerant Fuel Concepts for Light Water Reactors

Proceedings of a Technical Meeting held at Oak Ridge National Laboratories, United States of America, 13–16 October 2014

IAEA
International Atomic Energy Agency

ACCIDENT TOLERANT FUEL CONCEPTS FOR LIGHT WATER REACTORS

The following States are Members of the International Atomic Energy Agency:

AFGHANISTAN
ALBANIA
ALGERIA
ANGOLA
ANTIGUA AND BARBUDA
ARGENTINA
ARMENIA
AUSTRALIA
AUSTRIA
AZERBAIJAN
BAHAMAS
BAHRAIN
BANGLADESH
BARBADOS
BELARUS
BELGIUM
BELIZE
BENIN
BOLIVIA, PLURINATIONAL STATE OF
BOSNIA AND HERZEGOVINA
BOTSWANA
BRAZIL
BRUNEI DARUSSALAM
BULGARIA
BURKINA FASO
BURUNDI
CAMBODIA
CAMEROON
CANADA
CENTRAL AFRICAN REPUBLIC
CHAD
CHILE
CHINA
COLOMBIA
CONGO
COSTA RICA
CÔTE D'IVOIRE
CROATIA
CUBA
CYPRUS
CZECH REPUBLIC
DEMOCRATIC REPUBLIC OF THE CONGO
DENMARK
DJIBOUTI
DOMINICA
DOMINICAN REPUBLIC
ECUADOR
EGYPT
EL SALVADOR
ERITREA
ESTONIA
ETHIOPIA
FIJI
FINLAND
FRANCE
GABON
GEORGIA
GERMANY
GHANA
GREECE
GUATEMALA
GUYANA
HAITI
HOLY SEE
HONDURAS
HUNGARY
ICELAND
INDIA
INDONESIA
IRAN, ISLAMIC REPUBLIC OF
IRAQ
IRELAND
ISRAEL
ITALY
JAMAICA
JAPAN
JORDAN
KAZAKHSTAN
KENYA
KOREA, REPUBLIC OF
KUWAIT
KYRGYZSTAN
LAO PEOPLE'S DEMOCRATIC REPUBLIC
LATVIA
LEBANON
LESOTHO
LIBERIA
LIBYA
LIECHTENSTEIN
LITHUANIA
LUXEMBOURG
MADAGASCAR
MALAWI
MALAYSIA
MALI
MALTA
MARSHALL ISLANDS
MAURITANIA
MAURITIUS
MEXICO
MONACO
MONGOLIA
MONTENEGRO
MOROCCO
MOZAMBIQUE
MYANMAR
NAMIBIA
NEPAL
NETHERLANDS
NEW ZEALAND
NICARAGUA
NIGER
NIGERIA
NORWAY
OMAN
PAKISTAN
PALAU
PANAMA
PAPUA NEW GUINEA
PARAGUAY
PERU
PHILIPPINES
POLAND
PORTUGAL
QATAR
REPUBLIC OF MOLDOVA
ROMANIA
RUSSIAN FEDERATION
RWANDA
SAN MARINO
SAUDI ARABIA
SENEGAL
SERBIA
SEYCHELLES
SIERRA LEONE
SINGAPORE
SLOVAKIA
SLOVENIA
SOUTH AFRICA
SPAIN
SRI LANKA
SUDAN
SWAZILAND
SWEDEN
SWITZERLAND
SYRIAN ARAB REPUBLIC
TAJIKISTAN
THAILAND
THE FORMER YUGOSLAV REPUBLIC OF MACEDONIA
TOGO
TRINIDAD AND TOBAGO
TUNISIA
TURKEY
TURKMENISTAN
UGANDA
UKRAINE
UNITED ARAB EMIRATES
UNITED KINGDOM OF GREAT BRITAIN AND NORTHERN IRELAND
UNITED REPUBLIC OF TANZANIA
UNITED STATES OF AMERICA
URUGUAY
UZBEKISTAN
VANUATU
VENEZUELA, BOLIVARIAN REPUBLIC OF
VIET NAM
YEMEN
ZAMBIA
ZIMBABWE

The Agency's Statute was approved on 23 October 1956 by the Conference on the Statute of the IAEA held at United Nations Headquarters, New York; it entered into force on 29 July 1957. The Headquarters of the Agency are situated in Vienna. Its principal objective is "to accelerate and enlarge the contribution of atomic energy to peace, health and prosperity throughout the world".

IAEA-TECDOC-1797

ACCIDENT TOLERANT FUEL CONCEPTS FOR LIGHT WATER REACTORS

PROCEEDINGS OF A TECHNICAL MEETING HELD AT OAK RIDGE NATIONAL LABORATORIES, UNITED STATES OF AMERICA, 13–16 OCTOBER 2014

INTERNATIONAL ATOMIC ENERGY AGENCY
VIENNA, 2016

For further information on this publication, please contact:

Nuclear Fuel Cycle and Materials Section
International Atomic Energy Agency
Vienna International Centre
PO Box 100
1400 Vienna, Austria
Email: Official.Mail@iaea.org

Printed by the IAEA in Austria
June 2016

IAEA Library Cataloguing in Publication Data

Names: International Atomic Energy Agency.
Title: Accident tolerant fuel concepts for light water reactors : proceedings of a Technical Meeting held at Oak Ridge National Laboratories, United States of America, 13-16 October 2014 / International Atomic Energy Agency.
Description: Vienna : International Atomic Energy Agency, 2016. | Series: IAEA TECDOC series, ISSN 1011–4289 ; no. 1797 | Includes bibliographical references.
Identifiers: IAEAL 16-01046 | ISBN 978–92–0–105216–2 (paperback : alk. paper)
Subjects: LCSH: Nuclear fuels. | Nuclear reactors — Safety measures. | Nuclear power plants — Accidents — Prevention. | Light water reactors.

FOREWORD

Nuclear fuel is a highly complex material that has been subject to continuous development over the past 40 years and has reached a stage where it can be safely and reliably irradiated up to 65 GWd/tU in commercial nuclear reactors. During this time, there have been many improvements to the original designs and materials used. However, the basic design of uranium oxide fuel pellets clad with zirconium alloy tubing has remained the fuel of choice for the vast majority of commercial nuclear power plants.

Severe accidents, such as those at the Three Mile Island and Fukushima Daiichi have shown that under such extreme conditions, nuclear fuel will fail and the high temperature reactions between zirconium alloys and water will lead to the generation of hydrogen, with the potential for explosions to occur, damaging the plant further.

Recognizing that the current fuel designs are vulnerable to severe accident conditions, there is renewed interest in alternative fuel designs that would be more resistant to fuel failure and hydrogen production. Such new fuel designs will need to be compatible with existing fuel and reactor systems if they are to be utilized in the current reactor fleet and in current new build designs, but there is also the possibility of new designs for new reactor systems.

This publication provides a record of the Technical Meeting on Accident Tolerant Fuel Concepts for Light Water Reactors, held at Oak Ridge National Laboratories (ORNL), United States of America, 13–16 October 2014, to consider the early stages of research and development into accident tolerant fuel. There were 45 participants from 10 countries taking part in the meeting, with 32 papers organized into 7 sessions, of which 27 are included in this publication. This meeting is part of a wider investigation into such designs, and it is anticipated that further Technical Meetings and research programmes will be undertaken in this field.

The IAEA wishes to thank the hosts and all the participants for their contribution to the meeting, in particular K. Terrani (ORNL) and J. Killeen (United Kingdom). The IAEA officer responsible for this publication was V. Inozemtsev of the Division of Nuclear Fuel Cycle and Waste Technology.

EDITORIAL NOTE

This publication has been prepared from the original material as submitted by the contributors and has not been edited by the editorial staff of the IAEA. The views expressed remain the responsibility of the contributors and do not necessarily represent the views of the IAEA or its Member States.

Neither the IAEA nor its Member States assume any responsibility for consequences which may arise from the use of this publication. This publication does not address questions of responsibility, legal or otherwise, for acts or omissions on the part of any person.

The use of particular designations of countries or territories does not imply any judgement by the publisher, the IAEA, as to the legal status of such countries or territories, of their authorities and institutions or of the delimitation of their boundaries.

The mention of names of specific companies or products (whether or not indicated as registered) does not imply any intention to infringe proprietary rights, nor should it be construed as an endorsement or recommendation on the part of the IAEA.

The IAEA has no responsibility for the persistence or accuracy of URLs for external or third party Internet web sites referred to in this publication and does not guarantee that any content on such web sites is, or will remain, accurate or appropriate.

CONTENTS

SUMMARY

INTRODUCTION

Nuclear fuel is a highly complex material that has been subject to continuous development over the past 40 years and has reached a stage of development where it can be safely and reliably irradiated up to 65 GWd/tU or more in commercial nuclear reactors. During this time there have been many improvements to the original designs and materials used. However, the basic concept of uranium oxide fuel pellets clad with zirconium alloy tubing has remained the fuel of choice for the vast majority of commercial nuclear power plants.

Severe accidents, such as those at Three Mile Island and Fukushima Daiichi have shown that under such extreme conditions, nuclear fuel will fail and the high temperature reactions between zirconium alloys and water will lead to the generation of hydrogen with the potential for explosions to occur, damaging the plant further.

Recognising that the current fuel designs are vulnerable to severe accident conditions, there is renewed interest in alternative fuel designs that would be more resistant to fuel failure and hydrogen production. Such new fuel designs would need to be compatible with existing fuel and reactor systems if they are to be utilised in the current reactor fleet and in current new build designs, but there is also the possibility of new designs for new reactor systems.

This report provides a record of a technical meeting, held in 2014 to consider the early stages of research and development into accident tolerant fuel. It is part of a wider investigation into such designs and it is anticipated that further technical meetings and research programmes will be undertaken in this field.

Fourty five participants from ten countries took part in the meeting. Thirty two papers were presented distributed between seven technical sessions. However, full texts of only twenty seven papers were submitted to the IAEA and included into the Proceedings of this meeting. But major findings contained in missing papers are overviewed in this Summary.

SUMMARY OF THE TECHNICAL SESSIONS

The first session, under the title Experimental Data and Modelling in Normal and Accident Conditions was chaired by John Killeen, the IAEA Consultant.

This session provided an overview of two of the major programmes in place to try to develop fuel that would be capable of withstanding a severe accident scenario, such as that at Fukushima Daiichi, potentially to avoid either fuel melt or to minimize the production of explosive hydrogen when the fuel temperatures rise in a steam environment. The consensus was that the approaches under consideration served to increase the time to restore cooling to the fuel in the case of severe accidents and this is, in itself, a significant benefit.

The first presentation on *Evaluation metrics applied to accident tolerant fuels* described a broad American project, led by the US Department of Energy (US DoE) to determine a set of metrics to help in the evaluation of suitable candidate designs for development as a more accident tolerant fuel than the current UO_2/zirconium alloy designs. The intention is to evaluate a new fuel design using a systems approach that would consider manufacture, normal operation and storage as well as response to severe accident conditions. It is seen that a new design must not affect the thermal hydraulics or the current fuel cycle under normal operation, but must show a benefit under accident conditions. The paper provided information about the US DoE programme and the expert panel that will provide a grid with weighting factors to assess the candidate projects for additional support after 2016.

The aim of the expert panel review is to ensure a proper quantitative assessment of the benefits and vulnerabilities of the different options available. Some provide minor benefits with a high likelihood

of success by using a continuous development model based on current fuel designs, whilst others consider a completely new ceramic cladding or fuel compound which would provide greater benefits if successfully developed through a longer and more risky development period.

It is clear that the requirements for accident tolerant fuel (ATF) were not simply defined and the term "more accident tolerant" was thought to be more appropriate. All fuel designs could fail under imagined scenarios and ultimately melt; the main issue is to improve the performance by lengthening the time that the fuel will remain intact under severe accident conditions. Some designs will provide much longer resistance to loss of cooling than others. Further it is realized that the various designs will provide differing responses to different accident scenarios, including less severe design extension conditions (DEC) faults, in old terminology- beyond design basis accidents-BDBAs, not recommended anymore after publishinging by the IAEA in 2012 of the "Safety Standards, Safety of Nuclear Power Plants: Design, Specific Safety Requirements No. SSR-2/1".

The second paper on *Development of fuels with enhanced accident tolerance* then provided information on the French programme, led by AREVA and the CEA. Their programme was based around improving fuel thermal conductivity and fission product retention and developing a clad that was less prone to hydrogen production whilst maintaining good geometry. They were participating in the US DoE ATF programme and were starting to move to product development with an enhanced conductivity pellet undergoing test reactor irradiations.

The programme includes research into innovative designs of cladding including SiC based claddings with a tantalum metallic liner to aid fission product retention which would resist oxidation under steam oxidation at 1200°C for over 100 h. Other cladding developments are more traditional, with oxidation resistant coatings being applied to zirconium alloy cladding. The pellet programme was looking at additives (up to 10%) which would improve the thermal conductivity of the pellets and lower the stored energy on reactor trip, improving the fission product retention, but this may require additional fuel enrichment to maintain current fuel cycles. Questions were raised about the technical details of the pellet behaviour, but any answers will depend on the results of the irradiation testing now being undertaken.

Session 2, titled as Metallic cladding accident tolerant fuel concepts was chaired by Lance Snead (ORNL) and Jean-Christophe Brachet (CEA). The main topic of this session was the various metallic cladding concepts under consideration and the attempts to design a cladding that would resist the oxidation of zirconium at high temperatures in a steam environment, avoiding cladding failure and hydrogen production.

The first paper on *Cladding behaviour during postulated design-basis LOCAs* from the USA described the Argonne experiments on oxidation and mechanical testing of current zirconium based alloys. The expectation for ATF was to improve cladding behaviour in design basis loss of coolant accidents (DB LOCA) where temperatures should always remain below 1204°C, and therefore hopefully the performance in design extension conditions (DEC). The data set included various commercial reactor alloys that had been pre-hydrided and some that had been irradiated to high burnup levels around 60 - 70 GWd/tU and the experiments were aimed at better defining a LOCA criterion for the USNRC.

The French experience with chromium coatings on zirconium alloy cladding tubes was described in detail in the second paper presented at Session 1. The intent of this work is to develop a cladding that is suitable for surviving a DB LOCA and slightly beyond and is a short- to mid-term research project. The idea is to limit the oxidation rate of the cladding so that it can meet the current DB LOCA criterion for several hours in steam environments at temperatures up to 1300°C, improving on the several minutes at 1204°C of current claddings. The current status of the work is that Cr coatings can be successfully applied to zirconium alloys and oxidation tests show significantly increased oxidation resistance. The time of onset of breakaway corrosion is significantly increased and the hydrogen pickup in the clad is reduced. However, several issues are still being considered, including the effects of irradiation and thermal cycling on the coating and the practicalities of commercially manufacturing zirconium alloy tubing with the coating.

The ORNL work on FeCrAl cladding material was presented by paper on *Optimization of nuclear grade fecral fuel cladding for light water reactors*. They have tested 20 alloys to help determine an optimum composition for an alloy with good resistance to oxidation and with suitable mechanical properties for use in reactor. So far they have developed an alloy with a minor improvement in mechanical properties compared with a zircaloy. Tensile testing shows little effect of the Cr/Al ratio in the alloys, but a minimum of 5% Al is needed for the oxidation resistance. Preliminary work has shown that satisfactory tubing can be manufactured. The results of computational thermodynamics for alloy design were presented and together with tensile testing of alloys with minor additives, have helped to optimize the mechanical properties.

Tensile test samples have been irradiated and tested, showing an increase in strength but had a variable effect on ductility. Detailed electron metallography has been undertaken and reliable trends of performance with alloy composition under irradiation have been found, but much further work is still to be done to determine the effects of, for example, irradiation temperature, dose and minor alloying elements. Irradiation tests of fuelled rodlets an optimized clad are planned to start in December 2014.

Electric Power Research Institute (EPRI) described a molybdenum clad design which requires a duplex tube with an oxidation resistant outer coat in paper on *Development of MO-based accident tolerant LWR fuel cladding*. Molybdenum cladding provides excellent mechanical properties, particularly at high temperatures, but there is significant uncertainty at this stage of its potential under oxidizing conditions.

Stainless steel cladding was the topic of the paper on *Characterization of advanced steels as accident tolerant fuel cladding for light water reactors* presented from GE in the USA. It was noted that the GE team was focusing on potential claddings under the US DoE ATF programme. The paper considers several steel alloys and uses zircaloy-2 as a comparator. A series of out of pile test have been carried out to examine crack potential, exposure to high temperature water with various water chemistry regimes and with steam. Chemical compatibility with fuel has been demonstrated to 80 GWd/tU.

The final paper of the session on *Development of co-pilgering process for manufacturing double clad tubes for accident tolerant fuel* came from India. It described the capabilities of the manufacturing facilities in India. In particular he described the potential to manufacture an ATF design of cladding made from duplex tubes of 9Cr-1Mo steel with a zircaloy-4 inner liner using pilgering. The presenter noted that any duplex tube can be made with this method.

Session 3 on Accident tolerant fuel screening was chaired by Andrew Sowder (EPRI) and Jeff Powers (ORNL). The main topic of discussion in this session was on the requirements to allow a selection of promising concepts for further research, without compromising work on concepts that would take many years to bring to commercial use, but had a high potential benefit.

A second paper from EPRI on *Challenges and opportunities for commercialization of enhanced accident tolerant fuel for light water reactors: a utility-informed perspective* was promoting international collaboration and noted that most ATF programmes are nationally based. EPRI noted that fuel changes have historically been driven by continuous improvement and incremental change. ATF changes are nuanced – it is necessary to consider fission product release, time and hydrogen generation. Stakeholders include the utilities, the vendors and regulators. Qualification of any new fuel is needed so the existing reactor lifetime is an issue as it can take 20 years for fuel development. An aggressive irradiation testing programme is needed, whilst keeping as many options open for as long as possible. There are many opportunities for international collaboration in materials characterisation and testing, but there needs to be a strong "pull" from vendors and utilities. Currently most programmes are government funded and not commercially pulled; for example, the US DoE programme is pulling universities and national labs into a programme with the utilities and vendors that has important milestones.

A multinational team presented a paper on *A safety assessment framework for prospective fuel technologies* that sets out structured guidelines on the issues that are needed to licence a new fuel type.

It is recognised that the existing safety criteria may well not be suitable for a new fuel design and it is necessary to think through the fuel safety assessment principles and requirements for a new fuel type in detail. Issues raised included mixed cores, where the new and old fuel must remain compatible throughout life. The discussion on this paper included concern that operators would take advantage of any improvement in fuel behaviour and simply exploit it through raised power or other operational manoeuvre and the safety advantage originally intended could become compromised.

The first paper of two papers from China on *Preliminary assessment of several candidates accident tolerant fuel* provided a current overview of China General Nuclear Power Group (CGN) R&D in the context of the larger Chinese activities and plans. CGN now has 11 operating plants and 13 under construction. CGN is in the process of expanding R&D investment with a reported 15 new R&D centres under development. In the nuclear fuel area, CGN activities encompass development of improved fuel assembly designs, advanced zircaloy cladding, nuclear fuel performance code, and accident tolerant fuel (ATF). China is pursuing greater international engagement on ATF-related R&D through multiple fora, including participation (with observer status) in OECD-NEA sponsored workshops beginning in 2012, bilateral discussions with US Department of Energy beginning in 2013, and the present IAEA Technical Meeting in 2014. In terms of national programmes, China is now launching two programmes in 2015, one of which is being led by CGN. Near-term Chinese cladding R&D is focused on advanced steels and coated (MAX phase) zircaloy. Longer-term focus is on ceramic (SiC/SiC composite) cladding materials. MAX phase coatings on metallics. For fuels, near-term interest is on advanced UO_2 formulations (via additives); longer-term concepts include high density uranium fuels (e.g., nitride and silicide compositions) and fully ceramic microencapsulated (FCM) fuel concepts. Other related efforts include severe accident code development.

The second paper from China on *Preliminary analysis of ATF concept design by NPIC* briefly reviewed the role of the Nuclear Power Institute of China (NPIC) as an established centre for nuclear fuel R&D and material testing and characterization. NPIC supplies all research reactor fuel in China and operates the largest test reactor in China – the High Flux Engineering Test Reactor (HFETR) and is currently constructing a new test reactor (HFETR 2), which should be operational in 2018. NPIC also operates 6 post-irradiation examination (PIE) facilities, radiochemistry laboratories, and hot cell facilities. While NPIC currently is not conducting ATF R&D funded under the current Chinese programme, NPIC does have experience with a wide range of advanced fuel concepts, including nitride, silicide, molybdate, and TRISO (Tri-layer coating for fuel particles used in high temperature reactors, in more details see T.D. Gulden, H. Nickel "Coated particle fuels", Nuclear Technology, vol. 35, Sept. 1977, pp. 206-213) compositions. NPIC is preparing for potential future work on ATF by conducting a scoping study and gap analysis spanning neutronics, fuel performance under normal operations, fuel response under design-basis and design extension accident conditions, and manufacturability and economics. In addition, NPIC is conducting some fuel performance modelling using the COPENIC 2.4 fuel performance code modified to handle SiC and UN materials. The Chinese nuclear safety authority, NNSA, has set a national goal for new nuclear plants to eliminate risk of large releases of fission products to the environment. This national policy provides an important driver for expanding and accelerating ATF R&D in China.

At the end of the session, a high level overview of the Nuclear Energy Agency (NEA) and a brief description of ongoing and new activities within NEA related to international ATF R&D were presented for the information of the participants (not included into the Proceedings). The primary activity related to ATF development at the NEA falls under the Nuclear Science Committee, which has been organizing workshops dedicated to information exchange since 2012. This activity has subsequently evolved as an expert group following approval of a formal charter by NEA governing bodies. Work by the Expert Group on Accident Tolerant Fuel for LWRs (EGATFL) is now underway and is organized under three task forces addressing ATF criteria, metrics, and assessment methods; cladding; and fuel. Initial products will likely be state-of-the-art reports. Another important activity at NEA supportive of international ATF collaboration is the updating of an NEA database on testing and characterization facilities. The NEA will continue to work with IAEA and other international programmes to coordinate activities and avoid unnecessary duplication of work.

Session 4 on Cross-cut testing was chaired by Shannon Bragg-Sitton (INL). This session focused on out-of-pile and in-pile testing of accident tolerant fuel and cladding concepts.

The second of the ORNL papers *High-temperature steam oxidation of accident tolerant fuel cladding candidate materials* provided information about high temperature steam oxidation of candidate ATF cladding materials, providing an excellent overview of the capabilities of the suite of high temperature steam testing facilities at ORNL. Key facilities are listed below, along with the limits on operating conditions:

- High pressure furnace (Keiser Rig): Examination of pressure effects on oxidation kinetics, up to 1400 °C, 2 MPa, 2 cm/s flow rate;
- Thermogravimetry: Generation of detailed oxidation kinetics information, up to 1550°C, atmospheric pressure, 2 cm/s flow rate;
- High temperature furnace: High temperature and high flow rate exposures, up to 1725°C, atmospheric pressure, 200 cm/s flow rate;
- Integral LOCA test station: Rapid temperature ramp to 1200°C, rod burst, quench, 1250°C (5-10°C/s ramp rate), atmospheric pressure, >10 cm/s.

The high temperature furnace and the integral LOCA test station are deployed in both ex-cell and in-cell versions for handling of clean, non-radioactive materials and materials after irradiation.

Oxidation test data generated using these test facilities for materials of interest to ATF cladding were presented. Results were focused on three protective barriers known to offer slow oxidizing species transport: chromia formers, alumina formers and silica formers. Data is relevant to both direct replacement of cladding and to coatings that might be applied to zirconium alloy cladding. Experiments indicated the following summary results:

- For Fe-based chromia formers, >25%Cr is necessary for good oxidation resistance;
- In FeCrAl alloys, a critical alloy concentration of Cr and Al is necessary to enable formation of protective oxides that in turn offer oxidation kinetics up to three orders of magnitude slower than Zr alloys;
- SiC, a silica former, exhibits exceptional oxidation resistance in water vapour up to 1700°C.

A paper on *Research on promising cladding materials for accident tolerant fuels at KIT* from Germany gave an overview of ATF cladding research that is being conducted at the Karlsruhe Institute of Technology (KIT). KIT performs research on candidate accident tolerant cladding materials under loss of coolant accident conditions.

KIT infrastructure allows experimental study of material behaviour at temperatures up to 2000°C. Integral tests on a scaled fuel rod simulator bundle are performed in the QUENCH facility to investigate thermo-hydraulic and material processes occurring during the LOCA or severe accidents (with or without control rods). Simulator bundles contain 21-32 fuel rods, ~2.5 m in length. An approximately 1 m section is electrically heating via heater rods inside ZrO_2 fuel simulator pellets to a maximum of 70 kW. Quenching can be performed using either water or saturated steam. Extensive instrumentation is available to monitor experimental and fuel simulator conditions.

KIT is currently performing research on SiC as candidate cladding material, including testing of prepared glasses as possible SiC joining material. KIT facilities are used to perform 4-point bend testing and high temperature oxidation and subsequent quenching of SiC, followed by x-ray and neutron radiography and tomography for sample analysis down to 1 μm resolution. Work is also being conducted in application of Fe-Cr-Al coatings on a zirconium alloy substrate using plasma spray followed by intense pulsed electron beam treatment. Coated zirconium alloys are currently being characterized and tested under steam oxidation.

Additional KIT test facilities include: NETZSCH steam furnace for thermogravimetric analysis (up to 100% steam, 1250°C or 1600°C in a dry atmosphere); BOX rig for investigation of materials at high temperatures (1700°C) in defined atmospheres (including steam); and single-rod QUENCH tests.

A report from Idaho National Laboratory (INL) provided an overview of ATF irradiation testing within the U.S. DOE programme (paper was not submitted for publication). The U.S. DOE is currently supporting the investigation of numerous fuel and cladding concepts within the national laboratories, industry, and universities. These concepts are currently undergoing feasibility studies (Phase 1), including both out-of-pile and in-pile testing, prior to the planned prioritization / down-selection in late 2016 that will lead to further development and testing of selected concepts in Phase 2. Irradiation testing of accident tolerant fuel and cladding concepts will go through multiple phases to collect the data necessary for licensing. The ATF-1 and -2 test series would be conducted in the INL Advanced Test Reactor (ATR), followed by the ATF-3 test series in the Transient Reactor Test (TREAT) Facility.

The ATF-1 series includes drop-in capsules to investigate the performance of a variety of proposed ATF concepts under normal LWR operating conditions. The ATF-1 capsules are filled with an inert gas and are designed to isolate fuel rodlets from the ATR primary coolant during irradiation. Hence, the test rodlet cladding will not be in contact with water coolant during irradiation. This test series is intended to investigate the irradiation behaviour of new fuels and their interaction with the cladding. Resultant data on fuel behaviour and fuel-cladding interaction will inform down-selection to one or more promising concepts prior to subsequent irradiation tests. ATF-1 will commence with the insertion of several ATF concepts supported by development teams that are led by industry partners Westinghouse Electric Company, AREVA, and General Electric (GE) Global Research and by Oak Ridge National Laboratory.

The ATF-2 series will further test the most promising concept(s) from ATF-1 in the INL ATR pressurized water loop. In an ATR loop, experimental fuel rods will be in direct contact with high-pressure water coolant with active chemistry control to mimic the conditions of pressurized water reactor (PWR) primary coolant. In addition to continuing the investigation of fuel behaviour and fuel-cladding interaction begun in ATF-1, ATF-2 will include cladding-coolant interaction. ATF-2 will be the most prototypic irradiation test possible in the ATR to assess the performance of ATF concepts under normal PWR operating conditions. The ATF-3 TREAT test series would then subject experimental ATF rods to reactivity-initiated accident (RIA) scenarios to investigate their integral performance under this class of accident conditions.

All irradiated concepts will go through a suite of post-irradiation exams (PIE), likely to be conducted at INL PIE facilities. Key fuel performance phenomena of interest include dimensional changes, fission gas production and release, fuel restructuring, constituent redistribution, and fuel-cladding chemical/mechanical interaction as a function of composition and burnup. Anticipated PIE includes standard non-destructive and destructive exams; additional PIE will include testing to measure thermal properties, mechanical properties, fracture toughness, microstructure, etc.

Session 5 titled as Advanced accident tolerant fuel pellets was cjaired by Rose Montgomery (TVA). The session on fuel pellets covered a wide range of concepts in three presentations. The first presentation from Korea on *Thermo-physical properties of micro-cell UO_2 pellets and high density composite pellets for accident tolerant fuel* considered microcell UO_2 where the thermal conductivity is improved by the addition of metallic or ceramic dopants which form an intersecting lattice on the grain boundaries. The team from KAERI has successfully manufactured pellets with oxides of silicon, titanium, aluminium and chromium and with metallic molybdenum and chromium. The team has demonstrated the effect of steam oxidation on these pellet variants. Their second approach is to support the development of uranium nitride pellets which have a high uranium density. They have prepared mixed uranium oxide and nitride pellets and s planning a series of irradiation tests.

Presentation from ORNL (paper was not submitted for publication) described the history of microencapsulated fuel. There is a long history of such carbon and silicon carbide coated particle fuel, and such fuel types have been used in high temperature gas cooled reactors. The use of TRISO particles in LWR could require an increase in enrichment to around 15%. Details were given of the manufacturing process for LWR applications, where the fuel particles would be embedded in a SiC matrix.

Information was provided on the mechanical and thermal properties of this fuel type and the irradiation testing of the fuel type with surrogate ZrO_2 kernels for the UO_2 in the fuel was described. It was noted that the thermal conductivity of the SiC matrix degraded with irradiation and that the swelling saturated at around 2% at 2-4 dpa. Overall it was shown that the fuel temperatures are expected to remain low, despite the conductivity degradation of the SiC matrix, and that fission product retention would be high. The fuel has an oxidation resistant matrix that has good stability under irradiation.

The final presentation in this Session from LANL in the USA (paper was not submitted for publication), considered USi as a fuel type, the additional uranium fuel density implied that it would be possible to utilize a cladding material with worse neutronics than zirconium based alloys. He had worked to understand the full phase diagram and looked at uranium silicide/nitride and boride mixes. He noted that oxidation was very easy for this uranium compound and that the powder was pyrophoric. An autoclave test at PWR type conditions would provide a go/no-go test of this material.

Session 6 on Accident tolerant fuelled system analysis chaired by Robert Montgomery (PNNL) and Michael Todosow (BNL). The session was focused on the analysis and modelling of ATF systems. The modelling teams all noted that additional work and data was required before accurate modelling of advanced fuel systems could be validated and verified.

A presentation from the University of Tennessee in the USA (paper was not submitted for publication) described an extensive programme of work supported by the US DoE. The code system BISON/MOOSE, within the NEAM/CASL framework, was a key tool for this investigation, utilizing the 3-D FEM capabilities to describe the geometry of the fuel variants, including TRISO particulate fuel and various coatings on the claddings. Neutronic modelling was also carried out on idealized fuel assemblies made from ATF using the SERPENT code. It was seen that it would be necessary to integrate aspects of fuel performance, neutronics and thermal hydraulics at intermediate scales (e.g. $\frac{1}{8}^{th}$ of the core) to enable system evaluations of ATF concepts. Typical results showed that oxidation resistant, coated claddings would increase fuel centre temperatures by around 30°C and give a small penalty on cycle length that could be compensated by increased enrichment. There remained a need for basic materials properties for many of the coatings proposed for ATF and for new techniques for modelling transient situations.

Brookhaven National Laboratories (BNL) used the US NRC code TRACE to analyse the performance of ATF in anticipated transients and accident conditions on *PWR plant model to assess performance of accident tolerant fuel in anticipated transients and accidents*. The code with a PWR model of a three loop Westinghouse plant was used. Point kinetics were generated using a 3-D core model. The PARCS code was used to calculate reactivity coefficients of uranium oxide and uranium nitride/silicide/boride fuel. Calculations showed that the fuel types had similar responses to some accident scenarios, e.g. steam generator tubes rupture (SGTR) or loss of off-site power.

Further work in support of the US DoE programme on ATF was reported from BNL in paper on *Reactor performance screening of accident tolerant fuel and cladding candidate systems*. This was focused on scoping calculations for advanced fuel and cladding materials in a state-of-the-art PWR. It is important to be able to fit the ATF into current design reactors. The work was directed towards UN-based ceramic fuels and several proposed advanced cladding materials. UN is chemically reactive with H_2O and must be *shielded* by a secondary phase. The work is limited to considering 17 × 17 Westinghouse PWR assembly geometry with an approximate 18 month cycle length. Reactor physics analysis of various advanced claddings (filled with UO_2 to provide a reference case) showed a burnup

penalty for all advanced clads, with the exception of SiC cladding, features such as resonance absorption (in Mo based clads for example) are not attractive, as the moderator temperature coefficient (MTC) is affected. Increased enrichment is a possible solution for this burnup penalty.

Various nitride fuel variants were considered, but it was necessary to use 100% enrichment to ^{15}N to remove the absorption penalty from other isotopes of Nitrogen. Cycle length and batch numbers were improved relative to UO_2 fuel because of the increased uranium density in the nitride and it may be possible to reclaim the enrichment penalty from the cladding. It was possible to design an ATF fuel variant that closely matched the behaviour of UO_2/Zr fuel types using an iron based cladding and a UN-U_3Si_5 fuel type. Key questions remain: do the secondary phases adequately shield the UN from H_2O and are the fuels viable from the perspective of the materials science (fabrication, properties, and radiation tolerance)?

The next paper (6.3) described the approach to ATF taken in the United Kingdom. It is part of a wider programme to consider fuel for Gen IV reactors as well as current and advanced PWRs. The aim is to select a suitable combination of advanced fuel and cladding and several candidate materials are being manufactured and tested. To quantify the potential benefits of ATF's and to explore the design optimization issues associated with a higher density, higher thermal conductivity fuel such as U_3Si_2 fuel, an in-reactor fuel modelling capability will be required. The fuel modelling programme ENIGMA has been used to explore the behaviour of various fuel types and to determine where materials properties are needed to allow accurate modelling. For some of the changes made to the code so that it could model advanced fuels, property measurements or post-irradiation examination (PIE) data were found in the literature on which new models could be based, but for others the absence of appropriate information meant that highly simplistic, or null, assumptions needed to be made. Examples of materials properties that are lacking for the U_3Si_2 fuel type include thermal expansion, creep, elasticity, densification and swelling, fission product diffusion rates, grain growth and others.

Core neutronic modelling was also undertaken to determine an optimized ATF based on UN fuel pellets. The determination of a suitable geometry depends on the moderator to fuel ratio and this was investigated to suggest that a ratio of 2.5 (compared with 1.9 for UO_2 fuel) would be suitable.

Overall economic assessments were also carried out for several options to show that ATF designs could have an economic benefit over UO_2/Zr fuel designs as well as their resistance to severe accident scenarios, but that there was a large amount of basic experimental work needed before this could be realized.

The final report in the Session was another paper from ORNL on *ORNL analysis of operational and safety performance for candidate accident tolerant fuel and cladding concepts* which provided an analysis of the operational and safety performance of various ATF concepts for PWRs. The reactor physics study of alternative cladding types showed that neutron absorption was a concern and that fuel enrichment above 5%E was likely to be needed to match the current fuel performance. SiC and FeCrAl cladding materials were potentially viable though they created changes to the neutron spectrum in the reactor. Further analyses in full core calculations, thermal hydraulics, fuel performance, accident behaviour and economics were needed.

The report also considered the performance of fully ceramic microencapsulated fuel. This fuel type is based on TRISO fuel particle technology, encased in a SiC matrix fuel pellet. The challenges include low uranium density and the consequent enrichment to around 20%. The analysis showed that this was a viable fuel concept, particularly if the fuel kernel was made from UN.

Severe accident calculations have been started using the MELCOR code to identify appropriate ATF concepts for BWR. There is a significant shortage of data for the analysis and much investigative work is needed to be able to properly model severe accident phenomena.

Session 7 on Silicon carbide based accident tolerant fuel concepts was chaired by Chairpersons: Sosuke Kondo (Kyoto University), Weon-Ju Kim (KAERI), Yutai Katoh (ORNL) and Mirco Grosse

(KIT). The final session was focused on the manufacturing issues associated with SiC based fuel cladding as well as materials properties and the effects of irradiation.

ORNL noted the positive benefits that could be obtained from SiC based cladding, such as oxidation resistance, lack of irradiation embrittlement and low neutron absorption (paper on *Systematic technology evaluation program FOR SiC/SiC composite- based accident-tolerant LWR fuel cladding and core structures*). The report noted the recent increase in industrial experience with the material which improves the potential to solve manufacturing difficulties for fuel tube and joining from other industries such as aerospace. However, the use of a ceramic cladding provides many challenges to an industry used to metallic clad materials and the relevant failure modes. Fuel performance calculations will have many issues to understand and model, such as the swelling of the clad, cracking (currently noted at around 20 GWd/tU), heat transport through the clad, fuel temperatures, fuel swelling interaction with the clad and others. The deployment of SiC cladding is definitely seen as a long term option for water cooled reactor systems.

There is wide international interest and collaboration in working with SiC to overcome some of the major manufacturing and compatibility issues. Other key issues are the statistical nature of failure and a need for a comprehensive performance analysis.

The commercial development of ATF fuel at Westinghouse was described in paper on *Progress on the Westinghouse accident tolerant fuel programme*. The programme has been running for over ten years but has accelerated following the Fukushima Daiichi accident. The development programme includes SiC cladding variants but is looking at a Ti_2AlC coating for zirconium alloys as a mid-term cladding option with SiC for use in the longer term. For fuel they were investigating U_3Si_2 for the mid-term and waterproofed UN for the long-term with commercial application targeted for 2030. In-pile and out-of-pile tests are being carried out with partner organisations, with results of irradiation testing of coated cladding due in early 2015.

The first of two reports from the Muroran Institute of Technology in Japan described the work undertaken there (paper on *R&D of SiC/SiC fuel pin at OASIS, Muroran Institute of Technology*). It described how work on SiC based claddings had been carried out for many years, where, the important role of high temperature non-metallic materials had been recognized as giving increased accident tolerance to LWR systems, but there was a new emphasis following the accident at Fukushima Daiichi. The paper introduced developments in the fabrication technology of Nano-Infiltration and Transient-Eutectic Phase (NITE) SiC/SiC composites. Under this programme it has been possible to manufacture SiC components, but the process is as much art as science. After the accident in 2011, SiC/SiC related activities have been accelerated under a programme named OASIS. The OASIS activities include a Government funded project, named SCARLET. The project aims to replace of zircaloy claddings with SiC/SiC based materials and to be able to manufacture such components reliably on an industrial scale.

A second paper from the Muroran Institute of Technology (paper on *Irradiation programme of SiC/SiC fuel claddings at Halden-reactor*) was presented to describe in detail the SCARLET (SiC fuel cladding/assembly research launching extra-safe technology) and INSPIRE (innovative SiC fuel pin research) projects. These were launched in 2012 as 5 year projects. INSPIRE is an irradiation testing project of SiC/SiC fuel claddings aiming to accumulate material, thermal and irradiation effect data of NITE-SiC/SiC in a BWR environment. Fuelled SiC/SiC cladding tube segments are installed in HBWR in Norway. The project includes preparing the NITE-SiC/SiC tubes, joining of end caps, preparation of rigs to control the irradiation environment to BWR condition and the instrumentation to measure the condition of rigs and pins in operation. Basic neutron irradiation data will be accumulated on SiC/SiC coupon samples currently under irradiation in BR2. The output from this project, presenting the potential of NITE-SiC/SiC fuel cladding, with the onset of fuel-cladding interaction, will become available within three years. The SCARLET project is aimed at industrialisation of the production of SiC based cladding tubes and end fittings. Currently tubes of up to 500 mm length are possible. An irradiation test in HBWR under PWR water condition will be started in early 2015, testing the environmental stability of SiC/SiC cladding by continuous DEMO

NITE (Nano-powder Infiltration and Transient Eutectic) process and joint stability with zircaloy endcaps.

A third Japanese paper on *Effect of constituents of silicon carbide composites on oxidation behaviour* from Kyoto University described the effect of constituents of silicon carbide composites on oxidation behaviour. He described how silicon carbide is a very attractive engineering ceramic, in particular for high temperature use and nuclear application. The superior stability of SiC under high temperature steam to that of metal is a critical motivation for light water reactor application. However, silicon carbide composites exhibit pseudo-ductile fracture behaviour by de-bonding and sliding at fibre/matrix interphase. Carbon (C) as the fibre/matrix interphase is the weakest link for severe environments including oxidation in steam, and SiC composites also include porosity and impurities, depending on the fabrication methods and conditions. Various kinds of SiC composites were prepared and then tested under high temperature oxidising conditions, some had a C interphase and others had residues from sintering additives. Air and steam oxidation conditions were used and significant weight reduction was observed for the composites with C interphase below 1000 ℃ depending on the amount of C. Significant degradation of mechanical properties were also observed for the composites with C interphase after exposure in air. The NITE (Nano-powder Infiltration and Transient Eutectic) composites deformed significantly after exposure in steam at 1200 ℃ due to significant oxidation. Degradation of mechanical properties was not observed for porous SiC composites without a C interphase.

A paper on *Mechanical property of triplex sic composite tubes and corrosion of CVD SiC in PWR-simulating water* from KAERI described testing of SiC composite tubes under normal operating PWR conditions. In particular this team studied the effect of dissolved hydrogen in the PWR water. The dissolved hydrogen dramatically reduced the corrosion rate of SiC compared with the water condition without the dissolved hydrogen. It was revealed that the dissolution of the surface oxide of SiC primarily contributed to the weight loss at the initial stage of corrosion. Further weight loss was limited for up to 120 days because the dissolved hydrogen effectively retarded the formation of SiO_2. A second series of tests on composite tubes investigated the stress response and showed that delamination could occur and that the hoop stress tended to be proportional to the volume fraction of the reinforced fibres in the composite.

A second paper on *Acceleration of the hot water corrosion of SiC by ion irradiation* from Kyoto University was presented which also considered hot water corrosion, but was interested in irradiation effects and tested ion-irradiated, high purity SiC material under varying water conditions. The results showed selective corrosion at crystallographic boundaries for both ion-irradiated and non-irradiated specimens, though it was clear that ion-irradiated regions were preferentially dissolved compared with non-irradiated regions, implying the operation of an irradiation enhanced corrosion mechanism.

A report (paper on *Silicon carbide behaviour under prototypic LWR chemistry/neutron flux and accident conditions*) from the Massachusetts Institute of Technology (MIT) described an extensive experimental and theoretical programme carried out there. Irradiation testing of SiC materials has been carried out since 2006. Exposure of SiC and SiC fibre composites in the MITR water loop facility has generated data on corrosion rates and property changes as a function of irradiation with some specimens achieving up to 600 days exposure. Monolithic Chemical Vapour Deposited (CVD) SiC show the lowest corrosion rates, however designs incorporating fibre composites offer better mechanical behaviour. The corrosion of the composite layers is driven strongly by details of their manufacturing and availability of the matrix and open porosity to the coolant; neutron irradiation also has an accelerating effect on this corrosion. Initial investigations into changes in strength indicate a trend due to composition and irradiation, but require large sample sizes due to statistical noise. Thermal diffusivity (and therefore conductivity) is a strong function of irradiation and composition. The composite and composite/monolith interfaces are important sources of thermal resistance and will significantly impact the heat transfer performance of SiC materials.

There have been tests to investigate LOCA conditions, with quench and burst tests carried out, including on composite tube samples and these tests are ongoing. The composite tubes are showing

low corrosion and good mechanical properties and different designs are being tested to optimise performance.

A second paper (*Technical and economic viability of ceramic multi-layer composite SiC cladding for LWRs*) from MIT was given that considered the technical and economic viability of ceramic multi-layer composite (CMC) SiC cladding for LWRs. CMC cladding is the only option among the proposed accident tolerant fuel concepts in the USA that could result in a fuel enrichment savings, and thus be compatible with the current enrichment infrastructure. CMC cladding could also result in additional economic benefit by avoiding the costs that might be incurred following a severe accident. However, due to its long development period and likely higher cost of manufacturing compared to zircaloy, its economics merits are uncertain.

The significant role that thermal conductivity degradation and swelling induced irradiation plays in performance of CMC cladding has already been documented. However, the impact of material properties on the performance of the neighbouring layers has been underrated and found recently to be critical for the viability of the concept. Analysis, using finite element software ADINA, shows that by considering the existing irradiation data for composite fibres and CVD SiC, a promising design can be achieved with an inner monolith surrounded by a fibre composite that compress the inner monolith layer followed by an environmental CVD barrier coating. A sensitivity study of the thermo-mechanical performance of such three layer cladding and its comparison to a two layer design with an inner composite and thick outer monolith layer was described.

The final presentation of the meeting was from the University of Tennessee and reported on recent results associated with a project funded by Nuclear Energy University Programs (NEUP) entitled, "Ceramic Coatings for Clad (The C^3 Project): Advanced Accident-Tolerant Ceramic Coatings for Zr-Alloy Cladding." The goal of this NEUP project is to develop an "accident tolerant" fuel concept based on an advanced ceramic coating for Zr-alloy cladding. The ceramic coatings investigated so far are primarily nitrides and carbides. Many of these samples were corrosion tested in a water-filled autoclave at 360°C for 3 to 14 days or in supercritical water at 542°C for 2 days. So far, titanium aluminium nitride (TiAlN) coatings coated with titanium nitride (TiN) have shown the smallest weight gains in 360°C water, suggesting that these coatings are the least susceptible to water-based corrosion. Paper was not submitted for publication.

ACCIDENT TOLERANT FUEL DEVELOPMENT PROGRAMME
(SESSION 1)

Chairperson

J. Killeen
(IAEA Consultant)

EVALUATION METRICS APPLIED TO ACCIDENT TOLERANT FUELS

S.M. BRAGG-SITTON
Idaho National Laboratory
Idaho Falls, Idaho
United States of America
E-mail: shannon.bragg-sitton@inl.gov

Abstract

The safe, reliable, and economic operation of the nation's nuclear power reactor fleet has always been a top priority for the United States' nuclear industry. Continual improvement of technology, including advanced materials and nuclear fuels, remains central to the industry's success. Decades of research combined with continual operation have produced steady advancements in technology and have yielded an extensive base of data, experience, and knowledge on light water reactor (LWR) fuel performance under both normal and accident conditions. One of the current missions of the U.S. Department of Energy's (DOE) Office of Nuclear Energy (NE) is to develop nuclear fuels and claddings with enhanced accident tolerance characteristics for use in the current fleet of commercial LWRs or in reactor concepts with design certifications (GEN-III+). LWR fuel with accident tolerant characteristics became a focus within advanced LWR research following the 2011 Great East Japan Earthquake, resulting tsunami, and subsequent damage to the Fukushima Daiichi nuclear power plant complex, and upon receiving direction from Congress. The overall goal of ATF development is to identify alternative fuel system technologies to further enhance the safety, competitiveness and economics of commercial nuclear power. Enhanced accident tolerant fuels would endure loss of active cooling in the reactor core for a considerably longer period of time than the current fuel system while maintaining or improving performance during normal operations. The U.S. DOE is supporting multiple teams to investigate a number of technologies that may improve fuel system response and behaviour in accident conditions, with team leadership provided by DOE national laboratories, universities, and the nuclear industry. Concepts under consideration offer both evolutionary and revolutionary changes to the current nuclear fuel system. Mature concepts will be tested in the Advanced Test Reactor at Idaho National Laboratory beginning in summer 2014 with additional concepts being readied for insertion in fiscal year 2015. This paper provides a brief summary of the proposed evaluation process that would be used to evaluate and prioritize the candidate accident tolerant fuel concepts currently under development.

1. INTRODUCTION

The goal of ATF development is to identify alternative fuel system technologies to further enhance the safety, competitiveness, and economics of commercial nuclear power. The development of an enhanced fuel system supports the sustainability of nuclear power, allowing it to continue to generate clean, low CO_2-emitting electrical power in the United States. Any new fuel concept must be compliant with and evaluated against current design, operational, economic, and safety requirements. The overall fuel cycle must also be considered, particularly for concepts that represent a significant departure from the current technology.

The complex multi-physics behaviour of LWR nuclear fuel makes defining specific material or design improvements difficult; as such, establishing desirable attributes is critical in guiding the design and development of fuels and cladding with enhanced accident tolerance. ATF designs would endure loss of active cooling in the reactor core for a considerably longer period of time than the current fuel system – depending on the LWR system and accident scenario – while maintaining or improving fuel performance during normal operations. Key requirements for advanced fuels relate to the nuclear fuel performance, cladding performance, and adherence to overall system constraints.

This paper provides a brief summary of a technical evaluation methodology proposed within the U.S. to aid in the optimization and prioritization of candidate ATF designs. A complete description of the proposed metrics and associated sensitivity studies is included in Ref. 1. As used herein, "metrics" describes a set of technical bases that will be applied to fairly evaluate multiple concepts against a common baseline and against one another. The proposed technical evaluation methodology will be applied to assess the ability of each concept to meet performance and safety goals relative to the current UO_2 – zirconium alloy

system. Evaluation of anticipated benefits will be based on characterization and test data available at the time the evaluation is performed. Potential vulnerabilities will also be scored based on known or anticipated operational vulnerabilities or currently unknown performance for a selected parameter. The resultant ranked evaluation will then inform concept prioritization, such that the most promising accident tolerant fuel design option(s) can continue to be developed for irradiation as a lead fuel rod (LFR) or lead fuel assembly (LFA) in a commercial reactor within the desired timeframe (by 2022). Concept prioritization is currently planned for late 2016.

2. ACCIDENT TOLERANT FUEL ATTRIBUTES

The desired ATF attributes highlight the performance of both the fuel and cladding under normal and postulated accident conditions. Fuel system design options must first maintain acceptable cladding and fuel thermo-mechanical properties, fuel-clad interactions, and fission-product behaviour. Targeting improvements in these attributes provides guidance in establishing the critical parameters that must be considered in the development of fuels and cladding with enhanced accident tolerance. Accident tolerant attributes include reduced steam reaction kinetics, lower hydrogen generation rate (or generation of other combustible gases), and reduced stored energy when compared to the current fuel system. A common set of qualitative metrics (versus specific quantitative targets for each property) will aid in design optimization and concept prioritization on a more quantitative basis.

Candidate fuel systems must first hold to the principle of "do no harm," meaning that the fuels must, under all operating conditions, perform as well as or better than the current fuel system. As such, a candidate fuel should preserve or improve upon:

- Burnup limits / cycle length (while maintaining criticality and fuel performance).
- Operational parameters (power distribution, peaking factors, safety margins, etc.).
- Reactivity coefficients and control parameters (shutdown margin, rod worths).
- Handling, transportation and storage (consideration of fuel isotopics, handling dose, mechanical integrity).
- Compatibility with existing infrastructure (e.g. fabrication facilities, loading, in-core operations, post- irradiation handling and storage, etc.; necessary to maintain acceptable economics).

To be considered for the "accident tolerant" moniker the fuel system must additionally provide improved response to anticipated operational occurrences (AOOs), DBAs (reactivity initiated accident, loss of coolant accident, station blackout) and BDBAs. Improved performance under normal operating conditions will be necessary to make an economic case for enhanced fuels that are likely to be more costly than the current fuel system. Economic viability must be maintained with respect to additional costs (e.g., fabrication) and potential cost reductions realized through improved performance (higher burnup for extended cycles and power upgrades) or increased safety margin.

3. GO/NO-GO CRITERIA

A large number of properties and performance parameters are considered in fuel development. Fuel performance is the result of a complex system with interaction between the components of the fuel, cladding, reactor configuration and protection systems. Fuel system performance cannot be evaluated in isolation. Some "go / no-go" criteria must be established for any fuel system prior to defining more specific performance targets. Briefly stated, these include:

- The fuel design must meet current LWR constraints without changing assembly thermal-hydraulics.
- The fuel must have a quantifiable benefit under accident scenarios (e.g. longer times to onset of fuel melt) relative to the current fuel system to be deemed "accident tolerant".
- Reactivity feedback coefficients must be similar in magnitude and parametric behaviour to the reference UO_2 – Zr alloy system to ensure backward compatibility in existing reactors. Reactivity coefficients for candidate fuels must not reduce the safety of the reactor system or the safety margin and should fall within the existing safety envelope for UO2 – Zr fuels.
- The fuel must maintain current cycle length and power output at allowable enrichment levels (increased cycle length, number of fuel batches in the core management scheme, and power density may be desirable but not required).

A concept that fails to meet one of these criteria would be omitted from further consideration. For example, a fuel enrichment requirement of 20% or higher (above the low enriched uranium [LEU] limit), as determined by neutronic calculations, would be "no-go." This equates to a vulnerability that cannot be overcome, hence removing the concept from consideration. A required enrichment of 5-20% would be assigned an increasing vulnerability as the enrichment requirement increases (i.e., 19.9% $\longrightarrow$ vulnerability of -5); see section IV for a description of how benefit and vulnerability scored would be applied in the evaluation of each concept.

4. PROPOSED EVALUATION METRICS

Assessment of the potential beneficial impact or unintended negative consequences of candidate ATF concepts must address the obvious "fuel-specific" characteristics of the concept and must also address how implementation of the concept may affect overall reactor performance and safety characteristics. This assessment would include neutronics and thermal-hydraulics analyses to ensure that the reactor would operate as intended with the candidate fuel system. Coupled thermal hydraulic-neutronic analysis of candidate ATFs is essential in understanding the synergistic impact of the thermal properties and reactivity feedback.

Detailed evaluation of each concept will gauge its ability to meet performance and safety goals relative to the current UO_2 – zirconium alloy system and relative to one another. This ranked evaluation will enable the continued development of the most promising ATF design options given budget and time constraints, with a goal of inserting one (or possibly two) concepts as a lead fuel rod in a commercial LWR by 2022.

Evaluation of proposed fuel system concepts will be conducted by an independent expert review panel. Results of this evaluation will inform a prioritization of fuel system concepts by late 2016. At the time the review is conducted, preliminary viability will have been determined via fundamental material characterization, benchtop scoping tests, preliminary irradiation, and associated neutronic and thermal hydraulic modelling. The convened expert review panel will be comprised of technology experts selected based on their knowledge of the technologies under review, reactor operations, and fuel fabrication plant operations. The review panel will include experts specializing in materials (metals and ceramics), neutronics, thermal-hydraulics, reactor operations, and severe accidents to enable assessment of the technology feasibility for near term development of each ATF design concepts.

An evaluation table will aid the panel in ranking the potential performance of multiple concepts across the fuel life cycle and range of potential operating conditions. The independent panel will be tasked with reviewing input (available data, analysis results, modelling and simulation results) provided by each concept design team and to make a qualitative assessment of the relative benefits or vulnerabilities associated with the candidate design for each "Performance Attribute" relative to the specified "Performance Regimes" including:

- Fabrication/Manufacturability (to include licensability and anticipated economics over the life cycle of the fuel);
- Normal Operation and AOOs;
- Postulated Accidents (DBA);
- Severe Accidents (BDBA);
- Used Fuel Storage/Transport/Disposition (to include potential for future reprocessing).

The concepts may be at varying stages of development upon initial review. It is unlikely that any of the concepts will have been fully characterized upon commencement of the review. The goal for the initial committee review is to have sufficient confidence in the assessment results to estimate the potential for success of a concept and to make preliminary estimates on the time and budget that may be required to develop the concept to maturity.

The proposed evaluation table (Table 1) is designed to separately identify "Benefits" and "Vulnerabilities" for each concept. The candidate fuel system should be ranked within each category on a scale of 0 to ±5. A score of "0" would indicate no notable change from the current fuel system; i.e. evaluation of UO_2 – Zr-alloy would result in an overall score of 0 for both benefits and vulnerabilities. A score of "+5" in the benefits column would indicate a significant benefit/improvement relative to the current system; a "-5" in the vulnerabilities column would indicate a significant data gap or potential issue for the indicated performance attribute. A "vulnerability" could be a known operational vulnerability that results from a particular fuel system behaviour or property, such as lower than desired melting temperature, or an attribute could be scored with high vulnerability based on currently unknown performance for a selected parameter. If a specific property or behaviour has not yet been measured or tested (or if it is not known conclusively), this would correspond to higher vulnerability and should be scored as such. For attributes that are currently unknown or assumed, recommended actions should then be noted by the Expert Panel to mitigate the associated risk.

Scoring of benefits and vulnerabilities is inherently subjective in nature. Selection of the panel members based on significant expertise in one or more areas relevant to fuel and reactor performance will be critical to development of an accurate review of all proposed concepts. It is not expected that any one reviewer would have expertise in all necessary areas. The purpose in establishing a range of possible scores from 0 to ±5 is to allow for more discretization by the review committee that will be necessary in ranking the various concepts. Scoring of benefits and vulnerabilities *separately* ensures that technologies can easily be parsed into categories of moderate benefit – low risk; moderate benefit – high risk; significant benefit – low risk; and significant benefit – high risk. The overall benefits score and vulnerabilities score *must not be added together*, as the anticipated benefits *do not* negate the noted vulnerabilities. If a decision is made to continue development of a concept despite noted vulnerabilities, any recommended actions should be resolved before convening a subsequent review panel.

The assessment table attempts to list key considerations under each performance regime, and the associated performance attributes for those regimes. Industry has provided input to these desired performance attributes, as described in Montgomery et al. [2]. *This list of attributes is not exhaustive, but is intended to identify the major contributors/considerations to the identified regime.* Some of these items may need to be modified for particular plant designs. In the absence of a specific plant design, which would include details of emergency response systems applicable to accident performance, these assessments must be made on a general basis.

The same screening table (Table 1) can be applied as the conceptual fuel system designs are matured and additional performance data becomes available. The level of uncertainty in each of the performance attributes would be expected to decrease at each evaluation stage, allowing quantitative estimates for some of the behaviours of interest as more property data become available. For high risk, potentially high payoff technologies, the vulnerability score and number of recommended actions would be expected to decrease significantly for each subsequent review, allowing a more informed decision to proceed (or not proceed) with further testing and development. There is also provision for "off-ramps" prior to subsequent expert review should a concept design or specific materials demonstrate that it cannot meet the minimum performance requirements during the fundamental scoping tests or core level analysis.

The "benefits" and "vulnerabilities" scores for each technology will result in a ranked, prioritized list of candidate technologies. The review panel may choose to report two prioritized lists: one for near-term technologies, fitting within the defined 10-year development window, and a second for longer term technologies that appear to have a significant benefit at this early development stage but are unlikely to meet the defined development timeframe. The number of technologies selected to proceed for additional testing and development will be dependent on budget availability.

TABLE 1. ASSESSMENT TABLE FOR CANDIDATE FUEL SYSTEM ATTRIBUTES

Performance Regime	**Performance Attributes (For large-scale deployment)**	**Expert Opinion Assessment**		**Recommended Actions**
		Benefit	Vulnerability	
Fabrication/Manufacturability *Considerations:* Millions feet of clad/year ~300 million pellets/year Economics - cost of raw materials and fabrication process Current fabrication plant enrichment limits	Manageable fissile material content			
	Compatible with large-scale production needs (material availability, fabrication techniques, waste, etc.)			
	Compatible with quality and uniformity standards			
	Licensibility			
	Anticipated life cycle costs			
Normal Operation and AOOs *Considerations:* Overall neutronics Linear Heat Generation Rate (LHGR) to centerline melt Power ramp, ~100 W/m/min Reduced flow (departure from nucleate boiling, DNB) Flow-induced vibrations Surface roughness effects Safe shutdown - earthquake External pressure (~2750 psi, 10%	Utilization or Burnup (12, 18, or 24 month/cycle)			
	Thermal hydraulic interaction			
	Reactivity control systems interaction			
	Mechanical strength, ductility (beginning of life and after irradiation)			
	Thermal behaviour (conductivity, specific heat,			
	Chemical compatibility (fuel-cladding) / stability			

Performance Regime	Performance Attributes (For large-scale deployment)	Expert Opinion Assessment	Recommended Actions
above PWR design pressure) Axial growth (less than upper nozzle gap)	Chemical compatibility with and impact on coolant chemistry		
	Fission product behaviour		
Postulated Accidents (Design Basis) *Considerations:* Prompt reactivity insertion Post-DNB behaviour (T > 800°C for Zr- UO_2 system) Loss of coolant conditions Thermal shock Steam reactions (~1000°C +)	Thermal hydraulic interaction		
	Mechanical strength and ductility		
	Thermal behaviour (conductivity, specific heat,		
	Chemical compatibility/ stability (e.g. oxidation behaviour)		
	Fission product behaviour		
	Combustible gas production		
Severe Accidents (Beyond Design Basis) *Considerations:* Thermal shock Chemical reactions Combustible gas release Long-term stability in degraded state	Mechanical strength, ductility		
	Thermal behaviour (conductivity, specific heat,		
	Chemical compatibility/ stability (including high temperature steam interaction)		
	Fission product behaviour		
	Combustible gas production		
Used Fuel Storage/ Transport/ Disposition *Considerations:* Handling, placement, and drying loads; future reprocessing potential	Mechanical strength, ductility		
	Thermal behaviour		
	Chemical stability		
	Fission product behaviour		

5. CURRENT STATUS AND PATH FORWARD

This paper described a proposed technical evaluation methodology that can be applied to assess the anticipated operational and safety performance of proposed accident tolerant fuel concepts relative to the current UO_2 – Zirconium alloy system. Rather than focus on individual properties, the approach considers the confluence of properties that results in a particular behaviour during all phases of possible operation and also considers challenges associated with fabrication of each concept. Evaluation tables completed for each concept will provide a clearer overview of each new concept relative to one another, highlighting expected benefits and vulnerabilities – which can be translated to the risk / benefit ratio for each concept and can be linked to the near term versus far term nature of the concept development. The intended goal of this exercise is to inform concept prioritization, such that the most promising accident tolerant fuel design option(s) can continue to be developed toward lead fuel rod insertion in a commercial reactor (targeted for 2022) and qualification.

ACKNOWLEDGEMENTS

This work was supported by the U.S. Department of Energy, Office of Nuclear Energy, under DOE Idaho Operations Office Contract DE-AC07-05ID14517, and was performed on behalf of the Fuel Cycle Research & Development Program Advanced Fuels Campaign. Significant contributions have been made to the metrics development effort by a number of individuals across the DOE complex. Contributors include Melissa Teague and Brad Merrill (INL); Larry Ott and Kevin Robb (ORNL); Mitch Farmer and Mike Billone (ANL); Robert Montgomery (PNNL); Chris Stanek (LANL); and Michael Todosow and Nicholas Brown (BNL).

REFERENCES

[1] BRAGG-SITTON, S.M., et al., "Enhanced LWR Accident Tolerant Fuel Performance Metrics", INL/EXT-13-29957, Idaho National Laboratory, prepared for the U.S. Department of Energy Advanced Fuel Campaign (2013).

[2] MONTGOMERY, R., et al., "Industry-valued Design Objectives for Advanced LWR Fuels and Concept Screening Results," Proceedings of 2013 LWR Fuel Performance Meeting/TopFuel, Charlotte, NC, USA (Sept 2013).

DEVELOPMENT OF FUELS WITH ENHANCED ACCIDENT TOLERANCE

J. BISCHOFF[*], P. BLANPAIN[*], J-C. BRACHET[**]
C. LORRETTE[**], A. AMBARD[***], J. STRUMPELL[+], K. McKOY[+]
[*]AREVA NP, Lyon
[**]CEA, Saclay
[***]EDF R&D, Ecuelles, France
[+]AREVA Inc., Lynchburg, Virginia, United States of America
E-mail: jean-christophe.brachet@cea.fr

Abstract

AREVA is involved in several projects for the development of fuels with enhanced accident tolerance. Through its participation in the DOE-NE ATF programme, AREVA is investigating with the University of Florida new UO_2 pellets containing SiC additives as whiskers or particles, and fabricated with Spark Plasma Sintering technique, which reduces fabrication times. These new pellets have the potential to increase the thermal conductivity by up to 60% of the conventional UO_2 pellet, which will therefore decrease the pellet temperature during operation and thus decrease fission gas release. Nevertheless, this still has to be confirmed at very high temperatures and especially under irradiation. Concerning potential cladding solutions the coating of zirconium alloy with a MAX phase is one option that is investigated. The goal is to limit the zirconium oxidation reaction and its production of hydrogen during high temperature steam corrosion. Additionally, AREVA is also involved as fuel vendor in the development of a molybdenum (Mo) cladding managed by the Electric Power Research Institute (EPRI) [1]. The latter uses the good high temperature thermo-mechanical properties of molybdenum (high thermal conductivity and mechanical strength) to improve accidental behaviour. Furthermore, AREVA is actively involved with the CEA and EDF in tri-partite R&D projects to develop the CEA's two potential cladding concepts of chromium coated zirconium alloys and sandwich SiC/SiC composite cladding [2, 3]. The chromium-coated zirconium alloys have shown great potential at inhibiting the high temperature steam oxidation reaction and preserving the cladding mechanical properties. The SiC/SiC sandwich cladding, initially developed for fast breeder reactor applications, exhibits low steam oxidation kinetics at high temperature, which would enhance the LWR fuel's accidental behaviour.

1. INTRODUCTION

For the past 50 years, the nuclear fuel rod concept for Light Water Reactors (LWRs) of UO_2 pellets enclosed in zirconium cladding has been used and optimized to improve its reliability and performance. At the same time, other types of fuel concepts have been investigated mainly for applications in research and fast breeder reactors, and more recently as part of the large international R&D effort on Generation IV reactors. During the Fukushima Daiichi accident in 2011 the fuel rods underwent the degradation stages of a severe accident, including the rapid oxidation of zirconium, which led on the one hand to the production of large quantities of hydrogen, and on the other hand to additional heat production [4]. As a consequence, the nuclear community decided to find and develop innovative fuel concepts that would exhibit enhanced resistance to accidental conditions, and particularly against exothermic cladding oxidation.

Fuel concepts defined as enhanced accident tolerant fuels are both cladding and fuel meat/pellet solutions which should exhibit the following properties:

- High melting temperature;
- Improved oxidation reaction kinetics with high temperature steam to reduce the heat and hydrogen production due to the high temperature oxidation of zirconium alloys;
- Improved cladding and fuel thermo-mechanical properties to maintain coolable geometry at high temperatures (limit ballooning and burst, and retain high post-quench ductility);
- Increased thermal conductivity of fuel meat;
- Enhanced retention of fission products.

AREVA is actively participating in the development of some innovative fuel concepts, which include three potential cladding solutions and one fuel meat/pellet concept. These developments are performed through two main collaborative projects consisting of:

- The DOE-NE Enhanced Accident Tolerant Fuels (EATF) programme, in partnership with Duke Energy, Tennessee Valley Authority (TVA), University of Florida (UF), University of Wisconsin (UW), Savannah River National Laboratory (SRNL) and the Electric Power Research Institute (EPRI) [5];
- The tri-partite R&D with the CEA, and EDF.

Additionally these developments are complemented by experiments performed at the AREVA Technical Centres as well as accidental behaviour analyses. This paper will present the different concepts investigated within these programmes.

2. DESCRIPTION OF THE CONCEPTS INVESTIGATED

As part of the DOE-NE EATF programme, AREVA is developing the following concepts:

- For the cladding:
  - Max phase coatings on zirconium alloys with savannah river national laboratory and the university of wisconsin;
  - Epri's molybdenum (mo) cladding;
- For the fuel meat/pellet:
  - SiC and diamond additives to UO_2 pellets using spark plasma sintering (SPS) to increase the pellet thermal conductivity with the University of Florida.

As part of the tri-partite R&D with CEA and EDF, AREVA is developing two potential cladding concepts:

- Chromium coatings on zirconium alloys;
- SiC sandwich cladding containing two layers of SiC composite surrounding a thin metallic layer.

2.1. Innovative cladding concepts

Overall, three main cladding concepts (coatings on zirconium alloys, EPRI's Mo cladding, and CEA's SiC sandwich cladding) are being investigated, each with a different range of potential performance during accident conditions and with various deployment times. The objective is to develop solutions ranging from evolutionary concepts (for example coatings on zirconium alloys) to revolutionary concepts (such as the SiC sandwich cladding) with gradually increased potential performance in accident conditions, which is correlated with a gradual increase in deployment time. Fig. 1 schematically describes this evolution of performance with implementation time.

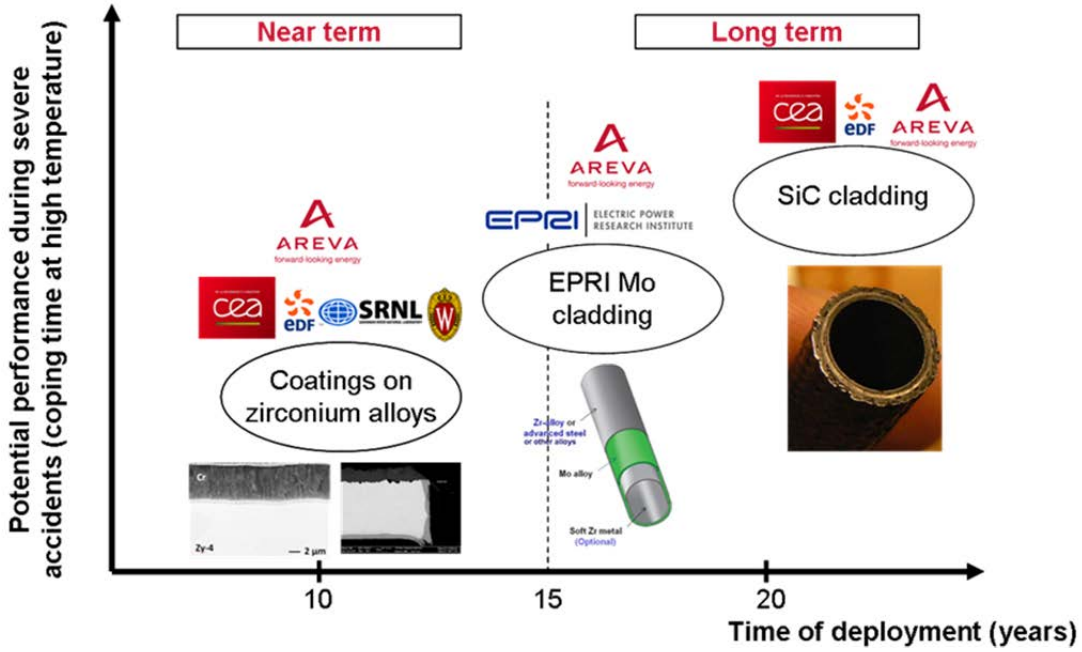

FIG. 1. Potential performance as a function of development time for the various cladding concepts investigated by AREVA.

2.1.1 CEA's chromium coating on zirconium alloys

Within the tri-partite R&D framework with CEA and EDF, AREVA is investigating the coating of a thin layer of chromium (between 8 – 20 µm thick) on zirconium alloys to improve the high temperature steam corrosion behaviour. The chromium layer is fabricated by Physical Vapour Deposition (PVD), which creates, for fresh material, a dense layer with good adherence to the substrate [2].

Overall the chromium coating serves as a protective oxidation barrier by providing the following properties:

- Significantly improved resistance to corrosion under nominal conditions in the usual 360°C water test;
- Reduced corrosion rates in high temperature steam;
- Increased post-quench mechanical behaviour due to a reduced ingress of oxygen within the metal to form the α(O)-Zr phase.

For example, Fig. 2 shows the comparison between uncoated and coated Zy-4 tubes after oxidation in 1200°C steam for 6000 s and quench. The uncoated sample exhibits a very thick oxide and has fragmented after the quench whereas the coated sample shows very little oxide and was not deteriorated after the quench.

FIG. 2. Overview of uncoated and coated Zy-4 tubes exposed to steam at 1200°C for 6000 s after quenching.

2.1.2 MAX phase coating on zirconium alloys

MAX phases are a group of ternary ceramic compounds composed of early transition metals (Sc, Ti, V, Cr, Zr, Cr, Nb, Mo, Hf, and Ta) as M, of elements in the A group (mainly Al, Si, P, S, Ga, Ge, As, In, Cd, Sn, Tl, and Pb) as A, and carbon or nitrogen as X [6, 7]. Research on these compounds began during the late 1990s so they are new materials but they exhibit very interesting properties by combining some of the advantages of metals and ceramics. For example, MAX phases have a good thermal and electrical conductivity, as well as good corrosion resistance and the good mechanical properties are maintained at high temperature.

Consequently, AREVA, along with the Savannah River National Laboratory and the University of Wisconsin, is investigating these MAX phases, in the form of Ti_2AlC, as a coating on zirconium alloys to reduce the high temperature steam oxidation and thus decrease the heat and hydrogen production. The coating is deposited on the surface of the sample using Cold Spray, a technique which forms relatively dense coatings but which makes it difficult to obtain a coating thinner than 50 µm. The coating is adherent to the substrate and shows good high temperature steam corrosion resistance. Fig. 3 shows a cross-section scanning electron microscopy (SEM) image of a one-sided coated sample expose tot steam at 1100°C for 4 min. Very little oxidation is observed under the coating compared to the un-coated edges of the sample.

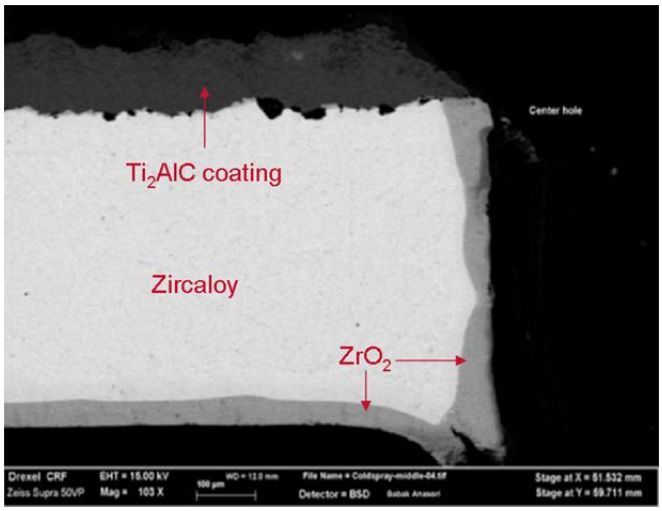

FIG. 3. Cross-section SEM image of a one-sided Ti_2AlC coated Zy-4 sample exposed to 1100°C for 4 min.

2.1.3 EPRI's Molybdenum cladding concept

Molybdenum is a refractory metal which melts at a temperature of 2623°C, which is close to the melting point of UO_2 (2850°C) and nearly 1000°C more than zirconium alloys (around 1850°C). Consequently, molybdenum can provide additional margins in terms of fuel melting. Additionally, it has a high thermal conductivity and preserves good mechanical strength and behaviour at high temperatures (1000°C and above), which can help maintain the coolable geometry of the rod by preventing ballooning and burst, a key property to improve the accident tolerance of the cladding.

Nevertheless, the neutron absorption cross section (more than 10x that of zirconium) of molybdenum is relatively high so thin tubes 0.2 mm thick are envisioned to partially compensate for the loss of reactivity. Additionally, the corrosion of molybdenum in water environment can be an issue due to material recession so two developments are being investigated: on the one hand zirconium or FeCrAl coatings are deposited on the surface to provide corrosion resistance leading to a duplex or triplex rod concept, and on the other hand more corrosion resistant molybdenum alloys are being developed with the goal to simplify the rod concept by not needing the coating [1]. Fig. 4 schematically shows the design of the triplex Mo cladding with Zr or FeCrAl coating.

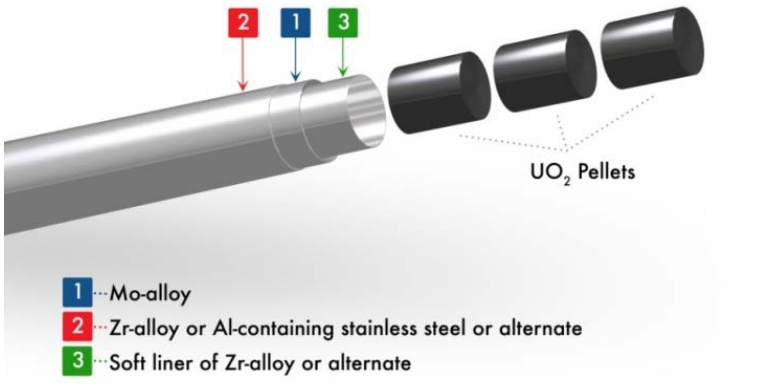

FIG. 4. Schematic of EPRI's Mo cladding concept.

2.1.4 CEA's SiC sandwich cladding

SiC/SiC composite cladding was investigated at first for Generation IV application in Gas Fast Reactors due to its very good high temperature properties and dimensional stability. Since the event at Fukushima Daiichi in 2011, this concept is being adapted for application in light water reactors (LWRs) with the aim to increase safety margins during accidental conditions. The main advantages for using SiC to improve accident tolerance are:

- Very low nominal and high temperature steam corrosion kinetics;
- High strength at high temperature;
- High sublimation temperature.

The cea sandwich concept contains a thin (50-100 µm) refractory metal liner in between two sic composite layers as described in Fig. 5. This sandwich design offers many advantages since the metallic liner provides the following g key features [3]:

- Leak-tightness of the cladding;
- Improved mechanical properties;
- Easier sealing of the cladding by conventional solutions such as welding.

Studies were performed to establish the corrosion behaviour of SiC composite under PWR conditions and showed very little oxidation compared to conventional zirconium alloys and the mechanical properties of the SiC cladding are preserved after such an oxidation. Furthermore, high temperature tests showed that SiC composite tubes exhibited very little weight change up to 110h in 1200°C steam whereas a standard Zy-4 tube was decomposed after only 4h. These results demonstrate the potential of this material, but significant studies and developments are still necessary due to new failure modes compared to conventional metallic cladding, which would also lead to new design rules.

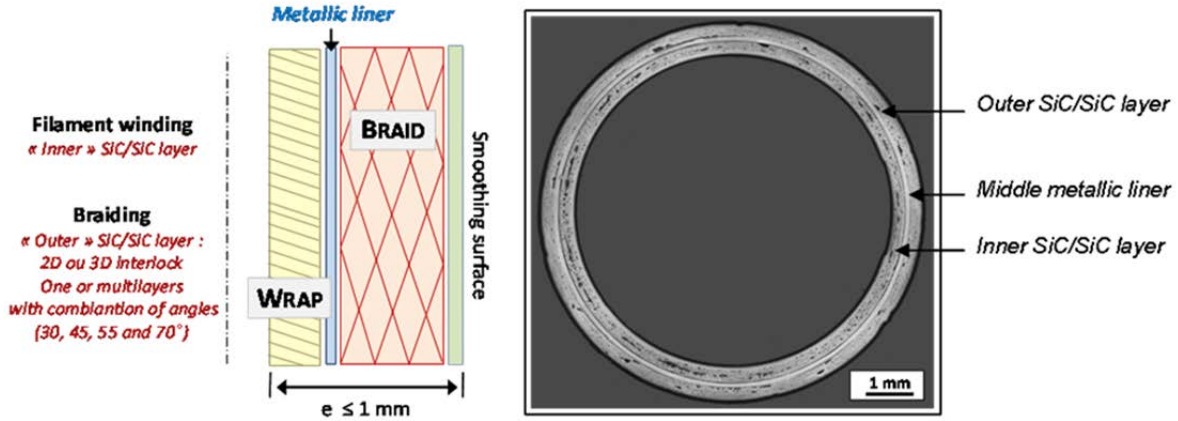

FIG. 5. Schematic of CEA's SiC sandwich cladding concept and cross-section of a manufactured prototype.

2.2. Innovative fuel meat concepts

AREVA is investigating with the University of Florida the addition of SiC (as whiskers or powder) or diamond particles in UO_2 pellets to enhance its thermal conductivity. Increasing the thermal conductivity of the pellet will decrease the average fuel temperature and reduce the radial temperature gradient, which will reduce the thermal stresses and cracking in the

pellets. Consequently, such a development would decrease the fission gas production and release.

The additive materials (SiC as powder or whiskers, and nano-diamond particles) were chosen for their small neutron absorption cross-section, chemical stability and high thermal conductivity. The amount of additives is limited to 10 vol% because it provides a significant improvement in conductivity in unirradiated samples (around 40%) while not infringing on the enrichment limit of 5% [8]. The composite pellets are fabricated using a Spark Plasma Sintering technique, which decreases fabrication time and increases pellet density to obtain an average of 95% of theoretical density. Fig. 6 shows SEM micrographs of UO_2 – 10 vol% SiC composites fabricated by the conventional oxidative sintering technique and the SPS technique [8].

These composite pellets (both UO_2 – SiC and UO_2 – diamond pellets) will be irradiated as rodlets in the Advanced Test Reactor (ATR) as planned by the DOE programme. The main goal of this irradiation is to assess the impact of irradiation on the thermal conductivity of the pellets.

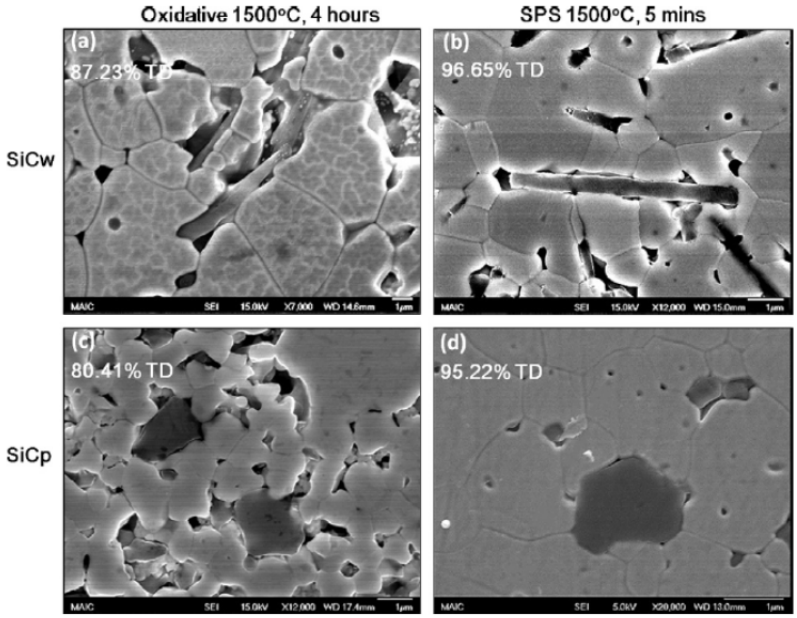

FIG. 6. Comparison of the UO_2-10 vol% SiC microstructure using the conventional oxidative sintering technique and the SPS technique at 1500°C for 4h and 5 mins, respectively [8].

3. CONCLUSION

After the Fukushima-Daiichi accident several international programmes have been launched to investigate and develop innovative fuel concepts that would exhibit enhanced resistance to accidental conditions. Within this framework, AREVA is actively involved in the development of several cladding and pellet concepts through collaborative projects as part of the DOE EATF programme and the French tri-partite R&D with CEA and EDF. For the cladding, three main concepts are being investigated: coatings on zirconium alloys (CEA's Cr coating and Cold Spray MAX phase coatings), EPRI's molybdenum cladding, and the CEA's SiC/SiC composite sandwich cladding. For pellets, AREVA is working with the University of Florida to develop enhanced thermal conductivity pellets containing SiC or diamond particle additives. Overall, the concepts investigated range from evolutionary solutions to long term

revolutionary concepts with gradually increased potential performance in accidental conditions.

ACKNOWLEDGEMENTS

Part of the work presented in this paper was performed for the Department of Energy (contract No DE-NE-0000567). The authors would like to thank Bo Cheng for his work on the molybdenum rod concept.

REFERENCES

[1] CHENG, B., "Fuel Behaviour in Severe Accidents and Mo-alloy Based Cladding Designs to Improve Accident Tolerance", EPRI, Proceedings of TopFuel Conference in Charlotte, NC, USA (2013).

[2] IDARRAGA-TRUJILLO, I., LE FLEM, M., BRACHET, J-C., LE SAUX, M., HAMON, D., MULLER, S., VANDENBERGHE, V., TUPIN, M., PAPIN, E., BILLARD, A., MONSIFROT, E., SCHUSTER, F., "Assessment at CEA of Coated Nuclear Fuel Cladding for LWRs with Increased Margins in LOCA and beyond LOCA Conditions", Proceedings of 2013 LWR Fuel Performance Meeting/TopFuel, Charlotte, NC, USA, Sept (2013) 15-19.

[3] SAUDER, C., MICHAUX, A., LOUPIAS, G., BILLAUD, P., BRAUN, J., "Assessment of SiC/SiC Cladding for LWRs", Proceedings of TopFuel Conference in Charlotte, NC, USA (2013).

[4] ORGANISATION FOR ECONOMIC COOPERATION AND DEVELOPMENT, "The Fukushima Daiichi Nuclear Power Plant Accident: OECD/NEA Nuclear Safety Response and Lessons Learnt", NEA N°7161, OECD (2013).

[5] AREVA FEDERAL SERVICES LLC, "Final Report for the Enhanced Accident Tolerant Fuels", RPT-3011235-000, Contract No. DE-NE-0000567 (2014).

[6] BARSOUM, M.W., BRODKIN. D., EL-RAGHY. T., Layered Machinable Ceramics for High Temperature Applications, Scrip. Met. et. Mater. **36** (1997) 535-541.

[7] BARSOUM, M.W., EL-RAGHY. T., Synthesis and Characterization of a Remarkable Ceramic: Ti_3SiC_2, J. Amer. Ceram. Soc. **79 (7)** (1996)1953-1956.

[8] YEO, S., McKENNA, E., BANEY, R., SUBBASH, G., TULENKO, J., Enhanced Thermal Conductivity of Uranium Dioxide-Silicon Carbide Composite Fuel Pellets Prepared by Spark Plasma Sintering (SPS), J. Nucl. Mater. **433** (2013) 66-73.

METALLIC CLAD ACCIDENT TOLERANT FUEL CONCEPTS
(SESSION 2)

Chairpersons:

L. Snead

(ORNL, USA)

J.-C. Brachet

(CEA, France)

CLADDING BEHAVIOUR DURING POSTULATED DESIGN-BASIS LOCAS

M.C. BILLONE, Y. YAN*, T.A. BURTSEVA, R.O. MEYER
Argonne National Laboratory
*Oak Ridge National Laboratory
United States of America
E-mail: billone@anl.gov

Abstract

A previous report by Argonne provided results on cladding embrittlement, breakaway oxidation, and ballooning with rupture under conditions of postulated loss-of-coolant accidents (LOCAs). This paper updates those results, provides additional results in those areas, and adds results of mechanical testing of cladding after ballooning, rupture, oxidation at elevated temperature, and quench. Significant conclusions are as follows. Embrittlement of high-exposure cladding is accelerated by hydrogen that is absorbed during normal reactor operation (i.e., pre-transient) and the acceleration has been quantified as an oxidation limit vs. pre-transient hydrogen content in the cladding metal. Breakaway oxidation, which leads to excessive hydrogen pickup and embrittlement during a LOCA transient, can occur during times that are relevant for these accidents. Conditions that lead to breakaway are only partially understood. Factors that contribute to increased susceptibility to breakaway oxidation – especially surface finish and scratches – have been investigated. Ballooning strains increase as rupture temperature decreases within the temperature range explored in this work. Rupture temperature depends primarily on internal gas pressure and to some extent on pre-transient hydrogen content, alloy composition, and heating rate. Four-point bend tests are effective for measuring post-quench failure limits for ballooned, ruptured, and oxidized cladding. The results indicate that strength and failure energy degrade significantly with increasing pre-transient hydrogen and transient oxygen levels, based on cross-section-average values for these parameters. Further, using the oxidation limit vs. hydrogen content derived for non-ballooned regions would ensure the preservation of strength for ballooned regions.

1. INTRODUCTION

Accident tolerant fuel rods are being developed to perform better than the current Zr-based cladding alloys during normal operation, design-basis (DB) accident events, and/or beyond-design-basis (BDB) accident events. The results presented in this paper apply to Zr-based cladding alloys subjected to DB loss-of-coolant accidents (LOCAs) as defined by the U.S. Nuclear Regulatory Commission (USNRC). In terms of USNRC acceptance criteria for DB LOCAs, the emergency core cooling system must limit the peak cladding temperature to ≤1204°C and the maximum oxidation level to 17% such that cladding post-quench ductility (PQD) is retained. Data generated by Argonne are being used by the USNRC to revise oxidation limits for maintaining PQD and to address excessive hydrogen pickup during breakaway oxidation. Also, the Argonne results serve as a baseline for accident tolerant fuel-rod design concepts, which are expected to experience less corrosion and hydrogen pickup during normal operation and/or decreased oxidation and hydrogen release during DB and BDB LOCAs.

LOCA-relevant data generated by Argonne up through May 2008 are documented in NUREG/CR-6967 [1]. These data include: (a) PQD results for as-fabricated (AF) cladding alloys, pre-hydrided (PH) cladding alloys, and cladding alloys from fuel rods irradiated to high burnup (HBU) in commercial light water reactors; (b) breakaway oxidation times and corresponding oxidation temperatures for AF cladding alloys; and (c) characterization of AF and HBU-fuelled cladding alloys in terms of ballooning strain, rupture temperature and corresponding pressure, oxidation, and secondary hydriding. The results from (a) were used to determine the ductile-to-brittle transition oxidation level as a function of pre-transient (i.e., pre-test) hydrogen content in the cladding metal.

Test results generated after May 2008 are being documented in a companion NUREG report. These include: (a) PQD data for PH and HBU cladding with intermediate hydrogen content (200 wppm to 400 wppm); (b) additional breakaway oxidation data for steady-state temperature histories and new data for transient temperature histories; and (c) new data for the mechanical behaviour of ballooned-and-ruptured cladding (AF and PH) following oxidation

and quench. This paper presents a summary of results from previously documented testing [1] and from the more current tests.

Materials and test methods are summarized in Section 2. PQD results for non-ballooned cladding samples are reported in Section 3. Breakaway oxidation results are presented in Section 4 for non-ballooned cladding. Results for ballooned-and-ruptured cladding are reported in Section 5.

2. MATERIALS AND TEST METHODS

2.1. Materials

Cladding materials included zircaloy-2 (Zry-2), zircaloy-4 (Zry-4), ZIRLO, and M5. As-fabricated materials received in the 1998-2002 timeframe were used to validate (VAL) the LOCA apparatus and test procedures. These materials included 8×8 Zry-2 and 17x17 M5 (0.57-mm wall thickness). As-fabricated materials received during the 2003-2010 timeframe were used as samples for oxidation and PQD tests, for breakaway oxidation (BO) studies, and for LOCA integral testing (LIT). Cladding from HBU fuel rods was received during the 2000-2006 timeframe. Table 1 summarizes the design, AF dimensions (outer diameter [D_{mo}] and wall thickness [h_m]), condition, and tests conducted with these materials. Zry-4 cladding materials are distinguished between vintage (V) materials, which were fabricated with rough inner and outer surfaces, and modern (M) materials, which had belt- or wheel-polished outer surfaces and sand-blasted inner surfaces. Other cladding materials listed in Table 1 had polished outer surfaces. The cladding wall thickness is significant because the oxidation level is determined as the equivalent cladding reacted (ECR), which treats all oxygen picked up by the metal as a surface zirconia layer and normalizes the cladding consumed by this layer to the pre-transient cladding wall thickness.

TABLE 1. SUMMARY OF CLADDING MATERIALS USED IN LOCA-RELEVANT TESTING

Cladding Materials	Design	D_{mo}, mm	h_m, mm	Condition	Tests
Zry-2 (Zr-lined ID)	8×8	12.27	0.82	AF	VAL
	9×9	11.28	0.71	AF, HBU	LIT
	10×10	10.29	0.66	AF	PQD, BO
Zry-4	M-17×17	9.50	0.57	AF, PH	PQD
	M-15×15	10.91	0.67	AF	PQD, BO
	V-15×15	10.77	0.76	AF, PH, HBU	PQD, BO
ZIRLO	17×17	9.50	0.57	AF, PH, HBU	PQD, BO, LIT
M5	17×17	9.50	0.57	AF, HBU	VAL, PQD
	17×17	9.50	0.61	AF	PQD, BO
	17×17	9.50	0.57	AF	BO

2.2. Test methods

The LOCA apparatus consists of a radiant-heating furnace with a 254-mm-high uniform heating zone, a 50-mm diameter quartz-tube stream chamber, containers with de-ionized water for the boiler and the quench system, a boiler designed to produce atmospheric steam, and a quench system for bottom flooding of the quartz chamber. Oxidation-quench tests were conducted with 25-mm-long non-deformed samples held in place near the axial centre of the furnace by a test train and subjected to two-sided oxidation. LOCA integral tests were conducted with longer (305-318 mm) pressurized cladding tubes partially filled with

HBU fuel or zirconia pellets. These samples, which had a small top plenum, were supported at the top and pressurized at the top by about 10 cm^3 of argon. Most of the pressurized argon was outside the furnace heating zone such that the pressure was essentially constant during the heating ramp until ballooning and rupture occurred. For the LOCA integral test, steam flowed along the outer surface of the cladding. Following rupture, some steam entered the inner region of the sample through the rupture opening. Due to axial heat conduction, the uniform temperature zone for the LOCA integral samples was about 100-125 mm long. Details of the LOCA apparatus and the oxidation-quench phase of the experiment are described in Ref. [1].

In order to generate high quality data, temperature control and monitoring are considered to be very important, especially for oxidation at 1200°C. For oxidation-quench tests with shorter samples, three thermocouples (TCs) were spot-welded to the Inconel holder just above the sample at orientations of 0°, 120°, and 240°. One of these served as the control TC whose output was used via a controller to adjust the furnace power to achieve desired heating rates, hold temperatures, cooling rates, and quench temperatures. Prior to conducting data-generating tests, two types of benchmark tests were performed. Thermal benchmark tests were conducted with two additional TCs spot-welded to the sample outer surface in order to set control parameters for the holder TC such that the target sample temperatures were achieved. Following thermal benchmark tests, weight-gain benchmark tests were conducted without TCs welded to the sample and with the fixed control parameters for the holder TC. The measured weight gain, as well as the measured outer-inner surface oxide layer thicknesses, was compared to Cathcart-Pawel (CP) correlation predictions for weight gain and oxide layer thickness [2]. At oxidation temperatures of 1100°C and 1200°C, the weight gain of all alloys tested agreed quite well (within 10%) with CP-predictions for accurately measured temperatures. At 1000°C, measured oxidation rates were found to be dependent on cladding alloy and test time. For this oxidation temperature, weight-gain benchmarks with Zry-4 were conducted for about 1500 s, which included the ramp from 300°C to 1000°C (about 100 s) and the hold time at 1000°C.

For LOCA integral tests, TCs were spot-welded directly onto the cladding outer surface at locations about 50-mm above (at 0° and 180° orientations) and below (at 90° and 270° orientations) the sample mid-span. One of the upper TCs was used to control the furnace power. Extensive thermal benchmarking was conducted for non-pressurized samples and for pressurized samples, which ballooned and ruptured. The outer-surface oxide layer thickness was measured at axial locations near the upper TCs and compared to CP-predicted values. These tests were conducted at a heating rate of 5°C/s, a peak oxidation temperature of 1200°C, a controlled cooling rate of 3°C/s from 1200°C to 800°C, and very rapid cooling via quench water bottom flooding at 800°C.

Although weight gains and oxide-layer thickness values were routinely measured, test results are presented in terms of the calculated ECR based on the CP-predicted weight gain (i.e., CP-ECR). For samples that ballooned and ruptured, the reported CP-ECR is the maximum value for the cross-section within the rupture region with the minimum average wall thickness.

For non-deformed oxidation-quench samples, ring compression tests (RCTs) were conducted with rings (about 8-mm long) sectioned from these samples. RCT loading induces a primary hoop bending stress and a secondary axial stress. The RCTs were conducted at 135°C and a controlled displacement rate of 0.033 mm/s (2 mm/minute). This slow displacement rate allowed enough time for the operator to stop the test after the first

significant load drop. For rings that cracked at only one orientation, the spring-back after removal of the load resulted in a very tight crack at the 12 or 6 o'clock orientation relative to the applied load orientation (see Fig. 1). For such samples, the post-test outer diameter in the loading direction (D_{of}) could be measured with reasonable accuracy and compared to the pre-test diameter (D_{oi}) in the loading direction to determine the permanent displacement (d_p) in the loading direction. This displacement was normalized to the pre-test outer diameter of the cladding metal (D_{mo}) to determine permanent strain (d_p/D_{mo}). Based on error analyses and data trends, cladding rings with <1% permanent strain were assessed as brittle and cladding rings with ≥1% permanent strain were assessed as ductile. For cladding rings that cracked simultaneously at 2 to 4 orientations, D_{of} could not be measured accurately and d_p could not be determined. For such cases, the offset displacement (δ_p) was determined from the RCT load-displacement curve and normalized to D_{mo} to determine the offset strain (δ_p/D_{mo}). As discussed in Ref. [3], this methodology has an inherent error because the unloading slope for the RCT is less than the loading slope used to determine δ_p. The ductility criterion used for the offset strain is based on an extensive database and is given by:

$$\delta_p/D_{mo} \geq 1.41\% + 0.1082 \cdot \text{CP-ECR} \quad (1)$$

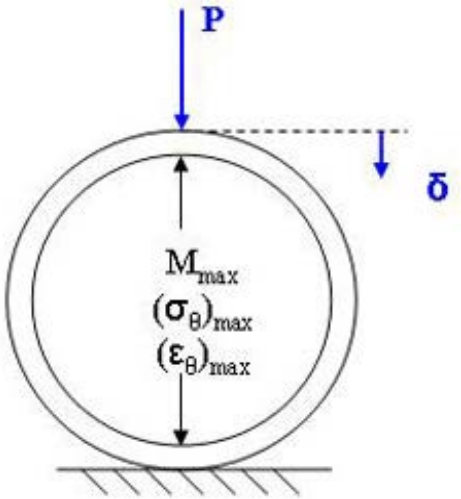

FIG. 1. RCT schematic showing the controlled displacement (δ) and the measured load (P) at the 12 o'clock orientation. Locations are shown for the maximum: hoop bending moment (M), elastic hoop stress (σ_θ), and elastic hoop strain (ε_θ).

For LOCA integral test samples, the four-point bend test (4-PBT) was used to assess the mechanical behaviour of ballooned, ruptured, oxidized, and quenched cladding. A schematic of the 4-PBT loading is shown in Fig. 2. As with the RCTs, the 4-PBTs were conducted at a controlled displacement rate (1 mm/s) and the load (P in N) was measured as a function of displacement. Also, tests were conducted at 135°C. For AF 17×17 cladding, the 4-PBT displacement rate of 1 mm/s gives the same maximum elastic strain (axial) rate as was achieved in the RCT (hoop) with 0.033 mm/s displacement rate. The span L_s was 150 mm and the span "a" was 50 mm. Under these conditions, the axial bending moment (M) is (0.025 m)•P along span L_s. The advantage of the 4-PBT loading is that the uniform bending moment span (L_s) includes the whole ballooned region and allows failure to occur at the weakest point along the sample (e.g., centre of rupture node or regions between edges of rupture opening and necks of balloons). Three metrics were used to assess the mechanical performance of ballooned and ruptured cladding samples following oxidation and quench: (a) maximum bending moment (M_{max} in N•m) prior to failure (i.e., severing of the cross section), which is a measure of strength; (b) failure energy (E_{max} in J), which is the area under the load-

displacement curve and a measure of toughness; and (c) offset strain (δ_p) which is a measure of plastic displacement.

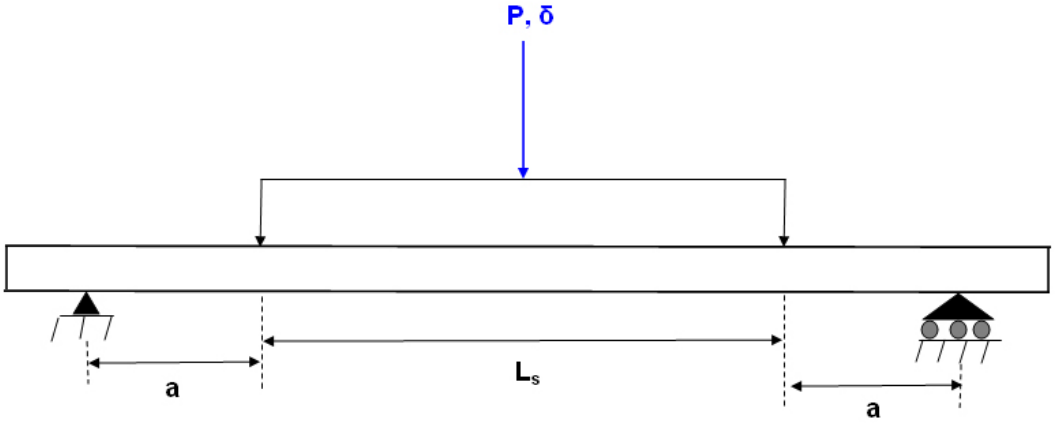

FIG. 2. Schematic of the 4-PBT.

3. EMBRITTLEMENT OF NON-BALLOONED CLADDING

Zr-based alloys oxidized in steam at 1000°C to 1200°C form an outer-surface oxide layer, an intermediate oxygen-stabilized alpha layer, and an inner beta layer. For double-sided oxidation, the beta layer is within pairs of inner- and outer-surface alpha-oxide layers. Prior to breakaway oxidation at the lower oxidation temperatures, the tetragonal-oxide phase is protective with regard to hydrogen pickup and is brittle at RCT test temperatures (≤135°C). The oxygen-stabilized alpha phase, which has a high affinity for oxygen and a low affinity for hydrogen, is also brittle at these RCT temperatures. The beta phase has a low affinity and solubility limit for oxygen and a high affinity and solubility limit for hydrogen. The solubility of oxygen in the beta phase is about 0.2 wt.% at 1000°C, about 0.4 wt.% at 1100°C, and about 0.6 wt.% at 1200°C for as-fabricated cladding with very low hydrogen content. Following cooling, the beta phase transforms to a low-oxygen-content alpha phase and is called the prior-beta phase. The prior-beta layer will retain PQD at 135°C if the oxygen content remains below about 0.6 wt.%. Thus, for AF cladding, the ductility of the RCT samples is highly dependent on the oxygen content in the prior-beta layer. This beta layer will retain PQD for AF cladding following oxidation at 1000°C and 1100°C due to its low oxygen content. As the oxidation time and CP-ECR increase at these temperatures, embrittlement will eventually occur due to excessive thinning of the prior-beta layer and/or hydrogen pickup during breakaway oxidation (see Section 4). For AF cladding oxidized at 1200°C, embrittlement will occur as the oxygen content in the prior-beta layer approaches the solubility limit. The decrease in ductility for AF cladding correlates quite well with increasing CP-ECR even though it is not a direct measure of the oxygen content in the prior-beta layer. However, CP-ECR has the same functional dependence on time and temperature as does the oxygen increase (due to diffusion) in the beta layer. Thus, it is a good surrogate for the effects on PQD of oxidation time at temperature prior to saturation of the prior-beta layer.

The presence of pre-transient hydrogen accelerates the embrittlement process. Hydrogen increases the oxygen solubility within the beta phase and the oxygen diffusion rate into this phase. There also appears to be an intrinsic embrittlement effect of hydrogen beyond the increases in solubility and diffusion. However, the presence of pre-transient hydrogen does not increase the weight-gain rate even though it has a very detrimental effect on PQD. As such, embrittlement thresholds in this work are expressed in terms of the transition CP-ECR as a function of pre-transient hydrogen content.

3.1. As-fabricated (AF) cladding alloys

AF 17×17 cladding alloys were oxidized at 1000°C, 1100°C, and 1200°C to CP-ECR oxidation levels of 5%, 10%, 15%, 17% and 20% prior to quench at 800°C and ring-compression testing. AF 10×10 Zry-2 was oxidized at 1000°C and 1200°C to similar oxidation levels. The other materials listed in Table 1 were oxidized at 1200°C prior to quench and ring compression testing. RCTs were performed initially at room temperature (RT). Samples oxidized at 1000°C and 1100°C exhibited PQD at RT up to the oxidation limits tested (20%). As such no further PQD tests were conducted at these temperatures. Additional testing was conducted at 1000°C for breakaway oxidation studies (see Section 4). The PQD was determined at 135°C for all alloys in Table 1 oxidized at 1200°C. Additional tests were conducted at intermediate oxidation levels to better determine the ductile-to-brittle transition level. Except for vintage 15×15 Zry-4, the transition oxidation level for maintaining 1% permanent strain was 19% to 20% CP-ECR for cladding alloys oxidized at 1200°C. Within experimental uncertainty, the embrittlement threshold for modern cladding materials was alloy independent. Also, based on samples oxidized at 1200°C and cooled without quench, PQD appeared to be independent of quench cooling for Zry-4, ZIRLO, and M5 [1].

3.2. Pre-hydrided (PH) cladding alloys

Initial tests conducted to determine the effects of pre-test hydrogen on PQD were performed with 17×17 Zry-4 and vintage 15×15 Zry-4. The oxidation temperature for these tests was 1200°C. However, because of the large axial variation in hydrogen content, tests were conducted to determine the ductile-to-brittle transition hydrogen content for fixed CP-ECR levels. In addition to variable hydrogen content, oxidation tests were conducted with a range of heating rates and quench temperatures. PQD results for PH Zry-4 were highly sensitive to heating and cooling rates: the transition hydrogen content decreased with increased heating and cooling rates.

More recent testing was conducted with ZIRLO samples pre-hydrided to 200−290 wppm. Due to improvements in the pre-hydriding process, the axial uniformity of hydrogen content was much better for these samples. Oxidation levels for 1200°C tests were 8−11%. For PH ZIRLO samples, the transition CP-ECR was: (a) 11% for 200 wppm hydrogen, (b) 10% for 240 wppm hydrogen, and (c) <9% for about 290 wppm hydrogen.

3.3. Cladding alloys from high-burnup (HBU) fuel rods

Cladding samples from fuel rods irradiated to high burnup (i.e., HBU cladding) were oxidized at ≤1200°C peak temperatures for pre-test hydrogen contents (in the cladding metal) of 140 wppm to 600 wppm. Hydrogen pickup during normal reactor operation is highly dependent on cladding alloy. Fuel burnup levels (63 GWd/t to 70 GWd/t) were above the licensing limit for all cladding materials tested. The target hold temperature for these tests was 1200°C, which was achieved before embrittlement occurred for samples with <400 wppm. For samples with 540 wppm to 600 wppm, embrittlement occurred following cooling during the heating phase at 1130−1180°C peak temperatures.

PQD results for HBU cladding are shown in Fig. 3, along with results for AF and PH cladding. The horizontal axis represents the pre-test hydrogen in the cladding metal. The vertical axis is the transition CP-ECR oxidation level for which minimum ductility (e.g., 1% permanent strain) was retained. Significant observations for embrittlement threshold oxidation levels include: (a) transition oxidation levels are highly dependent on pre-test hydrogen content in the cladding metal and independent of fuel burnup; (b) results are alloy

independent; (c) PH cladding is a good surrogate for HBU cladding, and (d) the current 10CFR50.46 limit (17%) is non-conservative.

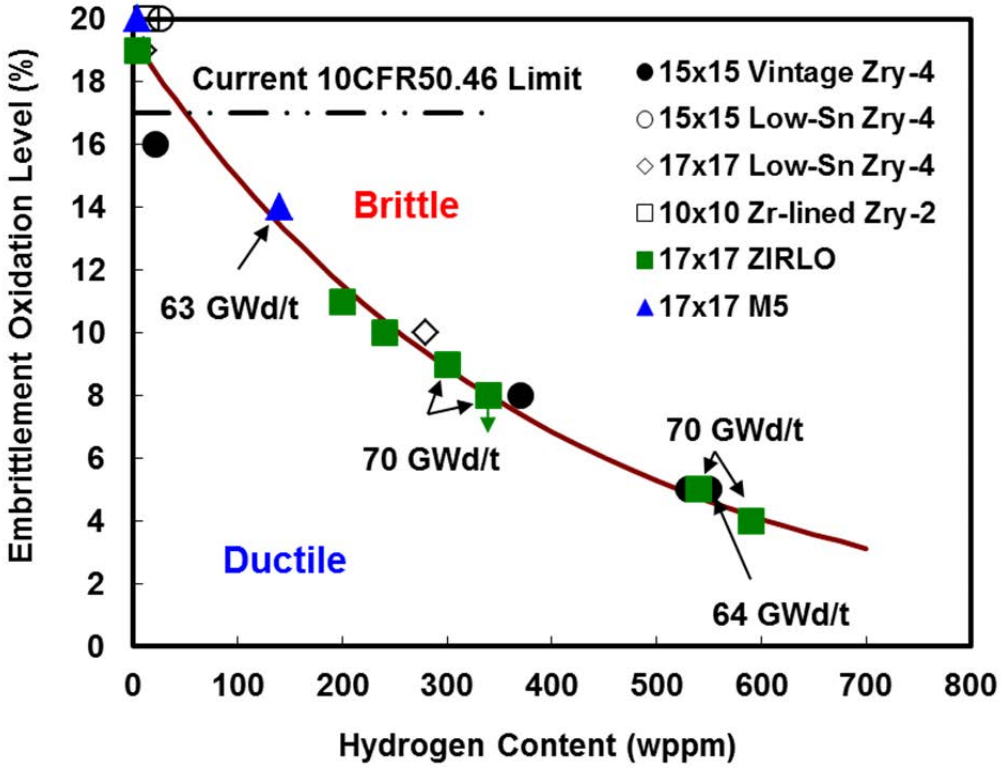

FIG. 3. Embrittlement oxidation levels vs. pre-transient hydrogen content for peak oxidation temperatures of 1200°C at <400 wppm hydrogen and 1130-1180°C at >400 wppm hydrogen.

4. EMBRITTLEMENT DUE TO BREAKAWAY OXIDATION

Zirconium dioxide (ZrO_2) can exist in several crystallographic forms and has a monoclinic structure at normal reactor operating temperatures. The tetragonal oxide that generally develops under LOCA conditions is dense, adherent, and protective with respect to hydrogen pickup. Although the monoclinic-to-tetragonal phase transformation temperature is nominally ≈1150°C, the tetragonal oxide phase can be stabilized at lower oxidation temperatures by compressive stress, hypostoichiometry, impurities (e.g., Ca, Mg, and Al), and to some extent grain size. There are, however, mechanical (e.g., local regions of tensile stress) and chemical (e.g., impurities, such as F, at or near the metal surface [4]) conditions that promote a transformation to the lower-temperature monoclinic phase that is neither fully dense nor protective. When these conditions are present, the tetragonal-to-monoclinic transformation can begin in an unstable way at local regions of the metal-oxide interface and grow rapidly throughout the oxide layer due in part to the local volume increase (≈5%) associated with the phase transformation. Because this transformation results in an increase in oxidation rate, it is referred to as breakaway oxidation. Along with this increase in oxidation rate due to cracks in the monoclinic oxide, there is significant hydrogen pickup. Hydrogen that enters in this manner during a LOCA transient has a similar effect on embrittlement as hydrogen from the normal burnup process.

Breakaway oxidation occurs in all zirconium-alloy cladding materials if the cladding is held for long times (minutes to hours) at certain constant temperatures between 650°C and 1100°C. It is often apparent from the visual appearance of the outer surface of the oxide layer. The time at which breakaway oxidation occurs is commonly determined from the increase in weight-gain rate. However, a more reliable and relevant indicator is the measured increase in

hydrogen concentration. It was demonstrated in Ref. 1 that 200-wppm hydrogen pickup is a good metric for determining breakaway oxidation time. Based on RCT results, embrittlement occurred at ≈450 wppm hydrogen pickup for cladding samples oxidized for long times at 970−1000°C. Although the 200-wppm hydrogen pickup criterion is conservative with respect to ductility retention, the oxidation time at 970−1000°C is relatively short for post-breakaway cladding to pick up the additional 250 wppm leading to embrittlement.

4.1. Steady-state oxidation

Argonne tests used to determine breakaway oxidation were generally initiated at 1000°C for steady-state oxidation times of about 5000 s (including about 100 s of ramp time from 300°C to 1000°C). For cladding samples that exhibited breakaway oxidation (>200 wppm hydrogen pickup), the test time was reduced to determine the minimum breakaway-oxidation time. This minimum time at 1000°C was then fixed for oxidation at lower (800°C and 970−985°C) and higher (1015°C) temperatures. If such samples picked up >200 wppm hydrogen, the test time at these temperatures was decreased until initiation could be directly determined or estimated by interpolation.

As discussed above, breakaway oxidation initiates very locally at the oxide-metal interface and propagates rather rapidly in the circumferential and axial directions for higher oxidation times. Because breakaway is an instability phenomenon, considerable data scatter is expected to occur with regard to local initiation time and hydrogen pickup. This is illustrated in Fig. 4 for AF ZIRLO oxidized at 1000°C for 4000 s. The sample on the left exhibited small yellow spots and streaks within a lustrous black matrix. The hydrogen pickup just below one of these yellow spots was about 280 wppm. Below the lustrous black spots, the hydrogen pickup was as low as 40 wppm. The 200 wppm hydrogen pickup criterion is based on the average hydrogen content for a 2-mm-long ring sectioned away from the ends and containing some of the yellow region. The average hydrogen pickup was 120±110 wppm (pre-breakaway) for the sample to the left and 400±120 wppm (post-breakaway) for the sample to the right in Fig. 4. Metallographic examination was performed for the pre-breakaway sample to confirm that local breakaway actually occurred on the cladding outer surface and that breakaway on, and hydrogen pickup through, the inner surface had not occurred. Fig. 5 shows local breakaway at the outer surface and confirms that breakaway had not occurred at the inner surface. Also important to observe in Fig. 5 is the “scalloping” at the oxide-metal interface, which is considered to be a precursor to breakaway oxidation [5].

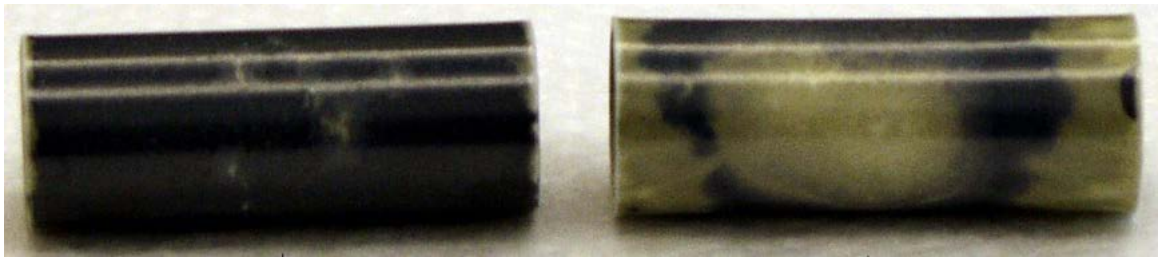

FIG. 4. AF ZIRLO samples following oxidation at 1000°C for 4000 s.

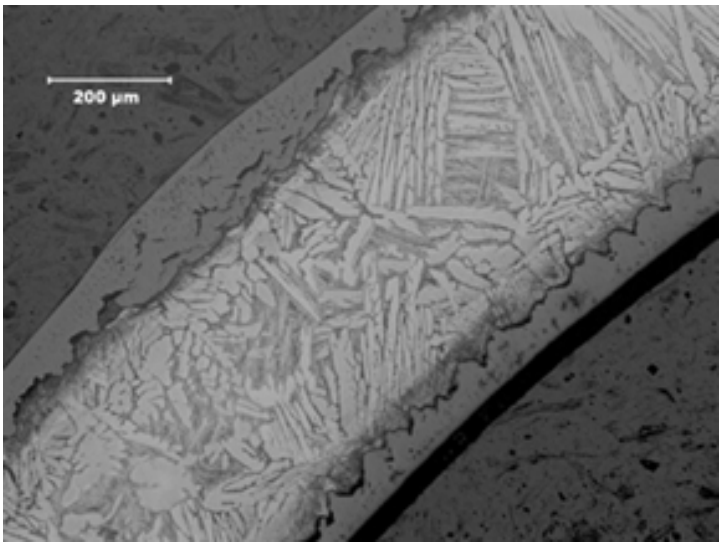

(a)

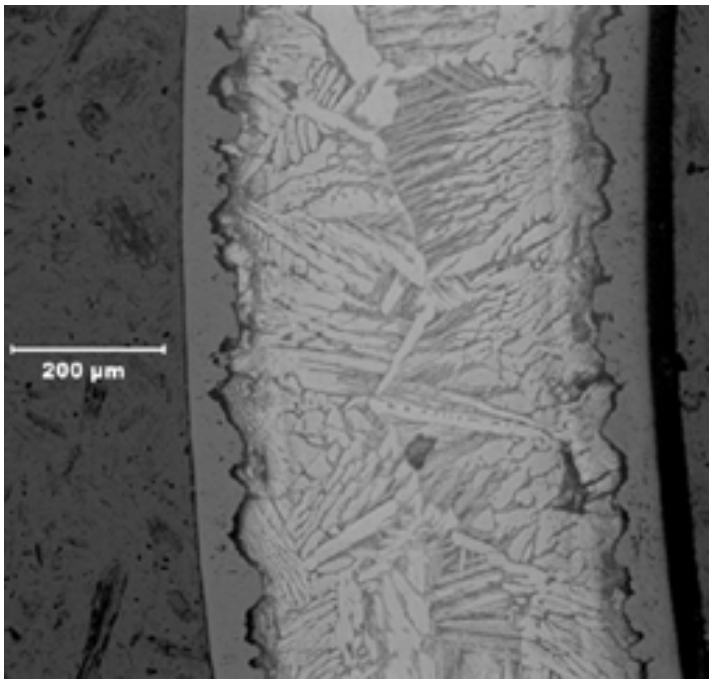

(b)

FIG. 5. Oxide layers for AF ZIRLO following oxidation at 1000°C for 4000 s: (a) local outer surface breakaway and (b) pre-breakaway scalloped metal-oxide interfaces.

Although there was a significant difference in hydrogen pickup for the samples shown in Fig. 4, the data scatter for the time to pickup 200-wppm hydrogen (i.e., minimum breakaway time) was much less: 4000±200 s. The larger data scatter for hydrogen pickup is based on time for very local initiation of breakaway oxidation, circumferential and axial propagation of breakaway, and hydrogen diffusion following local breakaway. Samples that met the 200-wppm hydrogen pickup generally had very large axial and circumferential variations in hydrogen content.

In addition to testing AF cladding alloys in the as-received condition, the effects of outer-surface treatments were also studied: pre-scratched (Zry-4, Zry-2, and ZIRLO with 20-µm deep scratches along the length of the samples), pre-filmed (ZIRLO with a 1-µm-thick

oxide layer grown at low temperature), and Ethanol vs. Alconox pre-test cleaning (ZIRLO). Although it was demonstrated that breakaway oxidation initiated along the scratched region for ZIRLO and Zry-4 due to the geometric irregularity, breakaway times were within the data scatter (near the lower times) for these materials. For pre-filmed samples, Ethanol-cleaned samples, and Alconox-cleaned samples, minimum breakaway oxidation times were also within the data scatter (closer to the average value).

Table 2 summarizes Argonne (ANL) results for minimum breakaway oxidation time, as well as results from other research efforts. The acronyms used in the last column refer to Leistikow and Shantz (L&S) and Westinghouse Electric Company (WEC). Data listed as "CEA" refer to collaborative efforts among CEA/Saclay, EdF, and AREVA. For vintage Zry-4, the Leistikow and Shantz time for breakaway oxidation at 1000°C is considerable lower than the ANL time for tests conducted at comparable long-time temperatures. However, their Zry-4 was much older, the surface roughness was not specified, and they pickled their samples in an HF-containing acid bath prior to oxidation. For polished Zry-4, ANL and CEA results are comparable for materials fabricated by AREVA. Using WEC 15×15 Zry-4, WEC results at 1010°C appear to be consistent with ANL and CEA results considering the scatter expected for different Zry-4 materials. For polished M5, ANL and CEA results are consistent. CEA results for M5 are recommended because of their data at longer test times. For ZIRLO, ANL and WEC results (≈4400 s for "fast"-ramp tests) are consistent for an oxidation temperature of 1000°C. However, for "slow"-ramp tests, WEC observed no breakaway oxidation for test times up to 4550 s.

TABLE 2. COMPARISON OF ARGONNE RESULTS FOR MINIMIM BREAKAWAY OXIDATION TIME AND RESULTS FROM OTHER RESEARCH EFFORTS

Material	Oxidation temperature, °C	ANL min. time for breakaway, s	Results from other research tests	
			Times	Reference
Vintage Zry-4	1000	–	1800	L&S [5]
	985	3800±100	–	
Polished Zry-4	1000	–	≈5400	CEA [6]
	1010	–	≈4400	WEC [7]
	985	≈5000		
Polished Zry-2	970-1000	>5000	–	–
Polished ZIRLO	1000	4000±200	≈4400	WEC [7-10]
	1000	–	>4550	WEC [7-10]
	970-985	3100±300	>4600	WEC [7-10]
Polished M5	1000	>4100	6500±500	CEA [11]
	980-985	>5000	–	

It is not at all clear why WEC observed a difference in breakaway time at 1000°C for *fast* vs. *slow* ramp tests. For both types of tests, the temperature ramp rate up to about 980°C was very fast. The difference was in the time to heat the samples from 980°C to 1000°C. Fast-rate tests were those for which the total ramp time was about 60 s while it took up to 270 s to heat up to 1000°C for slow-ramp tests. Most of this time difference occurred in heating from 980°C to 1000°C. From a mechanistic point of view, it is difficult to understand how and why the material would *remember* this ramp rate difference over 4000 s later in the oxidation process.

The ANL and WEC differences in results for oxidation temperatures just below 1000°C are more difficult to understand, especially as both research facilities used the same material. WEC observed no breakaway oxidation at oxidation temperatures of 980°C and 990°C for test times ranging from 3800 s to 4400 s. For oxidation temperatures of 970°C to 985°C, ANL found minimum breakaway oxidation times of 3100±300 s based on a large number of tests. It is possible to explain these differences if the minimum breakaway oxidation time occurs within a very narrow temperature band. WEC used a conventional furnace, which likely had temperature uniformity in the circumferential direction. ANL used a radiant heating furnace with circumferential variations in temperature of about 10°C. Therefore, ANL tests with average temperatures of 970°C, 980°C, and 985°C included all temperatures within the range of about 965°C to 990°C while WEC tested at discrete temperatures of 960°C, 980°C, and 990°C.

4.2. Transient oxidation

During a LOCA transient, temperatures are not constant. The issue addressed with ANL transient testing was whether or not changing temperatures would decrease the minimum breakaway time. Tests were conducted with step changes in temperature (1045°C→980°C and 975°C→1000°C) for total test times of 4000 s. No breakaway oxidation was observed after 4000 s total test time. These results suggest that cladding must remain at the critical temperature for an extended period of time to develop breakaway oxidation and not merely pass through the critical temperature for a short period of time during a temperature transient. A second set of tests was conducted with temperature cycling of 100°C (i.e., 5 short cycles from 930°C to 1030°C) and with a long-time temperature of 980°C. These tests were not representative of any particular LOCA transient. Rather, they were designed to disturb the stress state in the oxide layer to determine if early breakaway oxidation could be induced. For the first cycling test, the temperature was held at 980°C for 1500 s (included about 100s ramp), cycled five times for about 400 s, and held for an additional 1400 s at 980°C. After 3300 s total test time, the hydrogen pickup was 427±36 wppm indicating a minimum breakaway time <3300 s. The second cycling test was similar except cycling was induced after 2000 s and the total test time was reduced to 2800 s. The hydrogen pickup was 225±79 wppm indicating a breakaway oxidation time close to 2800 s. As this minimum time was within, but at the lower end, of the isothermal breakaway time of 3100±300 s, it was concluded that transient temperature histories would not lower the minimum breakaway times determined from results of isothermal tests. As shown in Fig. 6 (2 red solid squares) temperature cycling had about the same effect on reducing breakaway oxidation time as surface-scratched samples (2 open blue circles) had on reducing the isothermal breakaway oxidation time. However, the reduction was only about 10% and within the data scatter shown in Fig. 6. This “conclusion” is really a matter of judgement and interpretation as only two data points are shown in Fig. 6 for scratched and cycled samples. A surface-scratched sample subjected to temperature cycling may have exhibited <2800 s breakaway oxidation time. Also, repeat tests under these conditions are likely to result in considerable data scatter for a total test time of 2800 s.

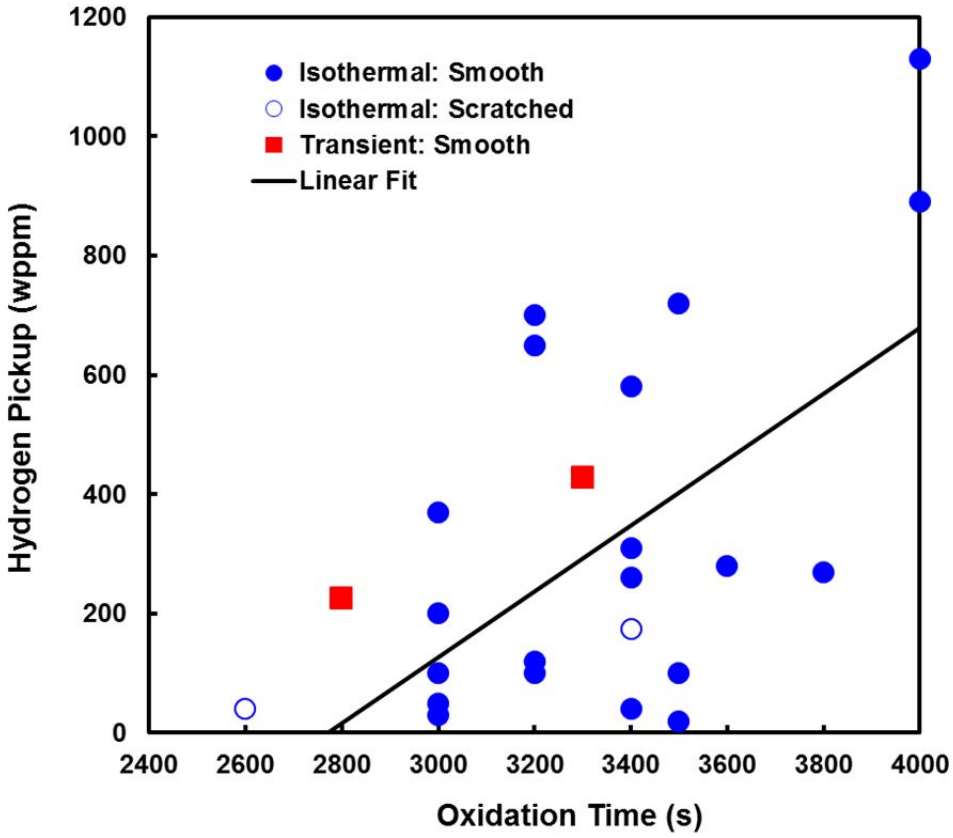

FIG. 6. Hydrogen pickup vs. test time for ZIRLO samples oxidized in steam at long-time temperatures of 970°C to 985°C.

5. BALLOONED AND RUPTURED CLADDING RESULTS

Test results are reported in Ref. [1] for ballooning strain and rupture temperature, pressure, and maximum width for AF 9×9 Zry-2 and fuelled, HBU 9×9 Zry-2. These samples were pressurized at 8.28 MPa (gauge) at 300°C and ramped at 5°C/s. With regard to ballooning strain and rupture temperature and pressure, no difference was found between AF samples and HBU samples with about 70 wppm hydrogen. For one HBU test sample, axial profiles of oxygen and secondary hydrogen pickup were characterized. For tests with AF cladding, two tests were terminated just after rupture and four test samples were oxidized in steam at 1200°C for 1 s to 300 s (9 to 21% CP-ECR) prior to cooling with (three tests) or without (one test) quench at 800°C. Post-oxidation 4-PBTs were conducted at RT for samples oxidized to 9% and 15% CP-ECR.

In this section, the focus is on more recent and more extensive test results for AF and PH 17×17 ZIRLO cladding (9.50 mm D_o, 0.57 mm h).

5.1. Ballooning and rupture

Eight scoping tests were conducted with and without oxidation to map out ballooning strain following rupture (i.e., rupture strain) and rupture conditions for AF ZIRLO as a function of pressure at 300°C. In the current work, the ballooning strain is defined as the change in circumference at the cladding mid-wall ($\Delta C_m = C_{mf} - C_{mi}$, where C_{mf} is the maximum mid-wall circumference of the ballooned-and-ruptured cladding metal) normalized to the initial mid-wall cladding circumference (C_{mi} = 28 mm). Fig. 7 shows the cladding cross section following a ramp-to-rupture test sample with 300°C gauge pressure of 9.66 MPa.

Routine post-test measurements include the maximum outer diameter (D_{max} = 15.0 mm from rupture tips at bottom to top of sample), the minimum outer diameter (D_{min} = 13.5 mm at an orientation 90° from D_{max}), and the rupture opening (δ_b = 6.2 mm). Based on metallographic examination, C_{mf} was measured to be 38.3 mm to give a maximum rupture strain of 40%. The wall thickness varied from ≈0 at the rupture tips to 0.45 mm, and the average wall thickness (h_f) was determined to be 0.38 mm. 10CFR50.46 specifies that the average wall thickness prior to oxidation be used to calculate CP-ECR. However, the detailed metallographic examination used to determine C_{mf} and h_f proved to be too tedious for a large test matrix. An empirical correlation was developed to determine these two parameters from measured values of D_{max}, D_{min}, and δ_b. For many of the tests, the outer circumference was measured directly by means of a thin stiff wire or string, and this value was corrected through an iterative process to give C_{mf} and h_f.

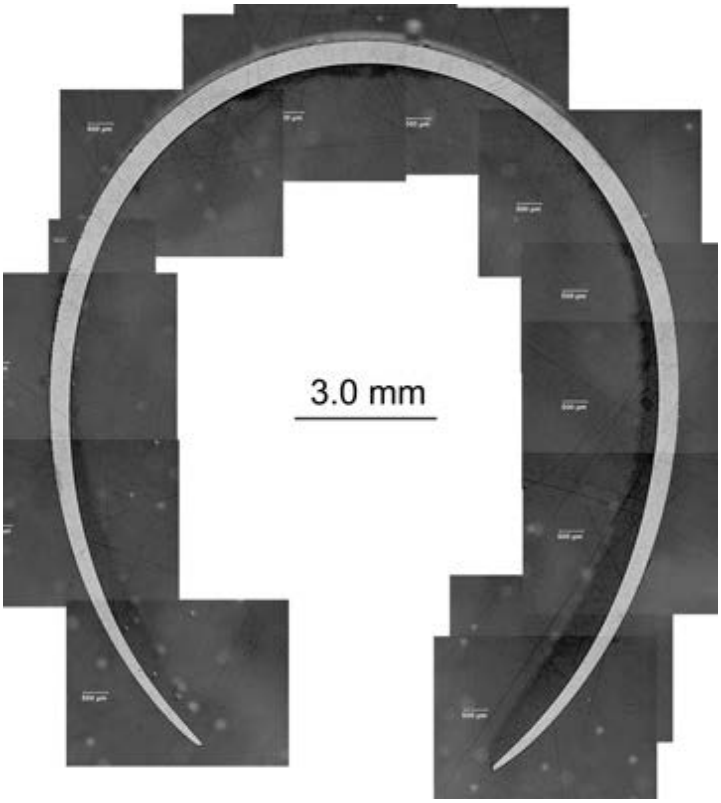

FIG. 7. Cross section of an AF ZIRLO sample following a ramp-to-rupture test.

For scoping tests, the 300°C fill pressures (gauge) were in the range of 2.76 MPa to 11.03 MPa. The highest ballooning strain (≈70%) occurred at 715°C for 11.03 MPa fill pressure and the lowest ballooning strain (≈20%) occurred at 845°C for 4.14 MPa fill pressure. Based on a full assessment of scoping-test results, data-generating tests were conducted at reference fill pressures of 8.28 MPa (10 AF and 5 PH) and 4.14 MPa (3 AF and 1 PH). Rupture temperatures and strains for AF ZIRLO samples were relatively consistent for these fill pressures: 750±7°C and 46±4% for 8.28 MPa fill pressure and 845±4°C and 23±4% for 4.14 MPa fill pressure. For PH ZIRLO, the presence of pre-test hydrogen resulted in higher rupture strains and lower rupture temperatures as compared to results for AF ZIRLO. For example, ZIRLO with 660 wppm pre-test hydrogen and 4.14 MPa fill pressure ruptured at 742°C (vs. 845°C for AF ZIRLO) with a rupture strain of 57% (vs. 23% for AF ZIRLO). Results from scoping and data-generating tests are shown in Fig. 8, where the minimum strain is believed to occur at a temperature corresponding to the middle of the mixed phase regime between lower-temperature pure alpha and higher-temperature (≈1000°C) pure beta. The

transition temperature between the alpha phase and the mixed phase depends on cladding alloy and hydrogen content.

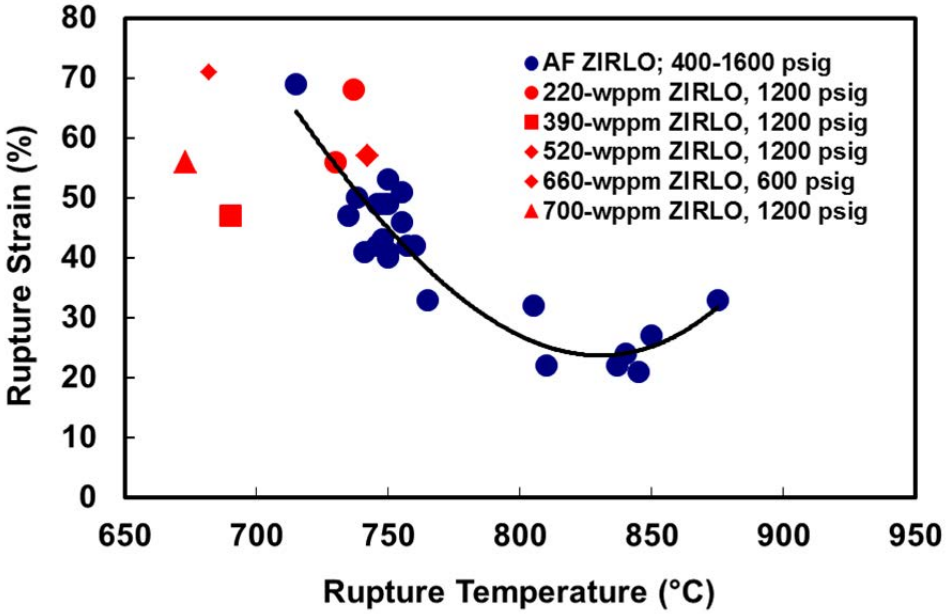

FIG. 8. Rupture strain vs. rupture temperature for AF and PH ZIRLO.

5.2. Oxidation and secondary hydriding

Although the prescribed (by 10CFR50.46) CP-ECR is calculated based on the average wall thickness, the calculated and measured local oxidation levels for the cross section shown in Fig. 7 would be relatively high near the thin balloon tips and relatively low near the thick back wall of the ballooned-ruptured region. This non-uniformity in local oxidation level has a dramatic effect on the response of the post-oxidation sample to 4-PBT loading, especially as tests were conducted with the maximum tensile stress aligned with the length of the rupture opening (i.e., maximum tensile stress acting on heavily oxidized balloon tips). This subject is discussed in Section 5.3.

The length of the ballooned region is defined by ANL as the axial extent for which the circumferential strains are ≥2%. These ends of the balloon regions are referred to as "necks." Steam that enters through the rupture opening is near static. Inner surface oxidation in this region releases hydrogen that is partially trapped. Most of this hydrogen diffuses within the sample inner area away from the rupture opening and is picked up by the cladding through the inner surface. This hydrogen pickup is commonly referred to as secondary hydriding. Steam also diffuses within the cladding to partially oxidize the cladding inner surface within the balloon region. Assuming that the diffusion of hydrogen is faster than the diffusion of steam, additional hydrogen becomes available for diffusion and pickup as oxidation progresses along the sample from edges of the rupture opening to the balloon necks. These phenomena result in a decrease in oxidation level and an increase in hydrogen level between rupture edges and balloon necks. Fig. 9 shows the measured axial distribution of oxygen content (in wt. %) and hydrogen content (in wppm) for a 4.14 MPa pressurized sample oxidized to a maximum CP-ECR of 17%. The maximum oxidation level occurred at an axial location corresponding to the largest circumferential strain and the widest rupture opening. The maximum hydrogen content occurred near the balloon necks. These results suggest that the weakest part of the sample may be where the oxidation level is highest (location of maximum wall thinning) and the hydrogen pickup is lowest or it may be at locations between the rupture edges and the balloon

necks where high oxygen and hydrogen levels are present. As shown in the next section, failure location depended on rupture strain with high rupture strains causing failure within the rupture-opening cross section.

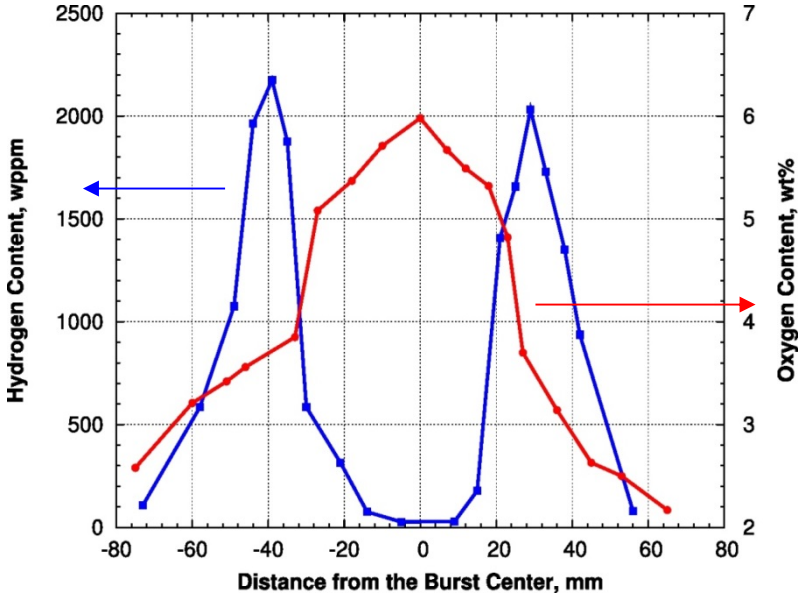

FIG. 9. Axial profiles of hydrogen and oxygen content in AF ZIRLO sample with 23% maximum rupture strain oxidized to 17% CP-ECR at 1200°C peak temperature.

5.3. 4-PBT results for ballooned and ruptured cladding

The 4-PBTs were conducted at 135°C, at a displacement rate of 1 mm/s (initially 2 mm/s) and to a total displacement of 14 mm. For tests in which the load dropped to zero, indicating severing of a cross section, the tests were manually terminated. Three ramp-to-rupture test samples (AF ZIRLO) were subjected to 4-PBT loading. These samples were highly ductile and survived 14-mm displacement without severing or even cracking. The maximum bending moments, maximum energies (i.e., area under load-displacement curves), and the offset displacements were essentially the same for rupture strains of 20% to 70%: M_{max} = 20 N.m, E_{max} = 8.1 J, and δ_p = 7.5 mm. These results demonstrated that oxidation is required to weaken and embrittle ballooned and ruptured cladding.

For one of the oxidation tests, a non-pressurized sample was oxidized (outer surface only) to 17% CP-ECR. The sample severed after about 8 mm displacement, but the strength (M_{max} = 24 N.m) was high. The toughness (E_{max} = 4.2 J) and the plastic displacement (δ_p = 0.4 mm) were reduced compared to ramp-to-rupture samples. This test demonstrated that oxidation alone did not weaken the cladding.

The post-oxidation/quench results for ballooned and ruptured cladding showed the expected decrease in strength and toughness with increasing oxidation level from 10% to 18% CP-ECR. Due to wall thinning, oxidation at 1000°C to 1200°C during the 5°C/s heating ramp, and oxidation at 1200°C to 1000°C during the 3°C/s cooling ramp, it was not possible to achieve oxidation levels <10% even with a hold time of only 1 s at 1200°C. With regard to plastic displacement, most of these test samples severed at one or two cross sections during the elastic loading phase (i.e. 0% offset strain) of the 4-PBT. Considering the varying wall thickness shown in Fig. 7, it is not surprising that AF ZIRLO failed without exhibiting plastic flow. Within the rupture-opening location, the local and average oxidation levels were high while the hydrogen pickup was negligible. Most of the AF cladding samples with rupture

strains >40% severed at the rupture location for which the cladding was thinnest and the oxidation level was highest. For an AF sample with 43% rupture strain oxidized to 12% CP-ECR, Fig. 10 shows the: (a) severed cross section, (b) high oxidation level at one of the crack tips, and (c) low oxidation level at the back region of the rupture cross section. The crack initiated at the rupture tips and propagated through the cross section without exhibiting plastic deformation because the more ductile part of the cladding did not have enough toughness to blunt crack growth.

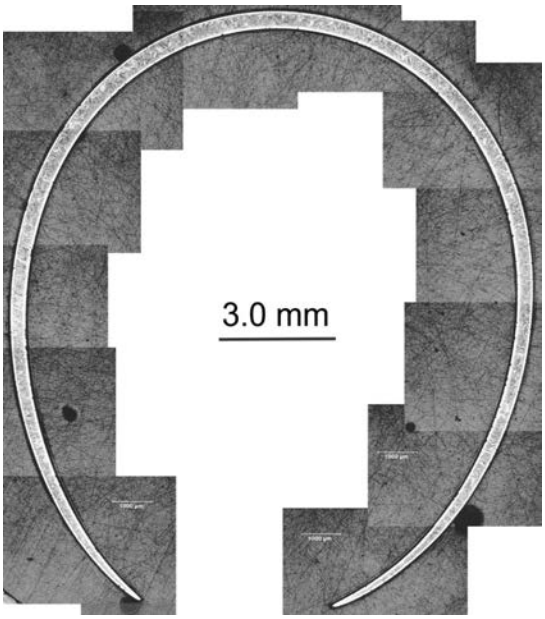

(a)

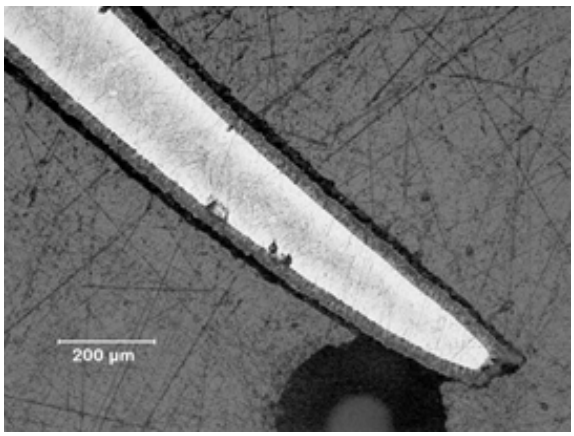

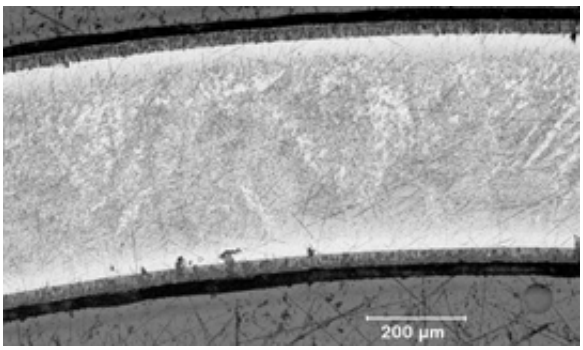

(b) *(c)*

FIG. 10. AF ZIRLO sample with 43% rupture strain oxidized to 12% CP-ECR: (a) cross section at failure location, (b) high oxidation level at rupture tip, and (c) low oxidation level at back region of rupture cross section.

For AF cladding with rupture strains in the range of 22% to 27%, severing occurred at two locations about ±25 mm from the rupture centre in regions with significant combinations of hydrogen pickup and oxidation level (see Fig. 11). For PH cladding with 220 wppm to 700 wppm, rupture strains were in the range of 56% to 71%. These samples all severed through the rupture node, which was weakened by wall thinning, high oxidation level, and pre-test hydrogen.

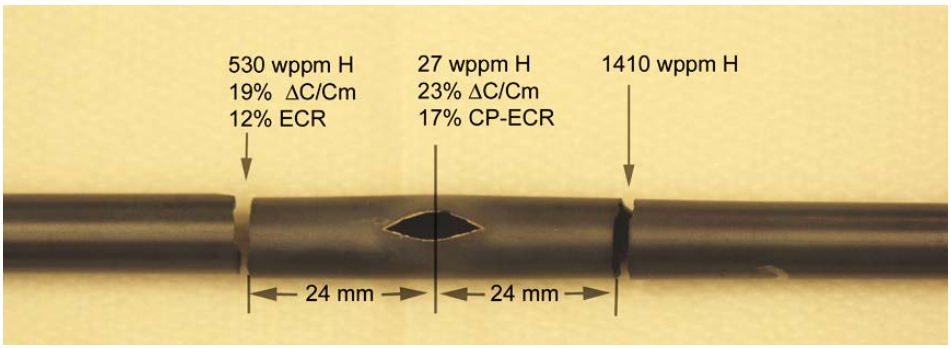

(a)

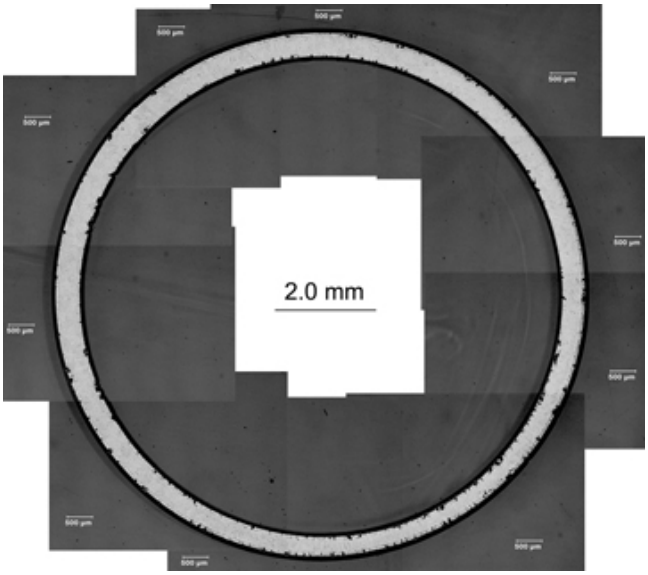

(b)

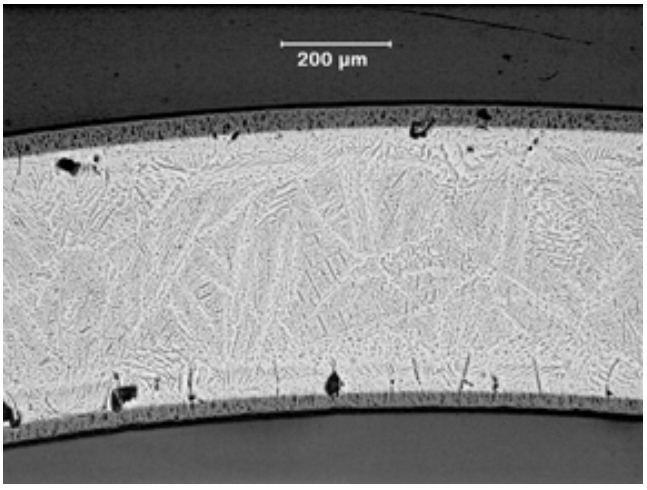

(c)

FIG. 11. Post-4-PBT results for AF ZIRLO sample with 23% rupture strain oxidized to 15% CP-ECR: (a) failure locations, (b) severed cross section at -24 mm (left), and (c) inner- and outer-surface oxide layers at -24 mm.

Fig. 12 shows the maximum bending moment vs. CP-ECR for AF and PH ZIRLO. Within data scatter, there was no significant difference in M_{max} for samples that severed along the cross section containing the rupture opening and for samples that severed at axial locations outside the rupture opening. Lowering of the rupture strain would tend to increase the strength of the rupture-opening cross section for a fixed oxidation level. However, this

merely shifted the location of the weakest part of the cladding to the rupture-edge/balloon-neck region with no appreciable increase in strength. Also shown in Fig. 12 are the maximum bending moments for PH ZIRLO samples. These results clearly demonstrate that cladding strength is degraded significantly by the presence of pre-test hydrogen. The failure-energy results shown in Fig. 13 indicate the same trends of decreasing toughness with increasing oxidation level and pre-test hydrogen content.

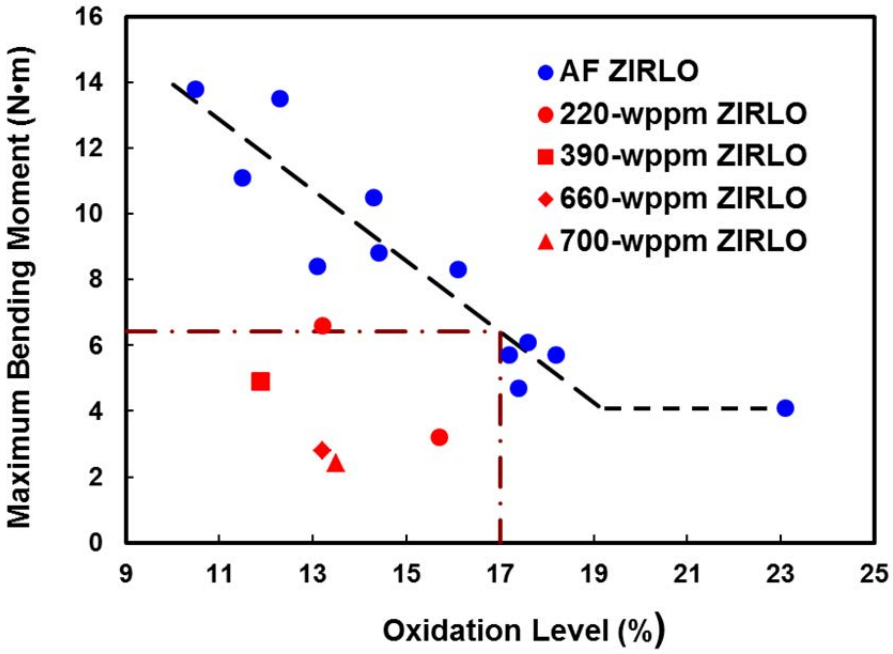

FIG. 12. Maximum bending moment vs. oxidation level (CP-ECR) and pre-test hydrogen content for ballooned and ruptured ZIRLO cladding.

As mentioned, Figs. 12 and 13 results were obtained from samples that failed during the linearized portion of the loading curve associated with elastic deformation of the 4-PBT sample. As such, offset strains (measure of plastic deformation) were essentially zero. From a structural point of view, the samples exhibited no measurable ductility even for regions (e.g., cross sections containing the rupture opening) that were expected to have local ductility (e.g., thick back of rupture-node cross section. Also, Fig. 9 suggests that there would be a region of about 100 mm to 120 mm within the balloon region that would be brittle based on the embrittlement results shown in Fig. 3.

While it is unlikely that the material between the rupture edges and the balloon necks retains "ductility" in response to 4-PBT and RCT loading, results shown in Fig. 12 clearly demonstrate that the material retains strength if oxidation levels and pre-test hydrogen content are limited. The issue of how much strength is needed to resist severing into two or three pieces is a difficult one to address as generally accepted structural analyses of degraded cores are not available.

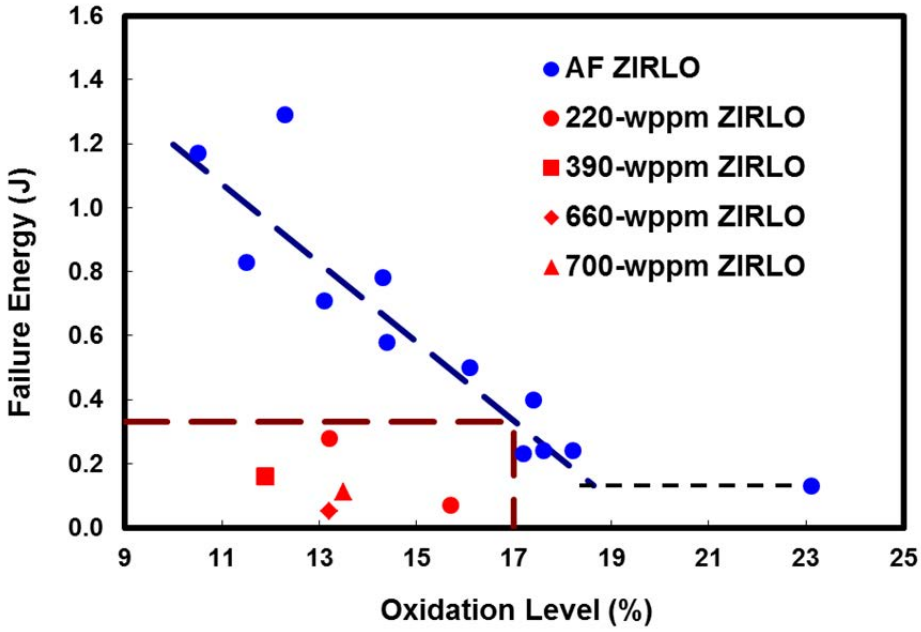

FIG. 13. Failure energy vs. oxidation level (CP-ECR) and pre-test hydrogen content for ballooned and ruptured ZIRLO cladding.

JAEA [12-15] has conducted oxidation-quench tests with ballooned and ruptured AF, PH, and irradiated 17×17 Zry-4 cladding samples. During cooling and quench (from 700°C to 100°C) phases of the tests, samples were subjected to full or partial (735 N, 540 N, or 390 N) constraint, which induced axial tensile loads and stresses. These tests simulated possible axial-contraction restraint at the grid spacers during cooling. The JAEA reference case, which is considered to be an upper bound on grid-spacer constraint load, was 540 N. Although full constraint (i.e., plane strain condition) is overly conservative, Argonne chose to use JAEA results from such tests. For AF Zry-4, oxidized at 1200°C to >10% CP-ECR, maximum recorded loads for samples that survived full-constraint loading were ≤2000 N. As shown in Ref. [3], the AF ZIRLO sample oxidized to 17% CP-ECR (see Figs 11-12) would have survived the JAEA full constraint test without severing. Based on measured M_{max} (5.7 N.m) for this sample, it would take an equivalent axial load of 2350 N to sever the sample. If the correlation value (6.4 N.m) had been used in the analysis, the axial load required to sever an AF cladding sample would have been 2630 N. Thus, AF cladding appears to be strong enough to survive full axial constraint if the oxidation level is limited to 17%.

For PH samples tested by Argonne, the results in Fig. 3 would limit cladding with 220 wppm pre-test (or pre-transient) hydrogen content to 11% CP-ECR. Linear extrapolation back to 11% of the two data points for 220-wppm ZIRLO gives a maximum bending moment of 9.6 N.m (>6.4 N.m). Thus, use of the oxidation limit shown in Fig. 3 would result in maximum bending moments larger than the value at 17% for AF cladding.

6. DISCUSSION

The data presented in this paper apply to as-fabricated and pre-hydrided Zr-based cladding alloys and cladding from fuel rods irradiated to high-burnup in commercial reactors. The datasets include: (a) oxidation limits vs. pre-oxidation hydrogen content based on preserving post-quench ductility for oxidation temperatures near the current limit (1204°C) in the Code of Federal Regulations (10CFR50.46), (b) time limits to prevent embrittlement due to breakaway oxidation at lower oxidation temperatures (970°C to 1015°C), and (c) oxidation

limits vs. pre-oxidation hydrogen content to preserve the strength of ballooned and ruptured cladding. The primary purpose of generating such data was to provide NRC with the technical basis for establishing oxidation and time limits for design-basis LOCAs to preserve post-quench ductility for cladding outside of the ballooned and ruptured region and for establishing limits to preserve post-quench strength in the ballooned and ruptured region.

The data generated by Argonne for cladding currently used in commercial reactors can also be used as a *measuring stick* for the evaluation of the performance of new cladding materials with *enhanced accident tolerance.* As an example, the effectiveness of coated Zr-based alloy cladding is discussed for 17×17 fuel assemblies irradiated in a pressurized water reactor (PWR).

Based on embrittlement results shown in Fig. 3, it is clear that reducing the hydrogen pickup during normal reactor operation would allow for higher oxidation levels and corresponding times at 1200°C. Hydrogen pickup in M5 is low relative to Zry-4 and ZIRLO cladding alloys. AREVA published results from a larger database showing corrosion-layer thickness values ≤25 μm and hydrogen content values <100 wppm for 17×17-array M5-clad fuel rods [16]. As a baseline, coated Zr-based alloy cladding that reduced corrosion layer growth and hydrogen pickup (<100 wppm) during normal operation would allow for residency times corresponding to >62 GWd/t burnup and would improve accident tolerance during design-basis LOCAs even if the coating was not effective in reducing the oxidation rate at LOCA relevant temperatures. For 17×17 AF cladding with 0.57-mm wall thickness, the embrittlement threshold is about 20% CP-ECR, which corresponds to 400 s double-sided oxidation time at 1200°C. This could be achieved by coated cladding that eliminated hydrogen pickup during normal reactor operation. The 400 s, which is based on embrittlement, could be extended to higher times if the coating were partially protective with regard to oxidation at 1200°C. However, if the cladding were coated only on the outer surface, there would still be oxygen pickup through the cladding inner surface. Typically, cladding irradiated to high burnup develops a thin oxide layer (10±3 μm)`on the inner-surface, which is bonded to the fuel. At elevated temperatures, this oxide layer is "reduced" by the Zr metal such that oxygen from this layer diffuses into the cladding. The fuel is also a source of oxygen as Zr has a higher affinity for oxygen than the fuel. Thus, the oxidation time at 1200°C could be further extended if an effective coating were also applied to the cladding inner surface.

Minimum breakaway oxidation times measured by Argonne were in the range of 3000 s to >5000 s for 970°C to 1015°C oxidation temperatures. These times were based on 200-wppm hydrogen pickup rather than the traditional increase in weight-gain rate. Data generated by AREVA, CEA, and EdF [11] showed breakaway oxidation times in the range of 6500±500 s for M5 oxidized at 1000°C. The time at elevated temperatures for design-basis LOCAs, especially small-break accidents, varies considerably from plant to plant. Although criteria should be developed to prevent embrittlement due to breakaway oxidation, it is not clear how to use the data to develop the criteria. A conservative approach would be to limit the total LOCA time above a certain temperature to be less than the minimum breakaway oxidation time. In evaluating the performance of enhanced accident tolerant cladding (e.g., coated Zr-based alloys), materials that extend the breakaway oxidation time to >6500 s would be an improvement relative to current alloys. Extension of breakaway oxidation time to >6500 s may be more relevant and more of a benefit during beyond-design-basis accidents involving longer-time under-cooling events.

Zr-based alloys coated only on the outer surface would likely experience ballooning and rupture during the heating ramp. Ballooning and rupture would result in inner-surface cladding metal directly exposed to near stagnant steam for low-burnup fuel and high-burnup fuel (after dissolution of the inner-surface oxide layer). Secondary hydriding would occur as a result of inner-surface oxidation. As it is not at all clear that the inner-surface oxide layer is protective, hydrogen pickup might occur through this layer prior to dissolution. Also, ballooning and rupture would challenge the integrity of the outer-surface coating, as well as that of an inner-surface coating if one was present. Although it would be difficult for coated cladding to protect the balloon-region cladding (<3% of the total cladding length) from embrittlement, adequate strength could be preserved for times corresponding to 17% CP-ECR if the outer-surface coating was effective in reducing hydrogen pickup during normal operation. From the perspective of beyond-design-basis under-cooling events, it would be beneficial if the outer-surface coating along 97% of the fuel rod were effective in reducing the oxidation rate and corresponding hydrogen release rates at temperatures ≥1200°C.

The issue of fuel behaviour during a LOCA transient is beyond the scope of this paper. Reference 17 is recommended for readers interested in this subject.

ACKNOWLEDGEMENTS

This work was supported by the USNRC Office of Nuclear Regulatory Research under contract V6199. The authors would like to acknowledge the guidance of H.H. Scott, who served as the USNRC manager for this project.

REFERENCES

[1] BILLONE, M., YAN, Y., BURTSEVA, T., DAUM, R., "Cladding Embrittlement during Postulated Loss-of-Coolant Accidents", NUREG/CR-6967, USNRC ML082130389 (2008).

[2] CATHCART, J.V., PAWEL, R.E., McKEE, R.A., DRUSCEL, R.E., YUREK, G.J., CAMPBELL, J.J., JURY, S.H., "Zirconium Metal-Water Oxidation Kinetics IV. Reaction Rate Studies", ORNL/NUREG-17, USNRC ML052230079 (1977).

[3] BILLONE, M.C., "Assessment of Current Test Methods for Post-LOCA Cladding Behaviour", NUREG/CR-7139, USNRC ML12226A182 (2012).

[4] YAN, Y., BURTSEVA, T.A., BILLONE, M.C., High-Temperature Steam-Oxidation Behaviour of Zr-1Nb cladding alloy E110, J. Nucl. Mater. **393** (2009) 433.

[5] LEISTIKOW, S., SCHANZ, G., Oxidation Kinetics and Related Phenomena of Zircaloy-4 Fuel Cladding exposed to High Temperature Steam and Hydrogen-Steam Mixtures under PWR Accident Conditions, Nucl. Eng. Des. **103** (1987) 65.

[6] MARDON, J.P., BRACHET, J.C., L. PORTIER, L., MAILLOT, V., FORGERON, T., LESBROS, A., WAECKEL, N., "Influence of Hydrogen Simulating Burn-Up Effects on the Metallurgical and Thermal-Mechanical Behaviour of M5™ and Zircaloy-4 Alloys under LOCA Conditions," Proc. 13th Intl. Conf. on Nucl. Eng., ICONE13-50457, Beijing (2005).

[7] GRESHAM, J.A., "Updated Westinghouse Breakaway Oxidation Testing/Behaviour" (non-proprietary), LTR-NRC-08-29, WEC, Jun. 12, 2008, USNRC ML081700587 (2008).

[8] GRESHAM, J.A., "Westinghouse Results from Study on Impact of Specimen Preparation on Breakaway Oxidation" (non-proprietary), LTR-NRC-09-24, WEC, May 7, 2009, USNRC ML091350581 (2009).

[9] GRESHAM, J.A., "Weight Gain Data for Zircaloy-4 and ZIRLO Breakaway Tests" (non-proprietary), LTR-NRC-11-10, WEC, Mar. 10, 2011, USNRC ML110800046 (2011).
[10] COMSTOCK, R.J., MUELLER, A.J., ROMERO, J., MITCHELL, D., "Assessment of the Breakaway Performance of ZIRLO® and optimized ZIRLO™ High Performance Claddings for Realistic Small Break LOCA Transients," Proc. WRFPM 2014, Sendai, Paper 100148 (2014).
[11] VANDENBERGHE, V., BRACHET, J.C., LE SAUX, M., GILBRON, D., MARDON, J.P., SEBARRI, B., "Sensitivity to Chemical Composition and Heating/Oxidation Mode of the Breakaway Oxidation in M5® Cladding Steam Oxidized at 1000°C (LOCA Conditions)," Trans. TopFuel-2012, Manchester (2012) 214.
[12] NAGASE, F., FUKETA, T., Effect of Pre-Hydriding on Thermal Shock Resistance of Zircaloy-4 Cladding under Simulated Loss-of-Coolant Accident Conditions, JNST **41** 7 (2004) 723.
[13] NAGASE, F., FUKETA, T., Behaviour of Pre-Hydrided Zircaloy-4 Cladding under Simulated LOCA Conditions, JNST **42** 2 (2005) 209.
[14] NAGASE, F., FUKETA, T., Fracture Behaviour of Irradiated Zircaloy-4 Cladding under Simulated LOCA Conditions, JNST **43** 9 (2006) 1114.
[15] NAGASE, F., CHUTO, T., FUKETA, T., Behaviour of High Burn-Up Fuel Cladding under LOCA Conditions, JNST, **46** 7 (2009) 763.
[16] MARDON, J-P., "Latest Results on M5™ Alloy under RIA and LOCA Representative Conditions," Proc. Euro. Nucl. Conf., Versailles, Paper 303 (2005).
[17] RAYNAUD, P.A.C., "Fuel Fragmentation, Relocation, and Dispersal During the Loss-of-Coolant Accident", NUREG-2121, USNRC ML12090A018 (2012).

OPTIMIZATION OF NUCLEAR GRADE FECRAL FUEL CLADDING FOR LIGHT WATER REACTORS

Y. YAMAMOTO, K.G. FIELD, L.L. SNEAD
Oak Ridge National Laboratory
Oak Ridge
United States of America
E-mail: yamamotoy@ornl.gov

Abstract

Development of nuclear grade, iron-based wrought FeCrAl alloys has been initiated. These FeCrAl alloys are expected to serve as a substitute for Zr-based alloys in order to provide enhanced accident tolerance as LWR fuel cladding. Ferritic alloys with sufficient amounts of Cr and Al additions can exhibit significantly lower oxidation kinetics in high-temperature steam environments when compared to Zr-based alloys. Development efforts have focused on the optimization of the Cr and Al contents by balancing the high-temperature (>1000°C) steam oxidation behaviour with typical cladding performance measures including strength at service conditions, mechanical stability under design-basis and beyond-design basis accident scenarios, fabricability, and radiation tolerance including phase stability and radiation induced hardening/embrittlement. Efforts were initiated to evaluate various properties of model FeCrAl alloys with minor Y additions to support optimization efforts (Phase I); such as processibility, oxidation resistance, mechanical properties, thermal stability, weldability, thin-wall tube fabricability, and radiation tolerance. A set of alloys containing 10-18% Cr, 3-5% Al, and 0-0.12% Y, in weight percent, were prepared by conventional arc-melting and hot-working processes to explore the effect of composition on the properties of FeCrAl+Y alloys. It was found that most of the properties were insensitive to the alloy compositions; however, the steam oxidation resistance strongly depended on both the Cr and Al content of the alloy. Similarly, the radiation testing of the model alloys revealed that lower Cr content (<15%) was preferred to minimize Cr-rich α′ formation which lead to radiation induced hardening at typical service conditions. Based on these results, an optimized composition space, which narrowed the selected Cr and Al contents, was determined. Further development efforts were initiated which specifically focused on strengthening within this composition space (Phase II). Minor alloying additions such as Mo, Nb, and Si together with optimized thermo-mechanical treatment were utilized to successfully achieve improved tensile properties combined with sufficient oxidation resistance at elevated temperatures.

1. INTRODUCTION

The commercial fleet of light water reactors (LWRs) utilizes zirconium based alloys as cladding in the UO_2 based fuel system. The cladding serves as a protective barrier for the UO_2 fuel and fission products to the primary coolant flow during normal operation. Zirconium based alloys have shown excellent properties under normal operation including aqueous corrosion, radiation stability as well as sufficient strength at service temperatures. However, at elevated temperatures, oxidation of zirconium alloys in a steam condition would be accelerated which leads to production of hydrogen gas due to decomposition of H_2O [1, 2]. The recent nuclear accident, which occurred in Japan in 2011, has highlighted that improvements could be made in the accident tolerance of the current fuel-clad system for LWRs. In particular, a reduction in hydrogen gas production and reduced oxidation kinetics of the cladding could significantly increase the safety margins during accident scenarios such as loss of coolant accidents (LOCAs) [3].

Several different fuel-clad systems have been proposed including Mo clad, SiC clad, U_xSi_x fuel, among others [3]. A fuel-clad system with promising initial properties is the FeCrAl-UO_2 fuel system. The FeCrAl class of materials has been widely used with success in many industries where high temperature oxidation resistance is needed including combustion of water materials and fossil fuel energy plants [4]. Due to the complexity of the fuel-clad system in typical LWR configurations, an 'off-the-shelf' alloy solution might not be readily available for the FeCrAl alloy system. Therefore, recent work has been initiated to develop FeCrAl alloys deemed 'nuclear grade'. Nuclear grade designation is used here to describe alloys with several important features for nuclear applications including good mechanical properties for extended periods of high temperature, oxidation resistance, radiation tolerance, long-term aqueous corrosion resistance, compatibility with the prototypical UO_2 fuel and

neutronics which do not significantly penalize the overall reactor operation. Furthermore, nuclear grade FeCrAl alloys should be formable including the ability to make thin-walled tubes and good weldability.

Initial work was conducted on the FeCrAl alloy system based on their corrosion resistance, radiation response, and fuel-cladding chemical interaction by General Electric in the 1960s [5-8]. Although the reports of this programme provide insight into the performance of simple Fe-Cr-Al and Fe-Cr-Al-Y model alloys, it does not provide sufficient foundation for a truly optimized, nuclear-grade FeCrAl alloy which exhibits exceptional normal operation performance combined with accident tolerance for LWR applications. The objective of this work is to find optimized alloy compositions of the nuclear-grade FeCrAl alloys for LWR fuel cladding with accident tolerance, including thorough evaluation of various properties of the candidate alloys. The nominal alloy composition of the model FeCrAl alloys ranges Fe-(10~20)Cr-(3~5)Al-(0~0.15)Y in weight percent. The higher Cr addition would be better for corrosion resistance or oxidation resistance to support the stability of alumina-scale in a wide temperature range [9], although it would increase potential embrittlement of the materials at relatively lower temperatures due to the formation of Cr rich α′ phases [10, 11]. The higher Al additions would also be beneficial for the oxidation resistance, especially at elevated temperatures, but it may raise the ductile-brittle transition temperature (DBTT) which could affect the room temperature fabricability [12].

This paper serves as a status update of the current alloy developments on FeCrAl alloys. It is segmented into two phases. The first phase (Phase I) includes the development of model alloy compositions to evaluate large open-ended questions, such as evaluation of the mechanical or functional properties, especially focusing on the fabricability and the oxidation resistance. Some of these evaluations have been reported in other works [13-15], here only the most pertinent details towards defining the useable composition space for nuclear applications are highlighted. The main purpose of Phase I is to provide detailed data to allow for down selection of base alloy compositions for development of engineering grade alloys (Phase II). Phase II focuses on optimizing mechanical properties within the composition space defined by Phase I. Alloy design for strengthening, microstructure control through thermo-mechanical treatment, and property evaluation results of the Phase II alloys compared to the reference materials are discussed.

2. PHASE I ALLOY OPTIMIZATION

2.1. Alloy development

Phase equilibrium of the Phase I alloys was initially calculated by using thermodynamic software JMatPro® (version 5) with Fe database. Thermodynamic calculations indicated no significant difference in the phase equilibrium of all alloys in the composition range of Fe-(10~20) Cr-(3~5)Al in weight percent. Thermodynamic calculations also indicated the ferritic body-centred-cubic (BCC) phase is expected with a melting point near 1500°C. Small variations in the melting point were predicted based on varying composition but the relative changes were insignificant. Based on these calculations, various alloy compositions were selected, and the alloys were cast by arc-melting in a back-filled argon gas atmosphere with pure element feedstock and/or pre-alloyed Y-Al to make 400-800 g button ingots. The ingots were flipped and melted several times to avoid any potential inhomogeneity in the ingots. Then the ingots were drop-cast in a back-filled argon gas atmosphere to a water-cooled copper mold with a size of 13 × 25 × 125 mm to make bar-shape ingots, or 36 mm diameter × 100 mm length to make a columnar ingot. Table 1 summarizes the analyzed chemistry of the alloys in as-cast status.

TABLE 1. CHEMISTRY OF THE PHASE I FECRAL ALLOYS

ID	Composition, wt%				Remarks
	Fe	Cr	Al	Y	
B105N	85.12	9.64	5.22	<0.001	Without Y
B134N	83.27	12.88	3.83	<0.0003	
B154N	80.84	15.16	3.98	<0.0003	
B203N	77.05	20.01	2.91	<0.001	
B104Y	86.12	9.99	3.83	0.040	With Y
F1C5AY	85.15	10.01	4.78	0.038	
B125Y	83.56	11.96	4.42	0.027	
B134Y	83.02	13.01	3.94	0.007	
T35Y	82.26	13.18	4.44	0.070	
T35Y2	82.26	13.15	4.44	0.120	
B135Y	82.10	12.91	4.90	0.031	
B154Y	81.18	14.86	3.85	0.012	
B154Y-2	80.99	15.03	3.92	0.035	
T54Y	80.9	15.08	3.90	0.090	
T54Y2	80.84	15.06	3.93	0.120	
B155Y	79.87	14.98	5.02	0.033	
F5C5AY	79.88	15.21	4.83	0.063	
B183Y	79.27	17.53	2.95	0.019	
B183Y-2	79.52	17.51	2.93	0.017	
B184Y	78.39	17.51	3.91	0.043	

It was found the grain size of select alloys were sensitive to the processing temperatures used to form the final plate product. For example, Figure 1 shows the microstructure of B154Y processed at different temperatures using hot rolling and a final anneal. They were hot-rolled at designated temperatures with 40 - 77% thickness reduction at 1050, 900, and 700°C and then annealed at the same temperatures for 10 or 15 min (1a, 1b, and 1c), or 1h at 700°C (1d). The recrystallization was observed above 700°C, although 15 min at 700°C was not enough time at temperature for the alloy to be fully recrystallized. The grain size decreased with decreasing final annealing temperature, from more than 1 mm at 1050°C to 50-80 μm at 700°C after 1 h annealing. The recrystallization kinetics also depends on the amount of thickness reduction, although no significant dependence of alloy compositions was observed. After various attempts of the thermo-mechanical treatment, the optimized process to obtain 20-50 μm grain size was found; the alloys should be hot-rolled at 700°C with more than total 90% thickness reduction, followed by annealing at 700°C for 1 h.

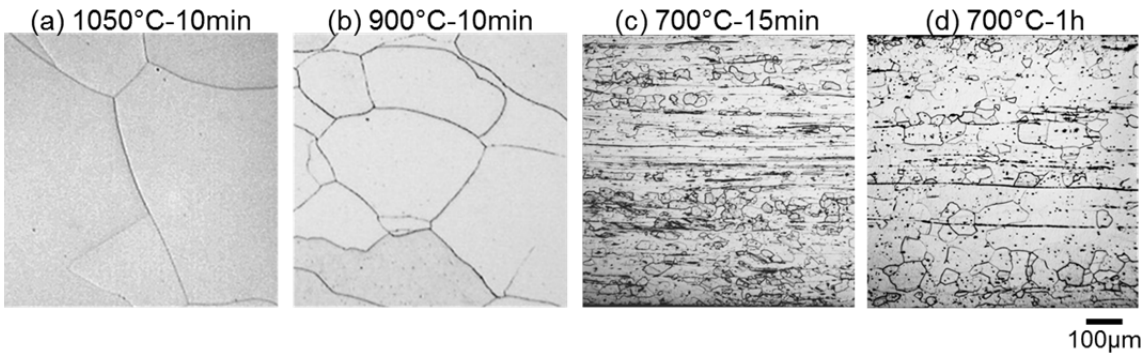

FIG. 1. Cross-sectional light optical micrographs showing the dependence of process temperature on microstructure of a FeCrAl alloy (B154Y); hot-rolled (total 40 or 77% thickness reduction) and annealed at designated temperatures for 10 min – 1 h.

2.2. Oxidation resistance

Fig. 2 illustrates the effect of Cr and Al contents on the oxidation resistance at 1200°C in Ar + 50% water vapour atmosphere, showing the oxidation features of the present model FeCrAl alloys together with commercially available FeCrAl based alloys [16]. Although there were a few exceptions, the protective feature without oxide nodule formation (indicating the formation of protective, external oxide layers on the surface) can be seen in relatively higher Cr and Al containing alloys together with the Y addition, with a limiting boundary drawn between around 17Cr-3Al and 10Cr-4.5Al (bal. Fe). The results indicate that promising oxidation resistance can be expected in a wide composition range of Cr and Al above the boundary, which would give a wide window for the alloy design to optimize the other types of required properties, such as fabricability, mechanical properties, weldability, environmental compatibility, and irradiation resistance. For example, the lower Cr would be preferred to avoid potential embrittlement at temperatures below 500°C due to the formation of Cr-rich α' under irradiation [17], but the high temperature oxidation resistance can be expected in the same alloy by combining sufficient amount of Al addition.

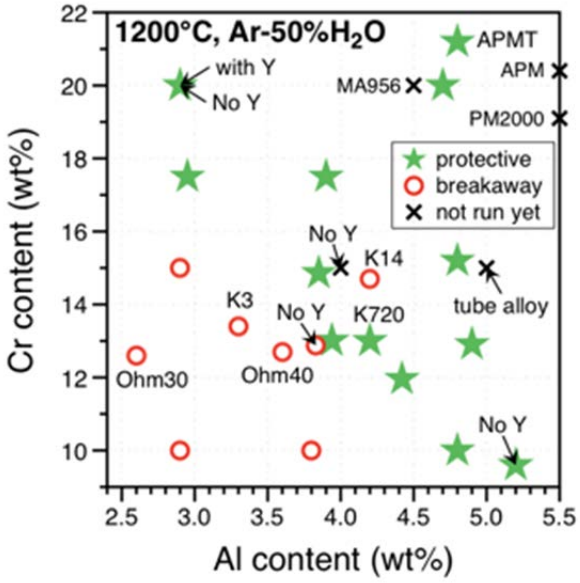

FIG. 2. Effect of Cr and Al content in commercial and model FeCrAl alloys on oxidation resistance at 1200°C in Ar-50%H_2O. Unlabeled points are cast, model FeCrAlY alloys from Table 1 [16].

2.3. Aging effect

Ageing studies were conducted on selected alloys to determine the susceptibility of FeCrAl alloys to Cr- rich α′ formation. Thermodynamic modelling indicated α′ is possible at temperatures below 500°C in the FeCrAl alloys of interest and small variations in the phase boundary can occur due to the composition variants. This prediction is inline with recent experimental work by Kobayashi and Takasugi [18] who used ternary diffusion couples to indicate the phase boundary for α-α′ in the Fe rich corner of the Fe-Cr-Al ternary. Similar precipitation effects were observed using small angle neutron scattering in select FeCrAl alloys by Messoloras et al. [19]. Cr-rich α′ has been known to harden and embrittle Fe-Cr alloys; this effect is historically known as the "475°C embrittlement" [10, 11]. The selected aging temperature of 400°C was slightly higher than the normal operation temperature (at 320°C) of LWRs, which was due to the expectation of faster kinetics of potential α′ formation. Fig. 3 shows the micro-Vickers hardness (300 g load) of the alloys plotted as a function of aging time. Initial (as-processed) hardness increased with increasing Al contents.

When focused on the time dependence, only B134Y (13Cr-4Al) alloy showed a peak of the hardness only after 1h, and then gradually weakened. This result indicates that the hardness of the alloy changes with competitive phenomena from the formation and dispersion of α′ precipitates (increase due to precipitate hardening) and recovery of the cold-worked material (decrease due to loss of work hardening). The latter effect on the B134Y seems strong among the alloys in the current study, indicating that the potential embrittlement due to Cr-rich α′ formation would be minimal for low Cr content FeCrAl alloys.

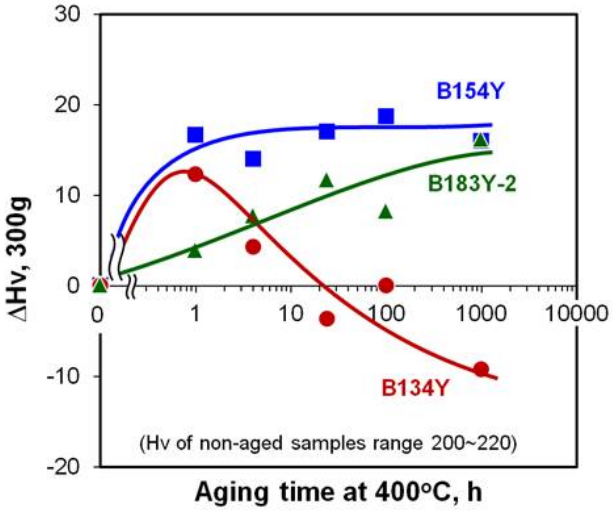

FIG.3. Micro-Vickers hardness of the ORNL FeCrAl alloys plotted as a function of aging time at 400°C.

2.4. Irradiation effects on properties

Four alloys were selected for irradiation in the High Flux Isotope Reactor to investigate the influence of radiation and temperature on the mechanical properties in the low damage dose (<5 dpa) regime. Due to the limited volume size of the target positions, sub-sized specimens of SS-J2 geometry were machined from the F1C5AY, B125Y, B154Y-2, and B183Y-2 feedstock. The specimens were irradiated to three neutron fluences, 3.7×10^{20} n/cm^2, 9.3×10^{20} n/cm^2, and 1.8×10^{21} n/cm^2 (all E>0.1 MeV) corresponding to a nominal dose level of 0.3 dpa, 0.8 dpa, and 1.6 dpa, respectively. The target irradiation temperature was 320 °C. Tensile specimens were mated with passive SiC thermometry to determine the nominal temperature of the irradiation. Dilatometric analysis of the SiC passive temperature monitors was utilized. The dilatometry was conducted up to 600 °C at a constant ramp rate of 1 °C/min using a Netzsch 402 CD dilatometer. Three SiC passive temperature monitors were run for each irradiation condition to provide a statistical mean of the nominal irradiation temperature. Based on the SiC thermometry the nominal irradiation temperature was ~340 °C for the 0.3 dpa samples, ~356 °C for the 0.6 dpa samples, and ~387 °C for the 1.6 dpa samples. The higher irradiation temperature in the 1.6 dpa samples is due to slightly higher neutron fluxes in the target position for those samples.

Irradiated specimens were tensile tested using shoulder loading at a crosshead speed of 0.0055 mm/s corresponding to a strain rate of ~10^{-3} s^{-1} on a screw-driven machine. The engineering strain was calculated from the recorded crosshead separation using the initial gauge length of 5.0 mm. The engineering stress was calculated by dividing the applied load by the initial cross sectional area. All tensile tests were performed at room temperature. The corresponding engineering stress-strain curves are provided in Fig. 4 for each irradiation

condition. It should be noted curves shown in Fig. 4 are from a single tensile test per sample per condition and therefore the results are not indicative of a statistical average. Given this, the results do provide some clear trends with an apparent irradiation induced hardening in the B125Y, B154Y-2, and B183Y-2 samples for all irradiation conditions investigated. Typically, radiation induced hardening was correlated with a loss of ductility in the alloys. The reduction of strength in the F1C5AY specimen irradiated at 387°C is most likely due to significant recovery of prior cold workcompared to the accumulated radiation induced defects. A similar effect was seen in the B134Y sample during aging in Fig. 3. The magnitude of the radiation induced hardening increased with increasing alloy Cr content, most likely due to more significant precipitation of the Cr-rich α′ phase. The formation of α′ has been shown to be Cr composition dependent with the number density increasing with Cr content [17, 20-23]. Furthermore, Bonny et al. [23] has shown irradiated Fe-Cr alloys with weight percent greater than 8 wt.% Cr are susceptible to α′ formation, and hence it is not unexpected in the FeCrAl alloys investigated here, although further characterization is needed. Nevertheless, the mechanical properties of the FeCrAl alloys appear to be dependent on the composition and hence an optimized alloy for nuclear applications should have reduced Cr content to have increased radiation tolerance.

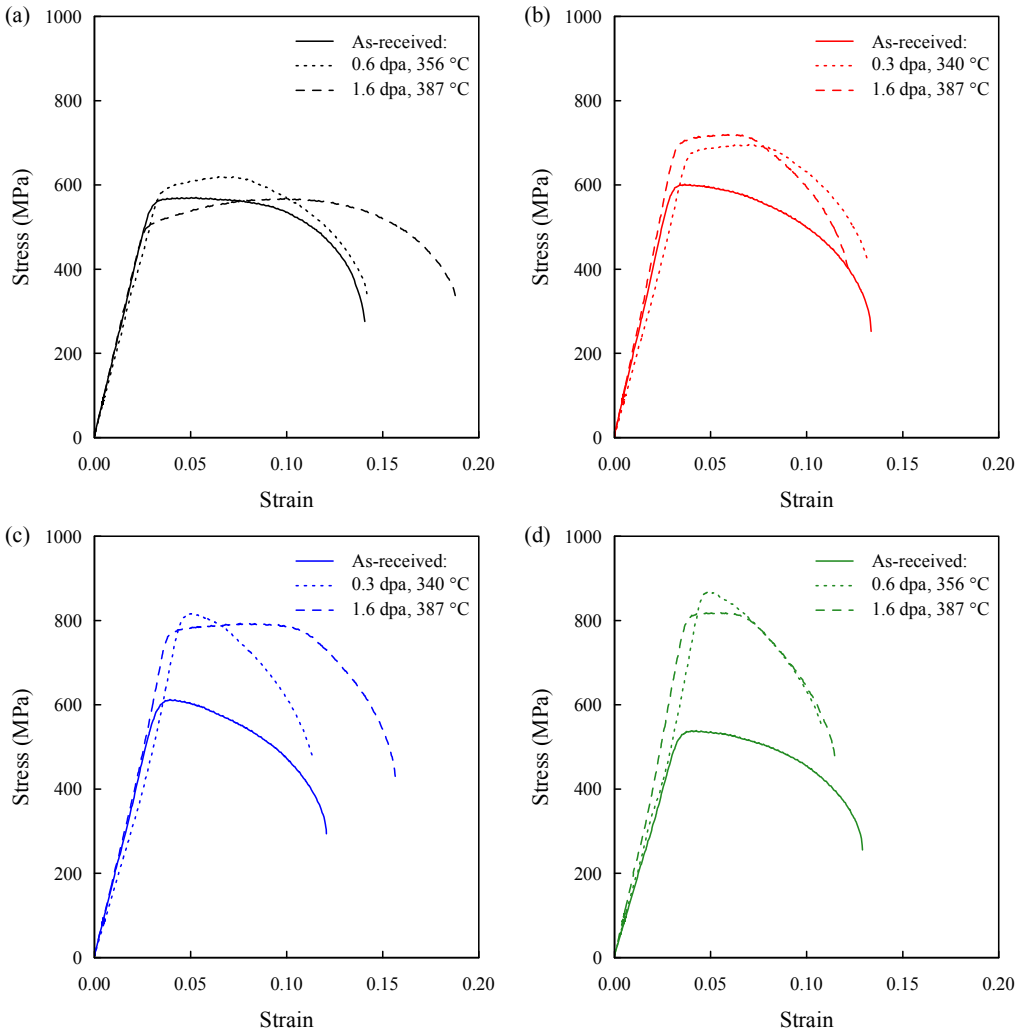

FIG. 4. Engineering stress-strain curves for as-received and irradiated FeCrAl alloys: (a) F1C5AY, (b) B125Y, (c) B154Y-2, (d) B183Y-2.

3. PHASE II ALLOY OPTIMIZATION

3.1. Alloy development

Table 2 summarizes the analyzed chemistry of the alloys in as-cast status. Note that T35Y2 is a Phase I alloy used as a reference material. All alloys were homogenized at 1200°C in Ar gas. The lab-scale heats were hot-forged at 1200 or 800°C to make disk-shape samples with ~8 mm thickness, rolled to make plate-shape samples with ~0.89 mm thickness (total more than 90% thickness reduction), and then annealed at the same temperature for up to 24h for recrystallization and grain size control. T35Y2 and C35MN5 were extruded at ORNL at 1050 and 800°C, respectively, and then annealed at 700 and 800°C, respectively. In order to control the microstructure of C35MN5, more than 97% of total area reduction was applied which was achieved by conducting the extrusion twice. Microstructure was characterized by using a light optical microscope and a scanning electron microscope (SEM) with back-scattered electron (BSE) mode. SEM-electron backscatter diffraction technique was used for crystallographic analysis of the obtained grain structure.

TABLE 2. NOMINAL AND ANALYZED COMPOSITIONS OF THE PHASE II FECRAL ALLOYS

Name		Fe	Cr	Al	Y	Mo	Si	Nb	C
T35Y2	Nominal	82.35	13	4.5	0.15	-	-	-	-
	Analyzed	**82.26**	**13.15**	**4.44**	**0.12**	**<0.01**	**0.01**	**<0.01**	**0.002**
C35M	Nominal	80.15	13	4.5	0.15	2	0.2	-	-
	Analyzed	**80.88**	**12.68**	**4.22**	**0.031**	**1.92**	**0.20**	**<0.01**	**0.003**
C35MC	Nominal	80.07	13	4.5	0.15	2	0.20	-	0.08
	Analyzed	**80.96**	**12.53**	**4.22**	**0.026**	**1.94**	**0.21**	**<0.01**	**0.089**
C35MNC	Nominal	79.83	13	4.5	0.15	2	0.20	0.3	0.02
	Analyzed	**80.41**	**12.77**	**4.31**	**0.065**	**1.95**	**0.20**	**0.24**	**0.026**
C35MN	Nominal	79.15	13	4.5	0.15	2	0.20	1	-
	Analyzed	**79.96**	**12.77**	**4.22**	**0.032**	**1.94**	**0.21**	**0.81**	**0.004**
C35MN5	Nominal	78.53	13	5.2	0.07	2	0.20	1	-
	Analyzed	**78.68**	**13.02**	**5.08**	**0.032**	**1.99**	**0.21**	**0.97**	**0.003**

Minor alloying additions are considered for refining the grain size compared to the reference alloy. Figure 5 summarizes the microstructure of the 2nd generation ATF FeCrAl alloys (C35~) processed at 800 and 1200°C, compared with the 1st generation FeCrAl model alloy (T35Y2) containing no minor alloying additions. The alloys processed at 1200°C showed fully recrystallized microstructure with more than 100 μm grain size, with a few Y-rich precipitate dispersions. No second-phases were observed, as, for the most part, predicted from the calculation. C35M processed at 800°C showed uniform grain size in a range from 30-50 μm which was smaller than that of the T35Y2 which was processed at a lower annealing temperature, indicating that the Mo addition could retard the recrystallization kinetics. C35MC and C35MNC were annealed for 24h at 800°C in order to obtain a fully recrystallized microstructure, and resulted in grain sizes of ~100 μm with relatively elongated grains along the rolling direction (parallel to the horizontal direction in the pictures). C35MN did not show recrystallization even after 24h annealing at 800°C. Figure 6 shows SEM-BSE images of the 2nd generation ATF FeCrAl alloys processed at 800°C. The predicted second-phases such as $M_{23}C_6$, MC, and Laves were observed in the alloys. Note that the size of $M_{23}C_6$ carbides were more than 10 μm which would not provide significant strengthening.

C35MN also exhibited very fine grain size microstructure with ~1-3 μm grain sizes, together with dispersion of sub-micron size Laves phase precipitates on the grain boundary.

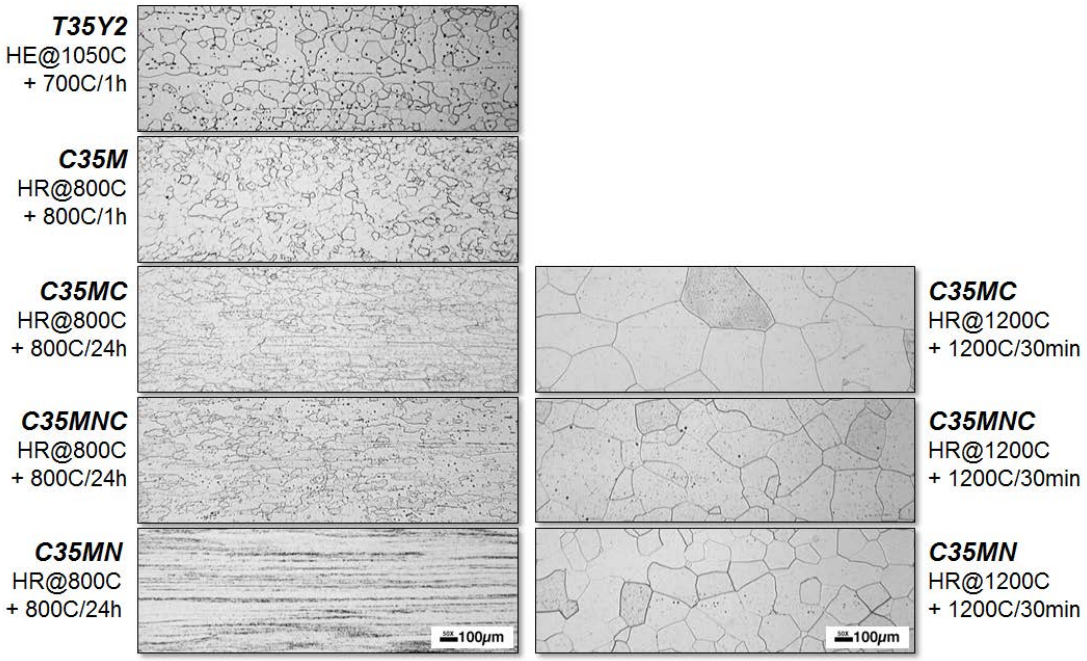

FIG. 5. Light optical micrographs showing the Phase II FeCrAl alloys processed at 800 (left-hand side) and 1200°C (right-hand side).

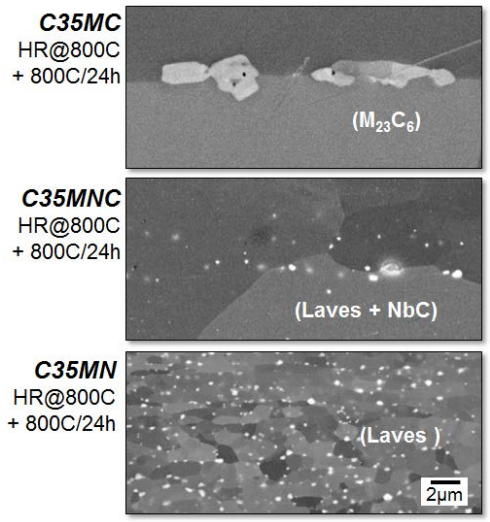

FIG. 6. SEM-BSE images showing the Phase II FeCrAl alloys processed at 800°C.

3.2. Mechanical properties evaluation

Tensile properties of the 2nd generation ATF FeCrAl alloys (C35~), corresponding to the materials shown in Figure 4, are summarized in Table 3. The results of T35Y2 are also shown for comparison purpose. Only slight improvement of the properties in C35M, C35MC, and C35MNC processed at 800°C were observed compared to T35Y2, indicating that the expected solid-solution strengthening or precipitate strengthening are not significant in the case of fully recrystallized microstructure tested at room temperature. On the other hand, the C35MN processed at 800°C showed more than 25% improvement of the yield and tensile strengths together with decent ductility. The properties of C35MC, C35MNC and C35MN

processed at 1200°C showed slightly improved properties compared with the 800°C-processed alloys even with the larger grain sizes, indicating that dissolution of minor alloying elements (C and/or Nb) contributed the solid-solution strengthening. However, the very fine grain size in the 800°C-processed C35MN seemed more effective for improving the tensile properties drastically.

TABLE 3. ROOM TEMPERATURE TENSILE PROPERTIES OF THE PHASE II FeCrAl ALLOYS

Name	Remarks	Process	GS (μm)	At room temperature YS (MPa)	TS (MPa)	UL (%)	TL (%)
C35MC	Mo+Si+C	HR800C + Ann 800C-24h	<100	412	549	14.3	23.0
C35MNC	Mo+Si+Nb+C	HR800C + Ann 800C-24h	<100	448	592	15.8	27.1
C35MN	Mo+Si+Nb	HR800C + Ann 800C-24h	~1	629	811	12.0	21.6
C35MC	Mo+Si+C	HR1200C + Ann 1200C-1h	300-500	589	633	1.7	3.9
C35MNC	Mo+Si+Nb+C	HR1200C + Ann 1200C-1h	100-300	445	562	16.3	27.6
C35MN	Mo+Si+Nb	HR1200C + Ann 1200C-1h	100-300	566	662	7.6	14.1

Figure 7 represents the temperature dependence of tensile properties of the Phase I (T35Y2) and Phase II alloys (C35MN, C35M). Note that C35MN were prepared through two different processing routes; by a hot-rolling or a hot-extrusion at 800°C, which exhibited similar microstructure to each other, as shown in Fig. 6c. For comparison purpose, a commercially available FeCrAl alloy (APMT, Fe-20Cr-6Al base ODS alloy) were tested at the same test condition. It clearly demonstrates the superior strengths of C35MN in a temperature range from room temperature to 500-600°C compared to the other FeCrAl alloys together with decent elongation of ~20%, indicating the advantage of mechanical properties around the operation temperatures of the LWR. The yield strengths of the developed FeCrAl alloys become lower than that of APMT in the higher temperature range than 600°C, which is due to the design nature of APMT (for high temperature creep strength) having more advantage in such temperature range.

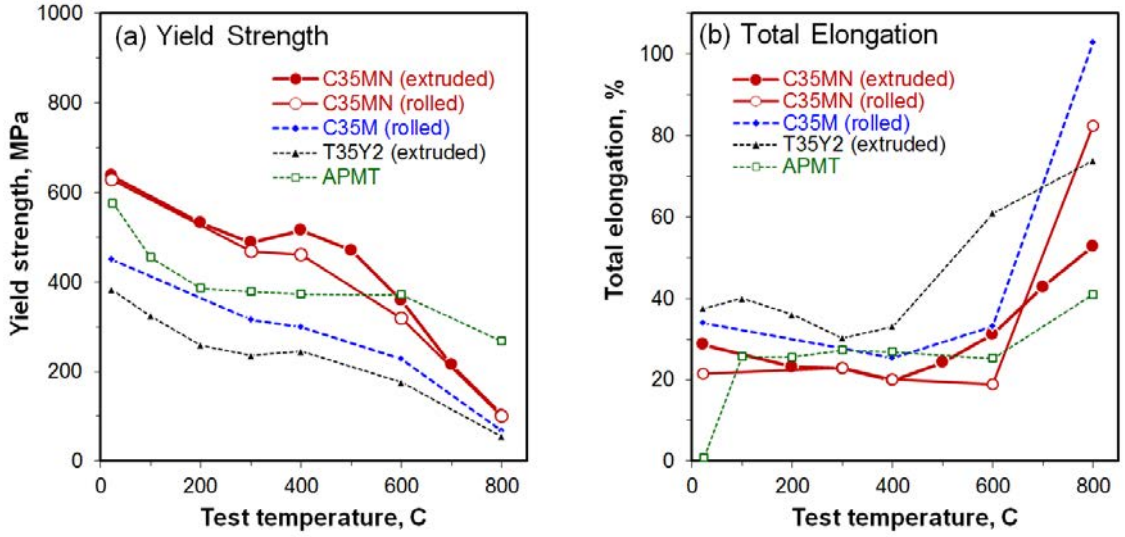

FIG. 7. Temperature dependence of FeCrAl alloys: (a) yield strength and (b) total plastic elongation.

4. CONCLUSIONS

Development of nuclear grade, iron-based wrought FeCrAl alloys has been pursued as the candidate materials for accident tolerant fuel cladding, substituting for the current Zr base alloys in the LWRs. Efforts were initiated to evaluate various properties of model FeCrAl alloys with minor Y additions to support optimization efforts (Phase I); such as processibility, oxidation resistance, mechanical properties, thermal stability, weldability, thin-wall tube fabricability, and radiation tolerance, by using lab-scale heats containing 10-18% Cr, 3-5% Al, and 0-0.12% Y, in weight percent. Most of the properties were insensitive to the alloy compositions in the range studied; however, the steam oxidation resistance strongly depended on both the Cr and Al content of the alloy. Similarly, the radiation testing of the model alloys revealed that lower Cr content (<15%) was preferred to minimize Cr-rich α′ formation which lead to radiation induced hardening at typical service conditions. Based on these results, Fe-13Cr-(4-5)Al+Y was down-selected as a base alloy composition for further development efforts (Phase II). Minor alloying additions such as Mo, Nb, and Si (C35MN) together with optimized thermo-mechanical treatment were utilized to successfully achieve improved tensile properties combined with sufficient oxidation resistance at elevated temperatures. Property evaluations of the developed Phase II alloy, such as weldability, creep rupture test, and tube fabrication, are currently in progress.

ACKNOWLEDGEMENTS

This research was funded by the U.S. Department of Energy's Office of Nuclear Energy, Advanced Fuel Campaign of the Fuel Cycle R&D programme. Authors would like to thank K. Terrani and B.A. Pint from Oak Ridge National Laboratory for their fruitful discussions.

REFERENCES

[1] MOALEM, M., OLANDER, D.R., Oxidation of Zircaloy by Steam, J. Nucl. Mater., **182** (1991) 170-194.

[2] FARMER, M.T., LEIBOWITZ, L., TERRANI, K.A., ROBB, K.R., Scoping Assessments of ATF Impact on Late-Stage Accident Progression Including Molten Core–Concrete Interaction, J. Nucl. Mater., **448** (2014) 534-540.

[3] ZINKLE, S.J., TERRANI, K.A., GEHIN, J.C., OTT, L.J., SNEAD, L.L., Accident Tolerant Fuels for LWRs: A Perspective, J. Nucl. Mater., **448** (2014) 374-379.

[4] EJENSTAM, J., HALVARSSON, M., WEIDOW, J., JÖNSSON, B., SZAKALOS, P., Oxidation Studies of Fe10CrAl–Re Alloys Exposed to Pb at 550°C for 10,000h, J. Nucl. Mater., **443** (2013) 161-170.

[5] GENERAL ELECTRIC, Progress Report No. 59, Fifth Annual Report – High Temperature Materials Programs: Part A, General Electric, Cincinnati, Ohio, (1966).

[6] COLLINS, J.F., ROBERTSHAW, F.C., "Advanced Long-Life Reactor Fuel Cladding and Structural Materials Development", Sixth Annual Report – High Temperature Materials Programs: Part A, General Electric, Cincinnati, Ohio, (1967), pp. 143-174.

[7] VANHOUTEN, G.R., BROZ, M.R., "Advanced Log-Life Reactor Fuel Element, Moderator, Control, and Shield Materials Development", Sixth Annual Report – High Temperature Materials Programs: Part B, General Electric, Cincinnati, Ohio (1967).

[8] KANGILASKI, M., "The Effects of Neutron Radiation on Structural Materials", Radiation Effects Information Center, Columbus, Ohio, (1967).

[9] PINT, B.A., Optimization of Reactive-Element Additions to Improve Oxidation Performance of Alumina-Forming Alloys, J. Am. Ceram. Soc.**86** (2003) 686-695.

[10] HEGER, J.J., 885F Embrittlement of the Ferritic Chromium-Iron Alloys, Metal Progress, (1951) 55-61.
[11] COURTNALL, M., PICKERING, F., The Effect of Alloying on 485 C Embrittlement, Metal Science, **10** (1976) 273-276.
[12] QU, H.P., LANG, Y.P., YAO, C.F., CHEN, H.T., YANG, C.Q., The Effect of Heat Treatment on Recrystallized Microstructure, Precipitation and Ductility of Hot-Rolled Fe–Cr–Al–REM Ferritic Stainless Steel Sheets, Materials Science and Engineering: A, **562** (2013) 9-16.
[13] PINT, B.A., TERRANI, K.A., BRADY, M.P., CHENG, T., KEISER, J.R., High temperature oxidation of fuel cladding candidate materials in steam–hydrogen environments, J. Nucl. Mater., **440** (2013) 420-427.
[14] FIELD, K.G., GUSSEV, M.N., YAMAMOTO, Y., SNEAD, L.L., Deformation Behaviour of Laser Welds in High Temperature Oxidation Resistant Fe–Cr–Al Alloys for Fuel Cladding Applications, J. Nucl. Mater., **454** (2014) 352-358.
[15] GEORGE, N.M., TERRANI, K., POWERS, J., WORRALL, A., MALDONADO, I., Neutronic Analysis of Candidate Accident-Tolerant Cladding Concepts in Pressurized Water Reactors, Annals of Nuclear Energy, **75** (2015) 703-712.
[16] PINT, B.A., UNOCIC, K.A., TERRANI, K.A., The Effect of Steam on the High Temperature Oxidation Behaviour of Alumina-Forming Alloys, Materials at High Temperature, in press, (2014).
[17] MATHON, M.H., DE CARLAN, Y., GEOFFROY, G., AVERTY, X., ALAMO A., DE NOVION, C.H., SANS, A., Investigation of the Irradiation-Enhanced α–α′ Phases Separation in 7–12 Cr Martensitic Steels, J. Nucl. Mater., **312** (2003) 236-248.
[18] KOBAYASHI, S., TAKASUGI, T., Mapping of 475°C Embrittlement in Ferritic Fe–Cr–Al alloys, Scripta Materialia, **63** (2010) 1104-1107.
[19] MESSOLORAS, S., PIKE, B.C., STEWART, R.J., WINDSOR, C.G., Precipitation in Iron-Chromium-Aluminium Alloys, Metal Science, **18** (1984) 311-321.
[20] BHATTACHARY, A.A., MESLIN, E., HENRY, J., PAREIGE, C., DÉCAMPS, B., GENEVOIS, C., BRIMBAL, D., BARBU, A., Chromium Enrichment on the Habit Plane of Dislocation Loops in Ion-Irradiated High-Purity Fe–Cr Alloys, Acta Materialia, **78** (2014) 394-403.
[21] BACHHAV, M., ODETTE, G. R., MARQUIS, E.A., α′ Precipitation in Neutron-Irradiated Fe–Cr alloys, Scripta Mat., **74** (2014) 48-51.
[22] FIELD, K.G., HU, X., LITTRELL, K., YAMAMOTO, Y., HOWARD, R.H., SNEAD, L.L., "Stability of Model Fe-Cr-Al alloys under the Presence of Neutron Radiation", Oak Ridge National Laboratory, Oak Ridge, TN, (2014), pp. 1-26.
[23] BONNY, G., TERENTYEV, D., MALERBA, L., On the α–α′ Miscibility Gap of Fe–Cr alloys, Scripta Materialia, **59** (2008) 1193-1196.

DEVELOPMENT OF MO-BASED ACCIDENT TOLERANT LWR FUEL CLADDING

B. CHENG[*], P. CHOU[*], Y.-J. KIM[**]
[*]Electric Power Research Institute, Palo Alto, CA
[**]GE Global Research Center, Shenectady, NY
United States of America
E-mail: bcheng@epri.com

Abstract

Accident tolerant fuel cladding must meet three basic requirements: (1) meet all fuel design, performance and reliability requirements, (2) maintain coolable core geometry at elevated temperatures (>1000°C) and (3) have high resistance to steam oxidation under accident conditions to significantly reduce hydrogen generation and avoid hydrogen explosion. The aim of developing accident tolerant fuel cladding is to provide significant coping time (10-72 hours) for a plant operator to recover from a severe accident condition, depending on the plant passive cooling system. Molybdenum (Mo) is a candidate because of its very high melting point and its high strength at elevated temperatures. At the same time, Mo and its alloys are known to be susceptible to the formation of volatile MoO_3 in oxidizing environments at temperatures >600°C. Therefore, this research programme uses a composite design in which the Mo alloy cladding is covered with an outer protective coating of either a Zr-alloy or an Al-containing alloy; both coatings will form protective oxides, either ZrO_2 or Al_2O_3 at elevated temperatures. Adherent coatings have been fabricated by PVD for proof-of-concept tests. Multiple lots of 0.2 mm wall thickness tubing, 2 m long, have been fabricated from pure Mo and La_2O_3-doped Mo-ODS. The feasibility of welding has been demonstrated. Test rodlets are being fabricated for irradiation in the Advanced Test Reactor (ATR) at Idaho National Laboratory in early 2015. This paper shares promising results from autoclave tests in simulated LWR environments; and from tests in 1000°C steam, steam plus hydrogen, and steam plus oxygen, for up to 4 days. Additional efforts are underway to optimize the properties of commercial Mo alloys, and to develop new Mo alloys with higher corrosion and oxidation resistance. Mechanical co-reduction to form duplex tubes is also planned.

1. INTRODUCTION

The events at Fukushima Daichi in 2011 have illustrated that hydrogen generation during a severe loss of coolant accident can significantly complicate the accident management effort [1]. The rapid oxidation and loss of mechanical strength of Zr-alloy cladding produces this rapid hydrogen generation, loss of core coolability and eventually fuel melting. The most effective approach in minimizing damage to the fuel and core is to extend passive core cooling system for as long as possible. An added defence is to enhance the capability of the fuel cladding to withstand high temperature steam oxidation and maintain fuel and core geometry to temperatures as high as possible, but with a minimum requirement of 1200°C. Dispersion of radioactive isotopes, particularly the volatile and soluble Cesium-137 and -134 due to the loss of fuel rod integrity and meltdown have would otherwise make the recovery effort much more difficult, as was seen at Fukushima Daiichi.

In BWRs, the main source of hydrogen is from the oxidation of Zr-alloy cladding and channel boxes. In a typical core with ~50,000 fuel rods, the total hydrogen generated from the oxidation of all fuel cladding in the core can exceed 1,000 kg. Following extensive evaluation of various options based on neutronic, thermal mechanical properties, fabricability and compatibility with the existing light water reactor design and operation, molybdenum alloy is identified as a candidate due to its high melting temperature (2623°C) and sufficient strength well above 1200°C. A well-known weakness of Mo-alloys is its tendency to form volatile molybdenum trioxide in oxidizing environments, which may be overcome by forming an outer protective layer, via coating or mechanical co-reduction. The outer coating is designed to be fully metallic with good corrosion resistance under normal operation and form an in-situ protective oxide of either ZrO_2 or Al_2O_3 in steam at accident temperatures.

Analyses of fuel behaviour under a station blackout (SBO) accident, in which all AC and DC power to the station was lost, have been performed using MAAP [2,3] and MELCOR

[4] codes. The results indicate that extending the availability of emergency core cooling is utmost important in delaying temperature rises and fuel damage. Current generation plants are generally designed to have 4 to 24 hour passive cooling capacity, and the Generation III+ plants under construction will have 72 hours passive cooling capacity. If the AC/DC power is not restored to supply cooling water after the battery-assisted passive cooling is lost, the fuel rod surface will start heating up. The time to start fuel rod melting after the loss of coolant is estimated by the MAAP code analysis to range from 3 to 11 hours as shown in Table 1.

TABLE 1. TIME TO INITIATION OF FUEL ROD MELTING AS A FUNCTION OF AVAILABILITY OF CORE COOLING [2]

Passive Cooling. hrs	Decay Heat, %Pre-scram Power	Time to First Melting, hrs after SBO
2	1.18	~3
24	0.67	~10
72	0.52	~11

Rapid hydrogen generation and fuel rod burst or collapse will occur at the temperature range of 800-1000°C. Both result from the inherent property of zirconium to (1) react with steam to form highly stable zirconium oxide and (2) lose its mechanical strength at that temperature range.

To enhance the tolerance of fuel rods to a severe loss of coolant accident, the following goals are considered: (1) reduce hydrogen generation rate, (2) maintain fuel rod integrity, i.e., preventing cladding burst or collapse, and (3) extend time to initiation of fuel rod melting, which occurs at >2000°C. Candidate cladding materials/designs to achieve these goals need to maintain chemical and mechanical stability at temperatures significantly exceeding ~800°C.

In the aftermath of TMI-1, Fineroth explored monolith Al_2O_3 tubes as a potential replacement for zircaloy fuel cladding to enhance fuel tolerance to accidents [5]. While, the ceramic is generally stable in steam at elevated temperatures, brittleness and irradiation instability of Al_2O_3, led Fineroth to pursue SiC composite as a candidate material over the last decade. For SiC composite cladding, significant challenges remain in fabrication of long, thin wall tubes and designing fuel rods with hermeticity to meet thermal-mechanical and reliability requirements [6, 7]. This research has focused on metals and alloys as candidate materials. A coated Mo-alloy cladding design has been proposed and under feasibility study since 2012[(2)].

2. CONSIDERATIONS OF CANDIDATE MATERIALS

The desired attributes for a practical ATF cladding material are quite stringent. In addition to good material properties at high temperature, the candidate material must be compatible with current fuel/core designs, and provide economic operation, including good neutronics. Moreover, from an operational perspective it must be highly reliable, corrosion resistance, and exhibit low embrittlement at high burnups. Lastly, the ATF fuel/cladding must meet all regulatory and safety requirements.

2.1. Temperature targets of ATF designs

The surface temperature of fuel rods at the peak nodes or core centre will increase rapidly when a reactor core reaches a dry steam condition in a SBO accident with no battery-assisted coolant flow. Preliminary analysis using the MAAP code [8] predicts Zr-alloy

cladding will burst at ~850°C in 1-5 hours and start melting at ~2600°C in 3-11 hours, depending on the duration of battery-assisted cooling. Figure 1 shows a case study assuming availability of 72 hour passive cooling for both PWR and BWR. The yellow line represents zircaloy cladding, the red line assumes a hypothetical ideal cladding which does not react with steam until melting, and the dashed lines represent hypothetic cladding with half of the steam reaction rates of zircaloy. It is seen from Figure 1 that fuel cladding designs with the capability of withstanding steam reaction and maintaining fuel rod integrity to ~1500°C may provide additional coping time of ~20 hours for a PWR and ~2 hours for a BWR. (Note: the situation is plant design specific and therefore the results do not necessarily represent all plants bearing the same design group).

Designing an ATF with lower temperature capability may or may not achieve one of the goals of (1) reducing hydrogen generation due to steam oxidation, (2) preventing dispersion of volatile fission products by maintaining fuel rod integrity, and (3) delaying time to fuel rod melting. The latter objective provides more coping time for emergency personnel to reverse or mitigate the accident.

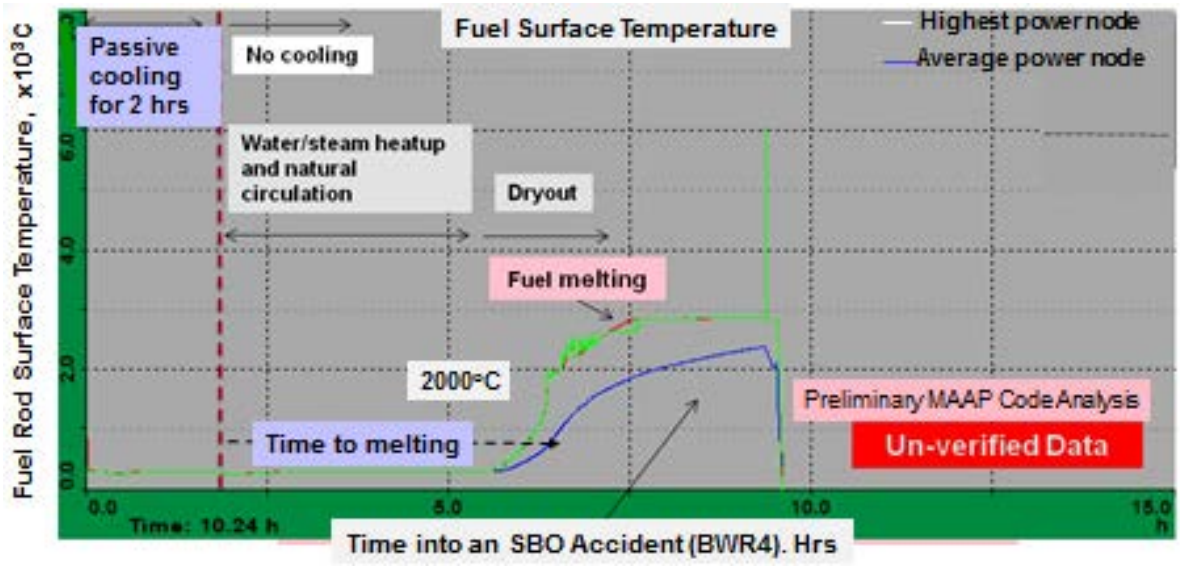

FIG. 1. Fuel rod surface temperature progression in a SBO accident as estimated using the MAAP code [8].

2.2. Identifying suitable cladding materials

It is highly challenging to find candidate ATF cladding materials to meet the requirements of (1) high oxidation resistance to 1200-1500°C, (2) sufficient mechanical strength to 1200-1500°C, (3) acceptable neutron absorption cross sections, (4) all performance requirements for normal operation at 300-350°C, and (5) abundant availability.

In jet and rocket engineering, Al_2O_3, SiO_2, and ZrO_2, as well as some complex oxides have been employed as surface protective layers [9]. The melting temperatures of these three oxide are substantially high at 2016, ~1600 and 2715°C, respectively. A class of Fe-Cr-(5-8 wt%)Al alloys have been developed for high temperature applications due to the formation of a highly protective Al_2O_3 at temperatures exceeding ~>1000°C. SiO_2 forms on SiC to protect SiC from oxidation at elevated temperatures. ZrO_2 forms on Zr-alloys will grow very rapidly at temperatures exceeding ~600-800°C due to the enormous solubility of oxygen in zirconium

(4-10%), which destabilizes the ZrO_2. ZrO_2 can only provide protection as a surface coating on metals with lower affinity to oxygen at elevated temperatures.

Table 2 shows the melting temperature of selected candidate materials. Zr-alloys will substantially lose all its strength and burst when under internal pressure at ~850°C. Molybdenum, one of the refractory metals, has substantially higher melting temperature than Zr-alloy and stainless steel. There also have no reported eutectic reaction of Mo with other common elements to lower its melting temperature.

TABLE 2. THERMAL NEUTRON CROSS SECTION, MELTING AND VAPORIZATION TEMPERATURES OF ATF CANDIDATE MATERIALS

	Neutron Absorption at Same Thickness	Melting, °C	Eutectic, °C	Phase Transition, °C	Volatility, °C
Zr	Low	~1800	~950 with Fe, Ni	~872 (Zr)	
Steel	Higher	~1500	1160 of Fe-B	~912 (Fe)	
Mo	~Steel	2623	1578 of Zr-Mo	None	
SiC	Lower	2730		None	~2000
UO_2		~2200-2600			

*All Zr will become ZrO_2

Molybdenum alloys have been the subject of R&D for nuclear energy applications for over 50 years [10-13]. Irradiation data of several commercial molybdenum alloys at LWR-relevant conditions have been obtained and very high strength molybdenum alloys have been developed, including some suitable for use at temperatures >1500°C. Metal trays made of Mo-alloys have been commonly used in fuel fabrication shops as containers to hold UO_2 pellets for sintering in hydrogen environment at ~1600°C. Some Mo-alloys are used as a thermal couple material in furnace under inert environments to ~2000°C. There are three outstanding concerns regarding the use of Mo-alloys in LWRs: (1) high reactivity in oxidizing environment at >~500°C, (2) higher neutron absorption cross section in comparison to zirconium. It is noted, however, Mo has a thermal cross section very close to that of iron, and (3) difficulty in making thin wall tubes.

Figure 2 shows the strength of Mo as a function of temperature. Un-irradiated Mo exhibits good properties in excess of 1500°C. For pure Mo and Mo-ODS, the room-temperature DBTT is low, maintains some post-irradiation ductility. Their strength and ductility, properties important to fabricability, are shown in Figure 3.

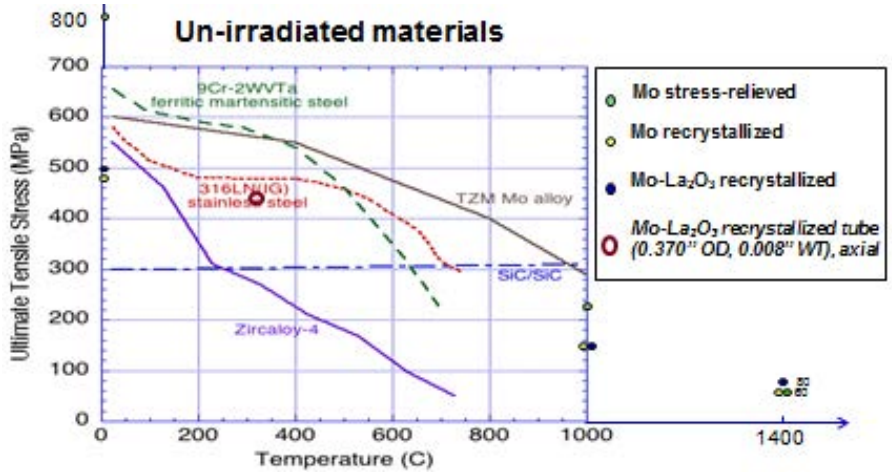

FIG. 2. Strength of Mo.

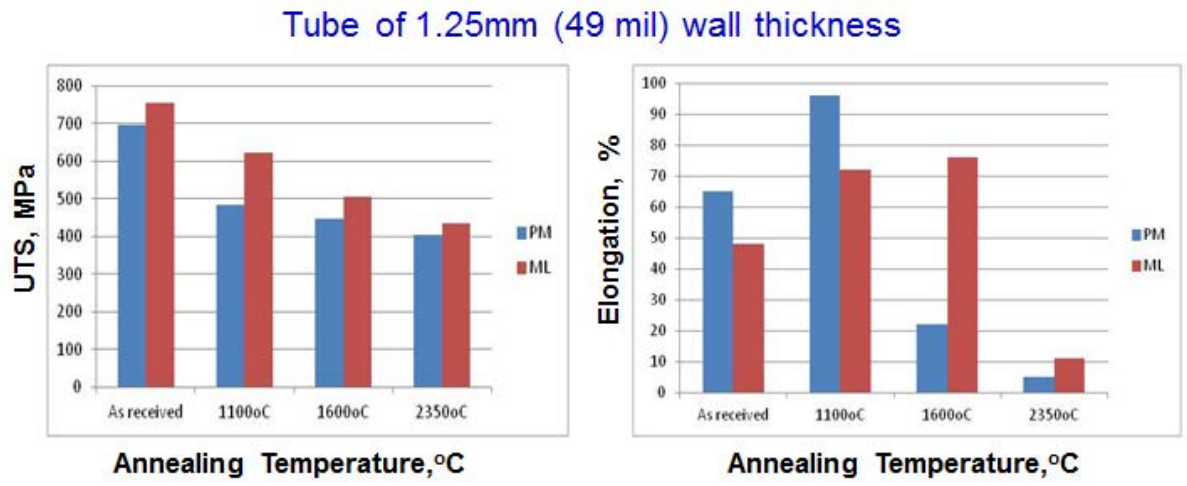

FIG. 3. Properties important for the fabrication of Mo and Mo-ODS.

2.3. Challenge in neutronic properties

Neutronic economic issue for fuel cladding material is not only dictated by the thermal neutron absorption cross section property. For example, lower thermal absorption cladding material with lower strength that requires thicker cladding wall will decrease the water volume in the core for neutron moderation, hence effectively reducing the production of thermal neutron and in effect reducing neutronic economy. Higher strength material, like molybdenum, may allow a significant reduction in the wall thickness to partially compensate neutronic affects by increasing water moderation and somewhat reducing neutron absorption.

Analyses of the effect of non Zr-alloy cladding on the reactivity have been performed using MCNP code [14]. Comparison is made of zirconium, molybdenum and stainless steel 304 grade. The stainless steel case provides a reference point, as stainless steel cladding was used at a few LWRs, particularly in the earliest PWRs and BWRs.

Table 3 shows the relative effect of stainless steel and molybdenum on the cycle average neutron reactivity, K-inf, calculated for a 17x17 PWR design with 4% initial enrichment and 1500 ppm startup boron as the base design case using the MCNP code [14]. Molybdenum actually has lower average neutron thermal cross section than stainless steel, but is higher for the epi-thermal neutron group. It can be seen from the data that the cladding wall thickness of Mo alloy cladding needs to be reduced from that of the current Zr-alloy cladding to minimize the effect of neutron absorption.

TABLE 3. COMPARISON OF EFFECT OF DIFFERENT CLADDING MATERIAL ON NEUTRON REACTIVITY

Cladding Material	Thickness, mm	K-inf.
zirconium	0.55	1.1131
stainless steel 304	0.4	1.05035
molybdenum	0.25	1.0488

In a case study for a BWR 10x10 design containing 14 Gd-containing rods, it is shown in Table 4 that an assembly with 10 mil (0.25 mm) Mo cladding will maintain sufficient reactivity with the current maximum 4.95% enrichment after one 24 month cycle at 21.5 GWd/MTU. It can also been seen that maintaining the current fuel pellet OD (same cladding ID), hence reducing the fuel rod OD with thinner wall cladding, will increase the availability of water for neutron moderation, hence will be more efficient economically. Another

approach to maintain neutron reactivity in fuel designs is to reduce the amount of burnable poison, such as reducing the number of Gd-containing rods, as shown in Table 5.

TABLE 4. EFFECT OF MO 10 MIL CLADDING WITH THE SAME OD OR ID AS THE CURRENT ZIRCALOY CLADDING ON THE ASSEMBLY REACTIVITY OF A 10X10 BWR FUEL ASSEMBLY CONTAINING 14 GD RODS AT 0 AND 21.5 GWD/MTU

Cladding Type	Thickness, mm	K-inf.	DK-inf./K_{Zr}
Fresh fuel assembly - 10x10			
Zr	0.66	1.04377	0
Mo OD same	0.25	1.00581	-0.0364
Mo ID same	0.25	1.01491	-0.0276
Once burned fuel assembly at 21.5 GWd/MTU			
Zr		1.19747	0
Mo OD same		1.14451	-0.0442
Mo ID same		1.12646	-0.0593

TABLE 5. EFFECT OF REDUCING THE NUMBER OF GD-CONTAINING RODS ON RESTORING THE ASSEMBLY REACTIVITY WITH 10 MIL MO CLADDING

Case	Cladding	Tickness, mils	k	Δk	Δk/kZr
1	Zr-14 Gd rods	26	1.04377	0	0
2	Mo-14 Gd rods	10	1.00581	-0.038	-0.0364
3	Mo-13 Gd rods	10	1.03395	-0.0098	-0.0094
4	Mo-12 Gd rods	10	1.05203	0.0083	0.0079

The case study indicates that using thin wall Mo as fuel cladding with the fuel enrichment within the 5% limit will not prohibit the design of fuel assemblies to meet the current long cycle length requirements. Due to the current extensive use of burnable poisons for extended cycle length designs, the extent of neutronic effects on the cycle economics will need more realistic fuel reload evaluations. Less Gd and other burnable poisons, or slightly higher enrichment, may be needed to achieve a 24-month fuel cycle. Using depleted Gd may also be an option.

Natural Mo has 7 isotopes. The higher neutronic cross section of molybdenum is mainly from Mo^{95}, as shown in Figure 4. Mo^{95} has ~16% abundance. With newly available isotope separation technology, the cost for removing Mo^{95} has been quoted to decrease significantly as the demand of volume increases. A price reduction by a factor of ~4-5 from the currently quoted cost may make the use of Mo^{95} feasible.

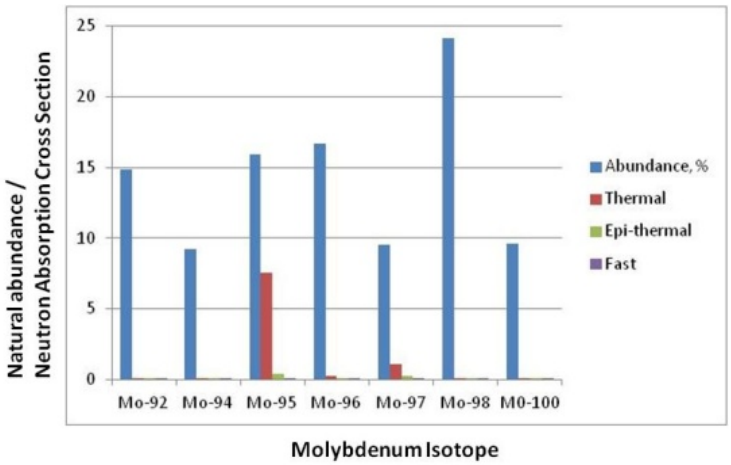

FIG. 4. Molybdenum isotopes, their natural abundance and neutron absorption cross section.

3. EXPERIMENTAL PROCEDURES

3.1. Coated Mo-alloy cladding designs

A novel concept that takes advantage of molybdenum's high melting temperature and high strength involves Mo-Zr or Mo-steel duplex and triplex metal cladding as shown schematically in Figure 5.

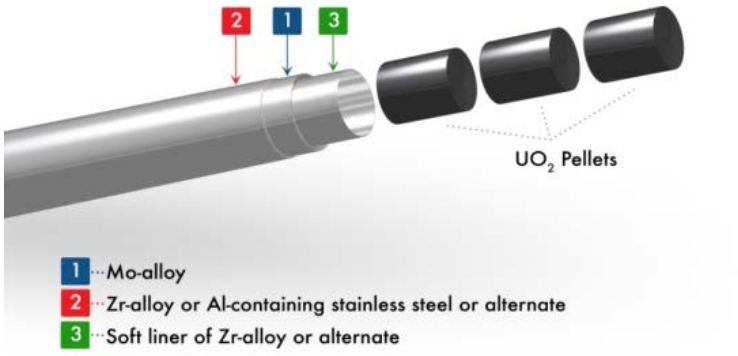

FIG. 5. Schematic of Coated Mo cladding for enhancing accident tolerance.

A high-strength Mo-alloy cladding is bonded with a thin zirconium alloy or Al-containing stainless steel on the outer surface to form a duplex cladding. A zirconium alloy outer layer (<0.15 mm), designed with similar or improved corrosion properties compared to current Zr-alloy cladding, will make the cladding fully compatible with LWR coolants. The outer Zr-alloy layer will be fully oxidized to ZrO_2 in the early stage of a severe accident (700-1000°C). The ZrO_2, due to its very high energy of formation, is expected to be stable in high temperature steam, providing protection to the underlying Mo alloy. An Al-containing stainless steel will provide superior corrosion resistance in steam up to ~1400°C [15]. Although Mo alloys have demonstrated good compatibility with UO_2 fuels, a triplex cladding including a thin inner layer of a Zr-alloy or other metals is also proposed. Duplex and triplex cladding will add to the complexity of cladding fabrication, and advanced fabrication techniques will need to be developed.

With the Mo-Zr duplex or triplex cladding, the total hydrogen released in a loss of coolant accident may be reduced by 90% from that of the current Zr-alloy cladding of 0.57 mm (22.5 mil) wall thickness for PWR fuel rods and more for BWRs, assuming ZrO_2 can be demonstrated to fully protect the Mo-alloy. An Al-containing stainless steel can substantially reduce the oxidation rate, and hence reducing the hydrogen generation rate by an order of magnitude when compared to monolithic Zr-alloy cladding [15]. The upper service temperature of Al-containing stainless steel is ~1400°C, beyond which melting of the Fe-based alloy will occur.

The high strength and creep resistance of Mo duplex and triplex cladding is anticipated to maintain the fuel rod geometry and, hence rod coolability to ~1400-1500°C. The Zr-alloy outer layer should be compatible with LWR coolant, and the Al-containing stainless steel will be tested for compatibility with the LWR coolant. The key properties of coated Mo-alloy for use as LWR fuel cladding is given in Table 6.

TABLE 6. CHECKLIST OF COATED MO-ALLOY FOR LWR FUEL CLADDING

Key Properties	Zr alloy	Mo	Al-containing SS
Melting Temperature, °C	~1800°C	2623°C	~1500°C
Tensile and Creep Strength	Nil at >800°C	to >1500°C	
Corrosion resistance	Good	Need Protection	Good?
Oxidation reistance	Poor (form ZrO_2)	Better (steam)	Excellent
Material cost	Average	Average	Average
Neutronic absorption	Low	Higher	Higher
Fabricability into long tube	Good	OK	OK
Welding	Good	Good	Possible
PCMI (Power ramp, RIA, Swelling)	Good	Appears OK	
Wear resistance	Adequate	Excellent	?
Irradiation embrittlement	Adequate	??	?
Radioactive waste issue	No	No	?

3.2. Thin wall Mo-alloy cladding fabrication and mechanical properties

A total of six lots of thin wall Mo-alloy tubes have been fabricated for testing. Tubes of 0.2 mm (8 mil) wall thickness and outer diameters of 9.4 mm (0.370") or 10 mm (0.393") have be fabricated of pure Mo, including low carbon arc cast (LCAC) and powder metallurgy (PM) molybdenum ingots, as well as Mo-ODS containing 0.35 wt% of dispersed La_2O_3. Examples of thin wall Mo-alloy tubes are illustrated in Figure 6, together with the microstructure. Research and development is in progress to optimize the microstructure with equi-axed grain structure to enhance the mechanical properties.

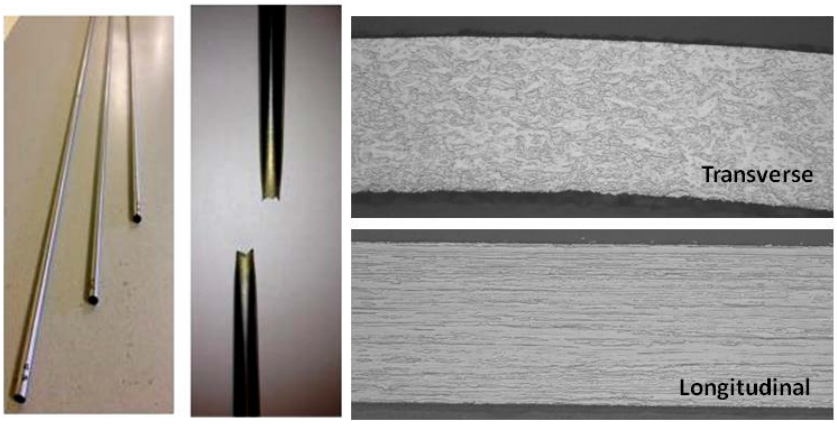

FIG. 6. Examples of thin wall Mo-alloy tubes and the microstructure.

The Mo-alloy tubes are controlled to have an ultimate tensile strength (UTS) of approximately 450 MPa in stress relieved condition and ~280 MPa in recrystallized condition when tested at 320°C, Table 7. The ductility in uniform elongation ranges from 7 to 14%. Because of its high melting temperature and single phase structure (i.e., absence of phase transition) until melting at ~2600°C, the mechanical strength will be maintained to much higher temperatures than that of common structural alloys including Zr, Fe and Ni based alloys.

TABLE 7. MECHANICAL PROPERTIES OF STRESS RELIEVED AND RECRYSTALLIZED MO-ALLOY TUBES TESTED AT 320°C

	Stress relieved		Recrystallized	
Test Temperature, °C	320	320	320	320
Crosshead Speed, cm/m	0.49	0.49	0.49	0.49
UTS, Mpa	441	448	280	283
0.2% Yield Strength, Mpa	373	376	157	158
Uniform elengation, %	7	7	12	14
Fracture elongation, %	11	10	15	16
Area of Reduction, %	38	39	64	66

Under development are tubes with a fine equiaxed grain structure through induction heat treatment for a very short duration. The goal is to achieve uniform ductility in the axial and diametrical dimensions. This may aid in reducing the propensity for axial cracking which may develop during drawing. The basis for this grain size control is given in Reference [16].

3.3. Coated Mo-alloy tubes

Mo alloys are stable in inert and reducing environments to near ~2000°C. However, for application in oxidizing environments over ~300-400°C, protection of the Mo surface from corrosion and oxidation will be necessary, until corrosion and oxidation resistance alloys are available. Surface coating or modifications are subject of the present feasibility study. Surface coating can be formed successfully by existing technologies. A hybrid fabrication process with coating and co-reduction mechanically will be evaluated under this study. For proof of concept of the current design for enhancing accident tolerance, coatings have been fabricated and evaluated using the following techniques: physical vapour deposition (PVD), vacuum plasma deposition (VPS), high velocity oxygen fuel (HVOF) deposition, and high velocity air fuel (HVAF) deposition. All processes can form very high density coating with good adhesion.

Figure 7 shows coatings of ~50 µm formed on Mo-ODS tube sample via a PVD process. Coatings of zircaloy-2, zircaloy-4 and Al-containing stainless steel or FeCrAl have been fabricated successfully. The coatings are formed on 8-20 cm long tubes. The uniformity of the coating thickness and density and adhesion has been excellent. The chemical compositions are also as expected[16]. Uniformly coated tubes of ~1 meter (36") long, using the existing PVD equipment has been fabricated, and fabrication of longer tubes is feasible with modifications of the coating equipment.

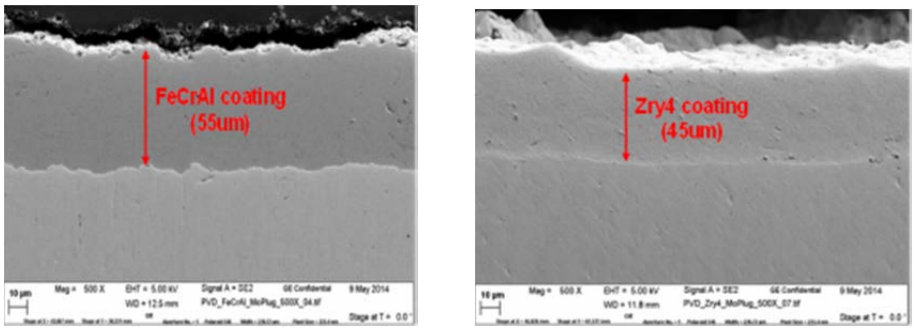

FIG. 7. Zircaloy-4 and FeCrAl coated on thin wall Mo-alloy tube.

3.4. Corrosion and oxidation properties

The bare (uncoated) and coated Mo alloy tubes have been subjected to characterizations of the properties required for service as fuel cladding in LWRs. The corrosion resistance of pure Mo and Mo-ODS in simulated BWR and PWR coolants at 290 and 330°C, respectively, in long term autoclave tests, and the oxidation resistance in steam and steam containing 10% hydrogen at 1000°C are discussed in details in another paper at this Conference [17]

Table 8 summarizes the corrosion data in LWR coolants. It is noted that the corrosion resistance of bare Mo-alloys in simulated BWR environments is excessively high and hence will require protection of the coating of Zr-alloy or Al-containing stainless steel. The corrosion resistance of bare Mo alloy in the simulated PWR water with 3.6 ppm dissolved hydrogen is substantially decreased to ~1 μm per month.

Some experimental Mo-alloys containing Nb have been found to significantly reduce the corrosion rate. As shown in Figure 8, Mo-alloy C has an order of magnitude lower corrosion rate (~0.5 μm/mo) than that of the bare, pure Mo tube.

TABLE 8 SUMMARY OF THE CORROSION RATE (IN μM PER MONTH) OF BARE AND COATED MO-ALLOY TUBES IN SIMULATED LWR COOLANTS

Test Condition	Mo/ML	Zr-coated	FeCrAl-coated
PWR: 330°C, 3.6 ppm	~1	Very low	Very low
BWR-HWC: 288°C, 0.3 ppm H_2	~5	Very low	Very low
BWR-NWC: 288°C,1 ppm O_2	~50	Very low	Very low

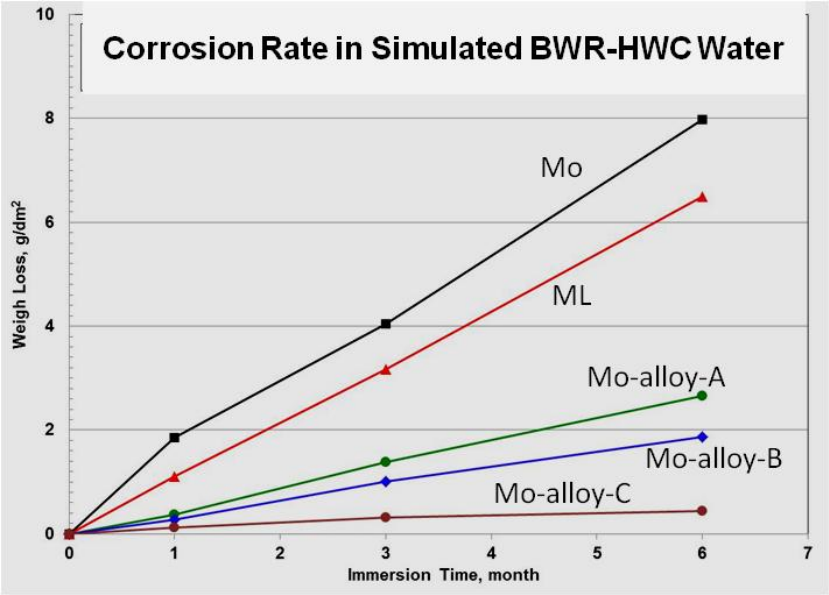

FIG. 8. Corrosion resistance of pure and ODS Mo tubes and Nb-containing Mo sheet samples in simulated a BWR coolant.

The steam oxidation resistance of pure Mo and Mo-ODS has been found to be much better than previous results reported in the literature. The oxidation rates from testing in 1000°C de-oxygenated steam for 6, 8, 24, 72 hours. zircaloy tube of 0.57 mm (22.5 mil) is expected to be fully oxidized in ~3 hrs at 1000°C[(13)]. In comparison, Mo oxidizes at a rate of ~25 μm or 0.025 mm per day. Reference 16 also reports that the Mo oxidation rate is reduced by ~20% in steam containing 10% hydrogen. The oxidation rates obtained in this programme

are similar to those recently reported by Nelson, et. al. obtained at the Los Alamos National Laboratory [18].

The coated Mo alloy tubes are stable in 1000°C steam for up 3-4 days, Figure 9. As expected, the ZrO_2 remains stable and protective to the Mo tube with no evidence of significant inter-diffusion or degradation at the interface of Mo and zircaloy. The Al-containing stainless steel forms a very thin protective Al_2O_3 to protect the Mo tube.

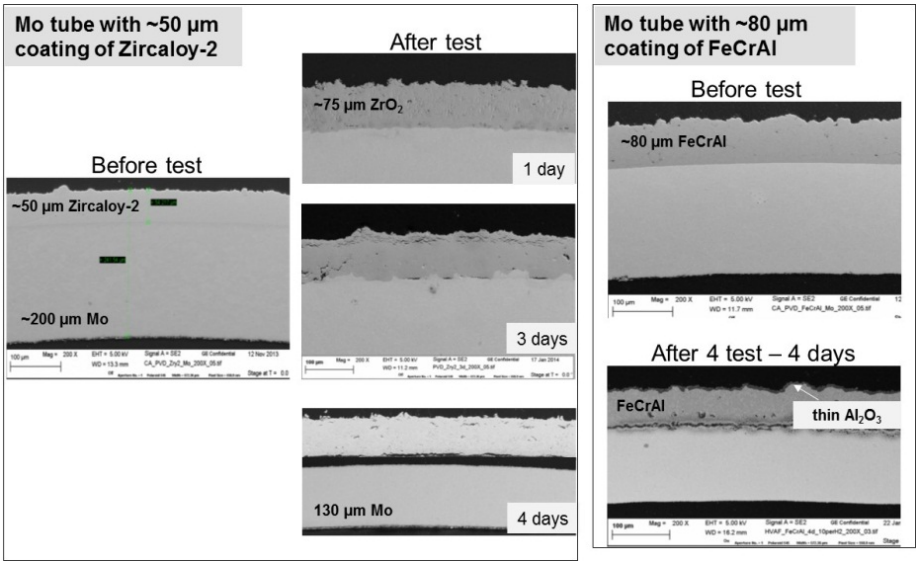

FIG. 9. Surface layer structure of coated Mo-alloy cladding exposed to de-aerated steam at 1000°C for up to 4 days.

The stability of coated Mo tubes in steam and hydrogen enriched steam will be tested at 1200 to 1500°C.

3.5. Tube to endcap welding

Welding of the thin wall Mo tube to an endcap has been successfully demonstrated using plasma welding, gas tungsten arc (GTAW) TIG welding and electron beam (EB) welding. EB welded tubes have been demonstrated to be leak-tight to 2800 psig (19 MPa) at room temperature.

Resistance projection welding, which can weld metals together via solid state inter-diffusion at the interface with causing large grain growth are also been explored. In the initial phase of this feasibility study, tube to endcap weld is to be performed between Mo tube and Mo endcap, and then the weld zone and the endcap is to be coated via PVD. In the longer term development, techniques to weld coated tube to coated endcap will be evaluated.

3.6. Tasks in progress and planned

The following tasks are in progress and planned as a part of this feasibility study:

- Optimization of the mechanical properties of Mo thin wall tubes are being evaluated through modification of tube thermal-mechanical reduction processes to achieve optimized texture and/or achieving equi-axed fine grain structure though induction heat treatment;

- Thin wall tubes will be subjected to burst and creep tests at temperatures up to ~1200°C to demonstrate their capability to maintain fuel rod integrity during a rapid power ramp as well as under accident conditions at elevated temperatures;
- Development of a combination of coating and mechanical reduction for thin wall tube fabrication is under evaluation to ensure availability of suitable technologies for large scale commercial production when needed. Feasibility assessment is underway;
- As a part of the U.S. DOE ATF programme, 4 fuel rod segments with Mo-alloy cladding are being prepared for insertion in the ATR core in 2015. The irradiation capsule containing the fuel rod segments will be filled with helium gas. The Mo rod irradiation task is made possible as a collaborative effort of EPRI, LANL, INL, and ORNL.

4. CONCLUSIONS

The feasibility studies have been carried out by EPRI since late 2012 have achieved encouraging results. Five lots of 2 meter long, thin-wall (0.2 mm) tubes of pure Mo and La_2O_3 doped Mo-ODS have been fabricated. Samples with high quality thin coating of zircaloy or Al-containing stainless steel on Mo-tube have been fabricated via several techniques including physical vapour deposition (PVD), vacuum plasma spray (VPS) and high velocity air or oxygen fuel (HVAF or HVOF) spray. The coatings formed by PVD have achieved the best results in coating density and adherence. In fact, a sub-micrometre inter-diffusion layer appears to form at the Mo and coating interface to prevent delamination throughout the feasibility tests. The corrosion resistance of bare and coated Mo-tubes has been tested in autoclaves with simulated LWR coolants. The oxidation resistance of bare and coated Mo tubes in 1000°C steam, steam plus hydrogen, and steam plus oxygen has been characterized for up to 4 days. Excellent corrosion and oxidation resistance of coated Mo tubes have been demonstrated. Additional tests in 1200-1500°C steam are planned. Welding of Mo-alloy tube to endcaps has been demonstrated, and a systematic study is under way to optimize the welding process.

An Irradiation test of four fuel rodlets with Mo-alloy cladding is under preparation for testing at the Advance Test Reactor (ATR) at Idaho National Laboratory, and tests at other reactors are planned in coming years. New Mo-alloys with potentially better corrosion and oxidation resistance are being prepared for testing and evaluated for the feasibility of fabricating into thin-wall tubes.

ACKNOWLEDGEMENTS

The authors gratefully acknowledge the important contributions of Todd Leonhardt (Rhenium Alloys Inc) for fabrication of thin-wall Mo-alloy tubes; of Ian Harris (EWI) for evaluation of welding techniques; of Stu Malloy and Andy Nelson (LANL) for steam test studies; of R. T. Chiang for neutronic calculations; of Chan Paik and Frank Rahn for MAPP code analyses. The authors thank Jeff Deshon (EPRI) for management support. EPRI Fuel Reliability Program and EPRI Technology Innovation Program provide funding support. Generous collaborations from the U.S. Department of Energy and the national laboratories are also appreciated.

REFERENCES

[1] MIZOKAMI, S., “Evaluation and Analysis of Fukushima Cores”, EPRI/INL/DOE Workshop on Accident Tolerant Fuel, San Antonio, February (2014).

[2] CHENG, B., “Fuel Behaviour in Severe Accidents and Mo-alloy based Cladding to Improve Accident Tolerance”, TopFuel (2012) paper#A0034.
[3] CHENG, B., CHOU, P., KIM, Y-J., “Development of Mo-alloy Cladding to Enhance Fuel Tolerance to Severe Accidents”, TopFuel, Charlotte, USA. (2013), Paper#8555.
[4] BRAGG-SITTEN, S., “Application of MELCOR to ATF Concepts for Severe Accident Analysis”, EPRI/INL/DOE Workshop on Accident Tolerant Fuel, San Antonio, February (2014).
[5] FINEROTH, H., “Passively Safe Commercial Nuclear Fuel”, Knowledge Foundation International Conference on Nuclear Power Safety, (2011).
[6] SNEAD, L., KATOH, Y., YUEH, K., TERRANI, K., BRAGG-SITTEN, S., “SiC development related to ATF Applications”, EPRI/INL/DOE Workshop on Accident Tolerant Fuel, San Antonio, February (2014).
[7] TERRANI, K., KATOH, Y., SNEAD, L., “Thermal Mechanical Modelling of SiC/SiC Composite Cladding”, EPRI/INL/DOE Workshop on Accident Tolerant Fuel, San Antonio, February (2014).
[8] RAHN, F., et. al., “MAPP Code Analysis of Behaviours and Current and Accident Tolerant Fuel in Severe Loss of Coolant Accidents”, EPRI, to be published.
[9] OPILA, E., JACOBSON, N,, MYERS, D., COPELAND, E., Predicting Oxide Stability in High-temperature Water Vapour, Metals & Materials Society, Jan. (2006).
[10] COOPER, R.H., Jr., HOFFMAN, E.E., Eds., Proc. Symp. on Refractory Alloy Technology for Space Nuclear Power Applications, CONF-8308130. Springfield, VA: NTIS, (1984).
[11] WHELAN, E.P., MISKA, K.H., Eds., “Physical Metallurgy and Technology of Molybdenum and its Alloys”. AMAX Specialty Metals Corp., Greenwich, CT, (1985).
[12] COCKERAM, B.V., SMITH, R.W., LEONARD, K.J., BYUN, T.S., SNEAD, L.L., J. Nucl. Mater. **382** (2008) 1-23.
[13] BYUN, T.S., LI, M., COCKERAM, B.V., SNEAD, L., J. Nucl. Mater. **376** (2008) 240-246.
[14] CHIANG, R.T., Neutronic Assessment for Mo-cladding Fuel Assembly. EPRI. To be published.
[15] PINT, B., TERRANI, K., YAMAMOTO, Y., FIELD, K., SNEAD, L., “ORNL Advanced Alloy Development (FeCrAl)”, EPRI/INL/DOE Workshop on Accident Tolerant Fuel, San Antonio, February (2014).
[16] LIU, G., et al., Nanostructured high-strength molybdenum alloys with unprecedented tensile ductility, Nature Materials, **12** (2013) 344-350.
[17] KIM, Y-J., CHENG, B., CHOU, P., “Molybdenum Alloys for Accident Tolerant Fuel Cladding: High Temperature Corrosion and Oxidation Behaviour”. WRFPM Conference in Sendai, Japan (2014) Paper #100144.
[18] NELSON, A.T., SOOBY, E.S., KIM, Y-J., CHENG, B., MALOY, S.A., High temperature oxidation of molybdenum in water vapour environments, J. Nucl. Mater. **448** (2013) 441-447.

CHARACTERIZATION OF ADVANCED STEELS AS ACCIDENT TOLERANT FUEL CLADDING FOR LIGHT WATER REACTORS

R.B. REBAK, P.L. ANDRESEN, Y-J. KIM, E.J. DOLLEY
GE Global Research, Schenectady, NY
United States of America
E-mail: kimyj@ge.com

Abstract

After the tsunami incident in Fukushima Daiichi in March 2011, the international community is set to identify appropriate nuclear materials with increased accident tolerance with respect to the traditional UO_2-zirconium alloy fuel system permitting loss of active cooling for a considerably longer time period, while maintaining or improving the fuel performance during normal operations. The researched safety characteristics of these advanced fuels are mainly: (a) Improved reaction kinetics with steam; (b) Slower hydrogen production rate; and (c) Enhanced retention of fission products. In the US the Department of Energy is supporting the development of an improved cladding advanced steels such as the iron-chromium-aluminium (FeCrAl) alloy system. Environmental test results show that FeCrAl alloys are highly resistant to corrosion and environmental cracking under normal operation conditions and extremely resistant to attack by steam under accident conditions. That is, the replacement of a zirconium alloy using a ferritic material containing chromium and aluminium appears to be the most near term implementation for accident tolerant fuels.

1. INTRODUCTION

Following the north east Japan events at Fukushima Daiichi in March 2011, the U.S. Department of Energy Office of Nuclear Energy (DOE-NE) is working to develop nuclear fuels and claddings with enhanced accident tolerance [1, 2]. A fuel may be defined as having enhanced accident tolerance if, in comparison with the current UO_2-zirconium alloy system, it can tolerate loss of active light water cooling in the reactor core for a considerably longer time period while maintaining or improving fuel performance during normal operations and operational transients, as well as in design basis and beyond design-basis events. The enhanced fuel material should have:

- Improved reaction kinetics with steam;
- Slower hydrogen production rate;
- Improved cladding and fuel properties;
- Enhanced retention of fission products.

The commercial nuclear energy in the United States had its origin in the nuclear navy [3]. The navy originally adopted zirconium based alloys over stainless steels for the fuel cladding mainly because of the higher transparency to neutrons of the former making the reactors more compact for submarine applications [4, 5]. In spite of the thermal neutron cross section of stainless steels being approximately 12-16 times higher than for zirconium alloys it is now understood that the fuel enrichment penalty incurred by the use of stainless steel cladding can be partially overcome by using thinner wall advanced stainless cladding because they are stronger than the zirconium alloys [5, 6]. The best steels would be ferritic since they do not contain the high neutron absorbing nickel [6]. The average thermal neutron absorption cross section for a zirconium alloy is 0.20, for the traditional type 304 SS it is 2.86, for the high nickel type 310 SS it is 3.21 and for the ferritic APMT alloy the cross section is 2.47 [6].

At the beginning of the nuclear navy programme, the susceptibility to cracking of sensitized stainless steels in high temperature water initially relegated the stainless steels in cladding material research and development as compared to the zirconium alloys. Six decades later, it is now understood that high strength ferritic stainless steels are resistant to environmental cracking and irradiation damage, which would not limit their application as fuel cladding in light water reactors [7]. Moreover, current significant progress in steelmaking practices shows that the chemical purity in modern steels can be highly controlled. Similarly,

there is an increased ability in the fabrication of these advanced steels into thin walled tubes, including readily joining (welding) by several techniques.

Terrani et al. cite several uses in the industry of non-zirconium alloys as fuel cladding, including type 304, 316 and 347 austenitic stainless steels and austenitic nickel based alloys such as Inconel 600 and Incoloy 800 [5]. Type 304 SS fuel cladding was used for some time in US commercial light water reactors, for example at the Connecticut Yankee and San Onofre 1 power stations [8]. The early cracking of type of 304 SS was linked to sensitization due to welding of high carbon alloys. The cracking phenomenon of sensitized stainless steels is now well understood and controlled and it is not a current concern in light water reactors.

The GE project is focused on developing a new metallic cladding material to replace the current zirconium based alloy. The GE project does not include fuel development. The GE proposal path to obtain an accident tolerant fuel is to use advanced ferritic steels (e.g. Fe-Cr-Al alloys) for the cladding of existing commercial uranium oxide fuel.

1.1. Behaviour of ferritic and austenitic steels in light water reactors

Austenitic stainless steels such as types 304 and 316 are highly susceptible to stress corrosion cracking in chloride containing environments, especially at temperatures higher than 60°C [9]. The most common tests used in the industry to determine susceptibility to chloride cracking are immersion of U-bend specimens (ASTM G 30) into hot solutions of chloride salts including magnesium chloride or sodium chloride (ASTM G 36 and G 123). Ferritic stainless steels such as types 405 and 430 are highly resistant to SCC in hot chloride solutions [9, 10].

Austenitic stainless steels such as type 304, 308, 316, 321 and 347 are used extensively worldwide as construction materials for light water power reactors [11]. In the USA the most common austenitic alloy may be type 304 SS (UNS S30403) and in Japan the preferred stainless steel is type 316 (S31603). European countries such as Germany may prefer to use titanium (Ti) or niobium (Nb) stabilized types of stainless steel such as type 321 (S32100) and 347 (S34700). Austenitic stainless steels are susceptible to stress corrosion cracking (SCC) in boiler water reactor (BWR) service and in a lesser extent in pressurized water reactor (PWR) service [11].

Austenitic stainless steel (SS) core internals components are susceptible to irradiation assisted stress corrosion cracking (IASCC) during service in nuclear power plants light water reactors [12, 13, 14]. One of the effects of irradiation is the hardening of the SS due to modifications in the dislocation distribution in the alloy [15, 16]. Irradiation also alters the local chemistry of these austenitic alloys, for example in the vicinity of grain boundaries by a mechanism of radiation induced segregation (RIS). The segregation or depletion phenomena at or near grain boundaries may enhance the susceptibility of these irradiated austenitic alloys to stress corrosion cracking (SCC) [17, 18]. The effect of the IASCC on austenitic stainless steels may impact the life extension of currently operating light water reactors due to the progressive dose accumulation by the materials [19].

In nuclear power plant applications, ferritic steels have superior void swelling resistance because they experience delayed void nucleation and they sustain less than 2% swelling even at irradiation levels close to 200 dpa [20]. On the other hand, austenitic stainless steels such as type 304 undergo the onset of significant void swelling and possible embrittlement at dose rates in the order of 20 dpa [17].

Besides the higher resistance of ferritic steels to radiation damage, other benefits that could make ferritic steels more attractive than the austenitic stainless steels in nuclear applications and specially as accident tolerant fuel (ATF) cladding include: (1) Ferritic materials have lower cost since they do not contain nickel (Ni), and generally contain lower chromium (Cr), (2) They do not contain nickel (Ni) or cobalt (Co) that could be become activated in commercial reactors, (3) They offer a lower coefficient of thermal expansion (CTE) that matches the CTE of pressure vessel ferritic alloys such as type A508, A516, or A533, and (4) Ferritic steels have higher thermal conductivity for heat transfer capabilities (Table 1, Fig. 1).

TABLE 1. PHYSICAL PROPERTIES OF FERRITIC AND AUSTENITIC STEELS

Material	CTE (0-538°C) μm/m/°C	Thermal Conductivity at 100°C (W/m.K)
Zircaloy-2	8.32 & 15.7 (orientation dependent)	13.8
Ferritic type 430 (16% Cr)	11.4	23.9
Austenitic type 304L (18% Cr)	18.4	16.2

FIG. 1. Desirable Characteristic of Ferritic Stainless Steels for ATF Cladding.

1.2. Reaction of cladding materials with steam

In the case of a loss of coolant accident (LOCA), such as in the Fukushima Daiichi situation, the cladding of the fuel will be exposed to steam. The zirconium alloy plus steam reaction has been widely studied under loss of coolant accident scenarios [5, 21, 22, 23, 24, 25, 26].

Zircaloy oxidizes in presence of steam to form zirconia and hydrogen following an exothermic reaction:

$$Zr + 2\ H_2O \rightarrow ZrO_2 + 2\ H_2 \qquad \Delta H = -586\ kJ/mole\ (-140\ kcal/mole) \qquad (1)$$

According to Baker and Just the chemical heat generated by the reaction of zirconium and steam in (Eq. 1) could exceed the nuclear heat generation during a destructive nuclear transient. Moreover, the hydrogen generated by the reaction could give rise to a pressure surge and might subsequently react explosively with air [22].

The oxidation behaviour of iron based alloys in steam was recently reviewed and updated comparing to the behaviour of zirconium alloys [5, 26]. At 1200°C, the degradation of APMT was practically nil (no mass change) after 8 h exposure at 1000°C while the degradation of zircaloy-2 was complete for the same period of time [26]. APMT offers extraordinary resistance to reaction with steam at temperatures higher than 1000°C because it allows first for the formation of a protective Cr_2O_3 scale which subsequently allows for the formation of a continuous protective Al_2O_3 scale between the metal and the Cr_2O_3 scale. It is this Al_2O_3 scale what protects the alloy against further oxidation in steam [26, 27, 28]. Cheng et al. studied the oxidation behaviour of several new cladding candidates (SiC, stainless steels 304 and 317, alloy PM 2000 and iron-based alloys with 15-25% Cr) at 800, 1000 and 1200°C [28]. They concluded that, aluminium in the PM 2000 alloy formed a very protective alumina layer which significantly reduced the mass loss compared to the other materials under superheated steam conditions [27]. Pint et al. also showed the effect of the content of Cr on the degradation of ferrous alloys [26]. It was reported that the content of Cr is important and that, in the absence of Al, at least a 25% of Cr may be required in the iron alloy to offer protection against steam [26]. However, it is likely that if the alloy also contains approximately 5% Al, lower amount of Cr may be needed to offer a similar resistance to oxidation.

1.3. Approach of GE research for the selection ATF cladding material

Based on the available literature information, General Electric has decided to select a few steels to characterize for the ATF cladding application. Table 2 gives the list of the materials studied with their nominal chemical composition. zircaloy-2 was also studied for comparison as a current base line material. Table 2 shows a list of ferritic materials containing from 9% chromium (Cr) (T91) to 27% Cr (Ebrite). Some of the ferritic materials also contain aluminium (such as MA956 and APMT) for resistance against superheated steam. The only austenitic material in the list is Alloy 33 (33% Cr) since previous data showed that it is highly resistant to environmental cracking in high temperature water (reactor design conditions).

TABLE 2. LIST OF MATERIALS STUDIED

	Alloy	Nominal Composition
A	Zirc-2 UNS R60802	Zr + 1.2-1.7 Sn + 0.07-0.2 Fe + 0.05-0.15 Cr + 0.03-0.08 Ni
B	Ferritic steel T91 K90901	Fe + 9 Cr + 1 Mo + 0.2 V
C	Ferritic steel HT9 S42100	Fe + 12 Cr + 1 Mo + 0.5 Ni + 0.5 W + 0.3 V
D	Nano ferritic alloys NFA	e.g. 14YWT; Fe + 14 Cr + 0.4 Ti + 3 W + 0.25 Y_2O_3
E	MA956 or UNS S67956	Fe + 18.5-21.5 Cr + 3.75-5.75 Al + 0.2-0.6 Ti + 0.3-0.7 Y_2O_3
G	APMT	Fe + 22 Cr + 5 Al + 3 Mo
H	High Cr Ebrite S44627	Fe + 25-27.5 Cr + 1 Mo + 0.17 (Ni + Cu)
J	Alloy 33 – UNS R20033	33 Cr + 32 Fe + 31 Ni + 1.6 Mo + 0.6Cu + 0.4 N

Figure 2 shows the systematic approach undertaken by GE to characterize the suitability of the materials for the cladding application. The first step is concerned with the suitability of the selected material to perform well under normal operation or design conditions of the reactor. If the material does not resist general corrosion or stress corrosion cracking in high temperature water (e.g. 300°C) it would not be a suitable material for the cladding. The second step in Fig. 2 is if the material will perform well under accident conditions or beyond design conditions when there is a lack of coolant (light water). That is, in presence of superheated steam (accident conditions) the candidate steel has to outperform the current materials such as zircaloy-2. Figure 3 shows the types of tests that were performed or will be performed for both design and beyond design conditions (e.g. Fretting and Quenching tests will be performed in the near future). At the moment we have demonstrated convincingly that several of the studied materials (such as APMT) in Table 2 pass both the first and second step in Figure 2, that is, they perform better than zircaloy-2 both under normal operation conditions and under accident lack of coolant conditions. The third step in Fig. 2 is Fabrication Feasibility, which will be addressed in more detail in the near future. Similarly, modelling and calculations will be performed to address the issue of neutronics and cost associated to the deployment of a new cladding rod into a commercial light water reactor.

2. BEHAVIOUR OF CANDIDATE MATERIALS UNDER NORMAL OPERATION CONDITIONS

2.1. Advanced steels resistant to general corrosion in high temperature water

During its lifetime performance under normal operation conditions it is essential that the cladding does not breach releasing fission products from the fuel into the water. That is, similarly to the actual zirconium based alloys, the candidate replacement alloys should not corrode excessively in water at ~300°C nor suffer environmentally assisted cracking under similar conditions. The life of a fuel bundle in a commercial reactor is generally less than 10 years, that is, under normal operation conditions the cladding should be able to maintain hermetic integrity for this period of time.

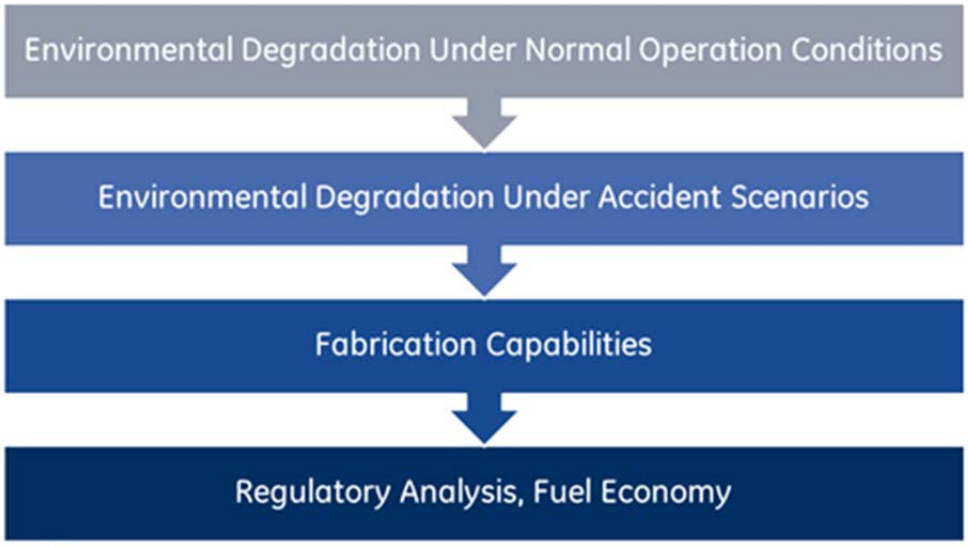

FIG. 2. Systematic Steps to Study and Rate the ATF Candidate Cladding Materials.

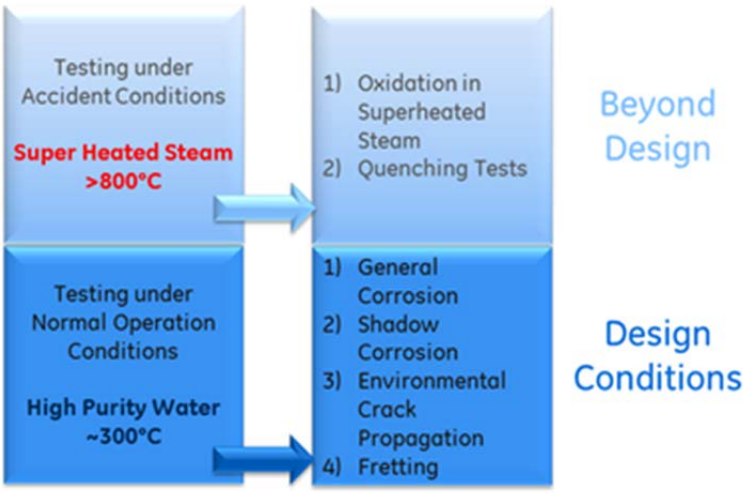

FIG. 3. Environmental Testing of ATF Candidate Cladding Materials performed under Normal Operation Conditions and Beyond Design (Accident) Conditions.

Coupons of the candidate materials were tested for general corrosion under laboratory simulated normal operation conditions of commercial light water reactors. Four sets of autoclaves were used (Table 3). The degradation of the immersion coupons is currently being evaluated by weight (mass) change, standard metallographic procedures and surface analysis techniques. The corrosion behaviour is also being evaluated by using electrochemical techniques such as monitoring the corrosion potential as a function of time. The corrosion potentials of coupons of all the alloys (including Pt) were continuously monitored using a zirconia membrane reference electrode containing copper and copper oxide, whose reference potential is 273 mV higher than the standard hydrogen electrode (SHE) in pure water at 550°F (288°C).

In all the autoclave systems (S-2, S-5, S-6, and S-14) the water was re-circulated at a flow rate of 100 cm^3/min and reconditioned (filtered) before entering again the autoclaves.

TABLE 3. IMMERSION TESTS UNDER SIMULATED NORMAL OPERATION CONDITIONS

Autoclave	Test Conditions at GE GRC	Alloys under Testing
2584 S-2	Simulated PWR, High Purity Water, 330°C	T91, 14YWT, APMT
2584 S-5	Simulated BWR, Hydrogen Water Chemistry (63 ppb H_2), 288°C	T91, 14YWT, APMT
2584 S-6	Simulated BWR, Normal Water Chemistry (2000 ppb O_2), 288°C	T91, 14YWT, APMT
2520 S-14	Simulated BWR, Normal Water Chemistry (2000 ppb O_2), 288°C	Zirc-2, T91, HT9, 14YWT NFA, MA956, APMT, Ebrite, Alloy 33

Results from autoclaves S-2, S-5 and S-6 are not reported here since they are still in testing. Figures 4 and 5 show the mass (weight) change for the alloys exposed to autoclave S-14 for incremental periods of 32 days, 121 days, 213 days and 366 days. The mass change is reported as mass gained per unit area per day. Figure 4 shows the mass change rate for two coupons each of zircaloy-2 (the current baseline material for cladding in commercial light water reactors) and the newly studied materials T91, HT9 and NFA (Table 2). As the exposure time increased the rate of mass gain for the four alloys decreased, showing that a

protective oxide film developed on the surface that slowed down the rate of material degradation (Fig. 4). Figure 4 also shows that up to one year exposure the mass change for T91 (9Cr1Mo) was comparable to the mass change for zircaloy-2. The mass change rate for HT9 (12Cr1Mo) and NFA (14Cr) were lower than for T91. That is, all the tested alloys in Fig. 4 showed equal or better corrosion resistance performance than the current zircaloy-2 material under normal operation conditions. Fig. 4 also shows the mass change trend according to a power fit for both zircaloy-2 and HT9.

Figure 5 shows the mass change rate for two coupons each of Zirc-2 (the current baseline material for cladding in commercial light water reactors) and the newly studied materials MA956, APMT, Ebrite and Alloy 33 (Table 2). It also shows the power law fit for the mass change rate for zircaloy-2 and APMT. It is clear again that all the new candidate alloys investigated in Fig. 5 had a mass gain rate lower than that for zircaloy-2. The data for one year exposure shows that the mass gain rate for APMT was approximately one order of magnitude lower than for zircaloy-2.

Figure 6 shows the corrosion potential as a function of time for eight materials including Zirc-2 and platinum. The lowest corrosion potential (most active) corresponded to zircaloy-2 and the highest corrosion potential (most noble) corresponded to platinum. All the seven iron containing materials had corrosion potentials that were in a narrow potential band of less than 50 mV. The lowest potential of the seven iron containing materials was for T91 (9Cr1Mo), the most active of the steels. The values of corrosion potential for the different materials in Fig. 6 agree well with the mass gain as a function of time shown in Fig. 4.

Results from Figs 4, 5 and 6 show that any of the tested steels in Table 2 will perform as good or better than zirconium alloy from the general corrosion point of view.

Figure 7 shows the aspect of the corroded coupons at X10,000 magnification after one year of immersion in 288°C water. Figure 7 shows that both HT9 and NFA had small oxide crystals on the surface of the tested coupons suggesting little oxide growth. On the other hand, alloy T91 had larger equiaxed crystals on the surface. The shape of the crystals seem to change comparing between APMT, Ebrite, MA956 and Alloy 33, probably because of the different elements (Fe, Cr, Al, etc.) present in the oxide film which form different crystallographic structures.

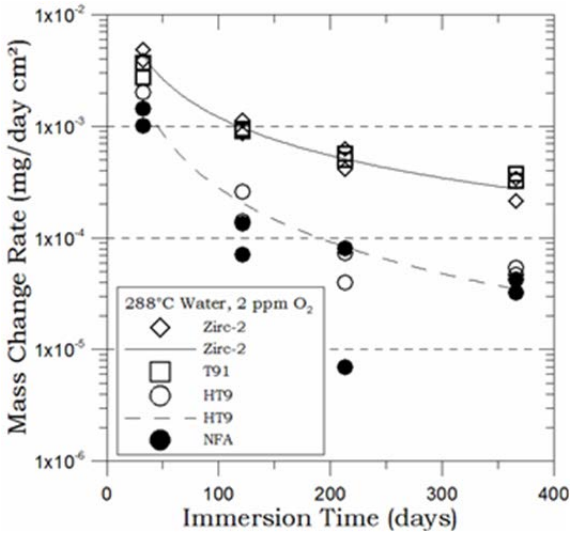

FIG. 4. Mass change per unit area and unit time for Zirc-2, T91, HT9 and NFA coupons exposed to pure water + 2 ppm O2 at 288°C for a total time of 366 days.

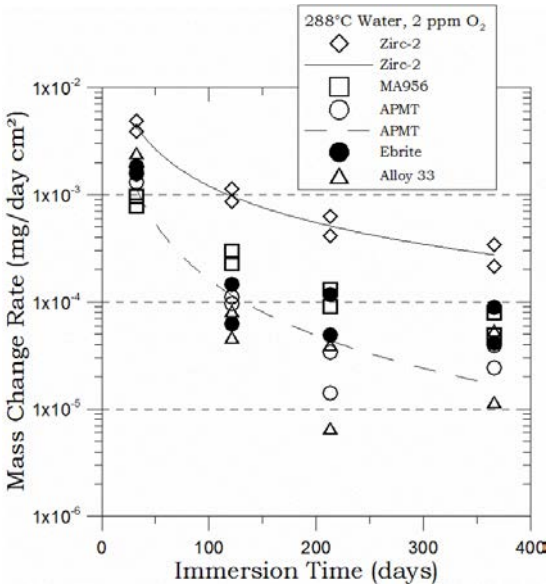

FIG. 5. Mass change per unit area and unit time for Zirc-2, MA956, APMT, Ebrite and Alloy 33 coupons exposed to pure water + 2 ppm O_2 at 288°C for a total time of 366 days.

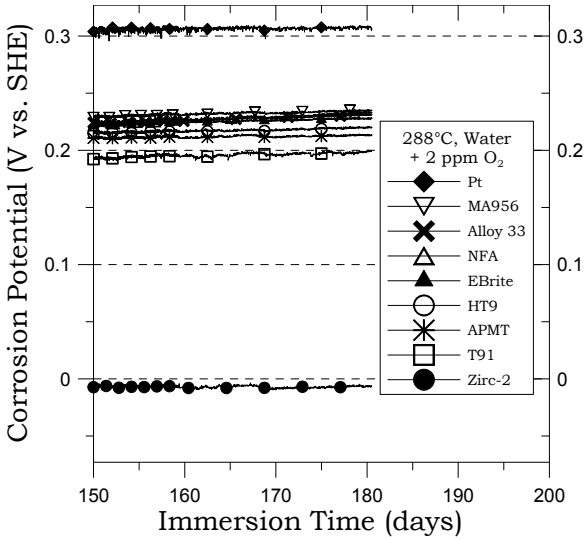

FIG. 6. Corrosion potential of Pt, Zirc-2 and seven candidate alloys exposed to pure water + 2 ppm O_2 at 288°C.

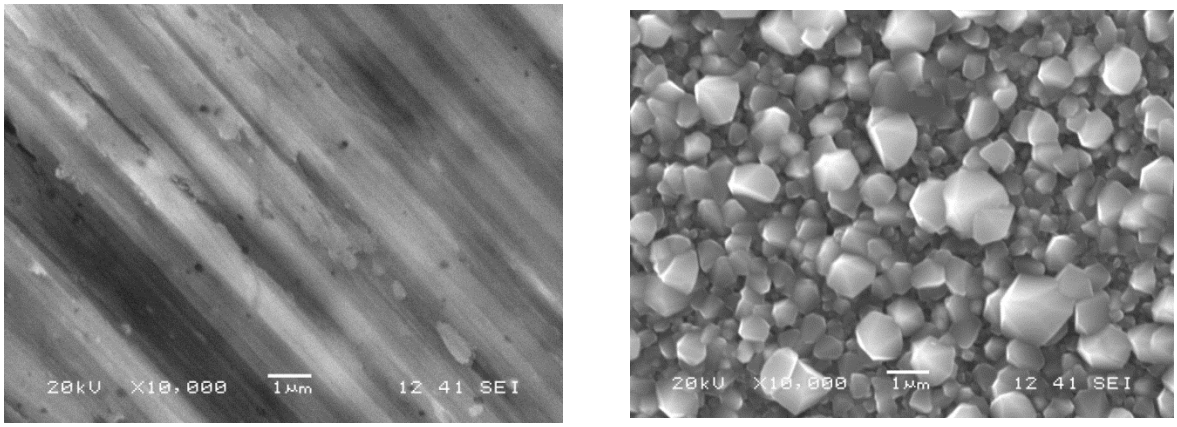

RA2, Zircaloy-2 RB2, T91

FIG. 7. SEM images at 10,000X of the coupons surface after exposure to pure water with 2 ppm O_2 at 288°C for 1 year (366 days) in system S-14.

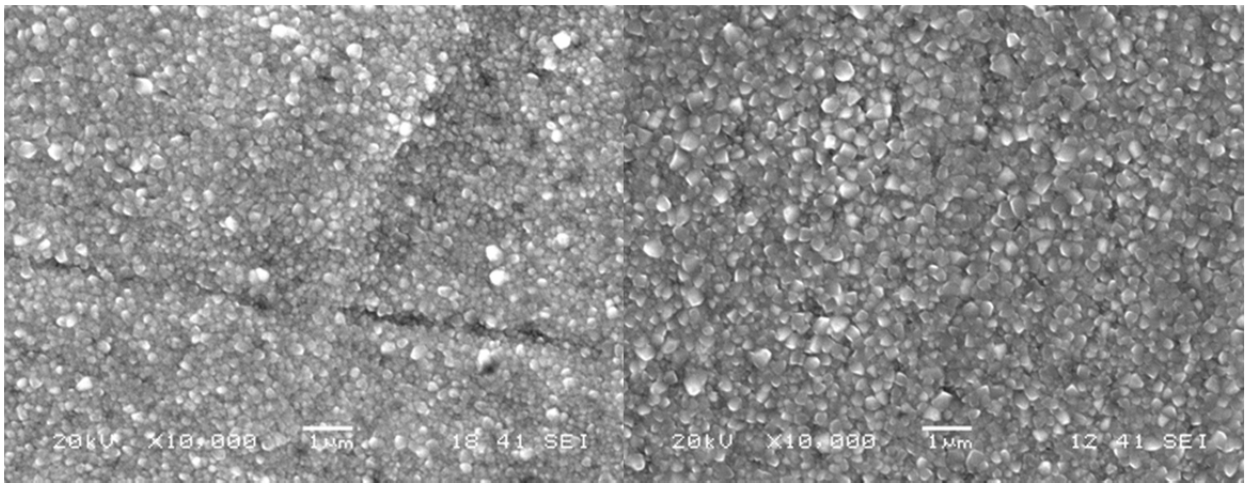

RC2, HT9 RD2, NFA

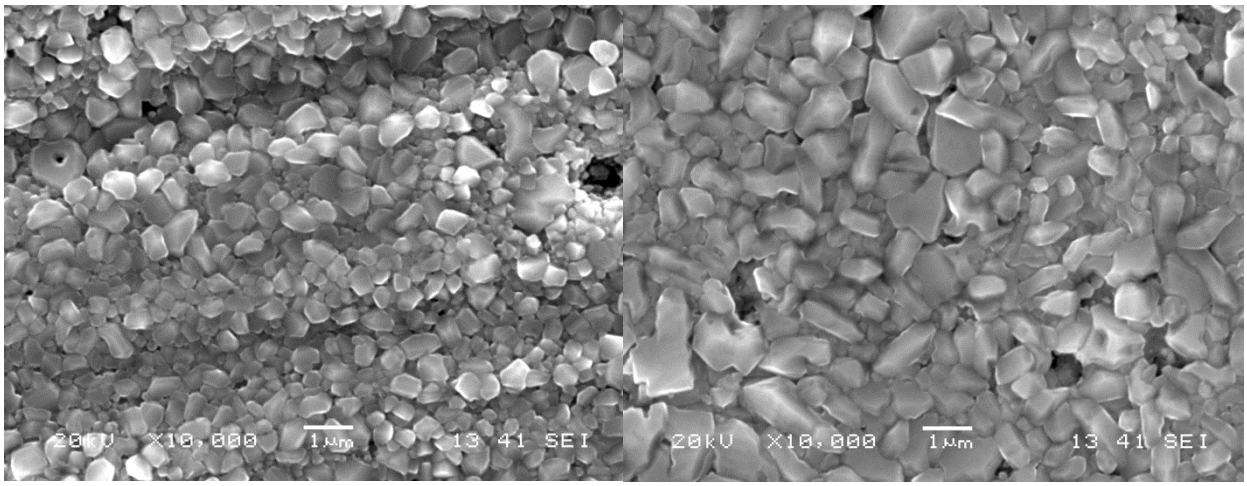

RE2, MA956 RG2, APMT

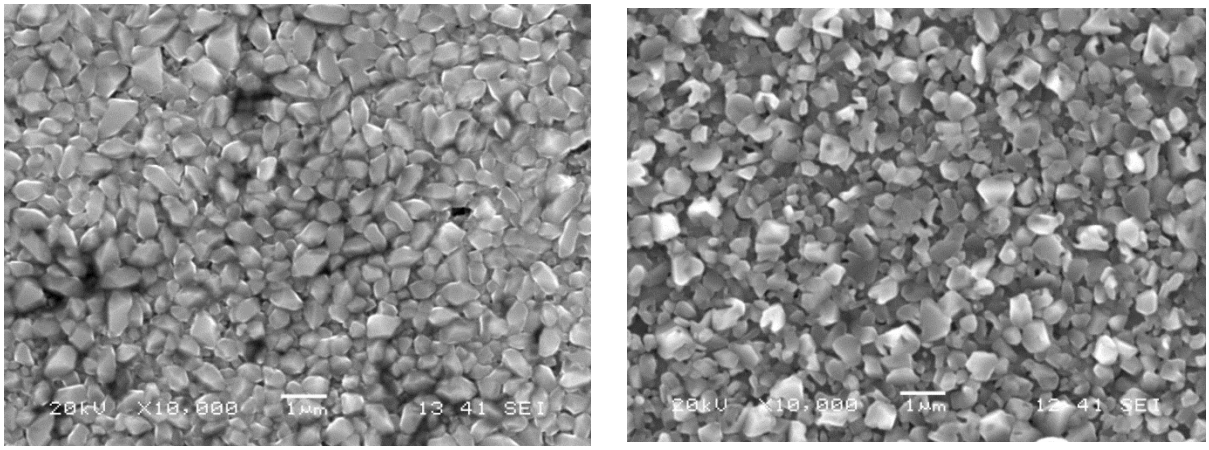

RH2, Ebrite RJ2, Alloy 33

FIG. 7. (cont). SEM images at 10,000X of the coupons surface after exposure to pure water with 2 ppm O_2 at 288°C for 1 year (366 days) in system S-14.

Figure 8 show representative images of the oxides formed in all the coupons side by side to compare morphology, thickness, and structure. Figure 9 is a chart comparing the average thickness (4-5 measurements on a 30kx field) of the oxides. From the chart, it can be

seen that there are three groupings of thickness: zircaloy-2/T91 >> MA956/E-Brite/Alloy 33/APMT > NFA/HT9. For the most part, all of the oxides appear dense and continuous across the alloy interfaces. Figures 8 and 9 show that the tested steels would be resistant to corrosion in high temperature water and form less oxide than the current zircaloy-2 material.

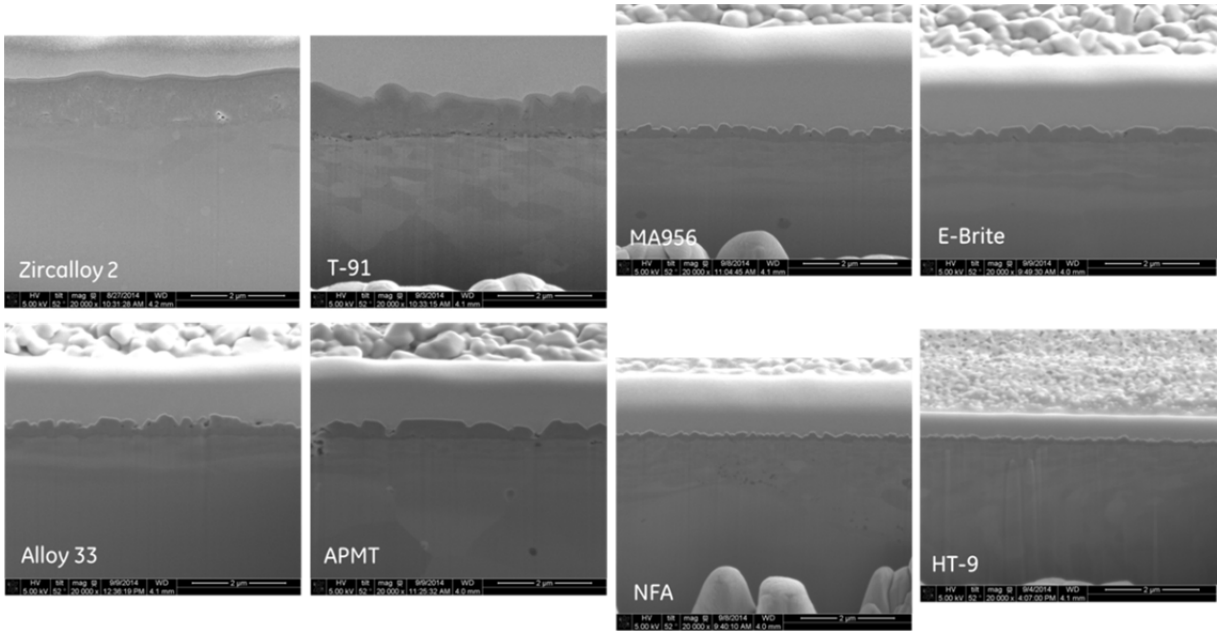

FIG. 8. Composite of tilted images of 90° cross-sections of all coupons (adjusted to the same magnification.) exposed to 288°C for one year.

2.2. Advanced steels resistant to shadow corrosion in high temperature water

In operating boiling water reactors, accelerated growth of ZrO_2 has been observed on a zirconium alloy component when it is in close proximity to a dissimilar material (e.g., Alloy X-750 and a stainless steel). This anomalous oxide growth is called “shadow corrosion” since the pattern of the enhanced corrosion resembles the shape of the adjacent metallic components. Several hypotheses have been proposed to explain this phenomenon, including a type of galvanic corrosion driven by the corrosion potential difference between dissimilar alloys (e.g., zircaloy-2 and Alloy X-750). In current reactors, irradiation of the zirconium and X-750 type of materials make that their respective corrosion potential move in opposite direction, thus increasing even more the potential gap between the dissimilar materials.

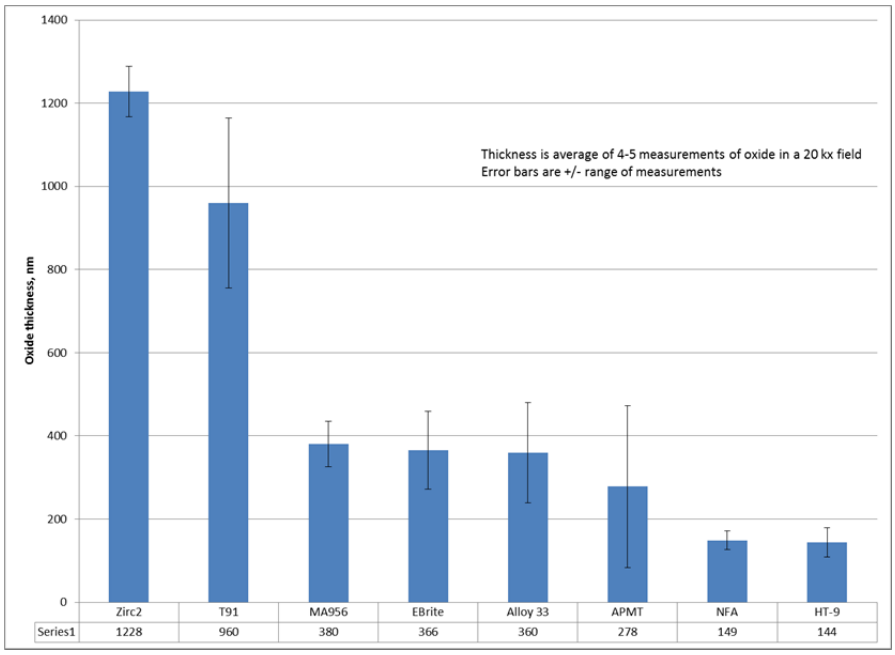

FIG. 9. Comparison of oxide thickness for the eight materials exposed to 288°C water for one year.

Testing has been conducted in high temperature BWR type water to explore if the proposed advanced steel materials would have similar high temperature behaviour as zircaloy-2 when coupled to X-750 spacers. The photo electrochemical response of oxidized surfaces was evaluated by introducing the UV light to the specimen through optical fibre glass. A schematic view of autoclave system and the high temperature water loop for electrochemical measurement under UV illumination are shown in Figs 10 and 11, respectively. The coupled electrodes for galvanic corrosion measurement had a gap of 1 mm between the anode electrode (zircaloy 2 or ferritic alloys) and the cathode electrode (X-750). The test specimen was irradiated through the sapphire window.

The corrosion potential of a metal in contact with high temperature water is dependent on the water chemistry conditions (e.g. presence of oxygen or hydrogen), the oxide surface nature, such as oxide thickness, composition, conductivity, structure, etc. Also, a change in electro-catalytic nature of the surface associated with the chemical compositions of the oxide layers can play a significant role in the corrosion potential behaviour of the materials. Figure 12 shows the corrosion potential behaviour of 304 SS, Alloy X-750, Pt and several advanced steels alloys such as APMT in 288°C water under various water chemistry conditions without UV illumination. Under oxidizing water chemistry conditions (0.6 ppm and 1 ppm O_2) and reducing water chemistry conditions (0.1 and 0.15 ppm H_2), the corrosion potential of advanced steels (APMT, Alloy 33, and NFA) were very similar to that of the well-known materials such 304SS and X-750. The corrosion potential of zircaloy-2 was always lower than that of other electrodes due to the formation of insulating oxide, ZrO_2 that limited the O_2 reduction kinetics. Based on the corrosion potential data, it is clear that the redox kinetics on ferritic advanced steel alloys behaves similarly to that of 304SS or X-750 in high temperature water.

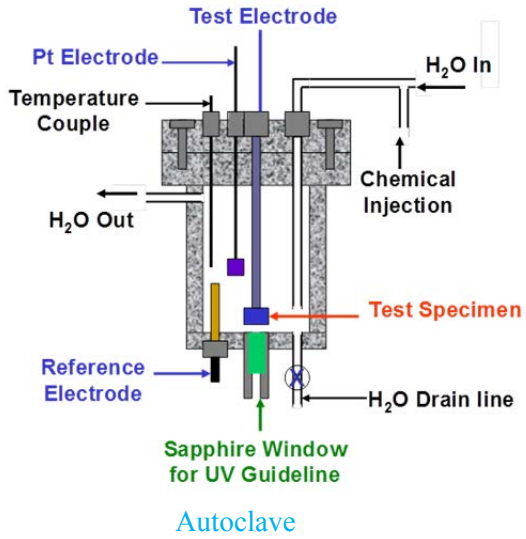

FIG. 10. Arrangement of the test electrodes in the autoclave for high temperature photo-electrochemical tests.

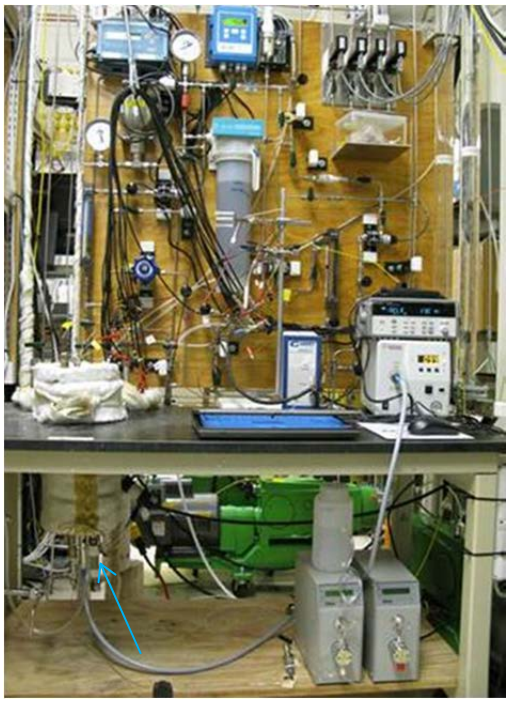

FIG. 11. High temperature water loop for photo-electrochemical measurements.

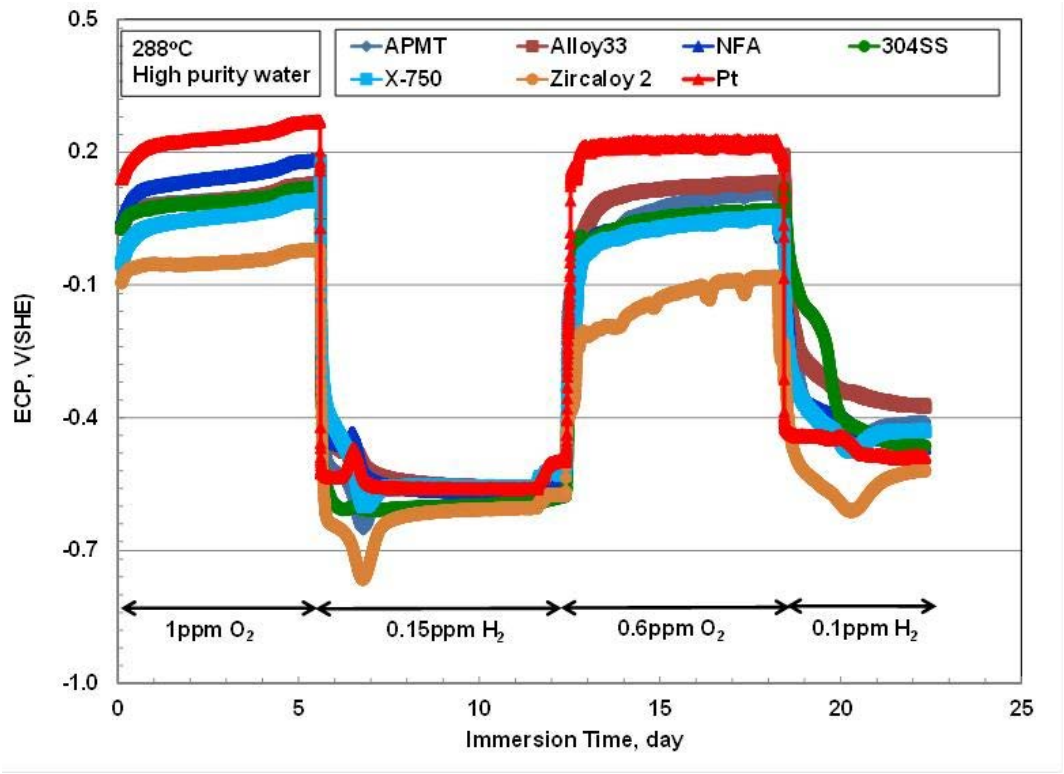

FIG 12. Changes in the corrosion potential of zircaloy-2, 304 SS, Alloy X-750, Pt and advanced steel alloys in 288°C water under oxygen and hydrogen water chemistry conditions.

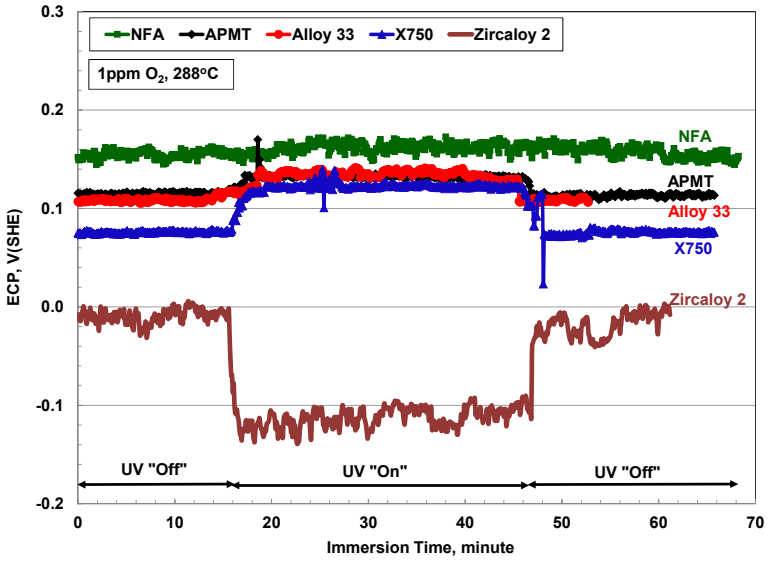

FIG. 13 Corrosion potential of zircaloy-2, X-750 and advanced steels ferritic alloys (APMT, Alloy 33 and NFA) in 288°C water containing 1 ppm O_2 with and without UV illumination.

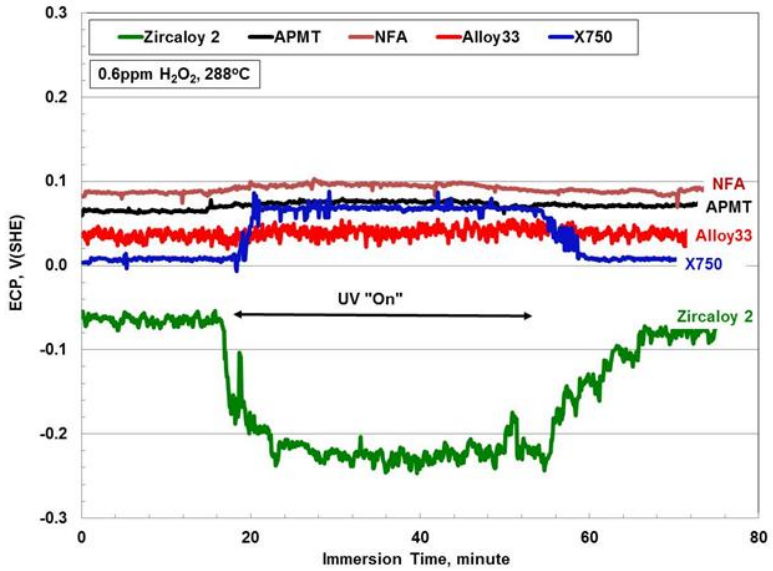

FIG. 14. Comparison of the corrosion potential behaviour of zircaloy-2, X-750 and advanced steel ferritic alloys (APMT, Alloy 33 and NFA) in 288°C water containing 0.6 ppm H_2O_2 with and without UV illumination.

The corrosion potential behaviour of zircaloy-2, X-750 and ferritic alloys was measured in 288°C water containing 1 ppm O_2 or 0.6 ppm H_2O_2 with and without UV illumination, as shown in Figs 13 and 14. The presence of UV light decreased the corrosion potential of zircaloy-2, but increased the corrosion potential of X-750 in high temperature water. This change in the corrosion potential in the presence of UV light can be explained by the photo excitation of *n*-type ZrO_2 formed on zircaloy-2 and *p*-type NiO on X-750. Also, the corrosion potential of both alloys returned to the previous value when the UV light turned off, indicating no significant residual effect of UV light on the oxide properties of ZrO_2 and NiO. Figures 13 and 14 also show that X-750 and advanced steel ferritic alloys behave in a similar way regarding the shift in their corrosion potential under both water chemistry conditions with and without UV. This means that a zircaloy-2 component coupled to a X-750 spacer may suffer shadow corrosion in presence of oxidants in the reactor because their corrosion

potential grow apart from each other when irradiation is present [30, 31]. However, Figs 13 and 14 show that a APMT cladding would not adopt a different corrosion potential of a X-750 spacer and therefore would not suffer shadow corrosion in the reactor core [30, 31].

2.3. Advanced steels resistant to environmental cracking in high temperature water

Table 4 shows the non-irradiated and irradiated materials that are being tested for resistance to environmental cracking. It includes from T91 (9% Cr) to Alloy 33 (33%Cr) (See Table 2 for compositions).

TABLE 4. IRRADIATED AND NON-IRRADIATED CT SPECIMENS TESTED AND UNDER TESTING AT GE GRC

Specimen ID	Material	Condition	Hours Tested
C642	Nano-ferritic	As-received	4,970 hours
C646	HT-9, irradiated	38.7 dpa	4,533 hours
C647	HT-9 ferritic	21% cold forged	8,585 hours
C648	APMT ferritic	23% cold forged	10,700+ hours
C649	T91 9%Cr ferritic	23% cold forged	4,624 hours
C680	HT-9, irradiated	7 dpa	1,312 hours
C689	HT-9, irradiated	38.7 dpa	6,500+ hours
C690	9% Cr ferritic	30% cold forged	2,457 hours
C691	20% Cr ferritic	20% cold forged	69 hours
C692	Alloy 33 austenitic	20% cold forged	5,600+ hours
C709	APMT ferritic	As-received	2,900+ hours
C710	Nano-ferritic	As-received	2,700+ hours

Most of the 0.5T CT specimens were machined from the plates so that the notch in the specimen was placed in the SL direction of the plate (ASTM E399). Most of the materials were cold forged (CF) by 20%, which increases their yield strength. The 20% cold reduction was performed to compare crack propagation results with literature data for austenitic steels, which are normally cold reduced. (Cold reduction is used to accelerate crack propagation rate and, therefore, minimize the time required for testing). For a plate material, the SL direction should be the most susceptible to environmentally assisted cracking, since the crack will have a tendency to separate the material along pre-existing rolling lines. 0.5T compact type specimens were machined with 5% side grooves on each side. The CT specimens were instrumented with platinum current and potential probe leads for DC potential drop crack length measurements. In this technique, current flow through the sample was reversed about once per second primarily to reduce measurement errors associated with thermocouple effects and amplifier offsets. The test was computer controlled using inputs from the relationship between the measured potential and crack length. Data were stored in a permanent disk file typically once every 0.69 hours. In addition to the data record number, total elapsed and incremental time, and crack length, the system measured and stored temperature, current, corrosion potential, dissolved gases, influent and effluent conductivity, load and time/date. Additionally, both operator and automated programme messages describing changes in the test conditions and test status were a permanent part of the data record [32-35].

The CT specimens were electrically insulated from the loading pins using zirconia sleeves, and within the autoclave a zirconia washer also isolated the upper pull rod from the internal load frame. The lower pull rod was electrically isolated from the autoclave using a

pressure seal and from the loading actuator using an insulating washer. Ground isolated instrumentation was used for the platinum current and potential probe attachments to the specimen. Testing was performed using servo-electric testing machines equipped with a single stage, low flow servo-valve to ensure optimal (non-noisy) response. Crack growth rates can be considered statistically meaningful when the crack growth increment is at least 10 times the resolution of the technique, which was typically 1 to 5 μm. Thus, crack length increments were typically > 50 μm, although for very low growth rate conditions, smaller increments were occasionally used to reduce testing time from several months per datum to several weeks. Generally, the lowest test time for each combination of variables (e.g. stress intensity) was in the order of 2 weeks or 3 mils (76 μm) of crack growth. The R^2 correlation coefficients from linear regression analyses of the crack lengths vs. time data from which growth rates are calculated were typically >0.90.

Deaerated, de-mineralized water was drawn through a demineralizer and submicron filter to ensure ultra-high purity (0.055 μS/cm or 18 MΩ-cm) and then into a glass column (6.4-cm diameter by 183 cm long). The volume of the column is approximately 4 L, which added to the volume of the autoclave and the piping results on a total volume of solution in the order of 7-8 L. A high pressure pump recirculated the water from the column to the autoclave and back to the column at a rate of approximately 100-200 cm^3/min (which represents two volumes replenishment of the autoclave each hour). The autoclave effluent was back-pressure regulated, then continuously monitored for conductivity and dissolved oxygen. The oxygen concentration was controlled by bubbling gas mixtures blended by mass flow controllers. Impurities of interest (such as 30 ppb sulfate ions as sulfuric acid) were added to the glass column using a metering pump, which was controlled via a preset value in the conductivity meter. The crack tests were performed in a 4-L (1 gallon) stainless steel autoclave at 550°F (288°C) and 1500 psia (10.3 MPa). The corrosion potentials of the CT specimen and a Pt coupon were continuously monitored using a zirconia membrane reference electrode containing copper and copper oxide, whose reference potential is 273 mV higher than the standard hydrogen electrode (SHE) in pure water at 550°F (288°C).

Once the specimen was loaded in the autoclave and connected to the leads, water recirculation started and the temperature and pressure were raised to 550°F (288°C) and 1500 psi (10.3 MPa), respectively. Cyclic fatigue started at a stress intensity of 25 ksi√in (27.3 MPa√m) using a trapezoidal wave at a frequency of 0.001 Hz, a load ratio (K_{min}/K_{max}) R = 0.6 and zero holding time. Ideally, once the crack front propagated 3 mils (76 μm) in the first step a holding time of 9000 s is applied for each cycle at the highest value of the stress intensity in that cycle. Again, ideally, after the crack advanced another 3 mils (76 μm), the stress intensity is kept constant at the highest value (or a static load, R = 1) and the crack advance is typically monitored for a minimum time of 2 weeks or a growth of 3 mils (76 μm). Current results show that these ideal situations cannot be fully applied for the alloys in Table 4 because they are highly resistant to environmental cracking and cracking generally stops growing once the high frequency loading is transitioned to low frequency loading.

Changes in the crack growth rate were also monitored when the water chemistry was changed from pure water to water contaminated with sulfuric acid to give 30 ppb concentration of sulfate ions or chloride ions. Similarly the crack propagation rate was also monitored under oxygenated conditions or normal water conditions (NWC or containing 2 ppm of dissolved oxygen) and under hydrogen water conditions (HWC or containing 63 ppb of dissolved hydrogen). The presence of oxygen or hydrogen controls the corrosion potential of the specimen under test. The crack propagation rate is generally lowered when the corrosion potential is lowered.

2.3.1. Results and discussion for ferritic alloys susceptibility to cracking

Stress corrosion cracking (SCC) testing was initiated on a nano-ferritic alloy (NFA) (specimen c642 in Table 4 and Fig. 15), containing 14% Cr and oxide dispersion hardened with Y_2O_3 in the as-received condition (not cold worked). The in-situ fatigue pre-cracking proceeded as anticipated. As the frequency was slowed to transition to intergranular SCC conditions, cracking slowed down and ceased [35]. The stress intensity and frequency had to be increased to re-initiate the cracking; however, as the loading frequency decreased, crack growth stalled (Fig. 15). Figure 15 shows that even at very high stress intensities of 45 ksi√in and an aggressive R value of 0.45 as the frequency of the loading was decreased below 0.001 Hz the crack stopped growing. That is the crack does not propagate under constant load conditions. This crack growth cessation behaviour at low frequencies was observed before for other ferritic steels containing 5, 9 and 13% Cr [32, 33, 34].

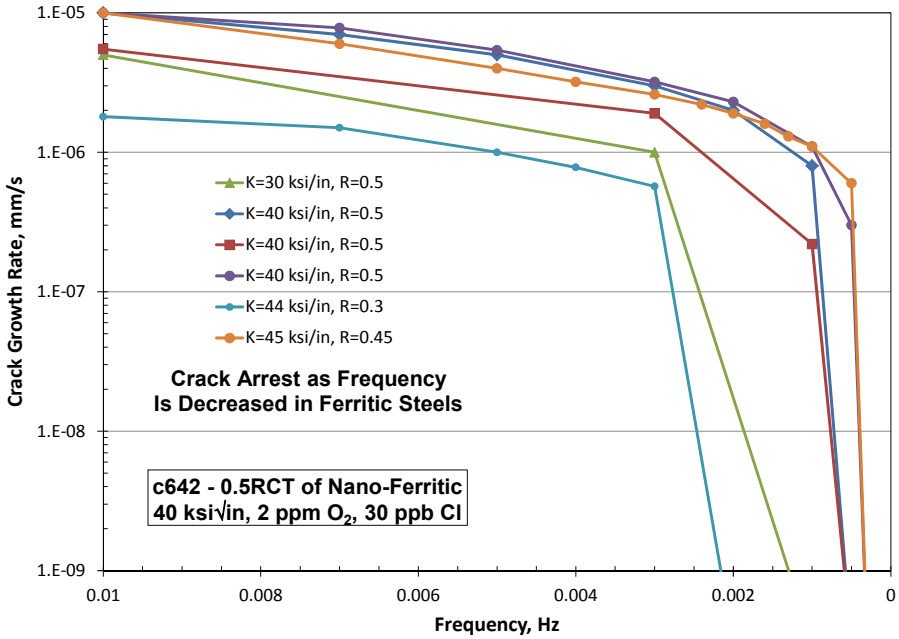

FIG. 15. Crack growth rate vs. frequency for specimen c642 a nano-ferritic ODS alloy tested in 288°C water containing 2 ppm dissolved oxygen and 30 ppb chloride as HCl showing that crack arrest occurs as frequency of the loading is decreased.

Table 4 shows also the SCC testing of highly irradiated specimen c646 made of HT9 and received from Pacific Northwest Laboratory. Despite the high neutron dose (38.7 dpa) the specimen c646 exhibited excellent resistance to SCC, even with elevated (2 ppm) dissolved oxygen and with 30 ppb sulfate or chloride. Figure 16 shows that even at very high stress intensities of 38 ksi√in and an aggressive R value of 0.4, as the frequency of the loading was decreased below 0.001 Hz the crack stopped growing. That is the SCC crack does not propagate under constant load conditions, even for highly irradiated ferritic alloys. This crack growth cessation behaviour at low frequencies was reported before for other ferritic steels containing chromium [32, 33, 34].

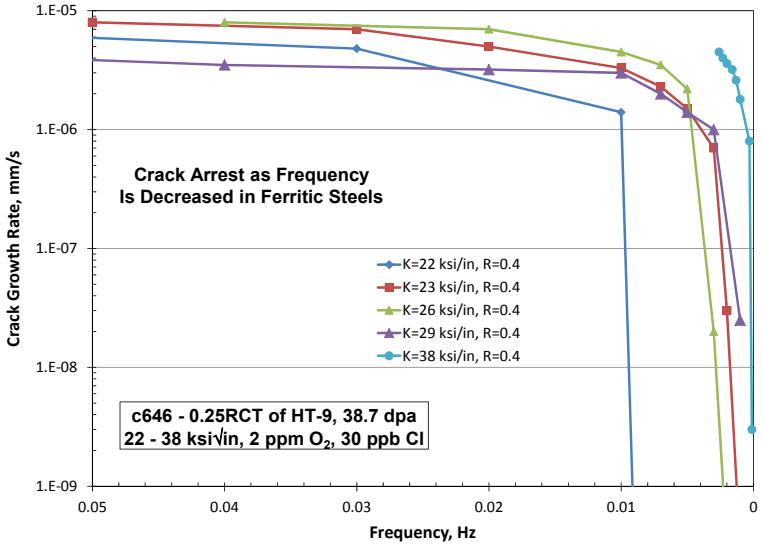

FIG. 16. Crack growth rate vs. frequency for specimen c646 of HT9 ferritic steel irradiated to 38.7 dpa tested in 288°C water containing 2 ppm dissolved oxygen and 30 ppb chloride as HCl showing that crack arrest occurs as frequency is decreased.

Testing was also initiated on HT9 ferritic steel with 20% cold work (specimen c647 in Table 4 and Fig. 17). Figure 17 shows that even at very high stress intensities of 40 ksi√in and an aggressive R value of 0.3, as the frequency of the loading was decreased below 0.001 Hz the crack stopped growing. That is the SCC crack does not propagate under constant load conditions even for this highly cold worked material. In an actual reactor application and because of radiation creep relaxation of constant displacement (e.g., weld residual) stresses, it is not anticipated that high K and high neutron fluence can co-exist in most cases. That is, the residual stresses that may exist in a component will relax as the exposure to radiation increases. Dynamic strain appears to play a dominant role in the environmental cracking response of ferritic alloys, and the dynamic strain that results from crack advance (and redistribution of the stress and strain field near the crack tip) does not sustain SCC as readily as is observed in austenitic alloys. Once crack arrest occurs, the ferritic steels require significantly more aggressive loading conditions to re-initiate cracking [35].

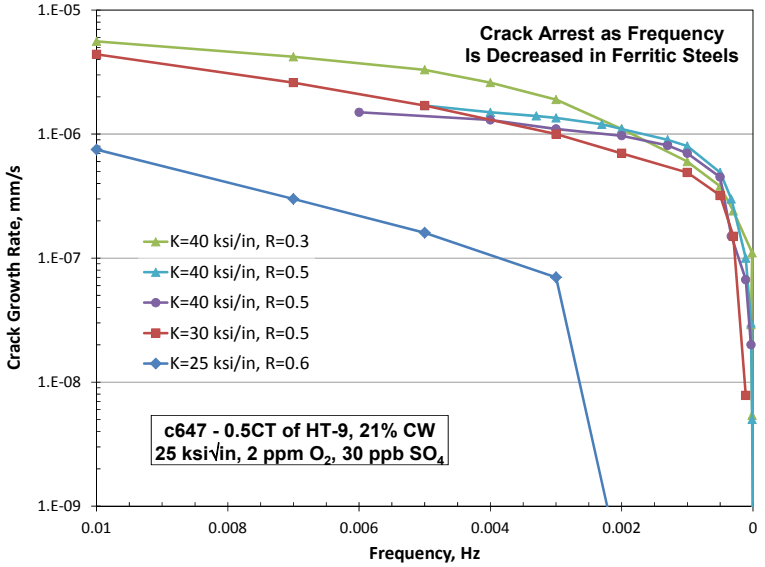

FIG. 17. Crack growth rate vs. frequency for specimen c647 of 21% cold worked HT9 ferritic alloy tested in 288°C water containing 2 ppm dissolved oxygen and 30 ppb sulfate as H_2SO_4 showing that crack arrest occurs as frequency of loading is decreased.

Specimen c648, 20% cold worked Alloy APMT (Tables 2 and 4) was tested for SCC resistance in high temperature water. The in-situ fatigue pre-cracking was very well behaved, and as the frequency was slowed to transition to SCC conditions, cracking was sustained, although the crack growth rate was relatively low, both compared to other ferritic steels and to reference austenitic materials like Alloy 600 and type 316 stainless steel [35]. As the frequency was steadily decreased and hold times at K_{max} introduced, the crack growth rate slowed but did not dramatically decrease at any step, or arrest. A subsequent change from 3000s hold at K_{max} to 9000s hold also reduced, but sustained, the growth rate. However, on changing to 85,400s hold at time 6188 h (Fig. 18), crack arrest occurred. The effect of frequency on crack growth rate and crack arrest is shown in Fig. 19. APMT shows a similar behaviour as other ferritic steels, that is, SCC crack propagation is not sustainable under non cyclic loading conditions, even for high applied stress intensity values of 40 ksi√in (Fig. 19).

All of the ferritic alloys being evaluated for SCC response in this programme have excellent resistance to stress corrosion cracking, even under quite aggressive conditions of elevated oxidants (2 ppm dissolved O_2) and 30 ppb sulfate or chloride (well above that allowed by the BWR water chemistry guidelines). All crack propagation reported here under cyclic loading condition can be considered fatigue cracking. Only under constant load conditions (R=1) the crack propagation may be recognized as environmentally assisted cracking or stress corrosion cracking (SCC). Current results show that ferritic steels containing chromium are extremely resistant to cracking in high temperature water.

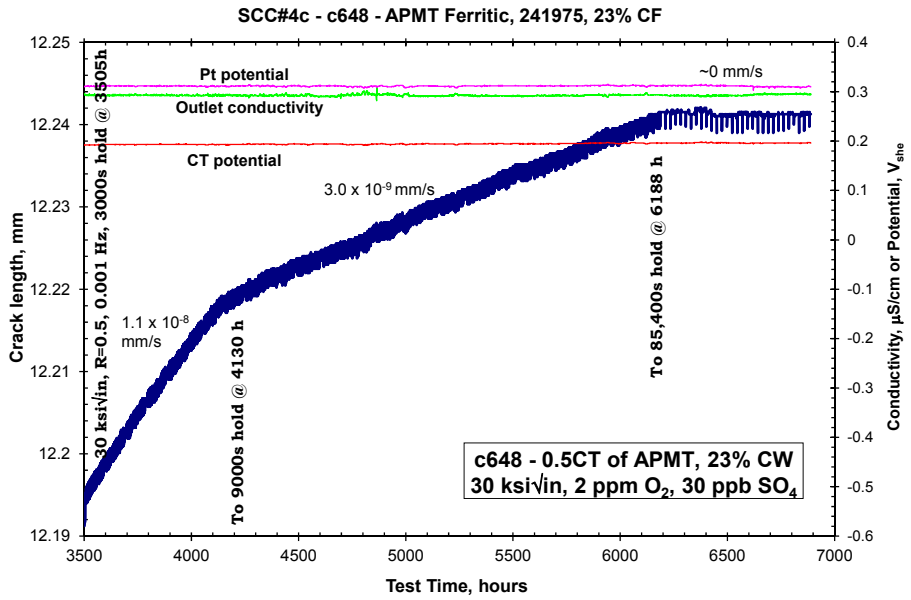

FIG. 18. Crack length vs. time for specimen c648 of a 23% cold worked APMT alloy in 288 C water containing 2 ppm dissolved oxygen and 30 ppb sulfate as H_2SO_4 showing that high growth rates can be observed at high ΔK or frequency, but as the loading conditions are made less aggressive, the cracking does not slow in a controlled fashion, but rather stops.

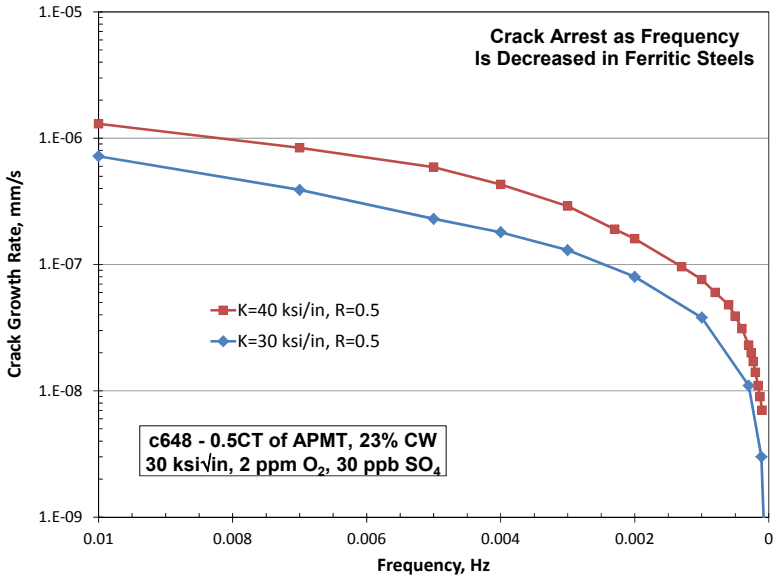

FIG. 19 Crack growth rate vs. frequency for specimen c648 of a 23% cold worked APMT alloy in 288°C water containing 2 ppm dissolved oxygen and 30 ppb sulfate as H_2SO_4 showing that crack arrest occurs as frequency is decreased.

3. BEHAVIOUR OF CANDIDATE MATERIALS BEYOND DESIGN CONDITIONS

3.1. Advanced steels resistant to oxidation in superheated steam

An extensive testing campaign was conducted to address the behaviour of several materials in superheated steam, a condition that may simulate an accident scenario with the loss of coolant in a reactor. Testing was conducted using commercial materials and also alloys fabricated especially for the testing. Results presented here were obtained at GE Global Research and they agree well with testing conducted at Oak Ridge National Laboratory and Los Alamos National Laboratory.

Initially all the tests were performed in 100% steam. The specimens were flat rectangular measuring approximately 25 x 8 x 2.3 mm with a total exposed area of 5-5.3 cm². The surfaces were ground on wet SiC paper up to 320 grid finish. All specimens were washed with solvents and dried. The weight (mass) of the specimens was measured with direct reading microbalance at room temperature before and after each test (3 readings), and the mass change due to exposure to steam was calculated. Figure 20 shows the superheated steam system (SSS). Some of main components include a vertical alumina retort where the five specimens were exposed to steam hanging vertically from a tree. Five thermocouples monitored continuously the temperature next to each specimen. The retort was connected to a steam generator where water was pumped at a rate of 2.5 g/min. The ultra-high purity (UHP or 18 MΩ) water was deaerated with argon before it was injected into the steam generator using a metering pump with a reciprocating piston design. The steam was forced to flow through four alumina diffusers to allow for the preheating and homogenization of the steam. The temperature of the retort was controlled by a three-zone furnace. The steam exited the retort through another set of alumina diffusers to avoid back convection of steam onto the specimens. The steam was condensed at the exit of the system and the volume of water collected was comparable to the amount of water injected into the steam generator.

Front *Back*

FIG. 20. Superheated Steam System (SSS).

Once the coupons were inserted in the retort and the system was sealed, the entire system was purged using a constant flow of pure argon (30 cm^3/min) for 1-2 hours and the gas flow was maintained while heating the chamber (from room temperature to the testing temperature). When the testing temperature was reached, the argon gas flow was stopped and the argon deaerated water injection to the steam generator was started. The top and bottom stainless steel caps of the retort were maintained approximately 150-180°C to avoid steam condensation. At the end of the test, the steam injection was stopped and the testing chamber was cooled down using a flow of dry argon (30 cm^3/min).

Figure 21 shows the appearance of the coupons before and after 8 hours exposure in steam at 800°C. After the test, the zircaloy-2 specimen was slightly bent, perhaps due to the growth of oxides on the surface. The zircaloy-2 oxide layer presented a white snake-like skin appearance and signs of spallation. Alloy T91, did not show any sign of deformation but small oxide spallation was evident. The nano ferritic alloy (NFA) exhibited a uniform black oxide scale whereas APMT and Alloy 33 showed minimal pink and light green discoloration, respectively.

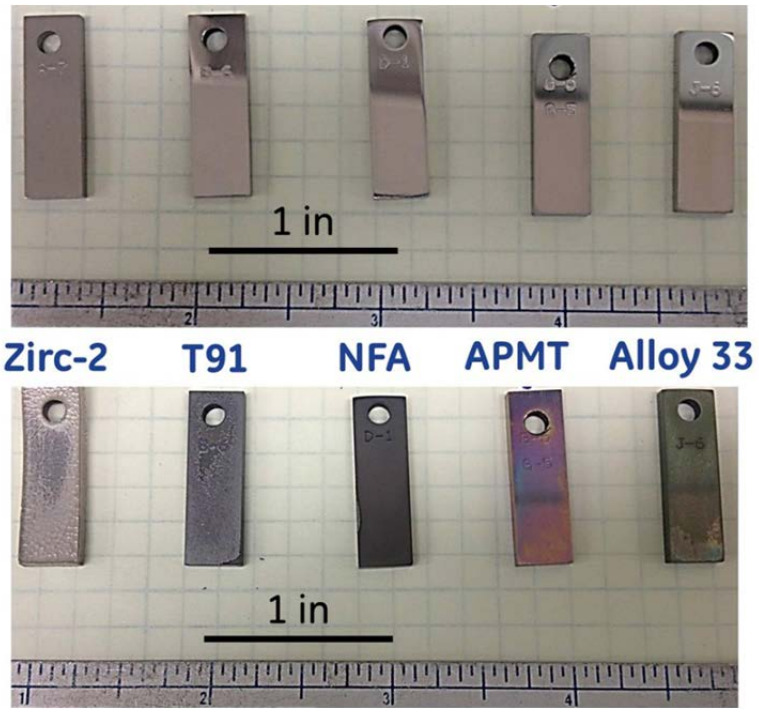

FIG. 21. Specimens before (top) and after (bottom) exposure to 100% steam at 800°C for 8 h.

Figure 22 shows the mass gain per surface area as a function of testing time for five alloys (Table 2). The zircaloy-2 coupon was consumed at the 48 h testing time; therefore there is no data in the plot. Figure 22 shows that there were two evident groups of alloys regarding resistance to degradation in steam. zircaloy-2 and T91 are in Group 1, with a higher oxidation rate, and Group 2 included NFA, APMT and Alloy 33 with an oxidation rate that was approximately two orders of magnitude lower than for Group 1. Overall, the highest oxidation rate was for zircaloy-2 and the lowest for APMT. The oxidation of the iron containing alloys seems to follow a parabolic law with an exponent coefficient close to 0.5. The coefficient was higher for the zirconium alloy, suggesting that oxidation was not controlled by diffusion through a protective oxide film on the surface.

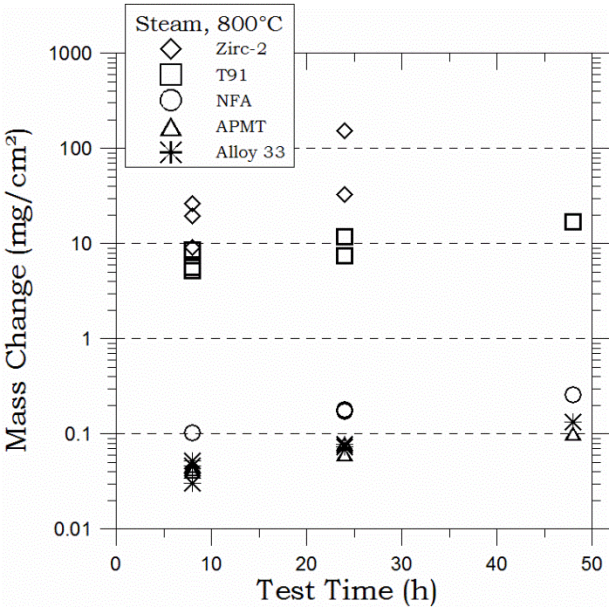

FIG. 22. Mass change as a function of test time in 100% steam at 800°C. The zircaloy-2 coupon was consumed after 48 h of testing.

Figure 23 shows the appearance of the zircaloy-2 and APMT coupons in a scanning electron microscope after the exposure to 100% steam at 800°C for 24 h. The magnification for zircaloy-2 is approximately 10 times lower than that for APMT. Figure 23 shows the evident difference in oxidation behaviour between these two materials. APMT had the lowest oxidation susceptibility in steam since marks from sample preparation are clearly discernible. On the other hand zircaloy-2 was completely covered by a cracked oxide film.

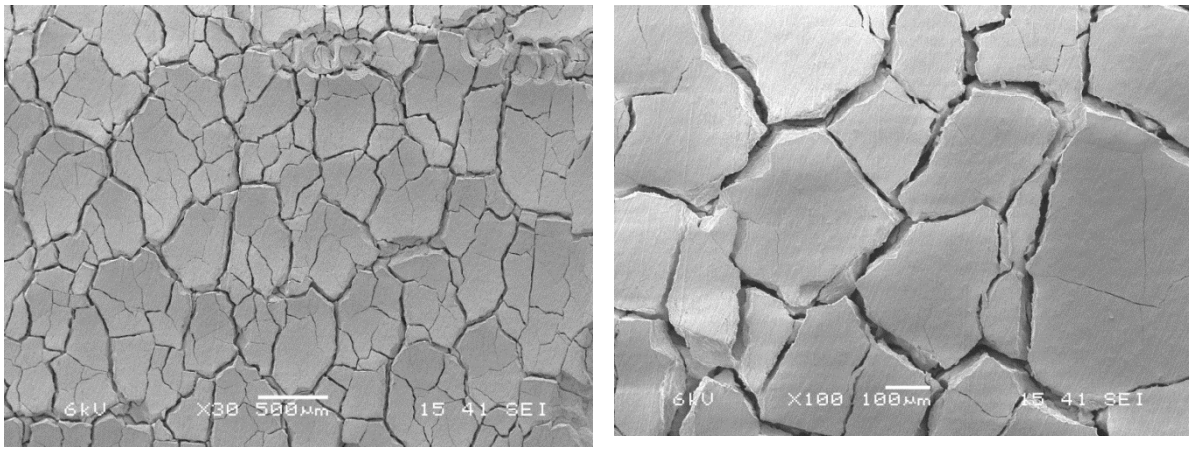

zircaloy-2, X30 (Specimen A12) zircaloy-2, X100 (Specimen A12)

FIG. 23. Appearance of coupons after testing in 100% steam at 800°C for 24 h.

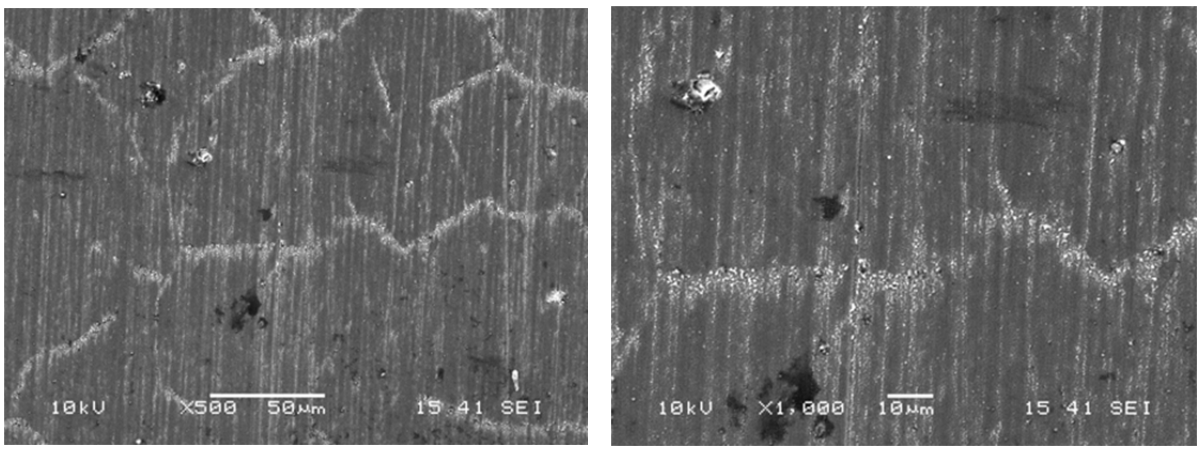

APMT, X500 (Specimen G9) APMT, X1000 (Specimen G9)

FIG. 23 (cont). Appearance of coupons after testing in 100% steam at 800°C for 24 h.

Figure 24 shows the appearance of coupons after testing for 24 h in 100% steam at 1000°C. Alloy APMT showed excellent resistance to oxidation while zircaloy-2 was completely transformed to oxide (the coupons were of identical size before the steam oxidation tests started).

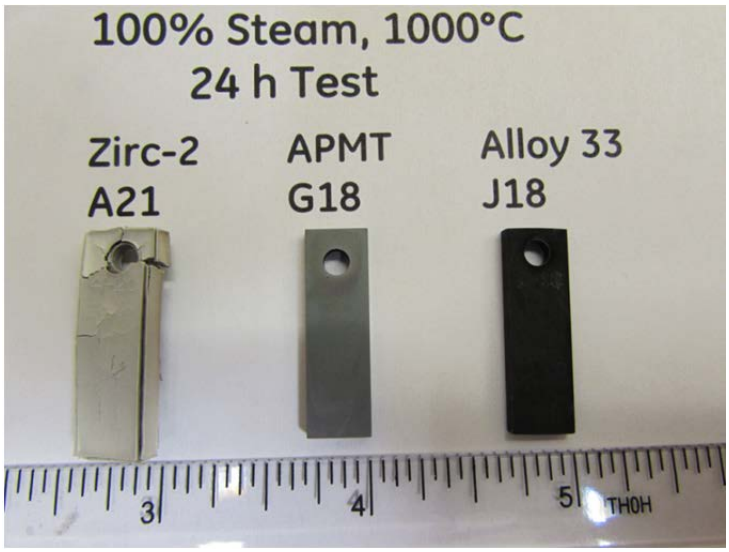

FIG. 24. Appearance of coupons after testing in 100% steam at 1000°C for 24 h.

4. SUMMARY AND CONCLUSIONS

The objective of the GE project is to demonstrate that advanced steels such as iron-chromium-aluminium (FeCrAl) alloys could be used as accident tolerant fuel cladding material in commercial light water reactors. The main findings are as follows:

- Under normal operation conditions the candidate alloys (e.g. APMT, Alloy 33) showed excellent resistance to general corrosion, shadow corrosion and to environmentally assisted cracking;
- Under accident conditions the selected candidate materials showed several orders of magnitude improvement in the reaction with superheated steam as compared with the current zirconium based alloys.

The replacement of a zirconium alloy using a ferritic material containing chromium and aluminium appears to be the most near term implementation for accident tolerant fuels.

ACKNOWLEDGEMENTS

The technical expertise of Dustin Ellis, Timothy Jurewicz, Paul J. Martiniano, Richard J. Blair, and Frank Wagenbaugh is gratefully acknowledged. The funding support from Kelly Fletcher and Steven J. Duclos is thankfully appreciated.

This material is based upon work supported by the Dept. of Energy [National Nuclear Security Administration] under Award Number DE-NE0000568. This report was prepared as an account of work sponsored by an agency of the United States Government. Neither the United States Government nor any agency thereof, nor any of their employees makes any warranty, express or implied, or assumes any legal liability or responsibility for the accuracy, completeness, or usefulness of any information, apparatus, product, or process disclosed, or represents that its use would not infringe privately owned rights. Reference herein to any specific commercial product, process or service by trade name, trademark, manufacturer, or otherwise does not necessarily constitute or imply its endorsement, recommendation, or favouring by the United States Government or any agency thereof. The views and opinions of authors expressed herein do not necessarily state or reflect those of the United States Government or any agency thereof.

REFERENCES

[1] CARMACK, J., GOLDNER, F., Forward for special JNM issue on accident tolerant fuels for LWRs, J. Nucl. Mater., **448, 1–3**, (2014), 373.

[2] BRAGG-SITTON, S., Development of advanced accident-tolerant fuels for commercial LWRs, Nuclear News, March (2014), pp. 83-89.

[3] HEWLETT, R.G., DUNCAN, F., Nuclear Navy 1946-1962, The University of Chicago Press, Chicago, IL (1974).

[4] BRAGG-SITTON, S.M., "Light water reactor sustainability program. advanced LWR nuclear fuel cladding system development technical program plan", Report INL/MIS-12-25696, Idaho National Laboratory, December (2012).

[5] TERRANI, K.A., ZINKLE, S.J., SNEAD, L.L., Advanced oxidation-resistant iron-based alloys for LWR fuel cladding, J. Nucl. Mater., **448, 1–3** (2014) 420–435.

[6] GEORGE, N.M., TERRANI, K.A., POWERS, J.J., "Neutronic analysis of candidate accident-tolerant iron alloy cladding concepts", Report ORNL/TM-2013/121 Oak Ridge National Laboratory (2013).

[7] ANDRESEN, P.L., REBAK, R.B., DOLLEY, E.J., "SCC resistance of irradiated and unirradiated high Cr ferritic steels," Paper C2014-3760, Corrosion/2014, San Antonio, TX, 09-13 March 2014 NACE International, Houston TX (2014).

[8] RIVERA, J.E., MEYER, J.E., "Stainless steel clad for light water reactor fuels", Energy Laboratory Report No. MIT-EL 80-021, July (1980).

[9] SEDRIKS, A. J., Corrosion of Stainless Steels, 2nd edition, John Wiley & Sons, Inc. New York (1996).

[10] BOND, A.P., MARSHALL, J.D., DUNDAS, H.J., Resistance of ferritic stainless steels to stress corrosion cracking, Stress Corrosion Testing, ASTM STP 425, American Society for Testing Materials, (1967) 116.

[11] ANDRESEN, P.L., "Stress corrosion cracking of current structural materials in commercial nuclear power plants", Paper C2012-0001929, Corrosion/2012, Salt Lake City, UT NACE International, Houston, TX (2012).

[12] CHUNG, H.M., SHACK, W.J., "Irradiation-assisted stress corrosion cracking behaviour of austenitic stainless steels applicable to LWR core internals", NUREG/CR-6892, Argonne National Laboratory and U.S. Nuclear Regulatory Commission, Office of Nuclear Regulatory Research, Washington, DC 20555-0001 (2006).

[13] COOKSON, J.M., CARTER R.D., Jr., DAMCOTT, D.L., ATZMON, M., WAS, G.S., Irradiation assisted stress corrosion cracking of controlled purity 304L stainless steel, J. Nucl. Mater., **202** (1993) 104-121.

[14] JACOBS, A.J., WOZADLO, G.P., NAKATA, K., KASAHARA, S., OKADA, T., KAWANO, S., SUZUKI, S., "Correlation of grain boundary composition in irradiated stainless steel with IASCC resistance", in Proc. 6th International Symposium on Environmental Degradation of Materials in Nuclear Power Systems - Water Reactors, pp. 597-606, Minerals, Metals & Materials Soc (TMS), Warrendale, PA, United States (1993).

[15] WAS, G.S., "Recent developments in understanding irradiation assisted stress corrosion cracking", Proceedings of the 11th International Conference on Environmental Degradation of Materials in Nuclear Systems, Stevenson, WA, 10-14 August (2003), 965-985.

[16] BRUEMMER, S.M., "New issues concerning radiation-induced material changes and irradiation-assisted stress corrosion cracking in light water reactors", Proc. 10th Int. Conf. Environmental Degradation of Materials in Nuclear Power Systems -Water Reactors, NACE International, Houston (2002).

[17] WAS, G.S., BUSBY, J., ANDRESEN, P.L., "Effect of irradiation on stress-corrosion cracking and corrosion in light water reactors", ASM Handbook, Volume 13C: Corrosion: Environments and Industries S. D. Cramer, B. S. Covino, Jr., (Eds), pp. 386-414 ASM International, Metals Park, OH. (2006).
[18] YONEZAWA, T., FUJIMOTO, K., IWAMURA, T., NISHIDA, S., "Improvement of IASCC resistance for austenitic stainless steels in PWR environment", Environmentally Assisted Cracking: Predictive Methods for Risk Assessment and Evaluation of Materials, Equipment, and Structures, ASTM 1401, R. D. Kane, Ed, American Society for Testing find Materials, West Conshohocken, PA (2000).
[19] HOJNÁ, A., Irradiation assisted stress corrosion cracking and impact on life extension, Corrosion: **69,** 10 (2013) 964-974.
[20] RAJ, B., VIJAYALAKSHMI, M., Ferritic steels for sodium cooled fast reactors: design principles and challenges, JOM, **62.9** (2010) 75-83.
[21] WHITMARSCH, C.L., "Review of zircaloy-2 and zircaloy-4 properties relevant to S.S. Savannah reactor design", Report ORNL-3281, UC-80 - Reactor Technology TID-4500 (17th ed.) (1962).
[22] BAKER, L., JUST, L.C., "Studies of metal–water reactions at high temperatures", ANL-6548, Argonne National Laboratory (1962).
[23] LEISTIKOW, S., SCHANZ, G., Oxidation kinetics and related phenomena of zircaloy-4 fuel cladding exposed to high temperature steam and hydrogen-steam mixtures under PWR accident conditions, Nuclear Engineering and Design, **103,1** (1987) 65–84.
[24] INTERNATIONAL ATOMIC ENERGY AGENCY, "Hydrogen in water-cooled nuclear power reactors", Final Report EUR 14037 EN (1992).
[25] GRANDJEAN, C., HACHE, G., "A state-of-the-art review of past programmes devoted to fuel behaviour under loss-of-coolant conditions". Part 3. Cladding oxidation. Resistance to quench and post-quench loads, IRSN Report SEMCA 2008-093, France (2008).
[26] PINT, B.A., BRADY, M.P., KEISER, J.R., CHENG, T., TERRANI, K.A., "High temperature oxidation of fuel cladding candidate materials in steam-hydrogen environments", Paper #89, Proceedings of the 8th International Symposium on High Temperature Corrosion and Protection of Materials Les Embiez, France, (2012).
[27] OPILA, E.J., Volatility of Common Protective Oxides in High Temperature and Unanswered Questions, Materials Science Forum, **461-464** (2004), 765-774.
[28] CHENG, T., KEISER, J.R., BRADY, M.P., TERRANI, K.A., PINT, B.A., Oxidation of Fuel Cladding Candidate Materials in Steam Environments at High Temperature and Pressure, J. Nucl. Mater., **427, 1-3** (2012) 396-400.
[29] ANDRESEN, P.L., JUREWICZ, T.B., REBAK, R.B., "Stress Corrosion Cracking Resistance of Ferritic Chromium Steels in High Temperature Water", Paper C2012-0001181, Corrosion/2012, Salt Lake City - UT, NACE International, Houston TX (2012).
[30] KIM, Y.J., REBAK, R.B., "Photoelectrochemistry of Zr Alloys in High Temperature Water - A Review", Paper 6509, Corrosion/2009, NACE International, Houston, TX (2009).
[31] KIM, Y.J., REBAK, R.B., LIN, Y.-P., LUTZ, D., CRAWFORD, D, KUCUK, A., CHENG, B., 16th International Symposium, Zirconium in the Nuclear Industry, ASTM International, STP 1529, BARBERIS P. & LIMBACK M. Eds., p. 91 (2011).
[32] REBAK, R.B., "Resistance of Ferritic Steels to Stress Corrosion Cracking in High Temperature Water", Paper PVP2013-97352, Proc. ASME 55706; Volume 6A: Materials and Fabrication, V06AT06A085, DOI: 10.1115/PVP2013-97352 (2013).

[33] REBAK, R.B., ANDRESEN, P. L., BLAIR, R.J., DOLLEY, E.J., “Environmentally Assisted Cracking Resistant Ferritic Steels for Light Water Reactor Applications”, Paper C2013-2599, Corrosion/2013, Orlando - FL, NACE International, Houston TX (2013).
[34] ANDRESEN, P.L., REBAK, R.B., DOLLEY, E.J., “SCC Resistance of Irradiated and Unirradiated High Cr ferritic steels”, Paper NACE-2014-3760, CORROSION 2014, San Antonio, Texas, USA (2014).
[35] ANDRESEN, P.L., REBAK, R.B., DOLLEY, E.J., “SCC Growth Rate of Irradiated and Unirradiated High Cr Ferritic Steels”, presented at Fontevraud 8, Contribution of Materials Investigations and Operating Experience to LWRs’ Safety, Performance and Reliability, Avignon, France (2014).

DEVELOPMENT OF CO-PILGERING PROCESS FOR MANUFACTURING DOUBLE CLAD TUBES FOR ACCIDENT TOLERANT FUEL

B. VISHNU VARDHAN REDDY, B. CHANDRASEKHAR
G.V.S. HEMANTHA RAO, N. SAIBABA, P.N. PRASAD*
Nuclear Fuel Complex, Hyderabad, *NPCIL, Mumbai
India
E-mail: vishnu@nfc.gov.in

Abstract

Accident Tolerant Fuels (ATF) are those that, in comparison with the standard UO_2 – Zr system, can tolerate loss of active cooling in the core for a considerably longer time period (depending on the accident scenario), while maintaining or improving the fuel performance during normal operations. ATF cladding development efforts focus on materials with more benign steam reaction. For this, advanced steels (e.g. FeCrAl), refractory metals (e.g. Mo), ceramic cladding (SiC), Innovative alloys with dopants, zirconium alloy with coating or sleeve are being developed. Single material like zirconium alloy as clad may not be compatible with both fuel and coolant at elevated temperatures in accident scenario. Double clad tube is one of the prime concepts which has to be explored to develop ATF cladding. Two different clad materials- one oxidant resistant (like FeCrAl) and the other, fuel compatible (like Zr-4) constitute together as outer and inner tube to form ATF cladding. Bonding two different tubes in controlled thickness ratios and with almost no gap in between is utmost difficult. Different types of processes are available for production of double clad tubes such as coating, co-extrusion, co-drawing, internal expansion/external compaction, explosive bonding, co-pilgering etc,. Nuclear Fuel Complex (NFC), India has successfully demonstrated manufacturing of double clad tube by co-pilgering process where in outer cladding is of modified 9Cr-1Mo Steel and inner liner is of zircaloy-4. Considering different deformation behaviour of above materials during pilgering, fabrication of double clad tube is very critical. Optimization of tube dimensions like outer diameter and wall thickness at pre and final stages during pilgering is very important to achieve the required overall tube dimension and bonding between the tubes. This paper gives the methodology of manufacture of Double Clad Tubes by pilgering and the bonding between the two materials achieved in this process.

1. INTRODUCTION

Nature has provided us with the unique but sufficient choice in the form of zirconium based alloys for nuclear power reactors. However, use of zirconium in nuclear reactor is not free of problems and poses several challenges to scientists and engineers. In light water reactors, zirconium alloy claddings are particularly susceptible to hydrogen embrittlement, pellet clad interaction and high temperature exothermic reaction with steam leading to generation of large amount of hydrogen. These circumstances accelerate the course of accident progression especially at high temperatures. Zirconium alloy as clad may not be compatible with both fuel and coolant at elevated temperatures in accident scenario. Accident tolerant fuel (ATF) cladding development focuses on materials like advanced steels (e.g. FeCrAl), refractory metals (e.g. Mo), ceramic cladding (SiC), innovative alloys with dopants, and zirconium alloy with coating or sleeve. These developments enhance safety in the event of accidents. One of the prime concepts to be explored for development of ATF cladding is development of double clad tube which comprises of two similar or different clad materials along with coatings and liners.

In India, double clad tubes are also being explored for pressurized heavy water reactors (PHWR), fast breeder reactors (FBR) and advance heavy water reactors for higher burnup and accident tolerance. In pursuit of developing advanced cladding for Indian FBRs, Nuclear Fuel Complex (NFC), Hyderabad, having pioneered in manufacturing various size and shapes of nuclear grade clad tubes and other seamless tubes, developed fabrication process for double clad tubes by cold pilgering with appropriate heat treatment cycles using different materials altogether – modified 9Cr-1Mo steel as clad and Zr-4 as inside liner.

2. MANUFACTURING METHODS

The prime concern in manufacturing double clad tubes is to achieve strong mechanical bonding at the clad interface for sufficient strength and ample heat transfer. Better bonding between the tubes can be achieved by introducing high compressive forces. Various methods available for manufacturing double clad tubes are briefed below:

- Coatings: Optimized chromium coating on zirconium alloy cladding exhibits very good resistance to both oxidation and hydrogen up-take and appears as a candidate for safety improvement in current reactors in near future;
- Co-extrusion: Improved bonding can be achieved by co-extrusion technology for a composite billet. However, it is difficult to achieve required geometrical dimensions. Hence, co-extrusion has to be followed by complex thermo-mechanical processes for bi-layer system to achieve improved bonding and geometry;
- Co-drawing: It is not possible to achieve good mechanical bonding in co-drawing as axial tensile forces play a major role in drawing operation where as high compressive forces on the layers is the requirement;
- Hydro forming: Hydraulic pressurization to inflate inner tube or deflate outer tube is a easy process to generate double clad tube. This method is suitable for smaller diameter and thin tubes only. Very high pressures are required for good bonding;
- Explosive bonding: Explosion is far less commonly used technique because of use of chemical explosives. It is a solid state welding process used for the metallurgical joining of dissimilar metals. Large areas can be bonded extremely quickly and the bonding itself is very clean;
- Co-pilgering: Simultaneous reduction of outer diameter and wall thickness of both tubes is possible with co-pilgering. Compressive forces act on outer diameter and inner diameter resulting in good mechanical bonding, provided the differences in mechanical properties are taken care;
- Magnetic pulse welding: Similar to explosive bonding, magnetic pulse welding is a solid-state shock welding process in which metallic bonds are created through the high-velocity impact created by magnetic forces. It presents high potential as a joining technology, especially for dissimilar materials. It is a relatively new technology for double clad tubes.

Out of the various methods available, NFC has chosen pilgering as the suitable method for manufacturing double clad tubes, as it gives good amount of compressive forces and controls diameter, thickness and texture.

3. MATERIALS

Zirconium alloys are considered as the proven structural material for nuclear applications primarily because of their unique combination of good corrosion resistance, low capture cross section for thermal neutrons and high compatibility with various nuclear fuel materials. Advanced steels are always having high mechanical strength, toughness and oxidation resistance at elevated temperatures. Hence, double clad tubes with zirconium alloy as inner layer and advanced steels as outer layer are proposed to be the best substitute for nuclear applications.

Modified 9Cr-1Mo steel with Zr-4 liner is selected to fabricate double clad tubes. Zr-4 tubes were made from raw material stage at NFC and modified 9Cr-1Mo steel tubes made from ingot manufactured with controlled chemistry. The chemical compositions and mechanical properties are shown in Tables 1, 2 & 3.

TABLE 1. TYPICAL CHEMICAL COMPOSITION OF ZR-4

Element	Sn	Fe	Cr	O	Fe+Cr	Zr
Composition	1.2-1.7%	0.18-0.24%	0.07-0.13%	800-1400 ppm	0.28-0.37%	Balance

TABLE 2. TYPICAL CHEMICAL COMPOSITION OF MODIFIED 9CR–1MO STEEL

Element	C	Si	Mn	P	S	Ni	Mo	Cr	V	Fe
Composition	0.08-0.12%	0.2-0.5%	0.3-0.6%	0.00-0.02%	0.000-0.010%	0.00-0.40%	0.85-1.05%	8.00-9.50%	0.18-0.25%	Balance

TABLE 3. TYPICAL MECHANICAL PROPERTIES OF ZR-4 AND MODIFIED 9CR–1MO STEEL

Property	Zirconium alloy – 4		Modified 9Cr–1Mo steel	
	At room temp.	At 300°C	At room temp.	At 525°C
0.2% Yield Strength (MPa)	485 (Min)	330 (Min)	420 (Min)	275 (Min)
Ultimate Tensile Strength (MPa)	710 (Min)	480 (Min)	585 – 760	370 (Min)
% Elongation	12 (Min)	12 (Min)	20 (Min)	10 (Min)

4. CO-PILGERING PROCESS

Pilgering is a cold working process chosen for its dimensional accuracy and favourable texture development, controlled by the ratio of diameter to thickness reduction. Co-pilgering is one of the methods for fabrication of double clad tubes because of its many advantages as high compressive forces are involved resulting in good mechanical bonding between two layers. At NFC, a three roll pilger mill was selected to fabricate double clad tubes due to smaller diameter and thin walled tubes. Experimental works have been carried out to optimize the parameters like feed rate, speed, working length, rotation angle and Q-factor (Fig. 1).

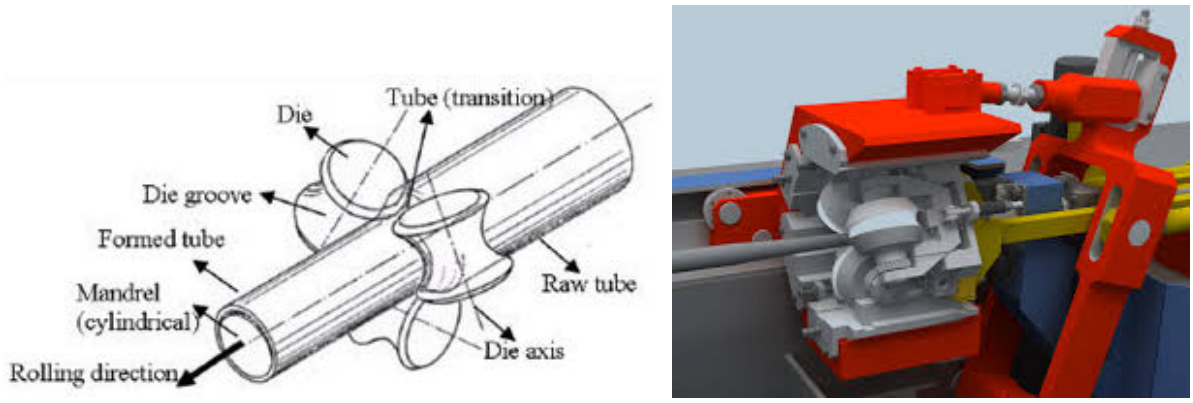

FIG. 1. Schematic of three roll pilgering process.

5. MATHEMATICAL MODELLING

Designing the pilgering pass schedules of modified 9Cr–1Mo steel and Zr–4 tubes is critical to obtain the required dimensions after co-pilgering. Due to different material characteristics, modified 9Cr-1Mo steel and Zr-4 show different behaviour during the deformation and heat treatment process. For better bonding between the materials, there should not be any slip between the different layers of the cladding. A mathematical model was developed to find the parameters for the input materials to equate the strains of the two materials during co-pilgering.

An analysis of the axial stress distribution in the working length while pilgering a single material, was done to calculate the strain distribution along the working zone. A programme was developed with outgoing tube dimensions and material properties as input to get ingoing tube dimensions as output while matching strain distribution along the working zone for both the materials. Optimum process parameters were found out for which relatively there is no slip at the clad interface while pilgering.

5.1. Approach and assumptions

Since pilgering is a very complex mechanical process, it is a herculean task to develop an exact model that simulates the working conditions of the process. A simplified analysis for parabolic profile and linear profile of the deformation zone was developed to determine the axial stresses in the clad materials. For this, the deformation zone is divided into 100 equal parts and "Slab Method" or the "Elementary Stress analysis technique" was used for each part. Corresponding strains were determined in each part using the stress-strain relations from the Theory of plasticity.

Following assumptions were made in developing the mathematical modelling:

- The material is isotropic, incompressible and the elastic strains are neglected;
- Deformation is homogeneous throughout the materials under study. A square grid placed in the deformation zone would be distorted uniformly into rectangular elements;
- Stresses on a plane normal to the flow are principal stresses;
- Strains in the circumferential direction are negligible i.e. Plane Strain conditions exist;
- Rolls and mandrel are rigid structures and there is no deformation in them during the process;
- All the material and interface properties are independent of temperature;
- Axial stresses are the major stresses and are solely responsible for the axial deformation;
- The intermediate layer follows the same profile followed by the top and the bottom layers;
- The rollers and the mandrel apply equal pressure on the tube.

5.2. Profile equations

In case two roll pilgering machine with parabolic profile mandrel, deformation zone of tube will be parabolic, Fig. 2. Similarly, in case of three roll pilgering machine with straight mandrel, deformation zone of tube will be linear, Fig. 3. With another assumption that interface layer also follows the same profile which the die and mandrel are following, the profile equations are derived for both parabolic and linear profiles in the deformation zone.

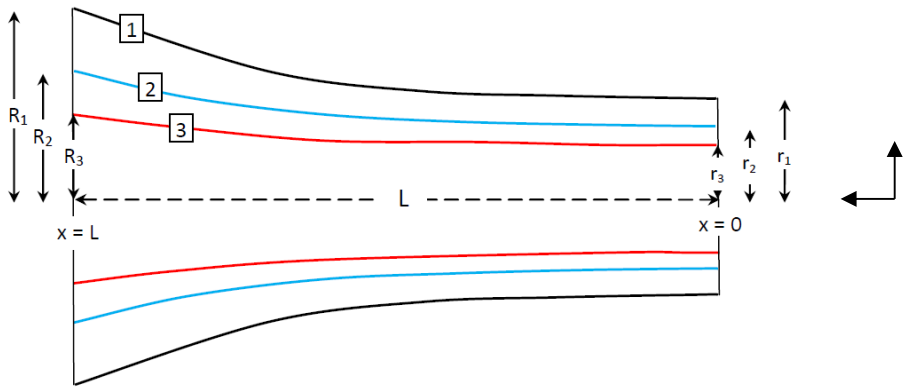

FIG. 2. Geometrical details of parabolic profile in the deformation zone.

Parabolic profile equation:

$$(\boldsymbol{x}+\boldsymbol{c})^{\boldsymbol{2}}=\boldsymbol{4ay} \tag{1}$$

Where $\boldsymbol{c}$ and $\boldsymbol{a}$ are proportionality constants and can be determined from boundary conditions.

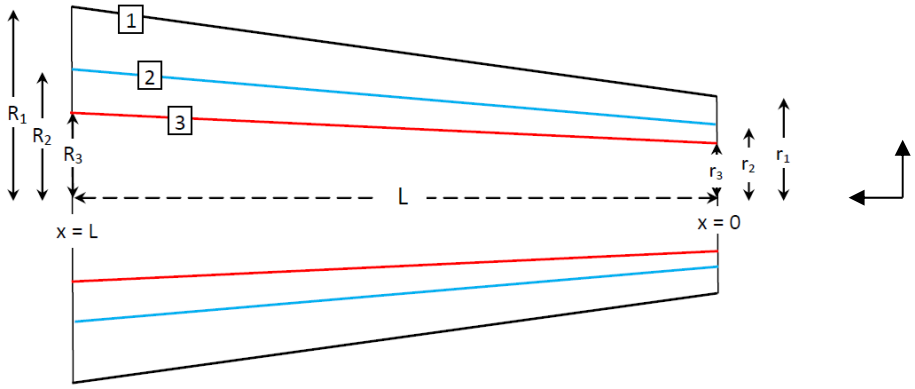

FIG. 3. Geometrical details of linear profile in the deformation zone.

Linear profile equation:

$$\boldsymbol{y}=\boldsymbol{mx}+\boldsymbol{c} \tag{2}$$

Where *m* and *c* are proportionality constants and can be determined from boundary conditions.

5.3. The von Mises' yield criteria

The von Mises yield criteria is given by

$$\boldsymbol{\sigma_0}=\sqrt{\frac{\boldsymbol{1}}{\boldsymbol{2}}((\boldsymbol{\sigma_1}-\boldsymbol{\sigma_2})^{\boldsymbol{2}}+(\boldsymbol{\sigma_2}-\boldsymbol{\sigma_3})^{\boldsymbol{2}}+(\boldsymbol{\sigma_3}-\boldsymbol{\sigma_1})^{\boldsymbol{2}}} \tag{3}$$

Where,

$\boldsymbol{\sigma_1, \sigma_2, \sigma_3}$ are the principle stresses;

$\boldsymbol{\sigma_0}$ is the yield strength of material.

In plane strain condition and at poisons ratio, $\boldsymbol{\nu = \frac{1}{2}}$,

$$\boldsymbol{\sigma_3 = \frac{1}{2}(\sigma_1 + \sigma_2)}$$

Thus,

$$\boldsymbol{(\sigma_1 - \sigma_2) = \frac{2\sigma_0}{\sqrt{3}}} \quad (4)$$

An infinitesimal element of length dx and thickness dh is considered on the deformation zone of the tube. It is subjected to an axial stress of σ_x and a radial stress of σ_r due to the die and mandrel pressures '$\boldsymbol{p}$', Fig. 4. A characteristic of the slab method is that these stresses are assumed to be principal stresses.

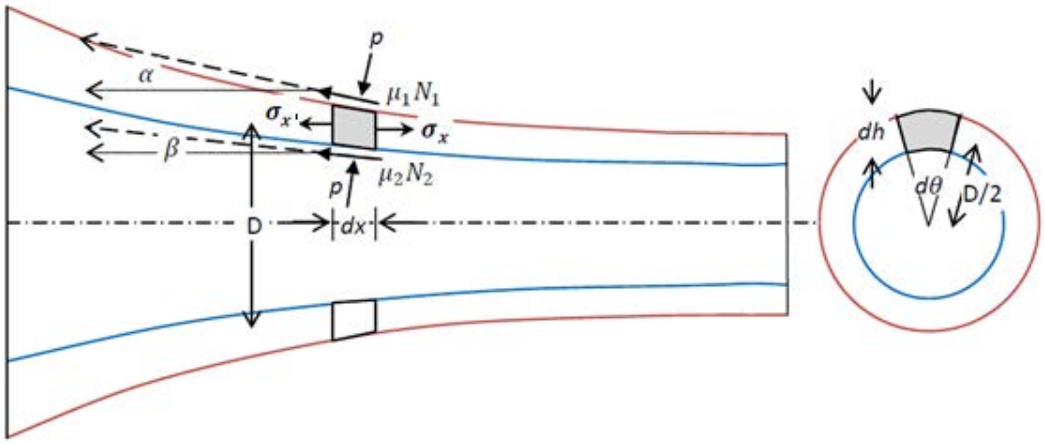

FIG. 4. A differential element of material in the deformation zone.

Equilibrium equation along the X-axis:

$$\boldsymbol{(\sigma_x + d\sigma_x)(h + dh)\pi D - \sigma_x h\pi D - (p\pi\mu_1 D + p\pi\mu_2 D)dx + (p\pi D \tan\beta - p\pi \tan\alpha)dx = 0} \quad (5)$$

Where,

h	is the thickness at the section;
D	is the mean diameter at the section;
p	is the die/mandrel pressure
μ_1	is the coefficient of friction between die and the tube;
μ_2	is the coefficient of friction between mandrel and the tube;
α	is the angle of the roller with the horizontal;
β	is the angle of the mandrel with the horizontal.

Equilibrium of forces in radial direction:

$$\boldsymbol{\sigma_r dx\pi D + p\cos\alpha\left(\frac{dx}{\cos\alpha}\right)\pi D = 0 \Rightarrow \sigma_r = -p} \quad (6)$$

Upon solving equations (4), (5) & (6) and applying boundary conditions, we obtain

$$\boldsymbol{\sigma_x = \sigma_{x^1}\left(\frac{h}{h_0}\right)^B - \frac{2\sigma_0}{\sqrt{3}}\left(\frac{B+1}{B}\right)\left[\left(\frac{h}{h_0}\right)^B - 1\right]} \quad (7)$$

Where,

$$\boldsymbol{B = \frac{(\mu_1+\mu_2)}{(\tan\alpha - \tan\beta)}} \quad (8)$$

The equation (7) can be written as

$$\boldsymbol{\sigma_x = \sigma_{x^1} S + K[S-1]} \quad (9)$$

Where,

$$\boldsymbol{S = \left(\frac{h}{h_0}\right)^B, \qquad K = -\frac{2\sigma_0}{\sqrt{3}}\left(\frac{B+1}{B}\right)}$$

This equation is used to determine the stress distribution in every section of the deformation zone.

Further, stress – strain relation:

$$\boldsymbol{\sigma = K\varepsilon^n \text{ or } \ln\sigma = \ln K + n\ln\varepsilon} \quad (10)$$

Where,

σ is the true stress;
ε is the true strain;
K is the strength coefficient i.e. the stress at ε = 1.0;
n is the strain hardening coefficient i.e. the slope of log-log plot.

$$\boldsymbol{\varepsilon = \int_{L_0}^{L}\frac{dL}{L} = \ln\left(\frac{L}{L_0}\right) = \ln(e+1) \text{ and } \sigma = s(e+1)} \quad (11)$$

Where,

e is the engineering stain;
s is the engineering stress.

From the equations (9), (10) & (11), a mathematical model has been developed to determine the stresses and strains across the deformation zone. The assumptions made to develop this model are applicable for both the materials of the clad under similar conditions. Hence, no significant effect on accuracy of the model is expected. This model was used to make the strains in both the clad materials relatively equal as shown in Fig.5 by choosing the optimum process parameters.

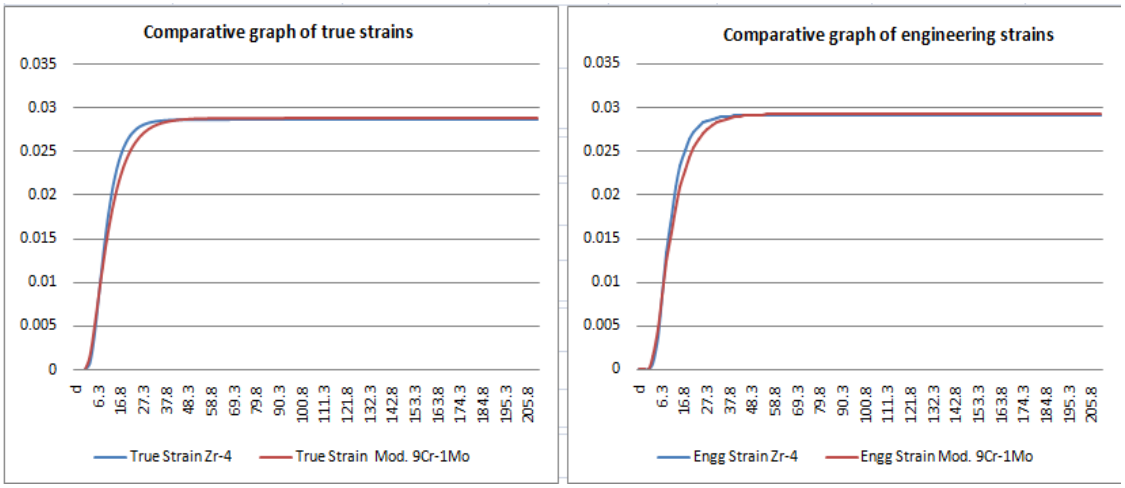

FIG. 5. Comparative strain graphs for linear profile deformation.

6. PROCESS FLOW

NFC is the only facility in India to produce zirconium and zirconium alloy products in large scale. Zr-4 tube required for the present process is produced from zircon sand, zirconium oxide powder, zirconium sponge at NFC. The required cladding tube is obtained through quadruple vacuum arc melting, machining, dual hot extrusions with intermediate heat treatment processes and multiple cold pilgering with intermediate annealing. Similarly, modified 9Cr–1Mo steel ingot was obtained and required cladding tube was produced through series of extrusion and cold pilgering cycles.

Zr-4 tube of size 8.1 mm OD×0.75 mm WT and modified 9Cr–1Mo steel tube of size 17.1 mm OD × 2.3 mm WT were considered as raw materials for double clad tubes. These tubes are tested for chemical composition, surface quality and dimensions. Then the tubes were processed to obtain pre-final sizes of 6.8mm OD × 0.2 mm WT for Zr-4 tube and 8.1mm OD × 0.65 mm WT for modified 9Cr-1Mo steel tube as shown in the FIG.6. Final modified 9Cr-1Mo steel tube is normalized and tempered to achieve desired mechanical properties. After visual and dimensional inspections, Ultrasonic testing and eddy current testing were carried out to detect flaws. Mechanical properties of the accepted tubes are evaluated to find optimized process parameters in co-pilgering.

Zr-4 tube was inserted inside the modified 9Cr–1Mo steel tube after thorough cleaning. Since pilgering process uses oil for lubrication, there is a chance of oil seepage between the layers. End fusion of the liner and clad was done using electron beam welding to reduce the relative slip and prevent oil ingress between two layers. Hydraulic pressurization was then carried out to close the gap between the liner and the clad. Finally, cold pilgering was carried out to manufacture double clad tube. Typical process flow sheet for double clad tube by cold pilgering process is shown in Fig. 6.

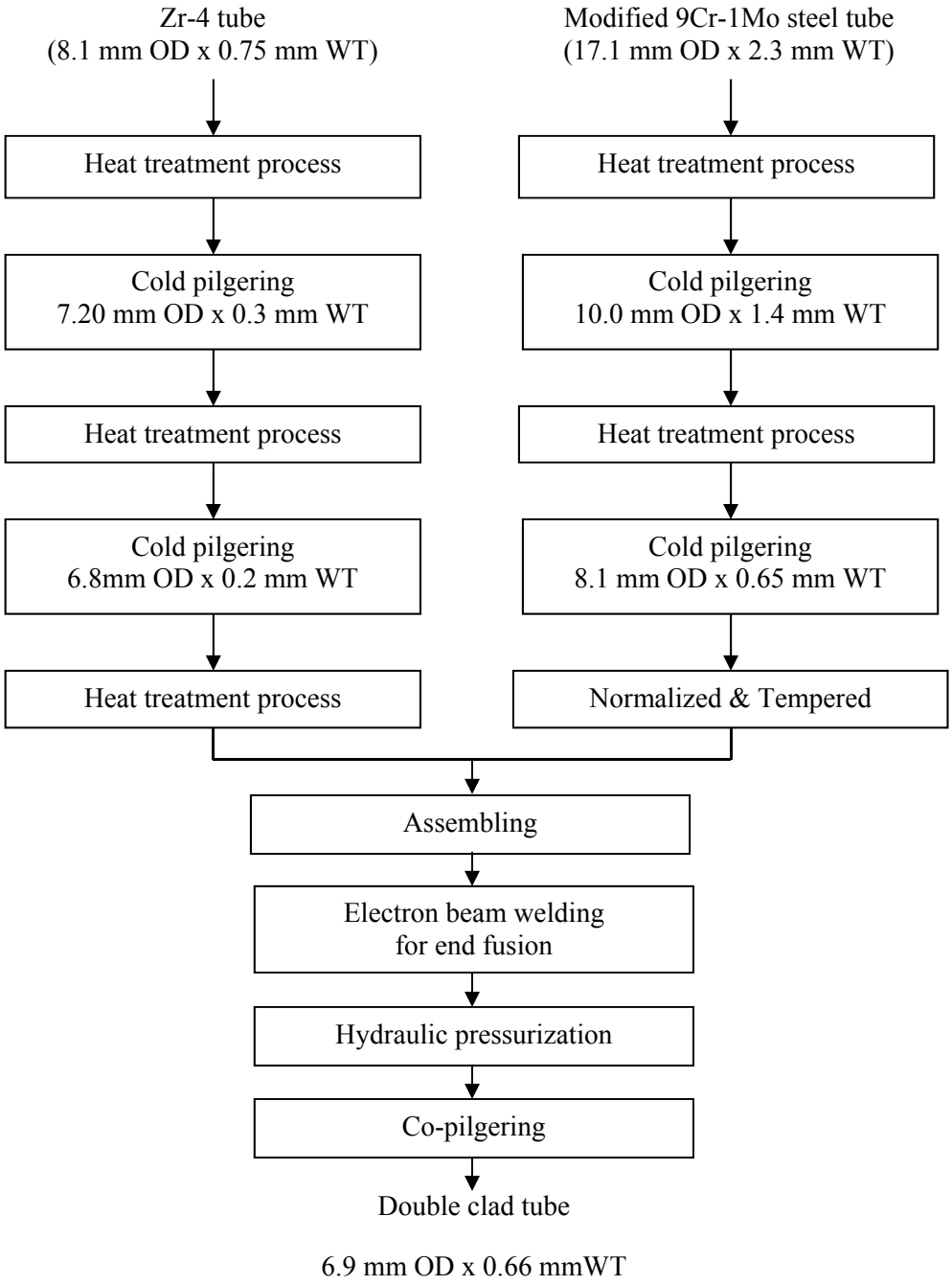

FIG. 6. Typical process flow for manufacturing of double clad tube.

7. EVALUATIONS & RESULTS

Visual and dimensional examinations, eddy current testing, surface roughness testing, bonding test, metallography and thermal cyclic study were conducted to evaluate the double clad tubes and the results were found to be satisfactory. Variation in OD was observed to be within 30 microns and Zr-4 liner thickness variation was within 15 microns. Maximum gap between clad and liner was found to be 2 microns. Eddy current testing has shown absence of gaps through the length of tube. Scanning electron microscopy (SEM) images as shown in Fig.7 have shown good bonding between the two layers.

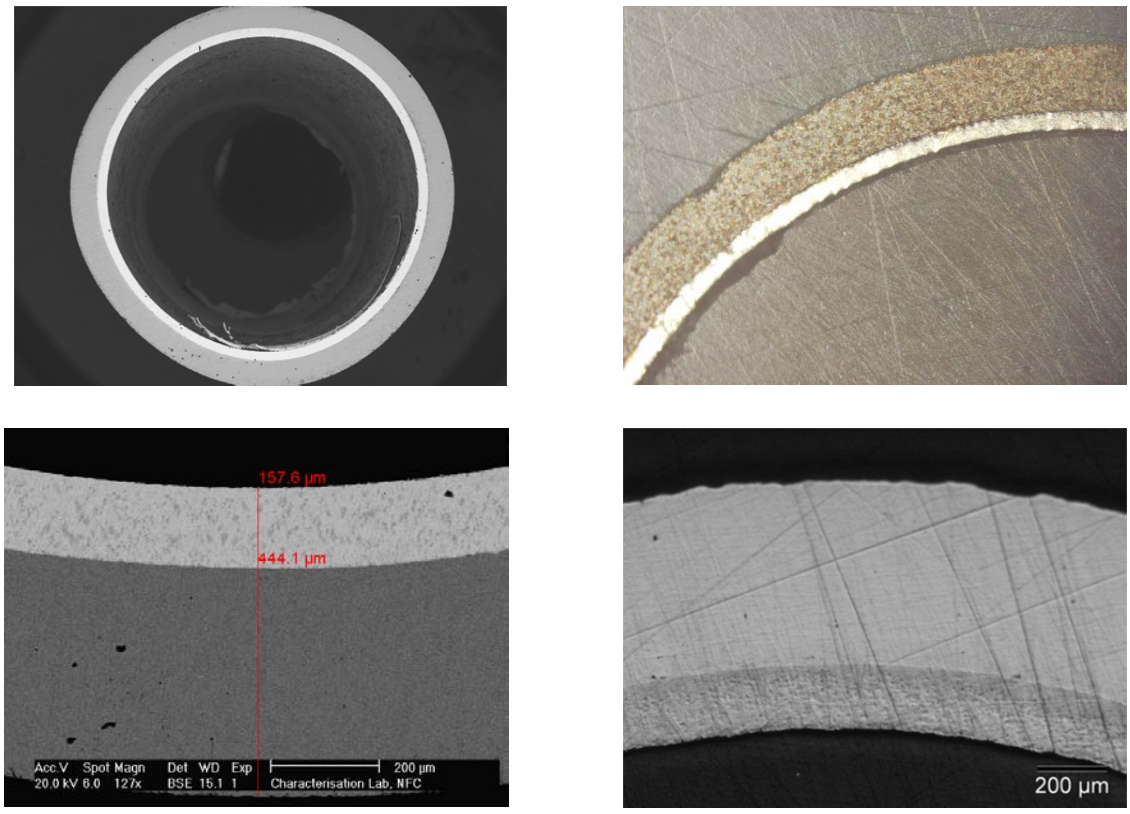

FIG. 7. Optical micrograph of double clad tube.

Another bonding test was carried out by slit opening as shown in the Fig.8. An increase in inner diameter (up to 0.06 mm) was observed after splitting the outer tube, because of elastic relaxation in liner. This infers good mechanical bonding between the clad and liner.

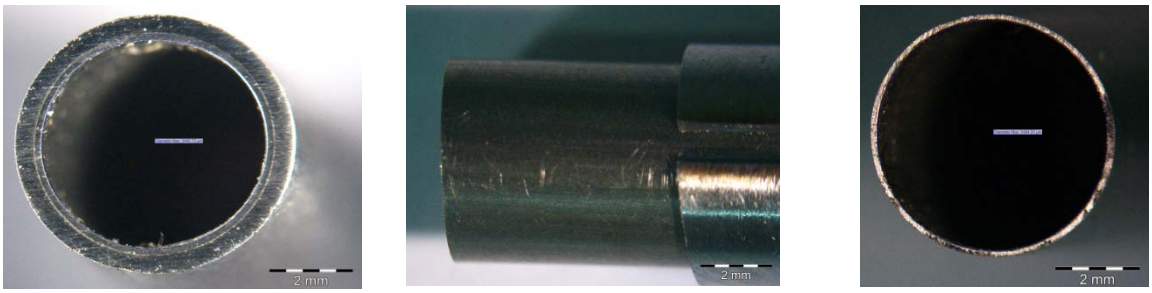

(a) (b) (c)

FIG. 8. Bonding test for double clad tube (a) as received tube (ID = 5.418mm), (b) slit opened condition and (c) after slit opening (ID = 5.484mm).

This double clad tube is also tested for cyclic heating between 500°C and 750°C as shown in the Fig.9 with heating rate of 20°C/min under flowing argon atmosphere with flow rate of 20 ml/min. After cyclic heating, it is observed that bonding between the layers is retained. The double clad tube with prototype fuel was irradiated in a test reactor and found to be satisfactory.

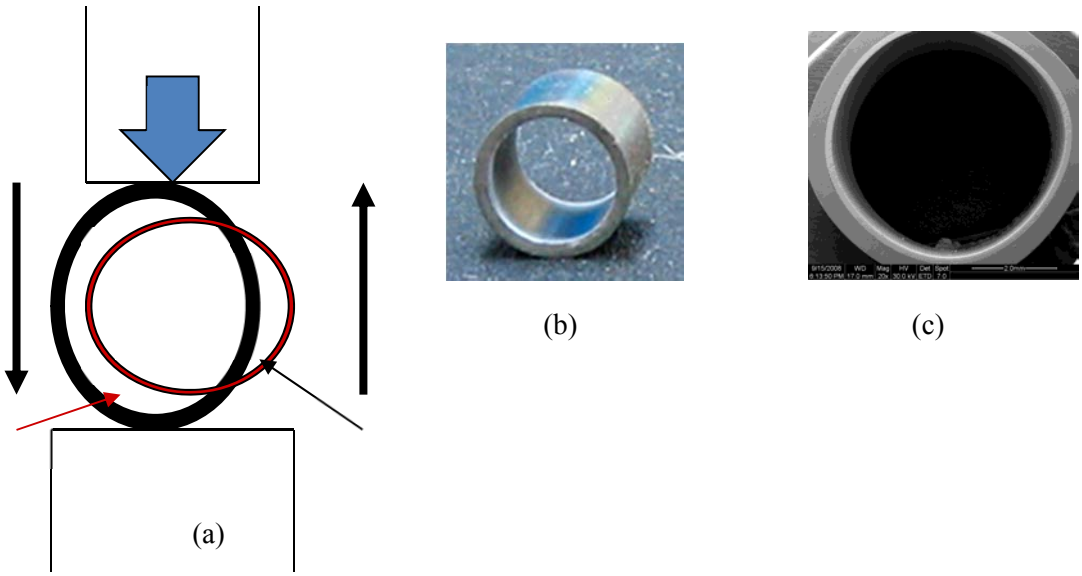

FIG. 9. Cyclic heating of double clad tube (a) Schematic testing of sample, (b) Sample before cyclic heating (c) Sample after cyclic heating.

8. CONCLUSIONS

In view of the post-accident effects in the nuclear reactors, it is crucial to develop accident tolerant fuel concepts to withstand beyond-design-basis LOCAs for much longer periods. Strengthening the clad tube without losing its compatibility with fuel or coolant is one of the principal concepts in developing ATF. Zirconium alloy as clad may not be well-suited for coolant at high temperatures. Double clad concept using appropriate dissimilar materials is most suitable for all circumstances.

NFC has successfully developed a co-pilgering process to manufacture double clad tubes with modified 9Cr–1Mo steel as clad and Zr-4 as liner. The materials are basically selected in pursuit of developing clad for Indian FBRs. Co-pilegering was selected as high compressive forces are involved in the process to give good mechanical bonding between two layers. A mathematical model was developed to find the optimized process parameters for co-pilgering. Multiple cold pilgering processes and heat treatment processes were established to obtain required mechanical properties for the clad. Double clad tube was manufactured with satisfactory bonding between the layers of clad and liner. Bonding test and SEM images confirms good bonding. Eddy current tests also prove absence of gaps in the full length tubes. These double clad tubes have shown satisfactory performance in thermal cycling and irradiation tests.

Co-pilgering can be used for manufacturing any type of double clad tubes for LWRs, PHWRs and AHWRs. Similar technology can be adopted for manufacturing cladding for accident tolerant fuel concepts. NFC is in the process of manufacturing double clad tubes through extrusion process to get good metallurgical bond between the clad tubes.

ACKNOWLEDGEMENTS

This work is supported by various organizations of Department of Atomic Energy, India such as NFC, BARC, IGCAR and NPCIL. The authors would like to express their sincere gratitude to all the scientists contributing towards the success of this project.

REFERENCES

[1] SURI, A.K., Material Development for India's Nuclear Power Programme, Sādhanā, Indian Academy of Sciences, **38.5** (2013) 859–895.

[2] ABE, H., TAKEDA, K., UEHIRA, A., ANADA, H., FURUGEN, M., "A New Fabrication Process for Zr-lined Zircaloy-2 Tubing", Zirconium in the Nuclear Industry: Tenth International Symposium, ASTM STP 1354, West Conshohocken, PA (2000) pp.425-459.

[3] KRISHNAN, R., ASUNDI, M. K., "Zirconium Alloys in Nuclear Technology", Proc. Indian Acad. Sci. (Eng. Sci.), **4.1** (1981) pp. 41-56.

[4] DIETER, G.E., Mechanical Metallurgy, SI Metric Edition, McGraw-Hill Book Company (1988).

[5] FURUGEN, M., HAYASHI, C., Application of Theory of Plasticity to the Cold Pilgering of Tubes, J. Mech. Work. Technol. (1984) pp. 273-286.

[6] HUMEL, P., FOGELHOLM, R., Simulation Model of Cold Pilgering, Journal of Materials Processing Technology **42.2** (1994) 167-173.

[7] HARADA, M., HONDA, A., TOYOSHIMA, S., Simulation of Cold Pilgering Process by a Generalized Plane Strain FEM, ASTM Standards and Engineering Digital Library (2005) 14.

[8] GHOSH, A., MALLIK, A.K., Manufacturing Science, Prentice Hall PTR (1990).

[9] ARTHUR, P.B., RICHARD, J.S., Advanced Mechanics of Materials, 6th Edition, John Wiley & Sons (2002).

ACCIDENT TOLERANT FUEL SCREENING
(SESSION 3)

Chairpersons:

A. Sowder
(EPRI, United States of America)

J. Powers
(ORNL, United States of America)

CHALLENGES AND OPPORTUNITIES FOR COMMERCIALIZATION OF ENHANCED ACCIDENT TOLERANT FUEL FOR LIGHT WATER REACTORS: A UTILITY-INFORMED PERSPECTIVE

A.G. SOWDER
Electric Power Research Institute (EPRI), Charlotte, NC
United States of America
E-mail: asowder@epri.com

Abstract

There is consensus within the global research and development (R&D) community that the barriers to deployment of accident tolerant fuel (ATF) for commercial use in the near-future are too high and carry too much risk for any one organization to succeed alone. International collaboration is needed to leverage existing and new resources and expertise. Efforts are now underway to bring key entities together to share experiences and identify gaps and opportunities to leverage resources. In the wake of Fukushima Daiichi, momentum and funding currently exist in many countries for R&D targeting enhanced accident tolerance fuel (and other non-fuel reactor components) for Generation II/III/III+ light-water reactors (LWRs) with the goal of fundamentally changing severe accident outcomes while also maintaining or even improving fuel and reactor system performance under normal operations. While funding and interest are relatively high at present, the long time frames required for implementing substantial changes to in-core components and fuel designs demand a stable and sustained R&D focus. Likewise, the geographic dispersion and scarity of key experimental and test facilities further highlight the need for coordination of experimental programmes and testing whenever possible and appropriate. Success in ATF development will come with the investment by, engagement of, and collaboration among the many key entities involved in the arduous path from early research through commercial deployment. As utilities are the ultimate customer for any new technology targeting enhanced performance and accident tolerance for LWRs, a clear understanding of nuclear plant operator needs and constraints is essential for the success of the global ATF R&D enterprise. Ultimately, the safety and performance benefits from ATF related investment will be realized only to the extent that new technologies are widely adopted and deployed in operating reactors.

1. INTRODUCTION

Research, development and demonstration (RD&D) seeking enhanced accident tolerant fuel (ATF) for light water reactors (LWRs) continues to expand. The majority fall under national programmes that individually face resource constraints and unique domestic requirements. These constraints along with down-selection pressures will inevitably leave many materials and concepts behind. Since some may hold great promise in the mid- to long-term, continued evaluation of such orphaned concepts may represent substantial value to the global ATF enterprise by keeping alternative RD&D paths open. EPRI's multi-decade experience leading international collaborative nuclear fuel research programmes, such as the Nuclear Fuel Industry Research (NFIR) program[1] has shown the value of coordinated international testing programmes for enhancing existing RD&D efforts through continued development of concepts and material testing not addressed elsewhere. Accordingly, EPRI sees the need for an international collaborative platform for testing and characterization of new materials and ATF concepts that facilitates access to and leverages the limited set of testing facilities available worldwide. This effort would focus on common need, pre-competitive data collection build upon international information sharing and assessment activities underway, e.g., at the OECD – NEA and IAEA, and is intended to complement – not compete with – current and emerging national and commercial R&D activities.

[1] The NFIR programme is entering its fourth decade and seventh phase. Its membership comprises industry leaders that include utilities, vendors and research laboratories. NFIR is focuses on providing fundamental material data to support performance and reliability of nuclear fuel and reactor core components.

2. PROBLEM DEFINITION

Changes to LWR fuel have been historically driven by clear goals, i.e., to improve fuel reliability with respect to in-service corrosion and wear and to improve fuel performance and utilization for improved economic operation via increased burnup, power uprates and cycle extension. Over 50 years of industrial experience with zirconium-based alloys for fuel cladding has resulted in a highly-optimized product that provides superior neutron economy, i.e., low parasitic absorption, manufacturability, and increased reliability even as duty and cycle lengths have increased.

The objectives for enhanced accident tolerant nuclear fuels are more nuanced and less defined – especially given the range of temperatures and other conditions enveloped by severe accident scenarios. As starting points for accident tolerant fuel development, the extension of core coolability under loss of coolant conditions and the elimination or reduction of hydrogen generation are widely recognized R&D endpoints for deployment. For accidents involving loss of active cooling for extended periods, commonly cited objectives include:

- Extending grace periods to allow more time for mitigation;
- Preserving fuel system integrity to allow reestablishment of core cooling and to maintain criticality control;
- Eliminating or significantly reducing hydrogen generation; and
- Reducing or eliminating fission product release.

As the drivers for enhanced accident tolerant fuel extend beyond those traditionally associated with nuclear fuel development, expectations for ATF expand and diverge among the many stakeholders. The three most important are:

- The regulator requiring adequate safety margins under normal, off-normal and design-basis accident conditions;
- The vendor seeking a commercially viable product that can be manufactured on an industrial scale and provides an acceptable return on investment; and
- The utility (the ultimate customer) demanding safe, reliable and economic performance under normal operations while also providing an adequate return on investment.

Meanwhile, ever present are external pressures and expectations from the public and decision-makers that can drive national policy for allocating vital resources to support early R&D, or their withdrawal. However attractive new ATF materials and concepts appear, the ultimate benefit accrues from their widespread adoption and use, which are in turn driven by the value for and compatibility with commercial operations.

The process for taking a new nuclear fuel concept from paper to batch reload in a commercial reactor is one that can require decades and involve substantial resources and business risk. Regardless of the specific design, objectives for development and qualification of new nuclear fuels remain constant [1].

- Provide fuel design specifications sufficient for manufacture;
- Understanding of fuel properties and behaviour under irradiation to define and constrain risks to ensure adequate safety for regulatory compliance and adequate performance and reliability for economic operation; and
- Demonstration that fuel manufactured according to specifications performs in accordance with licensing basis and operator requirements in real world environment.

Underlying these objectives and a successful path to commercialization are the fundamental data from testing and characterization of new materials, designs, and applications.

Important lessons have been learned from over the five decade development, industrialization, and optimization of the zirconium-based fuel system. Since the1970s, the evolution beyond early commercial fuels has included significant lag phases from design to commercial fleet-wide deployments. For example, development to deployment of mixed uranium-plutonium oxide (MOX) fuels and advanced niobium-based zirconium alloy claddings, such as optimized ZIRLO™ and M5™, spanned 20 ± 5 years [2-4]. While the nuclear fuel industry has refined the fuel development process significantly through parallel development and testing approaches, further acceleration of the fuel development process will likely be limited by stages and sequences of fixed length, such as irradiation. For example, a three-cycle irradiation of a lead test fuel assembly in a commercial reactor will likely require 5+ years followed by post irradiation examination (PIE) and analysis. And since the commercial experience with fuel qualification and licensing largely assumes compatibility with existing fuel and core designs with incremental modifications and invariant geometry, significant departures from the current fuel and core component paradigms in terms of metallic cladding, existing assembly configurations and geometries, and compatibility with coolant chemistry, may increase emphasis on irradiation programmes performed in material test reactors.

As a specific example, the development of barrier fuel to resolve severe pellet-cladding interaction phenomena leading to widespread fuel failures in BWRs in the 1970s provides several useful lessons. Development to deployment for barrier fuel spanned 13 years from 1973 to 1986 [5, 6]. Key attributes of this successful programme included:

- Narrow problem definition, i.e., fuel failure from PCI;
- Strong organizational commitment and stable leadership;
- Portfolio R&D approach to avoid dead ends;
- Early introduction of concepts into power reactors as segmented rods; and
- Aggressive testing in terms of numbers and severity.

Throughout the programme, access to testing, irradiation and post-irradiation examination facilities was paramount, which included six test reactors distributed across four countries (Figure 1):

- Japan: the Nuclear Safety Research Reactor (NSRR);
- Norway: the Halden Reactor;
- Sweden: the R2 test reactor; and
- United States: the General Electric Test Reactor (GETR), EBR II, and the Power Burst Facility (PBF) reactor.

One key lesson from this commercial programme is that even with a well-defined, commercially driven objective, development to deployment of barrier fuel for BWRs required over a decade. A second, and perhaps more poignant message from this example, comes from the simple fact that all but one of these irradiation facilities are now shut down and/or decommissioned. And while some new test reactors have come online or are under construction, the general trend is one of aging and increasingly scarce and dispersed testing facilities. The IAEA Research Reactor Database reports that over 50% of the world's test reactor fleet is 40 years or older [7].

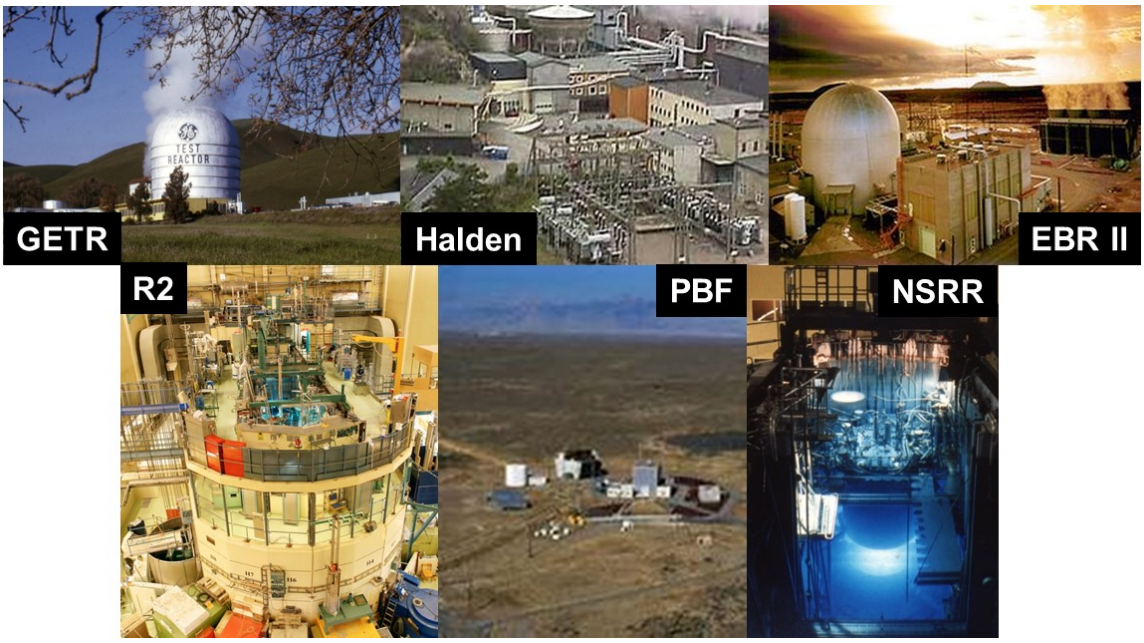

FIG. 1. Six test reactors used in GE's BWR barrier fuel development programme in the 1970s and 1980s. All but one of these reactors are now shut down (adapted from [6]).

3. CHALLENGES

Timing is a major challenge for efforts to rollout new fuel system concepts that can meaningfully enhance the accident tolerance of currently operating LWRs. The ultimate relevance of (and therefore commercial driver for) ATF with respect to existing reactor fleets is limited by economic plant life, which is incompatible with development timeframes for deployment of any new fuel/cladding. Figure 2 below is a projection of reactor retirements based on assumption of 60 and 80 year lifetimes for U.S. reactors operating in 2014.

Moreover, while post-Fukushima Daiichi support and funding for ATF RD&D are relatively high, the underlying political and programmatic support may be perishable. Therefore, it is important to demonstrate real progress in the near-term in order to maintain funding and support for longer-term efforts in the ATF RD&D domain. Bottom line is that there is a limited window of opportunity to derive substantial and compelling benefits from the adoption of ATF in the existing LWR fleet.

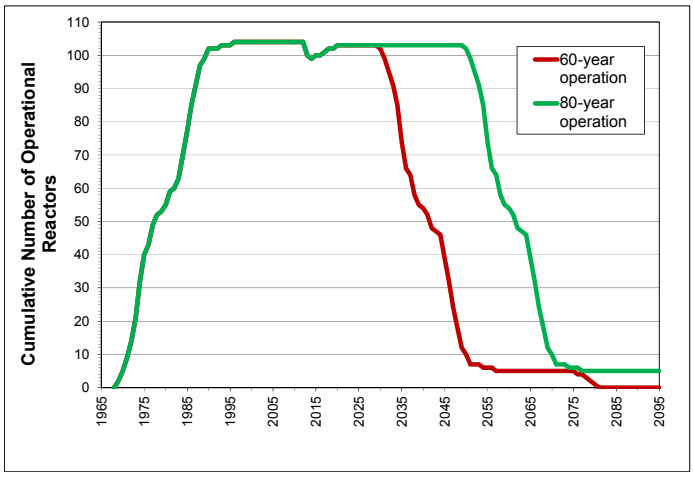

FIG. 2. Operational status for U.S. LWR fleet for 60- and 80-year lifetimes (plant data from [8]).

The scale of and resource demands associated with the RD&D effort required to bring any new enhanced accident tolerant fuel to market is enormous and will, by most accounts, exceed the resources and risk appetite of any one entity. This condition implicitly indicates the need for and value of a collaborative effort organized and executed on the international scale in order to coordinate and pool knowledge, facilities, and other resources and to avoid unintentional duplication of work.

The U.S. Department of Energy is providing substantial support for initial R&D on accident tolerant fuel concepts with an aggressive target of a lead test assembly (LTA) or rod (LTR) in a U.S. LWR by 2022 [9]. DOE sponsored work encompasses a range of fuel, cladding and coating technologies that will be narrowed through multiple gate reviews until one or two of the most promising are selected for demonstration in commercial reactors as LTAs or LTRs.

Figure 3 is a DOE graphic that offers a useful illustration of the tension that exists between the desire for nearer-term deployment and substantial, i.e., “game changing”, improvements in performance in the event of a severe accident. The figure illustrates that with marked improvements in enhanced accident tolerance comes great uncertainty, deployment times and ultimately overall programmatic risk. Given the anticipated shorter timeframes described above for existing Generation II plants, more incremental solutions appear to be the most viable. Those concepts offering the greatest potential benefit also represent substantial departures from current LWR technology and therefore also involve far greater timeframes and uncertainties.

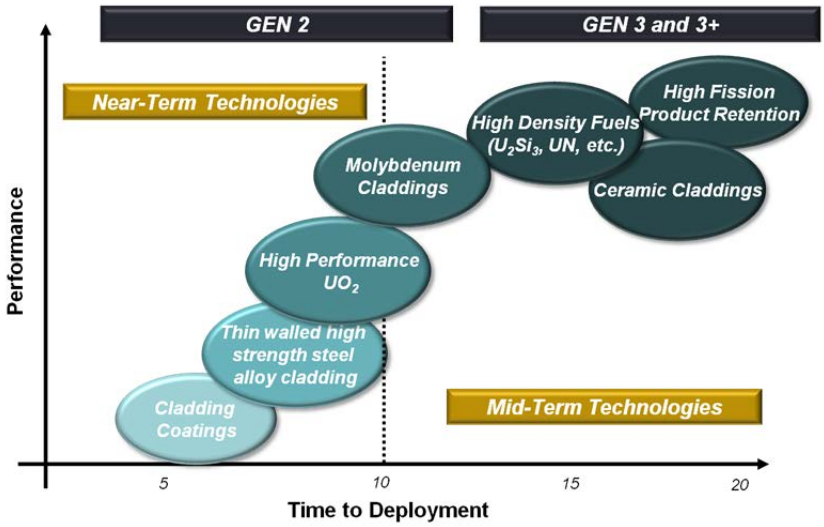

FIG. 3. Comparison of major accident tolerant fuel concepts in terms of relative benefit versus challenge illustrating anticipated relevance of technologies to current and new build light-water reactors. Adapted from U.S. DOE graphic [10].

Ultimately, DOE and other national research and development (R&D) programmes will narrow the field of candidate technologies through some down-selection process – no one has resources to simultaneously pursue all options beyond early screening and evaluation R&D.

4. GAPS

Based on extensive engagement with national and commercial interests, EPRI has identified the lack of a coordinated, international testing and characterization programme for ATF as an important programmatic gap that could delay and limit sustainability of the global ATF RD&D enterprise. This gap threatens the successful development and maintenance of ATF technology options by restricting:

- Development of promising concepts left behind following down-selection;
- Collection of fundamental material characterization data needed to support development, licensing, commercialization and operation through material and concept testing and evaluation;
- Availability of data to support use and future evolution of the technology; and
- Availability of viable alternative pathways.

Given that most major ATF RD&D programmes are – and will likely remain – nation-centric, a cross-cutting effort to leverage to the extent possible access to scare and geographically dispersed testing and characterization facilities.

5. OPPORTUNITIES

While the primary focus of RD&D to date has been on cladding and fuel improvements, there are a number of other potential paths to improve outcomes following a severe accident at an LWR that include modifications to other fuel hardware and core internals. These include BWR fuel channels, PWR assembly guide tubes, and PWR control rods and BWR control blades. Examples currently under development include SiC composite BWR channels and control rods. Another important benefit of investigating non-fuel components is the opportunity to obtain earlier introduction of and additional in-core experience with new

materials, like SiC, as these applications should prove less challenging in terms of licensing – and perhaps utility comfort as well.

More broadly, the early state of ATF technology maturity provides many opportunities for international collaboration in this pre-commercial RD&D domain. Advancing any new material or concept for use in a commercial reactor from early R&D through demonstration and deployment requires collection and analysis of a substantial amount of basic testing and characterization data. Moreover, continued testing of materials and fuels after deployment is required to address problems that inevitably arise and to support continued produce evolution and improvement. Meanwhile, unlike the original period for nuclear technology development, there may be many opportunities to benefit from RD&D in allied fields and associated with other nuclear and non-nuclear applications of new ATF materials and concepts, including:

- Generation IV fission and fusion reactor technology;
- High temperature non-nuclear power generation; and
- The aerospace industry.

An illustrative example from the aviation industry is the expanded use of carbon fibre composite materials in major structural components of commercial aircraft. Initially, carbon fibre components were deployed in limited applications, such as vertical tail and the rudder assemblies. This experience with incremental scale applications and further development resulted in revolutionary changes in aircraft construction. Carbon fibre reinforced composites comprise half of the 787 airframe [11].

6. IMPORTANCE OF GLOBAL COLLABORATION

Engagement by key international developers of new accident tolerant technologies has begun through the OECD – NEA [12] with the formation of an expert group on accident tolerant fuel for light water reactors (EGATFL). This forum is facilitating mutliple, important early activities needed to propel new materials and concepts from early R&D stages to in-core demonstration and ultimate commercial adoption. Currently, the IAEA is rolling out a new coordinated research programme (CRP) focused on ATF-related R&D [13] the Analysis of Options and Experimental Examination of Accident Tolerant Fuels for Water Cooled Reactors (ACTOF). Long-standing and ongoing international collaborative programmes of potential relevance and value for ATF efforts include the Halden Research Project [14] and the EPRI Nuclear Fuel Industry Research (NFIR) Program. Such coordination among international stakeholders is essential for more than information exchange. Rather, collaboration on a global scale can drive activities and engagement that otherwise would not take place. Such activities include:

- Sharing status of R&D plans and technology maturity;
- Establishing common understanding of metrics and criteria;
- Identifying barriers and gaps in knowledge and R&D activities;
- Sharing of basic material property data;
- Modelling and simulation exercises and benchmarking of codes; and
- Coordination of material characterization and fuel testing programmes.

7. CONCLUSIONS: EPRI PERSPECTIVE

A unique opportunity currently exists to enhance LWR fuel performance under normal and accident conditions through the pursuit of enhanced accident tolerant nuclear fuel

concepts and other core components while post-Fukushima Daiichi support remains high and funding remains available. However desirable enhanced accident tolerance appears, compatibility with commercial deployment and operation in terms of safety, manufacturability, reliability and economics remains paramount. Any new LWR fuel technology will, at a minimum, need to (1) be compatible with the safe, economic operation of existing plants and (2) maintain acceptable or improve nuclear fuel performance under normal operating conditions. Moreover, any benefits from enhanced accident tolerant fuel will be realized only with widespread commercial adoption.

Timing is critical, resources are limited, and barriers are high. Given the early stage of maturity, public sector support continues to be essential for "de-risking" the necessary RD&D in order to make commercialization a possibility. Among the global ATF community, there is general agreement that the challenge of ATF commercialization on a relevant timeframe is such that no single entity or group will succeed alone. The challenge calls for sustained collaboration to foster an environment for cooperation and innovation and to leverage limited and globally dispersed resources. Regardless of the concept or sponsor, timely and successful development and qualification of new nuclear fuels and non-fuel core components will require adequate testing and characterization data.

Ultimately, a strong pull from utility and vendor community needed for successful commercialization of ATF technologies. EPRI can facilitate this engagement and is considering an international programme based on its time-tested collaborative model to coordinate and sustain pre-competitive characterization and testing of ATF-related materials and concepts.

REFERENCES

[1] CRAWFORD, D.C., et al. An approach to fuel development and qualification. J. Nucl. Mater., **371** (2007) 232-242.

[2] ORGANISATION FOR ECONOMIC CORDINATION AND DEVELOPMENT-NUCLEAR ENERGY AGENCY, Increased Accident Tolerance of Fuels for Light Water Reactors, Workshop Proceedings, OECD-NEA Headquarters, December 10-12, 2012, Paris: NEA/NSC/DOC(2013)9.

[3] SANNEN, L., DEN BERGHE, S.V., VERWERFT, M., "50 years of Nuclear Fuel Qualification at SCK-CEN". Presentation at ENC2012, Manchester, UK: December 9-12, (2012). https://www.euronuclear.org/events/enc/enc2012/presentations/L-Sannen.pdf

[4] SABOL, G.P., ZIRLO™ – An alloy development success. J. ASTM Inter. **2** (2005) 2942-2955.

[5] ARMIJO, J.S., COFFIN, L.F., ROENBAUM, H.S., "Development of zirconium barrier fuel cladding". Zirconium in the Nuclear Industry: Tenth International Symposium. GARDE, A.M., BRADLEY, E.R., Eds. ASTM International: (1994). pp. 3–18.

[6] ARMIJO, J.S., "A perspective on accident tolerant fuel based on experience of invention, development/demonstration and commercial implementation of barrier fuel cladding". EPRI/INL/DOE Joint Workshop on Accident Tolerant Fuel, San Antonio, TX, USA (2014).

[7] INTERNATIONAL ATOMIC ENERGY AGENCY, IAEA Research Reactor Database. Report: Reactors by Age, Flux, Power and Utilisation per Year. Vienna. Accessed December 2014. http://nucleus.iaea.org/RRDB/Reports/CategoryList.aspx

[8] US NUCLEAR REGULATORY COMMISSION, "NRC Information Digest" (NUREG-1350, Volume 26), Appendices A-B: U.S. Commercial Nuclear Power Reactors - Operating Reactors. U.S. Nuclear Regulatory Commission, Volume 26: (2014-2015) NUREG-1350.

[9] U.S. DEPARTMENT OF ENERGY, "Advanced fuels campaign light water reactor accident tolerant fuel performance metrics". U.S. Department of Energy, Washington, D.C. FCRD-FUEL-2013-000264 (2014).

[10] GRIFFITH, A., "Accident tolerant fuel – overview from the U.S. Department of Energy". ICONE 22, Prague (2014).

[11] BOEING. Boeing 787 from the Ground Up. Boeing AERO Quarterly. (2006) 17-22. http://www.boeing.com/commercial/aeromagazine/articles/qtr_4_06/article_04_2.html

[12] ORGANISATION FOR ECONOMIC CORDINATION AND DEVELOPMENT-NUCLEAR ENERGY AGENCY. Start-up Meeting of the OECD-NEA Expert Group on Accident Tolerant Fuels for LWRs. OECD-NEA Headquarters, April 28 – 29, 2014, Paris. https://www.oecd-nea.org/science/egatfl/atf-public/atf2014-public/

[13] INTERNATIONAL ATOMIC ENERGY AGENCY, Summary Report. IAEA Technical Working Group on Fuel Performance and Technology Intermediate Meeting, Vienna, April 24-25, (2014). http://www.iaea.org/OurWork/ST/NE/NEFW/Technical-Areas/NFC/documents/TWGFPT/2014/Summary_Report.pdf

[14] ORGANISATION FOR ECONOMIC CO-OPERATION AND DEVELOPMENT-NUCLEAR ENERGY AGENCY. Halden Reactor Project. OECD-NEA, Paris. August 25, (2014). https://www.oecd-nea.org/jointproj/halden.html

A SAFETY ASSESSMENT FRAMEWORK FOR PROSPECTIVE FUEL TECHNOLOGIES

J.F. KELLY[*], H. DRUENNE[**], G. ROSSITER[***], J.P. MALONE[+],
A. DONALDSON[++], S. BRAGG-SITTON[+++]
[*]Thor Energy, Norway
[**]GdF-Suez, Belgium
[***]NNL, United Kingdom
[+]Lightbridge & IBC, United States of America
[++]Rolls Royce, United Kingdom
[+++]Idaho National Labs., United States of America
E-mail: shannon.bragg-sitton@inl.gov

Abstract

New technologies are being developed to improve the safety and economics of nuclear fuels for commercial water-cooled reactors. Standard fuel comprises uranium dioxide ceramic pellets sealed in a zirconium alloy cladding tube. This fuel-form serves the industry very well and has an exceptional safety record; however, it is recognized that new fuel materials and design features could provide greater levels of accident tolerance. Cost savings may also be possible once testing and qualification phases are complete and when the complete fuel cycle is considered. Nuclear utilities are the ultimate users of nuclear fuel and they put a high premium on both reliability and safety margin. Any fuel they use must offer high margin to failure in both normal and postulated accident conditions. For a new fuel variant to be viable it must be cost-effective and provide an improved safety rating as standard nuclear fuel. Significantly higher safety margins can justify a higher fuel price, but the additional margin must be attainable without requiring excessive input of resources. Determining the overall safety level for a nuclear fuel is non-trivial because it requires an understanding of how constituent materials behave during long periods in a reactor core, and this is complex due to the multiple, high energy, interdependent effects that take place. Fuel properties may even provide opposing safety merit in different conditions. Despite the difficulties, it is important for the fuel technology community to be able to assess — at least qualitatively — the safety performance credentials for the new types of fuel underdevelopment. Currently, there is no focused, peer-reviewed guidance to help perform such assessments. This paper introduces a framework of safety 'Premises', 'Principles' and 'Other Considerations' that are specifically tailored for the fuel technology community. The framework can serve as an informal methodology to help compare the safety features of different (new) nuclear fuels. It is expected that fuel developers can use this framework as a basis for suggesting appropriate formal safety assessment criteria when it comes to qualifying their fuel.

1. INTRODUCTION

New technologies are being developed to improve the safety and economics of nuclear fuels for commercial water-cooled reactors. Standard fuel comprises uranium dioxide ceramic pellets sealed in a zirconium alloy cladding tube. This fuel-form serves the industry very well and has an exceptional safety record; however, it is recognized that new fuel materials and design features could provide greater levels of accident tolerance. Cost savings may also be possible once testing and qualification phases are complete and when the complete fuel cycle is considered.

Nuclear utilities are the ultimate users of nuclear fuel and they put a high premium on both reliability and safety margin. Any fuel they use must offer high margin to failure in both normal and postulated accident conditions. For a new fuel variant to be viable it must be cost-effective and provide an improved safety rating as standard nuclear fuel. Significantly higher safety margins can justify a higher fuel price, but the additional margin must be attainable without requiring excessive input of resources.

Determining the overall safety level for a nuclear fuel is non-trivial because it requires an understanding of how constituent materials behave during long periods in a reactor core, and this is complex due to the multiple, high energy, interdependent effects that

take place. Fuel properties may even provide opposing safety merit in different conditions[1]. Despite the difficulties, it is important for the fuel technology community to be able to assess — at least qualitatively — the safety performance credentials for the new types of fuel under development. Currently, there is no focused, peer-reviewed guidance to help perform such assessments.

This paper introduces a *framework* of safety 'Premises', 'Principles' and 'Other Considerations' that are specifically tailored for the fuel technology community. The framework can serve as an informal methodology to help compare the safety features of different (new) nuclear fuels. It is expected that fuel developers can use this framework as a basis for suggesting appropriate formal safety assessment criteria when it comes to qualifying their fuel.

2. ASSESSING THE SAFETY OF NEW FUELS

New types of nuclear fuel incorporate various safety enhancement features such as more inert cladding, or higher thermal conductivity 'fuel meat' (pellet). To assess the overall safety standing for a prospective new fuel it is necessary to consider the *'fuel meat'* | *cladding* | *coolant* system in its entirety (sometimes referred to as the 'fuel system').

The OECD-Nuclear Energy Agency (NEA) has been continually assessing and revising safety criteria for standard nuclear fuel (see Appendix). An updated Technical Review of these criteria was published in 2012 [1]. The NEA document is exclusively focused on uranium dioxide fuel with zirconium alloy cladding and within this domain it provides comprehensive coverage of the safety significant considerations for such fuel. It also provides a good basis for describing safety issues for nuclear fuels more generally.

The various NEA criteria can be sorted according to five broad groups of factors that must be addressed when assessing the safety of a fully deployed fuel assembly:

- Neutronic design parameters (eg, reactivity coefficients);
- In-core behaviours and changes – induced by both chemical and physical processes;
- Mechanical factors (eg, seismic resistance);
- Activity inventory (ie, the amount of dispersible radioactivity within the fuel);
- Other factors (in particular, thermal hydraulic safety credentials).

While all safety attributes are important when refining standard nuclear fuels, it is the second group of factors concerning in-core fuel behaviours that is most useful in any comparative assessment of safety credentials for various new types of LWR fuel.

Operationally, linear heat generation rate (LHGR) limits for fuels are a global quantitative indicator of fuel safety margin, and these can be compared, but they are only established late in the fuel qualification process and thus are not relevant to the new-fuel technology community – at least until advanced testing phases are underway.

[1] For example, built-in cladding porosity may have the disadvantage of allowing a low level of fission product gas to pass through the cladding wall, while also offering the advantage of overall resistance to gross failure in beyond design basis accidents.

2.1. Focus on fuel behaviours

The developer of any nuclear fuel concept is concerned mainly with how the new fuel will behave under various operational conditions. Numerous changes are induced in nuclear fuel due to the rather harsh thermal, chemical and radiation environment in which it operates. The successful development of the fuel is dependent on ensuring that these changes do not threaten the safe operation of the reactor.

Ultimately, the concern is the release of radioactive material to the environment. It is the fuel meat itself and its cladding that provide the primary barriers to this end-point — hence the safety significance of the degradation experienced by these fuel components during in-core life and throughout long-term storage. It is important to show that the fuel performs well under both normal and postulated accident conditions when its physical properties are at their most vulnerable, and that this behaviour is both reliable and predictable.

The fuel safety framework proposed in this report comprises a comprehensive list of safety- significant fuel properties and behaviours. These apply to a wider set of fuel meat and cladding materials than those used in standard fuel; thus the framework is applicable to fuel types being developed for commercialization in light/heavy water reactors in the post-Fukushima Daiichi era.

3. A SAFETY FRAMEWORK FOR ASSESSING NEW NUCLEAR FUELS

The framework of behaviour-based fuel safety considerations was prepared as a tool for screening the safety credentials of new fuel technologies with enhanced safety features. The framework comprises:

- A set of ‘Premises’ outlining a number of fundamental fuel attributes that can be assumed as necessarily being in place — and without which no fuel is viable. Accepting these Premises simplifies the comparative assessment of various innovative fuel meat | cladding | coolant systems;
- A set of ‘Behaviour Principles’ describing the important safety-related behaviours that need to be specifically addressed when assessing the safety credentials of a new fuel type. These behaviour principles are categorized into key stages of operational life for any nuclear fuel: normal operation; accident conditions; beyond design basis accidents; and in spent fuel storage conditions;
- A number of ‘Other Safety Considerations’ that are relevant for some nuclear fuel designs, but which are unlikely to manifest as show-stoppers or differentiating factors, before the fissioning fuel material itself is shown to perform well.

In terms of using the framework, it is expected that a fuel designer will concentrate on the various fuel safety ‘Behaviour Principles’ when assessing the safety credentials for a new nuclear fuel.

3.1. Premises

TABLE 1. FUEL DEVELOPMENT SAFETY PREMISES

	Specific Considerations
Safe neutronic and thermal-hydraulic parameters are in place	- Reactivity coefficients are satisfactory; - Shutdown margin is satisfactory; - Power rating and heat transfer properties of the fuel meat and the cladding are satisfactory; - Fresh fuel enrichment limits are met (for criticality safety).
The fuel is able to be stored, moved and/or reprocessed according to national used fuel management strategies	- Used fuel can be moved to storage or other facilities with minimal risk of damage; - Able to be reprocessed - if desired; - Long term fuel behaviour is consistent with repository design.
The fuel can be designed to have a high degree of resistance to abnormal mechanical loads	- Seismic/blowdown loads can be safely absorbed; - Assembly hold-down force exceeds requirements;
The fuel can be designed such that it is mechanically compatible with existing reactor internals	- Effective debris trapping measures can be put in place.

In the safety assessment of a new fuel system, it can be assumed that these conditions are (or will be) met without difficulty. The wording of some of these Premises reflects that used in NEA criteria [1].

3.1.1. Neutronic and thermal-hydraulic parameters

Safe neutronic and thermal-hydraulic operation is so fundamentally important for all nuclear fuel that it can be assumed any proposed new fuel design will have cleared this requirement, before further development. Fuel components should have adequate resonances in the epithermal neutron energy range to ensure sufficient Doppler effect for the core to be intrinsically stable in fast reactivity accidents. Excessive neutron capture should be avoided to limit reactivity penalty and to minimize the risk of positive void coefficient or positive moderator temperature coefficient. Designed power ratings should be such that sufficient margin is maintained from the level where the cladding surface loses thermal conductivity (through dry-out).

It is assumed that new fuel designs will conform to national criticality safety regimes.

3.1.2. Used fuel management strategies

A fuel design must not contravene national used nuclear fuel management strategies in the country where it is used. There may be a requirement that the fuel can — in principle — be chemically processed to separate fission products and/or actinide components. In such a policy environment this should be possible using current technology or with processing technology that is expected to mature in time for application when needed. In any case, it should be possible to demonstrate that a new nuclear fuel form is suitable for permanent disposal in an underground facility, and also in interim, dry storage conditions.

All such conditions are assumed as being met.

3.1.3. Mechanical load resistance

Fuel must be robust at an assembly level, as well as at the fuel meat/cladding/coolant level. A fuel structure has to be able to absorb sizable impact energies without allowing breach of the fuel rods themselves. NEA criteria specify such resistance in the form of seismic loads, among other such forces.

For the purposes of developing new fuel technologies with advanced claddings and fuel matrix systems, it can be assumed that the mechanical design for any new fuel will be such that impact resistance criteria are met.

3.2. Behaviour principles

TABLE 2. FUEL DEVELOPMENT SAFETY PRINCIPLES

Fuel circumstance	Behavioural considerations
A(1). The fuel system is to retain its full integrity while operating under normal reactor conditions and during anticipated operational occurrences (AOOs); A(2). Furthermore, under normal operating conditions & AOOs, changes in the fuel system are to be slow, predictable and well within cladding failure margins.	- Cladding oxidation and hydriding; - Cladding strain, fatigue & growth; - Cladding collapse; - Cladding lift-off; - Cladding stress from fuel-meat impact; - Chemical damage to cladding from fuel-meat derived species; - Fuel-meat retention of fission products; - Fretting resistance; - Crud deposition.
B. The fuel system is to retain its bulk integrity during defined 'design basis' transient accidents involving; loss of coolant (LOCA) or reactivity insertion (RIA). Cladding breach resistance should be maintained for a number of hours after the transient. Particular attention is to be paid to fuel that has attained appreciable burn-up.	- Chemical damage to cladding from fuel-meat derived species; - Cladding stress from fuel-meat impact; - Cladding oxidation & embrittlement; - Fuel fragmentation and dispersal; - Explosive gas production; - Fuel melting &/or fuel matrix damage from localized heating.
C. The fuel system must be resistant to cladding breach failure during extended non-cooled periods (hours) comprising a beyond design basis accident (BDBA) event. Furthermore, the fuel must be able to resist dispersion of active fuel material following any such failure.	- Cladding embrittlement & strength loss; - Fuel melting; - Explosive gas production at credible temperatures.
D. The fuel is to retain its full integrity while in extended wet or dry storage following its discharge from the reactor core, and during subsequent transportation. Particular attention is to be paid to fuel that has attained appreciable burn-up.	- Strain from creep; - Oxidation & hydriding; - Gap source term.
E. The fuel should demonstrate adequate post-closure behaviours in permanent geological final disposal.	- Penetration radiotoxicity – per unit energy generated.

The behavioural considerations in the right column can serve as a useful check-list for qualitatively assessing the safety credentials of a new fuel system. The fuel circumstance groupings serve as useful operational context.

3.2.1. Fuel circumstance A: Normal operating conditions

All fuel must demonstrate high safety margins in both normal operating conditions and during 'anticipated operational occurrences' (AOO). This is a key Principle for a new fuel type and it is split into two distinct parts: the first states the obvious expectation that fuel must retain its full integrity in these situations, and the second states that its behaviours should be steady and predictable — recognizing that fuel does undergo considerable change throughout its in-core life. AOOs may result in conditions that lead to the release of activity to the reactor coolant. This may be acceptable if the activity does not lead to contravention of relevant regulatory limits. In terms of design guidance, the acceptability of these AOO-induced behaviours is inversely related to the probability of the AOO occurring and fuel failing as a result.

3.2.1.1. Cladding oxidation and hydriding

Fuel cladding undergoes chemical transformations in the high energy core environment. Oxidation and hydriding reactions can occur on metal claddings such as zirconium alloys. The reactions have safety significance because resultant oxide and hydride products can compromise the strength, corrosion resistance and heat transfer properties of the cladding barrier. Of further concern, these reactions may produce combustible products (e.g., hydrides).

Developers of fuels with cladding that is not susceptible — or has reduced susceptibility — to damaging chemical deterioration can claim a significant safety margin benefit. Resistance to oxidation needs to be considered separately to hydriding resistance. The extent of cladding interactions with a number of key reactive species needs to be taken into account, including those associated with water radiolysis and corrosion products suspended/dissolved in the coolant.

While inherent chemical inertness is always desirable for a cladding material, expectations for clad corrosion resistance can be downgraded if the operating fuel environment reduces or eliminates the corrosion mechanism, e.g., due to a particular coolant chemistry.

3.2.1.2. Cladding strain, fatigue and growth

Fuel cladding loses ductility when strained beyond an elastic limit[2]. The strain results mainly from stress imposed by fuel pellet swelling but there are also thermal expansion and fission gas pressure terms. Strain limits are established according to the specific fuel environment and design burn-up (and may even be beyond the elastic limit).

Irradiation-induced processes cause zirconium alloy fuel cladding to gradually lengthen while operating in-core. This growth is tolerable, but should not be excessive and it

[2] By way of contrast, for zirconium alloys this is ~1% strain in the circumferential direction and 2.5 – 3.5% axially.

must not result in interaction with fuel structure components at either end of the fuel assembly. The use of the term 'growth' as opposed to 'elongation' (as in NEA criteria) is deliberate since it distinguishes irradiation-induced processes from thermal expansion.

Cladding also has fatigue limits that dictate the number of power ascension cycles or local power changes (e.g. associated with control rod movements) that a fuel can safely undergo before the probability of failure exceeds an acceptable level.

New fuels can be credited with safety margin benefits if they use claddings that are demonstrably more able to accommodate these slow dimensional changes. Such cladding will ideally be less prone to irradiation-induced (axial) growth, yet have higher strain limits in the radial direction. It should also offer good power cycling tolerance. For some monolithic fuel forms the safety relevance of these behaviours may be greatly reduced.

3.2.1.3. Cladding collapse

Free-standing claddings (as in LWR fuel) should be resistant to collapsing onto the underlying fuel due to system/coolant pressure, despite the effect of the neutron flux (and associated heating). Resistance to collapse is a function of the strength of the cladding material (including that deriving from its thickness) and is also dependant on the initial internal pressure for the new fuel design.

The response of cladding creep is related to that of rapid collapse, however, creep takes place over much longer timeframes and can be beneficial to the heat removal properties of the fuel system if it occurs in a steady, predictable manner, and does not lead to unacceptable pellet-clad mechanical interaction (see *3.2.1.5.*). For this reason it is preferable to treat in-core creep separately as a distinct response in a fuel safety assessment.

For other fuels (notably those for pressurised heavy water reactors), cladding may be designed to collapse onto the underlying fuel-meat under reactor system pressure. For such fuels, cladding collapse considerations do not apply. Fuels with stronger cladding can generally claim a safety benefit. Such margin may be used to limit fuel pre-pressurization.

3.2.1.4. Cladding lift-off

A pellet-based fuel operating under normal conditions should reach its end-of-cycle life with an internal gas pressure that does not challenge the 'lift-off' limitations of the cladding material. In other words, the gap between the pellet and the cladding wall should never increase by 'ballooning' of the cladding tube due to excessive fission gas pressure. The probability of cladding lift-off can be reduced by: (i) reducing the release of volatile fission products from the fuel-meat material, and (ii) using a cladding material with high strength.

Considerable safety merit can be attributed to a fuel system if it can be demonstrated that – for normal power rating conditions – ballooning of the cladding will not occur for expected internal pressures resulting from fission gases released from the fuel-meat throughout the in-core life of the fuel. Safety assurance/margin may be derived from a high fission gas retention capability within the fuel-meat and/or high strength and ductility of the cladding material. An assessment of cladding lift-off resistance should determine the net effect of both these factors; indeed, fission gas retention capability is of such importance to a fuel safety assessment that it warrants separate consideration, as *3.2.1.7*.

3.2.1.5. Cladding stress from fuel-meat impact

Pellet-based fuel undergoing a rapid power ascent will suffer clad-tube stress from the impact of the expanding pellet and gases against the inner cladding wall – often referred to as 'pellet-clad mechanical interaction' (PCMI). This stress should be minimal, manageable, and not threaten to breach the cladding at any time throughout the life of the fuel. The effect is of concern mainly during reactivity insertion accident (RIA) scenarios; however, it can be relevant for high burn-up fuel under normal power operations. High burn-up fuel contains significant amounts of fission gas (mainly in the pellet rim) and may have lower cladding strength (due to oxidation) or increased brittleness (due to hydride precipitation).

The fuel-meat expansion is due to the combined thermal expansion from fission gases in the fuel matrix (in the rim region especially), and from expansion of the bulk fuel itself. Fission gas in the fuel rod's free-volume also expands. Resistance to PCMI can be derived from any of: lower thermal expansion tendency on the part of the fuel material; softer pellet material; lower fission gas inventory; and higher cladding ductility. Fuels incorporating material with these properties can claim some safety margin credit against PCMI damage.

3.2.1.6. Chemical damage to cladding from fuel-meat derived species

As fuel operates in normal or AOO conditions it should manifest either minimal chemical interaction between the fissioning fuel material and the cladding, and/or the chemical interactions that occur between the fissioning fuel material and the cladding should be demonstrably benign in terms of threatening cladding integrity.

Chief among the chemical mechanisms known to cause zirconium cladding damage is ‘stress corrosion cracking’ (SCC) in which aggressive chemical species (such as iodine) preferentially oxidize a metal where it is under mechanical stress, as at an incipient or existing crack.

Chemical degradation at the pellet-clad interface is referred to in the NEA criteria using the collective term “PCCI/SCC”. New fuels having higher resistance to PCCI and SCC can be credited with additional safety margin.

3.2.1.7. Fuel-meat fission product retention

Explicit consideration (further to that in *3.2.1.4* and *3.2.1.5*) of the fission product retention capabilities of the fuel meat/matrix should be taken. This is justified by the fact that deposition of fission products within the fuel causes extensive changes to its structural properties. The resulting physical and chemical effects mostly reduce the fuel's integrity.

3.2.1.8. Fretting

Fuel rods should be highly resistant to ‘fretting’ wear between cladding tube and fuel assembly contact points, and between the cladding tube and debris or foreign material that may be trapped by a structural member of the fuel such as a spacer grid. Such wear results from flow-induced movement and the resulting friction between the contacting surfaces. Analysis of the extent of this wear can be based on tribological properties of both the cladding outer surface and the contact pressure, taking into account changes in those properties that may have occurred while operating in-core.

A demonstrated resistance to fretting wear can be claimed as a safety benefit for a new fuel system. In general, the occurrence of this type of degradation is being reduced by better reactor operation practices (mainly through foreign material exclusion controls) and via novel grid, spacer and nozzle design.

3.2.1.9. Crud Deposition

"Cruds" are complex materials deriving from dissolved and suspended substances in the aqueous reactor coolant. These ill-defined materials may deposit/precipitate on cladding surfaces if water chemistry (e.g., pH), local temperature and flow turbulences allow. This typically occurs near the top of the fuel where it is associated with (sub-nucleate) boiling. Cruds form a porous layer that can capture boron from the coolant, thereby inducing local flux depression ('crud induced power shift') which in turn can cause local burn-up shadow, fuel reconditioning and rapid power ramps if the crud is dislodged.

Crud deposition has safety consequences relating to operational safety margins, including shutdown margin (through resulting burn-up redistribution). Also, cruds can be released into the coolant during or after a reactor shutdown, thereby dispersing activated material in the cooling system. This can cause dose issues during refuelling and maintenance outages, as well as the possibility of sudden local power changes when the core is returned to power.

The source of crud is not within the fuel meat, nevertheless, its build-up can depend on the material properties and local heat flux of cladding surfaces where deposition is most likely.

Fuel developers should address this phenomenon and can claim some safety credit if their fuel system is less susceptible to crud accumulation.

3.2.2. Fuel circumstance B: Accident conditions

A set of behaviour principles pertains to the response of a new nuclear fuel during accident conditions — in particular, in the two reference accident scenarios of a large-break loss of coolant accident (LOCA) and a reactivity insertion accident (RIA). These can both result in fuel materials being subjected to temperatures and stresses that approach or exceed physical design limits. The specific principles all describe physical/chemical changes that are inflicted on the fuel because of the extra energy deposited in the fuel as a result of the power transient (RIA) or absence of heat removal pathways (LOCA).

In considering detrimental chemical changes that may be inflicted on a new fuel system during a transient/accident, focus should be made on the post-event period. This is partly because such changes generally occur more slowly than the accident itself, but more importantly it is because fuel that endures an accident needs to be safely stored and managed over long periods.

3.2.2.1. Chemical damage to cladding from fuel-meat derived species

Cladding integrity can be threatened by chemical attack during power ramps and transients, as well as during normal operation (as discussed in *3.2.1.6.* above). In particular, corrosion by aggressive species (most notably iodine) at stress-induced cracks can cause rapid cladding breach and fuel failure. Certain fuel technologies help minimize this threat via better fission gas retention within the fuel material and/or by using cladding materials that are more resistant to specific stress corrosion cracking attack. Developers of

fuels incorporating PCCI resistance measures can claim an accident tolerance safety benefit.

3.2.2.2. Cladding stress from fuel-meat impact

In pellet-based fuels, PCMI can pose a serious threat to fuel integrity during transient and/or RIA accident conditions, i.e., those in which large and rapid temperature rises cause pellets and gas to expand and apply large forces on the cladding wall. This damage mechanism (see earlier description in *3.2.1.5.*) is one of the most important to understand in a RIA scenario since it can be a limiting fuel design factor.

Consideration of the vulnerability of a new fuel to PCMI in accident conditions needs to be more rigorous than when the fuel operates in normal/AOO conditions. In the more severe RIA event it is not only high burn-up 'rim structure' fuel that can inflict damaging force on the cladding wall. Other lower burn-up fuel may also threaten such damage.

The NEA defines a criterion called "RIA cladding failure", though this is a statistical concept relating to the number of fuel rods in a core that could suffer fatal PCMI and/or cladding strain failure in the event of a RIA.

As for the normal operation scenario, PCMI resistance can be derived from improvements in the properties of both cladding and fuel materials. A new fuel that is capable of demonstrating strong resistance to PCMI failure through to high burn-up levels can claim considerable safety margin credit.

3.2.2.3. Cladding oxidation & embrittlement

The resistance of a cladding to detrimental oxidation processes was considered in 3.2.1.1 for normal reactor operation conditions. In accident scenarios, however, there are distinct oxidative degradation pathways to assess, especially if the new fuel uses a metal-alloy cladding prone to high temperature oxidation. In such materials, the oxidation reaction can produce hydrogen (H_2) which can dissolve in the metal while it is at elevated temperature. This not only reduces cladding strength, but when the temperature drops the hydrogen may form metal-hydride particles that precipitate within the metal, causing it to become brittle and prone to fracture and failure.

Both oxidation rate (H_2 production) and H_2 dissolution increase with temperature, thus, licences limit the temperature that a zirconium-clad fuel can attain, both during a LOCA, and during a non-LOCA power transient event. Separate temperature limits apply for the two accident scenarios, and the NEA review [1] treats them as two distinct criteria, although the initiating cause remains the same (massive oxidation).

Degradation due to high temperature oxidation and subsequent embrittlement is of significance well after a RIA event. A new fuel surviving a RIA will need to be safely stored for long periods during which its strength/integrity needs to be assured.

Fuels can acquire resistance to this degradation pathway by using cladding material/s that offer any or all of: (i) reduced potential for reacting with water to produce H_2; (ii) reduced solubility of H_2 in the cladding material; (iii) reduced potential for forming hydride phases; (iv) greater overall mechanical strength.

Such resistance can be credited as a significant safety feature.

3.2.2.4. Fuel fragmentation and relocation

High burn-up pellet fuel has a tendency to fragment, particularly around the pellet rim. If this occurs, fuel pieces can relocate to areas where cladding lifts away from the fuel, as may occur during a LOCA or RIA. In a subsequent event where the cladding ruptures, fragmented fuel can be dispersed, potentially worsening radiological consequences. In the event that fuel has ballooned during the LOCA, but not ruptured, internally relocated fuel pieces can cause 'hot spots' that exceed cladding temperature limits.

Certain new fuel technologies may offer resistance to this degradation behaviour by virtue of any or all of: (i) greater fuel-meat toughness (less tendency to fragment), (ii) pellet-clad bonding, or (iii) a lower tendency for the cladding to balloon. Such resistance provides safety margin credit in LOCA scenarios.

3.2.2.5. Explosive gas production

A low thermo-chemical potential for producing hydrogen (H_2) or other explosive gases is a highly desirable feature for any new fuel type. Safety margin credit can be claimed for fuels using cladding material that is less inclined (than zirconium alloys) to chemically react to produce H_2. Particular attention should be paid to exothermic reaction pathways with steam at high temperature, since these may lead to positive feedback energy production loops during accidents.

3.2.2.6. Fuel melting & fuel matrix damage from localized heating

Fuel safety criteria specify that no part of a fuel can melt in the event of a power transient (or during normal operation). This is a conservative rule since it has been established that localized melting within a fuel pellet does not necessarily cause overall fuel failure. Nevertheless, the no-melt criterion remains an appropriate regulatory guideline since it rules out overheated zones, molten fuel-to-cladding contact, and piercing risk.

For fuels with non-homogeneous fuel-meat, i.e., those with appreciable 'granularity' and/or two distinct phases, a safety assessment should take into account whether partial melting of distinct phases may be possible within the fuel-meat, and/or whether the fuel matrix is damaged (without melting) by localized deposition of heat in the fuel meat, e.g., near fissile-rich particles. A further consideration is that of the possible existence of eutectic mixtures of fuel-meat components and whether these may cause low temperature melting regions within the fuel.

A higher margin to melting and heat damage can be derived from a higher melting point for the fuel-meat (and associated eutectics), and/or a lower operating temperature for the fuel in normal and AOO conditions (this stemming mainly from higher thermal conductivity).

3.2.3. Fuel circumstance C: Beyond design-basis accidents

A new nuclear fuel system must manifest a satisfactory response during a beyond design basis accident (BDBA) scenario. Such accidents are not defined explicitly, but can be regarded as rare, extreme cases of a LOCA (or RIA + LOCA) event in which the fuel experiences high LOCA-type temperatures for an extended period – longer than a few hours. In such severe conditions a fuel can be expected to degrade.

The BDBA safety performance of a new fuel should be assessed according to: (a) the time it can resist failure; (b) the amount of activity it is likely to release upon failure in the extended LOCA conditions; and (c) the mechanistic nature of the failure and whether this

leads to or contributes to the dispersal of activity (e.g., if coupled to melting or gas detonation processes). Assessing the BDBA safety performance for a new nuclear fuel system requires the use of credible time-temperature accident progression predictions that have been generated for the particular fuel/reactor system. Fuel performance analysis for regulatory licensing purposes can refer to the fact that such beyond design basis accidents for reactors are very rare.

3.2.3.1. Cladding embrittlement and strength loss

As noted for the fuel behaviour principle *3.2.2.3.*, cladding embrittlement is the result of extensive oxidation of metallic (e.g. zircaloy) cladding materials at high temperature. The metal picks up hydrogen while at elevated temperature and hydrides precipitate when the temperature drops, resulting in a loss of strength. Higher resistance to oxidative cladding degradation will give a new fuel better BDBA tolerance.

3.2.3.2. Fuel melting

Fuel systems (i.e., including cladding) with a higher melting point and/or higher thermal conductivity are inherently advantageous in terms of the time before parts of the fuel will melt after an extreme/beyond design basis LOCA. A safety advantage can be claimed against this principle for new fuels that may be less inclined and/or slower to melt in a severe BDBA scenario; however, it is not possible to extrapolate such an advantage to a broader claim of resistance to fuel damage in general. See the description for fuel life stage 3.2.2.6 explaining the fuel melting issue in transient conditions, including consideration of eutectics and fuel granularity.

3.2.3.3. Minimized explosive gas production

As described in *3.2.2.5.*, a low thermo-chemical potential for producing hydrogen or other combustible gas is a desirable feature for any fuel system. This principle has even higher significance in the BDBA scenario due to the large volumes of hydrogen that can be rapidly generated in such conditions. Safety margin credit can be claimed for fuels using cladding material that has a limited tendency to react to produce gases that have the potential to cause explosive reactions such as carbon monoxide and H_2.

Particular attention should be paid to exothermic reaction pathways with steam at high temperature since these lead to positive feedback energy production loops during severe accident scenarios.

3.2.4. Fuel circumstance D: Post-discharge storage

A new nuclear fuel system must behave in a safe and predictable manner in all conditions in which it is to be stored and transported in the period after fuel is discharged from its reactor core. Fuel technology developers must take into account the safety relevant changes that can take place in the used fuel form. Consideration should be given to both wet and dry storage conditions and also to the impact on/by handling operations therein.

3.2.4.1. Strain from creep

A fuel system must have adequate mechanical strength after it has been discharged from a reactor core. It is particularly important that this strength imparts high resistance to creep strain caused by stresses associated with gas pressure within used-fuel rods during the first decades of dry storage. During this period decay heat production is still high and can

result in high fuel rod temperatures which may facilitate cladding creep mechanisms and increase the overall creep rate. A fuel technology developer should assess creep strain vulnerability at the time of discharge and also whether this vulnerability changes over any extended storage period, factoring in the heat transfer capabilities of the storage system.

Demonstrated adequacy of long-term mechanical strength is an important safety attribute for a new fuel system in the context of its post-discharge handling.

3.2.4.2. Oxidation and hydriding

A key cause for the weakening of zirconium alloy cladding in used fuel over long periods is the formation of microscopic hydride phases. These hydrides can lead to excessive embrittlement directly (such that the cladding can fail during handling) and/or they may cause a damage phenomenon called delayed hydride cracking. The latter damage pathway is of concern mainly in dry storage conditions — existing circumferential hydrides dissolve at the start of dry storage (or during any prior vacuum drying) when clad temperatures are high, then re-precipitate as radial hydrides at a later date when the decay heat, and hence clad temperatures, fall. This only occurs when the clad hoop stresses are sufficiently high at the time of re-precipitation (since otherwise the hydrides tend to re-precipitate in a circumferential direction, in which case they are no more damaging than the original hydrides formed during irradiation).

A demonstrated resistance to this or any other type of chemically driven degradation is a positive safety attribute for any new fuel system.

3.2.4.3. Gap source term

Source terms are not normally regarded as being operational safety criteria, however, for used nuclear fuel in extended storage it is important to consider the quantity of each of the fission nuclides that are most easily released from the fuel matrix to the remaining internal space of the fuel rod (gap source term). In oxide fuel it is volatile/mobile caesium and iodine isotopes that are of key concern. Despite having a high activity and yield, the vast majority of strontium is retained within the fuel matrix and so does not contribute significantly to the gap source term. Estimation of nuclide inventories should be made at various points in time after discharge – up to ~50 years – such that these can be assessed and compared when fuel movements are foreseen.

Comparison of this source term between different fuel system designs at the end of their service life is of considerable interest to regulators, since it is a determining factor in the threat posed by the loss of fuel integrity during storage (and transport). A lower gap inventory of caesium and iodine will be considered as a safety-positive feature for a new fuel.

3.2.5. Fuel circumstance E: Long-term storage

To properly assess the viability of permanent disposal of a fuel in a geological repository, specific consideration needs to be made of: (a) the inventory of spent fuel per unit of energy generated; (b) the mass fractions of each radionuclide (including fission products, actinides, and activation products); (c) the instant release fraction of each radionuclide; (d) the fuel matrix dissolution rate; (e) transport of the radionuclides in groundwater; and (f) the dose uptake by each of the various uptake mechanisms for each of the released nuclides. The nuclides ^{129}I, ^{135}Cs, ^{36}Cl, ^{59}Ni and ^{14}C are particularly important, but new fuel types may differ in these ‘key’ isotopes from a dose uptake point of view.

3.2.5.1. Penetration radiotoxicity

Penetration radiotoxicity is an expedient measure of the radiotoxicity of the suite of radioisotopes that are released upon the postulated penetration of a used fuel canister by groundwater. This metric is derived by assessing factors (a) to (c) in the previous paragraph. It includes consideration of an 'instant release fraction' which typically includes contributions from the rod free volume, the cladding (pessimistically assumed to have corroded away before spent fuel canister penetration) and fuel grain boundaries. A new fuel demonstrating a high fission product retention capability will have a lower penetration toxicity, thereby offering a safety benefit. In principle, a more robust cladding could also be counted towards a lower penetration toxicity.

The longer term release of radionuclides (in particular the actinides) occurs by fuel matrix dissolution in groundwater (issue (d) above), so a more insoluble fuel matrix can serve as a separate safety credential for new nuclear fuel concepts.

3.3. Other safety considerations

TABLE 3. ADDITIONAL SAFETY CONSIDERATIONS FOR FUEL TECHNOLOGY DEVELOPERS

		Specific Considerations
A.	Self-healing/annealing of radiation damage.	- There may be extra resilience for new fuel materials in the high power context; - A self-annealing capability may be absent at low power, possibly impacting safety behaviour in an under-rated operating mode.
B.	Operability of the fuel in a transition core.	- Compatibility of new and existing fuel-types co-residing in the core.
C.	Satisfactory safety-related behaviour of failed fuel.	- Fuel matrix leachability.

3.3.1. Self annealing

Nuclear fuel operates in a severe environment and sustains extensive structural damage to material lattices due to the impact of high energy particles and fission fragments. Nevertheless, there is a competing reverse process in which the particle flux causes a degree of self-annealing and repair of some lattice defects. Self-annealing effects are temperature and flux dependent but it is not possible to reliably predict their extent. Different fuel materials are expected to manifest different levels of self-healing and it may be possible to claim a safety margin benefit if this can be demonstrated.

On the other hand, it is possible that if a fuel system is operated with an unusually low power rating (lower fluxes and temperature) this could have a negative impact on fuel behaviour and safety, because the self-healing processes occur to a lesser extent. This is probably unlikely, but it highlights a need to assess the safety performance of a new fuel-type in operational conditions that include lower-than-standard/full power ratings.

3.3.2. Transition core

A new fuel design must be compatible with current fuel types since it will generally be phased in over several core reloads. A compatibility assessment must address: neutronic aspects, thermal hydraulic aspects and chemical compatibilities.

3.3.3. Failed fuel

Nuclear fuel is deemed to have failed if its cladding becomes ruptured and radioactive material leaks into the coolant/moderator. In such an event remedial action may be taken (in BWRs) by the reactor operator to minimize the amount of radioactivity released by the failed fuel rod. No feature of a new nuclear fuel system should impede such remedial action. Conversely, a fuel that limits further activity release after a cladding breach can likely claim a safety benefit for such a feature.

In the event that a fuel rod loses integrity and is exposed to the coolant, volatile fission products will escape from the gap/rod plenum, as will some fission products on the surface of the exposed fuel-meat. Different fuels have different leachabilities of fission products and actinides from the fuel matrix and this will generally result in differing levels of safety credit.

4. FUTURE FUEL SAFETY ASSESSMENT APPROACHES

A framework for qualitatively assessing the safety credentials for new nuclear fuels has been outlined in this report. At its heart is a comprehensive list of safety significant 'Behaviour Principles' that are grouped according to how the fuel should perform in different operational and storage conditions. Addressing each of the fuel safety principles can be done on a stand- alone basis or with reference to standard zirconium alloy clad uranium dioxide fuel. Judging fuel safety attributes in this manner yields a 'safety matrix' that could facilitate and standardize discussion of the relative merits for various LWR and PHWR fuel technologies currently under active development.

Eventually, fuel safety performance claims must be demonstrated experimentally. Nuclear operators and the regulatory community will expect that qualitative safety margin assessments for new fuel systems are backed up by physical data from instrumented irradiation trials and post-irradiation examination. The material property / behaviour information deriving from new-fuel performance tests will enable developers and future users to get an idea of eventual operating limits for the fuel-system in question. Nonetheless, given the disparate nature of the new nuclear fuel systems being studied for commercial LWR deployment, it is not currently possible (or desirable) to set quantified safety limits on either: (i) material properties or the extent of irradiation behaviours specific to a new fuel system (or component thereof); or, (ii) reactor operating limits that are based on specific new fuel properties or behaviours.

4.1. Towards quantified limits for new nuclear fuels

At some point, however, there will be an appetite among the fuel development community for quantitative guidance on the 'safe behaviour envelope' for specific new-fuel materials &/or material arrangements in advanced fuel systems. This is a laudable goal but it will take time to; perform the targeted irradiation testing (including in simulated accident scenarios), undertake the PIE, analyse results, and, translate the data into relevant limits.

After new fuel-systems have been tested more extensively in power reactor conditions, linear heat generation rate limits can be derived and these should have value in comparing

new fuel systems that have advanced closer to commercialization. Another possible pathway to quantifying fuel safety credentials is by linking their performance to current probabilistic safety cases for the reactors in which the fuels (will) operate. As an example of such reasoning:

Standard fuel can withstand temperatures below W°C indefinitely and can withstand a higher temperature of X°C for T_1 minutes in a steam environment. A reactor safety case may demonstrate a very low probability of beyond design basis accidents giving rise to temperatures higher than X°C, or to temperatures above W°C but below X°C for periods longer than T_1 minutes. Now consider an advanced fuel that can safely withstand higher temperatures of Y°C (>X°C) indefinitely, or Z°C (>W°C) for a time T_2 minutes in a steam environment. The reactor safety case may demonstrate that the probability of exceeding these more severe conditions is significantly lower than the probability corresponding to the conditions justified for the standard fuel. Such quantification in terms of a probability difference establishes a case in favour of adopting the superior fuel.

It is evident from the various safety-significant fuel behaviours presented in this report that determining overall safety levels for different nuclear fuel systems is not trivial. Nevertheless, in order to qualify an advanced fuel it needs to be rigorously assessed in terms of its safety-related behaviours in operational, accident and storage conditions. This framework should be a useful tool for efficiently performing initial safety credential assessments for new nuclear fuel systems.

ACKNOWLEDGEMENTS

The authors thank the World Nuclear Association for initiating a project to examine the issue of how 'enhanced safety' nuclear fuel systems should have their safety credentials assessed.

REFERENCES

[1] OECD-NUCLEAR ENERGY AGENCY, Nuclear Fuel Safety Criteria Technical Review (second edition), Paris (2012), ISBN 9789264991781, http://www.oecd-nea.org/nsd/reports/2012/nea7072-fuel-safety-criteria.pdf.

[2] OECD-NUCLEAR ENERGY AGENCY, Nuclear Fuel Safety Criteria Technical Review, results of OECD/CSNI/PWG2 Task Force on Fuel Safety Criteria, NEA/CSNI/R(99) (2000), http://www.oecd-nea.org/nsd/docs/1999/csni-r99-25.pdf.

Appendix

OECD-NEA TREATMENT OF FUEL SAFETY CRITERIA

In 2000 the NEA published a review of existing nuclear fuel safety criteria [2] focused exclusively on fuels for current LWRs. A key aim of this exercise was to determine whether these needed re-definition in order to be applied to 'new' nuclear fuels. Twenty existing criteria were analyzed according to: (i) their relevance to normal, transient and/or accident conditions, and (ii) their relevance to various 'fuel design elements' / fuel technology directions (e.g. new cladding alloys, MOX use). The philosophy of the study was to question how fuel design elements affect fuel criteria, not vice versa.

After several years' work to update the safety criteria, NEA approved a revised listing in December 2011 — complete with more detailed descriptions of the various criteria and their relevance to different operating and accident conditions. A set of 'Other Considerations' is also included, describing issues that are relevant to safe fuel performance but not being criteria in themselves. Examples of these non-universal considerations include the impact of certain core management practices, and issues relating to the use of MOX fuel. These updated criteria were published in mid-2012 [1].

TABLE A.1. NEA FUEL SAFETY CRITERIA, LISTED IN THE RIGHT HAND COLUMN EXACTLY AS PUBLISHED IN [1]. THEY ARE GROUPED ACCORDING TO A NUMBER OF ARBITRARY CATEGORIES

Arbitrary grouping	NEA fuel safety criteria
Neutronic design & handling	Reactivity coefficients, Criticality & shutdown margin, Critical heat flux, Fuel enrichment
In-core behaviours & changes	Oxidation & hydriding, Stress/strain/fatigue, Rod internal gas pressure, Thermal-mechanical loads & PCMI, Pellet cladding interaction (PCI), Fuel melting, RIA cladding failure, Fuel fragmentation, Non-LOCA cladding embrittlement/temperature, LOCA cladding embrittlement, Crud deposition
Mechanical factors	Seismic/blowdown/transportation loads, Assembly hold-down force, Fretting wear
Activity inventory	Source term, Gap activity, Coolant activity
Other	Burn-up, LHGR Limits

PRELIMINARY ASSESSMENT OF SEVERAL CANDIDATES ACCIDENT TOLERANT FUEL

Y. WANG, T. LIU, Q. REN
China Nuclear Power Technology Research Institute
Shenzhen, Guangdong
China
E-mail: liutong@cgnpc.com.cn

Abstract

After the Fukushima Daiichi events, the enhanced accident tolerance fuel became a hot topic. This paper analyses three candidate fuel systems FCM-SiC, U_3Si_2-SiC, and UO_2+BeO-FeCrAl. Through the analysis shows that they have better performance than UO_2-Zr system during the LOCA and SBO conditions. During the LOCA condition, the cladding's peak temperature of FCM-SiC system is lower than standard UO_2-Zr system 257K. The amount of hydrogen generated is also decreased due to the stability of FeCrAl and SiC. All fuel systems's failure time have been put off. The fast failure system is UO_2+BeO-FeCrAl during SBO condition. It's still 2000 seconds later than the standard UO_2-Zr system. By the preliminary analysis shows that FCM-SiC is the best one.

1. INTRODUCTION

In the post-Fukushima Daiichi era, enhancing the accident tolerance of LWR becomes a hot topic. During severe accident condition, the performance of the fuel is top priority for the reactor's tolerance. As a result, the U.S. Congress directed DOE-NE to give "priority to developing enhanced fuels and cladding for light water reactors to improve safety in the event of accidents in the reactor or spent fuel pools" [1].

Accident tolerant fuels are defined as fuels that can tolerate a severe loss of active cooling in the reactor core for a considerably longer time period than the current UO_2/Zr system. There are several desired ATF attributes:

- Improved Cladding Properties:
    - Low heat of oxidation and oxidation rate;
    - Low steam interaction during the high temperature;
    - High strength and thermal conductivity.
- Improved Fuel Properties:
    - Low swelling;
    - High strength, thermal conductivity and melting point.

The R&D of ATF is a technological revolution which will promote the upgrading of fuel system. Since 2013, many nuclear power organizations of the world have invested a lot of manpower and financial resources to ATFs. As a new research, China also pays high attention to this study. At the sixth Round of the China-US civil nuclear energy cooperation action plan in August 2013, a special working group was established to focus on ATFs. By the end of 2013, China National Energy Administration held the first "Accident Tolerance Fuels Technology Seminar" in Shenzhen. Participating units include:

- Companies: CGNPC (China General Nuclear Power Group), CNNF (China North Nuclear Fuel), etc.;
- Research institutes: CAS (Chinese Academy of Sciences) , CAEP(China Academy of Engineering Physics), etc.;

- Universities: Xi'an Jiaotong University, National University of Defence Technology, etc.

During this meeting, there are extensive discussions of the international and domestic experience on the development of advanced cladding, pellet, fuel design, materials and processing technology. They agreed that "We need make enterprise as the main body of innovation, the demand of industrialization as the traction to call all possible resources and technologies to focus on the R&D of ATF"

As the initial sponsor in china, CGNPC proposed several materials. The purpose of this paper is to illustrate the performance of the candidate fuel/cladding materials during the BDBA (Beyond design basis accident) conditions. Section 2 provides a brief overview of thermal properties. Section 3 presents the performance of ATFs during BDBA.

2. CANDIDATE MATERIALS AND PROPERTIES

2.1. Several candidate pellets

According to current status of the study, the candidate pellets can be divided into two categories: improved technology, innovative technology. Improved technology is based on the current mature technology to improve the performance. It is focused on pellet's microstructure, preparation technology and additives. Compare to current UO_2 material system, Innovative technology use a new uranium compounds. Such as U_3Si_2, UN and UMo alloy. There are some candidate pellets:

2.1.1. UO_2+BeO

$BeO+UO_2$ is the representative of improved technology. It's UO_2 doped with a small amount of BeO to form a two-phase mixture. The amount of BeO must be controlled within a certain range to reduce the loss of uranium loading. To enable the thermal conductivity of the pellets is significantly improved, the BeO should form a continuous phase in the two-phase mixture [2]. Since actual data for the $BeO+UO_2$ are not currently available, except we assume the physical properties consistent with UO_2 except thermal conductivity.

2.1.2. U3Si2

As a representative of innovative technology, U_3Si_2 has the following advantages: high uranium density (11.3gU/cm^3); high melting point (1665℃); high thermal conductivity (twice the UO_2 at room temperature); good compatibility with the coolant; and low coefficient of thermal expansion etc. [3]. The only one caveat is that the irradiation swelling will significant increase when the temperature exceeds 500℃.

2.1.3. Fully Ceramic Microencapsulated (FCM) Fuel

The concept of FCM fuel was initially from the high temperature gas cooled reactor fuel TRISO. TRISO fuel has decades of application experience, a high degree of technical maturity, so FCM pellet also has good feasibility.

2.2. Candidate claddings

2.2.1. SiC

Compare to zirconium alloy, SiC has obvious advantages during accident conditions. Resistance to irradiation and high thermal conductivity can make it take longer cycle or higher power density than Zr. In addition, SiC still with good strength at 1300℃ and its economy of neutron is good for about 25% than the zirconium alloy [4, 5, 6 and 7]. Although SiC has many advantages, there are many problems must be studied, such as the tube's sealing and welding, processing precision.

2.2.2. FeCrAl

As a highly promising PWR cladding material, FeCrAl has excellent comprehensive performance. It has good mechanical properties, higher strength and toughness than Zr, excellent machining and welding properties. Under high temperature conditions, it will form an aluminium oxide layer on its surface so as to has a good corrosion resistance during high temperature steam.

2.3. Thermo-physical properties of candidate materials

In this study, we assumed the properties of FCM and SiC are same, because there are no actual data of FCM. This is a reasonable assumption since the FCM fuel pellet is largely SiC [8]. Due to the lack of vaild datas, we think the other properties of UO_2+BeO are consistent with UO_2, expect the thermal conductivity.

Thermal conductivity is a key parameter, during analysis the fuel rod performance. It determines the temperature gradient and the heat transfer between the fuel and coolant. By the influence of temperature, it also affects the mechanical and the thermodynamic state. High thermal conductivity will reduce the centreline temperature to avoid the melting of the pellets and claddings. The thermal conductivity and melting point are shown in Figs 1 and 2.

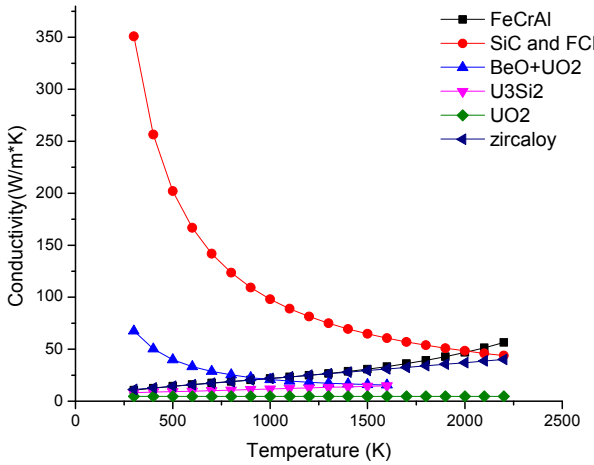

FIG. 1. Thermal conductivity of candidate materials.

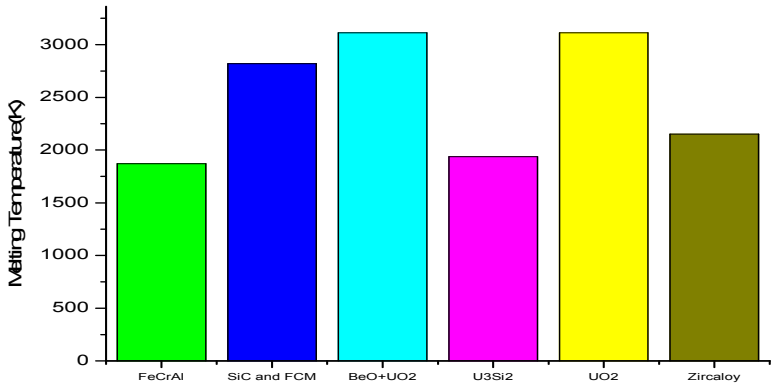

FIG. 2. Melting temperature of candidate materials.

As shown above, the thermal conductivity of FCM is the highest but with the rise of the temperature it dropped rapidly. The melting point of FCM is the highest in candidate cladding materials. Although the U_3Si_2's melting is lower than UO_2, its high conductivity will reduce the centreline temperature. Section 3 presents the detailed analysis results.

Volumetric heat capacity (VHC) describes the ability of a given volume of a substance to store internal energy while undergoing a given temperature change. It plays a critical role in LOCA condition. The higher VHC, the lower temperature rising. The density and specific heat of the candidate materials are shown in Figs 3, 4 and 5.

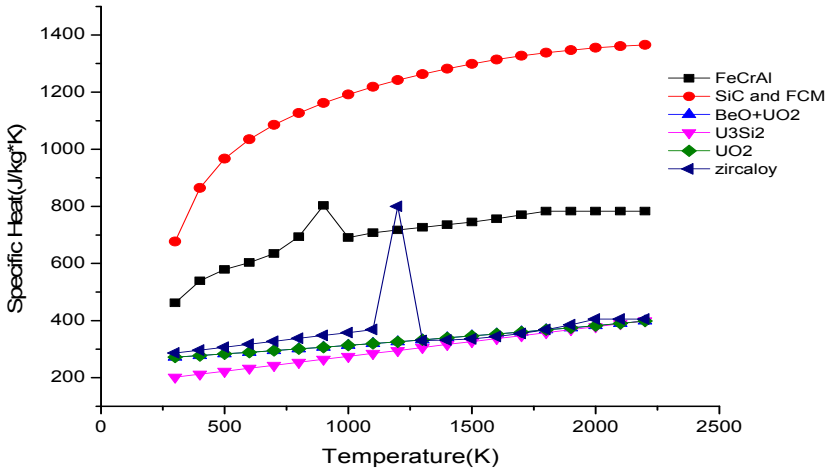

FIG. 3. Specific heat of candidate materials.

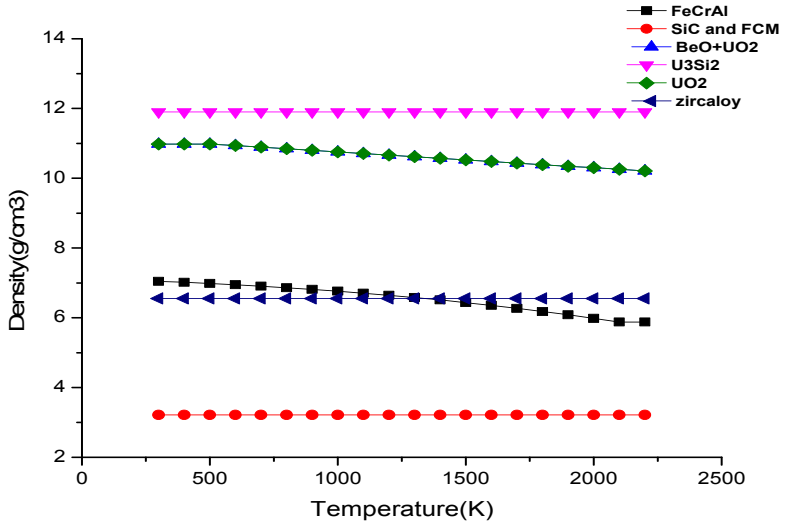

FIG. 4. Density of candidate materials.

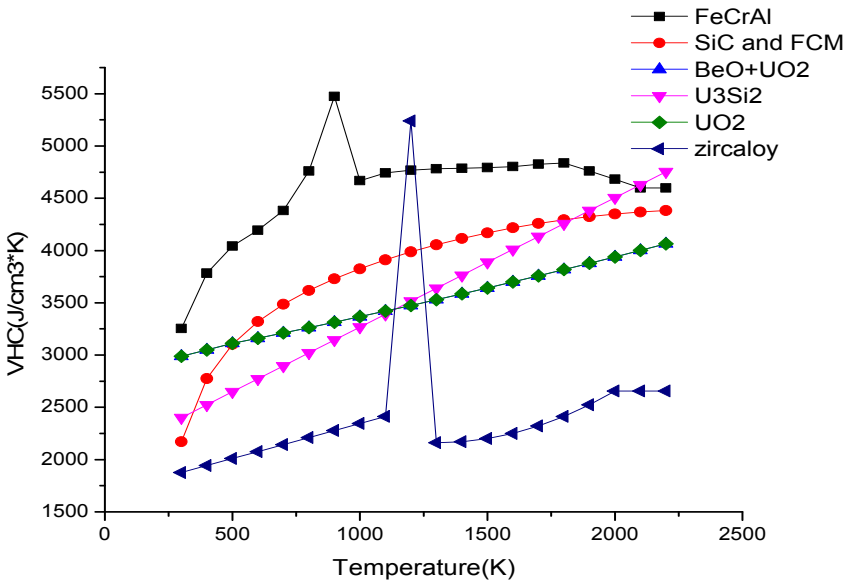

FIG. 5. VHC of candidate materials.

From figures we can see that FeCrAl has the highest VHC than other candidate materials and FCM is the second. Therefore, when the same volume of candidate materials absorbs the same energy, the temperature of FeCrAl is smallest. But we have to consider the impacts of other properties. The further analysis is provided in section 3.

3. PERFORMANCE DURING ACCIDENT ANALYSES

The new fuels are designed to be used in the conventional PWR, with the System CPR-1000 reactor selected as the reference plant. For purposes of comparison, we assume that new fuels do not affect the geometry of the core material. In this study we select the LOCA and SBO events. According to Appendix K 10CFR50.46, the failure temperature of Zr is 1477K during this analysis. Because of there are no clear guidelines for new fuels, we take the melting point to failure criteria. The three candidate fuels failure criteria as follow: FCM-

SiC's 2818K (the melting temperature of FCM), U_3Si_2-SiC's 1938K (the melting temperature of U_3Si_2), UO_2+BeO-FeCrAl's 1672K (the melting temperature of FeCrAl).

2.4. LOCA analysis

The LOCA event is a postulated accident that spans a range of primary system pipe breaks leading to a reduction in the coolant inventory. There are two main LOCA events: the large break LOCA (LBLOCA) and the small break LOCA (SBLOCA). The Three Mile Island nuclear accident belongs to this condition. Usually to open the ECCS to ensure the safety of the core. Before water from the ECCS reaches the bottom of the core, the temperature of cladding will rise rapidly due to the exposure of the core. The reaction of water and Zr will accelerated during this environment. The core will be reflooded when the water of the ECCS reach the core. The cladding may be brittle fracture by the thermal shock. If the ECCS failure during the LBLOCA, the reactor core will be completely bare. It will become a serious accident during a very short time.

This analysis assumes that the break appears in the horizontal portion of the cold pipe, break area is 0.78 m^2.

LBLOCA: The water of RWST (refueling water storage tank) is depleted, the low pressure safety injection pump will get the cooling water from containment sump to ensure the safety of core. As shown in Fig. 6, the candidate claddings' peak temperatures are lower than Zr. FCM-SiC has the lowest temperature. When the thickness of FeCrAl claddings is thicker, the temperature is higher. Detailed data are shown in table 1.

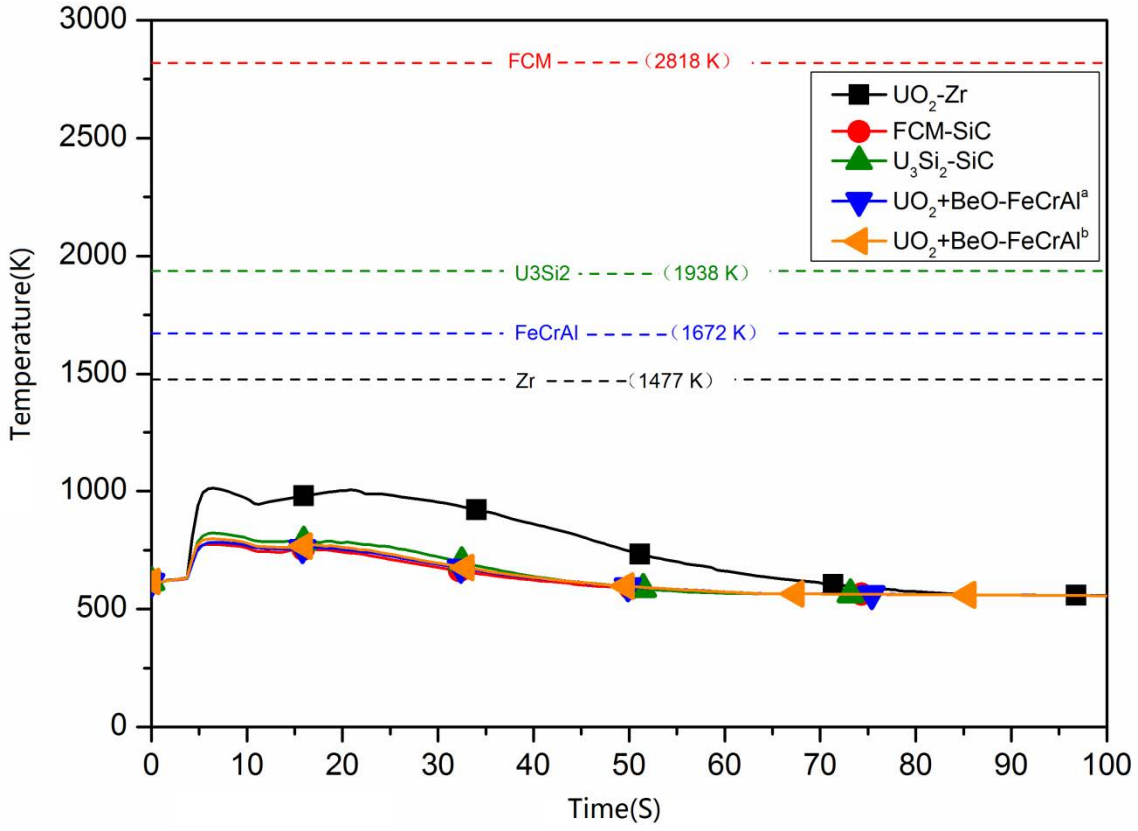

FIG. 6. Cladding temperature, LOCA.

TABLE 1. CLADDING TEMPERATURE: LOCA

Candidate ATF Concepts	The Peak Temperature of Cladding (K)	Deviation
UO_2-Zr	1012	0
FCM-SiC	755	-257
U3Si2-SiC	822	-190
UO_2+BeO-FeCrAl[a]	783	-229
UO_2+BeO-FeCrAl[b]	798	-214

[a] cladding thickness is 0.57mm, [b] cladding thickness is 0.45mm

LBLOCA without Safety Injection: While one HPSI and one LPSI are activated in the design basis LBLOCA, no SI system is available in this extreme scenario. Without the active inventory makeup, the core is depleted and heats up rapidly. The temperature of pellet and cladding are shown in Figs 7 and 8.

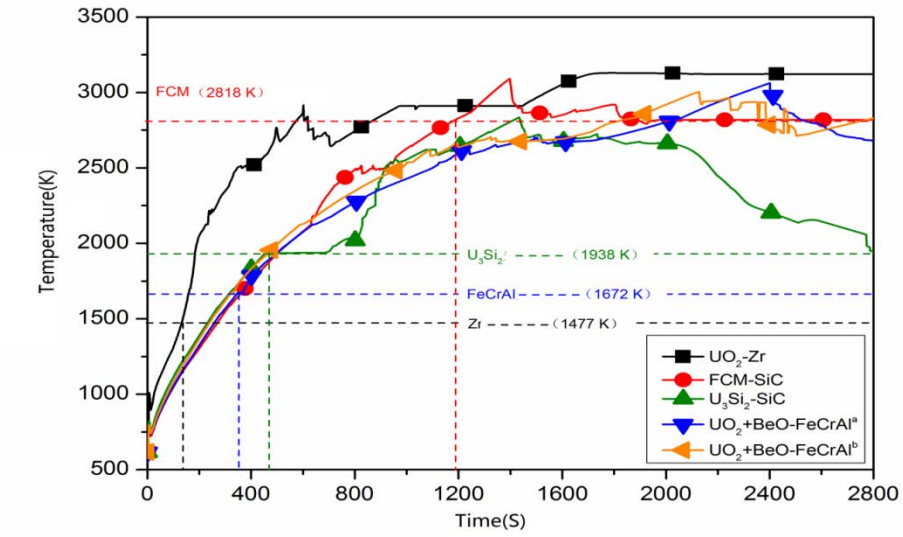

FIG. 7. Cladding temperature, LOCA without safety injection.

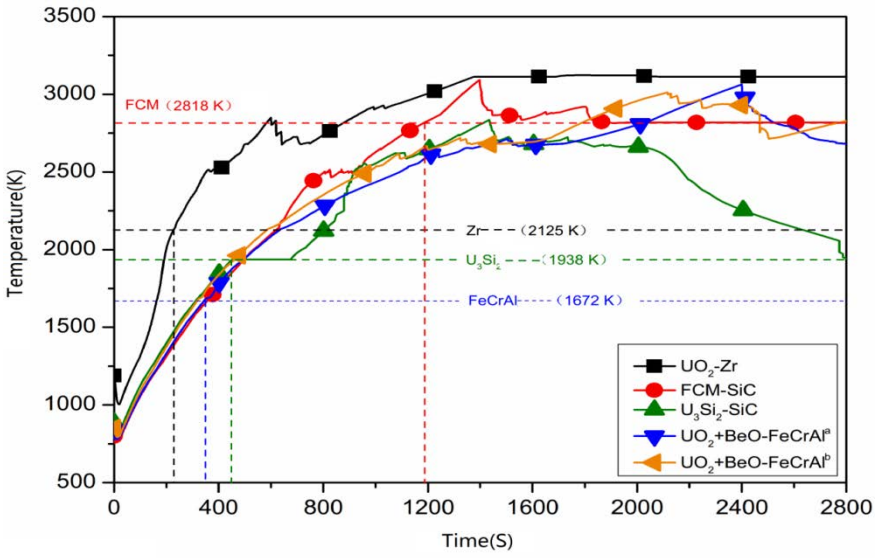

FIG. 8. Pellets temperature, LOCA without safety injection.

The cladding material will react with the water during the high temperature and pressure steam phase. Unlike Zr and FeCrAl which only produce H_2, the SiC reaction with water will produce CO and H_2. The amount of hydrogen generated by different claddings is shown in Fig. 9. The amount of CO generated by SiC is shown in Fig. 10.

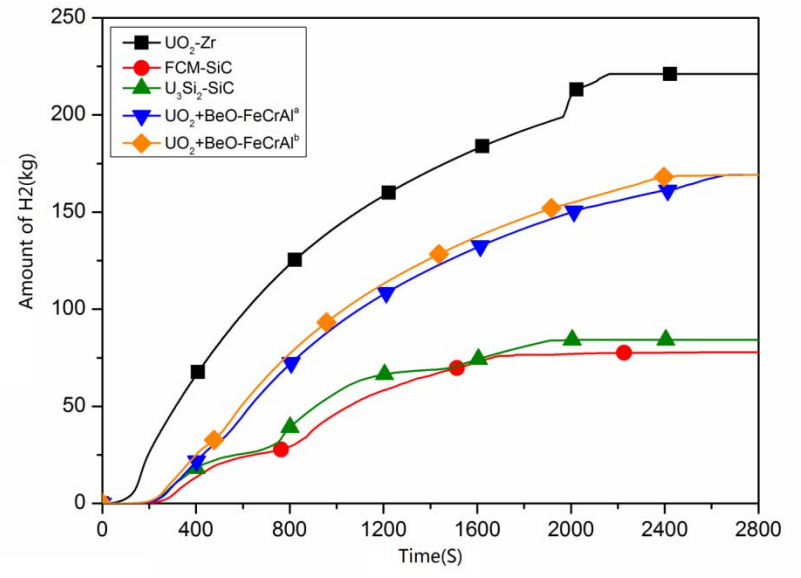

FIG. 9. In-core hydrogen generation, LOCA without safety injection.

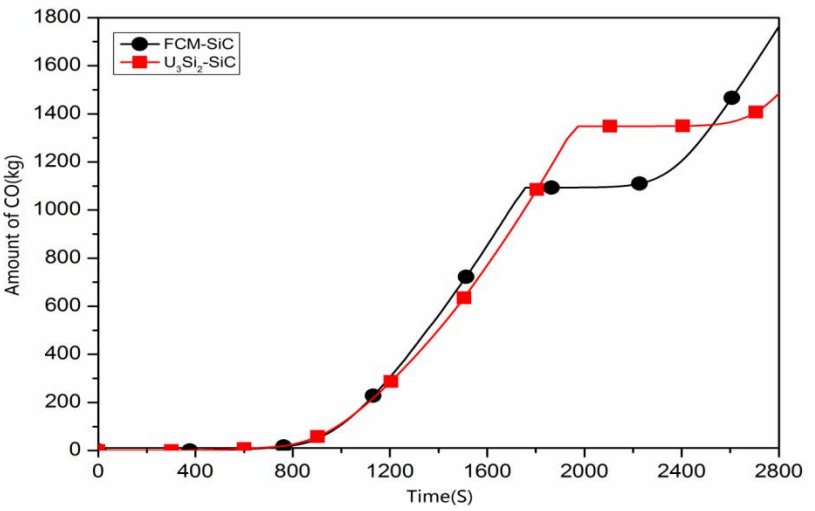

FIG. 10. In-core CO generation, LOCA without safety injection.

2.5. SBO analysis

The SBO event is an accident caused by the loss of all available electric power. The temperature of cladding and fuel will continuously increase due to the lack of coolant. Table 2 shows the event time.

TABLE 2. THE EVENT TIME

Event	UO_2-Zr	FCM-SiC	U_3Si_2-SiC	UO_2+BeO-FeCrAl[a]	UO_2+BeO-FeCrAl[b]
			Time(s)		
Loss of power	1000	1000	1000	1000	1000
Valve closed	3091	1159	1156	1162	1162
Core uncover	7510	7705	7676	7703	7696
Hot leg rupture	10709	13322	13093	13206	13131

The temperature rapidly rise in about 8000s due to the core is uncovered. Then the safety injection tank began to cool the reactor core. After the accumulator water depleted, the temperature will rise again. Figs 11 and 12 show the temperature of claddings and pellets.

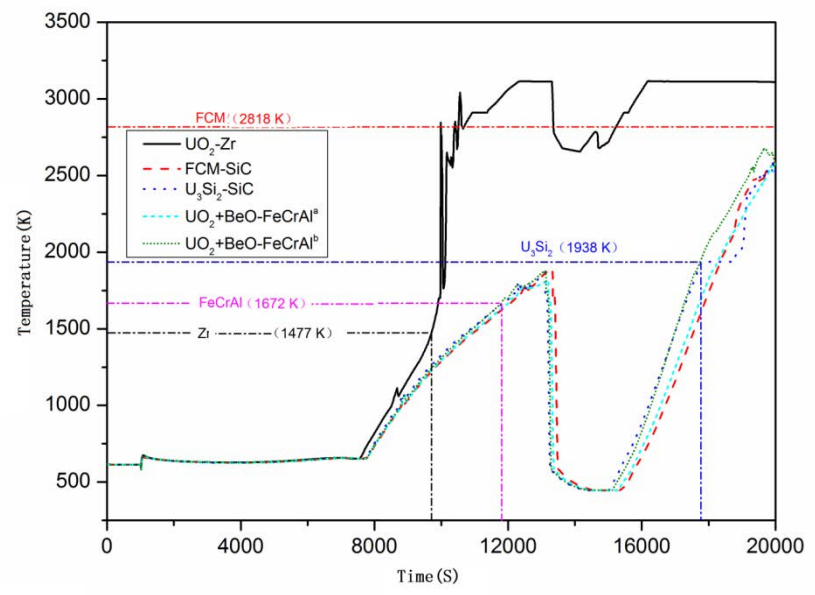

FIG. 11. Cladding temperature, SBO.

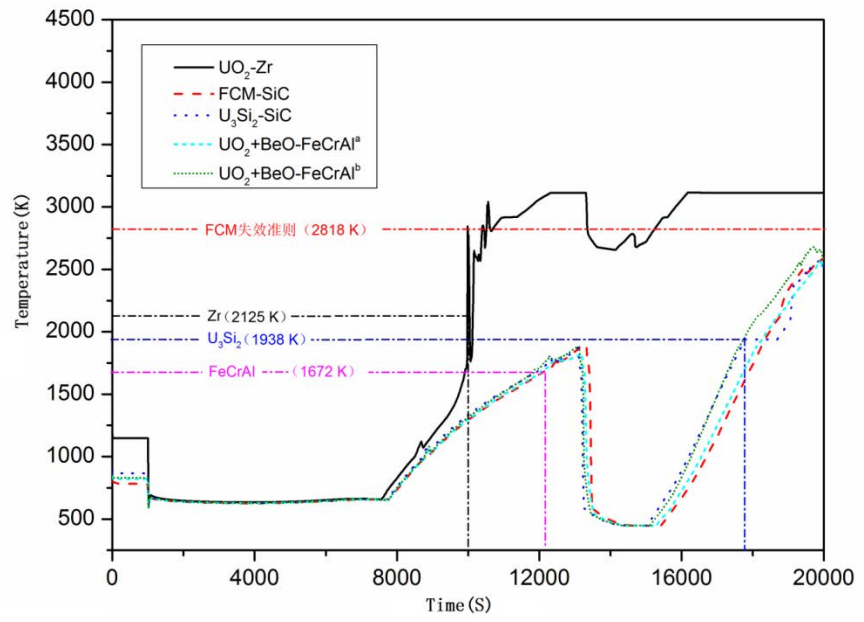

FIG. 12. Pellet temperature, SBO.

The Failure time of fuel systems are shown in Table 3. From the table we can see that even the first failure system UO_2+BeO-FeCrAl[b] is still 2000 seconds later than the standard UO_2-Zr system.

TABLE 3. FAILURE TIME OF FUEL SYSTEMS

Event	UO_2-Zr	FCM-SiC	U_3Si_2-SiC	UO_2+BeO-FeCrAl[a]	UO_2+BeO-FeCrAl[b]
			Time (s)		
Cladding temperature reach 1477K	8716.0*	9982.0	9756.0	9925.0	9811.0
Cladding temperature reach 1672K	8907.0	11074.0	10887.0	11048.0*	10843.0*
Pellet temperature reach 1938K	8987.0	17194.0	16916.0*	17269.0	16744.0
Pellet temperature reach 2818K	8987.0	>19000.0 *	>19000.0	>19000.0	>19000.0

*failure time

4. CONCLUSIONS

Under the accident conditions, all the candidate ATF systems show the excellent performance compare to the standard UO_2-Zr system. The LOCA studies indicate that the peak cladding temperatures could be reduced by 257K for FCM-SiC system. Hydrogen generation, which can exacerbate the accident, is also slowed by the candidate fuels. But there have some CO been generated by the SiC during the accident, which required further study. The results during the SBO accident show that all the new materials could delay the failure time of fuel systems. Even the fastest failure system, i.e. UO_2+BeO-FeCrAl[b] is still 2000 seconds later than the standard UO_2-Zr system.

In this paper, although there is not enough experimental data to support the theoretical analysis, the preliminary assessment also widely shows the outstanding accident tolerance performance of ATF concepts. To better assess the actual availability of the ATF systems, more theoretical analysis and experimental studies need to be performed.

REFERENCES

[1] BRAGG-SITTON, S., "Advanced fuels campaign. Light water reactor accident tolerant fuel performance metrics. Executive summary" (No. INL/EXT-13-30226). Idaho National Laboratory (INL). (2014).

[2] McCOY, K., MAYS, C., Enhanced thermal conductivity oxide nuclear fuels by co-sintering with BeO: II. Fuel performance and neutronics, J. Nucl. Mater. **375** (2008) 157–167.

[3] SHIMIZU, H., "The Properties and Irradiation Behaviour of U_3Si_2". Technical Report NAA-SR-10621, Atomics International, (1965).

[4] SNEAD, L.L., INOZAWA, T., KATOH, Y., BYUN, T-S., Handbook of SiC properties for fuel performance modelling, J. Nucl. Mater. **371** (2007) 329–377.

[5] TERRANI, K.A., PINT, B.A., PARISH, C.M., SILVA-CHINTHAKA, M., SNEAD, L.L., KATOH, Y., Silicon carbide oxidation in steam up to 2 MPa, J. Am. Ceram. Soc., **97(8)** (2014) 2331-2352.

[6] LIU, R., LIU, B., ZHANG, K., LIU, M., SHAO, Y., TANG, C., High temperature oxidation behaviour of SiC coating in TRISO coated particles, J. Nucl. Mater. **453** (2014) 107–114.

[7] http://en.wikipedia.org/wiki/Silicon_carbide.
[8] OTT, L.J., ROBB, K.R., WANG, D., Preliminary assessment of accident-tolerant fuels on LWR performance during normal operation and under DB and BDB accident conditions, J. Nucl. Mater. **448 (1)** (2014) 520-533.

PRELIMINARY ANALYSIS OF ATF CONCEPT DESIGN BY NPIC

W. LI, P. CHEN, Z. LIU, L. LV, M. LI, S. DU
Nuclear Power Institute of China
Science and Technology on Reactor System Design Technology Laboratory
Shuangliu, Sichuan
China
E-mail: lwj280@163.com

Abstract

Recently NPIC has launched a research project on Accident Tolerant Fuel concept design and preliminary scoping evaluation, as a first step to develop next generation PWR with enhanced safety under normal and accident conditions. Various fuel and cladding materials are combined together as conceptual designs. A technical screening of these designs was performed based on an 18 month fuel cycle in a typical PWR NPP in China. Some preliminary analysis on reactor physics, fuel behaviour and safety under server accident of these combinations were performed by NPIC to provide an insight of potential benefits which might be brought by these designs and a basis to more detailed designs. In order to facilitate scoping/ranking of these designs, a set of performance indicators was employed in this to compare fuel performance and safety margin in normal and accident conditions. In last ten years, NPIC has initiated some research on preparations of UN, U3Si2 and U-Mo fuel pellets as alternative fuel materials. These efforts are briefly introduced in this paper, which may provide a good foundation to our ATF fuel development. Besides, NPIC's irradiation capability such as High Flux Engineering Test Reactor and post irradiation examination facilities necessary for ATF development is also introduced. NPIC is willing to push development of ATF with cooperation of IAEA and other organizations.

1. INTRODUCTION

Nuclear Power Institute of China (NPIC), a subsidiary to China National Nuclear Corporation (CNNC), is China's most comprehensive R&D base which works on the research, design, test, operation for nuclear reactor engineering and small batch of production. For last three decades, NPIC has been devoted to nuclear fuel and material research, fuel element/assembly design and test. It is one of our missions to provide safe and reliable fuel products to research reactors and nuclear power plants in China. NPIC has participated in continual improvement of fuel technology, including advanced materials and nuclear fuels, which is very important to the industry's success. NPIC noticed that recent development of ATF concept, which may provide enhanced safety of current NPPs in accidents conditions like what happened in Fukushima Daiichi, and may also help to solve problems we encountered in GEN IV reactors, such as high temperature corrosion, high thermal margin and high dose irradiation stability. Therefore, NPIC is very interested in the fundamental research and development of ATF featured assembly. Considering the high cost and risk in ATF development, NPIC realized it is important to cooperate with other organizations to share experiences and leverage resources.

As a first step to develop next generation PWR fuel with enhanced safety under both normal and accident conditions, a research project focusing on ATF concept design and preliminary scoping evaluation is launched in NPIC early this year. Based on technique readiness levels and future demands of China's nuclear fuel market, a two-stage ATF development plan is proposed to meet the requirements of near-term and mid-term. The near-term design is intended to be applied in Generation II+ and Generation III plants in China, while the mid-term design is more applicable to Generation III+ and Gen IV plants.

There are a number of material options for both designs, according to our knowledge of existing or under developing fuels and claddings. Therefore, this paper is intended to assess fuel performances of different combinations of materials in current PWR conditions. Although it is dependent on experimental development, in and out-of pile qualification tests to decide which material should finally be used, theoretical analysis of these conceptual

designs is necessary to demonstrate adequate performance during normal operation and worthwhile improvements in severe accident scenarios and to inform concept down selection. On the other hand, this analysis helps to identify gaps in our knowledge of candidate materials and critical issues in each ATF concept designs. Outcomes of this analysis will be necessary reference in making ATF development strategy and help to make the qualification tests programme more purposely.

2. PERFORMANCE METRICS AND ANALYSIS METHODS

Considering the operating experiences and matured manufacturing of standard fuels, the near term concept design is mainly based on improvements of UO_2 pellets and surface modifications of zircaloy claddings. With additives like BeO and SiC fibers, thermal conductivity is increased and fission gas is better retained. With coating layer like MAX phase materials and monolithic SiC, high temperature oxidation resistance of cladding under accident conditions is to be improved. Although additives and coatings may have some influence on neutronic economics, considering the relatively small weight fractions of them, impact on fuel management strategy can be ignored while fuel performance and safety in accident conditions will be significantly improved. For the mid term concept design, both neutronic economics and accident tolerance are to be improved with high U content fuels like UN or U_3Si_2 and SiC composite cladding with better mechanical performance and corrosion resistance at high temperature.

In order to assess the ability of each concept to meet performance and safety goals relative to standard fuel system and relative to one another, a preliminary analysis on the performance of various ATF concept designs during normal and accident conditions is presented. In order to better understand the in-core performance and to guide new fuel designs, the properties of the new materials collected from literatures are implemented into fuel performance codes and other computational methods.

AFA-3G assembly was selected as a reference design to find out how the adoption of various fuel-cladding material combinations (as shown in Table 1) would change neutronics economics, fuel rod thermal-mechanical performance and safety performance. In order to facilitate comparing the results of concept designs with standard fuels, the evaluation is performed for an 18 months refueling cycle in a typical NPP of China.

TABLE 1. COMBINATIONS OF FUEL-CLADDING CONSIDERED FOR ATF CONCEPT DESIGN

Design name	Fuel material	Cladding material
REF	UO_2	zircaloy
ATF1-1	UO_2+SiC fibre(10w/o)	zircaloy with SiC coating layer
ATF1-2	UO_2+BeO (1.2 w/o)	zircaloy with SiC coating layer
ATF2	U_3Si_2	zircaloy with SiC coating layer
ATF3	UN	SiC composite cladding
ATF4	UN+30%w.t. U_3Si_2	SiC composite cladding

Fuel assembly geometric parameters of all fuel-cladding combinations are set the same as those of AFA 3G for simplicity and to avoid influence on thermal hydraulic performance. Geometry optimization of concept design will be performed in a next phase. The surface wettability of the cladding material will affect thermal hydraulic performance

and is certainly different for zircaloy, coating layer, and SiC composite, but for this preliminary analysis, the effect of surface wettability is not considered.

The following performance indicators are applied to assess the evaluation results of various fuel-cladding combinations:

- Enrichment needed for maximum fuel discharge burnup;
- Reactivity coefficients versus burnup;
- Maximum cladding strain and stress during transients;
- Maximum fuel temperature in normal and accident conditions;
- Maximum temperatures on the inner and outer surfaces of the cladding;
- Thermal margin from fuel melting in RIA.

3. PERFORMANCE ASSESSMENT

3.1. Neutronics analysis

These analyses are performed at the fuel-assembly level on a core physics computation platform SARCS (version 4.1) developed by NPIC. The search of enrichment and reactivity curve calculations were performed by using KYLIN (version 1.012) programme, at a steady condition of 15.5 MPa and 311°C. The effect of ^{15}N enrichment on neutronics was evaluated with RMC programme (version 0115) at normal pressure and normal temperature.

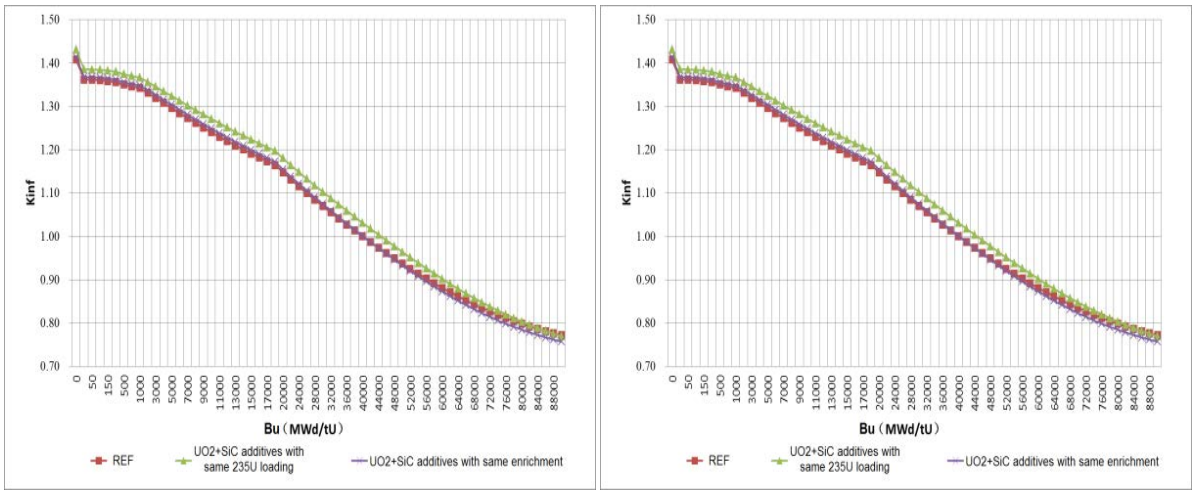

FIG. 1. Reactivity coefficient versus burnup for UO_2 with SiC and BeO additives.

Figure 1 shows the reactivity curves of ATF1-1 and ATF1-2. Due to the low absorption cross section of SiC coating layer and relatively small thickness, the effect of coating layer on neutronics is ignored here. Two assumptions were adopted in the calculation which generated different curves, i.e. same ^{235}U loading per fuel assembly as indicated by green curves, or same enrichment per fuel assembly as indicated by purple curves. If enrichment is maintained the same as that of reference PWR fuel assembly, reactivity curves of ATF1-1 and ATF1-2 are very close to that of reference fuel, which means no significant impact on neutronic economics. If ^{235}U loading is maintained the same, which means enrichment has to be increased, the reactivities of them are higher than that of reference fuel.

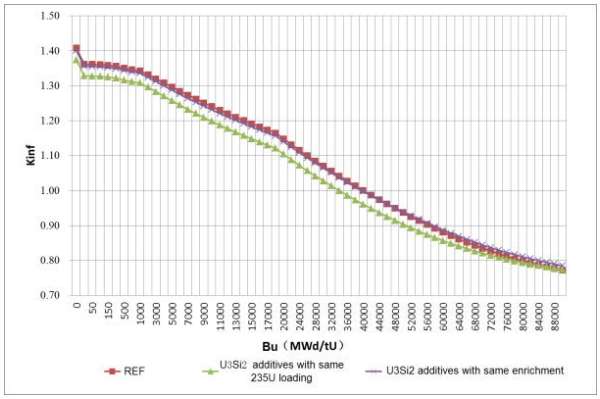

FIG. 2. Reactivity coefficient versus burnup for ATF2.

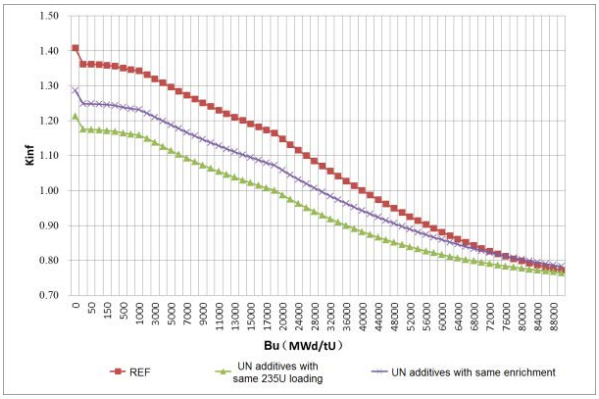

FIG. 3. Reactivity coefficient versus burnup for UN.

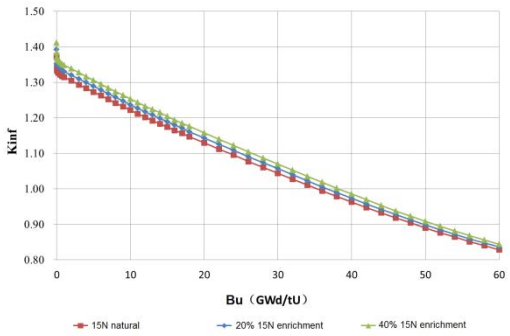

FIG. 4. Reactivity coefficient versus burnup for ATF3 with different ^{15}N enrichment.

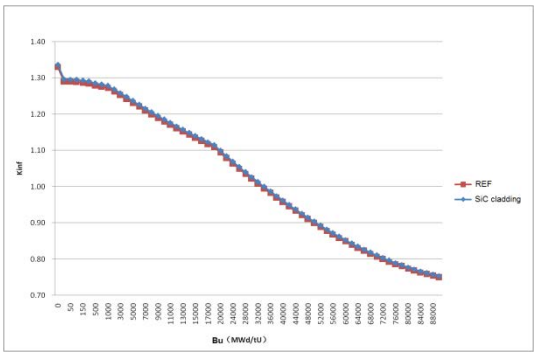

FIG. 5. Reactivity coefficient versus burnup for different cladding.

Figure 2 shows the reactivity curves of ATF2. Due to higher U density of U_3Si_2 than UO_2, enrichment can be lower (3.8% for U_3Si_2 and 4.45% for UO_2) maintain the same ^{235}U loading. If enrichment is maintained the same as that of reference PWR fuel assembly, reactivity curve of ATF2 is very close to that of reference fuel, with a deeper burnup or a longer time of full power output.

U density of UN is even higher than U_3Si_2, but reactivity curves, as showed in Figure 3, are much lower than that of reference fuel, mainly because of self-shielding effect and larger absorption cross section of N compared with O. ^{15}N has a lower cross section than other nitrogen isotopes. Figure 4 shows the significant effect of ^{15}N enrichment on reactivity curves. Blue colour represent 20% enrichment of ^{15}N, green colour represent 40% enrichment of ^{15}N ,and red curve colour represent none enrichment of ^{15}N. The effect of SiC cladding on reactivity coefficient is comparably small, as shown in Figure 5 by comparing its reactivity curve with zircaloy cladding. In order to achieve a discharge burnup of 75 GWd/tU, the enrichment has to be increased to 8% with a final reactivity around 0.92520, as shown in Figure 6. To improve the waterproof ability of UN pellet, a composite pellet by encapsulate UN kernels with U_3Si_2 is proposed by other researchers and its reactivity is evaluated here, as shown in Figure 7. In order to achieve a discharge burnup of 75 GWd/tU, the enrichment of ATF4 should be 7.5%, which is even lower than that of pure UN.

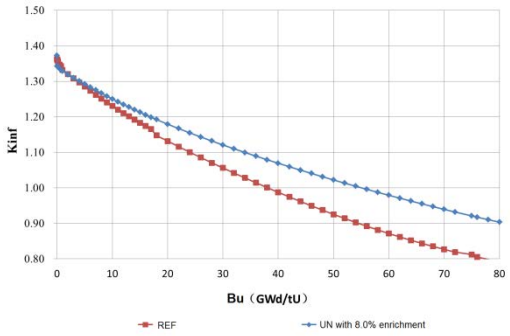

FIG. 6. Reactivity coefficient versus burnup for ATF3 with higher enrichment.

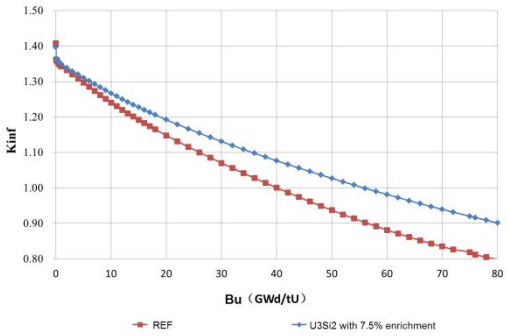

FIG. 7. Reactivity coefficient versus burnup for ATF4 with higher enrichment

3.2. Fuel behaviour at normal operating conditions

The COPERNIC2.4 fuel performance code is used in the analysis of ATF fuel behaviours under normal operating conditions in a PWR environment. The thermo-physical property models of SiC and UN were collected from literatures and implanted into COPERNIC code. Material properties required by COPERNIC were (1) elasticity constant, (2) Poisson's ratio, (3) strain due to swelling, (4) thermal strain, (5) thermal conductivity, (6) creep strain, (7) yield stress, (8) rupture strain, (9) specific heat at constant pressure, (10) density, (10) solidus-liquidus melt temperature, (12) heat of melting, (13) emissivity. The modified COPERNIC was exercised on a case that fuel rods experienced local power transients in the end of cycle to evaluate thermal responses of different combinations, and another case that fuel rods experienced a Condition 2 transient (Excessive Load Increase) to evaluate mechanical responses.

In the first case, although fuel rod power history remains steady until the end of fuel cycle, the axial power distribution is greatly changed by a transient, as shown in Figure 8. The peak local power is 51.1 kW/m and generates a high temperature in the third node of the fuel rod, as shown in Table 2. In order to see the effect of SiC composite cladding on thermal response, a new design - ATF3*, which uses SiC coated zircaloy cladding and UN pellets, is also evaluated here. Compared with reference fuel, all ATF designs exhibit lower temperature and larger margin from melting temperature, which shows the effect of enhanced thermal conductivity. The results also indicate lower fission gas release as a result of lower operating fuel temperature, but fission gas behaviour models are not so valid for ATF designs.

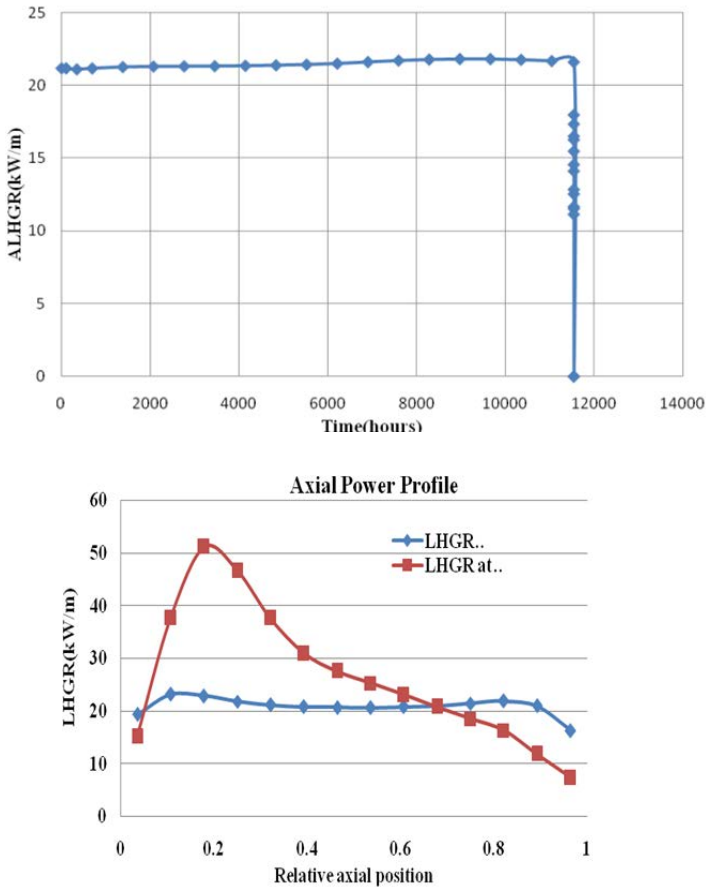

FIG. 8. Fuel rod power history before and at the transient.

TABLE 2. PEAK FUEL TEMPERATURE OF VARIOUS ATF CONCEPT DESIGNS IN CASE 1

Design name	Max. Pellet Temp., °C	Margin from melting, °C
REF	1893	697
ATF1-1	1521	1069
ATF1-2	1530	1060
ATF3*	618	2144
ATF3	803	1959

In the second case, all fuel rods experienced an Excessive Load Increase transient, which was the most challenging power history for Pellet Cladding Mechanical Interaction in case of reference fuel. Maximum strain energy density, maximum Tresca stress at inner side of cladding and maximum strain of all ATF designs and reference fuel are shown in Table 3. PCMI are eased because of lower temperature in the pellet also as a result of enhanced thermal conductivity. It is noted that ATF3 has a positive strain while ATF3* has a negative strain, mainly because it was assumed in this study that SiC composite cladding doesn't creep during irradiation and leaded to a larger gap size and higher pellet temperature than that of zircaloy cladding. The average pellet temperature in ATF3* is lower than any other design so that the pellet thermal expansion is smaller and cladding move inwardly even during the

transient. SiC cladding is a fragile material and is assumed to fracture at a strain over 0.2% and a stress over 220 MPa. For the ELI transient, ATF3 exhibits much lower stress and strain than reference fuel. But as burnup is increased, the situation is totally inversed. A rod drop transient at the end of 3rd cycle, which only induced a small SED for reference fuel, as shown in Table 4, is enough to bring ATF3 to failure. As burnup increase, the pellet cladding gap size deceases faster than that of reference fuel due to the higher swelling rate of UN. SiC cladding will lost the accommodation ability of pellet expansion under power transient in this case. This implies the most challenging case of PCI criteria for SiC cladding mostly happened at fuel rods with highest burnup. For reference fuel, the most challenging case is usually dependent on magnitude of power transient.

TABLE 3. CLADDING STRESS AND STRAIN OF VARIOUS ATF CONCEPT DESIGNS IN CASE 2A

Design name	Max. SED, MPa	Max. Tresca Stress, MPa	Max. Strain, %	Pellet Avg. Temp., °C
REF	2.479	561.7	0.468%	1014
ATF1-1	1.010	470.6	0.0847%	877
ATF1-2	1.073	478.3	0.097%	874
ATF3*	0.013	65.1	-0.497%	514
ATF3	1.45E-4	29.5	0.165%	692

TABLE 4. CLADDING STRESS AND STRAIN OF VARIOUS ATF CONCEPT DESIGNS IN CASE 2B

Design name	Max. SED, MPa	Max. Tresca Stress, MPa	Max. Strain, %	Pellet Avg. Temp., °C
ATF3 (EOC3)	0.3898	303.96	0.501%	586
REF (EOC3)	0.9314	393.44	0.445%	850

3.3. DB accident analyses

The preliminary evaluation of the design basis accident performance of various fuel/cladding combinations was performed by modelling PWR cores operating with these new materials. Currently, the knowledge of cladding and fuel components is incomplete because information such as in-core material performance is unknown. However, a preliminary study of the safety performance of ATF fuel designs can be performed by using currently available material properties and making a relative comparison to current materials and components. For this paper only a Reactivity Insertion Accident (RIA) was analyzed by using a modified COMBAT code. Figure 9 shows the power history during a RCCA ejection accident at the end of an equilibrium cycle. The temperature profile of various ATF designs and reference fuel during this accident cycle are summarized in Table 5.

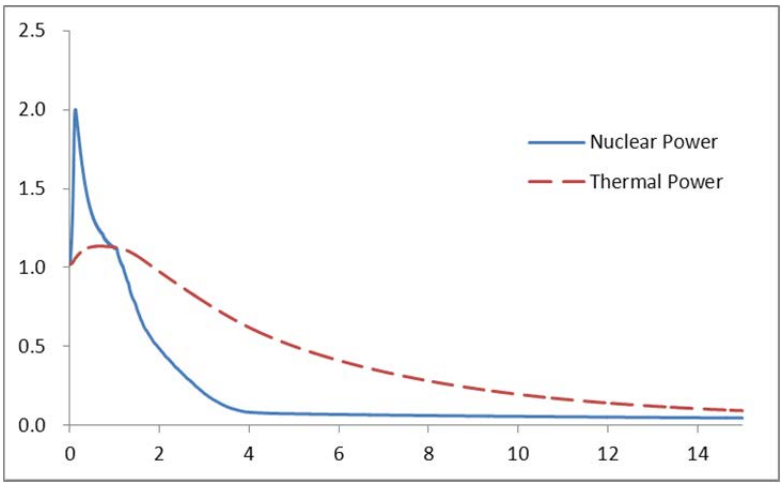

FIG. 9. Nuclear Power and Thermal Power at RCCA ejection accident.

TABLE 5 TEMPERATURE PROFILE OF VARIOUS ATF CONCEPT DESIGNS IN RIA

Design name	Pellet Center Temp., °C	Pellet Aver. Temp., °C	Cladding Inner Temp., °C	Cladding Outer Temp., °C
REF	2350.5	1704.9	982.9	954.0
ATF1-1	1575.0	1300.2	1010.4	980.0
ATF1-2	1603.8	1313.0	1011.4	981.0
ATF2	1120.1	1078.1	1024.9	995.0
ATF3	1287.6	1230.4	1163.2	985.0

3.4. BDB accident analyses

Modelling of an extended station blackout event (SBO) was performed as an approach to determine how an advanced cladding would respond to an accident similar to what occurred at the Fukushima Daiichi nuclear power plant in Japan in March 2011. Currently only the analysis with coated zircaloy was performed. As shown in Figure 10, compared with uncoated zircaloy, peak cladding temperature of coated fuel rod is lower and peak time is delayed, mainly because the assumption that coating layer stop the cladding-steam reaction and reduce the heat generated. Nevertheless, coated cladding will collapse if accident progress continues. The main contribution of coated cladding in the accident process is the reduction of hydrogen generated in the high temperature range before cladding failure happens.

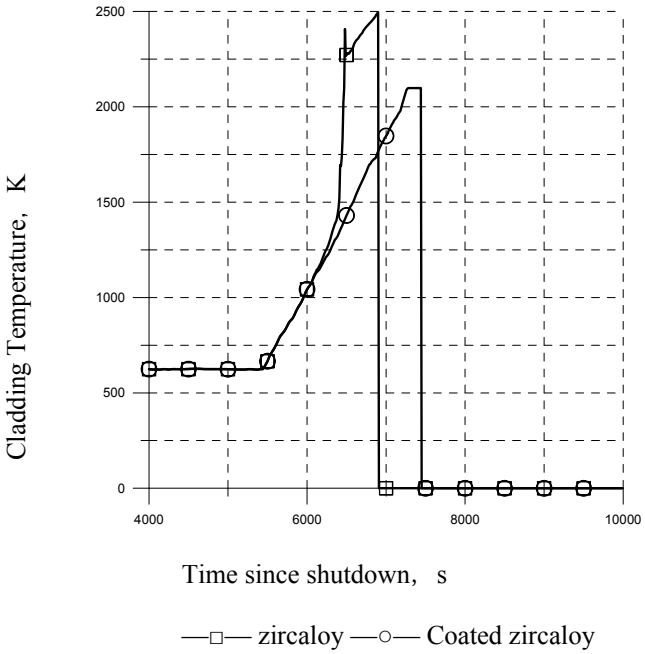

FIG. 10. Peak Cladding temperature at SBO.

4. CONCLUSIONS

NPIC has performed a preliminary evaluation on various combinations of fuel and cladding materials from respects of neutronics, fuel performance and accident safety behaviours. The conclusions of this paper are:

- The effect of coating layer (such as SiC or MAX phase material) on neutronics economics can be ignored. No significant effect on neutronic economics is observed with a small amount of additives in UO_2 pellet.
- High density fuels with increased enrichment (>5%) can increase the economic attractiveness of ATF by allowing longer refuelling cycle and deeper discharge burnup (75 GWd/tU). However, additional effort is required for UN. More specifically, ^{15}N enrichment is required to achieve an acceptable neutron economy. To improve oxidation resistant to reactor coolant, a composite pellet consists of UN and U_3Si_2 is feasible and even better than pure UN from the view of neutronics.
- Fuels with enhanced thermal conductivity (such as UO_2 with BeO or SiC fibre additives, UN) and better structural stability operates at much lower temperatures under normal operations and DB accidents (RIA) conditions. Coated Zr cladding offers significant improvement in fuel reliability during normal operations and moderate safety improvement during accidents, mainly on the reduction of hydrogen.
- SiC cladding offers significant oxidation resistance improvement under accident conditions. Due to the low thermal conductivity under irradiation, SiC should be applied with high thermal conductivity pellet. As a result of its fragile nature and very low irradiation creep, the most challenging rod and time for PCI criteria are different for SiC cladding compared with those of zircaloy cladding.

As mentioned earlier, the material properties models used in this preliminary evaluation are collected from literatures and many key irradiation behaviours are based on assumptions, such as the swelling rate and fission gas release of UN. Due to the variety of SiC composites and manufacture methods, there is a lot uncertainty in SiC cladding models,

like irradiation induced swelling, thermal conductivity, fracture strain. Further research and development efforts are needed to identify the best SiC composite candidate for LWR cladding applications to reduce the cost of production and to fully understand its performance under irradiation.

REFERENCES

[1] CARPENTER, D.M., "An Assessment of Silicon Carbide as a Cladding Material for Light Water Reactors". PhD thesis. Massachusetts Institute of Technology. (2010).

[2] SNEAD, L.L., et al., Handbook of SiC properties for fuel performance modelling. J. Nucl. Mater., **371** (2007) 329-377.

[3] PENG, X., et al., "Preliminary Assessment of Accident Tolerant Fuel Performance at Normal and Accident Conditions", IAEA Technical Meeting on Modelling of Water-cooled Fuel Including Design Basis and Severe Accidents, 28 October–1 November, Nuclear Power Institute of China, Chengdu, China (2013).

[4] OTT, L.J., et al., Preliminary assessment of accident-tolerant fuels on LWR performance during normal operation and under DB and BDB accident conditions. J. Nucl. Mater., **448** (2014) 520-533,

[5] PEIMAN, W., PIORO, I.; GABRIEL, K., "Thermal Aspects of Conventional and Alternative Fuels in Supercritical Water-Cooled Reactor (SCWR) Applications", Nuclear Reactors, MESQUITA, A.Z. Ed., INTECH, Rijeka, Croatia, (2012), pp.123-156.

[6] KATOH, Y., SNEAD, L., GOLUBOV, S., LARA-CURZIO, E., "Analyzing Irradiation-Induced Creep of Silicon Carbide", Mechanical Properties and Performance of Engineering Ceramics and Composites III, Wiley, (2007).

[7] BEN-BELGACEM, M. et al. Thermo-mechanical analysis of LWR SiC/SiC composite cladding, J. Nucl. Mater. **447** (2014) 125–142.

[8] KATOH, Y., et al., Continuous SiC fiber, CVI SiC matrix composites for nuclear applications: properties and irradiation effects, J. Nucl. Mater. **448** (2014) 448–476.

CROSS-CUT TESTING
(SESSION 4)

Chairperson:

S. Bragg-Sitton

(INL, United States of America)

HIGH-TEMPERATURE STEAM OXIDATION OF ACCIDENT TOLERANT FUEL CLADDING CANDIDATE MATERIALS

K.A. TERRANI, B.A. PINT, L.L. SNEAD, Y. YAMAMOTO
Oak Ridge National Laboratory, Oak Ridge
United States of America
E-mail: terranika@ornl.gov

Abstract

High temperature steam oxidation behaviour of accident tolerant fuel (ATF) candidate cladding materials is the foremost parameter that should be evaluated toward realization of an ATF concept. A survey of oxidation kinetics of these materials in high-temperature steam environments is provided in this paper and compared to that of Zr-based alloys. Specifically, candidate cladding materials that form protective chromia, alumina, or silica scales are examined. This survey is made possible via utilization of a set of complementary modules at the severe accident test station (SATS) at ORNL.

1. INTRODUCTION

Enhancing safety margins during light water reactor (LWR) severe accidents is currently the focus of a number of international R&D programmes. Specifically, alternative fuel and reactor core constituents that can potentially offer slower and less severe degradation than the current UO_2/Zr-based alloy cladding system are being examined. These advanced concepts are dubbed accident tolerant fuels (ATFs). The basis for development of ATFs is the notion that chemical and physical degradation of the fuel and core internals during a severe event exacerbate the accident's progression [1]. The current UO_2/Zr-based alloy fuel system is particularly susceptible since the Zr-based cladding experiences rapid oxidation kinetics in steam at elevated temperatures [2]. Therefore, alternative cladding materials that offer slower oxidation kinetics and a smaller enthalpy of oxidation can significantly reduce the rate of heat and hydrogen generation in the core during a coolant-limited severe accident [3-5]. Note that hydrogen generation cannot be eliminated in the core since oxidation of any element via the steam molecule releases hydrogen. The logic is that the rate and total amount of hydrogen generation is directly proportional to the oxidation rate of the fuel assembly structures, and therefore can be reduced if a transition away from Zr-based alloys and toward significantly more oxidation resistant materials is made.

The focus of this study is to provide a survey of oxidation kinetics of a set of ATF candidate cladding materials. The majority of the detailed steam oxidation kinetics reported here are the results from tests conducted at ORNL's Severe Accident Test Station (SATS). Therefore, initially, a brief overview of this facility is provided. Following that, the candidate ATF cladding materials are categorized into the three groups based on the protective external oxide or scale that forms in high temperature steam on these materials: chromia, alumina, and silica. The mechanism of steam oxidation and the corresponding kinetics of these materials are then discussed and compared to one-another. As a starting point, the oxidation resistance goal for ATF materials is two orders of magnitude lower than Zr-based alloys at temperature above 1000ºC.

2. SEVERE ACCIDENT TEST STATION

The SATS is a modular facility located at ORNL. It consists of four separate yet complementary modules meant to provide the ability to comprehensively examine oxidation kinetics and accident response of cladding materials. Figure 1 provides a schematic of the modules. The first module is a thermogravimetry analysis (TGA) unit that offers continuous mass change data for a specimen exposed to 1 bar steam. The second module is the high temperature furnace that is capable of exposing samples to 1 bar steam at up to 1700°C with

faster flow rates. The third module is the high-pressure or Keiser (named after its builder) rig that enables steam exposures up to 30 bar. The last module is the integral LOCA test furnace that enables rapid ramp rates owing to its infrared furnace technology and is capable of burst testing and quenching of tube specimens. Table 1 provides a summary of operating parameters for these various modules.

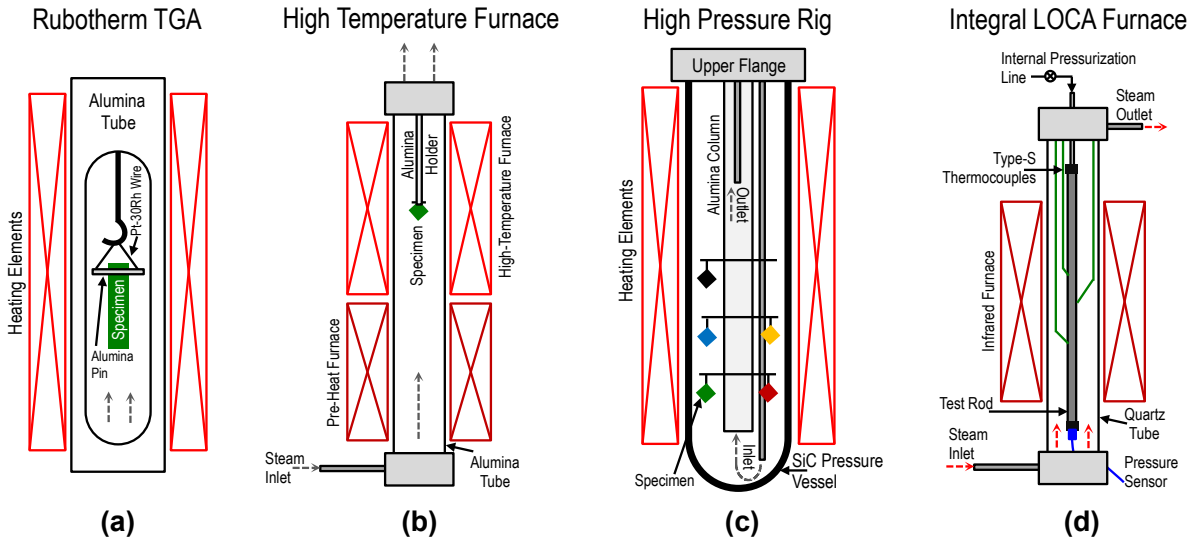

FIG. 1. Schematic drawing of the SATS modules.

TABLE 1. OPERATING PARAMETERS FOR THE VARIOUS MODULES OF SATS

	Integral LOCA Furnace	High Temperature Furnace	High Pressure Furnace	Thermogravimetry
Max Temperature [°C]	1200	1700	1400	1550
Max Pressure [MPa]	0.1	0.1	2	0.1
Max Flow Velocity [cm/s]	50	200	2	5
Max Ramp Rate [°C/min]	300	20	20	20
Capable of 100% steam	x	x	x	x

3. OXIDATION KINETICS OF CANDIDATE CLADDING MATERIALS

High-temperature oxidation resistance is achieved by the formation of a protective oxide barrier that forms on the surface of the materials and acts as a solid state diffusion barrier. A protective scale such as Cr_2O_3, Al_2O_3 or SiO_2 can form as a result of reaction of the oxidant with Cr, Al or Si in the bulk material, or a surface coating. However, protective coatings are limited, particularly coatings on Zr-based alloys, because the reservoir of scale-forming elements is finite and, when consumed, will only delay the rapid attack of the underlying substrate. Coating limitations are particular acute for this application where the metal cladding is sure to experience burst during temperature ramp upwards and the bulk underlying cladding will be exposed to steam. At the same time, detrimental interaction (e.g. eutectic formation) between the coating and the cladding should also be considered.

Protective scales that form on the surface of materials under oxidizing conditions have three important features. First, they remain dense and adherent such that the oxidation reaction becomes rate limited by solid state diffusion through the scale. Second, the diffusion rate through these oxides is slow resulting in a slow oxidation rate. And third, the oxide is thermodynamically stable in the steam environment or experiences only a slow volatilization.

If one of these three conditions is not met, the oxide layer will not be protective. Take for instance the ZrO_2 layer that form on the surface of Zr-based alloys. It exhibits excellent adherence to the underlying metal (certainly above 1100°C) and is exceptionally stable in steam, thereby meeting the first and third requirement. However, zirconia is a fast oxygen conductor, rapidly supplying the oxidant to the metal resulting in a rapid oxidation rate [6].

For the three protective scales, Cr_2O_3, Al_2O_3, and SiO_2, their adhesion is primarily dependent on the difference in thermal expansion coefficient between the oxide and the substrate. All three offer exceptionally slow oxygen diffusion rates and are very stable oxides. However, in the presence of water vapour and/or O_2, they can exhibit volatilization. Specifically, chromia may volatilize as CrO_3 or $CrO_2(OH)_2$ [7], while silica and alumina volatilize as $Si(OH)_4$ and $Al(OH)_3$, respectively [8-9], although the later only significantly occurs above 1400°C. The thermodynamic stability of these oxides in the presence of water vapour rank as $Al_2O_3 > SiO_2 > Cr_2O_3$; however, the latter is most strongly attacked in environments that contain both O_2 and H_2O, so better stability occurs in steam environments.

2.1. Steam oxidation of chromia-forming alloys

The results from this section are applicable to the behaviour of Fe-Cr, Ni-Cr and Fe-Cr-Ni alloys in high-temperature steam environments. Pint et al. [10] have established that a critical Cr content is necessary to form protective Cr_2O_3, as shown in Figure 2 where the lowest mass gains reflect protective behaviour and higher mass gains the rapid formation of FeO_x. In particular, for model Fe-Cr alloys, a Cr content of 25wt.% was necessary for protective behaviour at 1200°C in steam. For austenitic Fe-Cr-Ni stainless steels with a fixed Cr content, an increase in Ni content enhanced oxidation resistance, as had been observed previously in air and exhaust gas environments. However, Cr contents above 20 wt.% are typically needed to achieve good oxidation resistance in these alloys at 1200°C.

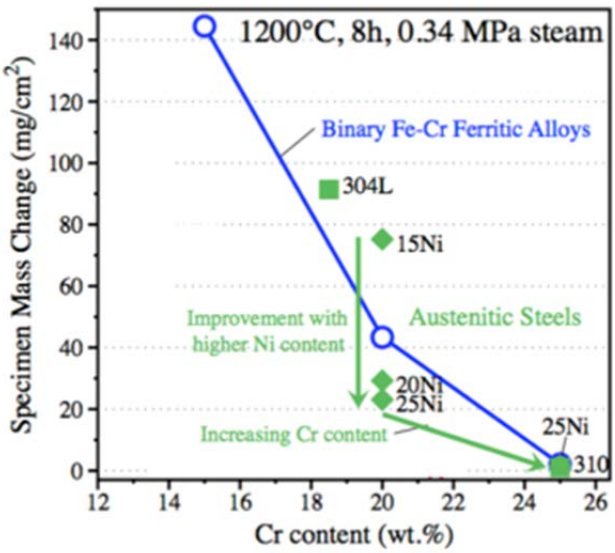

FIG. 2. Mass change in Fe-Cr and Fe-Cr-Ni alloys after 8h exposure in 1200°C and 0.34MPa steam (reproduced from Ref. [10]).

A steam pressure effect was also observed on the oxidation behaviour of 317SS (Fe-19Cr-12Ni-3Mo-0.6Mn-0.4Si); this behaviour is different from what is observed for Zr-based and alumina-forming alloys at 1200°C [11]. Figure 3 shows the metal consumed on 317SS specimens oxidized as a function of steam pressure during 8 h exposures at 1200°C in steam.

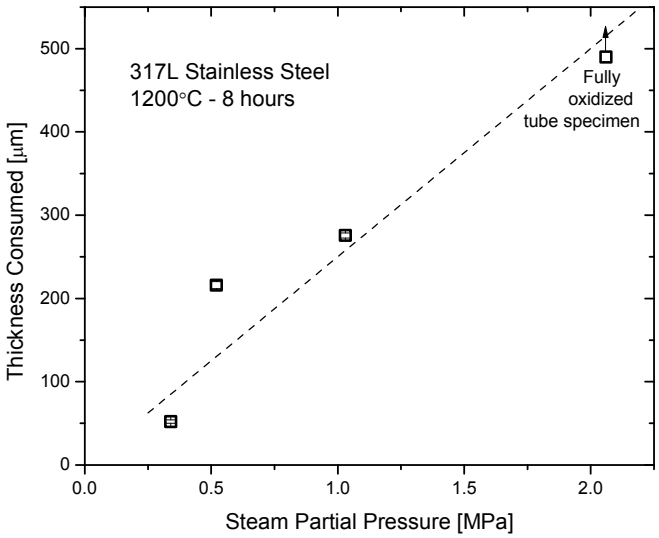

FIG. 3. Thickness of 317SS consumed as a function of steam pressure during 8 h 1200°C steam tests.

The high Cr content (~25wt%) in the Fe-Cr and FeCr-Ni alloys required to achieve oxidation resistance two orders of magnitude below Zr-based alloys can prove problematic in neutron irradiation environments. Specifically, in the case of Fe-Cr alloys, neutron irradiation at LWR operating temperatures results in formation of α′ precipitates. These Cr-rich precipitates increase with Cr content and severely degrade the ductility of the material intended for the cladding application [12]. In case of austenitic alloys, the high Cr content requires a high Ni content in turn to preserve the austenitic (FCC) structure. However, Ni has a high thermal neutron absorption cross-section that further increases the neutronics penalty of this class of cladding.

2.2. Steam oxidation of alumina-forming alloys

Because of the issue with Ni-base alloys, this section mainly focuses on the oxidation behaviour of FeCrAl alloys in high-temperature steam environments while a small set of data on behaviour of Al-bearing MAX phase materials is also mentioned. The excellent oxidation resistance of FeCrAl alloys has been known for more than 50 years [13]. The addition of Cr allows for relatively low Al contents to form alumina, compared to Fe-Al alloys which tend to form brittle intermetallic phases [14]. These alloys generally contain a small amount of oxygen-active or "reactive" elements (i.e. <0.5wt% Y, Zr or Hf) that improve the alumina scale adhesion and decrease the oxidation rate [15].

At elevated temperatures, the Al in the alloy diffuses to the surface and is selectively oxidized to form the alumina scale. As shown in Figure 4, aside from the reactive element, Al has the highest affinity for oxygen among the alloy constituents. However, if the amount of Al in the alloy is insufficient, FeO_x nodules form on the surface of the alloy and rapid oxidation takes place. In fact, Pint et al. have recently shown that a critical combination of Cr and Al is necessary in the alloy to achieve formation of a protective alumina layer at elevated temperatures [16-17], Figure 5.

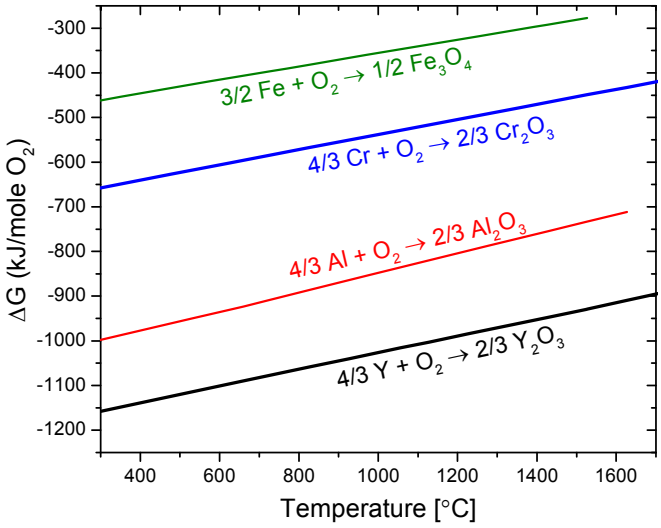

FIG. 4. Ellingham diagram for Fe, Cr, Al, and Y.

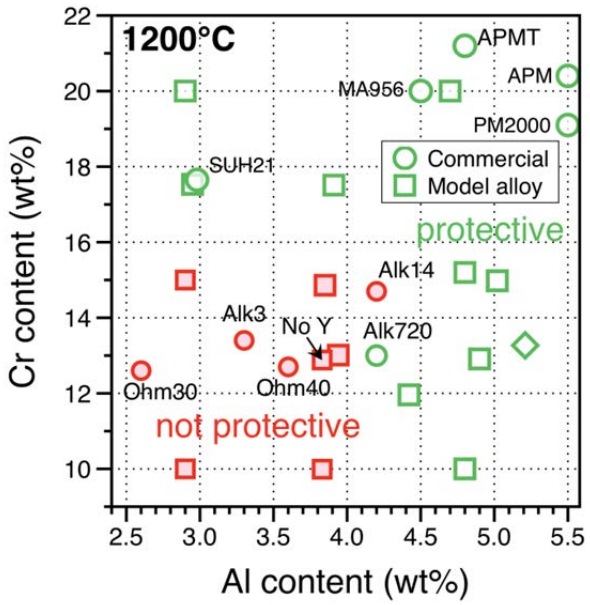

FIG. 5. Map of protective/unprotective oxidation behaviour in FeCrAl alloys as a function of Cr and Al content in the alloy at 1200°C steam (reproduced from Ref. [16]).

Two MAX phase materials, Ti_2AlC and Ti_3SiC_2 were also examined in the TGA module of the SATS. The Al-bearing variant formed a protective alumina scale, although the rate of oxidation proved slightly faster than typical FeCrAl alloys and improved with the starting material purity and stoichiometry [16]. The Si-bearing variant, however, did not yield a protective scale and rapid formation of titania was accompanied by significant mass gains.

2.3. Steam oxidation of silica-forming materials

The only material considered in this section is high-purity SiC as Si-containing alloys generally form silica scales beneath chromia scales and high Si levels in an alloy result in poor mechanical properties and fabricability. The oxidation behaviour of SiC in water vapour containing environments was initially examined in detail by Opila et al. [9]. The material recession is governed by paralinear oxidation kinetics that consists of oxide formation and subsequent volatilization. The former is diffusing-limited (parabolic kinetics) and the latter is

surface reaction limited (linear kinetics); hence the paralinear kinetics. Recent tests at ORNL have focused on 100% steam and steam-hydrogen environments with temperatures extending to 1700°C and over a wide range of pressures and flow velocities [18]. Although silica volatilizes in flowing steam, the overall recession kinetics remain slow in atmospheric pressures up to ~1700°C, beyond which the oxide layer melts. The oxidation rate accelerates greatly under high-pressure steam conditions (as low as 0.34 MPa) where interconnected defects form in the oxide layer and render it unprotective. Overall, however, even in the high-pressure conditions, the oxidation rate of SiC is well below that of Zr-based alloys. This attribute, combined with high-temperature strength of these materials, proves them as one of the leading ATF cladding concepts under examination.

2.4. Comparison of parabolic oxidation and linear volatilization rates

Figure 6 provides a side-by-side comparison between the parabolic oxidation and linear volatilization rate of the various chromia, alumina, and silica formers discussed in this study. The results are compared with the oxidation rate of Zr-based alloys. Volatilization rates of silica and Mo are also compared to one another.

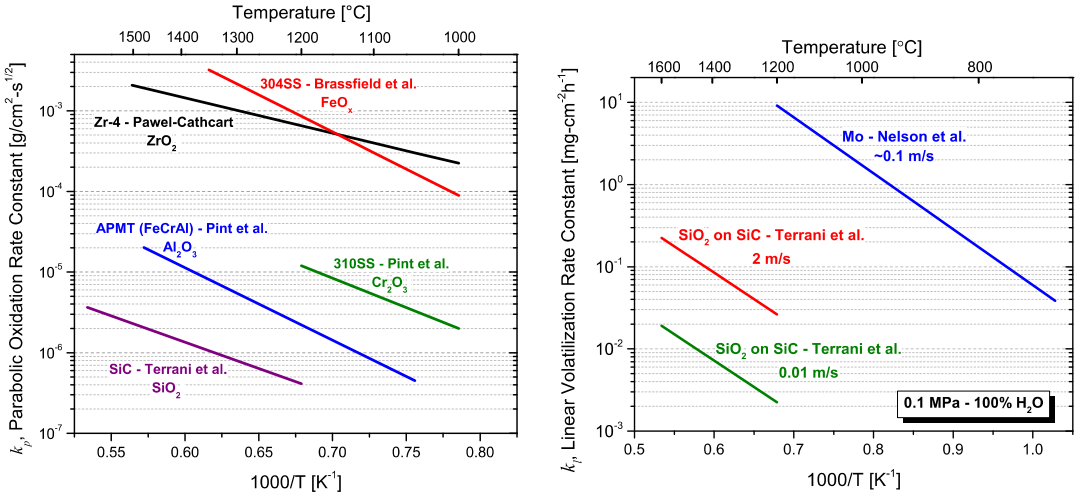

FIG. 6. Left: parabolic oxidation and Right: linear volatilization kinetics of ATF candidate cladding materials [2, 10, 18-20].

4. SUMMARY

Accident tolerant fuel cladding materials are under examination to replace Zr-based alloys in LWRs. An ATF cladding should reduce the rate of heat and hydrogen generation in the core and therefore lower the burden on safety systems and enhance the safety margins. Three different strategies involving protective barriers exist to enable high-temperature steam oxidation resistance via formation of protective scales of chromia, alumina or silica. For Fe-based chromia formers, ~25%Cr is necessary for good oxidation resistance. In FeCrAl alloys, a critical alloy concentration of Cr and Al is necessary to enable formation of protective alumina that in turn offers oxidation kinetics up to 3 orders of magnitude slower than Zr alloys. SiC, a silica-former, exhibits exceptional oxidation resistance in water vapour up to 1700°C.

ACKNOWLEDGEMENTS

The aid and technical insight of Mike Howell and James Keiser at ORNL is gratefully acknowledged. Sebastien Dryepondt provided useful comments on the manuscript. This work was supported by the Advanced Fuels Campaign of the Fuel Cycle R&D programme in the Office of Nuclear Energy, US Department of Energy.

REFERENCES

[1] ZINKLE, S.J., TERRANI, K.A., GEHIN, J.C., OTT, L.J., SNEAD, L.L., Accident tolerant fuels for LWRs: a perspective, J. Nucl. Mater. **448** (2014) 374-379.

[2] CATHCART, J.V., PAWEL, R.E., McKEE, R.A., DRUSCHEL, R.E., YUREK, G.J., CAMPBELL, J.J., et al. "Zirconium Metal–Water Oxidation Kinetics, IV: Reaction Rate Studies", ORNL/NUREG-17, Oak Ridge National Laboratory, (1977).

[3] OTT, L.J., ROBB, K.R., WANG, D., Preliminary assessment of accident-tolerant fuels on LWR performance during normal operation and under DB and BDB accident conditions. J. Nucl. Mater. **448** (2014) 520-533.

[4] TERRANI, K.A., ZINKLE, S.J., SNEAD, L.L., Advanced oxidation-resistant iron-based alloys for LWR fuel cladding, J. Nucl. Mater. 448 (2014) 420-435.

[5] FARMER, M.T., LEIBOWITZ, L., TERRANI, K.A., ROBB, K.R., Scoping assessments of ATF impact on late-stage accident progression including molten core-concrete interaction, J. Nucl. Mater. 448 (2014) 534-540.

[6] MOALEM, M., OLANDER, D.R., Oxidation of Zircaloy by steam, J. Nucl. Mater. 182 (1991) 170-194.

[7] TEDMON, C., The effect of oxide volatilization on the oxidation kinetics of Cr and Fe-Cr alloys, J. Electrochem. Soc. **113** 8 (1966) 766-768.

[8] OPILA, E.J., MYERS, D.L., Alumina volatility in water vapor at elevated temperatures, J. Am. Ceram. Soc. **87** (2004) 1701-1705.

[9] OPILA, E.J., HANN, R.E., Paralinear oxidation of CVD SiC in water vapor, J. Am. Ceram. Soc. **80** 1 (1997) 197-205.

[10] PINT, B.A., TERRANI, K.A., BRADY, M.P., CHENG, T., KEISER, J.R., High temperature oxidation of fuel cladding candidate materials in steam–hydrogen environments, J. Nucl. Mater. **440** (2013) 420-427.

[11] PAWEL, R.E., CATHCART, J.V., CAMPBELL, J.J., The oxidation of zircaloy-4 at 900 and 1100° c in high pressure steam, J. Nucl. Mater., **82 (**1979) 129-139.

[12] MATHON, M., DE CARLAN, Y., GEOFFROY, G., AVERTY, X., ALAMO, A., DE NOVION, C., A SANS investigation of the irradiation-enhanced α–α′ phases separation in 7–12 Cr martensitic steels, J. Nucl. Mater. **312** 2 (2003) 236-248.

[13] WUKUSICK, C., COLLINS, An iron-chromium-aluminium alloy containing yttrium, J., Mater. Res. Std. **4** (1964).

[14] STOTT, F., WOOD, G., STRINGER, J., The influence of alloying elements on the development and maintenance of protective scales, Oxidation of Metals **44** 1 2 (1995) 113-145.

[15] PINT, B., Experimental observations in support of the dynamic-segregation theory to explain the reactive-element effect, Oxidation of Metals **45** 1-2 (1996) 1-37.

[16] PINT, B. A., TERRANI, K.A., YAMAMOTO, Y., SNEAD, L.L., Material Selection for Accident Tolerant Fuel Cladding. Metallurgical and Materials Transactions E (2014).

[17] PINT, B.A., UNOCIC, K.A., TERRANI, K.A., Mater. High Temp. **32** (2015) 28-35.

[18] TERRANI, K.A., PINT, B.A., PARISH, C.M., SILVA, C.M., SNEAD, L.L., KATOH, Y., J. Am. Ceram. Soc. **97** (2014) 2331-2352.

[19] BRASSFIELD, H.C., WHITE, J.F., SJODAHL, L., BITTEL, J.T., "Recommended Property and Reaction Kinetics Data for Use in Evaluating a Light-Water-Cooled Reactor Loss of Coolant Incident Involving Zircaloy-4 or 304SS Clad UO_2", GEMP-482, General Electric Co., Apr 1968, (1968).
[20] NELSON, A.T., SOOBY, E.S., KIM, Y.-J., CHENG, B., MALOY, S.A., High temperature oxidation of molybdenum in water vapor environments, J. Nucl. Mater. **448** (2014) 441-447.

RESEARCH ON PROMISING CLADDING MATERIALS FOR ACCIDENT TOLERANT FUELS AT KIT

M. GROSSE, V. AVINCOLA, A. JIANU, S. AHMAD, M. STEINBRÜCK
Karlsruhe Institute of Technology, Karlsruhe
Germany
E-mail: mirco.grosse@kit.edu

Abstract

Research on nuclear materials has a long tradition at the Karlsruhe Institute of Technology (KIT) and its precursors, the Research Centre Karlsruhe and Nuclear Research Centre Karlsruhe. Examples of the common research fields are the study of material processes occurring during loss of coolant and severe accidents and the development of materials for GEN-IV reactors. These experiences have inspirited the application of the existing knowledge to develop and test candidate materials for so called accident tolerant fuel (ATF) claddings. Silicon carbide, alumina-forming modified layers and ternary carbides coatings (e.g. MAX-phases) on zirconium alloys are some of the considered solutions for this novel cladding systems which should be able to sustain very high temperature, beyond designs basis. At KIT different solutions are nowadays under investigation. An approach called GESA method, consists of Al-containing layers deposition followed by intense pulsed electron beam processing. This method can be used to manufacture alumina-forming modified layers. . Moreover, different deposition methods are currently under evaluation for ternary carbides coatings (V-, Zr-Based). Other major topics of these studies are the investigation of the high temperature oxidation and quench behaviour of silicon carbide (SiC) as monolith and composite cladding tubes. Despite the studies already performed on these materials, assessments are still required concerning the joining feasibility and the behaviour in case of severe accident scenarios (beyond design basis conditions). Hence, steam oxidation studies along with quench tests at temperature between 1600°C and 2000°C have been performed. This work is aimed at implementing bundle experiments in the QUENCH facility, already available at KIT. The joining of SiC based components for assembling complex structures is a scientific and engineering challenge since conventional welding processes cannot be applied due to their non-wetting nature. Yttrium-aluminosilicate glasses have shown promising potential to be used as solder for joining SiC components. These glasses have good mechanical properties, inertness to radiation and their thermal expansion coefficient closely matches with SiC at higher temperature. In our project, aluminosilicate glasses containing Yttrium and different rare earths were prepared by melt-quench technique. Different rare earth elements were used to evaluate the effect of ionic radius differences on the properties and structures of the glasses. The quantitative and qualitative studies of the prepared glasses were conducted to determine their properties and to establish a structure-property relationship. These prepared glasses were used to join the SiC assemblies via laser supported joining method. The properties and the chemistry of the joints were evaluated by examining the interface between solders and SiC.

1. INTRODUCTION

Research on nuclear materials has a long tradition at the Karlsruhe Institute of Technology (KIT) and its precursors, the Research Centre Karlsruhe and Nuclear Research Centre Karlsruhe. Examples of the common research fields are:

- The study of material processes occurring during loss of coolant and severe accidents by code calculations including model developments and experimentally by several large-scale facilities like the QUENCH-, LIVE-, DISCO- MOCKA- or hyka facilities.
- The development and testing of materials for GEN-IV reactors in various environments like liquid metals, supercritical water or helium.

These experiences inspirit applying the existing knowledge to the development and testing of materials being candidates ATF claddings. Particularly, in the KIT-QUENCH programme investigating processes occurring during the early phase of nuclear accidents like cladding rod burst, cladding oxidation and interactions between cladding, guide tube and absorber materials, as well as the debris bed formation gives a powerful framework for the new investigated topics. Commonly, a lot of systems are under discussion as possible candidates for accident tolerant fuels. They can be divided into three groups:

- Sic composites,
- Ternary carbides (e.g. MAX phase), alumina forming alloys, and advanced steels,
- Coatings to improve the performances of zirconium alloys.

Whereas many experimental data are already available on the behaviour of these materials under operation and design basis accident (LOCA) conditions, there is still a lack of information concerning the behaviour under beyond design basis (severe accident) conditions. On the other hand, the behaviour of the commonly used zirconium alloys is satisfying. Therefore, the material behaviour under beyond conditions is the most important argument for development and application of accident tolerant fuels. The paper presented gives first an overview of large-scale and laboratory-scale facilities relevant for testing of ATF claddings. In the second part examples of the common KIT research on promising cladding materials is given.

2. OVERVIEW OF KIT FACILITIES RELEVANT FOR TESTING AND CHARACTERIZATION OF ATF CLADDING MATERIALS

At KIT long term experiences exist in the investigation of material processes occurring under transient accident conditions. Examples of former investigation are the CORA and the REBECCA programmes. Nowadays the high temperature behaviour of common claddings alloys are studied in the QUENCH programme These investigations comprises separate-effect measurements of oxidation kinetics in various atmospheres relevant for nuclear accidents (steam, air, steam/nitrogen), the hydrogen uptake and release by the cladding material and eutectic reactions between zirconium alloys, steel and boron carbide.

The investigations are performed at laboratory-scale in order to study the effects separately or at fuel rod bundle scale in the QUENCH facility to simulate the whole behaviour including fuel rod interaction.

The facilities described in the following sections are available for own KIT research on promising ATF cladding materials as well as for partners on the basis of scientific cooperation or on subcontracts for international projects.

2.1. Laboratory-scale facilities for experiments on high-temperature oxidation and materials interactions

At the KIT institute IAM-AWP three thermo-balances are available allowing in-situ measurements of sample mass changes up to 1600°C. They can be connected with a mass spectrometer to measure the off-gas composition. Different furnace parts can be applied including one allowing using steam as oxidant up to 1250°C. An additional thermo-balance is available at KIT-IHM. The maximal temperature of this facility is 1750°C. Reducing, inert or oxidizing atmospheres including wet gases can be applied. Examples for applications are given in [1, 2].

The INRRO (In-situ Neutron Radiography Reaction Oven) is a horizontal tube furnace dedicated to perform in-situ neutron radiography investigations of reactions in different atmospheres including steam at temperature until 1500°C [3, 4]. The compact design allows mounting the furnace at neutron radiography facilities. By means of neutron radiography it is for instance possible to measure the full quantitative concentration and distribution of hydrogen in zirconium with a spatial resolution up to 25 µm and a time resolution up to 10 s. Former applications were for instance investigations of the hydrogen diffusion in zircaloy-4, the measurement of the hydrogen uptake of various zirconium alloys during steam oxidation or the dependence of the hydrogen uptake and distribution on the mechanical stress state of the sample. However, in-situ neutron radiography experiments depend on the availability of beam-time at neutron radiography facilities.

The BOX furnace is a horizontal tube furnace connected with a state of the art mass spectrometer to measure on-line the off-gas composition. This off-gas composition often provides information about the actual reaction rate in the furnace. The furnace can be used for isothermal experiments at temperatures up to 1600°C or transient tests up to 1700°C [2, 5].

The inductively heated LAVA furnace allows experiments in inert or reducing atmospheres up to temperatures of 2000°C. The off-gas composition can be measured by a mass spectrometer as well. It was used for instance for hot extraction measurements of the hydrogen concentration in zirconium alloys as well as for the study of metallic melt - ceramics interactions.

The most powerful laboratory scale facility for separate-effect tests is the QUENCH Single Rod facility QUENCH-SR. In the quartz tube of this vertical furnace samples with sizes between 20 and 200 mm can be applied. The transparent quartz tube allows the optical observation of the sample behaviour during the experiment in reducing, inert and oxidizing atmospheres including steam. The off- gas composition can be analyzed by means of a state of the art mass spectrometer. The facility offers the possibility of water quenching inside the facility by bottom flooding. Experiments were already performed at temperatures up to 2000°C with SiC cladding segments. Table 1 provides an overview of the laboratory scale facilities.

TABLE 1. OVERVIEW OF THE LABORATORY FACILITIES AT KIT AVAILABLE FOR THE INVESTIGATIONS OF ACCIDENT TOLERANT FUEL CLADDINGS

Furnace	T max for isothermal investigations, °C	T max for transient investigations, °C	Atmospheres	Special features
Thermo-balances	1250	1250	Steam, oxidizing, inert and reducing atmospheres	DTA measurements possible
	1600	1600	oxidizing, inert and reducing dry atmospheres	DTA measurements possible
INRRO	1500	1500	Steam, oxidizing, inert and reducing atmospheres	Special windows transparent for neutrons to perform in-situ neutron radiography experiments
BOX	1600	1700	Steam, oxidizing, inert and reducing atmospheres	Air lock for changing the sample at test temperature
LAVA	2000	2000	Inert and reducing atmospheres	
QUENCH-SR	2000	2000	Steam, oxidizing, inert and reducing atmospheres	Possibility to perform water quenching inside the facility under well-defined conditions

2.2. The large-scale QUENCH facility

The QUENCH facility at KIT is dedicated to simulate experimentally design basis and severe accidents on fuel rod bundle scale. Fig. 1 gives a scheme of the facility.

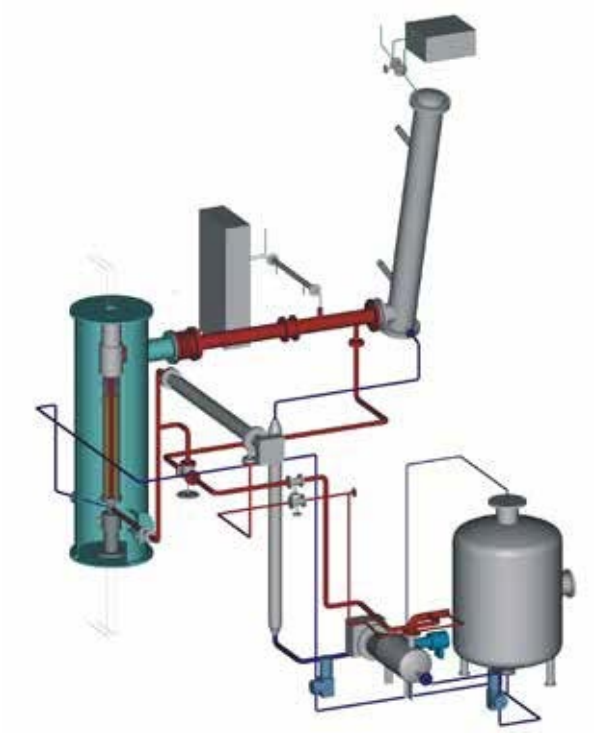

FIG. 1. Scheme of the QUENCH facility.

A typical QUENCH bundle consists of 21 to 31 fuel rod simulators depending on the core geometry of the simulated reactor type. Fig. 2 gives a scheme of the QUENCH-L0 bundle with 16 × 16 German KONVOI reactor geometry. The colours represents the different inner pressures in bar. The 2.5 m long fuel rod simulators consist of original claddings filled by ring shaped zirconia pellets with tungsten or tantalum heater rod (see Fig. 3). The bundle is surrounded by a shroud tube to simulate further rods. The experiments are instrumented by about 70 thermo-couples measuring the temperature at various axial and radial positions. Temperatures and other parameters like inner pressures of the rods, outer pressure in the bundle or water level height are measured with a frequency of 5 Hz. More details about the QUENCH facility are given in the open access reports of the QUENCH tests [7] or in various publications, e.g. [8–12].

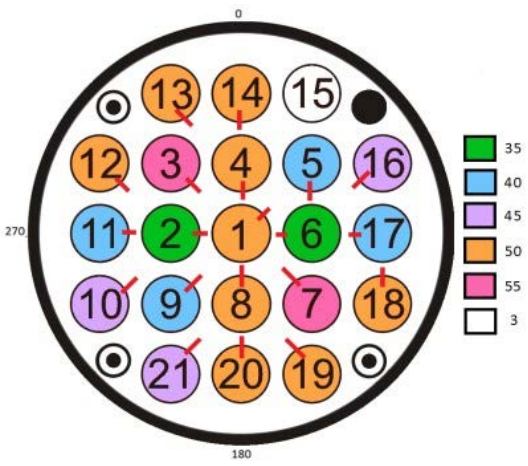

FIG. 2. Scheme of the bundle cross section for 16 × 16 KONVOI geometry.

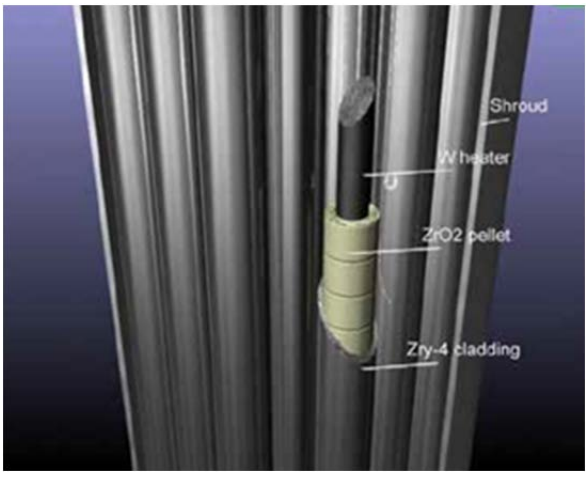

FIG. 3. Scheme of the fuel rod simulators.

Up to now, 17 severe accident and 5 LOCA simulations tests were performed. Main objectives of the large-scale tests are the determination of the hydrogen source term, the validation of models describing reactions occur during the scenarios, the verification of severe accident simulation codes like ASTEC, ATHLET-CD, MAAP, MELCOR, SCDAP/RELAP or ICARE/CATHARE, the investigation of the material behaviour and interaction during LOCA and severe accidents, the analysis of effects occurring during air ingress, the determination of the hydrogen uptake and embrittlement during LOCA, the comparison of the different cladding alloys commonly used in Europe and the investigation of the debris bed formation [8].

One main outcome of the programme is that the hydrogen source term is one to two orders of magnitude higher if cladding melting occurs compared to scenarios without melt formation. Cladding melt formation occurs if the temperature at which the quenching is initiated is too high, the water injection is insufficient (less than 1 g/s/rod), eutectic interactions occur (e.g. steel/B_4C, zircaloy/steel) or the oxide layer at the cladding growth with a non-protective morphology (breakaway effect, air oxidation). The LOCA simulation tests already performed showed that at both sides of the burst opening hydrogen enrichments are formed. These bended hydrogen enriched bands are non-symmetrical oriented to the tube axis [8, 10, 12].

3. EXAMPLES OF KIT RESEARCH ON PROMISING MATERIALS FOR ACCIDENT TOLERANT FUEL CLADDINGS

In this section, examples of KIT research on promising materials for ATF claddings such as high temperature oxidation of SiC, joining of SiC, production, modification and testing of alumina forming Fe-Cr-Al alloys and MAX phases will be given.

3.1. High temperature oxidation of SiC

3.1.1. Theoretical background of SiC oxidation by steam

Silicon carbide can react at high temperature with steam, oxidizing in two ways, called passive and active oxidation. The active oxidation occurs for very low water vapour partial pressure (<10 Pa) [13]. In case of higher oxidant partial pressure, the SiC undergoes reaction (1) developing a dense protective layer of silica (SiO_2):

$$SiC + 3H_2O = SiO_2 + 3H_2 + CO \quad (1)$$

This dense oxide layer slows down the oxidation of the substrate material. The developing of the silica layer is combined with the volatilization of the SiO_2 [13], following mainly equation (2). The volatilization process is strongly dependent on the external conditions.

$$SiO_{2(s)} + 2H_2O_{(g)} \rightarrow Si(OH)_{4(g)} \quad (2)$$

$$SiO_{2_{(s)}} + H_2O_{(g)} \rightarrow SiO(OH)_{2_{(g)}} \quad (3)$$

$$SiO_{2_{(s)}} + \frac{1}{2}H_2O_{(g)} \rightarrow SiO(OH)_{(g)} + \frac{1}{4}O_{2(g)} \quad (4)$$

Hydrogen production is occurring as part of reaction (1). This reaction is raising concerns on the safety characteristic of this cladding material. The formation of the silica layer (1) follows parabolic kinetics which is combined with linear kinetics (2) when volatilization starts to take part in the process. This is described with the para-linear equation (5).

$$\frac{dx}{dt} = \frac{k_p}{2x} - k_l \tag{5}$$

Where k_p is depending on the steam partial pressure and k_l on the steam flow velocity and the total pressure [13]. Among the forms in which silica is appearing, its formation on SiC results in a first vitreous layer and in a subsequent porous non-protective cristobalite scale [14]. The silica layer appeared fully crystallized at 1400°C after 100 h [15].

3.1.2. Oxidation experiments

SiC cladding samples, 2.5 cm length, were provided by Ceramic Tubolar Products LCC. The structural design is the so-called TRIPLEX, consisting of three SiC layers; the inner layer is a monolith tube operating as fission product release barrier and providing strength to the cladding; SiC fibre-SiC matrix composite is the middle layer, which is giving pseudo-ductility. The external layer consists of a deposited SiC as environmental barrier coating. For each test mentioned in Table 2, the temperature was raised at a rate of 10 K/min until the required test temperature was reached.

TABLE 2. SAMPLE TABLE, ATMOSPHERE AND TEMPERATURE DURING QUENCH TESTS

Sample	Atmosphere	T (°C)	Result
CTP13_m1	Argon	2000	Broken
CTP13_m2	Argon+Steam	2000	Broken
CTP13_m3	Argon	2000	Intact
CTP13_m4	Argon	2000	Intact
T11C	Argon+Steam	2000	Intact
T2C	Argon+Steam	2000	Broken
T10C	Argon+Steam	2000	Intact
T4D	Argon+Steam	1600	Intact
T4D_b	Argon+Steam	2000	-

The samples have been heated in an induction furnace. The annealing has been conducted in inert atmosphere up to 1400°C (argon 40 l/h). At this temperature steam has been introduced (63 g/h). The furnace is connected with a mass spectrometer (MS), which allows monitoring the exhausted gases. The volumetric flow rates have been calculated using argon as reference. The temperature is measured directly on the sample surface by means of a two-color pyrometer. After reaching 2000°C, the samples have been quenched by water at 90°C from the bottom with a velocity of 1 mm/s. During this procedure the samples are facing thermal stresses due to radial and axial temperature gradients. The thermal stress occurred in the cladding has been calculated using finite elements analysis. After the test, samples have been analyzed by X-ray and neutron tomography in order to investigate the presence of cracks, which would compromise the fission gas retention. These techniques allow internal

inspection of the sample depending on the total mass attenuation of the elements atomic number. The evaluation and analysis have been done using imaging software (ImageJ, VGstudio).

3.1.3. Results and discussion

In Fig. 4 a typical mass spectrometer measurement is presented. It can be noted that the production of hydrogen and other gases can be correlated with the steam injection at 1400°C. After a first peak when the steam injection is introduced and the oxidation starts, the H_2 flow decreases. This can be explained considering the formation of the silica layer (reaction 1). Starting at 1700°C, the hydrogen production increases. The temperature read by the pyrometer is also showing a change, which is probably due to the silica melting occurring at 1710°C. Moreover, the development of bubbles on the SiC surface prevent from the correct temperature reading. The hydrogen production at temperatures higher than 1800°C can be due to the reaction between graphite susceptor and steam, probably due to the weaving connection between the caps and the silicon carbide, which were preventing from water interaction with the graphite.

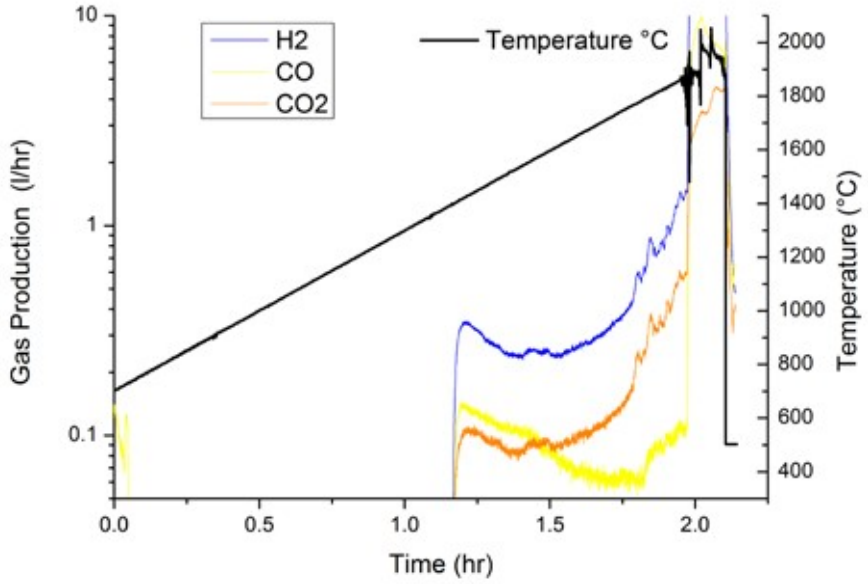

FIG. 4. Exhausted gas measurement during quench of T10C sample in steam.

The integral hydrogen release of sample T10C is presented in Fig. 5. Between the points A and B, parabolic shape production can be seen, due to the developing of SiO_2. After the B point, the value is increasing, probably due to the loss of the protective oxide scale. Comparison with hydrogen produced by zircaloy has been attempted. The area from A to B (1400°C to 1600°C) has been considered. Among the different available correlations, correlation determined at KIT has been chosen to calculate the hydrogen release from zircaloy [16]. Numerical code allowed to calculate the hydrogen production following the experimental conditions already described.

The resulted hydrogen production is given in Fig. 6: 0.003 kg/m^2 are produced by steam oxidation of SiC, 0.12 kg/m2 by oxidation of zircaloy. Accordingly to these data, the hydrogen produced by SiC is 30 times lower than in zircaloy.

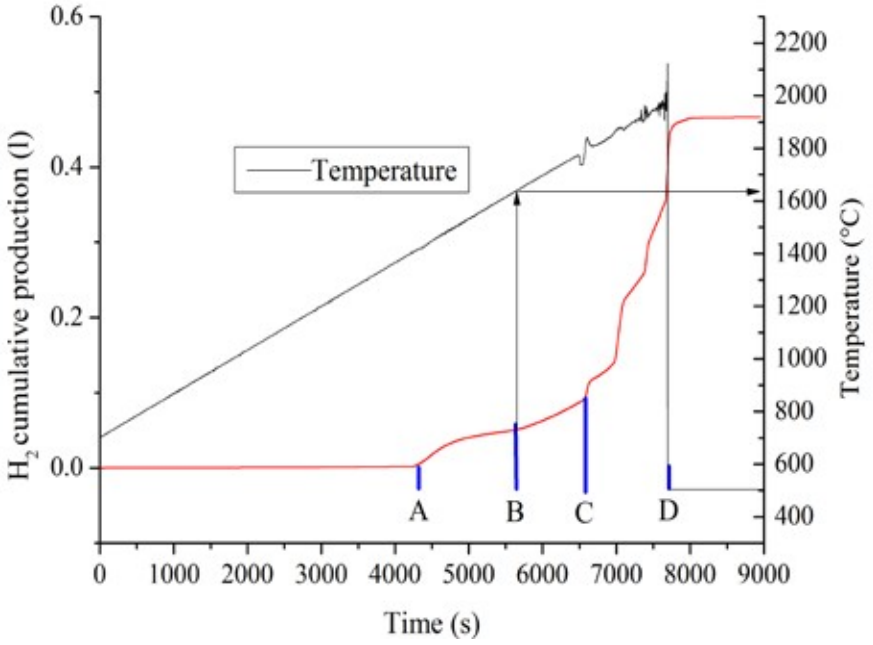

FIG. 5. Integral of the hydrogen production, sample T10C.

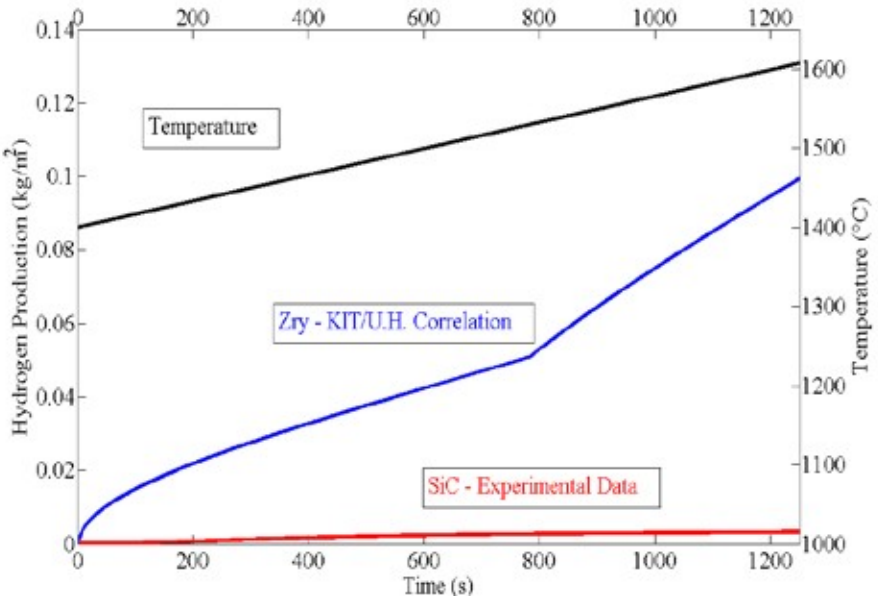

FIG. 6. Hydrogen produced by zircaloy and SiC in non-isothermal conditions.

In point C quenching with water occurs. During the quench procedure, the sample faces high thermal stresses. Under optical inspection, the samples are intact, with the exception of one, which was broken. Post-test analyses by X-ray radiography/tomography have shown that cracks are formed in the inner monolith layer of sample T10C (see Fig. 7). It can be assumed that thermal stresses faced during the quenching, generated cracks along the inner monolith layer. Considering the thermal stress due to the temperature gradient in the cladding thickness, lowering the temperature from 2000°C to 1600°C, will reduce the stress by 20 %. For this reason, the last test has been run at this temperature and no cracks have been detected.

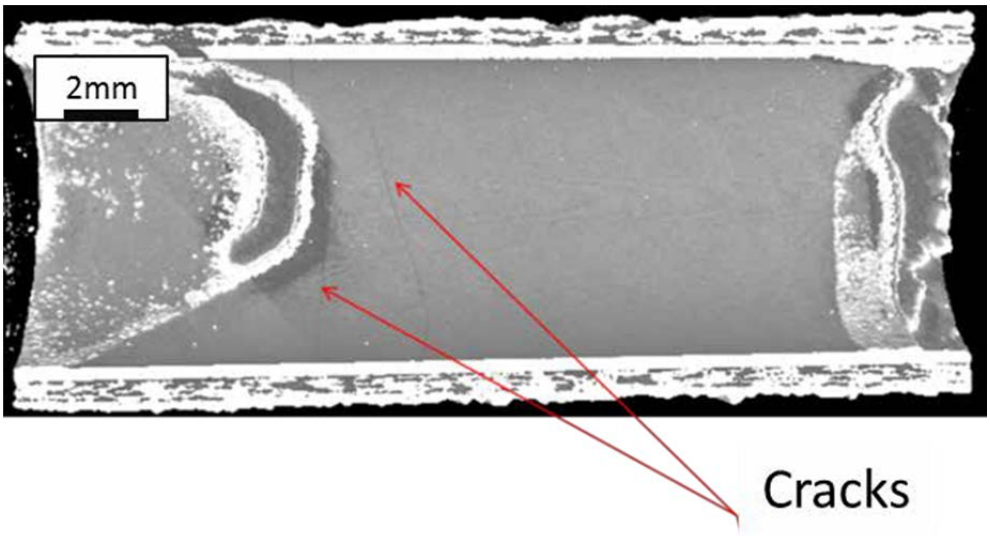

FIG. 7. 3D reconstruction on the basis of X-ray tomography data of sample T10C.

3.2. Joining of SiC

SiC does not show melting phase therefore it cannot be joined by conventional fusion welding processes. It is an important technological challenge to produce the complex geometry structure by assembling SiC components [17]. There are different processes that are being used in industry for joining of SiC components such diffusion bonding, chemical reaction bonding, application of pre- ceramic polymer, use of metals/metal alloys as filler for the brazing the SiC components and use of spark plasma sintering etc. The diffusion bonding and chemical reaction bonding processes need high temperature and pressure for longer interval of time. Secondly, the joining of components in these processes depends on the geometry of the kiln. The application of pre-ceramic polymer reduce the higher value of temperature and produce SiC structure in the joint but this joint is porous structurally and can affects the joint strength [17–19]. Metals/metal alloys are widely used in industry as an alternative choice for joining of ceramic bodies as they can induce the ductility in the joint and enhance the property profile of the joint, even though the thermal expansion coefficient mismatch between metals and ceramics is still an issue [20]. In our experiments, glasses are used as solders for joining of SiC components. There is a large number of natural elements that show attraction towards each other to prepare glasses. The properties of these glasses can also change to some extent by varying their compositions. Lipmann et al. [21] used different glass compositions for joining of SiC components and they found yttrium aluminosilicate glasses (Y_2O_3-Al_2O_3-SiO_2) as good choice material to be used as solder for joining of SiC. The coefficient of thermal expansion of this glass system matches with SiC on wider range of temperature. Secondly, the glass formation temperature of yttrium aluminosilicate glasses is around 900°C and they showed good strength, hardness and inertness to radiations [22, 23]. We prepared six different rare earth glasses with melt-quench techniques. These glasses were used for joining SiC components via laser supported process and then the properties of the joint profiles were evaluated.

TABLE 3. COMPOSITIONS OF PREPARED GLASSES (IN MOLE.%)

Specimen	Al_2O_3	SiO_2	Y_2O_3	Sc_2O_3	Yb_2O_3	Nd_2O_3	Dy_2O_3	Ho_2O_3	Tm, (°C)
AlSiY	22	65.82	12.18	---	---	---	---	---	1385
AlSiSc	22	65.82	---	12.18	---	---	---	---	1650
AlSiYb	22	65.82	---	---	12.18	---	---	---	1460
AlSiNd	22	65.82	---	---	---	12.18	---	---	1290
AlSiDy	22	65.82	---	---	---	---	12.18	---	1350
AlSiHo	22	65.82	---	---	---	---	---	12.18	1372

3.2.1. Glass preparation

Commercially available pure fine powders of Al_2O_3, amorphous SiO_2 and Re_2O_3 (Re= Y, Sc, Nd, Ho, Dy, Yb) were used for the preparation of glass samples. The oxides powders were mixed in isopropanol according to the composition given in Table 3 and homogenized for 30 min in an ultrasonic bath. Later, isopropanol was evaporated in a drying oven at about 100°C. The green bodies of small cylindrical shape were produced by cold isostatic pressing.

These cylinders were melted in platinum crucible up to 1450-1650°C (depending upon compositions). This temperature was held for 1h in order to achieve melt homogenization. The melted samples were quenched in water to obtain the glass splinters as shown in Fig. 8.

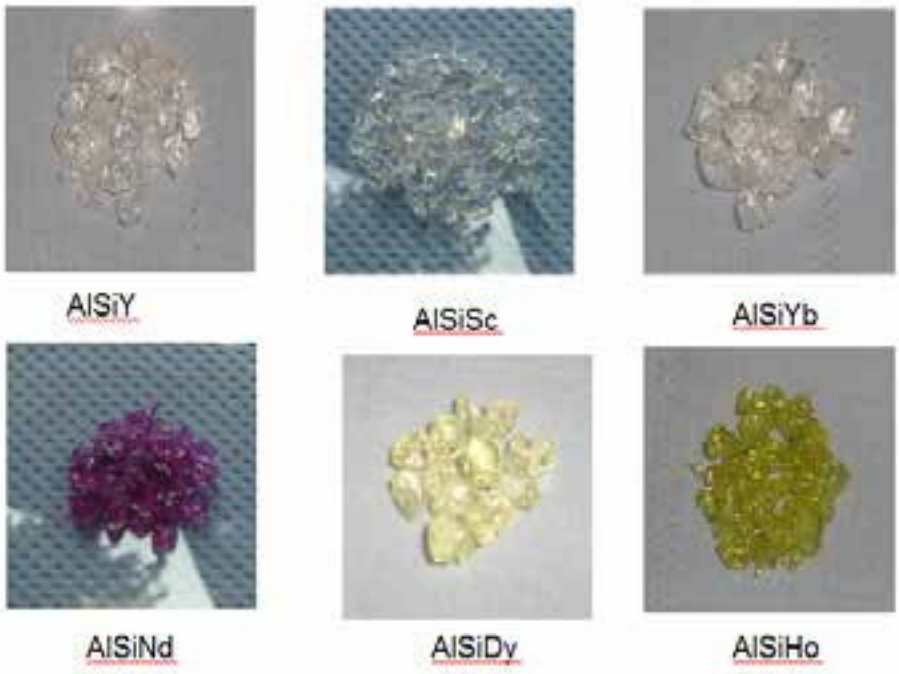

FIG. 8. Prepared glasses.

3.2.2. Results and discussion

3.2.2.1. Characterization of prepared glasses

The structural analyses by XRD of these prepared glasses showed amorphous structures. The glass splinters were grounded in a ball mill to get fine glass powder of less

than 5 micron diameters. Differential scanning calorimetry (DSC) analyses were carried out by using DSC 404 Netzsch to determine glass transition temperatures (Tg) and crystalline temperatures (Tc) for prepared glasses. It was found that the value of glass transition temperature increased by lowering the ionic radii of rare earth ions (Fig. 9, Table 4). Hot stage microscopy experiments were carried out to find out the softening temperature of these glasses under laser conditions.

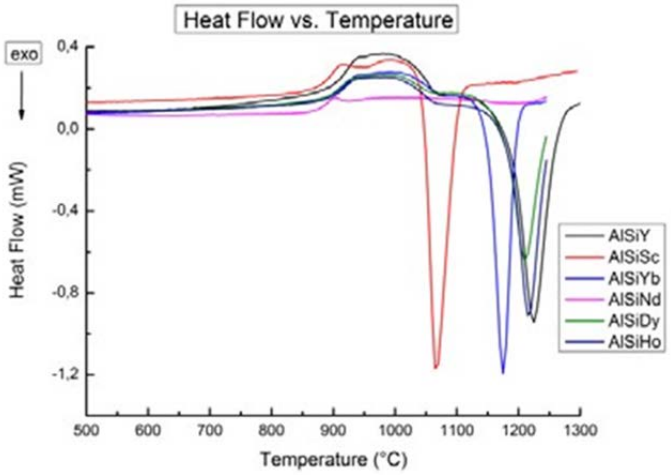

FIG. 9. DSC curves of prepared glasses.

TABLE 4. DSC VALUES OF PREPARED GLASSES

Specimen	Tg (°C)	Tc (°C)
AlSiY	917.2	1224.6
AlSiSc	893	1066.9
AlSiYb	918.1	1175
AlSiNd	884.3	---
AlSiDy	909.7	1210.3
AlSiHo	912	1216.9

3.2.2.2. Joining of SiC components

These glass powders were mixed with ethanol to make slurry that was pasted around the parts of SiC to be joined. SiC components were fixed in the jaws of holder and a little pressure (25 mN) was applied to hold the specimens (Fig. 10) and rotated around their axis with optimized speed of 120 rpm. Diode laser (wave length 808 + 940 nm) was scanned on the pasted slurry. This localized heating melts the glass slurry within 1 min. After that laser was switched off, the temperatures fall down to below 600 °C in next 40 s. This fast cooling rate (25 K/s) produced glassy structure in the joint layer. An infrared camera was used to measure the temperature during joining process. It is a fast joining process that completed within few minutes and does not require any surface preparation of SiC components before joining.

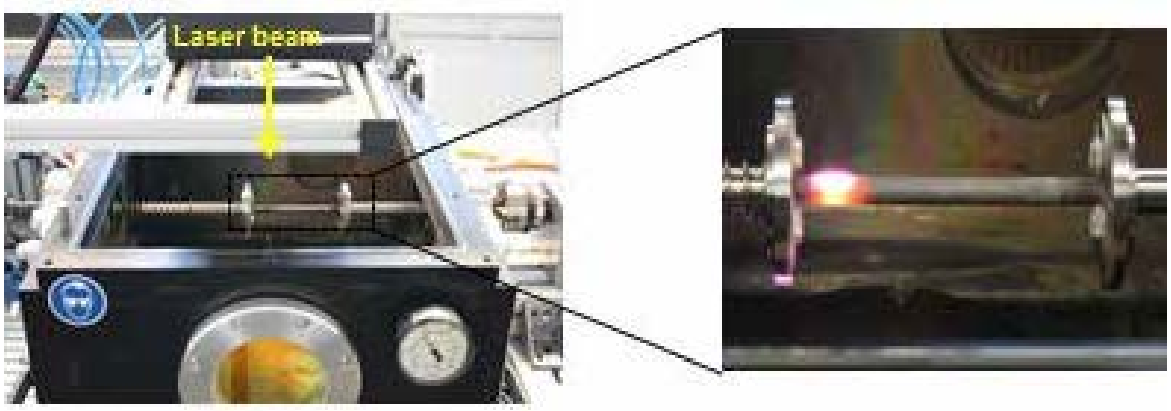

FIG. 10. Experimental joining set-up.

3.2.2.3. Characterization of the joint layer

Characterizations of the joint made with yttrium aluminosilicate glasses were carried out. The melted glass showed good wettability with SiC components (Fig. 11). It was found that the formation of pores in the joining layer depends on the composition of the solder and gap width. The high-temperature strength of the braze joint is indirectly proportional to the thickness of the joint. The strength of the joint was determined with 4-point bending test and found up to 70 % of the reference SiC material. Moreover, the structure of re-solidified solder does not depend on the absorption properties for the laser wavelength. He leakage rate (gas tightness) of joint was found up to 2×10^{-8} mbar.s^{-1}.

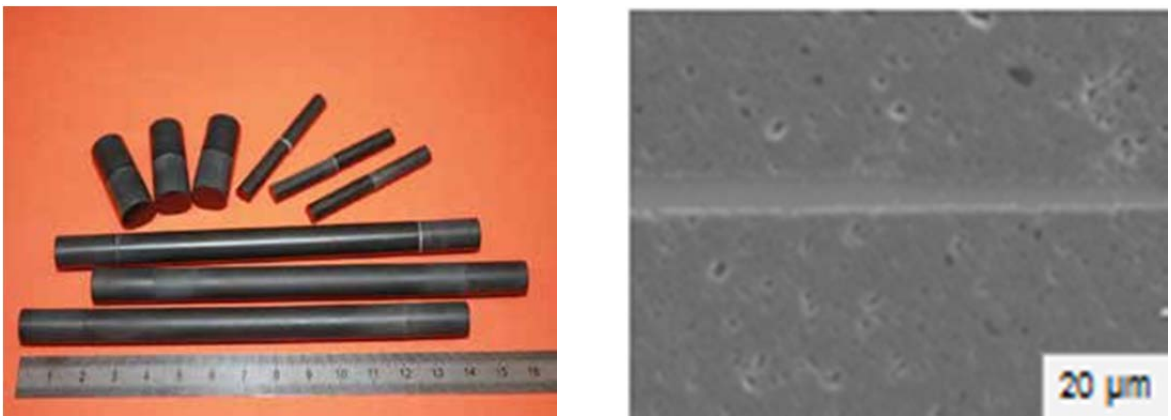

FIG. 11. (a) Joined SiC components (b) Joint layer made with Y_2O_3-Al_2O_3-SiO_2 solder.

3.2.3. Conclusion

Six different rare earth aluminosilicate glasses were prepared and their characterization was carried out by using different tools. These glasses were used for the joining of SiC components via laser supported process. The characterization of the joint layer was carried out. The success of that joining process depends on the solder composition and the thickness of the joint layer.

3.3. Protective coatings on zirconium-based alloys

Besides SiC claddings, zircaloy with protective coating seems to be promising as candidate material for ATF claddings. At KIT MAX phases and alumina forming alloys are investigated.

3.3.1. Fe-Cr-Al alloys

Alumina-forming Fe-Cr-Al alloys are of large interest for practical applications at high-temperatures in reactive atmospheres [24-27]. The role of Cr is to lessen the content of Al required to form a protective Al_2O_3 layer (third-element effect) [28, 29]. The alumina stability domain was defined for Fe-Cr-Al alloy systems (with low Al content) after exposure in gas atmosphere at temperatures higher than 800°C [25, 30] and after exposure to oxygen-containing liquid lead in the 400-600°C temperature range [31].

Experimental data concerning the oxidation behaviour of Fe-Cr-Al alloy systems under high- temperature steam exposure are available. Alumina-forming Fe-Cr-Al alloys are very resistant to this environment and form protective alumina scales up to 1475°C [32, 33]. In order to counteract the neutronic impact of this material, thinner cladding walls are required, which constitutes a challenging technological requirement. This is why alumina-forming Fe-Cr-Al layers can be considered as a good solution for protection of Zr-based cladding tubes.

An approach called GESA (abbreviation of the German name “Gepulste Electronstrahl Anlage” = pulsed electron beam facility), developed at KIT, consisting in deposition of an Al-containing layer on the substrate, followed by intense pulsed electron beam processing, can be used to manufacture alumina-forming modified layers [34 - 36]. Fig. 12 shows the cross section of the Fe-Cr-Al-Y layer deposed by low pressure plasma spray (a) and modified by intense pulsed electron beam (b).

The modification by intense pulsed electron beam consists in melting the layer together with some micrometres of the substrate surface. The processing leads to surface smoothening, pores removal and metallic bonding between the substrate and the layer. A structural and compositional gradient up to 30-50 micrometres can be obtained at the materials surface.

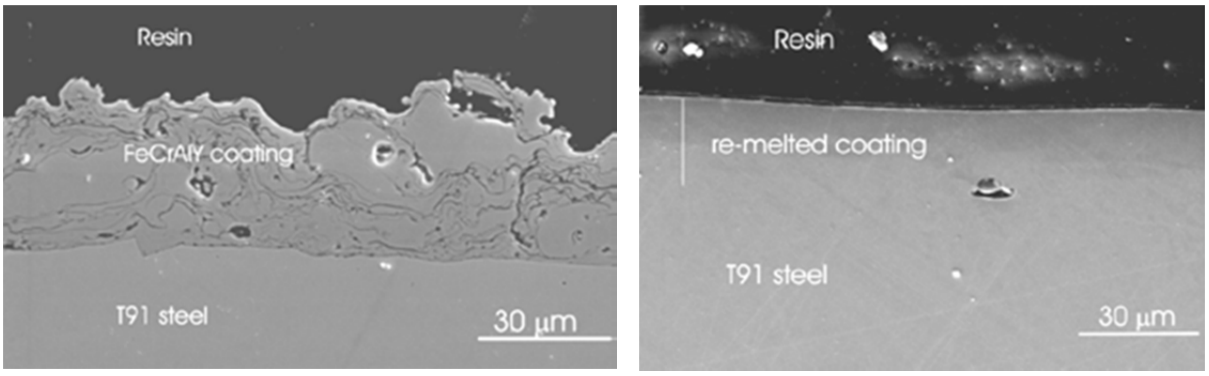

(a) *(b)*

FIG. 12. The deposed Fe-Cr-Al-Y layer (a) and the Fe-Cr-Al-Y layer after modification by melting with intense pulsed electron beam (b).

3.3.2. *Alumina coatings*

Another project deals with the direct deposition of an alumina coating at zircaloy. In order to obtain such protective coating, 40 µm thick aluminium layers has been deposed at zircaloy samples by means of PVD techniques. The samples were tested inside a thermo-balance. A first pre-oxidation was performed in order to form an Al_2O_3 layer on the aluminium. The heating rate was 10 K/min until a temperature of 500°C was reached. A steam flow of 3 g/h was introduced and the samples were held at this temperature for 2 h. One sample was returned to room temperature at this point in order to act as a reference. Afterwards, the temperature increased again to 1200°C. One sample was raised at a rate of 5 K/min, while the other sample was raised at a rate of 30°C/min. The sample of zircaloy without an alumina coating was also raised at 30 K/min. Upon reaching 1200°C, the samples were held for 120 min or until approximately 30 % mass gain occurred, as 30 % mass gain indicated full oxidation of the zircaloy. After the isothermal period at 1200°C was completed, the steam flow was switched off, and the sample was cooled down to room temperature.

Fig. 13 shows the mass gains and temperatures as a function of time for the zircaloy and alumina- coated zircaloy samples. The highest mass gain was recorded for the alumina-coated sample which was heated at a rate of 30 K/min, and the second highest one was for the other alumina-coated sample which was heated at a rate of 5 K/min. For both alumina-coated samples, the test concluded due to almost full oxidation before the full two-hour isothermal period at 1200°C was completed. In contrast, the sample of zircaloy without alumina coating oxidized significantly slower, completing the full isothermal period and yet still having a lower total oxidation than the other two samples. The reason for this is likely due to the deposited aluminium layer being too thick. Aluminium melts at 660°C, and therefore the bond between the alumina and the sample would be lost.

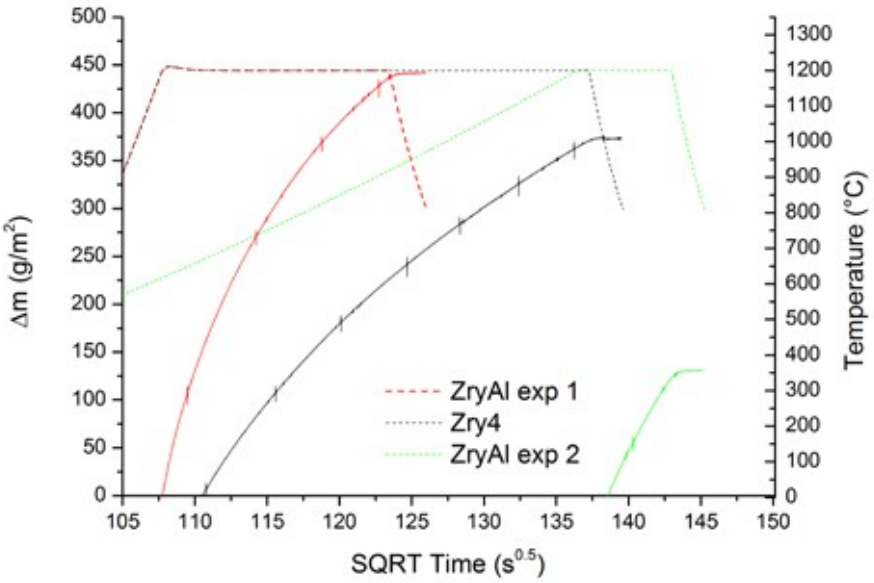

FIG. 13. The mass gain per unit area plotted against the square root of time for the three samples at 1200°C. The slopes determine the rate constant in units of g/($m^2 \cdot s^{½}$).

3.3.3. *MAX phases*

(M_y + 1 A X_y) phases (where M is an early transition metal, A is an A group element, X is C or N and y = 1 to 3), also known as MAX phases, are considered as promising materials

for structural applications at high temperatures [37 - 39]. Among these, V and Zr-based MAX phases can be considered as protective coatings for zirconium cladding tubes.

For ternary carbides coatings different compositions (V-, Zr-based) and deposition methods are under evaluation. Synthesis of V-based MAX-phases by different methods, such as pressureless sintering (either conventional- or microwave-assisted) and spark plasma sintering, are currently under development. Fig. 14 shows the XRD pattern of V_2AlC Max phase obtained by spark plasma sintering (SPS) at 1400 °C with 30 minutes holding time. A fully dense, single-phase V_2AlC samples were successfully obtained starting from mixed powders with non-stoichiometric molar ratio (2:1.2:0.9).

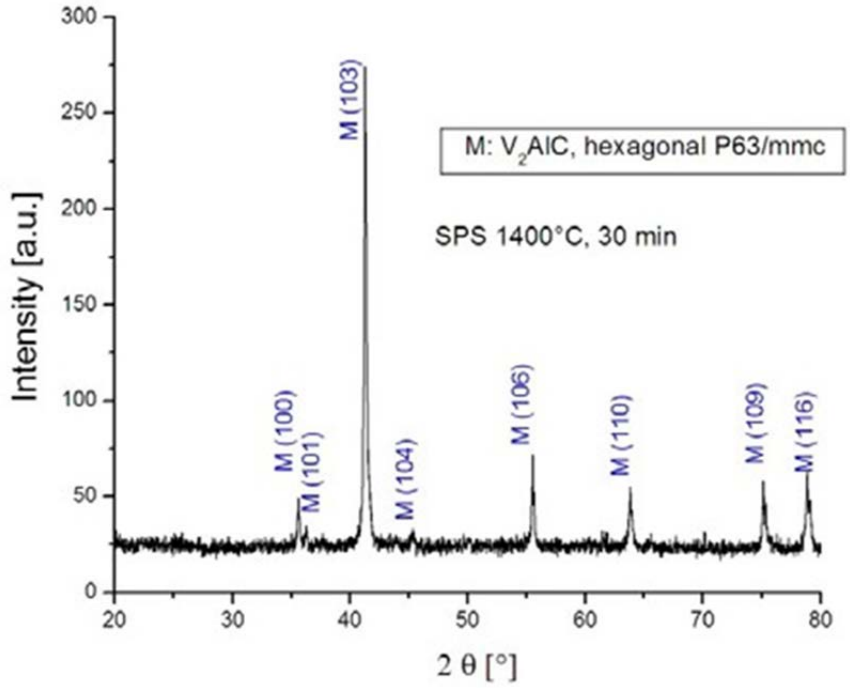

FIG. 14. XRD pattern of V_2AlC MAX phase obtained by SPS.

4. CONCLUSION

The long tradition and the high experience of KIT in the field of material research as well of design basis and severe nuclear accident is a good basis for applying the knowledge to the development and testing of promising accident tolerant fuel cladding materials. A lot of state of the art laboratory-scale facilities are available for separate-effect tests like the determination of the high-temperature oxidation or thermo-shock behaviour or the interaction between different structural materials applied in nuclear reactors. The facilities are used for in-house research but they are open for cooperation as well. However, assessments are still needed to meet industrial requirements. Some open issues are for instance the mechanical behaviour of a SiC cladding tube itself and the joining stability in case of thermo-shock.

Coated zircaloy claddings are a promising short-term solution. However, the high temperature oxidation kinetics, the thermo-shock behaviour, the adhesion between zircaloy and coating and the cladding behaviour of a damaged coating resulting from friction in the spacer grids or in case of fretting is not yet known enough to commercially employ these solutions.

REFERENCES

[1] STEINBRÜCK, M., Oxidation of zirconium alloys in oxygen at high temperatures up to 1600°C, Oxidation of Metals, **70** (2008) 317.

[2] STEINBRÜCK, M., Prototypical experiments relating to air oxidation of zircaloy-4 at high temperatures, J. Nucl. Mater. **392** (2009) 531.

[3] GROSSE, M., VAN DEN BERG, M., GOULET, C., LEHMANN, E., SCHILLINGER, B., In- situ neutron radiography investigations of hydrogen diffusion and absorption in zirconium alloys, Nucl. Instr.& Meth. In Phys. Res. **A651** (2011) 253.

[4] GROSSE, M., STEINBRÜCK, M., LEHMANN, E., VONTOBEL, P., Kinetics of hydrogen absorption and release in zirconium alloys during steam oxidation, Oxidation of Metals **70** (2008) 149.

[5] STEINBRÜCK, M., Degradation and oxidation of B_4C control rod segments at high temperatures, J. Nucl. Mater. **400** (2010) 138.

[6] HOFMANN, P., et al., "Quench Behaviour of Zircaloy Fuel Rod Cladding Tubes. Small-Scale Experiments and Modelling of The Quench Phenomena", Report FZKA-6208, Forschungszentrum Karlsruhe (1999).

[7] http://quench.forschung.kit.edu

[8] STUCKERT, J., GROSSE, M., RÖSSGER, C., KLIMENKOV, M., STEINBRÜCK, M., WALTER, M., QUENCH-LOCA program at KIT on secondary hydriding and results of the commissioning bundle test QUENCH-L0, Nuclear Engineering and Design **255** (2013) 185.

[9] GROSSE, M., STEINBRÜCK, M., STUCKERT, J., KASTNER, A., SCHILLINGER, B., Application of neutron radiography to study material processes during hypothetical severe accidents in nuclear reactors, J. Mat. Sci. **47** (2012) 6505.

[10] GROSSE, M., STUCKERT, J., ROESSGER, C., STEINBRUECK, M., WALTER, M., KAESTNER, A., Analysis of the secondary cladding hydrogenation during QUENCH- LOCA tests and its influence on the cladding embrittlement, ASTM STP **1543** (2014) doi:10.1520/STP154320120155.

[11] STEINBRÜCK, M., GROSSE, M., SEPOLD, L., STUCKERT, J., Synopsis and outcome of the QUENCH experimental program, Nuclear Engineering and Design, **240** (2010) 1714.

[12] GROSSE, M., STUCKERT, J., STEINBRÜCK, M., KAESTNER, A., Secondary hydriding during LOCA – Results from the QUENCH-L0 test, J. Nucl. Mater., **420** (2012) 575.

[13] OPILA, E.J., HANN, Jr., R. E., Paralinear oxidation of CVD SiC in water vapor, J. Am.Ceram. Soc. **80** (1997) 1.

[14] TORTORELLI, P.F. and MORE, K.L., Effects of high water-vapor pressure on oxidation of silicon carbide at 1200°C, J. Am. Ceram. Soc. **86** (2003) 1249.

[15] OPILA, E.J., Variation of the oxidation rate of silicon carbide with water-vapor pressure, J. Am. Ceram. Soc. **82** (1999) 625.

[16] GROSSE, M., Comparison of the high temperature steam oxidation kinetics of advanced cladding materials, Nucl. Trans. **170** (2010) 272.

[17] KATOH, Y., SNEAD, L.L., CHENG, T., SHIH, C., LEWIS, W.D., KOYANAGI, T., HINOKI, T., et al., Radiation-tolerant joining technologies for silicon carbide ceramics and composites, J. Nucl. Mater. **448** (2014) 497.

[18] SNEAD, L.L., NOZAWA, T., KATOH, Y., BYUN, T-S., KONDO, S., PETTI, D. A., (2007). Handbook of SiC properties for fuel performance modelling. J. of Nucl. Mater., **371** (2007) 329., doi:10.1016/j.jnucmat.2007.05.016.

[19] HENAGER, C.H., SHIN, Y., BLUM, Y., GIANNUZZI, L.A., KEMPSHALL, B.W., SCHWARZ, S.M., Coatings and joining for SiC and SiC-composites for nuclear energy systems, J. Nuclear Materials, **367-370** (2007) 1139., doi:10.1016/j.jnucmat.2007.03.189.
[20] MARTINELLI, A.E., & BUSCHINELLI, A.J.A., Review Article : Recent advances in metal-ceramic brazing, **49** (2003) 178.
[21] LIPPMANN, W., KNORR, J., WOLF, R., RASPER, R., EXNER, H., REINECKE, A-M., NIEHER, M., et al., Laser joining of silicon carbide - a new technology for ultra-high temperature resistant joints, Nucl. Engin. & Design, **231** (2004) 151, doi:10.1016/j.nucengdes.2004.03.002.
[22] HERRMANN, M., LIPPMANN, W., & HURTADO, A., High-temperature stability of laser- joined silicon carbide components, J. Nucl. Mater. **443** (2013) 458. doi:10.1016/j.jnucmat.2013.07.067.
[23] HERRMANN, M., LIPPMANN, W., HURTADO, A., Y_2O_3–Al_2O_3–SiO_2-based glass-ceramic fillers for the laser-supported joining of SiC, J. European Ceramic Soc., **34** (2014) 1935., doi:10.1016/j.jeurceramsoc.2014.01.019.
[24] MINER, R.G., NAGARAJAN, V., The morphology of oxidation of alumina-forming iron- base alloys containing chromium and aluminium, Oxid. Met. **16** (1981) 313.
[25] TOMASZEWICZ, P., WALLWORK, G.R., The oxidation of high-purity iron-chromium- aluminium alloys at 800°C, Oxid. Met. **20** (1983) 75.
[26] GOLIGHTLY, F.A., WOOD, G.C., STOTT, F.H., The early stages of development of α- Al_2O_3 scales on Fe-Cr-Al and Fe-Cr-Al-Y Alloys at high temperature, Oxid. Met. **14** (1980) 217.
[27] DEVAN, J.H., TORTORELLI, P.F., The oxidation-sulfidation behaviour of iron alloys containing 16–40 at% aluminium, Corros. Sci. **35** (1993) 1065.
[28] STOTT, F.H., WOOD, G.C., STRINGER, J., The influence of alloying elements on the development and maintenance of protective scales, Oxid. Met. **44** (1995) 113.
[29] ZHANG, Z.G., GESMUNDO, F., HOU, P.Y., NIU, Y., Criteria for the formation of protective Al_2O_3 scales on Fe–Al and Fe–Cr–Al alloys, Corros. Sci. **48** (2006) 741.
[30] ZHANG, Z.G., ZHANG, X.L., SHENG, L., TENG, X., The effect of the third element Cr on oxidation behaviour of Fe-xCr-10Al (AT.%) alloys at 900°C, Open Corros. J. **2** (2009) 37.
[31] WEISENBURGER, A., JIANU, A., DOYLE, S., BRUNS, M., FETZER, R., HEINZEL, A., DELGIACCO, M., AN, W., MUELLER, G., Oxide scales formed on Fe-Cr-Al-based model alloys exposed to oxygen containing molten lead, J. Nucl. Mater., **437** (2013) 282.
[32] TERRANI, K.A., PARISH, C.M., SHIN, D., PINT, B.A., Protection of zirconium by alumina- and chromia-forming iron alloys under high-temperature steam exposure, J. Nucl. Mater. **438** (2013) 64.
[33] PINT, B.A., TERRANI, K.A., BRADY, M.P., CHENG, T.J., KEISER, R., High temperature oxidation of fuel cladding candidate materials in steam–hydrogen environments, J.Nucl. Mater. **440** (2013) 420.
[34] MÜLLER, G., SCHUMACHER, G., ZIMMERMANN, F., Investigation on oxygen controlled liquid lead corrosion of surface treated steels, J. Nucl. Mater. **278** (2000) 85.
[35] WEISENBURGER, A., HEINZEL, A., MUELLER, G., MUSCHER, H., ROUSANOV, A., T91 cladding tubes with and without modified FeCrAlY coatings exposed in LBE at different flow, stress and temperature conditions, J. Nucl. Mater. **376** (2008) 274.
[36] ENGELKO, V., MUELLER, G., RUSANOV, A., MARKOV, V., TKACHENKOV, K., WEISENBURGER, A., KASHTANOV, A., CHIKIRYAKA, A., JIANU, A.,

Surface modification/alloying using intense pulsed electron beam as a tool for improving the corrosion resistance of steels exposed to heavy liquid metals, J. Nucl. Mater. **415** (2011) 270.

[37] BAO, Y.W., WANG, X.H., ZHANG, H.B., ZHOU, Y.C., Thermal shock behaviour of Ti_3AlC_2 from Between 200 and 1300°C, J. Eur. Ceram. Soc. **25** (2005) 3367.

[38] HU, C.F., HE, L.F., ZHANG, J., BAO, Y.W., WANG, J.Y., LI, M.S., ZHOU, Y.C., Microstructure and properties of bulk Ta_2AlC ceramic synthesized by an in situ reaction/hot pressing, J. Eur. Ceram. Soc. **28** (2008) 1679.

[39] HU, C.F., HE, L.F., LIU, M.Y., WANG, X.H., WANG, J.Y., LI, M.H., BAO, Y.W., ZHOU, Y.C., In situ reaction synthesis and mechanical properties of V_2AlC, J. Am. Ceram. Soc. **91** (2008) 4029.

ADVANCED ACCIDENT TOLERANT FUEL PELLETS
(SESSION 5)

Chairperson

R. Montgomery

TVA, United States of America

THERMO-PHYSICAL PROPERTIES OF MICRO-CELL UO2 PELLETS AND HIGH DENSITY COMPOSITE PELLETS FOR ACCIDENT TOLERANT FUEL

J-H. YANG, D-J. KIM, K. S. KIM, Y-H. KOO
Korea Atomic Energy Research Institute
Yuseong-gu, Daejeon
Republic of Korea
E-mail: yhkoo@kaeri.re.kr

Abstract

This study presents the design and fabrication of micro-cell UO_2 fuel pellets and high-density fuel pellets and also evaluates their out-of-pile performance. Micro-cell UO_2 pellets are characterized by enhanced retention capability of their fission products and/or thermal conductivity. High-density pellets are composite pellets consisting of oxide and nitride components and they are expected to offer enhanced uranium density and thermal conductivity.

1. INTRODUCTION

KAERI has launched a research programme to develop advanced LWR fuel pellets with enhanced accident tolerance [1]. The objectives of this project are to design and select potential candidates for ATF fuel pellets, test out-of-pile performance, and establish a database for fuel materials, as well as to evaluate the irradiation performance of selected samples in research reactors. Micro-cell UO_2 pellets and high density composite pellets are being developed under this research programme to increase the accident tolerance of nuclear fuels under severe accident conditions as well as normal operating conditions. In this study, we evaluated the thermo-physical properties of micro-cell and high density pellets. We fabricated sample pellets in which the micro-cell and composite concepts were successfully implemented. The thermal diffusivity and thermal expansion of the samples have been measured. A corrosion test in high temperature steam to evaluate the chemical compatibility with water is also conducted.

2. MICRO-CELL UO_2 PELLETS

Accident-tolerant pellets that maintain reliability during normal operation and moreover exhibit enhanced retention of fission products even in severe accidents are highly desirable, since the primary objective of developing such pellets is to minimize the release of radioactive materials into the environment during severe accidents. It should be noted that the fuel pellet is both the source of these radioactive fission products and the first barrier for blocking their release to the environment [2, 3].

KAERI has designed a microcell UO_2 pellet to enhance the retention capability of highly radioactive and corrosive fission products and/or increase the thermal conductivity of pellets [4]. The key idea of micro-cell UO_2 pellets is that the thin cell walls located in a pellet act as multiple chemical traps to immobilize volatile fission products (FPs) such as Cs and I, and/or as an enhancer of the thermal conductivity of the pellets to reduce the pellet temperature and chemical diffusivity of FPs. Fig. 1 shows a conceptual schematic illustration of a microcell UO_2 pellet in which all UO_2 grains or granules are enveloped by thin cell walls. The thin walls located among the grains act as chemical traps or physical barriers to the movement of fission products. Depending on the materials composing the cell wall, both ceramic and metallic microcell UO_2 pellets have been designed.

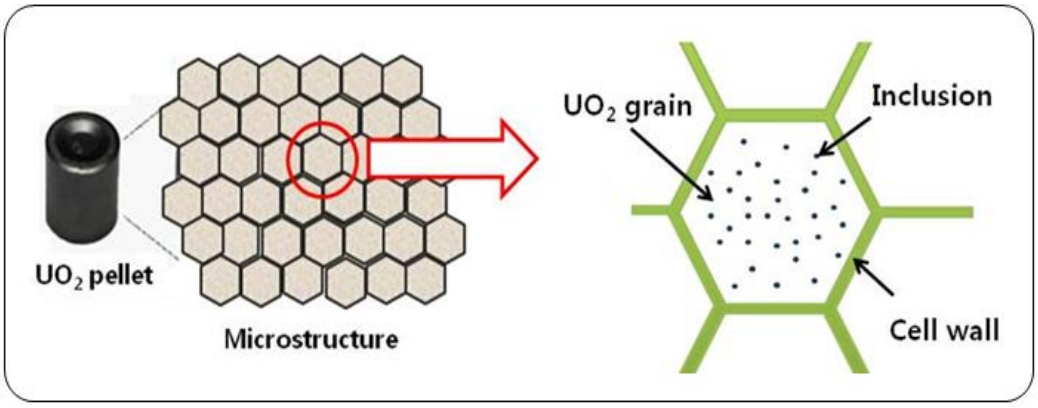

FIG. 1. Conceptual schematic illustration of microcell UO_2 pellets.

The main purpose of the ceramic microcell UO_2 pellets is to reduce the release of fission products to the outside of the pellets. Improved retention capability of fission products would reduce stress corrosion cracking at the cladding inner surface caused by I and/or Cs as well as by the internal pressure of the fuel rod. These benefits are expected to enhance the robustness of the fuel rods during severe accidents as well as normal operation. A mesh-like rigid wall structure is also expected to prevent massive fragmentation of pellets during severe accidents, thereby reducing the release of radiotoxic fission products to the environment. A conventional liquid-phase sintering technique has been applied to fabricate ceramic microcell UO_2 pellets. A powder mixture of UO_2 and additives was pressed into green pellets. These pellets were then sintered at an elevated temperature at which the additives for wall materials formed a liquid phase, penetrating through grain boundaries and enveloping UO_2 grains to make the proposed microcell. The wall materials require chemical affinity to Cs and/or I so that the wall is able to capture or form stable compounds with the incorporated Cs and/or I. Since Cs interacts with I to form caesium iodide precipitates and the fission yield of Cs is roughly ten times larger than that of I, the chemical affinity of the wall to Cs may have a considerable impact on the capability to retain fission products. Insolubility of the wall in UO_2 is also an important requirement to maintain the microcell structure during long-term irradiation in a nuclear reactor. It was suggested that SiO_2 can chemically trap volatile Cs fission products and form relatively stable compounds. Several kinds of SiO_2-based additives were selected in this study. Fig. 2 shows the typical microstructure of fabricated ceramic microcell UO_2 pellets in which the microcell concept is successfully implemented.

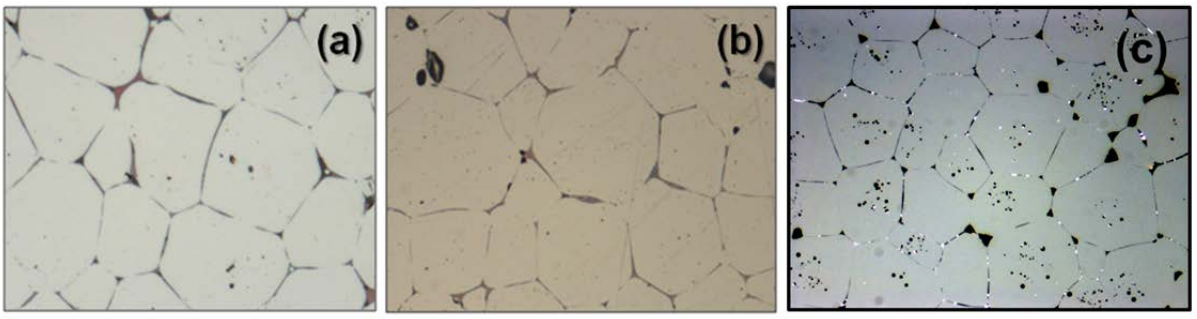

FIG. 2. Typical microstructure of manufactured ceramic microcell UO_2 pellets:(a) Si-Ti-O;(b) Si-Ti-Al-O; (c) Si-Cr-O.

The thermal conductivity of microcell pellets can be increased by adopting a cell wall material with high thermal conductivity. Metallic microcell UO_2 pellets with metallic cell walls of high thermal conductivity would reduce the operating temperature of the fuel pellets.

The use of such cold pellets would reduce not only the diffusivity of fission products but also stresses caused by thermal expansion of pellets or gas in a fuel rod. Moreover, the reduction of stored energy due to the low temperature would significantly increase the safety margin in design basis accidents such as LOCAs [5].

Mo and Cr have been selected for the metallic cell wall because they have a relatively high melting temperature and good thermal conductivity. The metallic microcell UO_2 pellets were fabricated by co-sintering of metal powder coated UO_2 granules. Metal powder coated UO_2 granules, prepared by mixing the metal powders and UO_2 granules, were pressed into green pellets. The green pellets were then sintered under a dry hydrogen atmosphere. The UO_2 granule density and size, metal powder size and content, and sintering temperature and time are being optimized to fabricate dense and sound pellets. Fig. 3 shows the typical microstructure of the produced pellets.

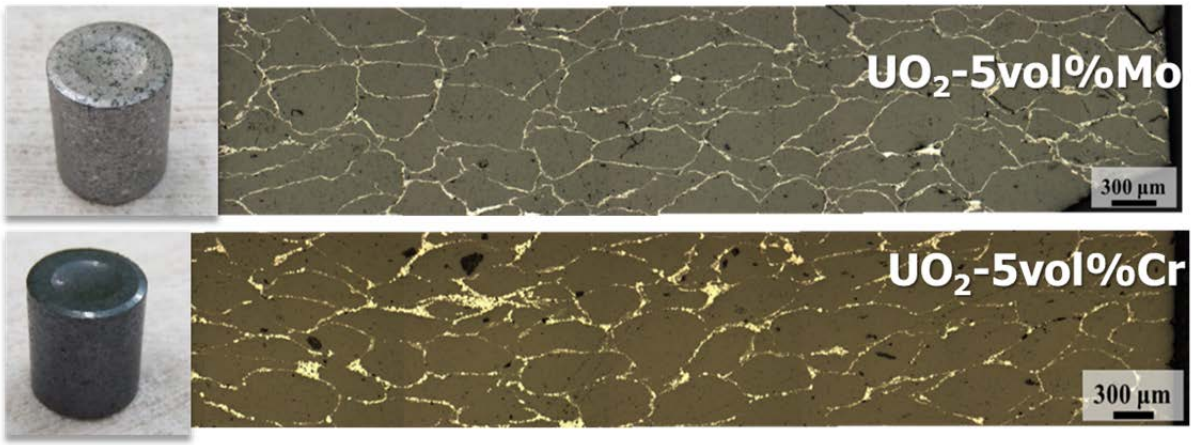

FIG. 3. Typical microstructure of metallic microcell UO_2 pellets.

3. HIGH DENSITY PELLETS

The high uranium density of fuel pellets generally allows a high burnup and long-life operation, leading to an enhanced fuel cycle economy and reduced spent fuel volume. In particular, the new ATF cladding might require a high uranium density fuel to compensate for the anticipated reduction of the fuel cycle length. For example, the ceramic composite cladding likely gives rise to a smaller volume for fuel pellets due to the thick cladding wall and low cladding thermal conductivity [6-7]. Advanced Fe-alloy cladding has a high neutron absorption cross section and thus may also require a high uranium density pellet [8].

Uranium-nitride based composite fuel pellets are being studied for the purpose of increasing both the thermal conductivity and the uranium density of the current UO_2 pellet. A major challenge related to the high density composite pellet is enhancing the corrosion resistance. Various nitride powders have been fabricated from atomized U alloys to assess the effects of alloying elements on the oxidation behaviour. UO_2-UN composite pellets in which a UN phase is embedded in a UO_2 matrix have been fabricated by hot press sintering. It is expected that the UO_2 layer that envelops the UN grains will act as a protection barrier for oxidation. Fig. 4 shows the XRD pattern for the (U, Nb)N powder and the microstructure of a UO_2-UN pellet.

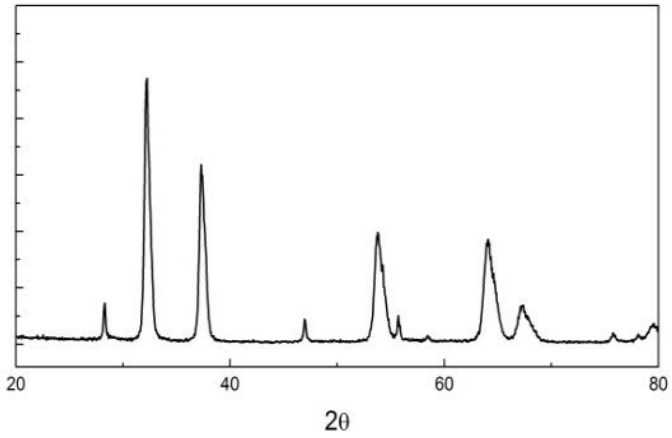

(a)

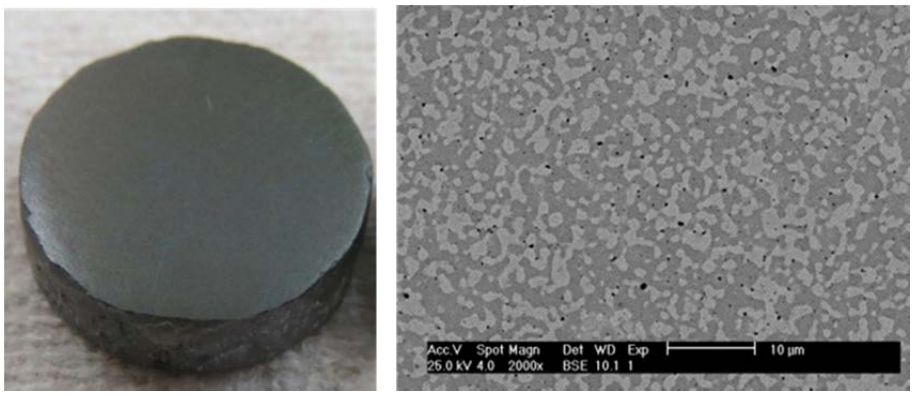

(b)

FIG. 4. (a) XRD pattern for (U, Nb)N powder, (b) shape and microstructure of a UO_2-UN composite pellet.

4. PERFORMANCE TEST RESULTS

4.1. Cs capture test of ceramic microcell UO_2 pellets

A simple annealing experiment was performed to test the Cs capture ability of the ceramic cell wall phase. A ceramic microcell UO_2 pellet and a piece of Cs ingot were annealed at 500°C for several hours inside an Ar-filled mini-autoclave. During the annealing, evaporated Cs is expected to react exclusively with the cell wall phase. The fractured surface of the annealed pellets was examined by SEM and EDS. The EDS spectrum from all mapping data points, shown in Fig. 5b, reveals the existence of Cs as well as cell wall components. The EDS element mapping image for Cs is shown in Fig. 5d. The yellow bright spots (colour online) indicate a high Cs concentration. The lines of high Cs concentration resemble the grain boundary image of Fig. 5c, indicating the preferential reaction of Cs with the grain boundary phase.

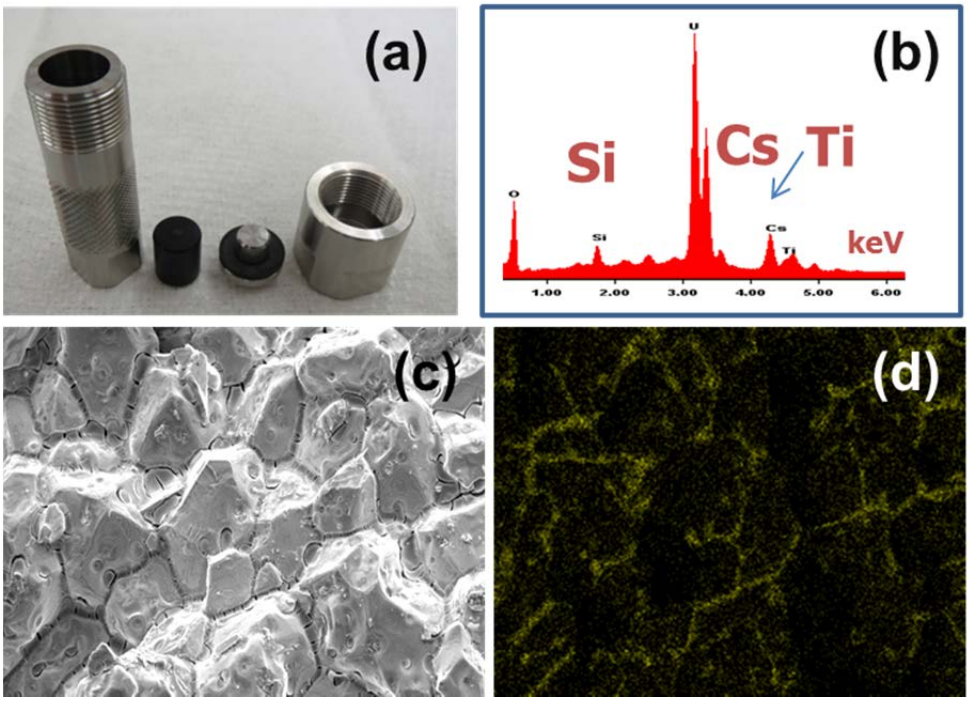

FIG. 5. SEM examination for Cs reaction test of ceramic microcell UO_2 pellet: (a) Test apparatus; (b) EDS spectrum; (c) SEM image; (d) area.

4.2. Thermo-physical property measurements

The thermal diffusivity measurement results shown in Fig. 6a indicate that the thermal transfer properties of the fabricated ceramic UO_2 pellets with microcells would be almost the same as those of standard UO_2 pellets. The thermal expansion measurement results for the ceramic microcell UO_2 pellets were similar to those obtained for the standard UO_2 pellets, as presented in Fig. 6b.

Figs 7a and 7b show the enhancement of the thermal conductivity in the metallic microcell UO_2 pellets. Fig. 7a reveals that the thermal conductivity of microcell UO_2 pellets containing 10 vol% of Mo is much higher than that of dispersed UO_2 pellets with 10 vol% of Mo. This indicates that the thermal conductivity is effectively enhanced by forming continuously connected metallic cell walls. The thermal expansion of UO_2 pellets containing 5 vol% of Mo was almost the same as that of the standard UO_2 pellet, as shown in Fig.7c. Fig. 8 shows the variation of the thermal conductivity as a function of the UN volume fraction at 600°C in the UO_2-UN composite pellets. Compared to the standard UO_2 pellet, the high density UO_2-UN composite pellet, in which the uranium density was increased by 13%, showed an increase in thermal conductivity of up to 100%.

Fig. 9 shows a comparison of the compressive creep deformation behaviour between ceramic microcell UO_2 pellets and standard UO_2 pellets. Because of the presence of the soft cell walls located along the grain boundaries, the ceramic microcell pellets deformed more easily than the UO_2 pellets. The use of soft ceramic microcell pellets is expected to reduce cladding strain during normal operation as well as transient operating conditions.

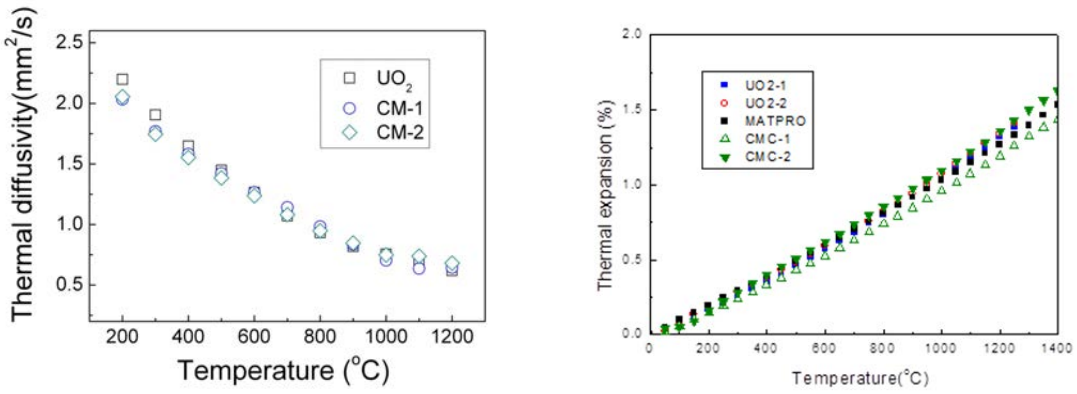

(a) *(b)*

FIG. 6. (a) Thermal diffusivity and (b) thermal expansion behaviour of the ceramic microcell UO_2 pellets as a function of temperature.

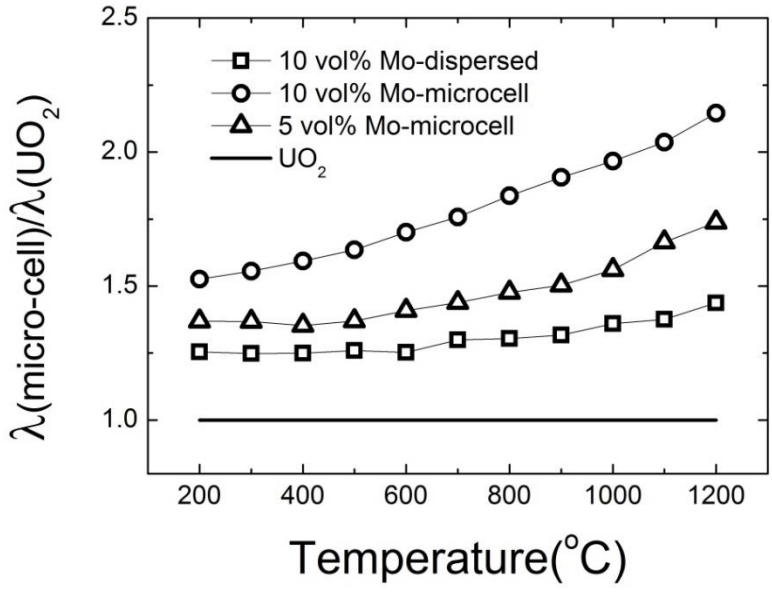

(a)

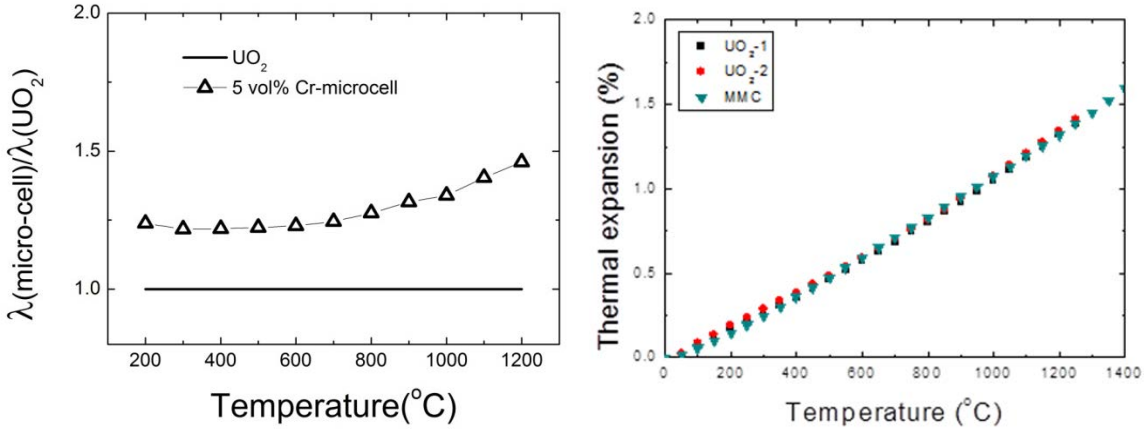

(b) *(c)*

FIG. 7. (a) Comparison of thermal conductivity enhancement in composite pellets containing Mo; (b) Thermal conductivity enhancement in microcell UO_2 pellets containing 5 vol% of Cr; (c) Thermal expansion behaviour of metallic microcell UO_2 pellets containing 5 vol% of Mo.

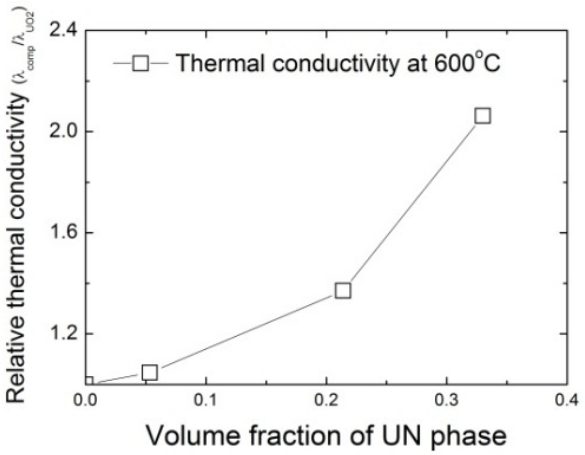

FIG. 8.Thermal conductivity enhancement of UO_2-UN composite pellets at 600°C as a function of volume fraction of UN.

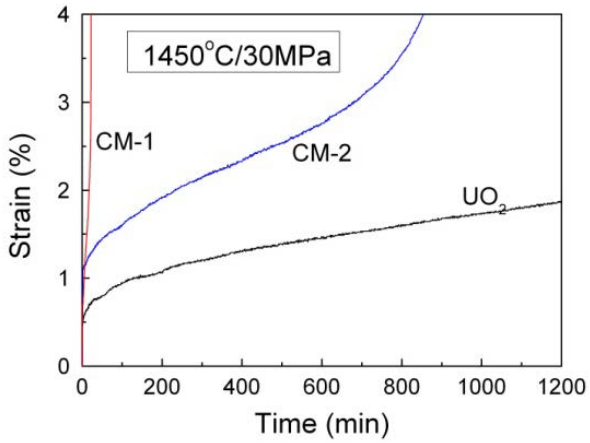

FIG. 9. Compressive creep deformation behaviours of a UO_2 pellet and ceramic microcell UO_2 pellets.

4.3. Steam oxidation behaviour

Maintaining dimensional stability under a high temperature steam environment is an important property that fuel pellets should have. The oxidation behaviour of the microcell UO_2 pellets under a steam environment was investigated. Test samples of metallic microcell pellets containing ceramic and 5 vol% of Mo were prepared by polishing the surface of the pellets. A standard UO_2 sample was also prepared for comparison. The pellets were annealed under a flowing steam environment at 500°C.

Fig. 10 shows the morphological changes of the polished surface of sample pellets after 24 h and 72 h annealing in 500°C steam. The polished surface of the standard UO_2 pellets became rough after annealing due to oxidation. In contrast, the microcell UO_2 pellets showed a shiny surface morphology even after 72 h annealing. Detailed surface morphological changes were investigated by using an optical microscope and SEM. Figure 11 shows the surface morphology evolution during steam oxidation. The surface of the standard UO_2 pellets was damaged due to oxidation along grain boundaries. A SEM image of the metallic microcell UO_2 pellets containing 5 vol% of Mo after 72 h annealing showed that the Mo wall was pitted by erosion. However, compared to the surface morphology of the standard UO_2

pellet after 72 h annealing, the oxidation of the UO_2 granules was significantly retarded in the metallic microcell UO_2 pellets. In the case of the ceramic micro-cell UO_2 pellets, the surface morphology was barely changed even after 72 h annealing.

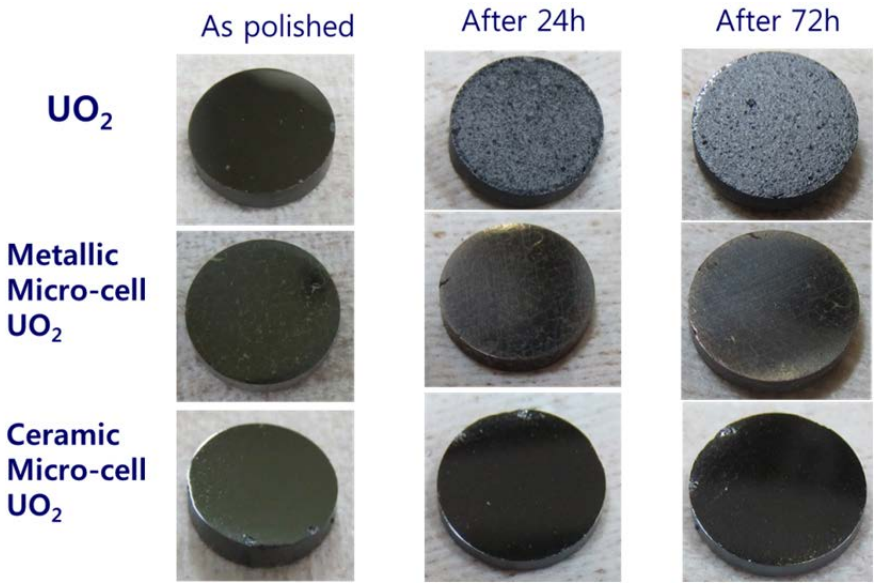

FIG. 10. Surface morphology evolution of UO_2 and microcell UO_2 pellets during steam oxidation at 500℃.

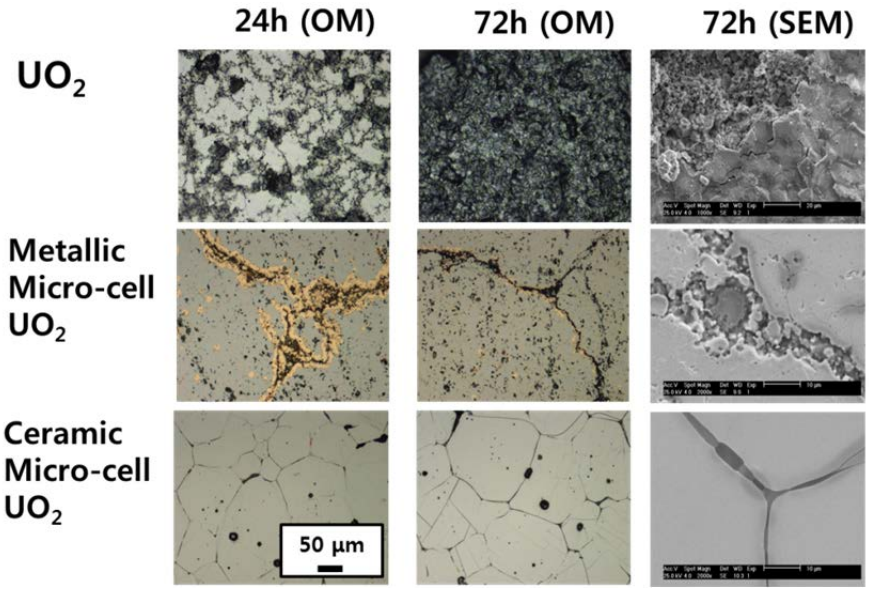

FIG. 11. Detailed surface morphological changes of UO_2 and microcell UO_2 pellets during steam oxidation at 500℃.

According to the literature, a volatile Mo hydroxide phase could be formed during the annealing of Mo under steam. It is believed that the formation and the evaporation of the volatile Mo hydroxide phase are responsible for the pitting of the Mo wall. However, a cross-sectional optical image of the tested sample pellets showed that the erosion depth was very shallow and the oxide phase did not penetrate the pellet interior, as shown in Fig. 12. Therefore, the pellet properties and stability may not be affected by the reaction between Mo and steam of 500°C.

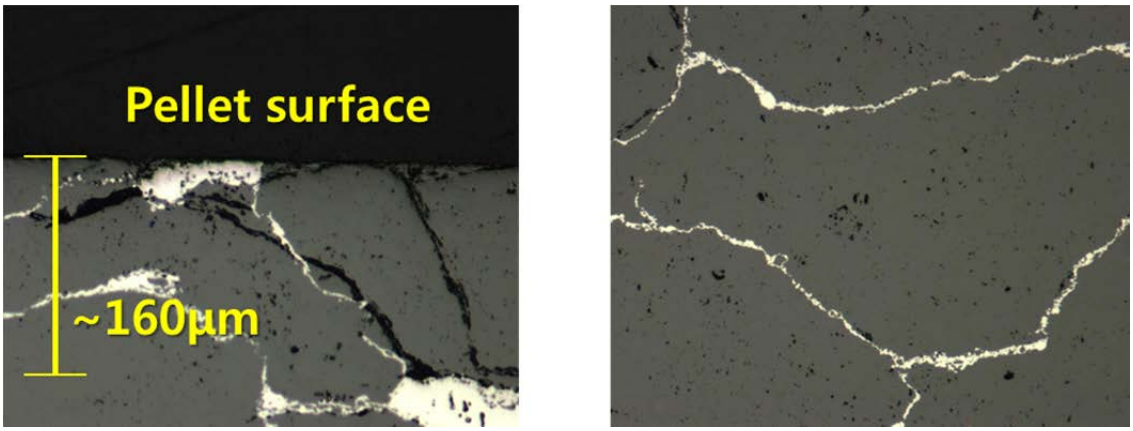

FIG. 12. Cross-sectional optical image of the tested metallic microcell UO_2 pellets.

Figure 13 shows the weight gain of UO_2 and microcell pellets during annealing in an 800°C steam environment. The XRD patterns shown in Fig. 14 for the UO_2 sample after the annealing test indicate that the weight gain in the UO_2 corresponds to the formation of a U_3O_8 phase. Figs 13 and 14 show that the weight gains were greatly reduced in both the ceramic and metallic microcell pellets, and no noticeable phase change was detected, compared to the UO_2 sample. The very low weight gain observed in the metallic microcell pellet appears to be due the formation and the evaporation of Mo hydroxide during the annealing.

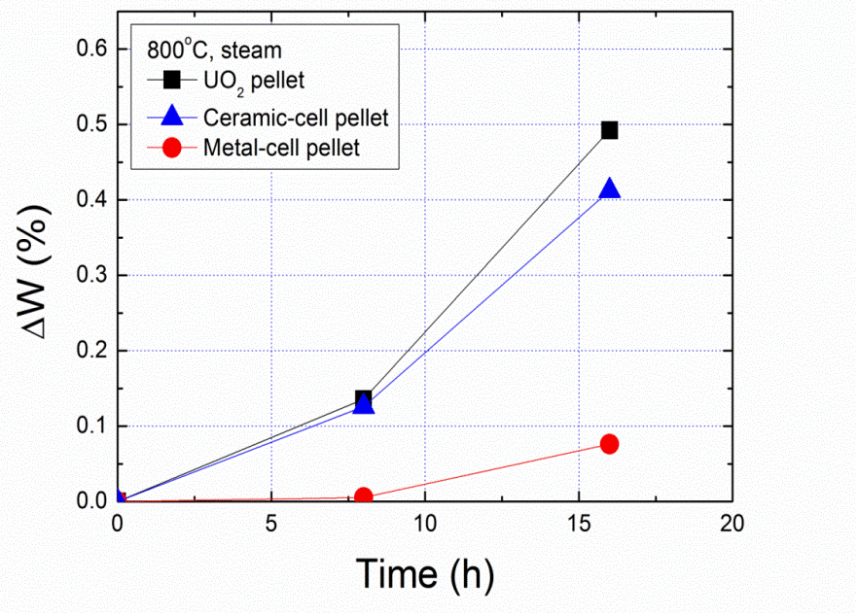

FIG. 13. Weight gains in test sample pellets during steam oxidation at 800℃.

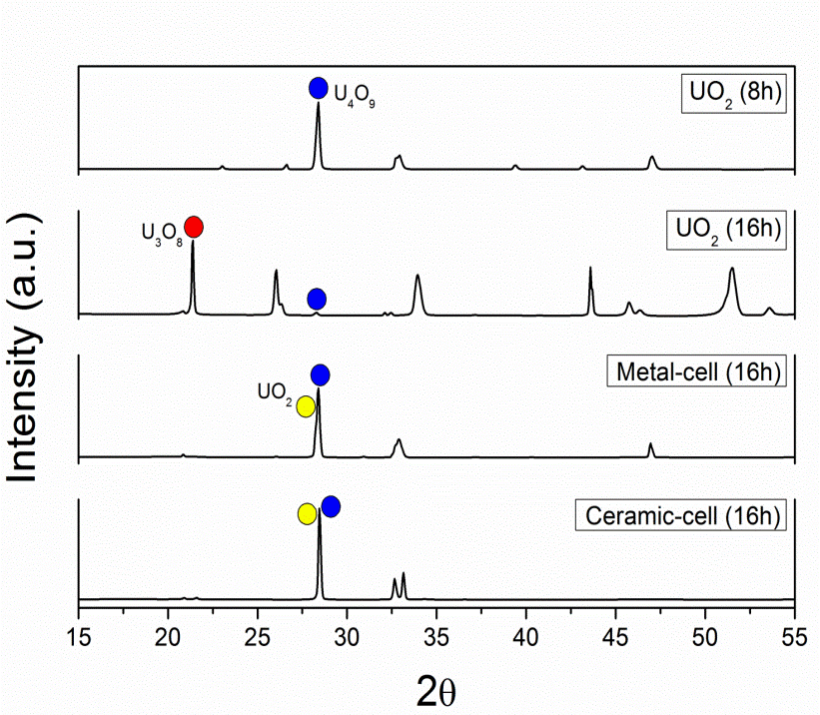

FIG. 14. XRD patterns of test sample pellets after steam oxidation at 800℃.

The observed oxidation resistance of the microcell UO_2 pellets in a steam environment is one of the representative benefits of microcell UO_2 pellets, which can enhance the fuel performance in normal operating conditions as well as accident conditions.

5. CONCLUSIONS

Accident tolerant micro-cell UO_2 pellets and UN-based high density pellets are being developed in KAERI. Micro-cell UO_2 pellets are characterized by enhanced retention capability of fission products and/or thermal conductivity. High-density pellets are composite pellets consisting of oxide and nitride components, and are expected to provide enhanced uranium density and thermal conductivity. Fabrication and performance feasibility test results showed that the micro-cell and high density concepts were successfully implemented. The newly developed ATF pellets with increased retention capability, thermal conductivity, and uranium density are expected to significantly enhance the fuel performance and the accident tolerance of LWR fuels.

ACKNOWLEDGEMENT

This work was supported by a National Research Foundation of Korea (NRF) grant funded by the Korean government (MSIP) (No. 2014000476).

REFERENCES

[1] KOO, Y-H., YANG, J-H., PARK, J-Y., KIM, K-S., KIM, H-G., KIM, D-J., JUNG, Y-I., SONG, K-W., KAERI's Development of LWR Accident Tolerant Fuel, Nuclear Technology **186,** (2014) 295-304.

[2] GOLDNER, F., "Overview of Accident Tolerant Fuel Development", Proc. OECD/NEA Workshop on Accident Tolerant Fuels of LWRs, Issy-les-Moulineaux, France, December 10–12, (2012).

[3] ZINKLE, S.J., TERRANI, K.A., GEHIN, J.C., OTT, L.J., SNEAD, L.L., Accident tolerant fuels for LWRs: a perspective, J. Nucl. Mater. **448** (2014) 374-379.
[4] YANG, J.H., KIM, K.S., KIM, D.J., KIM, J.H., OH, J.S., RHEE, Y.W., KOO, Y.H., "Micro-cell UO_2 Pellets for Enhanced Accident Tolerant Fuel", TopFuel 2013, American Nuclear Society, Charlotte, September 15-19 (2013).
[5] TERRANI, K. A., WANG, D., OTT, L. J., MONTGOMERY, R. O., The effect of fuel thermal conductivity on the behaviour of LWR cores during loss-of-coolant accidents, J. Nucl.Mater., **448** (2014) 512-519.
[6] KIM, W-J., KIM, D., PARK, J.Y., Fabrication and material issues for the application of SiC composites to LWR fuel cladding, Nucl. Eng. Tech. **45** (2013) 565-572.
[7] RAY, S., JOHNSON, S.C., LAHODA, E.J., "Preliminary Assessment of the Performance of SiC Based Accident Tolerant Fuel in Commercial LWR Systems", LWR Fuel Performance Meeting, Top Fuel 2013, American Nuclear Society, Charlotte, September 15-19 (2013).
[8] TERRANI, K.A., ZINKLE, S.J., SNEAD, L.L., Advanced oxidation-resistant iron-based alloys for LWR fuel cladding, J. Nucl. Mater. **448** (2014) 420–435.

ACCIDENT TOLERANT FUEL SYSTEM ANALYSIS
(SESSION 6)

Chairpersons

R. Montgomery

PNNL, United States of America

M.Todosow

BNL, United States of America

PWR PLANT MODEL TO ASSESS PERFORMANCE OF ACCIDENT TOLERANT FUEL IN ANTICIPATED TRANSIENTS AND ACCIDENTS

L.Y. CHENG, A. CUADRA, N. BROWN
Nuclear Science and Technology Department,
Brookhaven National Laboratory, Upton, NY
United States of America
E-mail: cheng@bnl.gov

Abstract

A PWR plant model based on the reactor system code TRACE has been assembled to enable the simulation of a broad spectrum of anticipated operational occurrences (AOO) and design basis accidents (DBA). The objective is to provide a simulation platform to support the development of advanced fuels and claddings and the deployment of accident tolerant fuel (ATF) in current PWR designs. The TRACE model simulates a Westinghouse 2308-MWt three-loop PWR, including standard primary and secondary loop components and various trips and control systems to model plant responses. Kinetics parameters for the standard UO_2 fuel and nitride fuel (UN-U_3Si_2-UB_4) have been developed from PARCS stand-alone full-core calculations to provide inputs to the TRACE point-kinetics model. Several transients have been analyzed to assess the performance of ATF relative to standard zircaloy-clad UO_2 fuel. These include complete loss of primary flow, steam generator tube rupture, small break (SB) and large break (LB) loss-of-coolant-accidents (LOCA). Among the accidents analyzed, the largest performance difference between the oxide fuel and the nitride fuel is in the LBLOCA where the peak clad temperature (PCT) for the nitride fuel is 30 K lower than that of the oxide fuel.

1. INTRODUCTION

A PWR plant model based on the reactor system code TRACE has been assembled to enable the simulation of PWR transients and accidents. The objective is to provide a simulation platform to support the development of advanced fuels and claddings and the deployment of accident tolerant fuel (ATF) in current PWR designs. The plant model is capable of assessing the safety and performance of different ATF designs in a broad spectrum of anticipated operational occurrences (AOO) and design basis accidents (DBA).

The purpose of accident analysis is to demonstrate compliance of plant performance against applicable regulatory acceptance criteria, thus assuring nuclear safety under postulated off-normal plant conditions. An example of regulatory acceptance criterion is that the calculated maximum temperature of fuel element cladding not be greater than 1200°C (2200°F) for light-water reactors (LWR) fuelled with uranium oxide pellets within cylindrical zircaloy cladding. There are generally two broad approaches in performing accident analysis, differentiated by using either conservative or realistic evaluation models. A realistic or best-estimate calculation uses modelling that attempts to describe realistically the physical processes occurring in a nuclear reactor. As a condition for using best-estimate calculations in licensing action, the U.S. Nuclear Regulatory Commission (USNRC) requires the licensee to demonstrate that the code and models used are acceptable and applicable to the specific facility over the intended operating range and must quantify the uncertainty in the specific application. In order to assure compliance with high probability that the calculated results will not exceed the acceptance criteria there is the requirement to consider the uncertainty and quantify it when comparing the results of the realistic or best-estimate evaluation model with the applicable regulatory acceptance criteria or limits. This assurance is further extended by specifying the operation envelope of the nuclear reactor to allow for a safety margin between a limiting safety parameter (e.g. the peak clad temperature (PCT)) and the applicable regulatory limit (e.g. PCT < 1200°C) under the most limiting postulated design basis accident conditions. In the context of our analysis, the safety margin is taken as the difference in physical units between the regulatory acceptance criteria and the results provided by the calculation of the relevant plant parameter after given considerations for conservatism or the uncertainties in the calculations. Figure 1 illustrates the relation among best-estimate result,

uncertainty, safety margin, and regulatory limit. Results from best-estimate calculations are used to assess the values of safety margins.

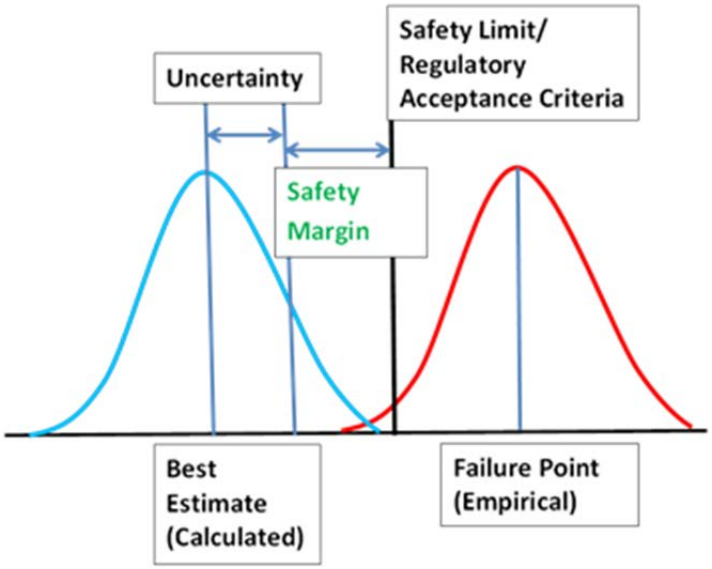

FIG. 1. Safety margin.

TRACE – *T*RAC/*R*ELAP *A*dvanced *C*omputational *E*ngine [1] is the latest, best-estimate reactor systems code developed by the USNRC for analyzing transient and steady-state neutronic-thermal-hydraulic behaviour in LWRs. It combines the capabilities of the USNRC's four main systems codes, TRAC-P, TRAC-B, RELAP5 and RAMONA. A TRACE PWR plant model, which simulates a Westinghouse 2308-MWt three-loop PWR, has been developed for the analysis of AOOs and DBAs. The following is a summary of the model development effort and results of four accidents: loss of off-site power (LOOP), steam generator tube rupture (SGTR), small-break loss-of-coolant-accident (SBLOCA), and large-break loss-of-coolant-accident (LBLOCA).

2. MODEL DEVELOPMENT

The basis for the TRACE model developed for the evaluation of ATF is an example PWR model described in the TRAC-M Users Manual [2]. The TRAC-M example PWR is a Westinghouse 2308 MWt, 3-loop plant. The original model has been transformed to comply with the functionality of the current TRACE input specifications. In particular, all the deprecated models are replaced with their current equivalents and in some cases, components are replaced or renodalized based on the current guidance for the modelling of reactors with TRACE. The PWR plant model, shown in Fig. 2, includes the following salient features:

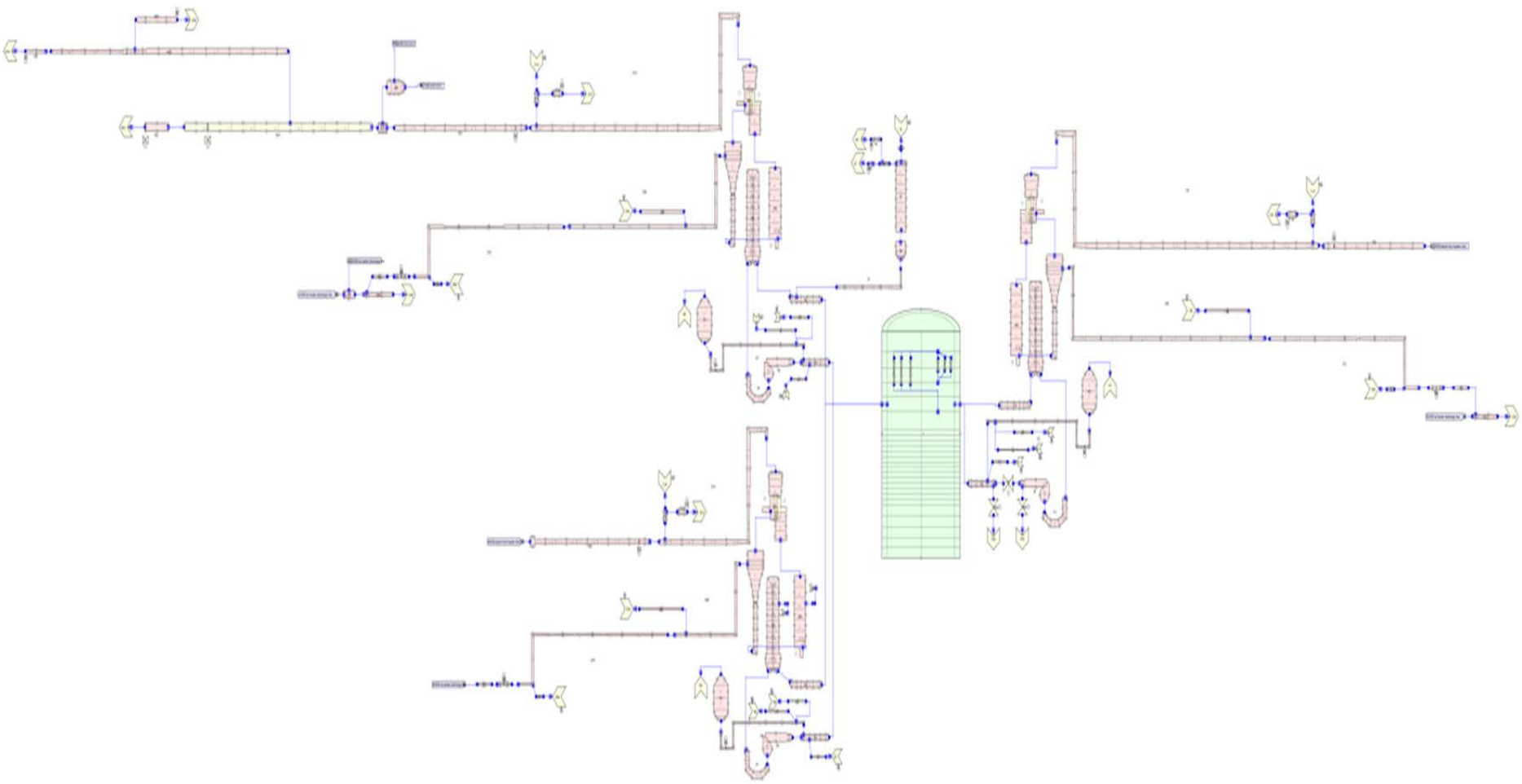

FIG. 2. TRACE PWR plant model.

- Three-dimensional reactor vessel (2 radial zones, 6 azimuthal sectors, and 12 axial levels);
- Powered-rod and unpowered-slab heat structures;
- Three primary- and secondary-coolant loops modelled individually;
- Makeup, letdown, and pressurizer-sprayer chemical and volume control system (cvcs) flows;
- Accumulator, low and high pressure safety injection (lpsi and hpsi) fills in each primary-coolant loop;
- Pressurizer and pressurizer power-operated relief valve (porv) and safety relief valve (srv),
- Main steam and steam-dump lines;
- Main and auxiliary feedwater systems;
- Various trips and control systems to model plant responses.

Figure 3 is a schematic representation of the primary system, showing the three primary loops, the steam generators (SG1 – SG3), the reactor vessel, and heat structures (HS801 – HS806) representing fuel assemblies in the core. The reactor vessel is modelled with two radial rings and six azimuthal sectors. The inner ring represents the core region and the outer ring represents the downcomer of the vessel. As shown in Fig. 3 the hot leg and cold leg of each loop are associated with two adjacent sectors. Each sector has one heat structure representing the fuel assemblies. The current model assumes uniform power for all six fuel assembly heat structures (HS 801 through 806). Each fuel assembly heat structure has two rod types, average and hot. The hot rod has a power factor of 1.678 times the average rods. Figures 4 and 5 present an expanded view of the components modelled in TRACE for the primary loop and secondary loop (main steam and feedwater loop) respectively. In this model, the pressurizer is connected to the hot leg of loop three.

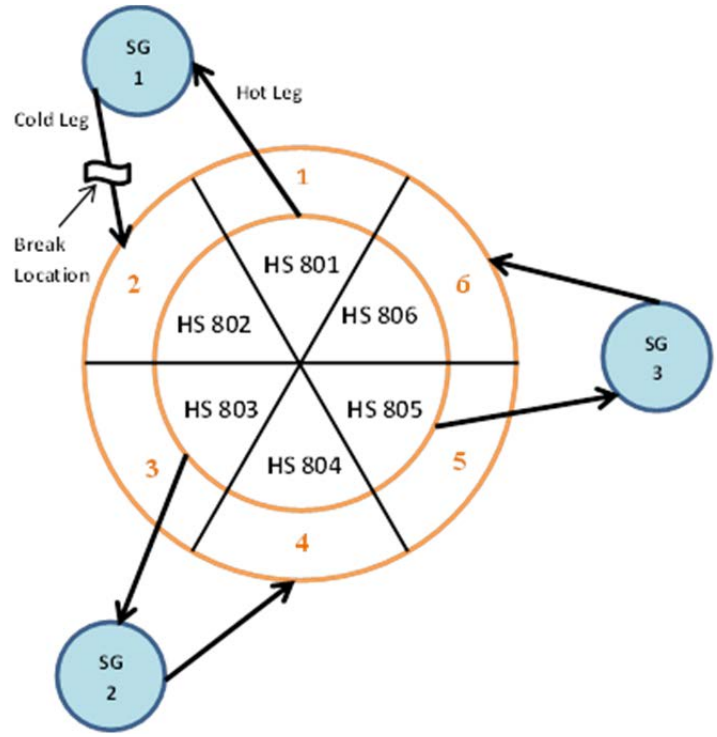

FIG. 3. Three-loop PWR model.

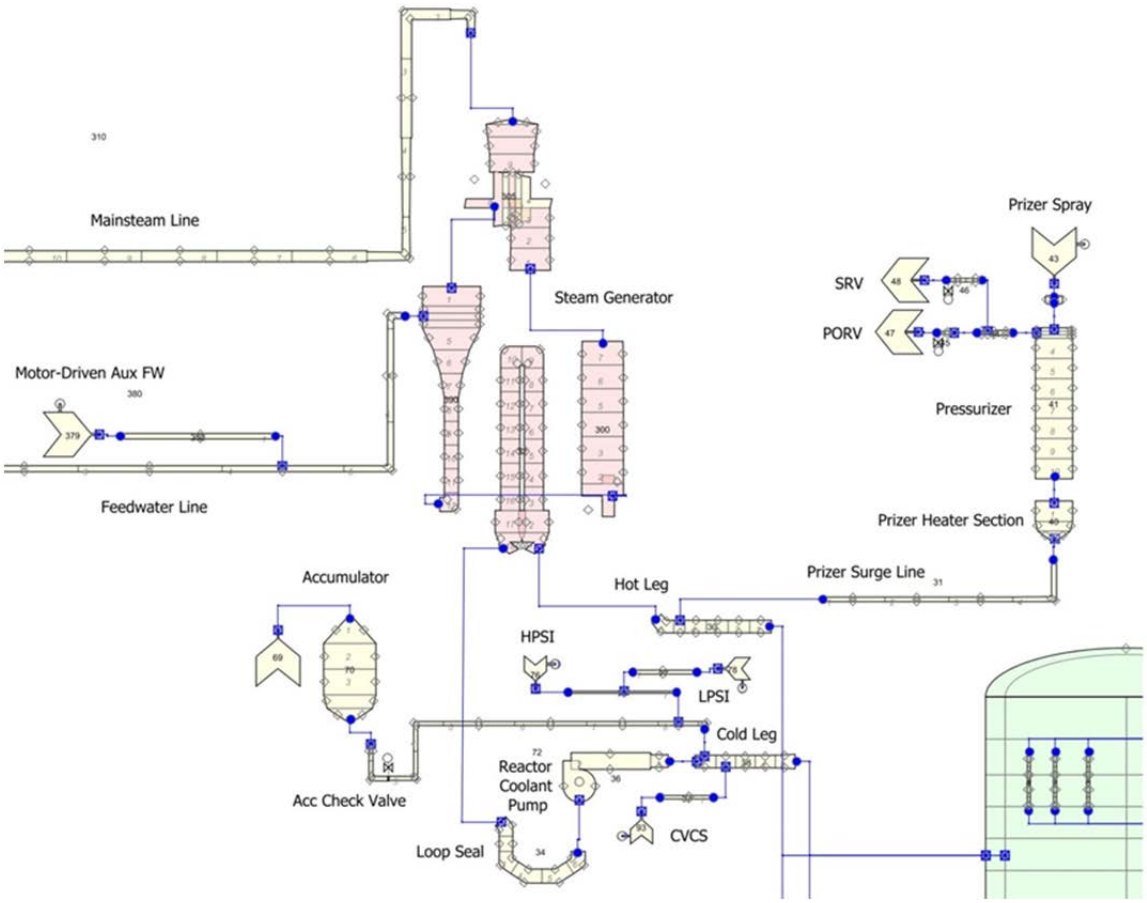

FIG. 4. Primary loop with pressurizer.

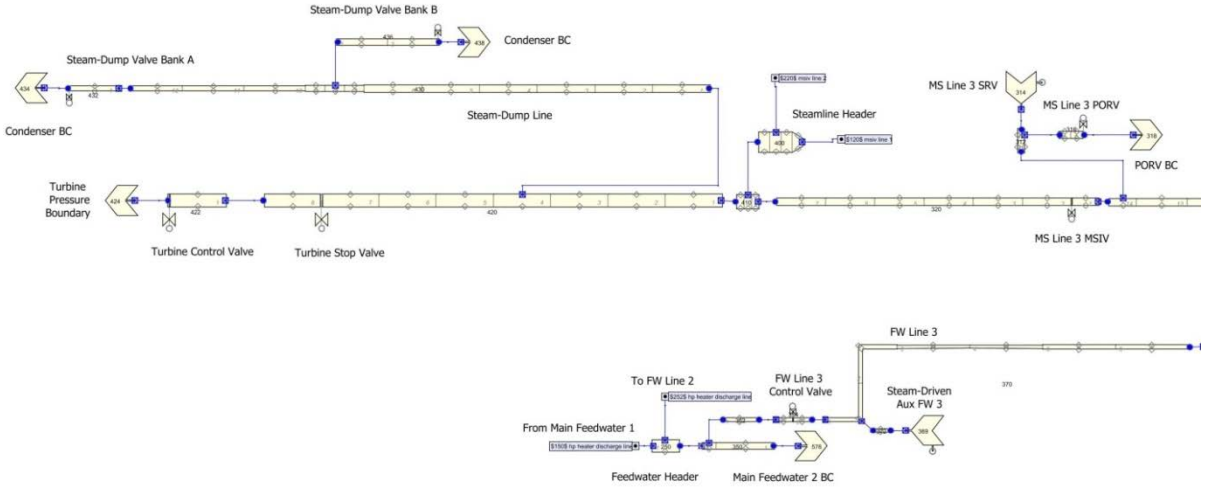

FIG. 5. Main steam line and feedwater line.

The steady-state operation of the PWR plant is maintained by a number of process control systems. The flow area of the turbine control valve is regulated to maintain the steam generator steam dome to a set pressure. The set pressure corresponds to the condition of the plant that produces the rated steam output, as specified in the plant thermal balance. A three-element control logic is implemented to regulate the feedwater flow to maintain the steam

generator water level to a set value. The logic processes the combination of water level error and the steam-feed mismatch to produce a bias adjustment to the feedwater valve flow area demand. The controller output is used to set the feedwater valve flow area.

The steady-state of the PWR plant is achieved by using the following tuning strategy:

- A reference plant is used for specifying the core thermal power, primary flow rate and feedwater temperature;
- The desired steam generator pressure is achieved by controlling the flow area of the turbine control valve;
- The desired water level in the steam generator is achieved by a three-element controller (steam flow, feed flow, and water level);
- The desired hot/cold leg temperatures are achieved by adjusting the effective tube-bundle heat transfer area of the steam generator;
- The desired recirculation ratio of the steam generator (ratio of total flow to steam flow) is achieved by adjusting the flow resistance in the steam generator.

3. KINETICS MODEL

Kinetic parameters for uranium oxide fuel and nitride fuel (UN-U_3Si_2) have been incorporated in the PWR model. Feedback coefficients included in the model are fuel temperature (Doppler), coolant temperature (spectral temperature), coolant density (void), and boron. PARCS [3] stand-alone full-core calculations provide kinetics parameter inputs to the TRACE point-kinetics model. These point kinetic parameters are for beginning-of-cycle conditions for an equilibrium cycle model based on a reference PWR. It is significant to note that the delayed neutron fractions (β) and other kinetics parameters of the two cores are different (for example, β_{UO2} = 0.00598 and $\beta_{UN\text{-}U3SI2}$ = 0.00612). In the PARCS core calculations, the few-group parameters were developed utilizing the TRITON/NEWT tools in the SCALE package [4]. A simplified set of branch cases was included in the few-group parameters. Separate sets of parameters (prompt-neutron lifetime and group constants for six delayed-neutron groups) have been calculated for the standard UO_2 fuel and the UN-U_3Si_2 fuel. In addition, SCRAM reactivity curves and reactivity coefficients are determined from PARCS kinetics calculations, assuming all control rods are Ag-In-Cd type. Table 1 shows the four reactivity coefficients (fuel temperature (T_f), moderator temperature (T_m), moderator density (D_m), and boron).

TABLE 1. FULL-CORE REACTIVITY COEFFICIENTS FOR CANDIDATE FUELS

	UO_2	UN-U_3Si_2
T_f (pcm/K)	-2.74	-2.83
T_m (/K)	1.93	0.862
D_m (pcm/kg/m^3)	14.2	14.0
Boron (pcm/ppm)	-5.99	-4.49

4. ACCIDENT ANALYSIS

Four accidents, one AOO and three DBAs, have been simulated to demonstrate the applicability of the TRACE PWR model to assess the safety performance of ATF zircaloy clad UO_2 fuel and nitride fuel (UN-U_3Si_2-UB_4) are considered. The four accidents are: loss of off-site power (LOOP), steam generator tube rupture (SGTR), small-break loss-of-coolant-accident (SBLOCA), and large-break loss-of-coolant-accident (LBLOCA).

4.1. Loss of off-site power

The loss of off-site power (LOOP) is an AOO. With the loss of electrical power, a primary pump trip at time zero initiated the transient and a reactor trip on low flow with a one-second time delay occurred at 3 s. Reactor power and primary flow are shown in Figs. 6 and 7 respectively. The decrease in reactor power before the scram is due to a negative reactivity feedback from the coolant heat-up (decrease in coolant density) because the pump trip reduced the primary flow. Figure 8 illustrates the fuel temperature response in an average fuel rod. The average fuel temperature is for an axial node near the core mid-plane (each fuel rod has sixteen uniform axial nodes). The UN fuel exhibits a lower average temperature than the UO_2 fuel because it has a higher thermal conductivity. A lower fuel temperature in the UN fuel also implies it has a lower stored energy than the UO_2 fuel. It is noted that the UN-U_3Si_2-UB_4 fuel and the UO_2 fuel have similar volumetric heat capacity at temperatures near the normal operating range. A lower initial temperature and a lower stored energy cause the UN fuel to have a lower fuel and clad temperatures than the UO_2 fuel after the reactor scram. The PCT for the two fuel types is compared in Fig. 9. Overall, the fuel response in an LOOP is relatively mild because the power decay is faster than the flow decay. The difference in the fuel temperature for the two fuel types is a reflection of the reduced stored energy and higher thermal conductivity for the nitride fuel.

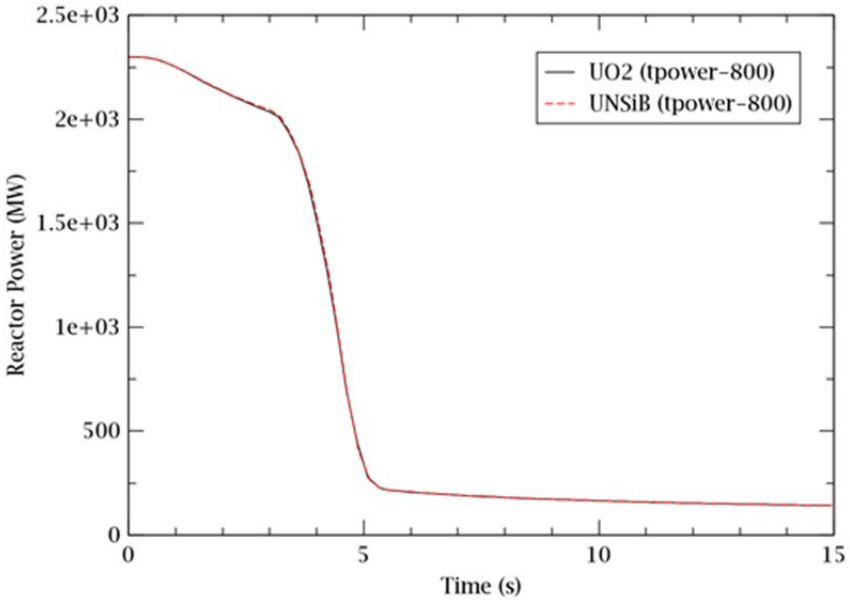

FIG. 6. Loss of off-site power – reactor power.

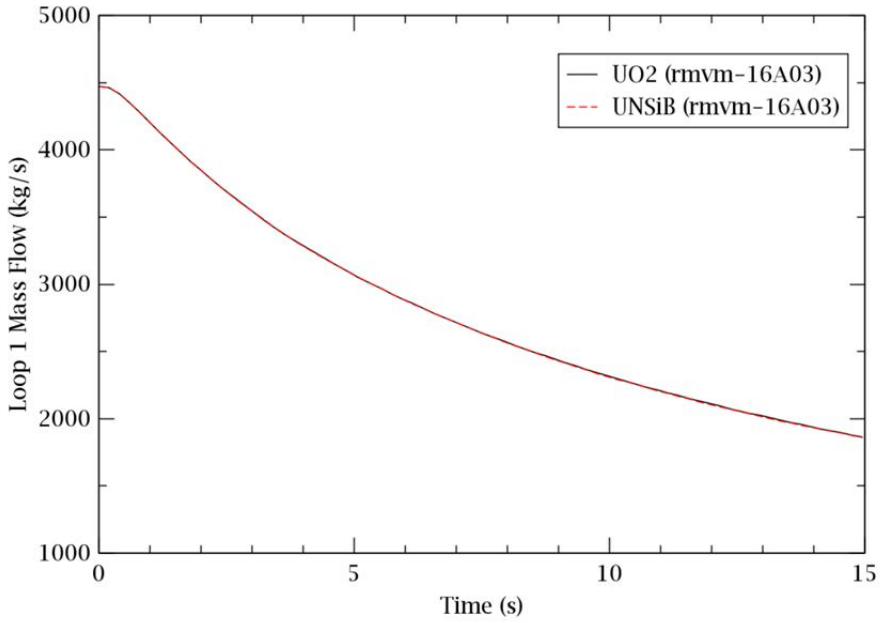

FIG. 7. Loss of off-site power – Loop 1 mass flow.

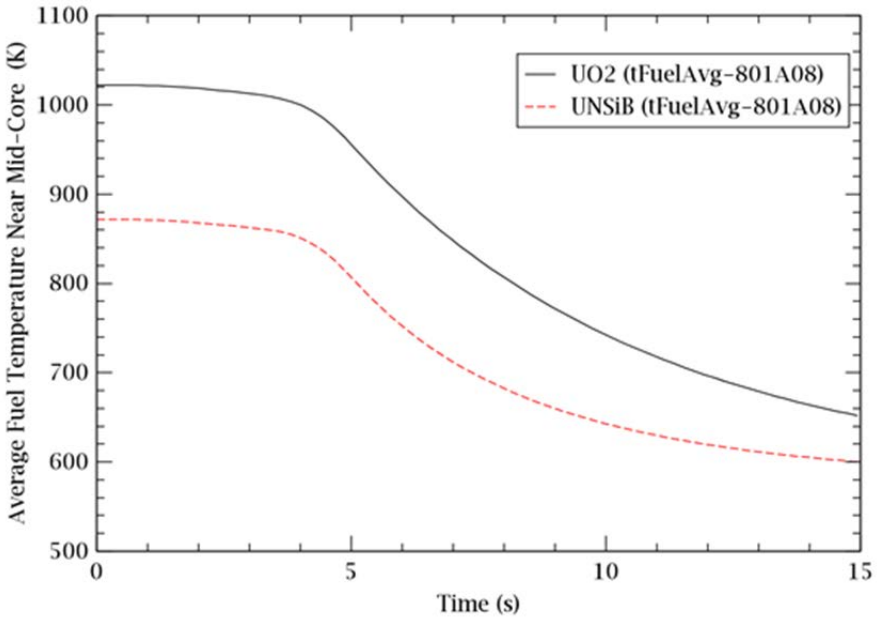

FIG. 8. Loss of off-site power – average fuel temperature in axial node 8.

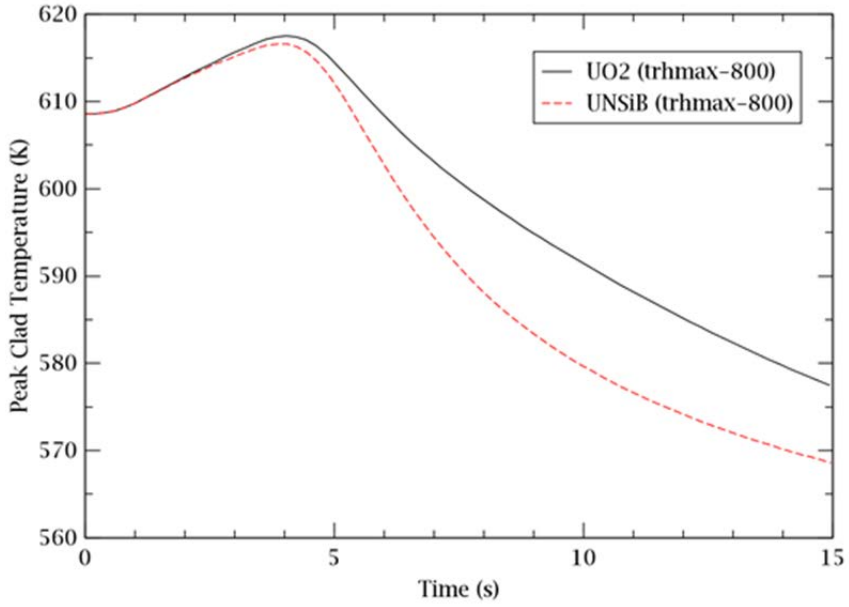

FIG. 9. Loss of off-site power – peak clad temperature.

4.2. Steam generator tube rupture

A steam generator tube rupture (SGTR) accident has been analyzed using the TRACE PWR model with point-kinetics. The single-tube rupture was simulated by a restart run in which a pipe was added to the model connecting the primary and secondary sides of the loop 2 steam generator. The location of the rupture connection is shown in Fig. 10. In the restart run, the new PIPE component provided a rupture flow area (6.087×10^{-4} m^2) equal to twice the flow area of a single tube, representing a double-ended guillotine break. In an SGTR transient, the reactor loses pressure due to leakage of the primary coolant to the secondary side of the steam generator.

The SGTR is a rather slow transient and the TRACE results have been examined to confirm the operation of various trips and controls. A comparison of the output against the input model verifies the sequence of trips generated by the SGTR transient. These trips include: reactor trip on low pressurizer pressure, turbine trip on reactor trip, initiation of safety injection (SI) on low pressurizer pressure, main feedwater pump trip on SI signal, initiation of motor-driven and steam-driven auxiliary feedwater pumps, and primary pump trip on low-low pressurizer pressure.

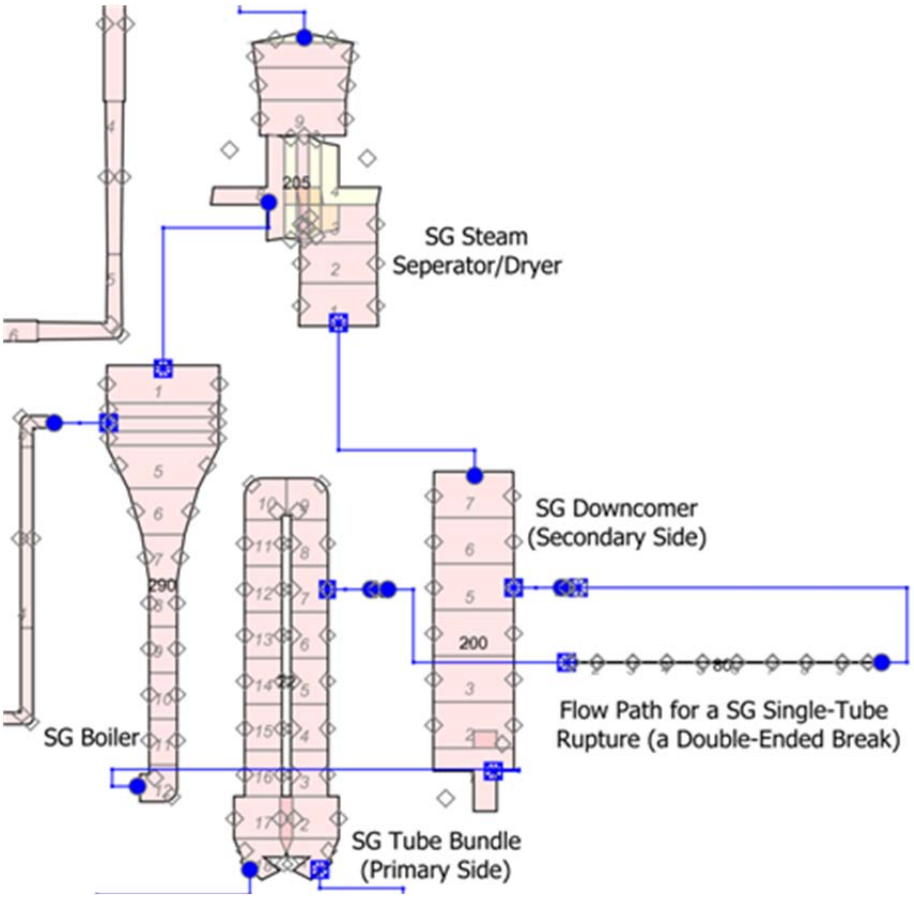

FIG. 10. Break connections for steam generator tube rupture.

Figure 11 compares the PCT for the oxide fuel and the nitride fuel. The PCT generally reflects the reactor power and core flow. It drops rapidly after the reactor trip at ~180 s and slowly increases after the primary pump trip at ~210 s. The reactor power, depicted in Figure 12, shows a slow decline until the scram when the power drops rapidly. Reactivity feedback from decreasing coolant density is the cause of the small decrease in reactor power before reactor trip. This is confirmed by a test case in which the moderator density reactivity was turned off. Result of the test case (no moderator density feedback) in Fig. 12 shows a steady reactor power until scram. The decrease in moderator density can be inferred from the core coolant mass in Fig. 13 (for the nitride fuel case). Before reactor scram, the coolant mass decreases with the decreasing reactor pressure (a lower density for lower pressure). After the reactor scram, steam generators continue to remove heat from the reactor and this leads to a decrease in the coolant temperature and an increase in the core coolant mass (a higher density for lower temperature). A subsequent decrease in the core coolant mass occurs after the primary pump trip that reduces both the primary flow and the heat removal by the steam generators.

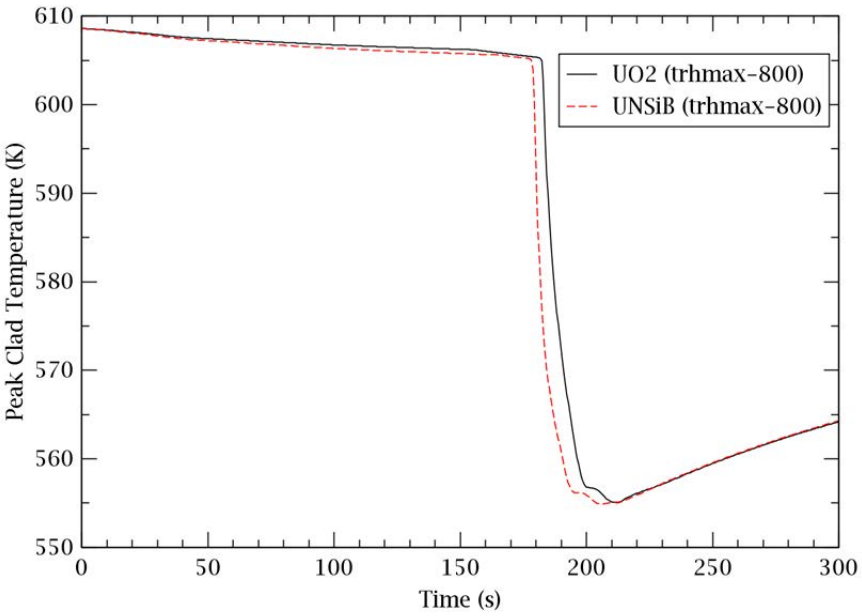

FIG. 11. Steam generator tube rupture – peak clad temperature.

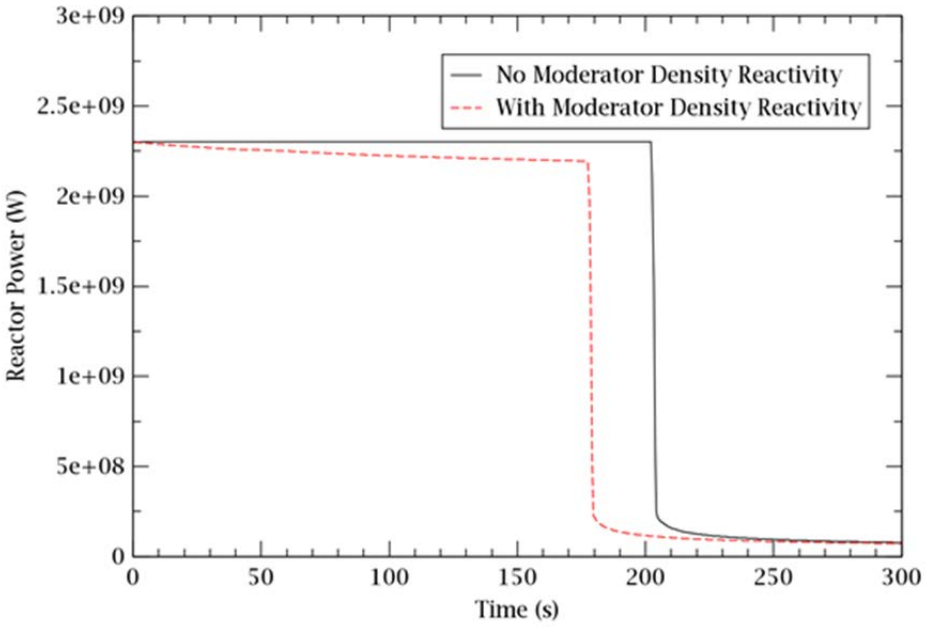

FIG. 12. Steam generator tube rupture – reactor power.

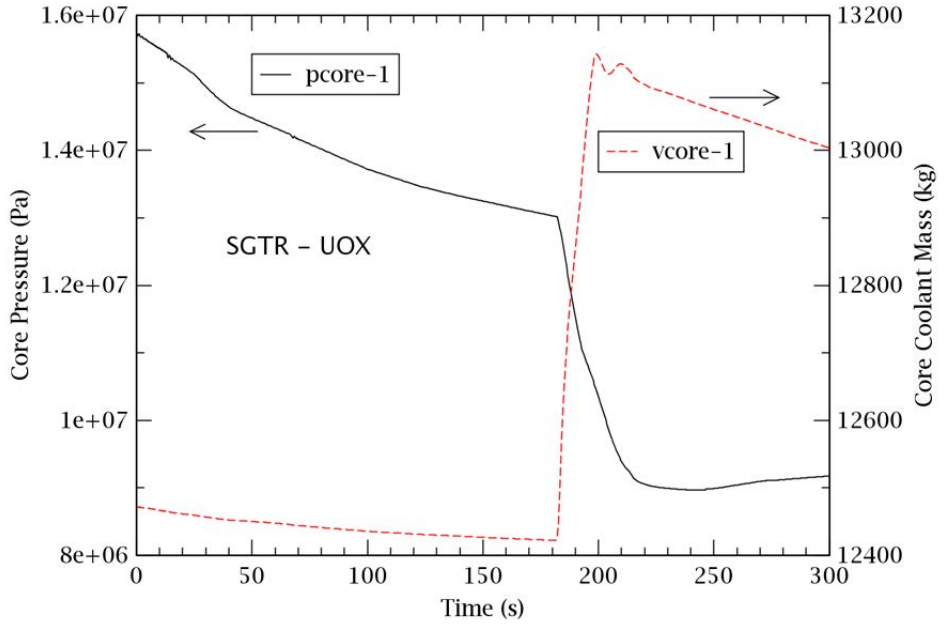

FIG. 13. Steam generator tube rupture – core pressure and core coolant mass.

4.3. Small-break LOCA

A small break in the cold leg of primary loop 1 was simulated with a loss of off-site power coincident with the reactor trip. The loss of off-site power assumption led to the tripping of primary pumps, main feedwater, and turbine stop valve. In the SBLOCA transient, the pipe rupture was initiated by opening a break valve (Valve 704 in Fig. 14) at time zero simulating a 0.1 m^2 break that opened completely in 0.001 s. This particular transient exercised a broad spectrum of systems in the model, including primary, secondary, and ECCS (emergency core cooling system).

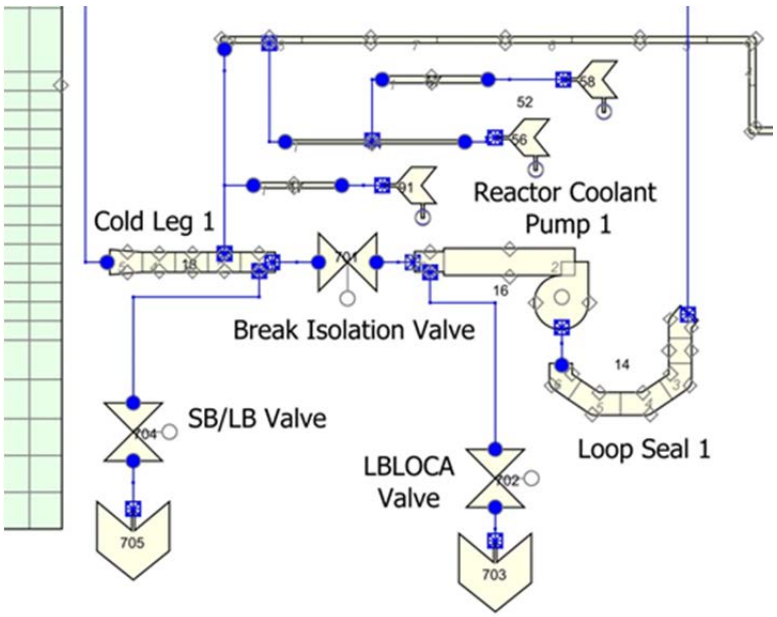

FIG. 14. Break connection for pipe rupture and double-ended break.

The SBLOCA analysis considered two types of fuel, the reference uranium oxide fuel (UO_2) and a nitride fuel (UN-U_3Si_2-UB_4). The progression of the SBLOCA for the two types of fuel is generally quite similar. Any variations are mainly due to thermal-physical property differences and thermal-hydraulic response of the system. Figure 15 shows the break flow and the total emergency core cooling system (ECCS) flow for this SBLOCA. The two flows are similar for the two fuel types in general. There are changes in the slope of the break flow at ~10 s and 45 s. The slowing down of the break flow at ~10 is due to the beginning of voiding in the cold leg in loop 1, i.e. the break flow changes from single-phase liquid to two-phase mixture. At ~ 45 s, the break flow increases again because of reduction in voiding in the cold leg of loop 1 due to significant injection of ECCS flow. In a SBLOCA, the break flow rate generally decreases with increase in voiding because of the choked flow condition at the break. High pressure safety injection (HPSI) was initiated at ~23 s but the ECCS flow was insignificant until the accumulator flow started at ~44 s. The reactor pressure in this analyzed accident did not decrease low enough for the low pressure safety system to begin injection.

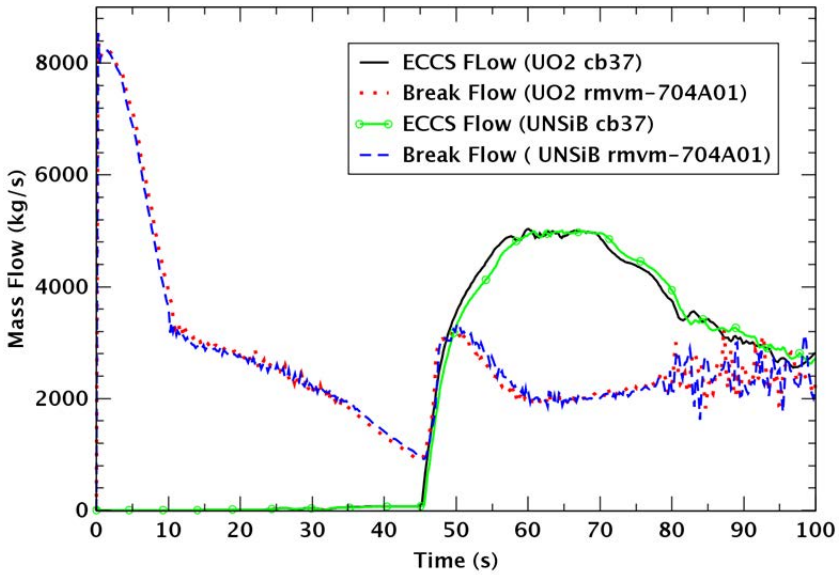

FIG. 15. SBLOCA – break flow and ECCS flow.

Figure 16 shows the peak clad temperature (PCT) for the two fuel types. For the oxide fuel, the PCT occurs in the hot rod in sector 2 (heat structure 802001). For the nitride fuel, it is the hot rod in sector 6 (heat structure 806001) that exhibits the PCT. In the SBLOCA, the nitride fuel shows a higher PCT than the oxide fuel. The magnitude of the PCT can be correlated with the duration of the state in which the fuel rod is uncovered i.e., not cooled by coolant. Figure 17 shows the location of the lower quench front for the two hot rods corresponding to the UO_2 fuel and the nitride fuel respectively. In Fig. 17, a location of 4.27 m corresponds to the top of the core and the zero corresponds to the bottom of the core. Heatup of the fuel, as seen in the rise in the PCT, begins when the quench front disappears to the bottom of the core and the subsequent recovery of the quench front brings a corresponding drop in the PCT. It is also informative to review the corresponding average fuel temperatures shown in Fig. 18. The nitride fuel with a higher thermal conductivity than the oxide fuel initially exhibits a lower temperature. By about 40 s, the two fuel types have reached about the same average fuel temperature. From that point on the PCT for the two fuel types begins to differ and the longer the fuel remained uncovered the higher the PCT becomes. Since the bottom quench front for the nitride fuel stayed below the core inlet for a longer period, its PCT reaches a higher value than the UO_2 fuel.

Results of the SBLOCA suggest that global system response alone does not provide sufficient information to delineate the fuel performance under accident conditions. In addition, the accident simulation model should have sufficient fidelity to provide local core conditions As seen in this SBLOCA, though the break flow and the ECCS flow are quite similar for the two fuel types, differences in the fuel response are driven by complex core thermal-hydraulics.

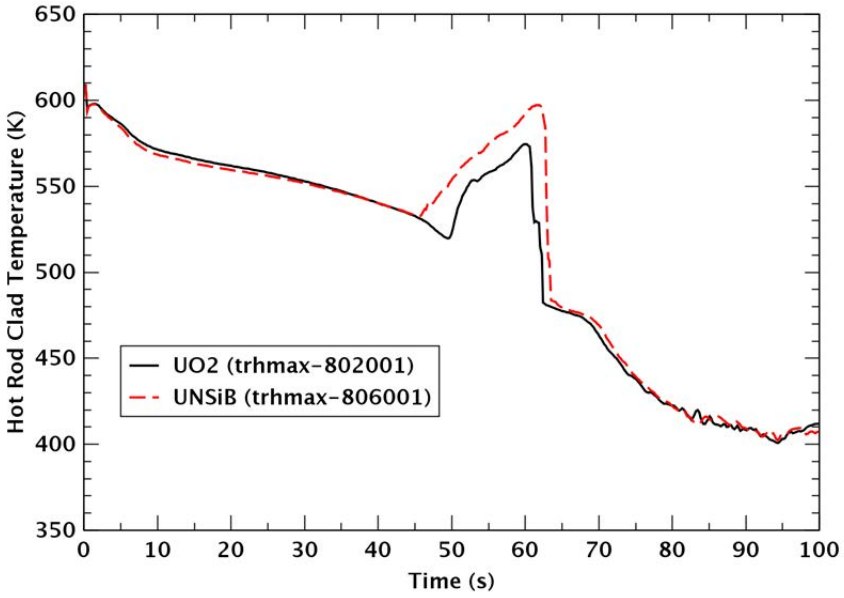

FIG. 16. Small-break LOCA – peak clad temperature.

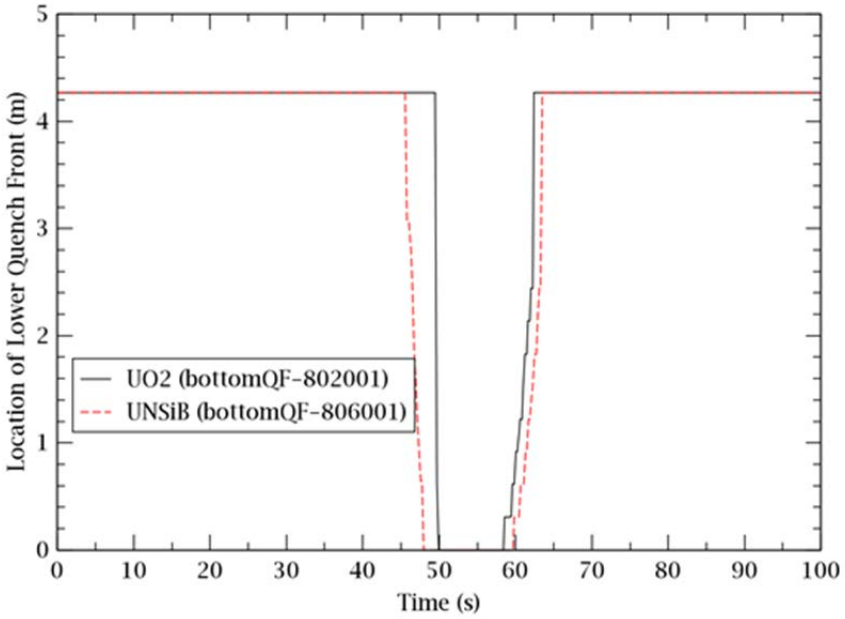

FIG. 17. Small-break LOCA – location of lower quench front.

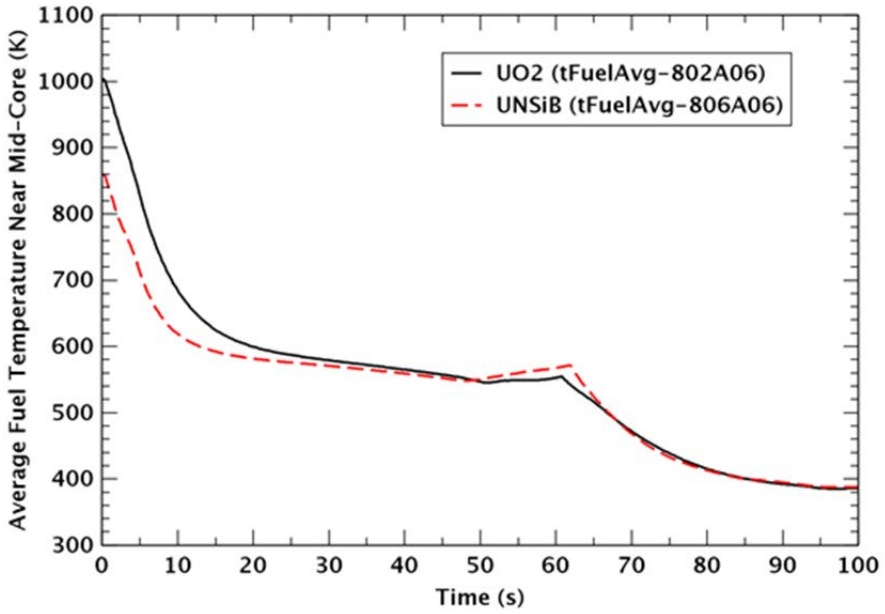

FIG. 18. Small-break LOCA – average fuel temperature near mid-core.

4.4. Large-break LOCA

A large break in the cold leg of primary loop 1 was simulated with a loss of off-site power coincident with the reactor trip. In the LBLOCA transient the double-ended pipe break was initiated at time zero by opening the two break valves in Fig. 14 (Valves 702 and 704) and closing the break isolation valve (Valve 701 in Fig. 14). For this fast transient the thermal-hydraulics and fuel thermal properties dictate the overall response more so than the reactivity feedback.

Figure 19 shows the PCT for the two fuel types. The PCT for the nitride fuel is ~30 K lower than the oxide fuel. Figure 20 shows the core liquid fraction. The initial blowdown causes the core to be uncovered with the core liquid fraction dropping to zero at about 20 sec. This leads to fuel heatup and a higher clad temperature. With the initiation of ECCS flow (see Fig. 21), the core liquid fraction begins to increase at ~35 s. Refilling and reflooding of the core quench the fuel rods with a consequential reduction in the clad temperature. The ECCS flow starts with flow from the accumulator followed by initiation of the high pressure and low pressure injection systems. In the LBLOCA simulation, the ECCS flow in loop 1 was disabled because the flow was assumed to leak out of the break and never reached the core.

It is of interest to note the asymmetry in the system response. Figure 22 shows the PCT for the hot rods in sectors 1 and 2. According to the loop layout in Fig. 3, all break flow has to pass through sector 1 first. Thus, sector 1 experiences the highest flow among the 6 sectors. As a result, the fuel rods in sector 1 receive the most cooling and register the lowest PCT among fuel assemblies in all 6 sectors.

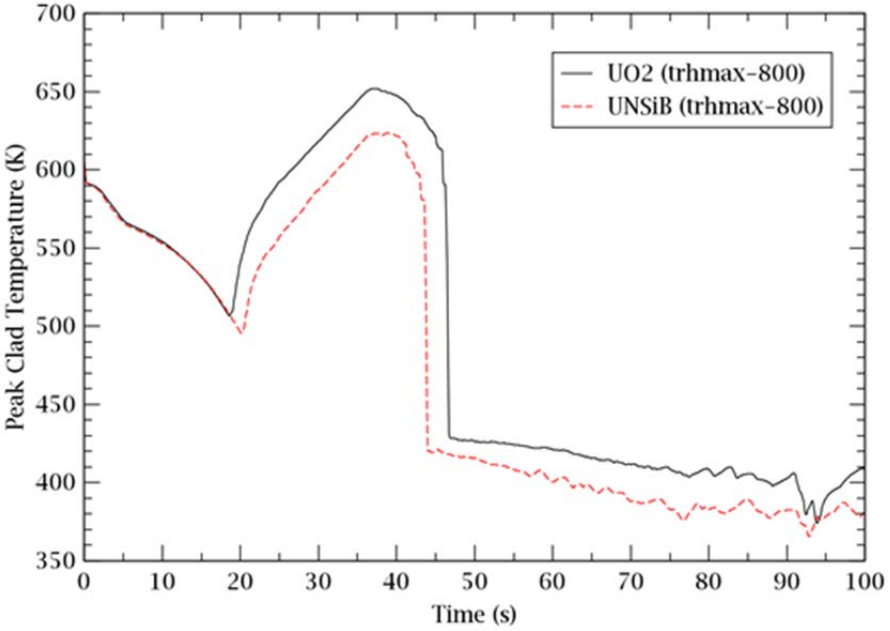

FIG. 19. Large-break LOCA – peak clad temperature.

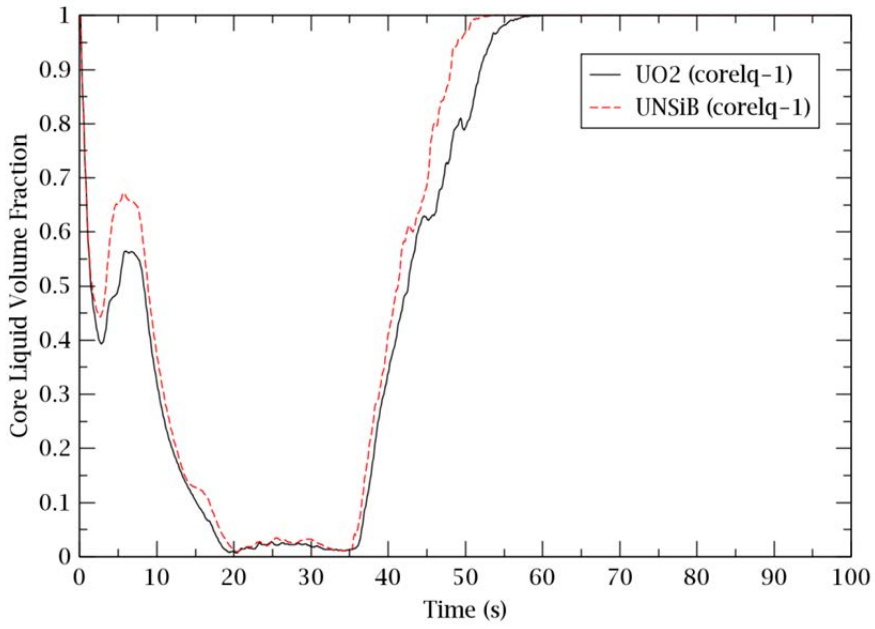

FIG. 20. Large-break LOCA – core liquid fraction.

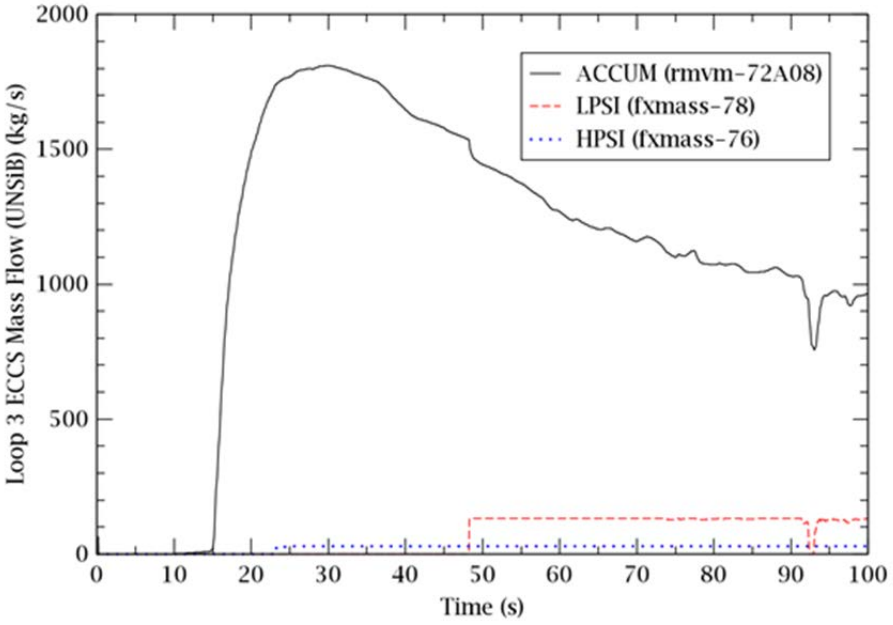

FIG. 21. Large-break LOCA – Loop 3 ECCS flow.

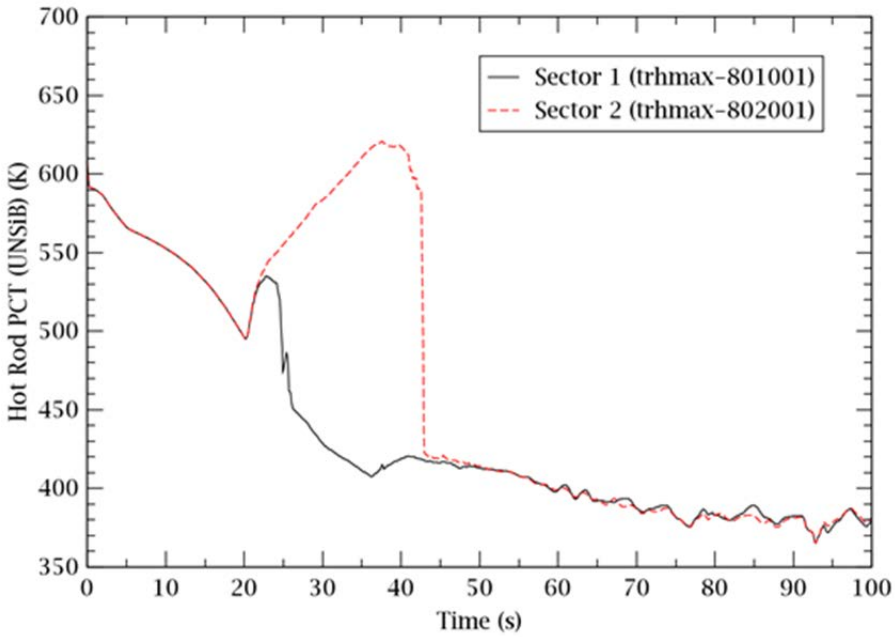

FIG. 22. Large-break LOCA – PCT in sectors 1 and 2.

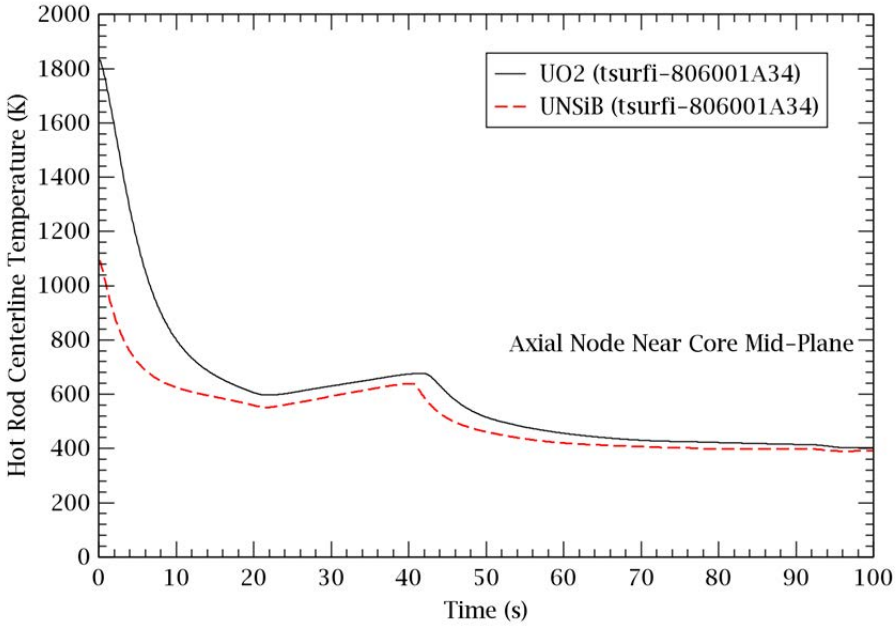

FIG. 23. Large-break LOCA – fuel centre-line temperature.

The fuel centreline temperature for the hot rod near the core mid-plane is shown in Fig. 23. In general, the nitride fuel is at a lower temperature than the oxide fuel because it has a higher thermal conductivity than the UO_2 fuel.

In addition to calculating the transient fuel and clad temperatures, this simulation also informs on the axial temperature distribution. Figures 24 and 25 show the axial distribution of the centreline temperature and the clad temperature respectively for the oxide fuel hot rod at various times during the LBLOCA. The heatup and quenching of the fuel are readily seen in their manifestation in the axial temperature distribution. In Fig. 25, the effect of top reflood is seen by comparing the clad temperature near the top of the core at 20 s and 30 s. The effect of bottom refill is seen by comparing the clad temperature in Fig. 25 near the bottom of the core at 30 s and 40 s.

The LBLOCA results again accentuate the influence of core thermal-hydraulics on the fuel response in an accident. The asymmetric core condition is seen to result in very different PCT. Core uncovery translates to core heatup. On the other hand, core refill and reflood provide the needed cooling to limit the PCT. Contrary to the result of the SBLOCA, in the case of the LBLOCA the period of core uncovery is shorter for the nitride fuel than the oxide fuel resulting in a PCT that is 30 K lower for the nitride fuel than the oxide fuel.

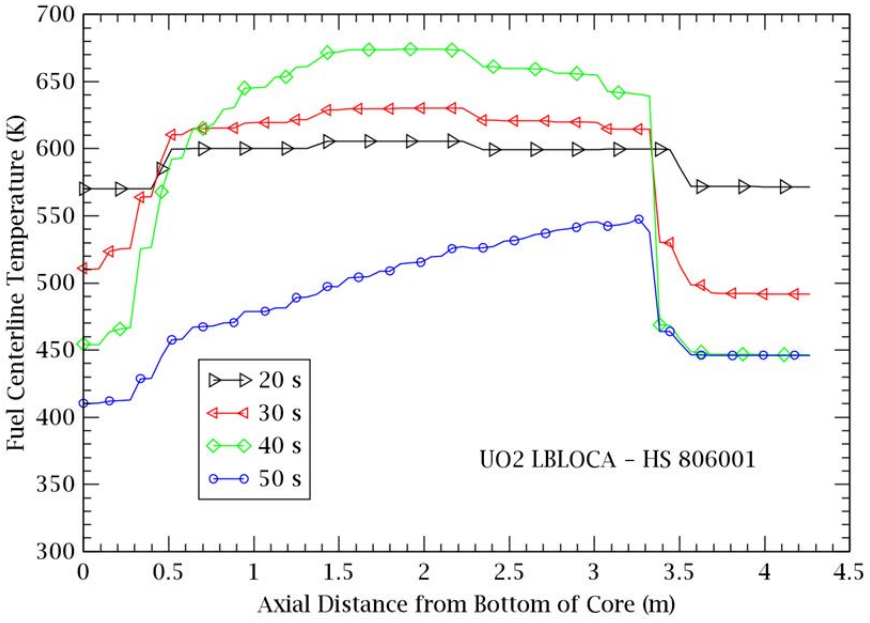

FIG. 24. Large-break LOCA – axial distribution of fuel centerline temperature.

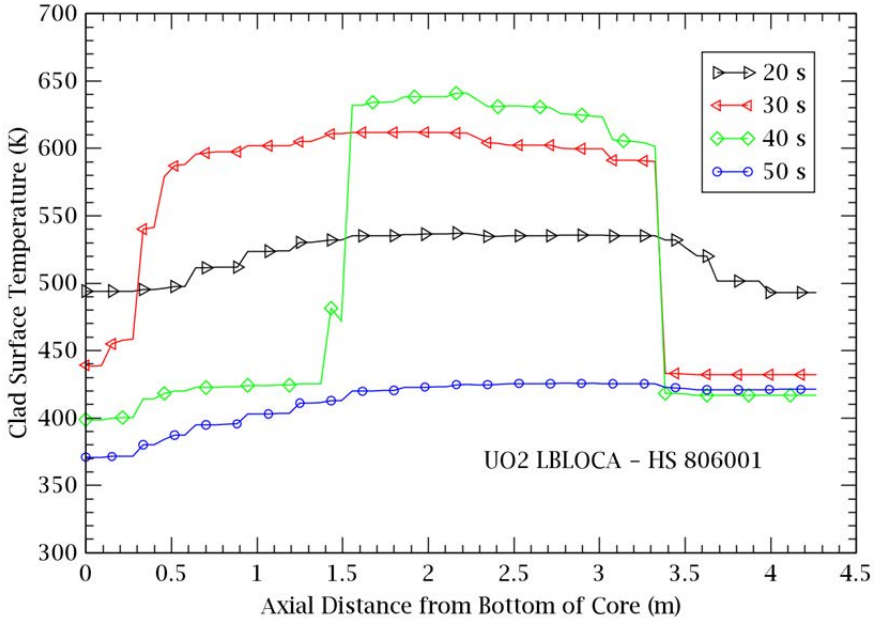

FIG. 25. Large-break LOCA – axial distribution of clad surface temperature.

5. SUMMARY AND CONCLUSION

A TRACE PWR plant model has been developed and applied to analyze different accidents and transients, including design basis accidents and anticipated operational occurrences. Its capability has been demonstrated and its fidelity is being improved with continuing development. This model is capable of providing transient and spatial temperature information for the fuel and cladding. This simulation platform supports the development of advanced fuels and claddings by providing a scoping capability to evaluate their impact on reactor performance and safety.

The transient and accident events show a very similar response for UO_2-Zr fuel-clad and UN-U_3Si_2-Zr fuel-clad. In the LBLOCA, LOOP, and SGTR the improved thermal properties

of UN-U_3Si_2 result in enhanced thermal margin, a lower peak clad temperature than the oxide fuel. Among the accidents analyzed, the largest performance difference between the oxide fuel and the nitride fuel is in the LBLOCA where the peak clad temperature (PCT) for the nitride fuel is 30 K lower than that of the oxide fuel. In the SBLOCA, the period of uncovered core lasted a little longer for the nitride fuel resulting in a higher PCT than the oxide fuel. Both the SBLOCA and the LBLOCA analysis accentuate the influence of core thermal-hydraulics on the fuel response in an accident. Among the four accidents analyzed, only the slower transients with delayed reactor scrams, namely the LOOP and the SGTR, do the effects of reactivity feedback become discernible.

ACKNOWLEDGEMENTS

This manuscript has been authored by employees of Brookhaven Science Associates, LLC under Contract No. DE-AC02-98CH10886 with the U.S. Department of Energy. The publisher by accepting the manuscript for publication acknowledges that the United States Government retains a non-exclusive, paid-up, irrevocable, world-wide license to publish or reproduce the published form of this manuscript, or allow others to do so, for United States Government purposes.

REFERENCES

[1] U.S. NUCLEAR REGULATORY COMMISSION, “TRACE V5.0 Theory Manual”, ADAMS Accession Number ML120060218 (4 June 2010).

[2] STEINKE, R.G., et al., “TRAC-M/FORTRAN 90 (Version 3.0) Users Manual”, LA-UR-00-834, Los Alamos National Laboratory (Feb. 2000).

[3] DOWNAR, T., et al., “PARCS: Purdue Advanced Reactor Core Simulator”, Proc. PHYSOR 2002 Seoul, Seoul, Korea (2002).

[4] BOWMAN, S.M., SCALE 6: Comprehensive Nuclear Safety Analysis Code System, Nucl. Technol. **174** 2 (2011) 126.

REACTOR PERFORMANCE SCREENING OF ACCIDENT TOLERANT FUEL AND CLADDING CANDIDATE SYSTEMS

N. R. BROWN, M. TODOSOW
Nuclear Science and Technology Department
Brookhaven National Laboratory, Upton, NY
United States of America
E-mail: nbrown@bnl.gov

Abstract

The present paper summarizes some recent efforts related to uranium nitride composite fuel concepts, where the uranium nitride is "shielded" from water by one or more secondary phases. This work shows selected results from the analysis of advanced cladding for UN-based composite fuels with various secondary phases, including U_3Si_5, U_3Si_2, UB_2, and UB_4. These fuels are analyzed with various cladding, including zircaloy, Stainless Steel, and several commercial alloys (Kanthal AF and APMT). Selected three-dimensional burn-up dependent equilibrium core analysis results with thermal feedback are compared for UO_2 and several UN-based composite fuels with UB_2 and UB_4. In this case, the UB_2 or UB_4 content as a tertiary phase has been optimized to match the performance of an Integral Fuel Burnable Absorber (IFBA).

1. INTRODUCTION

In the aftermath of Fukushima Daiichi, the DOE-NE Advanced Fuels Campaign has supported development of advanced nuclear fuel and cladding options with potentially improved accident performance. Analytical evaluation of these fuel and cladding options is vitally important, because it identifies whether the options have at least equivalent performance as the present UO_2-Zr fuel system under nominal conditions.

An assessment of the viability and potential attractiveness of advanced nuclear fuels must include consideration of how proposed concepts will impact the nominal reactor performance and safety characteristics. This assessment includes reactor physics analyses to evaluate the impact on performance parameters (e.g., cycle length/burn-up) and safety-related characteristics (e.g., reactivity and control coefficients, kinetics parameters). BNL has developed and demonstrated a methodology to perform screening of performance and safety of candidate fuel concepts based on assembly and full-core equilibrium cycle three-dimensional reactor analyses [1 – 3]. With the post-Fukushima Daiichi focus on fuels with enhanced accident tolerance for implementation in commercial light-water reactors the methodology has been refined and expanded to allow a more complete analysis of performance under a wide spectrum of potential transients and accidents, up to, but not including, Beyond Design Basis Accidents.

This paper summarizes screening efforts for uranium nitride composite fuel concepts, where the uranium nitride is "shielded" from water by one or more secondary phases. All nitride composite analyses in this paper assume 100% enrichment in ^{15}N. The use of natural nitrogen (which presents a significant reactivity penalty due to ^{14}N) has also been studied but is not presented here. This work shows selected results from the analysis of advanced cladding for UN-U_3Si_5 fuel, a fuel concept proposed by Los Alamos National Laboratory. Similar evaluations of advanced cladding have been performed at Oak Ridge National Laboratory, but focused on UO_2 fuel where the neutron energy spectrum is softer and the heavy metal loading is lower [4].

Selected equilibrium core analysis results with thermal feedback are compared for UO_2, UN-U_3Si_2, and UN-U_3Si_2-UB_4 fuels. In this case, the UB_4 content as a tertiary phase has been optimized to match the performance of an Integral Fuel Burnable Absorber (IFBA). This is highly relevant due to a recent Westinghouse patent in this area [5].

2. ANALYSIS OF SS304 CLADDING WITH UN-U_3SI_5 FUEL

We evaluated the potential for stainless steel 304 (SS 304) cladding as a possible pairing with UN-U_3Si_5 fuel. We performed lattice-level neutronic analysis for a 17 x 17 PWR assembly with 4.9% enriched ^{235}U using the SCALE package [6] to assess the impact of these advanced cladding materials on reactivity, safety coefficients, and cycle length/burn-up. In this set of calculations, the UN phase constitutes 80% of the fuel volume, the U_3Si_5 phase 10% of the fuel volume, and the porosity is 10%. Changes in the volume percent or porosity of the individual phases will impact the specific result values. However, the qualitative physics-based conclusions remain valid. SS 304 has attractive properties relative to Zr alloy cladding, including potentially reduced oxidation rates in high temperature steam. SS 304 also has more than a decade of operational experience in LWRs, and experienced very low failure rates, especially in PWRs [7]. Five assembly level cases were compared as a function of burn-up (the fission gas gap was maintained at the same thickness for all cases):

- UO_2 with Zr alloy cladding:
  - Fuel pellet outer radius (OR) = 0.4096 cm, clad thickness = 0.0572 cm;
- UN – U_3Si_5 with Zr alloy cladding:
  - Fuel pellet OR = 0.4096 cm, clad thickness = 0.0572 cm;
- UN – U_3Si_5 with SS304-based cladding:
  - Fuel OR = 0.4096 cm, clad thickness = 0.0572 cm;
  - Fuel OR = 0.4096 cm, clad thickness = 0.0419 cm;
  - Fuel OR = 0.4249 cm, clad thickness = 0.0419 cm.

The three-batch cycle length and discharge burn-up is shown in Table 1. The infinite multiplication factor as a function of burn-up is shown in Figure 1. The initial reactivity penalty and parasitic neutron absorption in SS 304 is very high, approximately ~10,000 pcm (percent millirho) at BOL. These calculations assume a three-batch fuel management scheme with no burnable absorber loading or soluble boron and 3% neutron leakage. The ^{235}U enrichment of the fuel is 4.9% in all cases. The key result from the analysis is that the higher fissile content in UN-U_3Si_5 with 0.0419 cm thick clad compensates for the poisoning impact of the clad and matches the cycle length of the reference UO_2-Zr system. However, the discharge burn-up, and therefore the resource utilization, is reduced. The soluble boron coefficient is shown in Figure 2. The soluble boron coefficient illustrates the dual impact of spectral hardening due primarily to the increased heavy metal density of the UN-U_3Si_5 fuel and secondarily to the increased neutron absorption in the clad. Reducing the cladding thickness compensates somewhat for this impact, but increasing the radius of the fuel pellet significantly reduces soluble boron worth. This implies the need for enriched boron in the coolant.

TABLE 1. THREE-BATCH CYCLE LENGTH FOR SS 304 CLADDING AND UN-U_3SI_5 FUEL IN VARIOUS FORM FACTORS

Fuel - Clad	UO_2 - Zr (0.4096 cm - 0.0572 cm)	UN - U_3Si_5 - Zr (0.4096 cm - 0.0572 cm)	UN - U_3Si_5 - SS304 (0.4096 cm - 0.0572 cm)	UN - U_3Si_5 - SS304 (0.4096 cm - 0.0419 cm)*	UN - U_3Si_5 - SS304 (0.4249 cm - 0.0419 cm)
Discharge burn-up (GWd/t)	61.6	60.9	45.7	50.8	45.8
Cycle length (EFPD)	533	656	492	547	571

* Note that this is the only calculation in this paper where the cladding outer diameter is modified resulting in a higher moderator-to-fuel ratio and similar performance to the case with a larger fuel pellet.

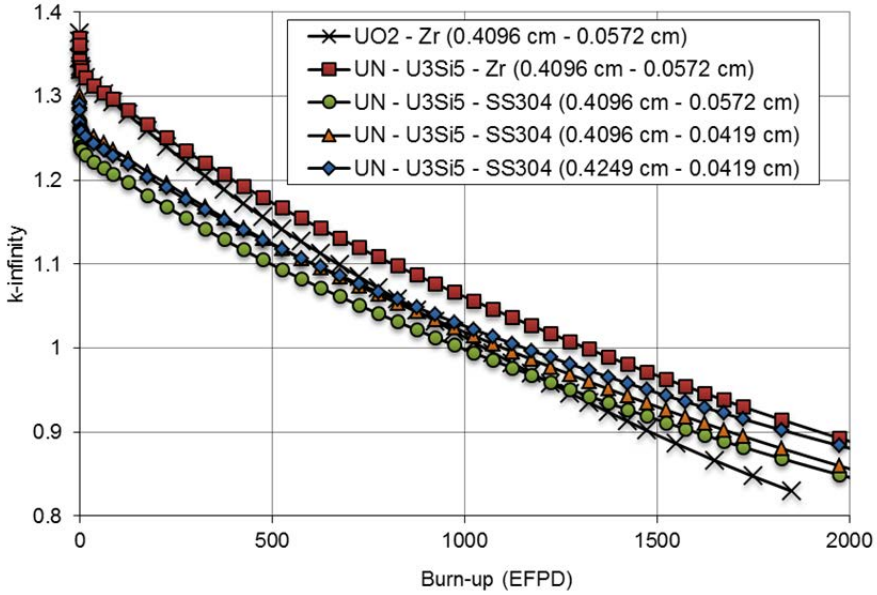

FIG. 1. Infinite multiplication factor as a function of burn-up for SS 304 cladding and UN-U_3Si_5 fuel in various form factors.

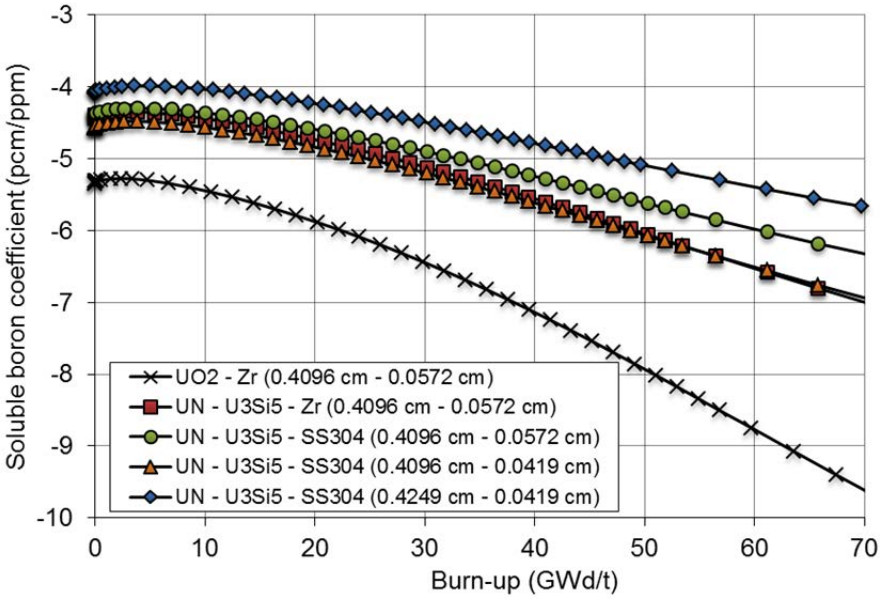

FIG. 2. Soluble boron coefficient as a function of burn-up for SS 304 cladding and UN-U_3Si_5 fuel in various form factors.

3. ANALYSIS OF ADVANCED IRON-BASED CLADDING MATERIALS WITH UN-U_3SI_5 FUEL

Several advanced iron-based claddings are under consideration due to increased oxidation resistance versus zirconium-based cladding. We analyzed several stainless steels with significant operational history in reactors, 304 and 316. In addition, we considered two commercial alloys, Kanthal AF (referred to as FeCrAl) and Kanthal APMT (referred to as APMT). The cladding thickness for the predominantly iron-based cladding materials is 0.0419 cm versus 0.0572 cm for zirconium-based cladding. The fuel pellet thickness is increased due to this change in cladding thickness. The reduced cladding thickness is relevant

given significant operational experience with iron-based cladding, such as SS304. Our analyses show that there is a large reactivity penalty due to these advanced claddings, as shown in Figure 3 plotted versus burn-up in GWd/t.

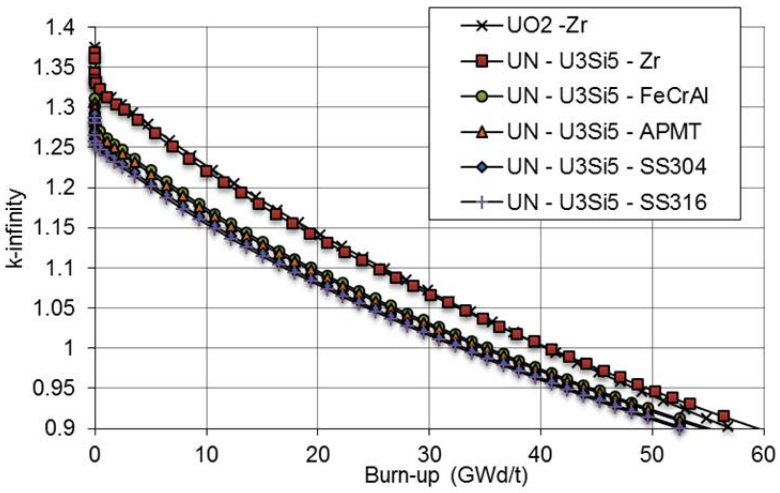

FIG. 3. Multiplication factor vs. burn-up (GWd/t) for UN-U_3Si_5 fuel and cladding combinations.

However, in terms of three-batch cycle length of nitride-composite fuels this reactivity penalty is compensated via the higher heavy metal loading and increased fuel pellet thickness, as shown in Table 2.

TABLE 2. THREE- AND FOUR-BATCH CYCLE LENGTH AND DISCHARGE BURN-UP FOR VARIOUS ADVANCED FUEL/CLADDING OPTIONS AT 4.9%-ENRICHED ^{235}U (NOMINAL UO_2-Zr VALUES ARE BOLDED)

Fuel	UO_2 - Zr	UN - U_3Si_5 - Zr	UN - U_3Si_5 - FeCrAl	UN - U_3Si_5 - APMT	UN - U_3Si_5 - SS304	UN - U_3Si_5 - SS316
			Three-batch			
Batch burn-up (GWd/t)	**20.5**	20.3	17.4	17.2	16.4	16.2
Discharge burn-up (GWd/t)	**61.6**	60.9	52.2	51.5	49.2	48.5
Cycle length (EFPD)	**533**	656	604	597	570	562
			Four-batch			
Batch burn-up (GWd/t)	**16.4**	16.1	13.7	13.5	12.9	12.7
Discharge burn-up (GWd/t)	**65.7**	64.3	54.7	54.0	51.5	50.8
Cycle length (EFPD)	**426**	519	475	469	448	442

4. EQUILIBRIUM CORE ANALYSIS FOR UN-U_3SI_2

We performed equilibrium core analysis of a variety of nitride composite fuel options, using a similar methodology as that described in Reference 1. This summary highlights a new proposed composite (UN-U_3Si_2-UB_4) with a tertiary component (UB_4) that has been tuned to match the performance of an assembly with 112 IFBA coated fuel rods. This type of configuration is relevant to a recent Westinghouse patent [5]. Three cases were compared in 17 x 17 assembly dimensions and an AP1000-like core: a nominal UO_2-Zr case with 112

IFBA coated rods, a UN/U_3Si_2-Zr case with 112 IFBA coated rods, a UN/U_3Si_2/UB_4-Zr case with 5 concentric depletion zones ("rings") per fuel pin. In the UN-U_3Si_2-UB_4 case the same mass of natural boron from the 112 IFBA coatings is conserved, but is dispersed throughout all 264 of the fuel pins in the assembly as UB_4. The PARCS regulatory-grade core simulator was utilized in a full three-dimensional model of the reactor core including thermal-hydraulic/fuel temperature reactivity feedback [8]. Equilibrium cycle fuel shuffling was performed with the fresh assemblies located near the periphery of the core and the once- and twice-burned assemblies located throughout the central core region. This is a relatively high-leakage loading scheme that is necessitated due to the simplified burnable absorber loading and desire to maintain reasonable power peaking. The radial assembly peaking factors as a function of burn-up in EFPD are shown in Figure 4.

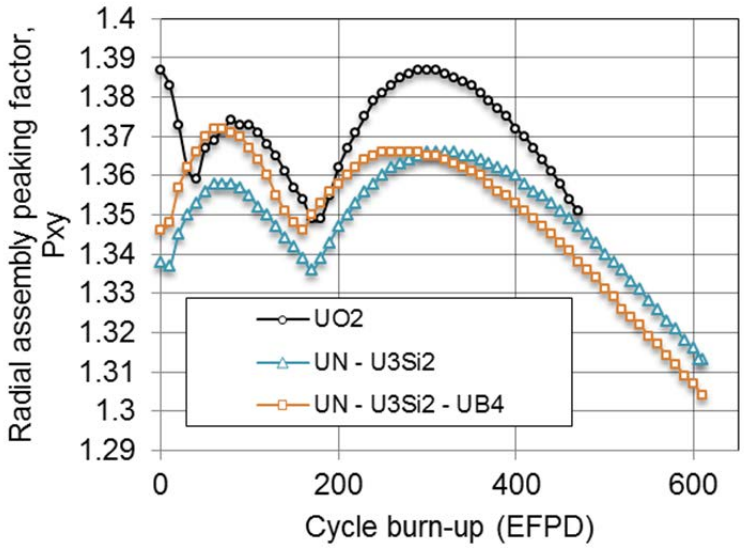

FIG. 4. Radial assembly power peaking as a function of burn-up (EFPD).

Radial power peaking in the core and End of equilibrium Cycle (EOC) is shown in Figure 5 for UO_2-Zr and UN/U_3Si_2/UB_4. Corresponding assembly-average fuel temperatures (assuming a gap conductance of 5,000 W/(m·K)) are shown in Figure 6. This analysis shows that this advanced composite fuel, even with burnable absorber integrated into the pin as a tertiary phase, can match the core performance of a nominal UO_2-Zr fuel. In addition, the fuel temperatures will be much lower due to the enhanced thermal conductivity of the fuel.

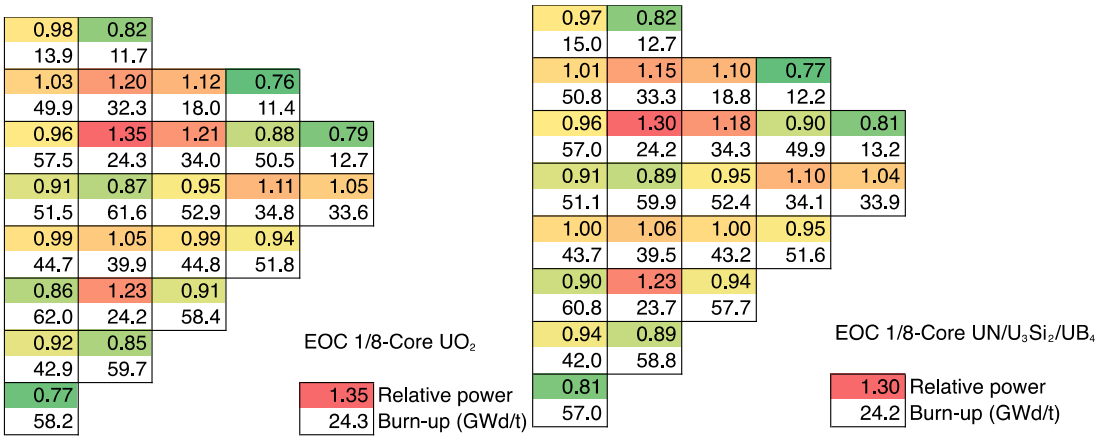

FIG. 5. Radial assembly power peaking at EOC for an AP1000-like reactor core.

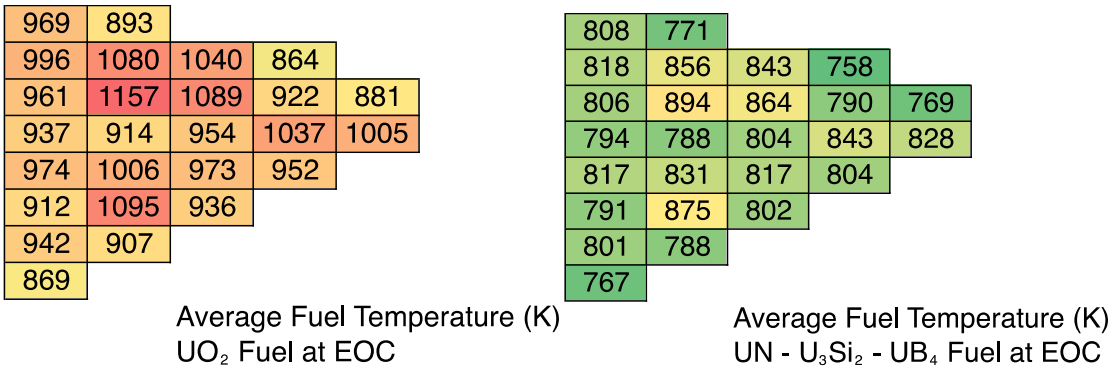

FIG. 6. Assembly average fuel temperatures for an AP1000-like equilibrium reactor core at EOC.

5. INITIAL EVALUATION OF UN-U_3SI_5 FUEL IN BOILING WATER REACTORS

As an initial screening study, the reactor performance of UN-U_3Si_5 was studied in the form factor of a Boiling Water Reactor (BWR). BWRs compose a significant fraction of the reactor fleet, and Fukushima Daiichi was a BWR. Evaluating performance in BWRs is more challenging than PWRs, due to the axial heterogeneity in void fraction profile and assembly design, large guide tubes, assembly shroud and inter-assembly gap, and control blades instead of control rods, among other differences. All of these result in significant intra- and inter-assembly shifts in the neutron flux spectrum. This causes high local pin power peaking that is mitigated via fuel pins that contain Gd_2O_3 absorber, enrichment zoning, and partial length fuel rods. An example BWR lattice is shown in Figure 7 and radial and axial flux and power distributions in Figure 8. All of these design considerations change considerably given the spectral shift cause by some accident tolerant fuels, such as UN-based ceramic fuels. In addition, the chemical compatibility of Gd_2O_3 absorber with some ATF concepts is unknown but is being studied.

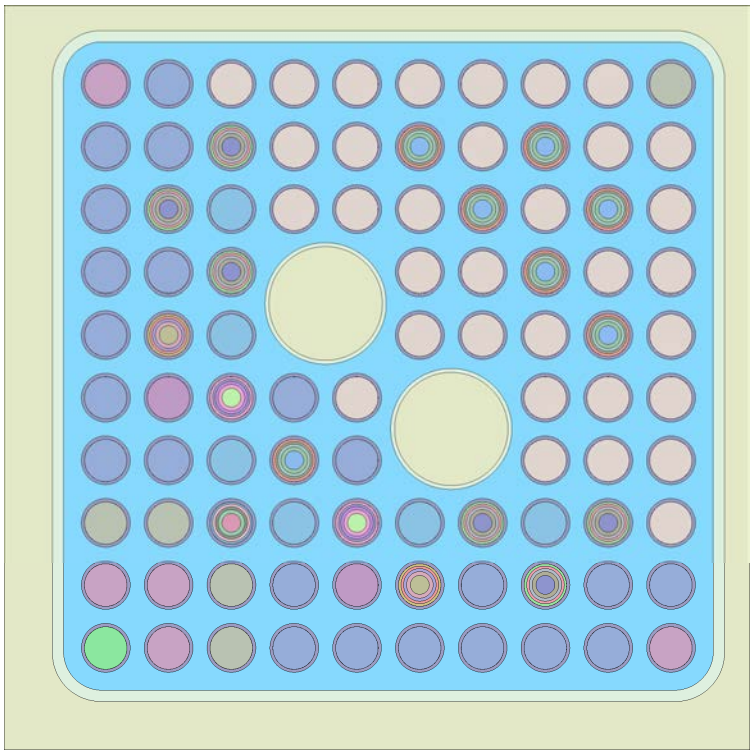

FIG. 7. Example BWR lattice model showing radial heterogeneity in lattice design.

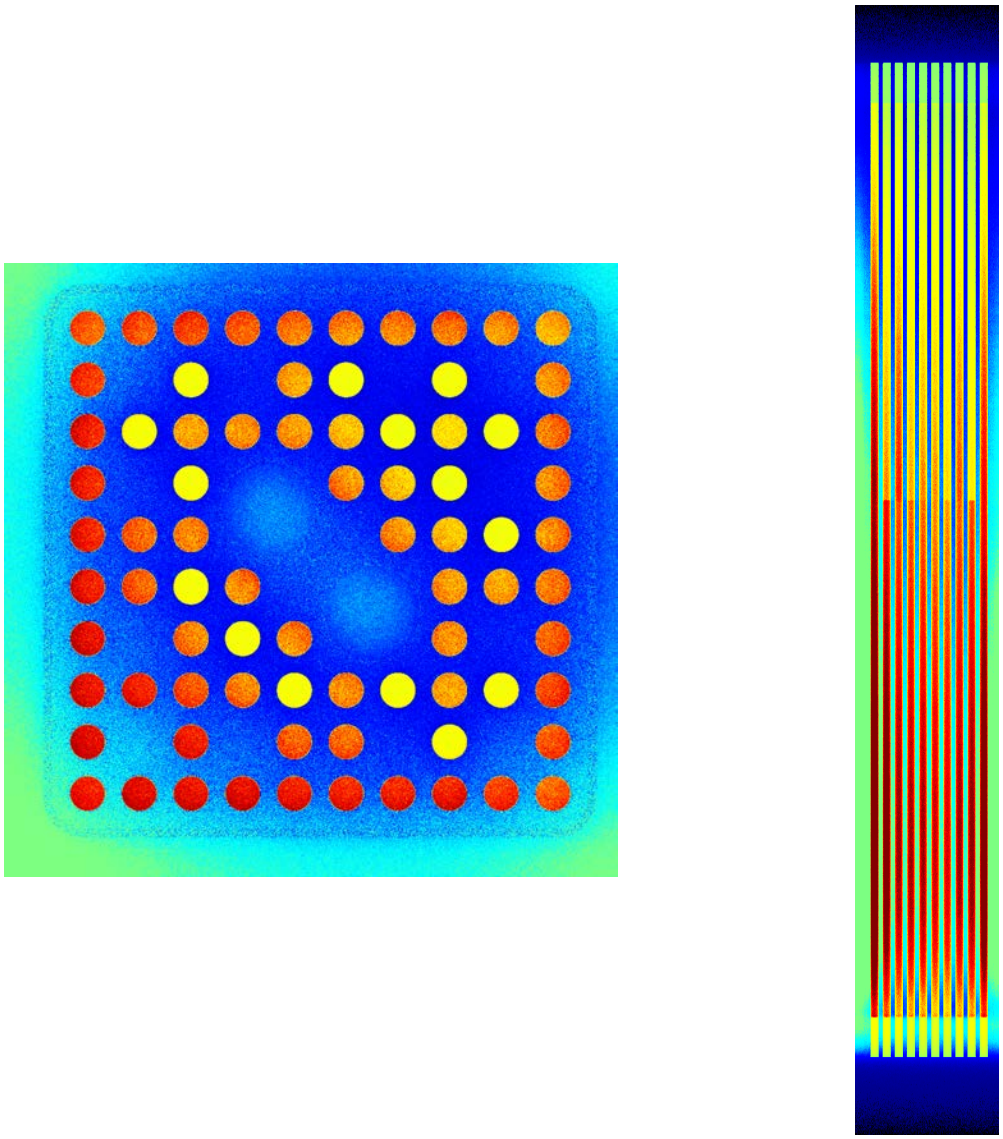

(Blue-Green Shades Represent Thermal Flux, Red-Yellow Shades Pin Power)

(a) (b)

FIG. 8. Thermal flux and power distribution contour plots, showing (a) radial and (b) axial heterogeneity in BWR.

As an initial scoping approach, an un-poisoned BWR lattice was considered with 40% void and UN-U_3Si_5 (80% UN, 10% U_3Si_5, and 10% porous) fuel with Zr cladding. For consistency with the existing studies the enrichment was assumed to be ~4.9% and the enrichment in ^{15}N was assumed to be 100%. The infinite multiplication factor is shown as a function of burn-up in GWd/t and in EFPD in Figure 9 and Figure 10, respectively. This analysis shows that the PWR-based conclusions about UN-U_3Si_5 fuel in terms of cycle length and discharge burn-up will also qualitatively hold for BWRs.

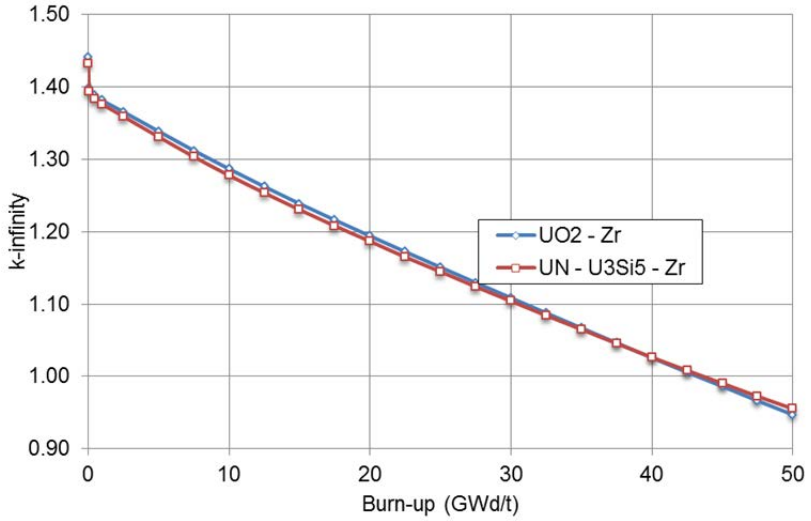

FIG. 9. Un-poisoned infinite multiplication factor as a function of burn-up (GWd/t) for a BWR assembly with UO_2 fuel and Zr alloy cladding and UN-U_3Si_5 fuel and Zr alloy cladding.

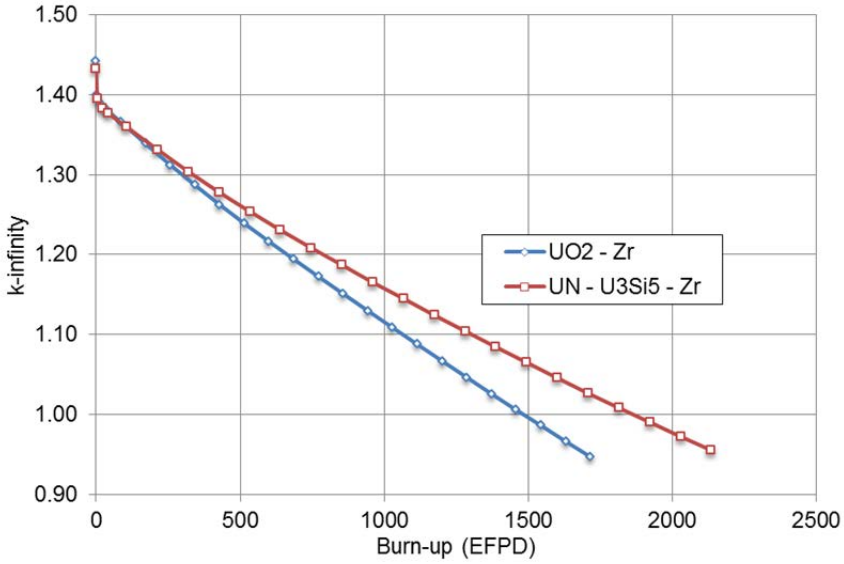

FIG. 10. Un-Poisoned infinite multiplication factor as a function of burn-up (EFPD) for a BWR assembly with UO_2 fuel and Zr alloy cladding and UN-U_3Si_5 fuel and Zr alloy cladding.

6. CONCLUSIONS

Assuming a constant enrichment, the higher density of UN-based fuels can compensate for the parasitic absorption in Fe-based cladding in terms of cycle length in EFPD relative to the UO_2-Zr system. However, there will still be a marginal penalty in discharge burn-up in GWd/t.

The reactivity control capability of a UB_4 admixture in a UN composite fuel can closely match an IFBA coating burnable poison configuration. Admixture of UB_4 as reactivity control offers potentially enhanced flexibility for many advanced PWR fuels, and a UB_2 or UB_4 phase could even reduce the peak rod gas pressure in UO_2-based fuel pins (compared with IFBA-coating) by distributing the boron throughout an increased number of fuel rods. These results are obtained with natural boron.

BWRs are challenging to evaluate due to heterogeneity in void distribution and assembly design, chemical compatibility of absorbers (e.g. Gd_2O_3) with possible fuel forms, and other issues. However, an initial assessment indicates fuel management conclusions about UN-U_3Si_5 fuel in PWRs are also applicable to BWRs. Further work is needed in this area.

ACKNOWLEDGEMENTS

This manuscript has been authored by employees of Brookhaven Science Associates, LLC under Contract No. DE-AC02-98CH10886 with the U.S. Department of Energy. The publisher by accepting the manuscript for publication acknowledges that the United States Government retains a non-exclusive, paid-up, irrevocable, world-wide license to publish or reproduce the published form of this manuscript, or allow others to do so, for United States Government purposes.

REFERENCES

[1] BROWN, N.R., ARONSON, A., TODOSOW, M., BRITO, R., McCLELLAN, K., Neutronic performance of uranium nitride composite fuels in a PWR, Nucl. Eng. Des. **275** (2014) 393-407.

[2] BROWN, N.R., LUDEWIG, H., ARONSON, A., RAITSES, G., TODOSOW, M., Neutronic evaluation of a PWR with fully-ceramic micro-encapsulated fuel, Part II: Nodal core calculations and preliminary study of thermal hydraulic feedback, Annals of Nuclear Energy **62** (2013) 548-557.

[3] BROWN, N.R., LUDEWIG, H., ARONSON, A., RAITSES, G., TODOSOW, M, Neutronic evaluation of a PWR with fully-ceramic micro-encapsulated fuel, Part I: Lattice benchmarking, cycle length, and reactivity coefficients, Annals of Nuclear Energy **62** (2013) 538-547.

[4] GEORGE, N.M., TERRANI, K.A., POWERS, J.J., "Neutronic Analysis of Candidate Accident-Tolerant Iron Alloy Cladding Concepts", ORNL/TM-2013/121 (2013).

[5] LAHODA, E. J., U.S. Patent 7,139,360 B2 (2006).

[6] OAK RIDGE NATIONAL LABORATORY, SCALE: "A Comprehensive Modelling and Simulation Suite for Nuclear Safety Analysis and Design", ORNL/TM-2005/39 (2011).

[7] TERRANI, K.A., ZINKLE, S.J., SNEAD, L.L., Advanced oxidation-resistant iron-based alloys for LWR fuel cladding, J. Nucl. Mater. **448** (2014) 420-435.

[8] DOWNAR, T.J., XU, Y., SEKER, V., HUDSON, N., "PARCS v3.0 U.S. NRC Core Neutronics Simulator Theory Manual", University of Michigan Technical Report, (2012).

DEVELOPMENTS IN REACTOR AND ECONOMIC MODELLING CONSIDERING THE PERFORMANCE OF ACCIDENT TOLERANT FUELS

D. MATHERS, I. PALMER, C. GROVE, M. THOMAS
National Nuclear Laboratory
United Kingdom
E-mail: daniel.p.mathers@nnl.co.uk

Abstract

Accident tolerant fuel (ATF) technology is being developed to enhance the safety performance of nuclear fuels and cladding. The development and testing of ATF materials by NNL through its Nuclear Fuel Centre of Excellence is being complemented by parallel developments in fuel performance modelling, in addition to reactor physics and economic calculations to optimise ATF fuel. An approach for preliminary optimisation of ATF fuel pin and cladding parameters, in typical commercial PWRs is described, including an initial optimisation of uranium nitride (UN) fuel pellet dimensions and enrichment (combined with zirconium cladding) and for silicon carbide composite (SiC) clad fuel (combined with uranium oxide fuel (UO_2)). In order to optimise pin reactivity, pellet diameter is less for UN compared with UO_2. A lower feed enrichment was required to give an equilibrium energy output close to the equivalent UO_2 fuel. Modelling this design indicates that there is a potential economic benefit, through lower fuel assembly costs, when using optimised UN fuel compared with standard UO_2 PWR fuel. For standard UO_2 fuel, full core calculations have examined the reactivity benefit when replacing zircaloy clad for SiC. Calculations assume idealised SiC clad thicknesses similar to those used with current zircaloy clads. An economic analysis, considering current cost estimates of SiC clad manufacture, indicates SiC clad fuel assembly costs are significantly increased. However, there remains scope for offsetting these increased fuel costs through optimised reactor operation by taking advantage of the reduced parasitic neutron absorption or higher temperature tolerance of SiC clad. An initial assessment is also undertaken of how the performance of the higher density uranium nitride fuel compares against key PWR safety measures: considering pin power peaking, shutdown margin, moderator temperature coefficients, boron reactivity worth, delayed neutron fractions and boration limits. All analyzed key safety parameters were within typical PWR limits.

1. REQUIREMENTS FOR ACCIDENT TOLERANT FUEL MODELLING

Accident tolerant fuel (ATF) technology is being developed that enhances the safety performance of nuclear fuels and cladding. Numerous aspects of ATFs are being studied, including ways in which the cost of this new technology may be offset. ATFs are primarily targeted at current Generation II and III light water reactors (LWRs). In addition, they could be of interest for Gen III heavy water reactors (HWRs), water-cooled small modular reactors (SMRs) and in future for Gen IV in particular the supercritical water reactor (SCWR). There are also predicted applications for some ATF materials for Gen IV fast reactors, ATF technology may also be utilised, across all current/future reactor types, with fuels containing plutonium (Pu) and/or minor actinides (MAs), such as those which have the potential for use in future sustainable closed fuel cycles.

As a first step towards deployment of ATFs the in-reactor performance of novel fuel-clad systems must be proven. Steps are being undertaken through various multi-national collaborative proposals to make the fuel-clad system components and then to test their properties and down-select fuel-clad pairings prior to coupled tests and subsequent irradiation trials. The performance of these fuels under test will require analysis and validation and will ultimately provide data for predictive models. These models will be used to predict the performance of ATF under different operating conditions, including accident scenarios. The performance of fuels in these modelling scenarios will determine whether ATF is further developed. Reactor test programmes require significant investment and therefore the testsneed to be designed to maximise value, for example, by testing the performance of ATF as applicable to code parameters with the largest effects or impacting uncertainties.

There are many different fuel and cladding concepts for high accident tolerance. Fuel concepts being considered include advanced uranium oxide, uranium silicide (U3Si2), uranium nitride (UN) fuels, coated particles and thorium containing fuels. The claddings

being considered include improved zirconium alloys (including surface treatment), standard and advanced steels (in particular FeCrAl alloys), silicon carbide composites (SiC-SiC) and MAX phase ceramics. The applicability of these concepts in terms of Technology Readiness Levels (TRLs) in comparison to other fuel and cladding types is summarised in Figures 1 and 2 below.

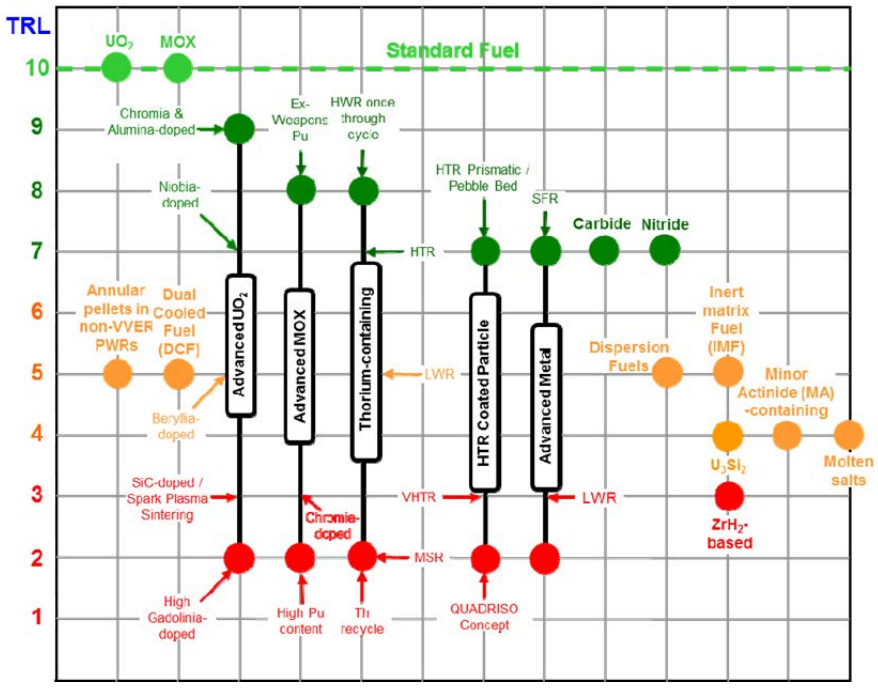

FIG. 1. Summary assessment of technology readiness.

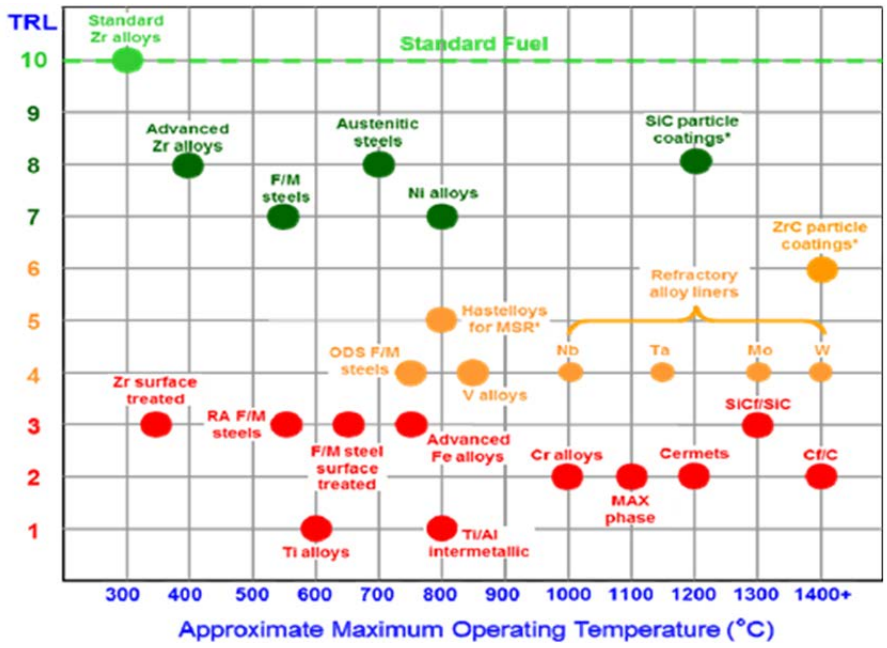

FIG. 2. Summary assessment of technology readiness for cladding.

Uranium dioxide (UO_2), with U-235 enrichments up to 5%, has been the fuel of choice for light water reactors (LWRs) for many years. Manufacturing routes are well established and challenging the status quo will require safety, environmental and economic benefits to be demonstrated to both fuel manufacturer and reactor operator. The potential

advantages of uranium silicide (U_3Si_2) and uranium nitride (UN) fuels in particular are evident from examining the basic properties of the materials (see Table 1). A higher thermal conductivity is beneficial in reducing the peak temperatures in the centre of the pellet during a beyond design basis accident as well as reducing thermal stresses during normal operations. A higher density is economically attractive because the amount of fissile atoms per unit volume is increased; this means that, for equivalent fuel enrichment, the fuel is more reactive and therefore burnup may be increased, or, the same cycle length can be attained with a lower enrichment fuel. These benefits need to be validated through a fuel qualification programme, combining fabrication, in-pile testing and modelling.

TABLE 1. A COMPARISON OF BASIC PROPERTIES OF UN AND U3SI2 COMPARED TO UO_2

Material	Theoretical density (TD) $Mg{\cdot}m^{-3}$	Difference in heavy metal TD compared to UO_2	Thermal conductivity at 1100°C $W{\cdot}m^{-1}{\cdot}K^{-1}$	Melting Point °C	Thermal expansion coefficient $x10^{-6}K^{-1}$
UO_2	10.96	-	2.8	2840	10
UN	14.3	+40%	22.8	2762	8
U_3Si_2	12.2	+18%	17.3	1665	15

The use of a novel ceramic composite cladding material to replace the zirconium alloy cladding currently used in all light water reactors would increase the “accident tolerance” of the cladding. Zirconium alloys have reasonable corrosion resistance at normal operating temperatures (below 350°C), but at higher temperatures the oxidation rate accelerates, and above 500ºC gross oxidation can occur. This is problematic in loss-of-coolant accidents such as those that occurred at Three Mile Island and Fukushima Daiichi, where cladding temperatures can exceed 700°C. Under these conditions, rapid oxidation of the cladding results in the evolution of large quantities of hydrogen that can explode, resulting in core damage and fission product release.

Ceramic claddings offer a promising alternative to zirconium-based alloys, and attention has focused on SiC because of a number of important advantages, including: much greater resistance to oxidation in water and steam, even at high temperatures; good radiation stability; low neutron capture cross-section; and greater mechanical strength at high temperatures.

Achieving increased safety as well as improved economic performance is the objective of ATF developments resulting in promising fuel and cladding combinations. SiC cladding has been demonstrated to be resistant to runaway oxidation at temperatures above those expected to be reached in the station blackout scenario at Fukushima Daiichi. The high density waterproofed UN/U_3Si_2 and U_3Si_2 have both the potential to provide significant economic advantages for utilities.

2. FUEL PERFORMANCE MODELLING

To quantify the potential benefits of ATF’s and to explore the design optimisation issues associated with a higher density, higher thermal conductivity fuel such as U_3Si_2 fuel, a basic in- reactor modelling capability will be required. ENIGMA is the UK's primary tool for thermal reactor fuel performance modelling under steady state and off-normal conditions. Its capabilities currently include the modelling of various fuel pellet types (including UO_2 and MOX) in various claddings (including zirconium-based alloys and steels). Work has now begun to extend ENIGMA's capabilities to include advanced fuel types based on U_3Si_2.

The specific aims of the work were as follows: to adapt and extend the fuel property models to include the best-available correlations for U_3Si_2, derived from measurements carried out in support of the use of U_3Si_2 dispersion fuels in research and test reactors; to test the adaptations in the revised version of the code; to document all the changes in an update to the code manual.

In total, twelve sets of changes were made to ENIGMA in order to create a first version capable of modelling U_3Si_2 fuel; this new version is uniquely identified as ENIGMA 7.8/B11. For some of the changes, property measurements or post-irradiation examination (PIE) data were found in the literature on which the new models could be based, but for others the absence of appropriate information meant that highly simplistic, or null, assumptions needed to be made. It should therefore be recognised that the new capability in ENIGMA is effectively only a first iteration, and at present remains unverified and unvalidated.

The twelve areas of change in the code are summarised below. The consequences of each change were examined in turn by running an idealised LWR fuel analysis through to high burnup and generating a set of standard plots of the key code predictions of interest (temperature, stress, strain, fission gas release etc). This allowed the relative importance of the different changes to be quantified. All code changes were documented in detail in the code manual.

The twelve code changes were as follows:

2.1. Revised input logic

A new input option was created to select U_3Si_2 fuel, together with some cosmetic adjustments and changes to house-keeping routines, to allow the user to access the new capability. This change has no effect on code predictions;

2.2. Neutronic modelling

Only a simplistic approach to modelling the neutronic differences between U_3Si_2 and UO_2 has been adopted thus far, and this is an area where further work is needed. As an interim approach, U_3Si_2 is modelled as UO_2 but with the supplied U-235 enrichment value multiplied by the U_3Si_2: UO_2 ratios of the theoretical densities and heavy metal contents, in order to give a first order approximation to the equivalent enrichment in a UO_2 fuel rod;

2.3. Thermal conductivity

The conductivity of U_3Si_2 is appreciably higher than that of UO_2 and increases with temperature rather than decreases (a factor which has the potential to significantly enhance accident tolerance). This is thought to apply over the whole relevant temperature range from room temperature to near its melting point at around 1600°C, though data at the highest temperatures is scarce. A simple linear relationship was therefore adopted in the code. Effects of porosity, irradiation and stoichiometry are currently unknown and hence have not yet been included in the model;

2.4. Thermal expansion

Measurements on U_3Si_2 are scarce, and show some variation depending on fabrication route, but do provide enough information to define a simple thermal expansion coefficient correlation. The thermal expansion of U_3Si_2 is thought to be about 50 percent higher than for UO_2 in the temperature range of interest;

2.5. Elasticity

Fixed values of Young's modulus and Poisson's ratio, independent of temperature and porosity, have been assumed, based on the limited literature data available. Young's modulus is significantly (about 60 percent) lower with U_3Si_2 fuel than with conventional oxide fuel, reflecting that as an intermetallic compound, its properties are more akin to those of a metal than a ceramic;

2.6. Creep

No published information was found on the creep properties of uranium silicide. As an interim measure, all components in the creep model (for both thermal and irradiation creep) were set to zero;

2.7. Density and heat capacity

The theoretical density of U_3Si_2 is 12.2 g/cm^3, compared with 10.96 g/cm^3 for UO_2. It contains 92.72 wt%U compared with 88.15 wt%U for UO_2. Concerning specific heat capacity, a linear correlation with temperature was adopted; the heat capacity of U_3Si_2 is lower than that of UO_2 at low temperature, but similar at high temperature;

2.8. Densification and swelling

Empirical evidence is available for the swelling rate of U_3Si_2 based on measurements on research reactor plate dispersion fuel. Such measurements are generally at very high burnup levels compared with those for LWR fuel, and also represent swelling inclusive of any densification and high burnup restructuring effects. The following assumptions were made: (a) densification is set to zero; (b) swelling reduction due to loss of volatile fission products is set to zero; (c) the solid fission product swelling rate is set to a literature-recommended value; (d) the code's existing model for gas bubble swelling is left unchanged, but noting that in practice this means that the swelling contribution will be small due to the low operating temperatures involved; (e) swelling associated with restructuring effects is set to zero;

2.9. Fission gas diffusion coefficient

No literature information was found on the measurement of fission product diffusion coefficient in U_3Si_2. Some data is reported on gas release levels from irradiation trials of U_3Si_2, but generally at conditions of temperature and burnup that are a long way removed from those expected in LWR. Given the temperature and burnup regime expected for LWR operation (centreline temperature around 600°C, burnups up to around 70 MWd/kgHM) release levels can be expected to remain low, though non-zero. In the absence of other information, ENIGMA's existing model of gas diffusion coefficient used for oxide fuel was also adopted for U_3Si_2;

2.10. Grain growth

No published information was found on in-pile grain growth behaviour in U_3Si_2. Pending the availability of suitable measurements, the grain growth model in ENIGMA has been disabled when the fuel type is U_3Si_2;

2.11. Helium absorption and re-release

Again, the model for this process has been disabled when the fuel type is U_3Si_2, in the absence of any relevant data;

2.12. Pellet cracking, wheatsheafing and relocation

Given U_3Si_2 is more akin to a metal than a ceramic, it would not be reasonable to assume that its cracking behaviour was the same as that of oxide fuel; the related phenomena of pellet wheatsheafing and relocation likewise. In the absence of other information, the most reasonable assumption would be that these effects don't occur. Pellet cracking and pellet wheatsheafing have therefore both been disabled for silicide fuel. An empirical also been disabled.

In summary, a new version of the ENIGMA thermal reactor fuel performance code has been created embodying a prototype modelling capability for U_3Si_2 fuel. The model changes have been tested and documented, and the effects on code predictions for a representative LWR case have been quantified. Figure 1 shows example calculations using the new code version (currently unverified), comparing the estimated centreline temperature evolution for oxide and silicide fuel for an idealised PWR irradiation.

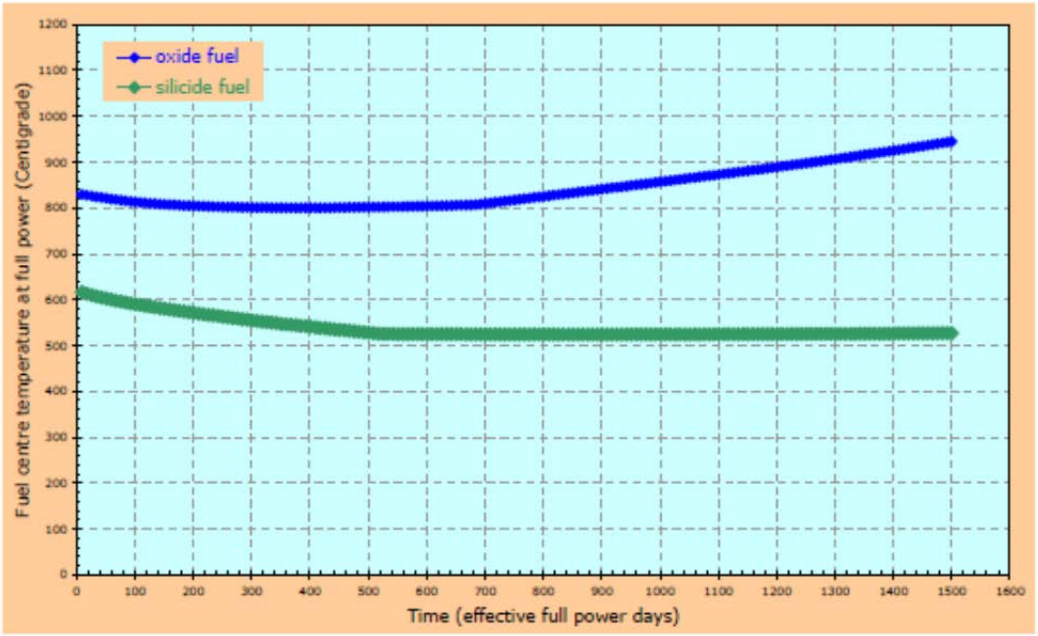

FIG. 1. ENIGMA temperature predictions for oxide and silicide fuels.

No attempt has yet been made to determine the optimum pin diameter for uranium silicide fuel in an LWR as has been performed for uranium nitride (section below). In spite of this, it can be assumed that as the neutron spectrum of U_3Si_2 fuel is intermediate between UN and UO_2, the optimum U_3Si_2 fuel pin diameter is likely to be smaller than that of UO_2 (0.950 cm) and greater than that of UN.

3. DETERMINATION OF OPTIMUM FUEL PIN DIAMETER WITH UN FUEL

A modelling study has also been carried out to investigate optimisation of the fuel pin diameter, but with a standard fuel assembly pitch. Uranium nitride fuel is investigated here, assuming that uranium nitride were to be used in place of industry-standard UO_2. UN is about 30 percent more dense than UO_2, decreasing the ratio of hydrogen to heavy metal (H:HM) if a standard UO_2 fuel assembly geometry is used to accommodate the UN fuel pins. In order to optimise the UN fuel assembly, the fuel pin diameter needs to be slightly decreased, thereby increasing H:HM which will tend to increase the reactivity of the fuel. The magnitude of the decrease in UN fuel pin diameter is a compromise between maximising the reactivity while ensuring the fuel maintains an inherent negative feedback mechanism, i.e., a negative moderator temperature coefficient such that any increase in temperature or coolant voidage will result in a decrease in reactivity.

An optimum fuel pin diameter for UN fuel has been determined in order to maximise reactivity. A Gen III+ pressurised water reactor (PWR), Westinghouse's AP1000, and its fuel design have been modelled neutronically using the CMS (Core Management System) commercial reactor analysis code suite provided by Studsvik Scandpower: Initially, INTERPIN-CS models the fuel performance of individual fuel rods in the core to obtain temperature data. Next, CASMO-4, a multi-group neutron transport theory code calculates the cross-sections and burnup characteristics of individual assemblies.

CMSLINK is then used to generate the nuclear data libraries from the CASMO-4 output containing the few-group cross sections required to model a LWR reactor core. Finally, SIMULATE-3 uses these cross sections to represent the reactor in three dimensions.

If UN fuel were to be used in an AP1000 in place of UO_2, the calculations demonstrate that the pin diameter should be decreased to optimise the fuel reactivity. However, if the pin diameter is decreased too much, a highly undesirable positive moderator temperature coefficient (MTC) is seen. Figure 2 plots the calculated beginning of cycle (BOC or zero burnup) multiplication factor '$k_{infinity}$' versus the moderator-to-fuel (M:F) ratio, where $k_{infinity}$ is a measure of reactivity defined as the ratio of the number of neutrons resulting from fission in the current generation to the number absorbed in the preceding generation in a system of infinite size. The figure shows that standard UO_2 fuel is optimised such that a decrease in the M:F ratio, for example due to the introduction of voidage or a temperature increase, leads to a decrease in reactivity.

The optimum value for the M:F ratio for UN fuel therefore lies to the left of the peak in the UN curve; a value around 2.5 was therefore chosen on the basis that at this ratio the MTC is negative. When an M:F ratio of 3.0 was chosen and analyzed using UN fuel, a positive MTC was seen.

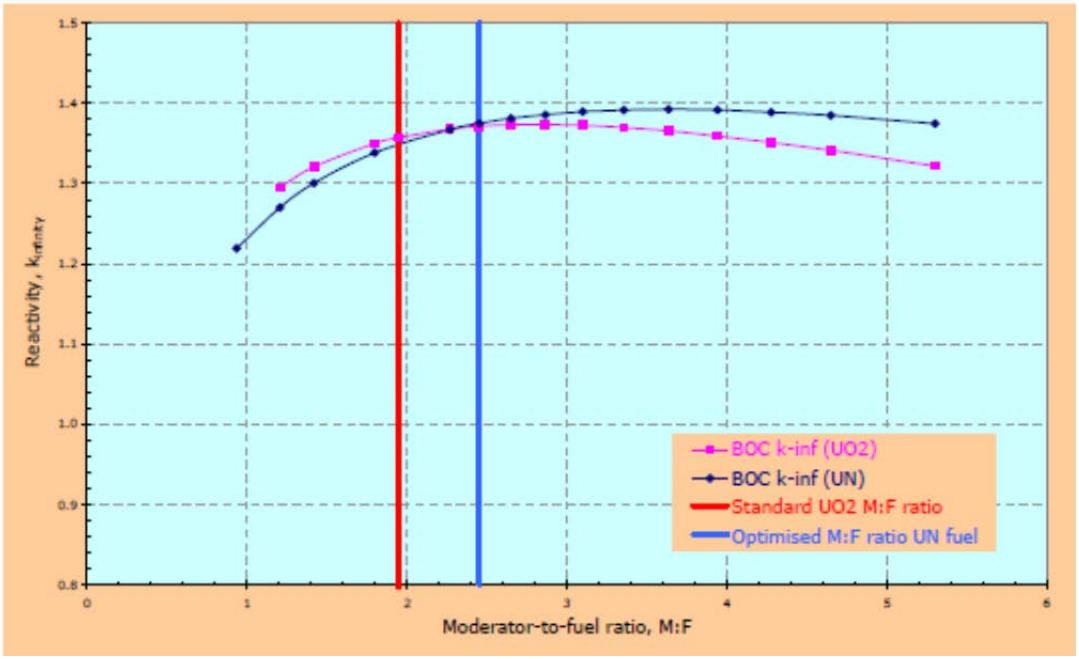

FIG. 2. $k_{infinity}$ versus moderator-to-fuel ratio at BOC for UN and UO_2. The results from these analyses indicate that the optimum fuel pin outer diameter (i.e. the cladding outer diameter) for UN fuel is smaller than the 0.950 cm value for UO_2. Similarly the UN fuel pellet diameter is optimal at a reduced value for UN compared with 0.819 cm for UO_2.

To get an indication as to whether a UN-fuelled AP1000 reactor core operated under an industry standard 18 month fuel cycle regime would satisfy a typical PWR safety case, key parameters were evaluated and assessed against typical PWR nuclear design limits:

- Radial Power Distribution Peaking Factor (FΔH) Limit at Full Power;
- Shutdown Margin with One Stuck Rod;
- Moderator Temperature Coefficient;
- Boron Reactivity Coefficient;
- Delayed Neutron Fractions;
- Boration Limits.

All of the design limits which were assessed were satisfied.

Natural nitrogen comprises 99.63% N-14 and 0.37% N-15. However, N-14 is a significant neutron absorber and leads to the production of radioactive C-14 and hydrogen, which can cause clad embrittlement. Therefore UN fuel designs proposed by industry to date have assumed a fuel composition enriched in N-15. An N-15 enrichment process is yet to be commercially implemented; however, an economic assessment was carried out using the predicted costs of potentially suitable processes. This assessment indicated overall that, with certain provisos, e.g., the price of N-15 extraction, there are potential economic benefits to using UN fuels compared with UO_2.

NNL's in-house fuel enrichment cost calculation tool 'ENRIC' has been used to calculate the relative cost of manufacturing UO_2 and UN fuel assemblies for AP-1000. Due to the increased density of UN fuel, the enrichment of the fuel can be reduced whilst maintaining an equivalent number of fissile atoms per unit fuel volume. A cost saving can be achieved through not having to enrich the fuel to as high a level as that required for UO_2.

Equivalent reactivity has been achieved using values of U-235 enrichment approximately 20% lower for UN fuel compared with UO_2 fuel. The reduced costs achieved through lower enrichment are partially offset by the requirement for (a) an increased fuel mass (UN fuel has higher density – the reduction in pellet diameter is not sufficient to circumvent a net increase in the fuel mass required), and (b) the additional cost associated with use of N-15 compared with natural N.

The finished assembly costs ($/assembly) are estimated at $1.87 million for UN fuel and $1.98 million for UO_2 fuel. The cost of using nitrogen enriched in N-15 is estimated to add an additional $40k to the cost of a finished fuel assembly.

Calculations of finished fuel costs generated by NNL compare the costs of a key option for accident tolerant fuel i.e. UN fuel assemblies with UO_2 fuel assemblies. Reactor plant savings of between $3 M and $7 M per 18 month reload are estimated. Extrapolating this to a 60 year reactor lifetime and assuming 90% utilisation gives an estimate of between $108 M and $252 M saving in using UN fuel for the lifetime of a reactor or between $1,728 M and $4,032 M for a 16 GWe fleet.

4. NEUTRONIC PERFORMANCE OF SIC-SIC CLADDING AND ASSOCIATED ECONOMIC IMPACT

The reactor core physics of the EPR has been analyzed deploying fuel assemblies made with silicon-carbide composite (‘SiC’ or ‘SiC-SiC’) as the cladding and spacer grid material.

Although SiC is not a novel material, nuclear fuel cladding is a new application and the immaturity of manufacturing technology makes estimation of a final likely cost and design difficult to determine at the current time. To date, no full-size SiC clad assemblies, or fuel rods, have yet been manufactured. The fuel clad dimensions used in this study (thickness 0.57 mm) are recognised to represent an ideal and that the thickness of SiC clad for the first fuel assemblies to come to market may be increased from those used in this study.

To determine the neutronic performance of the clad and the effects on a full core, Studsvik Scandpower’s state-of-the-art core management system (CMS) suite of codes [1, 2] was used to model the EPR. Two parallel cases were modelled: one with SiC-SiC clad and another with standard zirconium alloy clad fuel assemblies. The reactor operation scheme used an identical fuel assembly loading pattern and the same number of fresh fuel assemblies per cycle. In this study, the calculated differences in achievable cycle length obtained through the use of SiC were solely due to the clad material.

The cycle length for an 18 month equilibrium loading pattern has been calculated and compared against that achieved using conventional zirconium alloy clad fuel (Fig. 3). Results show an approximate 19 effective full power day (EFPD) increase in cycle length. Fuel specification has not been changed from that specified for zirconium alloy clad fuel. Cladding dimensions are also unchanged. The SiC cladding’s predicted enhanced in-core performance results from its lower neutron absorption compared with zirconium alloy.

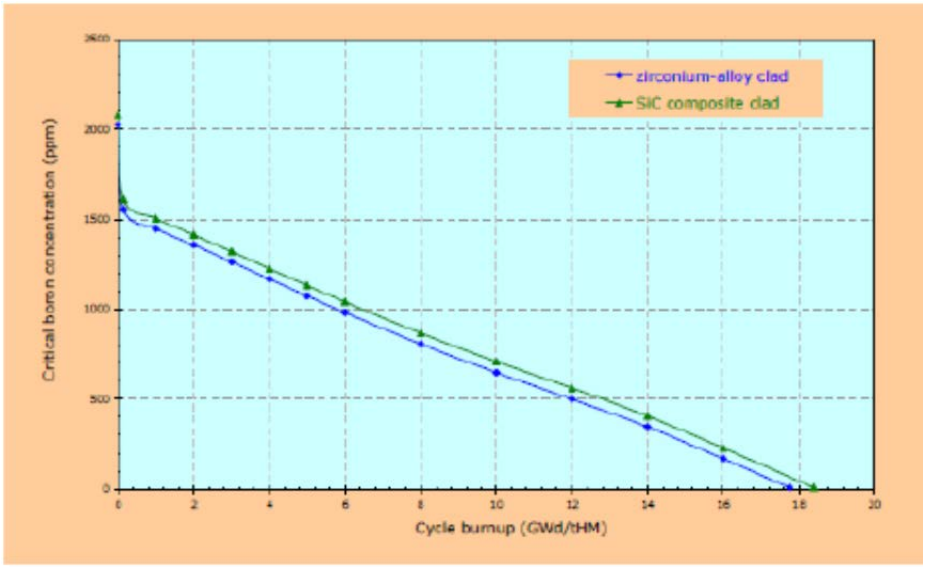

FIG. 3. Comparison of cycle length achieved for two assembly types.

A literature search has been undertaken to estimate the total cost of SiC clad fuel assemblies. Cost estimates for both zirconium alloy clad fuel and SiC clad fuel have been taken forward and used in conjunction with the reactor model to estimate the attractiveness of SiC clad use from an economic prospective. The search revealed cost estimates of £0.7 million for zirconium alloy clad and £1.2 million for SiC clad finished fuel assemblies (Figs 4, 5).

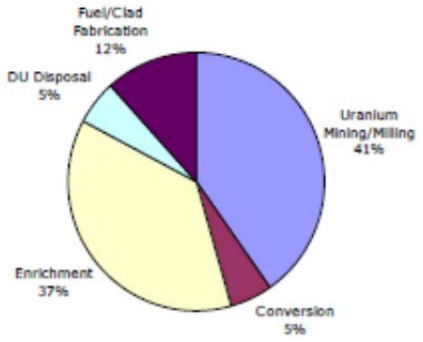

FIG. 4. Estimated cost breakdown for zirconium alloy clad fuel assembly.

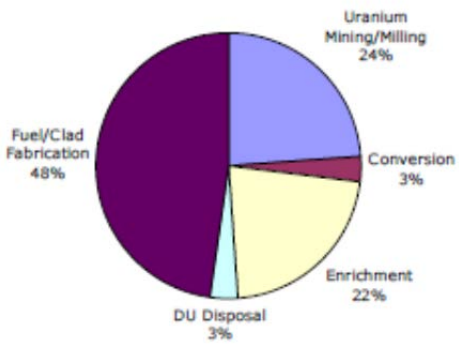

FIG. 5. Estimated cost breakdown for SiC-SiC clad fuel assembly.

The increase in cost for SiC clad fuel is solely due to the expense of the material. Several ways to mitigate the additional cost of SiC fuel use have been examined. The economic attractiveness has been investigated when using SiC clad fuel to increase cycle length on both an individual cycle and reactor lifetime basis. Results show that when using a simplified SiC clad design (0.57 mm thickness), with a UK specific electrical selling price of £89.50 per MWhe, additional revenue generated over a single cycle is more than sufficient to counteract the increased fuel costs - demonstrating scope for economic benefit with alternative, thicker, SiC clad designs. However, over the lifetime of a reactor, translating a small increase in cycle length to an economic benefit is not so clear. Cost estimates do not take account of research and development costs.

SiC's increased melting point and reduced neutron absorption (compared to current zirconium alloy clad) allow scope for increased power output from the reactor. Several alternative methods (specifically reducing the number of assemblies loaded per cycle and up-rating of core power) were analyzed as a potential way to gain an economic benefit through SiC clad use.

Core safety bounding limits have been examined by means of calculation of key safety parameters: the reactivity parameters calculated using SIMULATE-5 do not demonstrate anything to suggest the use of SiC clad in core would cause any particular problems with regard to overall reactor physics performance of the core.

5. SUMMARY OF SIC CLAD ECONOMICS

At the current time, no SiC-SiC cladding has been manufactured. Manufacturing sufficiently thin, hermetically sealed, clad is a technical challenge and is likely to remain expensive for the immediate future. The first SiC-SiC clad fuel assemblies that come to market are therefore likely to be significantly more expensive (estimated around 1.5x in this study) than current, zirconium alloy clad, fuel.

However, aside from the increased accident tolerance properties of SiC, there exists scope to mitigate some of the additional fuel costs associated with SiC clad use. The studies undertaken by NNL demonstrate that there is reduced neutron absorption for SiC clad; to exploit this, economic analysis undertaken by NNL, using the assembly price estimates mentioned above, has shown that (on a cycle-by-cycle basis) additional revenue generated during the period of increased cycle length is more than sufficient to recoup the additional cost of SiC clad use. Additional changes to fuel or reactor operating regime (such as loading fewer assemblies per cycle or decreasing fuel enrichment) have been noted. In addition, uprating of core power may be considered due to the increased margin achieved through SiC's elevated melting point. The potential economic benefits must be considered in the context of the speculative nature of the clad modelled. Further research and development of SiC claddings will provide information on the most probable specification of SiC cladding that can.

6. CONCLUSIONS

The development and testing of accident tolerant fuel and clad materials (ATF) by NNL through the Nuclear Fuel Centre of Excellence is being complemented by parallel developments in modelling. This includes research into new techniques, but also the evolution of established codes. In the latter category, the UK's primary fuel behaviour modelling tool, ENIGMA for thermal reactor steady state performance analysis is in the process of being developed to treat various new and advanced fuel and cladding materials, examples of which

are briefly outlined here. Reactor physics calculations are also being undertaken to help optimise ATF fuel cycle performance and economics.

A new version of the ENIGMA thermal reactor fuel performance code has been created embodying a prototype modelling capability for U_3Si_2 fuel. The model changes have been tested and documented, and the effects on code predictions for a representative LWR case have been quantified – for example calculating the lower fuel centre temperature of silicide fuel.

Uranium nitride (UN) fuel has been modelled in a PWR reactor. Due to the increased density of UN, the number of fissile U-235 atoms per unit volume is increased compared to UO_2 for fuel of equivalent enrichment and therefore, the studies have shown that the same cycle length can be achieved using UN fuel with a lower enrichment compared to UO_2 fuel. In addition, the denser UN fuel requires optimisation of the moderator-to-fuel ratio in order to obtain the most efficient fuel usage during the total irradiation time. This has been achieved by means of a small reduction in the pellet diameter (M:F ratio is not completely optimised due to the need to maintain a safe margin on positive reactivity feedback effects).

Economic analysis of UN fuel has shown that, given certain assumptions regarding UN fuel cost, there is a moderate saving per assembly achieved when using UN fuel. This saving arises through the reduction in fuel enrichment. Calculations of finished fuel costs generated by NNL compare the costs of a key option for Accident Tolerant fuel (i.e. UN fuel assemblies) with UO_2 fuel assemblies. Reactor plant savings of between $3 M and $7 M per 18 month reload are estimated. Extrapolating this to a 60 year reactor lifetime and assuming 90% utilisation gives an estimate of between $120M and $280 M saving in using UN fuel for the lifetime of a reactor or between $1,728 M and $4,032 M for a 16GWe fleet. This work is based on preliminary modelling to design a UN fuel pin, resulting in a smaller diameter, lower enriched fuel designed to observe reactivity constraints and key reactor safety tests including margins for shut down, moderator temperature conditions, boron reactivity and delayed neutron fractions.

Using UN fuel with enrichment equivalent to UO_2 fuel may compromise savings in fuel assembly costs (due to increased fuel mass requirement). There could be further scope to increase fuel burnup by using such fuel. However, the economic benefit of doing this would need to be carefully assessed against the increased fuel costs.

Concerning in-reactor fuel behaviour modelling, it should be noted that the ENIGMA code does not as yet include models for the properties and behaviour of UN as has been performed for U_3Si_2 (discussed in Section 1). This is an area where further similar work will be required if UN fuel is judged to be a viable alternative to UO_2 fuel.

Additionally, an economic study of SiC cladding deployment in a LWR (example used is EPR), undertaken by NNL, indicates that SiC's reduced neutron absorption (compared to current zirconium alloy clad) allows scope for increased power output from the reactor, and/or reduced fuel enrichment or total fuel requirement, over a full cycle of irradiation. These benefits are potentially sufficient to more than off-set the increased fuel fabrication costs, with SiC cladding fuel estimated to be approximately 1.5x the cost of standard zirconium alloy clad fuel. This increase in fabrication costs is due to the cost of SiC. Improvements in manufacturing technology needed to make thin, sealed tubes suitable for use in a nuclear reactor are required before studies with more certain specification of SiC can be undertaken.

The studies outlined in this paper do not include any consideration of combinations of accident tolerant fuels and enhanced cladding. The exact nature of the benefits from these and of other concepts requires further analysis and underpinning from test fabrication, irradiation tests and iterative modelling – included in this and related international collaborative studies.

REFERENCES

[1] STUDSVIK SCANDPOWER, "CASMO-5: A Fuel Assembly Burnup Program: User's Manual". SSP-07/431, Revision 3; (2011).

[2] STUDSVIK SCANDPOWER, "SIMULATE-5: Advanced Three-Dimensional Multigroup Reactor Analysis Code". SSP-10/438, Revision 3 (2012).

ORNL ANALYSIS OF OPERATIONAL AND SAFETY PERFORMANCE FOR CANDIDATE ACCIDENT TOLERANT FUEL AND CLADDING CONCEPTS

J.J. POWERS[*], A. WORRALL[*], K.R. ROBB[*], N.M. GEORGE[***], G.I. MALDONADO[***]
[*]Oak Ridge National Laboratory, Oak Ridge, Tennessee
[**]University of Tennessee, Knoxville, Tennessee
United States of America
E-mail: powersjj@ornl.gov

Abstract

Enhanced accident-tolerant fuels (ATFs) are being developed by the US Department of Energy Office of Nuclear Energy Fuel Cycle Research and Development Program to replace standard Zircaloy cladding and/or UO_2 fuel in light water reactors. Proposed ATF concepts seek to reduce severe accident (SA) risks by increasing the coping time available to operators for accident response, reducing the extent and rate of heat and hydrogen production from steam oxidation, or enhancing fission product retention. Candidate ATF concepts require analyses to demonstrate adequate performance during normal operation and worthwhile improvements in SA scenarios. Two key ATF areas are being developed at Oak Ridge National Laboratory: (1) alternate cladding materials, including advanced iron-chromium-aluminium (FeCrAl) alloys and silicon carbide (SiC) composites, and (2) fully ceramic microencapsulated (FCM) fuel, which uses coated fuel particles embedded in an SiC matrix. Reactor physics analyses examining candidate ATF clad materials in a pressurized water reactor (PWR), with preliminary assessments of combinations of fuel enrichment and cladding thickness required to match existing cycle lengths and economic factors such as fuel costs, are presented. SA analyses including updated analyses of how FeCrAl cladding and channel box impact SA scenarios in a boiling water reactor (BWR) are also discussed.

1. INTRODUCTON

Enhanced accident-tolerant fuels (ATFs) are being developed by the United States (US) Department of Energy Office of Nuclear Energy (DOE-NE) Fuel Cycle Research and Development programme to replace standard zirconium-alloy (Zircaloy) cladding and/or UO_2 fuel in light water reactors (LWRs) [1, 2]. Proposed ATF concepts seek to reduce severe accident (SA) risks by increasing the coping time available to operators for accident response, reducing the extent and rate of heat and hydrogen production from high-temperature (HT) steam oxidation, or reducing severe accident consequences by enhancing fission product (FP) retention. In addition to experimental development and qualification programmes, candidate ATF concepts require thorough analyses to demonstrate that they maintain adequate performance during normal operation and achieve worthwhile improvements in SA scenarios [3]. This work focuses on two important types of ATF concepts being developed at Oak Ridge National Laboratory (ORNL): (1) alternate cladding materials, including advanced iron-chromium-aluminium (FeCrAl) alloys and silicon carbide (SiC) composites, and (2) fully ceramic microencapsulated (FCM) fuel, which consists of uranium nitride (UN)-fuelled tri-structural isotropic (TRISO) coated particles embedded in an SiC matrix.

Reactor physics and SA analyses have been performed to assess alternate cladding material and FCM fuel ATF concepts. Reactor physics analyses examined ATF candidates in a pressurized water reactor (PWR) and included preliminary assessments of achievable cycle lengths, combinations of fuel enrichment and cladding thickness or particle packing fraction required to match existing cycle lengths, and economic factors such as fuel costs. SA analyses focused on assessing improvements during various accident scenarios using updated modelling of a boiling water reactor (BWR) with FeCrAl cladding and channel boxes. Preliminary conclusions from these analyses help to identify some of the most promising high-impact attributes to pursue in candidate ATF technologies and to assess the potential performance of ATF candidates during normal operation and SA scenarios. Detailed calculations are needed in the future to confirm these preliminary conclusions. In addition to fuel and cladding materials, other core components (e.g., control rods or blades) will also need to be designed to enhance the safety and accident tolerance of the overall reactor system.

2. CANDIDATE ATF CONCEPTS OF INTEREST

All proposed ATF concepts seek to accomplish the same goals: increased coping time during SA scenarios, reduced HT steam oxidation rates, and/or enhanced FP retention; however, numerous approaches exist to try to accomplish one or more of these objectives, including changing the cladding to improve performance during SA scenarios and/or changing the fuel to either directly improve performance or overcome obstacles introduced by changing the cladding material. Possible cladding changes include coating standard Zircaloy cladding with a thin ceramic or metallic layer to decrease oxidation rates or changing the cladding material entirely to an alternate material (e.g., iron-based alloys or ceramic composites). Modifications to the fuel could include changes to UO_2 to improve performance (e.g., adding dopants to increase the thermal conductivity) or changing the material entirely to enhance fission product retention (FCM fuel) or increase the heavy metal (HM) loading density (e.g., UN or U2Si3). These fuel and cladding concepts offer different levels of performance improvements and would require different amounts of time before commercial deployment. Figure 1 provides a visual summary of estimated performance improvements and time to deployment for a wide range of candidate ATF technologies.

ORNL technology development and analysis efforts have focused on two key types of LWR ATF concepts, which are the focus of this paper: (1) using UO_2 fuel pellets with alternate cladding materials (FeCrAl alloys and SiC ceramic cladding), or (2) changing the fuel material itself to FCM fuel to enhance FP retention. These three technologies (FeCrAl cladding, SiC cladding, and FCM fuel) are shown with red dashed boxes and labels in Fig. 1 to indicate where they fall on potential performance improvement and time to deployment. These three key technologies were chosen because ORNL has experience with them and has judged them to be both potentially feasible and effective. In addition, this set of ATF technologies spans a range of risk and reward, with a lower-risk, medium-benefit option (FeCrAl cladding) and potentially higher-benefit options that would require longer time periods for development and deployment (SiC cladding and FCM fuel).

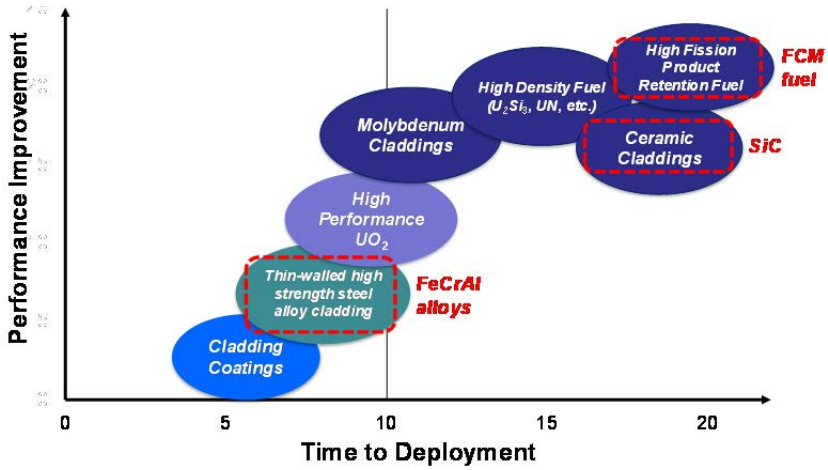

FIG. 1. Visual summary of the estimated potential performance improvements and time to deployment for a number of candidate ATF technologies, adapted from Ref. [1] with added emphasis on ORNL activities.

3. PHYSICS IMPACTS OF ALTERNATE CLADDING MATERIALS

Candidate LWR ATF technologies includes alternate fuel cladding materials that could replace Zircaloy [4]. Alternate cladding materials seek to reduce severe accident risks by increasing the coping time available to operators for accident response and reducing the

extent and rate of heat and hydrogen production during accidents. While many candidate ATF cladding materials have been proposed, this work will focus on comparing FeCrAl and SiC with reference UO_2/Zircaloy fuel/cladding pins using results for depletion calculations, spectral analyses, reactivity coefficient calculations, radial fission power, and plutonium breeding analysis. Lastly, estimated variations in fuel costs among the cladding material options are shown based upon relative uranium mass and enrichment needed in each design.

3.1. Description

Early analyses of PWR ATF cladding concepts included SiC and two types of iron-based alloys: austenitic stainless steels and ferritic alloys. The SiC cladding material was based on a SiC/SiC composite (SiC fibers embedded in a SiC matrix) [5] and represents a range of SiC concepts investigated for use in LWRs [6–8]. Austenitic stainless steel type 310 (310SS), included in these analyses largely due to its wide consideration by other organizations, contains more chromium (Cr) and nickel (Ni) than 304SS and forms a protective Cr_2O_3 scale in HT steam [4]. The ferritic FeCrAl alloys contain aluminium and form an even more protective Al_2O_3 scale in HT steam [9]. A generic FeCrAl alloy (labeled simply as FeCrAl in all tables, figures and text) was the main analysis example; some early analyses also included a specific APMT™ alloy [10] that was dropped from further analyses because its physics performance was very similar to generic FeCrAl. Zircaloy and historic 304SS cladding materials were also analyzed and were used as reference points for comparisons. Zircaloy represents zirconium alloys used as cladding in LWRs throughout the world. The 304SS represents generic 18Cr-8Ni type austenitic stainless steels used as fuel cladding in both PWRs and BWRs in the US through the early 1980s [11].

These candidate alternate cladding materials offer several advantages relative to using Zircaloy in a PWR, including significantly slower oxidation kinetics in HT steam [4,9,12,15] and superior HT strength for the metallic candidates; however, their use as LWR cladding also introduces several challenges. FeCrAl and 310SS exhibit increased neutron absorption cross sections compared with Zircaloy, which negatively affects the neutron economy. Maintaining cycle length therefore requires design changes, including using a thinner FeCrAl or 310SS cladding, as supported by their increased strength and the reduced thicknesses used by historic iron-based cladding [11], or using increased uranium enrichment. Figure 2 shows continuous-energy macroscopic neutron absorption cross sections for the clad material options, calculated using JANIS 3.4 with ENDF/B-VII.1 data and without any flux weighting to keep them problem-independent. The thermal macroscopic absorption cross sections for FeCrAl, 304SS, and 310SS are over an order of magnitude higher than those for SiC and Zircaloy. Although the absorption cross section for SiC looks promising, low thermal conductivity in SiC leads to elevated fuel temperatures [5, 13] and a large temperature gradient across the cladding that in turn induces large thermal stresses across the cladding thickness [14]. Table 1 summarizes several parameters for Zircaloy, 304SS, 310SS, FeCrAl, and SiC, including elemental composition, density, macroscopic thermal neutron absorption cross section ($\Sigma_{\mathrm{abs}}^{\mathrm{therm}}$) taken at a neutron energy of 0.253 eV, parabolic oxidation rate (POR) constant in 1200°C steam, and some of the known benefits and challenges including effect on SA performance. To fully capture the extent of SiC oxidation, a linear volatilization term also needs to be taken into account, which is omitted here for simplicity but reported elsewhere [15].

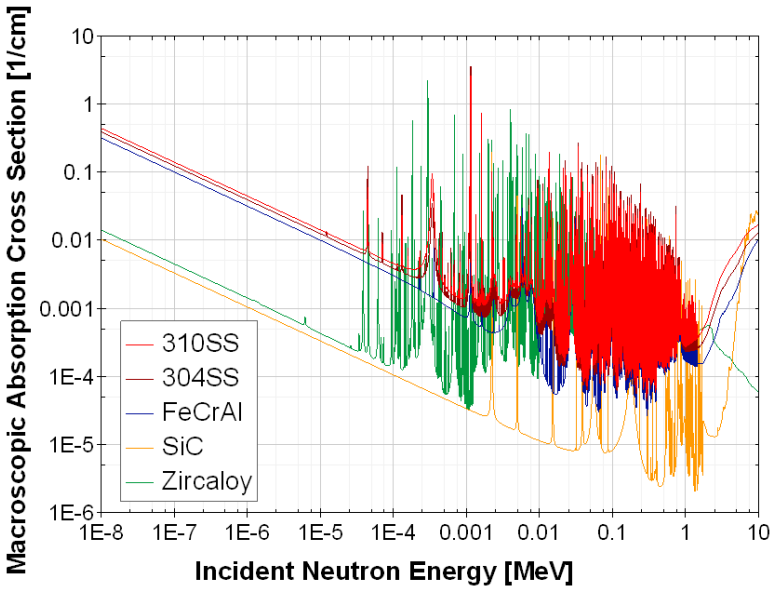

FIG. 2. Macroscopic neutron absorption cross sections for several clad material options of interest.

TABLE 1. SUMMARY OF RELEVANT DATA FOR CLADDING MATERIAL OPTIONS

Clad material	Density [g/cm^3]	Composition [wt %]	Σ_{abs}^{therm} [cm^{-1}]	POR constant in 1200°C steam [mg] [a]	Likely benefits [b]	Known challenges
Zircaloy	6.56	98.26 Zr, 1.49 Sn, 0.15 Fe, 0.1 Cr	0.0028	6.5×10^{-4}	Used in existing LWRs	SA performance
304SS	7.9	71.35 Fe, 18.9 Cr, 8.35 Ni, 0.7 Mn, 0.42 Si, 0.27 Mo	0.0778	8.5×10^{-4}	Improved HTS	SA, increased Σ_{abs}^{therm}
310SS	8.03	52.55 Fe, 25.22 Cr, 19.51 Ni, 1.9 Mn, 0.7 Si, 0.12 Mo	0.0880	1.3×10^{-5}	Lower OR, improved HTS	Increased Σ_{abs}^{therm}
FeCrAl	7.1	75 Fe, 20 Cr, 5 Al	0.0634	1.8×10^{-6}	Lower OR	Increased Σ_{abs}^{therm}
SiC	2.58	70.08 Si, 29.92 C	0.0021	3.7×10^{-7} [c]	Lower OR, low Σ_{abs}^{therm}	Fuel reliability

[a] Based upon data from Refs. [4] and [15].
[b] HTS: high-temperature strength, OR: oxidation rate
[c] As noted in the text, a linear volatilization term is omitted here that needs to be taken into account to fully capture the extent of SiC oxidation [15].

3.2. Preliminary reactor physics assessment

The scope of the present study has been limited to a preliminary assessment using models for a single PWR fuel rod, with a small number of quarter-lattice calculations performed to show that the same trends from pin-cell analyses would hold true at larger scale; future work should use assembly-level and core-level analyses. Further details of this PWR ATF cladding assessment work may be found elsewhere [16, 17]. Other researchers have also looked at ATF cladding with UO_2 fuel in PWRs [18], with results that generally exhibit good

agreement with the trends found in this present work. Subsequent work has begun to examine ATF cladding in BWRs [19, 20], but those studies are currently ongoing as of the writing of this document.

Two-dimensional (2D) pin cell analyses were performed using SCALE/TRITON from SCALE 6.1.2 with ENDF/B-VII.0 nuclear data [21, 22]. Figure 3 shows the TRITON pin cell model, which was based on a Westinghouse 17×17 PWR fuel rod; the inner red region is the UO_2 fuel pellet, the thin green ring represents the gas gap, the gray ring is the fuel cladding, and the blue outer region represents the borated water coolant. An analytical method was applied to the single-pin depletion results to approximate a multibatch loading scheme in a typical modern Westinghouse 17×17 PWR using three fuel batches and 18-month cycles. This method uses an integral reactivity approach over the fuel lifetime rather than assuming a linear reactivity, in order to increase the fidelity of cycle length estimations and appropriately reduce the importance of low reactivities that typically occur in high-exposure fuel at the core periphery in traditional very-low-leakage core loading patterns.

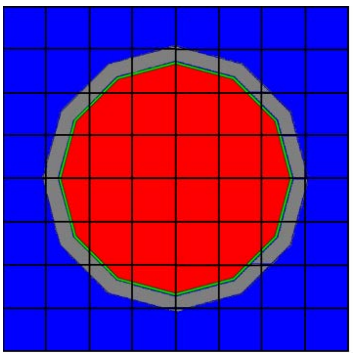

FIG. 3. TRITON pin cell model of a PWR fuel rod.

To verify the pin cell results, a 2D quarter-lattice of a Westinghouse 17×17 assembly was modeled in TRITON with reflective boundary conditions. Initial results indicate a small eigenvalue bias between pin cell and lattice calculations; however, the overall trends observed in the pin cell studies remain consistent at the assembly level.

3.2.1. Analysis objectives and constraints

There were two primary objectives in this study: (1) assess the impact of directly replacing Zircaloy cladding in PWR fuel rods with candidate ATF cladding materials while maintaining the clad thickness and fuel enrichment of the reference fuel rod and (2) estimate what combinations of cladding thickness and fuel enrichment would be needed to maintain the operational cycle length of the reference UO_2/Zircaloy fuel/cladding system. For the same cycle length, it would be desirable to minimize enrichment while maintaining a cladding thickness that might reasonably satisfy thermomechanical fuel performance constraints. An early estimate of reasonable 310SS and FeCrAl cladding thickness was obtained from recent work that included an historical perspective on past steel cladding in LWRs [4].

Throughout this study, the pitch-to-diameter ratio (P/D), clad outer diameter, and pellet-cladding gap were kept constant at 1.326, 9.4996 mm, and 82.55 μm, respectively. The reference cladding thickness was 571.5 μm. In cases where cycle length requirements were not met, the cladding thickness was adjusted to achieve the desired cycle length; this was achieved by adjusting the fuel pellet radius and the inner radius of the cladding in tandem in order to maintain a constant gap thickness and cladding outer diameter. For the metallic alloys (Zircaloy, 310SS, and FeCrAl), the assumed average fuel temperature was 900 K while the

cladding and gap were modeled at 600 K [23]. For the SiC models, the fuel temperature was raised to 1100 K and the temperature of the clad and gap to 700 K to account for the reduced thermal conductivity of the clad [14]. The borated water in the system was modeled at 580 K (0.7119 g/cm^3) with 630 ppm boron for all cases; this concentration is representative of the average value over an entire fuel cycle for a typical PWR. Cladding material compositions from Table 1 were used to model each option. UO_2 fuel pellets were modeled with a density of 10.47 g/cm^3 (~96% of theoretical density) and 4.9 wt% ^{235}U enrichment; current batch-average enrichment levels in fresh US PWR assemblies may be slightly lower, but trends continue to show increasing enrichment levels. Cladding thickness and enrichment variations were applied to each ATF cladding material option considered; thinner clads were looked at for iron-based alloys (310SS and FeCrAl) while thicker cladding options were assessed for SiC cladding to represent the thicker cladding structures demonstrated to date for SiC-based materials [24].

Fuel enrichments above 5% would require substantial licensing efforts because of the 5% limit currently in place for commercial facilities in the US. In addition, increased pellet diameters may exceed dimensions of existing fuels and could therefore require retooling at fuel fabrication plants. Both of these factors would increase costs and could impact fuel performance as well, but the extent has not been quantified in the work performed to date.

3.2.2. Neutronic impacts of direct introduction of alternate cladding materials

Figure 4 shows the infinite multiplication factor (k-infinity) as a function of effective full power days (EFPD) for each clad material of interest; these results were obtained from depletion calculations using the reference fuel pin geometry for all of the cladding materials listed in Table 1. Figure 5 shows the difference in k-infinity (in units of pcm) between Zircaloy cladding and each alternate clad material as a function of EFPD. The reactivity penalty for the metallic cladding materials decreases over the lifetime of the fuel because they absorb more thermal neutrons and yield a harder neutron spectrum in the fuel pellet, which increases conversion of U-238 to Pu-239. The impact of each cladding material on the beginning of life (BOL) neutron flux spectrum is shown in Fig. 6. End of life (EOL) reactivity penalties for austenitic stainless steels were found to be –4.2% (304SS) and –4.8% (310SS), while the penalties for ferritic alloys were slightly less negative at –3.2% (FeCrAl) and –4.0% (APMT). SiC cladding produced a +0.6% change in EOL reactivity.

Using the pin cell model described above, the moderator temperature coefficient (MTC) and void coefficient were calculated over a range of fuel burnup values using the previously-specified 630 ppm boron concentration in the coolant. An MTC calculation was also performed for fresh fuel with a boron concentration of 1300 ppm in the coolant. Initial results indicate that the reactivity coefficients for all alternate clad materials being considered appear to be approximately equal to, or more negative than, those for Zircaloy. Future work will include full-core analysis of realistic multibatch loading patterns with alternate clad materials and calculate other reactivity coefficients (e.g., fuel temperature coefficient boron coefficient).

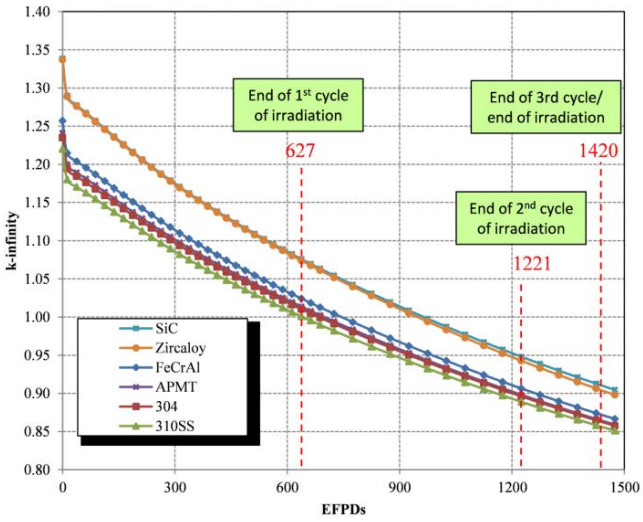

FIG. 4. Infinite multiplication factor (k-infinity) as a function of EFPD for several clad material options using reference geometry for a Westinghouse 17×17 PWR fuel rod.

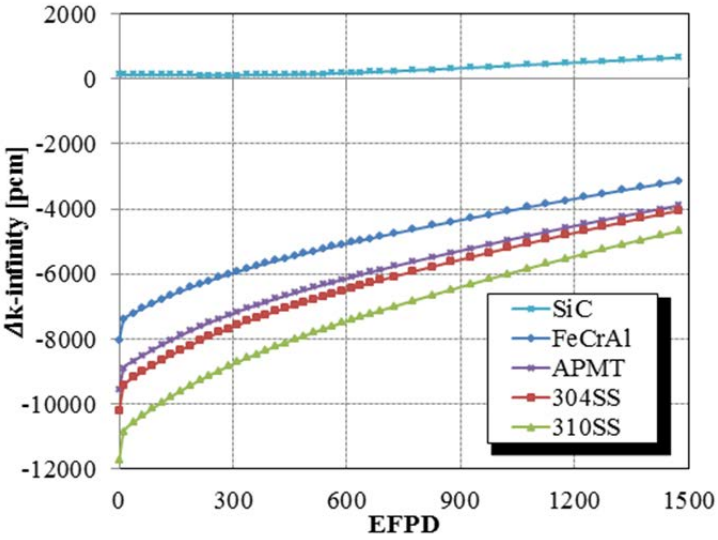

FIG. 5. Difference in k-infinity between Zircaloy and alternate clad materials as a function of EFPD.

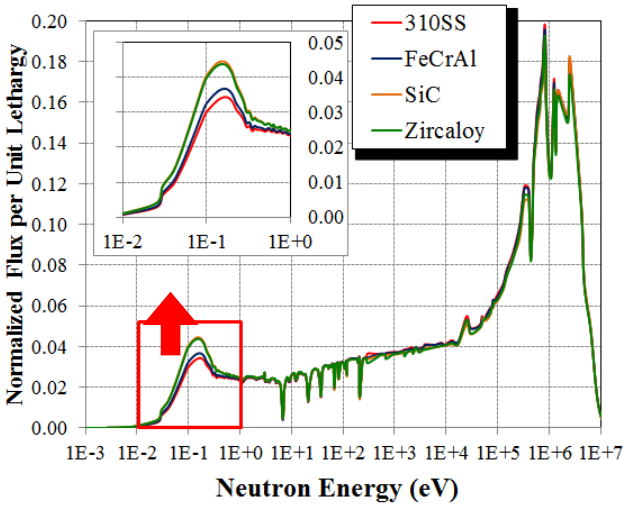

FIG. 6. Neutron flux spectrum at BOL for a PWR pin cell using different cladding material options.

3.2.3. *Maintaining reference pwr cycle length by varying clad thickness and enrichment*

A series of depletion calculations were performed to determine combinations of cladding thickness and enrichment that would enable each clad material option to achieve the same cycle length as Zircaloy. Three specific cases of interest were considered for each candidate alternate clad material with regard to matching the Zircaloy cycle length:

- What cladding thickness would be required if the reference 4.9% enrichment were maintained?
- What enrichment would be required if the reference cladding thickness (571.5 μm) were maintained?
- What enrichment would be required if the clad thickness were set to a reasonably conservative value (350 μm for iron-based alloys, ~900 μm for SiC)?

The results (cladding thickness and enrichment combinations) for each of these cases are summarized in Table 2 and illustrated in Fig. 7. Combinations of enrichment and clad thickness to the left and upward of the linear trend line shown for each material in Fig. 7 are expected to meet or exceed PWR cycle length requirements. Reduced neutron absorption in SiC cladding enabled an enrichment of less than 4.9% to match the Zircaloy cycle length with the reference clad thickness (Case II). The amount of clad thinning assumed in Case I was calculated purely on a neutronics basis to meet the required cycle length; it does not explicitly account for any fuel performance constraints.

TABLE 2. TABULAR SUMMARY OF FUEL PARAMETER COMBINATIONS THAT MATCH ZIRCALOY CLADDING CYCLE LENGTH IN A PWR

Material	Case I		Case II		Case III	
	Clad thickness [μm]	Uranium enrichment [%]	Clad thickness [μm]	Uranium enrichment [%]	Clad thickness [μm]	Uranium enrichment [%]
Zircaloy	571.5	4.9	571.5	4.9	571.5	4.9
310SS	226.3	4.9	571.5	6.38	350	5.39
FeCrAl	302.2	4.9	571.5	5.86	350	5.06
SiC	606.7	4.9	571.5	4.81	889	5.5

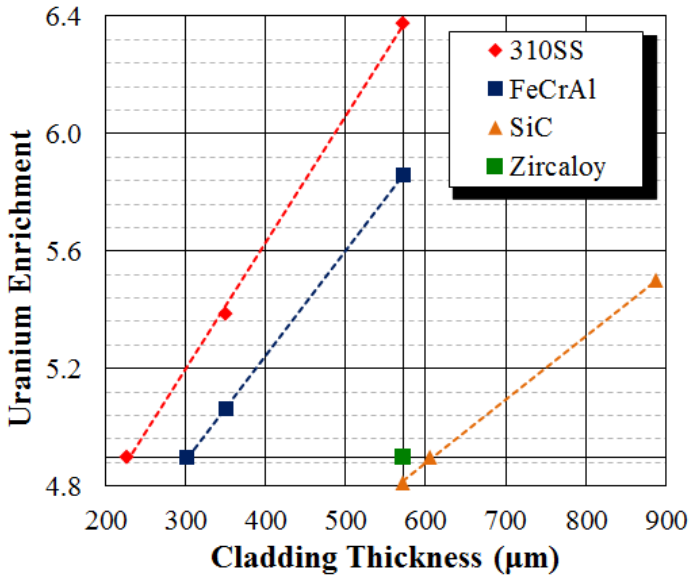

FIG. 7. Visual summary of fuel parameter combinations that match Zircaloy cladding cycle length in a PWR.

Concerns about possible material or fuel performance issues associated with deviating from the well-understood properties and microstructural evolution of conventional PWR fuel pellets, including the formation of a high-burnup structure (HBS) at the pellet periphery, led to an examination of the radial power profile within a fuel pellet for each clad material option. A model with ten concentric radial rings of equal area in a single fuel pellet was used with cladding thicknesses of 350 μm for 310SS and FeCrAl and 571.5 μm for SiC and Zircaloy. All four clad materials exhibit similar fission power distribution trends, with relatively flat BOL power profiles evolving to EOL profiles with a strong narrow peak near the pellet outer surface due to increased plutonium production there. This indicates that despite differences in neutron absorption between the clad materials, the relative radial fission power distribution will not differ significantly. Fuel pellets in these alternate cladding material options should therefore perform similarly to those in Zircaloy-clad fuel with respect to fuel-specific behavior (e.g., forming a high burnup structure) other than impacts from changes such as higher fuel temperatures with SiC cladding. Thermomechanical performance of the clad itself, however, could differ substantially. Further analyses and experiments are needed to explicitly examine the fuel performance impacts of alternate cladding materials, including possible performance issues related to mechanical and chemical pellet-cladding interactions.

In an effort to provide a preliminary analysis of the economic impacts of the alternate cladding material designs identified in Table 3, fuel pellet costs for several design options were calculated and were compared with those of the Zircaloy cladding design. Due to a lack of information about manufacturing and material costs for advanced cladding, this analysis does not account for fuel assembly material and fabrication costs (e.g., cladding and grid spacers); it focuses entirely on the costs of the enriched UO_2 fuel pellets. The ore, conversion, and enrichment unit costs assumed were \$35/lb, \$8.5/lb, and \$100/kg respectively, and are based on spot market prices [25]. Results are shown in Table 3 for cases that meet PWR cycle length requirements. Designs containing 310SS or FeCrAl would require an increase of 15% to 36% in UO_2 fuel pellet costs, although options from Table 2 with clad thicknesses below 350 μm could be cheaper but were excluded here because of cladding integrity concerns. SiC design options yield approximately the same fuel pellet costs as Zircaloy.

TABLE 3. ASSESSMENT OF FUEL PELLET COSTS FOR DIFFERENT DESIGN OPTIONS

	Clad thickness (μm)	Uranium enrichment [%]	HM per Assembly [MTU]	Uranium enrichment cost ($/kgU)	Enriched UO_2 cost ($/assembly)	Cost difference vs Zircaloy [%]
Zircaloy	571.5	4.90	0.470	1,990	934 614	-
FeCrAl–A	571.5	5.86	0.470	2,449	1 150 185	23.1
FeCrAl–B	350	5.06	0.522	2,068	1 079 144	15.5
SS310–A	571.5	6.38	0.470	2,699	1 267 566	35.6
SS310–B	350	5.39	0.522	2,223	1 160 028	24.1
SiC–A	889	5.50	0.400	2,277	910 032	-2.63
SiC–B	571.5	4.81	0.470	1,947	914 418	-2.16
SiC–C	606.7	4.90	0.462	1,990	918 584	-1.72

3.3. Summary

A preliminary reactor physics assessment of alternate cladding material options indicates that iron-based alloys require increased uranium enrichments and/or decreased cladding thicknesses to match the PWR operational cycle length attained with Zircaloy cladding. FeCrAl offered the smallest reactivity penalties, whereas austenitic steel (310SS)

showed large negative reactivity impacts. SiC performed well using the standard Zircaloy thickness, but large increases in clad thickness would have negative impacts on reactivity and fuel temperatures. Fuel pellet relative radial power distributions were similar for all clad options studied. Fuel pellets in these alternate clad material designs should therefore exhibit performance similar to Zircaloy-clad pellets, though clad performance itself may differ substantially. An economic assessment found that 310SS or FeCrAl cladding could increase fuel pellet costs by 15% to 36%, whereas SiC-clad fuel pellet costs would be similar to those for Zircaloy-clad fuel. Full-core physics and several other analyses are needed in the future to evaluate design margins under both standard operation and accident scenarios for neutronic, thermal-hydraulic, and fuel performance parameters.

4. PHYSICS IMPACTS OF FCM FUEL

FCM fuel consists of microencapsulated coated fuel particles embedded in an SiC matrix [26-28]. The microencapsulated fuel is generally TRISO coated fuel particles, although other fuel forms could be considered. FCM fuel has been proposed as an LWR ATF concept because it could accomplish multiple ATF goals: the particle coating layers and SiC matrix reduce SA consequences by providing additional barriers to radionuclide release, and the response time available to operators before fuel failure should increase because the FCM fuel pellets and clad should survive longer than standard LWR fuels.

4.1. Description

TRISO fuel particles consist of an inner fuel kernel surrounded by a buffer coating region and three structural coating layers, as shown in Fig. 8. The first coating layer is a porous carbon buffer region that attenuates recoil fission fragments, accumulates internal gases released from the kernel, and accommodates dimensional changes in the particle. Three bonded coating layers surround the buffer: a dense inner pyrolytic carbon (IPyC) layer, an SiC layer, and a dense outer pyrolytic carbon (OPyC) layer. The SiC layer acts as a pressure vessel and diffusion barrier, preventing the release of FPs. The PyC layers protect the SiC layer from chemical attack, act as additional FP diffusion barriers, and form part of the thermomechanical system along with the SiC pressure vessel layer. A detailed description of TRISO particles, including their material properties and behaviors as well as key failure mechanisms, may be found elsewhere [29, 30].

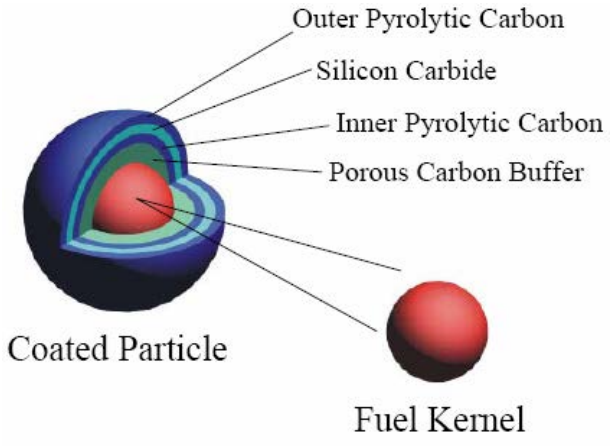

FIG. 8. Illustrative cutaway diagram of a TRISO fuel particle.

Historically, TRISO particles have been utilized in fuel elements consisting of spherical pebbles or hexagonal prismatic blocks with graphite used as a matrix and coating for

the fuel element; however, FCM fuel consists of TRISO fuel particles embedded in an SiC matrix. Using SiC as a matrix instead of graphite improves the radiation tolerance of the fuel matrix while also enhancing FP retention. Current FCM fabrication forms the matrix using SiC nanopowder and a small amount of oxide sintering agents in a Nano-Infiltration Transient Eutectic-phase (NITE) process [31, 32]. The NITE process results in a dense, radiation-tolerant matrix that forms at temperatures below 1900°C; limiting the processing temperature avoids microstructural and physical damage to the coated fuel particles. Extensive details on early processing techniques are available elsewhere [28]. LWR FCM fuel designs use fuel fabricated as pellets that will be stacked and placed inside a fuel rod, similar to standard UO_2/Zircaloy fuel rods. Figure 9 provides an illustrative comparison of these two LWR fuel rod designs. LWR FCM rods could use a variety of cladding materials, including SiC composites or FeCrAl. FCM fuel could also be fabricated into various other fuel forms (e.g., pebbles or plates) for different applications.

FIG. 9. An illustration comparing standard UO_2/Zircaloy fuel (left) and an FCM fuel pin (right), as reproduced from Ref. 28.

FCM fuels could use a wide range of fuel kernel materials, including typical TRISO fuels such as UO_2 or mixtures of UO_2 and uranium carbide (UO_2 + UC, often referred to as UCO). Advanced fuel options include plutonium and/or minor actinides, thorium, or uranium mononitride (UN). UN kernels have been fabricated and characterized with kernel diameters around 830 μm and above 90% of the theoretical density of UN [33]. Coating processes to produce fuel particles from UN kernels will differ from traditional TRISO particles; efforts to adapt existing processes or develop new ones for UN kernels are under way.

4.2. Preliminary reactor physics assessment

Numerous studies have examined the reactor physics aspects of using LWR FCM fuel as an ATF candidate [36–43], ranging from steady-state radiation transport calculations to depletion calculations and using different levels of geometric detail for assembly designs for at least three types of PWRs. Conclusions indicate that the low HM loading density of FCM fuel makes it challenging to maintain the same cycle length and that there may be some assembly power peaking issues due to the low reactivity in FCM assemblies near end of cycle, but design changes and optimization may address these issues, and other results (e.g., reactivity coefficients) appear reasonable. A study performed by ORNL and the

University of Tennessee using a simple pin cell model is shown below with some analysis, discussion, and then key conclusions.

4.2.1. Analysis objectives and constraints

A study was performed to identify FCM PWR fuel lattice designs that provide performance similar to current Westinghouse 17×17 UO_2 fuel designs with respect to reactivity, pin peaking, and power-sharing factors. Pin cell and 2D quarter-lattice calculations were performed to understand the impact of changing fuel design parameters, including particle geometry and fuel composition. The low HM loading density of particle-based fuels led to the use of uranium with a 19.75% ^{235}U enrichment. After initial studies using 500 µm diameter UO_2 fuel kernels, subsequent studies identified UN fuel kernels with a diameter of 800 µm or larger as offering the most attractive performance due to increased HM densities.

4.2.2. Results

Calculations comparing several FCM designs to that of a standard UO_2/Zircaloy PWR pin cell produced the results shown in Fig. 10, assuming a kernel diameter of 1000 µm. The increased enrichment used in FCM fuel makes the ^{235}U loading density comparable to that found in standard PWR fuels, but the reduced ^{238}U concentrations and masses result in less plutonium breeding. Therefore, due to the reduced ^{239}Pu fission contributions, the reactivity of the FCM fuel drops more sharply near EOL than the reactivity of typical LWRs.

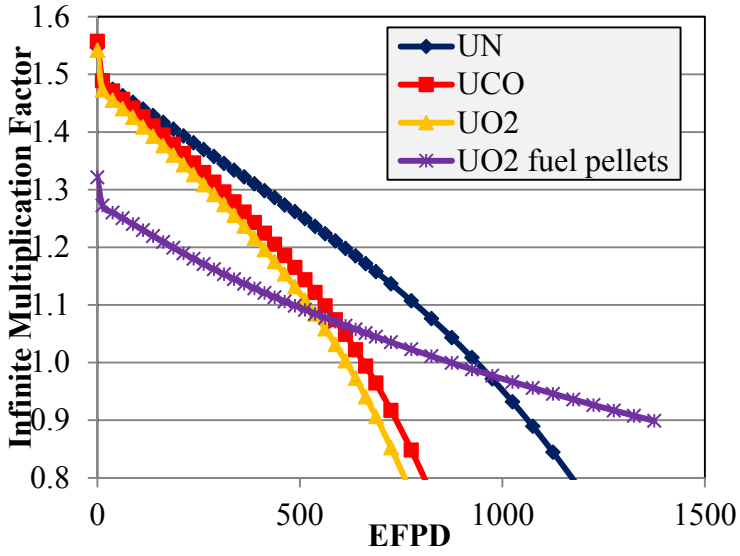

FIG. 10. Infinite multiplication factor for FCM fuel with several different fuel kernel types (UN, UCO, and UO_2) compared to that of solid UO_2 fuel pellets, as reproduced from Ref. [36].

Single-pin depletion calculations determined the achievable cycle length for a range of particle layer thicknesses, kernel diameters, and packing fractions. The results indicated that cycle length was affected more by the amount of fissile material present than any of the individual manipulated design parameters; trends showed that 19.75% enriched FCM fuel would require 10% more fissile material than 5% enriched UO_2 fuel to reach three 18-month PWR cycles. In order to meet cycle length requirements with a 17×17 lattice, FCM fuel would likely need to use UN fuel with a kernel diameter of about 900 µm and a particle packing fraction of about 50%.

Quarter-lattice calculations for UN FCM fuel found maximum BOL relative pin powers to be slightly lower than values calculated for standard UO_2 fuel. Color-set calculations were made using a checkerboard-type arrangement representing quarter lattices at the intersection of two fresh and two once-burned lattices arranged in the layout pictured in Fig. 11. Slightly higher assembly-average peaking factors were found for FCM lattices than for standard PWR lattices. These results indicate that power peaking within an FCM assembly may be less than in a standard PWR assembly; however, power sharing between fresh and once-burned FCM fuel assemblies may not be as good as in standard PWR assemblies because of the steeper reactivity trajectory (higher BOL reactivity and lower EOL reactivity) in FCM fuels. FCM fuel lattice optimization should decrease power peaking, but full-core analysis would add assembly power peaking factors that would exacerbate power peaking issues.

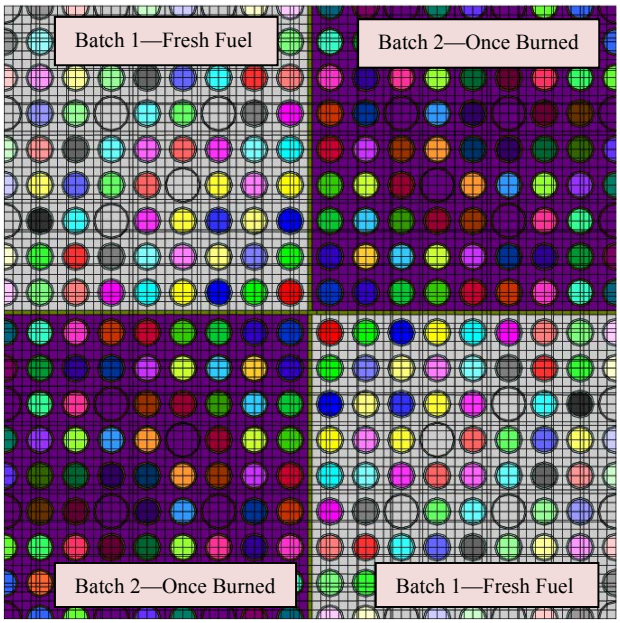

FIG. 11. Color-set model with fresh and once-burned FCM fuel lattices [36].

The neutron flux spectra of FCM fuel and conventional PWR fuels were calculated using the average flux across an entire pin-cell at BOL and EOL. These flux results, normalized per unit lethargy, are shown in Figs 12 and 13 as a function of energy. The FCM thermal neutron peak starts out significantly lower than standard UO_2 PWR fuel at BOL but becomes greater by EOL, indicating that the FCM spectrum softens from BOL to EOL while the conventional UO_2 fuel spectrum slightly hardens. The behaviors differ largely because the change in the amount of fissile material present between BOL and EOL is much bigger in the FCM fuel assembly design than it is in UO_2/Zircaloy fuel assemblies. FCM calculations modeled TRISO particles with an 800 μm diameter UN fuel kernel, a 70 μm buffer, a 35 μm thickness for other coating layers (IPyC/SiC/OPyC), and a 42% particle packing fraction. An enlarged fuel pellet radius (0.558 cm) was used to provide sufficient fissile material to meet PWR cycle length requirements, which enables a fair comparison between FCM and UO_2 fuel spectra.

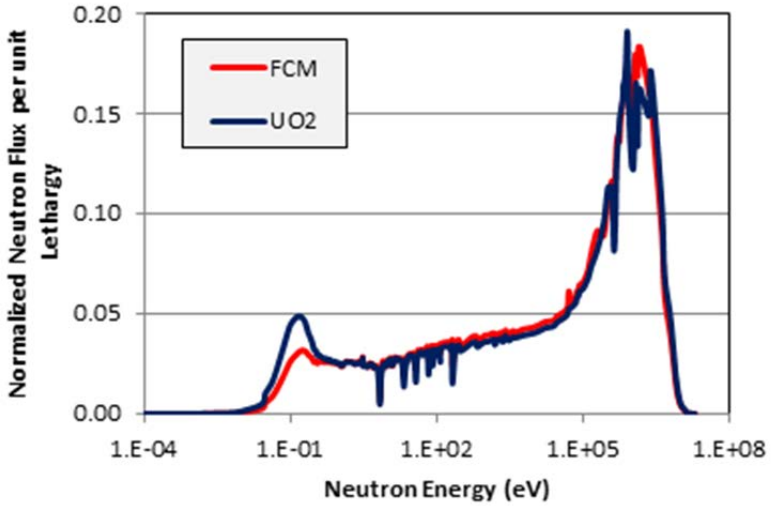

FIG. 12. Average BOL scalar flux for FCM and UO_2 lattices [36].

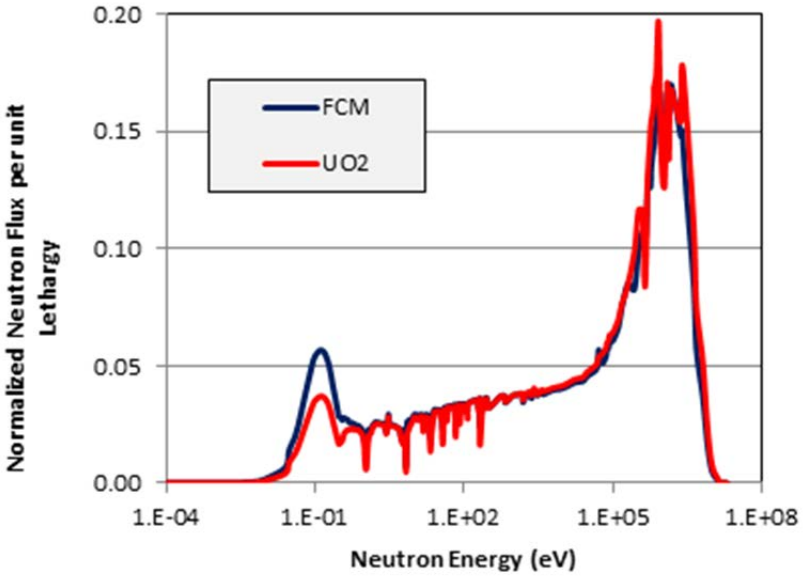

FIG. 13. Average EOL scalar flux for FCM and UO_2 lattices [36].

4.2.3. Discussion

The study above demonstrates potentially encouraging results for PWR FCM fuel, although the fuel design parameters needed to maintain the required PWR cycle length are aggressive and a multitude of other design options exist for FCM as an LWR ATF fuel that could be analyzed in greater detail. FCM designs for PWR ATF application need to continue to evolve as other analyses (e.g., thermal-hydraulics and severe accident modeling) and experiments uncover new information about FCM fuels. As an example, results from irradiation experiments could lead to significant FCM design changes. Another example is that the benefit of enhanced FP retention in FCM fuels remains unquantified at present; quantifying the benefit of various levels of enhanced FP retention via SA calculations could substantially influence particle designs and manufacturing tolerances (e.g., if only minor benefits are found for significantly enhanced FP retention, then particle designs and manufacturing tolerances may be relaxed or simpler non-TRISO particle designs could be considered). In addition to PWRs, FCM designs could be pursued for BWR cores.

It is worth noting that the best application of FCM fuel as an ATF in LWRs (including small modular LWRs) may be in new reactor concepts rather than backfitting FCM fuel into existing LWRs or those designs being built today; existing studies quite reasonably focus on fuel designs compatible with existing plants due to the overall goals of the ATF programme, but the limitations of that requirement impedes the overall design flexibility and performance of FCM fuel. A new fuel/cladding system might be reasonably expected to interact differently with the LWR system and therefore could push system design optimization in directions that are slightly different those taken for reactors that assumed the use of UO_2/Zircaloy fuel assemblies. Efforts to analyze FCM fuel in new LWRs, including small modular reactor (SMR) concepts, that still retain a high degree of flexibility in reactor design and lattice designs (e.g., going to a smaller number of thicker pins per assembly/bundle) may prove to be the area with the largest possible performance gains.

4.3. Summary

FCM fuel exhibits numerous potential benefits compared to standard UO_2 fuel pellets in LWRs [27]: it retains FPs better than UO_2 pellets due to FP containment within the particles, offers better irradiation stability than UO_2, and may offer lower oxidation rates compared to standard UO_2/Zircaloy fuels, depending upon which cladding material is used for FCM. The SiC matrix in FCM fuel may also offer several potential benefits relative to historical particle-based fuels including improved FP retention and better irradiation stability than a graphite matrix, especially in terms of decreased dimensional changes. In addition, the engineered microencapsulated fuel particles in FCM fuel may offer a higher HM loading density than historical coated-particle fuel if the large UN kernels and high particle packing fractions demonstrate acceptable performance during and after irradiation. These benefits could be important for LWR FCM fuel as well as FCM applications in advanced reactors [35].

LWR FCM fuel also introduces new challenges that either do not exist for UO_2/Zircaloy fuel/cladding designs or that become much more difficult with FCM fuel designs, chief among these being the low HM loading density of particle-based fuels. The low HM density, combined with the constraint of needing to be strictly compatible with the same fuel rod and lattice design of UO_2/Zircaloy assemblies, makes it very difficult to load enough fuel into an LWR core to maintain criticality and match the standard LWR cycle length. This significant challenge must be overcome with a combination of optimizing FCM assembly designs, increasing uranium enrichments, and engineering better particle-based fuels capable of using large diameter UN kernels at high particle packing fractions.

5. SEVERE ACCIDENT MODELING AND ANALYSES

ATF concepts are expected to provide substantial gains over the existing fuel (UO_2-Zircaloy), with respect to severe accident prevention, progression, and/or mitigation. To assess the potential gains afforded by ATF concepts, severe accident scenarios have been analyzed and compared with simulations using the existing fuel. Beyond design basis accidents that progress to core damage (severe accidents) are inherently multiphysics and multiscale processes, involving interactions between the reactor, primary and secondary systems, safety systems and engineered barriers, instrumentation and controls, operators, and accident mitigation measures. While testing and analysis of specific fuel characteristics (i.e., material properties) are important, the performance of the ATF concept needs to be analyzed in a coupled system to fully understand the potential benefits.

MELCOR is a system-level code that models the progression of severe accidents in light water nuclear power plants [44]. The code encompasses various phenomena that can

occur during a severe accident, including the thermal-hydraulic response; the heat-up, degradation, and relocation of the core material; transport of radionuclides; and hydrogen generation and combustion. MELCOR is primarily used to estimate the source term from severe accidents. Previous preliminary scoping simulations [45] of the FeCrAl ATF concept were performed in MELCOR 1.8.5. A number of modeling improvements were incorporated into version 1.8.6 of MELCOR. One key modeling change was the treatment of the reactor vessel bottom head. The current analyses were performed in MELCOR 1.8.6, which is widely used internationally.

This SA work used a BWR model despite the neutronics work above focusing on PWRs because ORNL had a BWR model readily available from its historic background in BWR severe accident analysis, PWR SA analysis would duplicate work being performed elsewhere, and BWR SA analysis needs to be performed as part of evaluating ATF concepts for both PWRs and BWRs. The MELCOR plant model used is for Peach Bottom (Unit 2 or 3), a BWR series 4 (BWR/4) with a Mark I containment. The model includes all major components, including the reactor; containment; reactor building; and various cooling systems (pumps, sprays, piping, tanks) as well as system and scenario control logic. An unmitigated long-term station blackout (LTSBO) was simulated in which the reactor is assumed to successfully shut down (time 0 h), all alternating-current (AC) power is lost at shutdown, and direct-current (DC) power is lost after 8 h. During the time period between reactor shutdown and loss of DC power, the steam-driven safety systems can inject cooling water. After the loss of DC power, the ability to inject cooling water ceases, and the reactor core eventually dries out, heats up, melts, and ultimately exits the pressure vessel onto the containment floor. The modeled scenario was unmitigated in that after 8 h the power was not restored and additional accident mitigation measures were not taken before the end of the simulation (32 h).

The ATF concept that was investigated involves the typical UO_2 fuel but with FeCrAl cladding. The cladding thickness was reduced by 50% from the reference Zircaloy cladding thickness by increasing its inner diameter. The amount of fuel was increased slightly to offset the change in cladding inner diameter. The channel box Zircaloy was replaced by FeCrAl while the dimensions of the channel box remained constant. The FeCrAl metallic material and its oxidized form were modeled as summarized in Table 4. Appropriate parabolic oxidation kinetics for FeCrAl was also employed.

TABLE 4. ASSUMED FeCrAl MATERIAL PROPERTIES FOR SEVERE ACCIDENT ANALYSIS

Assumed Material Properties	FeCrAl	FeCrAl Oxide
Melting Point (K)	1773	1901
Heat of Fusion (J/kg)	275000	687463
Density (kg/m^3)	Kanthal APM	5180
Thermal Conductivity (W/m K)	(Function of Temperature)	4.0
Specific Heat (J/kg K)		900.0
Heat of Reaction, H_2O @ 298 K (kJ/kg_{FeCrAl})	1247	—

The results of the accident progression timing are provided in Table 5 for two cases, one utilizing the FeCrAl ATF concept and the other utilizing the standard UO_2-Zircaloy system. The FeCrAl concept provides approximately 1 to 4.5 h of additional time to key stages of the accident progression. This additional time could be used to recover power, to employ accident mitigation and stabilization measures, and/or for evacuations.

TABLE 5. SIMULATION RESULTS FOR LONG-TERM STATION BLACKOUT

Event Timing (relative to shutdown)	Base UO_2-Zr (h)	FeCrAl (h)	Additional Time Margin (h)
First cladding gap release	12.4	12.6	0.2
Onset of core oxidation	12.3	13.5	1.2
100 kg of hydrogen generated	13.2	16.3	3.1
First cladding melting	13.8	17.2	3.6
Lower head failure	23.1	25.2	2.1
Containment failure	20.8	25.3	4.5
Onset radionuclide release to environment	20.9	25.3	4.4

The hydrogen generation over the course of the accident is provided in Fig. 14. Due to the slower oxidation kinetics of FeCrAl, considerably less hydrogen is generated. Hydrogen is a concern during severe accidents in that it is both combustible and noncondensable. Being noncondensable contributes to the pressurization and potential failure of containment. Once hydrogen leaves the inerted containment, combustion of the gas could exacerbate an accident and inhibit accident mitigation measures. In addition to the decreased amount of hydrogen generated, significantly less heat is generated from oxidation of the cladding and channel box material. Figure 14 also illustrates the amount of heat generated due to fission, decay heat, and oxidation. The difference between the cases around 15 h is equivalent to more than 200 GJ, which is approximately equivalent to 2.5 GJ of decay heat around 16 h. When FeCrAl is used, the deceased heat load and hydrogen generation allow containment to fail approximately 4.5 h later than for the case employing Zircaloy. In general these results are consistent with early scoping simulations [45]. The FeCrAl concept, due to its slower oxidation kinetics, could provide enhanced accident tolerance for a BWR during station blackout severe accidents.

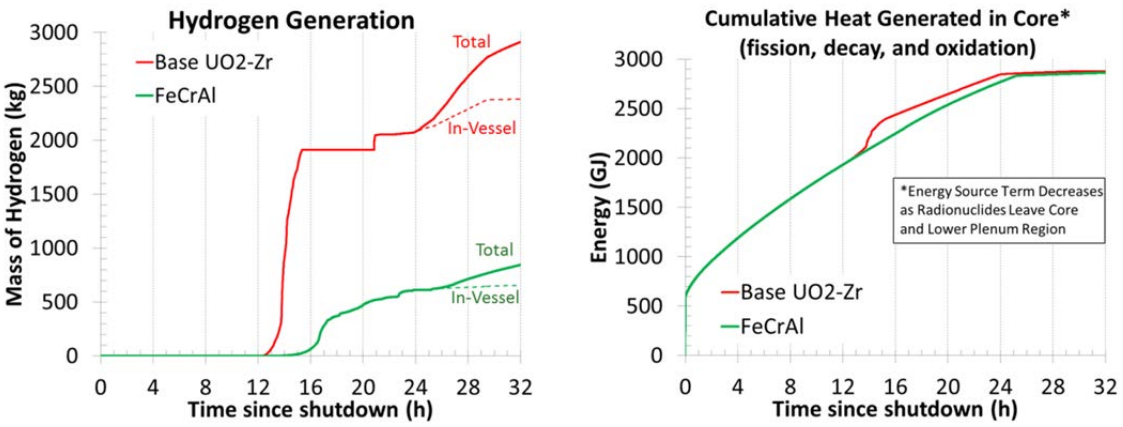

(a) (b)

FIG. 14. (a) Hydrogen generation and (b) heat generation during a severe accident.

6. CONCLUSIONS

Analysis of proposed ATF concepts at ORNL has thus far focused on reactor physics and severe accident analysis of two main types of candidate ATFs: alternate cladding materials such as FeCrAl alloys or SiC-based composites assuming continued use of standard UO_2 fuel, or the introduction of a complete new fuel/cladding system built around FCM fuel. A preliminary reactor physics assessment of alternate cladding materials indicates that

FeCrAl alloys require increased uranium enrichments and/or decreased cladding thicknesses to match the PWR operational cycle length attained with Zircaloy. Austenitic steel (310SS) showed negative reactivity impacts large enough to preclude it from further study when considering the better neutronic and oxidation performance of FeCrAl. SiC performed well using the standard Zircaloy thickness, but large increases in clad thickness would have negative effects on reactivity and fuel temperatures. An economic assessment found that FeCrAl cladding could increase fuel pellet costs by about 15% to 25%, whereas SiC-clad fuel pellet costs would likely be similar to those for Zircaloy. Full-core physics and several other analyses are needed to evaluate design margins based on thermal, reactivity, and fuel performance parameters, under both standard operation and accident scenarios. Reactor physics analyses of LWR FCM fuel found several challenges, the largest one being a low HM loading density. It appears possible to maintain the reference UO_2/Zircaloy cycle length despite the HM loading density issue by using engineered TRISO particles with large UN kernels, a high particle packing fraction, and increased uranium enrichment. Future work needs to evaluate the thermomechanical fuel performance of FCM fuel, the economic aspects associated with fuel fabrication and enrichment costs, and severe accident performance gains from enhanced FP retention. Severe accident analyses using updated computer codes and models as well as better material property correlations for FeCrAl in a BWR establish a proof-of-principle level of understanding that FeCrAl cladding may in fact offer enhanced accident tolerance through performance gains such as lower system temperatures and an increased margin in time before the onset of core degradation during a range of possible SA scenarios.

Future work includes establishing Technology Implementation Plans covering the material technology development and analysis phases and tasks needed to deploy FeCrAl cladding and FCM fuel and a Systematic Technology Evaluation Program for SiC composite cladding. These documents will be owned and driven by the community rather than belonging to ORNL specifically and will help further the development and readiness for deployment of these technologies. As part of that effort, a great deal of additional analysis work is needed, including full-core neutronics analysis for both PWRs and BWRs, thermal-hydraulic analysis, thermomechanical fuel performance analysis, system-level analysis (e.g., coolant chemistry and MELCOR) across a set of plant operating conditions ranging from normal operations to design basis accidents and beyond design basis accidents. In some of these areas, parametric studies may be needed to help guide material selection and development efforts instead of just assessing specific point designs. Developing a thorough fundamental understanding of (1) what dominant factors drive core degradation processes for different SA scenarios and at different timescales and (2) what the weak point in the overall system evolves to be as the fuel and cladding designs become more resilient stand out as two extremely crucial but difficult work areas for ORNL, the broader US ATF programme, and international ATF programmes collaborating worldwide. The effects of ATF concepts on the overall nuclear fuel cycle, including impacts on enrichment and fabrication facilities, fuel storage and transportation, and geological disposal, also need to be assessed.

ACKNOWLEDGEMENTS

The authors gratefully acknowledge the key insights and contributions of Kurt Terrani, Lance Snead, and Jess Gehin in helping to frame and guide aspects of this work. Valuable feedback was provided to portions of this document by numerous ORNL staff members, including Brian Ade, Steve Bowman, Matthew Francis, Andrew Godfrey, and Germina Ilas. The work presented in this paper was supported by the Advanced Fuels Campaign, which is

part of the Fuel Cycle Research and Development programme within the US DOE Office of Nuclear Energy.

REFERENCES

[1] CARMACK, W.J., GOLDNER, F., BRAGG-SITTON, S.M., SNEAD, L.L., "Overview of the U.S. DOE accident tolerant fuel development program," Proc. 2013 LWR Fuel Performance Meeting/TopFuel 2013, Charlotte, North Carolina, USA, September 15–19, 2013, American Nuclear Society (2013) 734–739.

[2] ZINKLE, S.J., TERRANI, K.A., GEHIN, J.C., OTT, L.J., SNEAD, L.L., Accident tolerant fuels for LWRs: A perspective, J. Nucl. Mater. **448** (2014) 374–379.

[3] BRAGG-SITTON, S., et al., Light Water Reactor Accident Tolerant Fuel Performance Metrics, Rep. FCRD-FUEL-2013-000264, Idaho Natl Lab., ID (2014).

[4] TERRANI, K.A., ZINKLE, S.J., SNEAD, L.L., Advanced oxidation-resistant iron-based alloys for LWR fuel cladding, J. Nucl. Mater. **448** (2014) 420–435.

[5] KATOH, Y., et al., Continuous SiC fiber, CVI SiC matrix composites for nuclear applications: Properties and irradiation effects, J. Nucl. Mater. **448** (2014) 448–476.

[6] YUEH, K., CARPENTER, D., FEINROTH, H., Clad in clay, Nucl Eng Int **55** (2010) 14–16.

[7] CARPENTER, D.M., An assessment of silicon carbide as a cladding material for light water reactors, Doctoral Thesis, Massachusetts Institute of Technology (2010).

[8] YUEH, K., TERRANI, K.A., Silicon carbide composite for light water reactor fuel assembly applications, J. Nucl. Mater. **448** (2014) 380–388.

[9] PINT, B.A., et al., High temperature oxidation of fuel cladding candidate materials in steam-hydrogen environments, J. Nucl. Mater. **440** (2013) 420–427.

[10] KANTHAL, Kanthal APMT (Tube) Material Datasheet, http://kanthal.com/en/products/material-datasheets/tube/kanthal-apmt/ .

[11] STRASSER, A., et al., An Evaluation of Stainless Steel Cladding for Use in Current Design LWRs, Rpt. NP-2642, Electric Power Research Institute (1982).

[12] CATHCART, J.V., et al., Zirconium Metal–Water Oxidation Kinetics IV. Reaction Rate Studies, Rpt. ORNL/NUREG-17, Oak Ridge Natl. Lab., TN (1977).

[13] SNEAD, L.L., et al., Handbook of SiC properties for fuel performance modeling, J. Nucl. Mater. **371** (2007) 329–377.

[14] BEN-BELGACEM, M., RICHET, V., TERRANI, K.A., KATOH, Y., SNEAD, L.L., Thermo-mechanical analysis of LWR SiC/SiC composite cladding, J. Nucl. Mater. **447** (2014) 125–142.

[15] TERRANI, K.A., PINT, B.A., PARISH, C.M., SILVA, C.M., SNEAD, L.L., KATOH, Y., Silicon carbide oxidation in steam up to 2 MPa, J. Am. Ceram. Soc. **97** 8 (2014) 2331–2352.

[16] POWERS, J.J., GEORGE, N.M., WORRALL, A., TERRANI, K.A., "Reactor physics assessment of alternate cladding materials," Transactions of the 2014 Water Reactor

Fuel Performance Meeting/Top Fuel/LWR Fuel Performance Meeting (WRFPM2014/TopFuel 2014), Sendai, Japan (September 14–17, 2014).
[17] GEORGE, N.M., TERRANI, K.A., POWERS, J.J., WORRALL, A., MALDONADO, G.I., Neutronic analysis of candidate accident-tolerant cladding concepts in pressurized water reactors, Ann. Nucl. Energy **75** (2015) 703–712.
[18] SHAPIRO, R., YOUNKER, I. FRATONI, M., Neutronic performance of accident tolerant fuels, Trans. Am. Nucl. Soc. **109** (2014) 1351–1353.
[19] GEORGE, N.M., POWERS, J.J., MALDONADO, G.I., TERRANI, K.A., WORRALL, A., Neutronic analysis of candidate accident-tolerant cladding concepts in light water reactors, Trans. Am. Nucl. Soc. **111** (2014) 1363–1366.
[20] GEORGE, N.M., POWERS, J.J., MALDONADO, G.I., WORRALL, A., TERRANI, K.A., "Demonstration of a full-core reactivity equivalence for FeCrAl enhanced accident tolerant fuel in BWRs," Proc. Advances in Nuclear Fuel Management V (ANFM V), Hilton Head Island, South Carolina, USA, March 29–April 1, 2015. American Nuclear Society (2014).
[21] OAR RIDGE NATIONAL LABORATORY, SCALE: A Comprehensive Modeling and Simulation Suite for Nuclear Safety Analysis and Design, Rpt. ORNL/TM-2005/39, Version 6.1, Oak Ridge Natl Lab., TN (June 2011).
[22] CHADWICK, M.B., et al., ENDF/B-VII.0: Next generation evaluated nuclear data library for nuclear science and technology, Nucl. Data Sheets **107** (2006) 2931–3060.
[23] GODFREY, A. T., VERA Core Physics Benchmark Progression Problem Specifications, Rpt. CASL-U-2012-0131-003, Oak Ridge Natl. Lab., TN (2014).
[24] BLOORE, D., "Reactor Physics Assessment of Thick Silicon Carbide Cladding PWR Fuels," Master's Thesis, Massachusetts Institute of Technology (July 2013).
[25] UX CONSULTING, The Nuclear Fuel Price Reporter, http://www.uxc.com.
[26] SNEAD, L.L., et al., Fully ceramic microencapsulated fuels: A transformational technology for present and next generation reactors—properties and fabrication of FCM fuel, Trans. Am. Nucl. Soc. **104** (2011) 668.
[27] TERRANI, K.A., SNEAD, L.L., GEHIN, J.C., Microencapsulated fuel technology for commercial light water and advanced reactor application, J Nucl Mater **427** (2012) 209.
[28] TERRANI, K.A., et al., Fabrication and characterization of fully ceramic microencapsulated fuels, J. Nucl. Mater. **426** (2012) 268.
[29] POWERS, J.J., WIRTH, B.D., A review of TRISO fuel performance models, J. Nucl. Mater. **405** (2010) 74.
[30] HANSON, D.L. (Ed.), A Review of Radionuclide Release From HTGR Cores During Normal Operation, Rpt. 1009382, Electric Power Research Institute CA (February 2004).
[31] TERRANI, K.A., SNEAD, L.L., GEHIN, J. C., Fully ceramic microencapsulated fuels for LWRs, Trans. Am. Nucl. Soc. **106** (2012) 1106–1107.
[32] SNEAD, L.L., et al., "FCM fuel development for LWR applications," Transactions of Reactor Fuel Performance 2012 (TopFuel 2012), Manchester, UK, September 2–6, 2012, (2012) 422–428.
[33] HUNT, R.D., SILVA, C.M., LINDEMER, T.B., JOHNSON, J.A., COLLINS, J.L. Preparation of $UC_{0.07–0.10}N_{0.90–0.93}$ spheres for TRISO coated fuel particles, J. Nucl. Mater. **448** (2014) 399–403.
[34] LINDEMER, T.B., VOIT, S.L., SILVA, C.M., BESMANN, T.M., HUNT, R.D., Carbothermic synthesis of 820μm uranium nitride kernels: Literature review, thermodynamics, analysis, and related experiments, J. Nucl. Mater. **448** (2014) 404–411.

[35] POWERS, J.J., TERRANI, K.A., "Uranium nitride: Enabling new applications for TRISO fuel particles," Transactions of the 2013 LWR Fuel Performance Meeting (TopFuel 2013), Charlotte, NC, USA, September 15–19, (2013).
[36] GEORGE, N.M., MALDONADO, I., TERRANI, K., GODFREY, A., GEHIN, J., POWERS, J., Neutronics studies of uranium-bearing fully ceramic microencapsulated fuel for pressurized water reactors, Nucl. Technol. **188** 3 (2014) 238–251.
[37] JO, C.K., CHANG, J., VENNERI, F., A neutronics feasibility study of using FCM on a LWR, Trans. Am. Nucl. Soc. **106** (2012) 689–691.
[38] LEE, W.J., SNEAD, L.L., VENNERI, F., "Fully ceramic micro-encapsulated (FCM) replacement fuel assembly for LWRs," Proceedings of 2013 the International Congress on Advances in Nuclear Power Plants (ICAPP 2013), Jeju Island, Korea, April 14–18, 2013, Korean Nuclear Society (2013).
[39] POWERS, J.J., et al., Fully Ceramic Microencapsulated (FCM) Replacement Fuel for LWRs, Rpt. ORNL/TM-2013/173, Oak Ridge Natl. Lab., TN (May 2013).
[40] BROWN, N.R., et al., Neutronic evaluation of a PWR with fully-ceramic micro-encapsulated fuel, part I: Lattice benchmarking, cycle length, and reactivity coefficients, Ann. Nucl. Energy **62** (2013) 538–547.
[41] BROWN, N.R., et al., Neutronic evaluation of a PWR with fully-ceramic micro-encapsulated fuel, part II: Nodal core calculations and preliminary study of thermal hydraulic feedback, Ann. Nucl. Energy **62** (2013) 548–557.
[42] LIANG, C., JI, W., "A neutronic feasibility study of AP1000 design loaded with fully ceramic micro-encapsulated fuel," Proceedings of 2013 International Conference on Mathematics and Computational Methods Applied to Nuclear Science & Engineering (M&C 2013), Sun Valley, ID, May 5–9, 2013, American Nuclear Society (2013).
[43] SHAPIRO, R.A., VINCENZI, M.J., FRATONI, M., "Optimization of fully ceramic micro-encapsulated fuel assembly for PWR," Proceedings of PHYSOR 2014, Kyoto, Japan, September 28–October 3, 2014.
[44] SANDIA NATIONAL LABORATORIES, MELCOR Computer Code Manuals, Version 1.8.6, Rpt. NUREG/CR-6119, Rev. 3 (September 2005).
[45] OTT, L. J., ROBB, K. R., WANG, D., Preliminary assessment of accident-tolerant fuels on LWR performance during normal operation and under DB and BDB accident conditions, J. Nucl. Mater. **448** 1–3 (2014) 520–533.

SIC BASED ACCIDENT TOLERANT FUEL CONCEPTS
(SECTION 7)

Chairpersons

Sosuke Kondo

Kyoto University, Japan

Weon-Ju Kim

KAERI, Korea, Republic of

Yutai Katoh

ORNL, United States of AmericaL

Mirco Grosse

KIT, Germany

SYSTEMATIC TECHNOLOGY EVALUATION PROGRAM FOR SIC/SIC COMPOSITE- BASED ACCIDENT-TOLERANT LWR FUEL CLADDING AND CORE STRUCTURES

YUTAI KATOH[1], KURT A. TERRANI[1,2], LANCE L. SNEAD[1]
[1]Materials Science and Technology Division,
[2]Fusion and Materials for Nuclear Systems Division
Oak Ridge National Laboratory
1 Bethel Valley Rd., Oak Ridge, TN 37831
United States of America
Email: katohy@ornl.gov

Abstract

High purity and crystalline SiC fiber/SiC matrix ceramic matrix composites (CMCs) are nuclear grade ceramic materials that do not undergo significant strength degradation up to at least many tens of dpa in neutron irradiation environments. Accordingly, they have been active subjects of research for high-temperature and high dose applications such as fusion reactor components. Given no degradation of strength up to at least 1400°C and high-temperature steam oxidation resistance, SiC/SiC CMCs are considered as attractive materials to substitute Zr alloys as accident tolerant LWR fuel and core constituents.

For a viable application of SiC/SiC CMCs as LWR fuel cladding or core components, many other development and feasibility areas remain that need to be considered. One of these areas is the hydrothermal corrosion of SiC-based materials in high-temperature and high-pressure water. SiC forms silica under these conditions, which subsequently dissolves into the coolant water. The corrosion rate of SiC is sensitive to water chemistry conditions and is increased in the presence of irradiation. Another important area that is of great importance is the ability of these CMCs to retain fission products for the fuel cladding application. This requires robust joining that does not degrade under irradiation or the coolant environment, as well as limiting micro-cracking that is a common occurrence in these brittle materials at relatively low levels of stress with a substantial probability (assuming fuel failure probability above 10^{-6} per fuel rod is unacceptable). The latter necessitates detailed thermo-mechanical models to estimate the stress distribution in these structures that incorporate irradiation evolution phenomena, which differ widely from metallic components. Once these stress levels are known, they can be used to predict failure probability in these structures. Finally, since much of the prior neutron irradiation data were conducted at higher temperatures, a renewed effort is necessary to examine low temperature irradiation effects (200-400°C) in these materials up to applicable doses for the LWR application (~15 dpa).

This paper reports the latest results in the areas identified above and sets the direction for future focused research towards viable application of SiC/SiC CMCs as LWR fuel cladding or core components.

1. INTRODUCTION

Fuels and core structures in the current light water reactors (LWR's) are vulnerable to catastrophic consequences in the event of loss of coolant or active cooling, as unfortunately evidenced by the March 2011 Fukushima Dai-ichi Nuclear Power Plant Accident [1-3]. This vulnerability is attributed primarily to the rapid oxidation kinetics of zirconium alloys in a water vapor environment at very high temperatures [1, 4]. Current LWR's use Zr alloys nearly exclusively as the materials for fuel cladding and core structures. Among the candidate alternative materials for the LWR fuel clads and core structures to enable so-called accident-tolerant fuels (ATF) and accident-tolerant cores (ATC), silicon carbide (SiC) – based materials, in particular continuous SiC fiber-reinforced SiC matrix ceramic composites (SiC/SiC composites or SiC composites), are considered to provide outstanding passive safety features in beyond-design basis severe accident scenarios [3, 5, 6]. The SiC/SiC composites are anticipated to provide additional benefits over the zirconium alloys, including the smaller neutron cross sections, general chemical inertness, ability to withstand higher fuel burn-ups

and higher temperatures, exceptional inherent radiation resistance, lack of progressive irradiation growth, and low induced-activation / low decay heat [7]. Presently, SiC/SiC composites are finding specialty applications as industrial materials as they mature and their application technologies grow [8]. Moreover, SiC and SiC/SiC composites are among the materials that have most extensively been studied for the effects of irradiation for nuclear applications [9].

However, application technologies for SiC/SiC composites for the LWR fuels and cores are very immature, since early concepts were introduced only recently [6, 10] and technically credible design concepts have not been formulated due to a lack of systematic technology development efforts until very recently [5]. For instance, while the potentially serious feasibility issues associated with swelling of SiC in the presence of steep temperature gradients in a nuclear environment had been pointed out in 2008 [11], a critical investigation had not been initiated until recently when a modeling study [12] and an experiment [13] predicted and demonstrated this issue, respectively. Moreover, an assessment of hydrothermal corrosion in LWR coolant environments had not been investigated until a recent set of experiments in the MIT Reactor [14], in which a severe mass loss in SiC/SiC composites in the boiling water reactor (BWR) coolant chemistry was identified. While these critical feasibility issues need to be thoroughly addressed in the relatively early stages in the course of the technology development, technically credible contingency plans will also be needed in case those issues appear to spoil the technical feasibility of certain baseline concepts.

The Systematic Technology Evaluation Program in support of the US Department of Energy's Advanced Fuels Campaign develops a technical program plan to address critical feasibility issues; to assess design and performance issues related with manufacturing, normal operation, and off-normal events; and to advance the technological readiness levels (TRL's) in essential technology elements for the SiC/SiC composite-based ATF and ATC. The present article provides high level overviews for the current technology, a critical technology gap analysis, and a draft technical program plan. The program plan was designed to systematically address the gap issues as identified by adopting a work breakdown structure, but also attempts to set a technical program toward steady progress in essential technology areas. Over the course of this exercise, it was recognized that the possible inability for fully ceramic structures to meet the performance requirement for ATF/ATC will create a critical turning point in the technology development roadmap. Therefore, discussion on the anticipated impact of the switch from a fully SiC ceramic clad/core to layered systems with a ductile environmental barrier coating is included.

2. TECHNOLOGY GAPS

2.1. Material properties

Despite the previous extensive studies on SiC and SiC/SiC composites including properties [15, 16], there has been insufficient understanding of their properties of particular interest for LWR core application for the nuclear-grade materials. Such properties include the statistical law for certain failure stresses such as for the matrix cracking, fission product transport, hydrothermal corrosion, fuel chemical compatibility, and thermal shock behavior. Moreover, the dimensional evolutions in a radiation environment are not understood to sufficient details.

2.2. Manufacturing technologies

SiC/SiC composite densification routes that have proved to produce radiation-resistant forms of composite materials are chemical vapor infiltration (CVI) and transient eutectic-phase sintering represented by NITE. CVI SiC/SiC is a mature technology that has already demonstrated scale components with very reasonable reproducibility up to large dimensions. The NITE SiC/SiC has more limited experiences, but has demonstrated fabrication of complex-shaped composites. However, manufacture of thin-walled tubes with a large length-to-diameter ratio remains a challenge for both fabrication routes. In addition to the manufacture of the tubes, end-plugging technologies that retain hermeticity and other functional integrity during operation remain to be developed.

2.3. Fuel performance

After decades of experience with metallic cladding components in thermal and fast reactors, the transition to use SiC composite cladding represents a revolutionary paradigm shift for fuels. With the conventional uranium dioxide fuel form, thermal issues arising from swelling of SiC need to be overcome. The viability of the fuel-clad systems with alternative fuel forms such as high metallic density and fully ceramic micro-encapsulated fuels needs to be carefully assessed via predictive fuel performance analysis. If the concept is deemed viable, the fuel performance analysis tools serve to guide the design process to optimize performance for the integral fuel module under normal and off-normal operating conditions. Note that when referring to "fuel" here, the integral structure consisting of the pellet, the cladding, and other fuel assembly components are all considered.

2.4. Codes and standards

For the purposes of establishing the properties database and qualify materials and components, a suite of standards are needed. The standards required likely include those for materials and component specifications, and test methods for all relevant mechanical, physical, thermal, and environmental properties. Currently only limited materials and test standards are available for ceramic matrix composites from international standardization organizations such as ASTM International and ISO. Moreover, certain design rules for SiC/SiC composite fuel cladding will have to be established.

3. CRITICAL FEASIBILITY ISSUES

The technology gaps discussed above can be categorized into the primary and non-primary technical issues. The primary gap issues are related with the critical technical feasibility, or go-or-no-go issues, which need to be addressed before further steps are taken in the non-primary technical issue areas. Three pressing issues have been identified to belong to this category with the hydrothermal corrosion and swelling-induced cracking at the most critical issues for the fully ceramic cladding systems and the fuel temperature issue that needs to be addressed by the research on fuel itself.

3.1. Hydrothermal corrosion

Thermodynamics always favors formation of silica (SiO_2) when water is put in contact with SiC under environments characteristic of normal operation in light water reactors. Silica dissolves in water likely forming silicic acid, $Si(OH)_4$, resulting in mass loss for SiC through the oxidation-dissolution process. Understanding the rate of material consumption is the key, since it determines the remaining thickness of the material in the cladding that continues to bear the applied loads and act as the first barrier to fission product release.

A number of out-of-pile autoclave tests have been performed to date that show mass loss in SiC materials as a function of time [17]. While the slowest mass loss rate was observed for CVD SiC, significantly higher rates were observed for sintered or reaction-bonded SiC variants. More pertinent to the fuel cladding application are the in-pile corrosion tests and autoclave tests on irradiated samples. While such data are rare, a recent in-pile corrosion test on CVI SiC/SiC composites at the MIT reactor under BWR NWC conditions [14] and an autoclave test in Japan with ion-irradiated CVD SiC samples [18] both indicate accelerated corrosion with irradiation. Previous in-pile tests at MIT reactor with open-ended composite samples where the fibers were exposed, in coolant chemistry close to PWR conditions (low oxygen potential) showed comparable corrosion with autoclave tests. Therefore, one can postulate that the radiolysis, products of which are much more significant under high oxygen potential conditions, has an important effect on SiC corrosion. On the other hand, the accelerated corrosion observed in the autoclave tests of ion-irradiated specimens indicate that radiation defects in SiC can play a role as well.

The current state of knowledge in the area of SiC corrosion in LWR coolant environments is very shallow, presenting what is perhaps the biggest gap at the moment for this technology. Systematic tests with well-defined samples under well-known conditions aiming to quantify the kinetics and identify the mechanism for corrosion are necessary.

3.2. Swelling-induced cracking

Fully crystalized SiC undergoes irradiation-induced swelling. The swelling occurs quickly after the start of irradiation and approaches saturation values before 1 dpa is reached [15]. The magnitude of saturation swelling is inversely correlated with irradiation temperature, at ~1% at 600°C and >2% at 300°C. The swelling of SiC accompanies a significant decrease in thermal conductivity because both of these irradiation-induced phenomena result from the accumulation of matrix defects. The differential swelling-induced stress or strain has been identified to be a serious threat for SiC-based fuel cladding in which a strong temperature gradient across the tube wall is inevitable due to the radial heat flux. Recent analysis by Ben-Belgacem et al. [12] also predicted very substantial tensile stress near the inner surface of cladding wall. While swelling itself does not result in material microcracking, the resulting thermomechanical stress can result in crack initiation and/or propagation. It is also noted that SiC composites possess intrinsic crack, such that irradiation-induced stress results in crack propagation.

The crack propagation radially through the clad wall is considered a fuel failure because it would immediately lead to a loss of fission product gas retention. More detailed investigation into this issue will require comprehensive modeling of fuel and clad behaviors, and a detailed and accurate understanding of swelling, irradiation creep, thermal conductivity change, and statistical failure of the clad material. Moreover, this potential weakness of the fully ceramic cladding highlights the need to explore clad design options involving hermetic seal coating with ductile materials.

3.3. Fuel temperature

Irradiation-induced swelling of SiC causes not only stresses arising from differential strain but results in an upward shift in the fuel temperature profile by two mechanisms: i) the clad swelling increases the physical gap between the pellet and the clad and ii) the low irradiated thermal conductivity of SiC/composite causes a large temperature drop across the clad wall. This increase in the fuel temperature is considered an important design issue since it exacerbates fission gas release from the pellet and could result in limited power rating for

the fuel to avoid melting at the pellet centerline which is a design limit by regulation. This issue may call for development of an engineering solution with the uranium dioxide fuel or alternative fuels that offer higher thermal conductivity and/or improved stability designed for reduced operating temperature as was investigated in Ref. [19]. Although this may be considered a less critical than other two issues, addressing the potential needs to modify the fuel form has to be initiated immediately. Note that the increase in pellet-cladding gap early in life has a positive feedback as well: delaying hard contact between the two to higher burnups compared to Zr-based cladding.

4. TECHNICAL PLAN

The initial technical program plan was developed to include three task categories of design and failure, environmental effects during normal operations, and off-normal environmental effects. The high level task items and their relevance with the critical gap issues for the SiC/SiC composite-based accident-tolerant fuel technologies for LWR's are summarized in Fig. 1. Each task consists of multiple subtasks as outlined below.

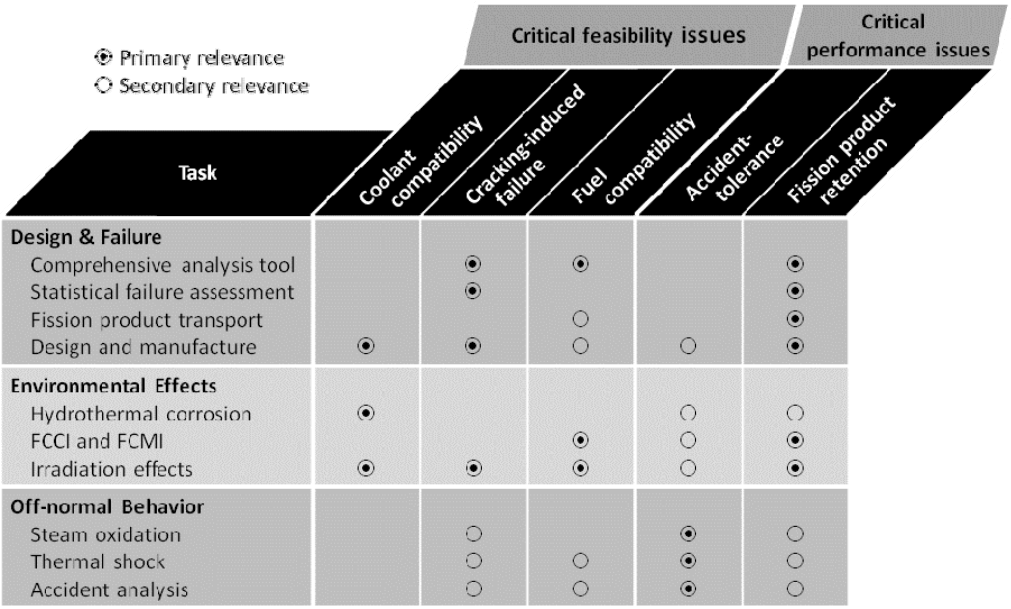

FIG. 1. Systematic technology evaluation program task items matrixed to the critical gap issues for SiC/SiC composite-based accident-tolerant fuel technologies for light water reactors.

4.1. Design and failure

Comprehensive performance analysis: An optimal SiC-based clad fuel assembly design is only possible when inputs from neutronics, thermal hydraulics, and materials are superimposed and integrated with one another. Therefore, an essential and useful activity is to examine the behavior of the cladding over the lifetime of the fuel to then gain insights into optimal designs for this component. As was shown by a recent study, the behavior of SiC ceramic cladding differs widely from the experience over the past six decades with Zr-based metallic cladding [12]. In this subtask, a full-scale simulation of the SiC-based cladding will be performed based on basic unirradiated and irradiated material property data and phenomenon that govern material evolution.

Statistical failure assessment: Information and understanding that are necessary to assess the failure probability, either matrix cracking or structural failure, are entirely missing

for SiC-based fuel rods. Specifically, the knowledge with regard to failure definition, probabilistic law that governs the failure, and the probabilistic parameters for failure of cladding tubes in relevant loading modes are critically important for establishing a predictive capability for failure probability. In order to achieve this goal, resources including the pertinent standard test methods for ceramic matrix composites and the quality assured experimental database are needed. This subtask will develop understanding in these areas.

Fission product transport: the ability of SiC to contain fission products has been studied for its application in high-temperature gas reactor fuels. The operating condition for SiC in LWR's is different with the lower temperature and the direct contact with fuel pellets. Although reactive transport can be ignored in case of noble gases and other species with low affinity for reaction with SiC, it needs to be taken into account for noble metals and other reactive species. This subtask will examine and quantify the susceptibility and rate for fission product transport through the SiC-based cladding. Transport of hydrogen isotopes into and out of the ceramic cladding will be studied as well. All transport mechanisms will ultimately be described in a form useful for component modeling.

Design and manufacture: The design and manufacture issues for SiC/SiC fuel rods include engineering of tubular composite structures, developing a method of end-plugging, manufacturing long tubes, and methods for quality assurance. These issues are specific to the pin-type nuclear fission fuels and thus have not previously been explored in other programs researching SiC such as fusion energy sciences. Additionally, due to concerns of unacceptable cracking probability for fully ceramic clad systems and hydrothermal corrosion rate, ductile metal-coated ceramic composite clad concepts will be explored.

4.2. Environmental effects

Hydrothermal corrosion: SiC recession as a result of corrosion in high-temperature water is a critical feasibility issue for fully ceramic cladding concepts because it leads to i) cladding thickness loss that could in turn result in increased loading on the structure and exposure of the pyrocarbon-filled fiber-matrix interphase, and ii) deposition of unwelcome corrosion products in the primary water circuit. Therefore, it is essential to quantify the rate of SiC recession along with its dependence on environmental conditions such as pH, oxygen potential, electrochemical potential, solutes in the aqueous systems, radiolysis, etc. While solubility of quartz in pure water has received extensive attention in the geochemistry field, the thermodynamic driving forces for amorphous silica dissolution in water chemistries representative of LWR conditions are not understood. This subtask will establish such a basis and verify against experimental observations, followed by developing water chemistry control strategies that limit corrosion to the extent that the cladding structure remains intact and the dissolved corrosion products do not present a problem to the overall system. It is also possible that the chemistry control is so challenging that any successful design will require a protective layer on the surface of the cladding that limits its corrosion.

Fuel-clad interactions: Fuel cladding chemical and mechanical interaction (FCCI and FCMI) affect the cladding structure and alter its loading state and therefore could be design limiting issues. FCCI could lead to stress corrosion cracking by causing corrosion-induced flaws in the material that dramatically reduce the reliability of the ceramic structure under tensile loads. FCMI that occurs once hard contact between the pellet and the cladding is established can easily lead to cladding failure by inducing significant loads on the structure. Consideration of FP interaction (particularly noble metals) with the cladding is of immediate importance. All aspects of the FCCI and FCMI will be examined through an integrated fuel performance modeling and experiments.

Neutron irradiation effects: Because most of the previous works on the effects of irradiation on SiC/SiC composites focused on high temperature operations, there remains serious lack of information on the irradiation effects at LWR-relevant temperatures. Therefore, the low temperature, high dose irradiation effects will be experimentally examined. Accurate determination of fluence- and temperature-dependent evolutions of swelling and the irradiation creep behavior will also be pursued. Understanding the effects of neutron irradiation on the end plug elements is considered essential. In case the ductile metal-coated SiC/SiC cladding concepts are pursued, the coated systems will be examined for the irradiation effects.

4.3. Off-normal environmental effects

Steam oxidation: SiC recession kinetics in atmospheric pressure steam up to 1700 °C have been shown to be at least two orders of magnitude slower and in high pressure steam (up to 2 MPa and 1350 °C) roughly one order of magnitude slower than Zr alloys [4]. Although the enthalpy of oxidation of SiC and Zr alloys is similar [20], the slower kinetics limits the extent of heat generation as a result of oxidation and provides additional safety margins during the course of a severe accident. The areas that will be subjected to further characterization are oxidation of composite structures with joints and flaws under stress to examine the ability for these structures to preserve their geometry and maintain coolability. If metal-ceramic hybrid structures are to be considered to achieve optimal operational performance under normal conditions, the integral high-temperature steam oxidation behavior of these structures will require investigation.

Thermal shock: To guarantee that the core remains controllable and coolable under design basis and beyond design basis accidents, demonstration of thermal shock resistance for SiC fuel assembly structures is necessary. Preliminary studies have been performed to date on this subject [21, 22], however those studies will be extended to consider irradiated SiC materials and pressurized cladding structures.

Accident analysis: Once oxidation kinetics, degradation modes, and integral structure response (capturing both physical and chemical degradation modes) under high-temperature, high-pressure, steam environments have been quantified and understood, this information will be injected into severe accident (SA) analysis tools to predict core behavior under such postulated events. SA analysis tools are necessary to identify limiting properties and configurations that reduce response time and safety margins. They are also an effective tool to consider various scenarios in an efficient manner and produce remedial actions and procedures to mitigate them.

5. CONCLUSIONS

The initial technical plan for the Systematic Technology Evaluation Program for SiC/SiC Composite Accident-Tolerant LWR Fuel Cladding and Core Structures was laid out. The primary objective of the planning was to develop a blueprint of a technical program that addresses the critical feasibility issues; assesses design and performance issues related with manufacturing, operating, and off-normal events; and advances the technological readiness levels in essential technology elements for SiC/SiC composite-based LWR fuel cladding and core structure concepts.

The presented planning exercise consisted of three main tasks: a technology review, a critical technology gap analysis, and a technical program planning. Various technical gap issues were identified during the technology review process and the analysis revealed that

many of them are related with the three key feasibility issues for SiC/SiC composite fuel cladding: hydrothermal corrosion, cracking failure, and fuel-clad system compatibility. Additional very important gap issues have also been identified and analyzed. A more detailed technical program plan is being developed with an objective of systematically addressing these key technology gaps and feasibility issues, and then lay out the tasks in a work breakdown structure, which consists of three top level categories: Design and Failure, Environmental Effects, and Off-normal Behavior. Simultaneously, the plan attempts to set an early technical program toward advancing the technological readiness levels of essential technologies in these three areas.

This technical program plan document is intended to receive continued updates beyond the current version. The future updates will incorporate input from broader community knowledge and reflect the evolving technology and findings.

ACKNOWLEGMENTS

Research sponsored by the Office of Fusion Energy Sciences, U.S. Department of Energy, under contract DE-AC05-00OR22725 with UT-Battelle, LLC.

REFERENCES

[1] PARISI, C., NEGRENTI, E., SEPIELLI, M. and DEL NEVO, A., Simulation & analysis of the severe accident of the Unit 1 of Fukushima Daiichi NPP, Energia, Ambiente e Innovazione, vol. **2**, pp. 56-61, 2012.

[2] WRAY, P., Materials for nuclear energy in the post-Fukushima era: An interview with John Marra, American Ceramic Society Bulletin, vol. **90**, pp. 24-28, 2012.

[3] ZINKLE, S. J., TERRANI, K. A., GEHIN, J. C., OTT, L. J. and SNEAD, L. L. Accident tolerant fuels for LWRs: A perspective, Journal of Nuclear Materials, vol. **448**, pp. 374-379, 2014.

[4] TERRANI, K. A., PINT, B. A., PARISH, C. M., SILVA, C., SNEAD, L. L. and KATOH, Y., Silicon Carbide Oxidation in Steam up to 2 MPa, Journal of the American Ceramic Society, vol. **97**, pp. 2331-2352, August 2014.

[5] BRAGG-SITTON, S., HURLEY, D., KHAFIZOV, M., MERRILL, B., SCHLEY, R., MCHUGH, K. et al., Silicon Carbide Gap Analysis and Feasibility Study, INL/EXT-13-29728, Idaho National Laboratory, Idaho Falls INL/EXT-13-29728, July 2013.

[6] SNEAD, L. L., KATOH, Y. and TERRANI, K. A., An Overview of SiC-Based Fuel and Cladding Technologies in Support of Accident Tolerant Fuel Development, EHPG13, 2013.

[7] KATOH, Y., SNEAD, L. L., SZLUFARSKA, I. and WEBER, W. J., Radiation Effects in SiC for Nuclear Structural Applications, Current Opinion in Solid State & Materials Science, vol. **16**, pp. 143-152, June 2012 2012.

[8] HALBIG, M. C., JASKOWIAK, M. H., KISER, J. D. and ZHU, D., Evaluation of ceramic matrix composite technology for aircraft turbine engine applications, in 51st AIAA Aerospace Sciences Meeting including the New Horizons Forum and Aerospace Exposition 2013, Grapevine, TX, 2013.

[9] NOZAWA, T., HINOKI, T., HASEGAWA, A., KOHYAMA, A., KATOH, Y., SNEAD, L. L., et al., Recent advances and issues in development of silicon carbide composites for fusion applications, Journal of Nuclear Materials, vol. **386**, pp. 622-627, April 30 2009.

[10] YUEH, K., CARPENTER, D. and FEINROTH, H., Clad in Clay, Nuclear EngINEERING INTERNATIONAL, PP. 14-16, 2010.

[11] MORLEY, N. B., KATOH, Y., MALANG, S., PINT, B. A., RAFFRAY, A. R., SHARAFAT, S., et al., Recent US research and development for the dual coolant blanket concept, Fusion Engineering and Design, vol. **83**, pp. 920-927, 2008.
[12] BEN-BELGACEM, M., RICHET, V., TERRANI, K.A., KATOH, Y., and SNEAD, L.L., Thermo-mechanical analysis of LWR SiC/SiC composite cladding, Journal of Nuclear Materials, vol. **447**, pp. 125-142, January 2014.
[13] DEMKOWICZ, P. A., HUNN, J.D., MORRIS, R.N., HARP, J., BALDWIN, C.A., WINSTON, P., et al., Preliminary Evaluation of Fission Product Release from AGR-1 Coated Particles, in American Nuclear Society 2012 Annual Meeting - Nuclear Fuels and Structural Materials for the Next Generation Nuclear Reactors, Chicago (2012).
[14] CARPENTER, D., SiC Water Corrosion Studies at the MIT NRL, in Workshop on SiC Technologies for Accident Tolerant Fuels, Oak Ridge, 2014.
[15] KATOH, Y., OZAWA, K., SHIH, C., NOZAWA, T., SHINAVSKI, R. J., HASEGAWA, A., et al., Continuous SiC Fiber, CVI SiC Matrix Composites for Nuclear Applications: Properties and Irradiation Effects, Journal of Nuclear Materials, vol. **448**, pp. 448-476, April 2014.
[16] NOZAWA, OZAWA, T., CHOI, K. Y. B., KOHYAMA, A. and TANIGAWA, H., Determination and prediction of axial/off-axial mechanical properties of SiC/SiC composites, Fusion Engineering and Design, vol. **87**, pp. 803-807, 2012.
[17] PARK, J.-Y.,KIM, I-H., JUNG, Y.-I., KIM, H.-G., PARK, D.-J. and KIM, W.-J., Long-term corrosion behavior of CVD SiC in 360°C water and 400°C steam, Journal of Nuclear Materials, vol. **443**, pp. 603-607, 2013.
[18] KONDO, S., LEE, M., HINOKI, T., HYODO, Y. and KANO, F., Hydrothermal Corrosion of Ion Irradiated SiC, in 39th International Conference on Advanced Ceramics and Composites, Daytona Beach (2015).
[19] BLOORE, D.A., Reactor physics assessment of thick silicon carbide clad PWR fuels, Massachusetts Institute of Technology (2013).
[20] FARMER, M.T., LEIBOWITZ, L., TERRANI, K.A. and ROBB, K.R., Scoping assessments of ATF impact on late-stage accident progression including molten core–concrete interaction, Journal of Nuclear Materials, vol. **448**, pp. 534-540 (2014).
[21] LEE, Y., Safety of light water reactor fuel with silicon carbide cladding, Massachusetts Institute of Technology (2013).
[22] YUEH, K. and TERRANI, K.A., Silicon carbide composite for light water reactor fuel assembly applications, Journal of Nuclear Materials, vol. **448**, pp. 380-388 (2014).

PROGRESS ON THE WESTINGHOUSE ACCIDENT TOLERANT FUEL PROGRAMME

J. P. MAZZOCCOLI[*], J. CHOI[**], P. XU[**]
[*]Westinghouse Electric Company, LLC Cranberry, Pennsylvania
[**]Westinghouse Electric Company, LLC Columbia, South Carolina
United States of America
E-mail: MazzocJP@westinghouse.com

Abstract

The Westinghouse led team on accident tolerant fuel (ATF) has made significant progress over the last decade on the development of economically attractive cladding and fuel options to utility customers that have the potential for increased tolerance for beyond design basis accidents. Since the occurrence of the Fukushima Daiichi accident in 2011, Westinghouse has become increasingly focused on ATF development and has accelerated the programme with support from the Department of Energy (DOE). The Westinghouse ATF designs have been motivated by significantly enhanced accident tolerance, simplified designs for future Nuclear Steam Supply Systems (NSSS), and substantially improved fuel cycle costs. To date, Westinghouse, working with its partners, has a basic concept for silicon carbide (SiC) ceramic cladding and advanced pellet designs and has also performed early tests to show viability of the chosen concepts. The Westinghouse ATF concepts include: deposition of oxidation resistant titanium-aluminium-carbide (Ti_2AlC) coatings on zirconium alloy as a mid-term cladding product and SiC composites as the long-term cladding product. Regarding fuels, uranium silicide (U_3Si_2) pellets are being developed as a mid-term fuel product, and waterproofed uranium nitride ($U^{15}N$) as the long-term fuel product. The Westinghouse ATF Program, in conjunction with its partner General Atomics, continues to advance SiC technology in the areas of fabrication, testing, and modelling. High temperature oxidation tests are ongoing at the Massachusetts Institute of Technology (MIT) to evaluate accident tolerance of this cladding. While initial efforts regarding the deposition of oxidation resistant coatings on zirconium alloy cladding did not perform as desired, the University of Wisconsin is continuing to optimize deposition parameters. Critical work also continues in the area of advanced pellet development on both U_3Si_2 and waterproofed uranium nitride fuels at Idaho National Laboratory (INL) and Texas A&M University, respectively. Radiation testing of U_3Si_2 pellets is planned in the near-term, and radiation of SiC cladding is currently underway and will end in early 2015. In September of 2014, the Westinghouse ATF Program won an award from the Department of Energy for continued cladding and fuel development, as well as the creation of a project plan for ATF lead test rods (LTR) activities.

1. INTRODUCTION

The Westinghouse led team on accident tolerant fuel (ATF) has made significant progress over the last decade on cladding and fuel options that will be both economically attractive to utility customers and have increased tolerance beyond design basis accidents such as Three Mile Island 2 and Fukushima Daiichi. Since the Fukushima Daiichi accident, the nuclear industry has been working closely with governments and regulators to make existing nuclear power plants more tolerant to beyond design basis accidents. It is also recognized by the industry that enhanced nuclear fuel plays a vital role in improving reactor safety and minimizing the consequences should an accident occur.

Starting in 2004, Westinghouse Electric Company had formed core teams to develop advanced ceramic cladding and pellet designs with enhanced safety margin. Westinghouse had initiated the development of a simplified reactor design, with passive safety features, that would not need to be so heavily dependent on the complex safety systems that are required in today's reactors. Since the occurrence of the Fukushima Daiichi accident in 2011, Westinghouse has become increasingly focused on ATF development and has accelerated the programme with support from the Department of Energy (DOE) and continued internal investment. Westinghouse has also established a work group with the focus on scientific studies for ATF called Collaborative Research on Accident Tolerant Fuel (CARAT), with over 30 international members across the world and has also been actively working with its parent company, Toshiba Corporation, in the development ATF technologies.

The Westinghouse ATF designs have been motivated by the following attributes:

- Significantly enhanced accident tolerance;
- Simplified designs for future nuclear steam supply systems (nsss);
- Substantially improved fuel cycle costs, providing an incentive for utilities to introduce new fuel designs.

In order to meet the above objectives, the programme has been focusing on both cladding and pellet design. To date, Westinghouse, working with its partners, already has a basic concept for SiC ceramic cladding and advanced pellet designs, and had also performed early tests to show viability of the chosen concepts. The Westinghouse ATF concepts include:

- Titanium-aluminium-carbide (Ti_2AlC) coatings on zirconium alloy as the mid-term cladding product;
- Silicon carbide (SiC) composites as the long-term cladding product;
- Uranium silicide (U_3Si_2) pellets as the mid-term fuel product;
- Waterproofed uranium nitride ($U^{15}N$) pellets as the long-term fuel product.

Each concept provides different levels of improvement on accident tolerance, while balancing the complexities in technology development, licensing risk and utility acceptance. The zirconium coating is expected to alleviate oxidation and hydriding degradation and to provide a moderate (~200°C) increased temperature tolerance in the case of a severe accident. The SiC composite cladding increases maximum tolerable cladding temperature from the current 1200°C to up to ~ 2000°C, and also increases corrosion resistance at normal operating conditions (~300°C). U_3Si_2 offers a 17% increase in ^{235}U and a 5 fold increase in thermal conductivity compared to UO_2, while waterproofed $U^{15}N$ offers up to a 35% increase in ^{235}U (estimate) and 10 fold increase in thermal conductivity. Details on these ATF concepts, proposed product specifications, and a preliminary safety evaluation were discussed in previous papers [1, 2].

In the current DOE ATF programme, Westinghouse is working closely with its partners to develop the aforementioned cladding and fuel concepts. Our core partners are as follows: General Atomics (GA) for the design and fabrication of SiC cladding and for SiC characterization and testing, the University of Wisconsin (UW) and Edison Welding Institute (EWI) for the fabrication and evaluation of coated cladding; the Massachusetts Institute of Technology (MIT) for oxidation tests and in reactor irradiation, Idaho National Laboratory (INL), Los Alamos National Laboratory (LANL), Texas A&M University, and National Nuclear Laboratory in the United Kingdom for the development and fabrication of U_3Si_2 fuel and waterproofed uranium nitride fuel. Also, our utility partner Southern Nuclear Company is evaluating and peer checking our fuel cycle cost and economic studies, and providing guidance on utility licensing requirements.

2. ACCIDENT TOLERANT FUEL CLADDING DEVELOPMENT

In the recent term, Westinghouse and its partner General Atomics have continued efforts regarding the evaluation of fundamental thermal and mechanical properties of SiC and have examined the failure mechanisms in multilayer cladding designs in which SiC monolith tubing is on the inside or outside of the cladding. Westinghouse has also been active with UW, EWI, and MIT on the development of oxidation resistant Ti_2AlC coatings

for zirconium alloy cladding. Recent developments for each technology area are discussed below.

2.1. Silicon carbide cladding architecture overview

It is commonly recognized that significant challenges have to be overcome for ceramic cladding, specifically, SiC ceramic matrix composites (CMC). One of the key challenges is to demonstrate hermeticity of the SiC cladding during normal operation, because low stress may cause microcracks to develop in normal usage. The team, under the leadership of our key partner General Atomics, has been working on the optimization of the SiC cladding designs and has made significant progress to overcome the insurance hermeticity for SiC cladding in both normal and accident conditions. Though designs may vary, the general philosophy is to use monolith SiC to provide hermeticity and the composite to provide structural integrity. Various SiC cladding designs were proposed using computational models, and short tubular samples were fabricated. The SiC cladding designs are listed in Table 1.

TABLE 1. CLADDING THICKNESS VARIATIONS BASED ON CLADDING MODEL

Model	Inner Monolith (μm)	Composite (μm)	Outer Monolith (μm)
Duplex	400	600	-
Standard	-	750	250
Intermediate	-	630	250
Thin	-	500	250

Fig. 1 shows the designs of SiC cladding with inner or outer monoliths in combination with the SiC composite. The duplex design contains the monolith SiC as the inner tube and the composite SiC as outer layer, while the standard design contains the composite SiC tube as the interior and the monolith SiC as the outer layer.

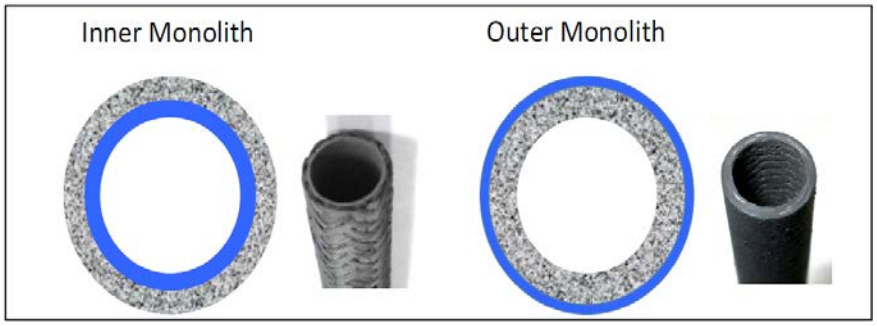

FIG. 1. Inner SiC monolith and outer SiC monolith designs with the blue giving the location and relative thickness of the monolithic layer. Duplex design on the left, standard design on the right.

2.2. Physical property development of SiC cladding

Recent efforts by General Atomics have focused on the experimental performance of various SiC cladding designs. A summary of some of these recent tests is provided in proceeding sections.

1.1.1. Thermal conductivity of SiC-SiC composite and duplex cladding

The thermal conductivity of an all SiC composite cladding and a duplex design that incorporates a SiC composite over an inner SiC monolithic have been measured. Both

cladding architectures have a thin pyrolytic carbon interface coating, but the amount of monolithic SiC varies. The measured thermal conductivity is provided in Fig 2.

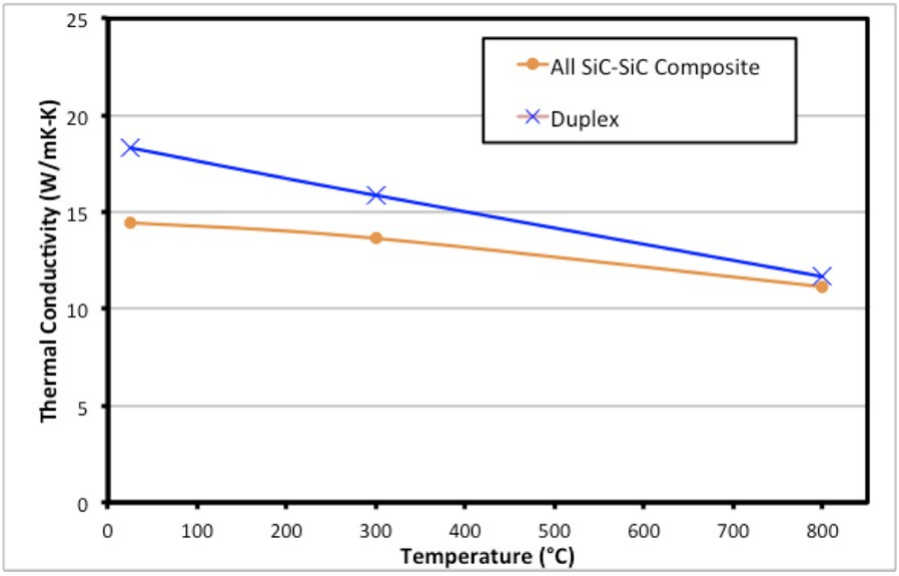

FIG. 2. Thermal conductivity of SiC-SiC composites and duplex cladding architectures

As may be expected, the duplex has the highest thermal conductivity due to the fact that the alpha SiC monolith accounts for ~30% of the thickness. Although duplex designs are not likely the final design, the data presented in Fig. 2 provides an upper bound of experimental conductivities that may be expected for a SiC cladding product.

1.1.2. Expanding plug stress test and permeability measurements

Expanding plug testing has been coupled to permeability testing to stress a sample with a monolithic outer overcoat. The internal pressure is the actual applied load from the expanding plug, assuming uniform compression of the plug. A specialized tube was fabricated, polished, and overcoated according to the baseline processes established and the tube was fabricated to accentuate possible difficulties that may arise from multilayer claddings so the overcoat was made thicker to examine cracking across layers. This produced a tube with a total thickness of 1.4 mm, with a SiC composite overcoat of 250-270 μm. These are not final architecture claddings, so the values here are being obtained to inform further development of the cladding. In particular, the outer monolith is expected to remain in compression or slight tension when evaluating the measurements below. All measurements were performed on the same sample and a cross-section of the tube is shown in Fig. 3.

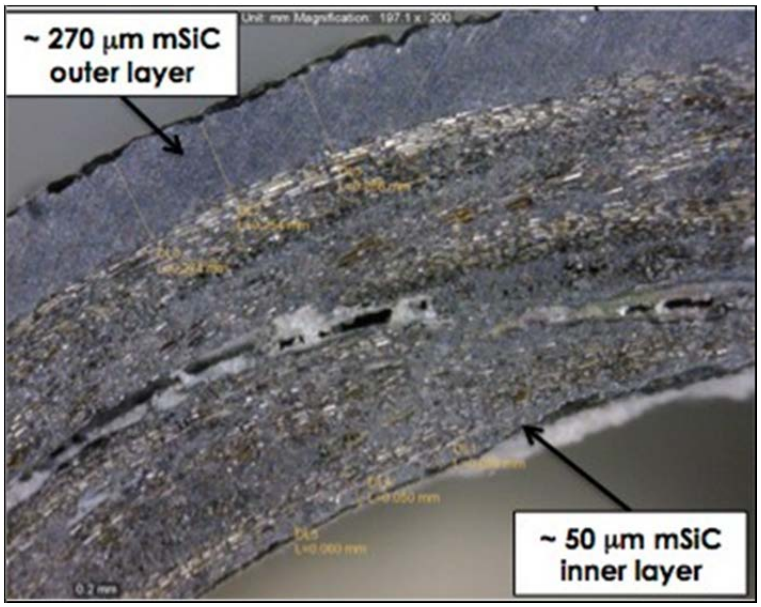

FIG. 3. SEM cross-section of the sample tested.

Table 2 provides the stress values calculated for the tube based on the applied internal pressure correlated with permeability measurements and shows that the cladding has demonstrated the ability to take up to 38 MPa of pressure, 3 times what is required for current nuclear fuel. This activity is part of the development of measuring meaningful stresses on multilayer tubes. As might be expected, the maximum calculated stress for the SiC-SiC composite is less than that of the monolith over the entire pressure range, due to the inherent stiffness of the monolith. Under all pressure conditions, the leak rate was very low and showed no appreciable correlation with increasing internal pressure. This process will be refined and used to test future samples.

TABLE 2. CALCULATED STRESS AND PERMEAIBILITY AS A FUNCTION OF INTERNAL PRESSURE FOR A SPECIALIZED TUBE

Internal Pressure (MPa)	Max Calculated SiC-SiC Stress (MPa)	Max Calculated Monolith Stress (MPa)	Leak Rate (Pa•cm3•sec-1)	Permeability Test Duration (hr)
0	0	0	< 1.01 × 10-7	144
7.8	20	35	< 1.01 × 10-7	12
15.1	40	70	< 1.01 × 10-7	12
22.1	60	100	< 1.01 × 10-7	12
30.3	85	140	< 1.01 × 10-7	12
38.3	105	175	< 1.01 × 10-7	12
45.8	125	205	>10.13	Seconds

2.3. Modelling of the multi-layered SiC cladding

General Atomics has developed a computer code to predict the failure of cladding due to a multilayer construction. This code accounts for a temperature-dependent swelling of the SiC due to thermal and neutron irradiation induced swelling effects. This swelling leads to a large stress gradient which goes from tensile at the inner wall to compressive at the outer wall. The combined results can lead to particularly large stresses at shutdown, as the loss of external pressure eliminates compressive stress, and the cessation of power generation eliminates the temperature-induced stress gradient, which is opposite to the swelling induced one and partially cancels it out. The conditions for beginning-of-life, end-of-life and

shutdown were examined. Analysis concluded that an outer monolithic design was the best option because it keeps the monolithic portion under compression.

Since February of this year, a number of changes have been made to the light water reactor (LWR) cladding model to better describe stresses on the inner composite layer. High stresses in the composite were occurring because they failed to model the true stress-strain behaviour of the SiC/SiC composite. Past the proportional limit, a simplified stress-strain curve was incorporated as this curve better represents composite behaviour, allowing the composite to become more compliant, which in turn transfers stress to the monolithic layer. Since the monolithic layer is already in compression, this does not result in unacceptably high stresses. In addition, the probabilistic failure model and the loading conditions have been updated to more accurately reflect the LWR fuel cycle. Current runs that include simplifying assumptions to account for the variation in the monolithic fracture stress and composite ultimate tensile strength have been promising. The next steps will be to continue to incorporate variation in strain limits and correlation between various values on the stress strain curve.

2.4. Oxidation resistant coatings for zirconium alloy cladding

The development of an oxidation resistant coating for zirconium alloy cladding has focused primarily on a titanium-aluminium-carbide ceramic with a 2,1,1 structure (Ti_2AlC). Rectangular ZIRLO® samples were coated using a cold-spray apparatus by the University of Wisconsin at temperatures of 600 and 790°C. The coated samples were then placed in a static steam autoclave at a temperature of 427°C and pressure of 10 MPa for periods up to 57 days to simulate extended exposure under normal reactor operation conditions. It was evident that the coated samples gained weight at a faster rate than the uncoated samples, indicative of undesirable performance. Additional characterization of the samples is currently being performed to determine the origin of the weight gain.

It should be noted that these results represent an exploratory stage of development in which particle size and spray conditions were not optimized. To obtain benchmark data on the oxidation rate of the pure Ti_2AlC sample, a single phase Ti_2AlC pellet with a density close to 100% was obtained from Sandvik, Inc. in Sweden. The pellet was exposed to 1200°C steam for 96 hours, and the regression was measured to be ~8 μm, so the regression rate was less than 0.8 $\mu m \cdot h^{-1}$. This low oxidation rate was comparable to literature values [3], and is an order of magnitude lower than for zirconium. The results suggest that Ti_2AlC is oxidation resistant up to 1200°C and is able to provide good protection for zirconium if the coating can be applied correctly, and the thickness can be as low as 20 μm. In the coming months, additional work will focus on the development of optimized spray and particle parameters to improve the density and robustness of the coating.

2.5. Irradiation testing

Irradiation capsules have been recently fabricated for General Atomics SiC tube samples as well as Ti_2AlC coated ZIRLO® samples. Fig. 4 shows an assembled test rig containing the samples. Irradiation testing began in April of 2014 at MIT and is to last ~240 reactor days, which ends in 2015.

FIG. 4. Images of modules prepared for the first irradiation cycle, flow shrouds removed to show samples.

3. ADVANCED PELLET DEVELOPMENT

In support of advanced pellet development, Westinghouse and its partners have made continued progress in the development of U_3Si_2 and waterproofed ($U^{15}N$) pellets. These developments include the optimization of U_3Si_2 fabrication processes in preparation for irradiation testing, as well as strides in the fabrication and characterization of the waterproofed pellets. A summary of these activities are discussed below.

3.1. U_3Si_2 pellets

One of Westinghouse's partners, Idaho National Laboratory has successfully fabricated pure phase U_3Si_2 pellets and has achieved an average density of >94% theoretical density after several iterations of process optimization. A representative image of the pellets is provided in Fig. 5. The results were reported in a paper published last year by Idaho National Laboratory [4].

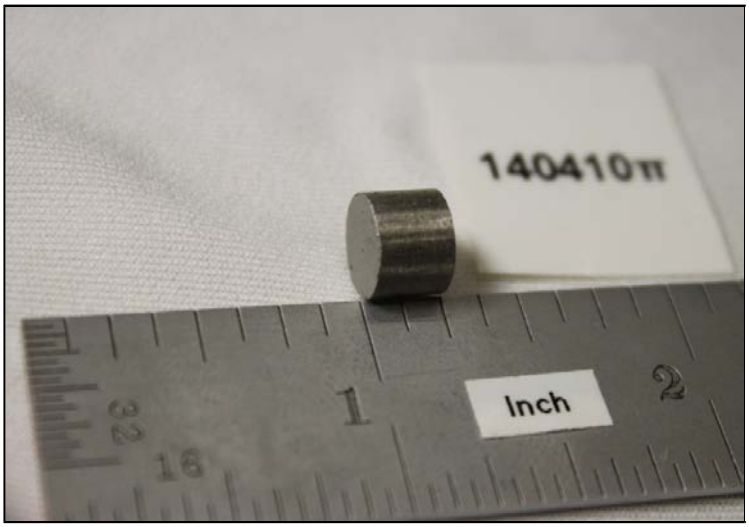

FIG. 5. U_3Si_2 pellet for radiation testing at ATR.

Final optimization of the pressing and sintering parameters was performed on available depleted uranium silicide stocks. An addition of 0.1 wt % polyox (polyox is a water-soluble, non-ionic polyethylene oxide polymer with a high-molecular weight) was shown to be an effective binder during the pressing process. The additional binder was needed to enhance the green strength of the pellets and helped to eliminate delamination and pellet chipping when the green pellets were removed from the die. Pellets sintered from the optimized process powder at the optimum sintering conditions have a measured density ranging from 11.60 to 11.93 $g \cdot cm^{-3}$ (±0.04). INL has completed and delivered U_3Si_2 pellets for irradiation experiments set to begin in Fall of 2014 at the Advanced Test Reactor (ATR) at INL.

3.2. Waterproofed $U^{15}N$ pellets

Westinghouse and its partners are developing waterproofed uranium nitride fuel through the introduction of uranium nitride/silicide pellet composites. Recent work performed by Texas A&M used longer sintering dwell times of 10 hours at 1775°C for pellets that had 25 and 32 wt% silicide resulting in bulk densities that reached 12.7 and 12.8 $g \cdot cm^{-3}$ to achieve theoretical densities of 92 and 94%, respectively. These densities were measured avoiding any high points in the pellet. Processing the samples in this manner reduced the overall swelling of the pellet; however it remained visible on top of the pellets as shown in Fig. 6. Further work involving calorimeter and interactions studies are planned.

FIG. 6. A waterproofed pellet with 32 wt % silicide sintered at 1775°C for 10 hours, density of 12.8 $g \cdot cm^{-3}$ or 94% of theoretical density.

Additional characterization of the waterproofed fuel was performed using scanning electron microscopy (SEM). Fig. 7 shows elemental mapping images of a 32 wt % silicide sample which was held at 1700°C for three hours. The regions circled in red show increased silicon content, and a slightly reduced uranium concentration compared to the rest of the silicon rich areas, which may be indicative of the presence of a minor phase.

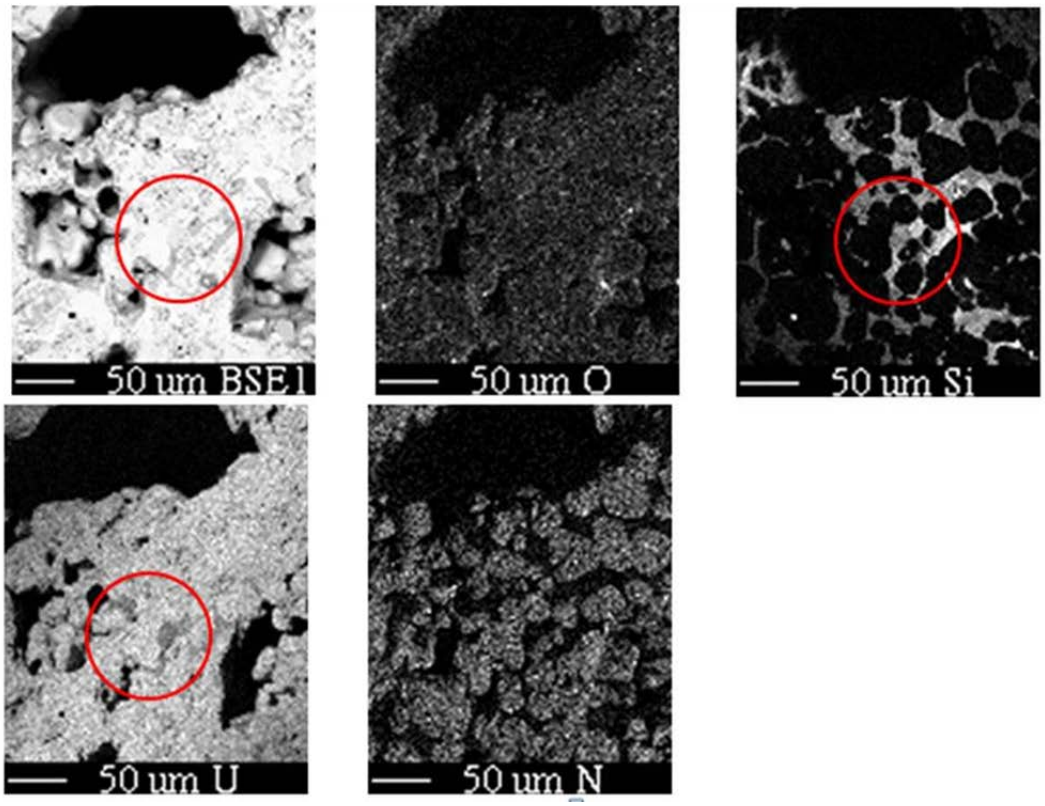

FIG. 7. Elemental maps of a 32 wt % silicide, 45-75 µm uranium nitride composite. The lighter within each image regions represent higher concentration of the respective element.

Analysis of additional pellets also showed some sensitivity of the silicide phase to oxidation with respect to the nitride phase. The oxidation may have occurred during sample preparation. SEM characterization is ongoing.

4. SUMMARY AND FUTURE WORK

The description of work included in this paper is intended to provide the reader with details about the recent progress that has been achieved regarding ATF cladding and fuel designs. The Westinghouse ATF Program, in conjunction with its partner General Atomics, continues to advance SiC cladding technology by optimizing fabrication techniques, performing thermal and mechanical tests, and expanding modelling of multilayered SiC architectures. High temperature oxidation tests are ongoing at MIT to evaluate accident tolerance of this cladding. The University of Wisconsin is continuing to improve spray and particle parameters for the deposition of Ti_2AlC to zirconium alloy and is poised to test and characterize these new samples after autoclave exposure. Critical work continues in the area of advanced pellet development on both U_3Si_2 and waterproofed uranium nitride fuels. Radiation testing of U_3Si_2 pellets is planned in the near term, and radiation of SiC cladding is currently at underway at MIT and will end in early 2015.

In September of 2014, the Westinghouse ATF Program won an award from the Department of Energy for continued cladding and fuel development in response to the Department of Energy Funding Opportunity Number: DE-FOA-0001063. The main cladding and fuel options that will be advanced during this phase are:

- A SiC wound fibre/SiC infiltrated/SiC monolithic composite cladding structure that allows for beyond design basis accident temperature of 1700°C;
- U_3Si_2 fuel that provides two to five fold increase in thermal conductivity, which significantly increases resistance to centreline melt during transient issues;
- The development of UN fuel with ~30% U_3Si_2 as the waterproofing agent which provides a five to ten fold increase in thermal conductivity which effectively eliminates centreline melt during transients as an issue

Additional objectives of this next phase of development include the generation of an ATF lead test rod (LTR)/lead test assembly (LTA) project plan for eventual incorporation of these components into an operating plant and activities that support licensing. The ultimate choice made among the various fuel and cladding options will be based on testing carried out in the current phase of ATF development and the results obtained from the next phase, which is to commence in October of 2014.

ACKNOWLEDGEMENTS

This material is based upon work supported by the Department of Energy under Award Number DE NE0000566.

DISCLAIMER

The authors would like to thank the funding agency, the Department of Energy, and the contributing partners in this contract, including General Atomics (GA), Idaho National Laboratory (INL), Massachusetts Institute of Technology (MIT), Texas A&M University (TAMU), Los Alamos National Laboratory (LANL), Edison Welding Institute (EWI), University of Wisconsin (UW), and Southern Nuclear Operating Company (SNC). The authors would also like to acknowledge the contributions from the Collaborative Research on Accident Tolerant Fuels (CARAT), a work group organized by Westinghouse with a focus on ATF research and development.

REFERENCES

[1] RAY, S., JOHNSON, S., LAHODA, E., "Preliminary Assessment of the Performance of SiC Based Accident Tolerant Fuel in Commercial LWR Systems", Paper #8490, Paper presented at 2013 LWR Fuel Performance Meeting, Charlotte, USA, September 15-19, American Nuclear Society, (2013).

[2] RAY, S., LAHODA, E., FRANCESCHINI, F., "Assessment of Different Materials for Meeting the Requirement of Future Fuel Designs", Paper A0115, Paper presented at LWR Fuel Performance Meeting, Manchester, UK, September 2-6, 2012, American Nuclear Society, (2012).

[3] BASU, S., OBANDO, N., GOWDY, A., KARAMAN, I., RADOVIC, M., Long-term Oxidation of Ti_2AlC in Air and Water Vapour at 1000-1300°C Temperature Range, J. Electrochem. Soc. **159** 2 (2012) C90-C96.

[4] HARP, J., LESSING, P.A., BLAIR, H., MAUPIN, J., "Preliminary Investigation of Candidate Materials for Use in Accident Resistant Fuel", Paper #8306, Paper presented at 2013 LWR Fuel Performance Meeting, Charlotte, USA, September 15-19, American Nuclear Society, (2013).

Note: This paper was presented at the IAEA Technical Meeting on Accident Tolerant Fuels. It is published by Westinghouse Electric Company as their report WCAP 9059, Westinghouse Non-Proprietary Class 3.

R&D OF SIC/SIC FUEL PIN AT OASIS, MURORAN INSTITUTE OF TECHNOLOGY

H. KISHIMOTO, A. KOHYAMA, J. S. PARK,
N. NAKAZATO, D. HAYASAKA, Y. ASAKURA
Muroran Institute of Technology
Muroran, Hokkaido
Japan
E-mail: hkishi@mmm.muroran-it.ac.jp

Abstract

The disaster in East-Japan, 2011 made a strong impact on nuclear energy policies all over the world. Accident tolerant fuel related activities have been initiated in these years as domestic programmes as well as international collaborative programmes. Where, the important role of high temperature non-metallic materials has been recognized for giving increased accident tolerance to LWR systems. R & D activities in Japan on SiC fibre reinforced SiC composite had been continued as an important option for nuclear safety. This paper introduces the fabrication technology developments of NITE SiC/SiC composites. Under the new trend toward ATF after the accident in 2011, SiC/SiC related activities have been accelerated under OASIS, Muroran Institute of Technology leadership. The OASIS activities including in MEXT fund based project, named as SCARLET is introduced. The project aims to replace of zircaloy claddings to SiC/SiC based materials.

1. INTRODUCTION

OASIS at Muroran Institute of Technology was launched in 2010. This organization aims to develop materials contributing for energy system and environment improvements. The most important material in OASIS is silicon carbide (SiC). SiC has been researched for long time, and there are many kinds of "SiC" and SiC/SiC composites [1-3]. A main technology of OASIS is "NITE" SiC/SiC composites. The NITE means "Nano-Infiltration & Transient-Eutectic Phase" method which is an applied liquid phase sintering method. The technology has developed in a Japanese programme at Kyoto University, CREST-ACE (Core-research for Evolutional Science and Technology- Advanced material for Conversion of Energy, 1997-2002) project [4]. The NITE method in CREST-ACE project was named as "Original" NITE process. Figure 1 is products of original NITE SiC/SiC composite produced in CREST-ACE programme. The original NITE method is able to produce SiC/SiC composites having following characters:

- Dense and robust structures better than PIP, CVI methods;
- Excellent gas tightness;
- Fairly high thermal conductivity, chemical stability;
- Flexibility in size and shape;
- Applicability of existing net-shaping techniques.

But the products in Figure 1 were actually not engineering products but products of art. The NITE method needed engineering process technologies to stabilize quality of products and establish mass production. OASIS at Muroran Institute of Technology was established to develop the "engineering" process technologies.

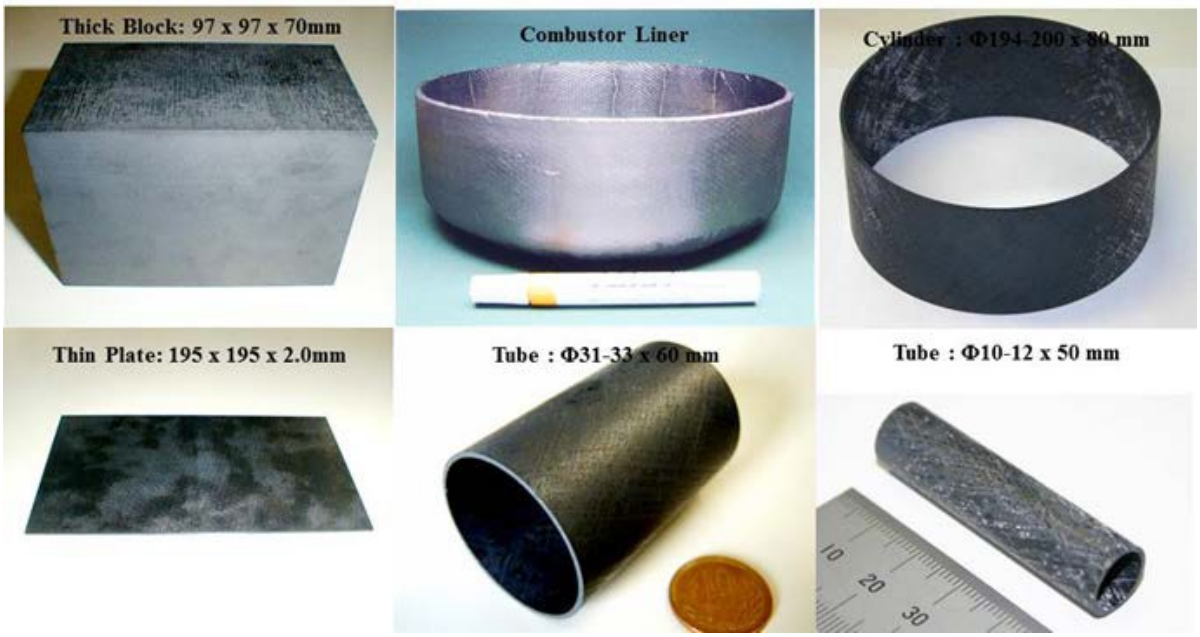

FIG. 1. Products of NITE SiC/SiC products produced by "original" NITE method.

2. OASIS PERSPECTIVE

OASIS discussed the direction of SiC/SiC developments. The original NITE process was summarized as followings.

- It is difficult to control and to stabilize the quality of products because of its wet process;
- Mass production by the process is almost impossible. It takes very long time to make one product;
- Quality of products depends on the technique of workers.

Figure 2 is a schematic image of deference between a metal use and a ceramic composite use. For the metal use, the processing from an ingot to a products progresses step by step. A material supplier normally does not need to know the detail of the last products. But in the case of a ceramic composite, the composite supplier sometime needs to discuss to the customer about the design and properties because the ceramic composites are hardly to be machined, bent, welded, etc. The composite customer needs to perform "near-net shaping" which is to apply a product the nearly final shape and properties which the customer designs. In the case of ceramic composites, especially NITE SiC/SiC composites, it is important whether the product is able to be formed or not. If there is an excellent coupon specimen, it is almost impossible to produce a tube with the same property as the coupon. On the other hand, it is possible to produce a coupon which has almost same property as the tube. Thus, product' fabrication technologies should have the highest priority. Investigations and improvements of properties need to follow it. OASIS determined to progress the developments of fabrication technologies aiming to stabilize the properties of the SiC/SiC and mass-production of them. The new NITE SiC/SiC composite developed at OASIS is named "DEMO" NITE SiC/SiC composites.

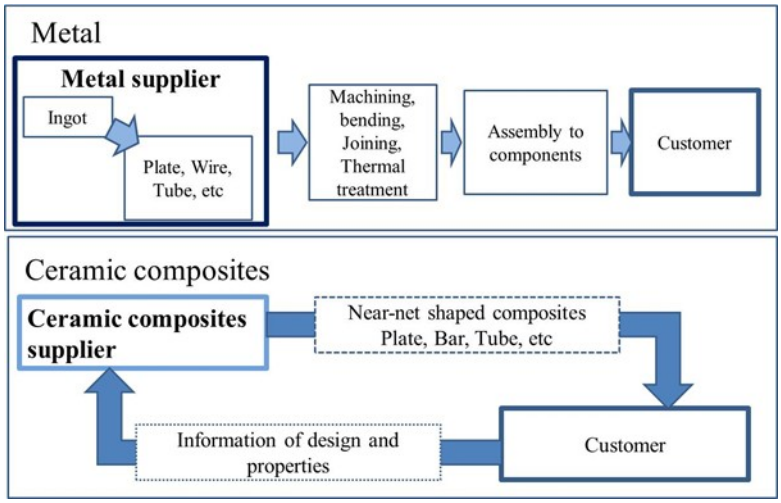

FIG. 2. Image of difference between metal and ceramic composite uses.

3. TECHNOLOGIES OF ORIGINAL NITE AND "DEMO" NITE PROCESSES

Figure 3 shows the process of NITE method. The original NITE process is a wet process using aqua based SiC slurry. SiC fibres are dipped into the slurry and dried to be a pre-preg sheet. The pre-preg sheets are stacked and sintered by hot-pressing. The issue of "original" NITE process is instability of products due to the use of the aqua-based slurry. After dipping and drying, there are many cracks on a pre-preg sheet. The sheet has non-flexibility, not-uniform thickness, unstable shape. It was difficult to fabricate a complex shape preform.

New intermediate SiC materials were necessary to apply complex shape and stabilize properties to a SiC/SiC composite. The slurry was changed from aqua-based one to polymer - based one. The polymer based-slurry is able to form to be a sheet because of its viscosity. A blade system was introduced to OASIS to produce the polymer-based slurry sheets, "SiC green sheets". The SiC green sheet shown in Figure 4 has flexibility and uniform thickness. SiC fibres are added to the green sheets to be a SiC pre-preg sheet. These are able to form tube-shaped, cylinder-shaped, corn-shaped and the other complex shaped preforms. The new intermediate material materials will contribute the automation of process and mass-production. The "DEMO" NITE processes are added in Figure 3. These technologies are defined as generation I of the DEMO NITE method.

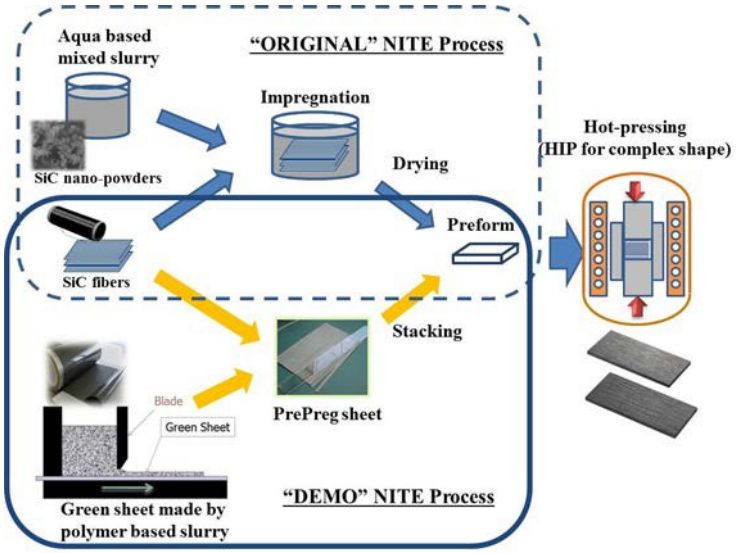

FIG. 3. Processes of NITE methods, "original" and "demo".

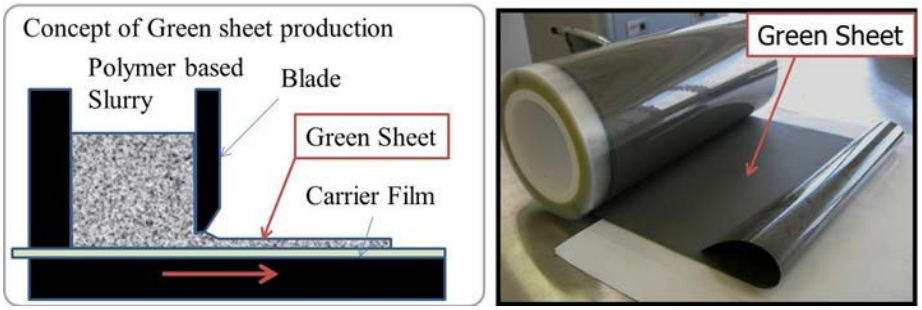

FIG. 4. SIC green sheet for "demo" NITE method.

4. SCARLET PROJECT AND SIC TECHNOLOGIES FOR CORE INTERNALS

The DEMO NITE SiC/SiC composite is not only for nuclear system but the other objectives. But after the severe accident at Fukushima Daiichi No.1 Nuclear Power Plant, SiC has been attracted as an innovative technology to secure the safety of nuclear systems. At Muroran Institute of Technology, a project to establish basic process technologies for SiC/SiC claddings has been launched in 2012. The project named SCARLET is Ministry of Education, Culture, Sports, Science and Technology in Japan (MEXT) fund-based 5 years termed project. The SCARLET is driven by five organizations of Hokkaido University, Tohoku University, Osaka University, JAEA and Muroran Institute of Technology.

There are 4 tasks:

- Fabrication technology development of SiC/SiC cladding tube;
- Assembly technology of SiC/SiC fuel pin;
- Compatibility with coolants and Neutron irradiation effects, and
- Nuclear safety and design were provided to the organizations and these are summarized in Figure 5.

This project mainly focus on cladding fabrications, some new technologies to tube have been developed. An intermediate SiC material was designed which was named "Pre-Composite Ribbon" (PCR). Figure 6 shows schematic images of the PCR production and images of a tube preform fabricated using the PCR. Preforms of Gen. I NITE SiC/SiC

claddings are hand-made, but a semiautomatic filament winding device is used for the fabrication of DEMO NITE SiC/SiC composites in SCARLET project. The use of these new technologies results in the fibre structure interwoven. A preform is densified by Hot Roller Press Form (HRPF) and a warm isostatic pressing (WIP). The HRPF is designed for the densification of preforms of long tube, and these technologies minimize fiber-architecture damages during the sintering process. Because a DEMO NITE SiC/SiC cladding of SCARLET project has interwoven fibre structure, and these technologies results in flexible strength design of a SiC/SiC cladding, the DEMO SiC/SiC claddings of SCARLET project are defined as generation II. Though the technique developments are on-going, basically, the Gen. II DEMO NITE method has better productivity than the Gen. I DEMO NITE method.

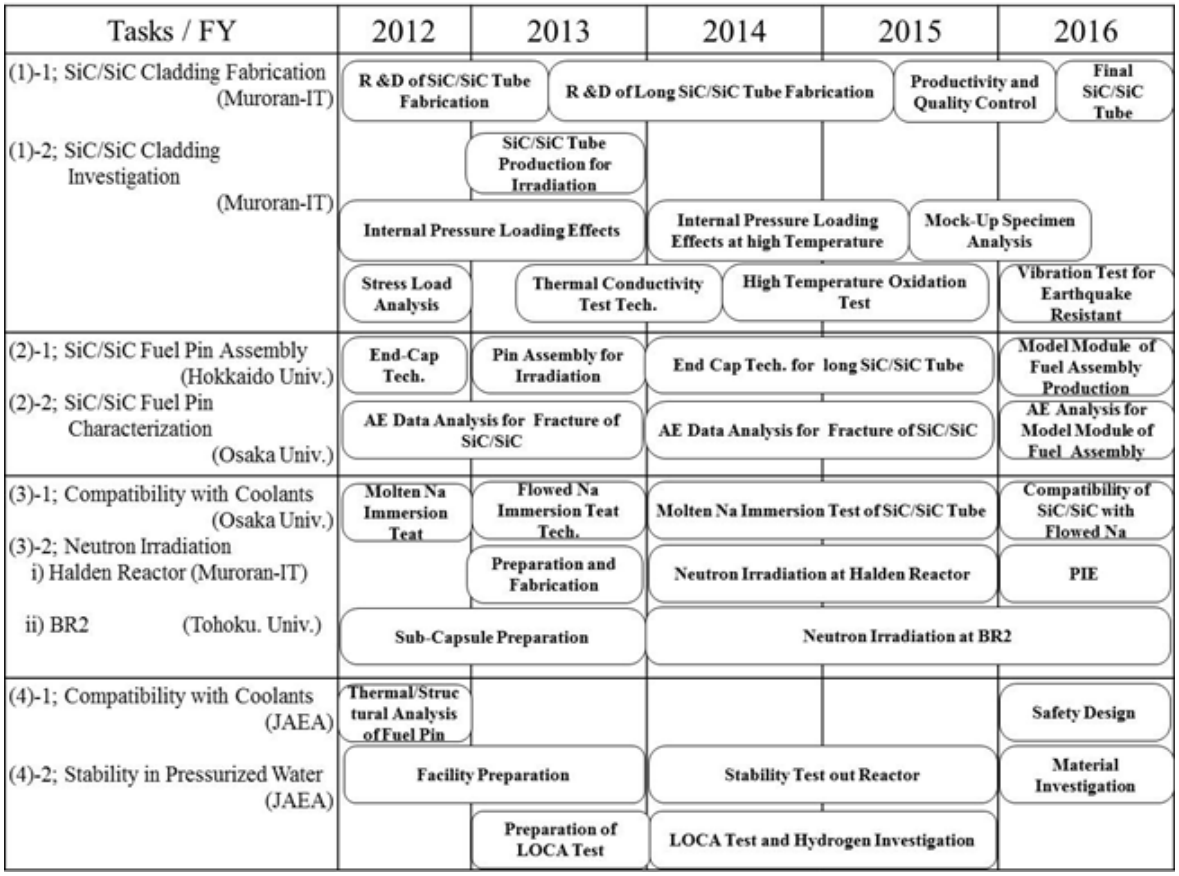

FIG. 5. Schedule of SCARLET project.

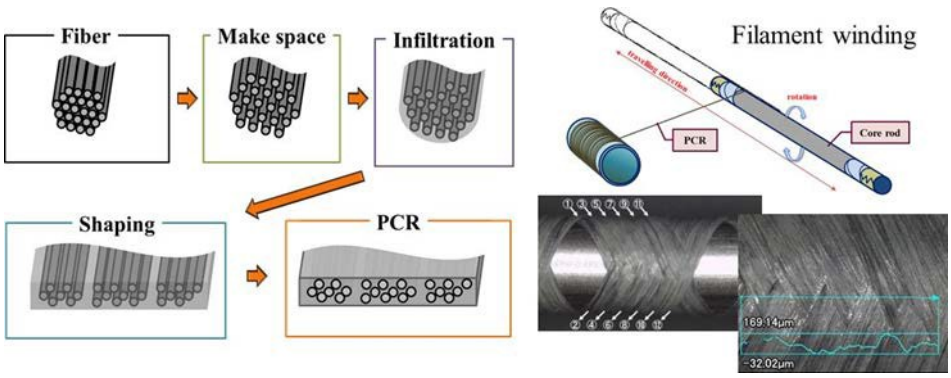

FIG. 6. Concept of PCR and a SiC/SiC preform made by PCR.

5. CURRENT STATUS OF CORE-INTERNALS FABRICATION TECHNOLOGIES AT OASIS

The current Gen I and II NITE SiC/SiC tubes have enough helium gas leak tightness as a cladding tube without metal liners. The claddings passed the helium gas leak tightness for the neutron irradiation experiment at Halden reactor, and the irradiation is planned to start in FY2014 [7]. For this experiment, brazing technologies also developed to connect SiC/SiC with zircaloy tubes. OASIS is able to produce 10-20 NITE SiC/SiC tubes in every one month. Strength and surface modification technology developments are also on-going. A continuous CVD carbon coating system for SiC fibre surface is now in operation. CVD system of SiC is also available. OASIS has several options to modify the environmental properties, and is making effort to establish SiC/SiC core internals.

TABLE 1. SUMMARY OF NITE SIC/SIC FABRICATION METHODS

		Original-NITE (-2002)	DEMO/NITE	
			Gen. I (2009-)	Gen. II (2012-)
PROJECT	Name	CREST-ACE	INSPIRE	SCARLET
	Objective of project	Fundamental study of technology	Radiation effect , Neutronics, FCI	Production technology, Environmental stabilities
NITE- SiC/SiC Cladding Fabrication	Intermediate Materials	Aqua based slurry only	Polymer based slurry, Green and Pre-preg sheets	Polymer based slurry, Pre-composite ribbons (PCR)
	Fabrication method	Hand-made	Hand-made	Semi-automatic filament winder
	Structure	Stack of SiC/SiC pre- preg sheets	Stack of SiC/SiC pre-preg sheets	Interwoven structure.
	Design of fibre structure	Limited	Limited	Flexible
	Helium gas tightness	Excellent	Excellent	Excellent

REFERENCES

[1] SNEAD, L.L., JONES, R.H., KOHYAMA, A., FENICI, P., Status of silicon carbide composites for fusion, J. Nucl. Mater., **233-237** (1996) 26.

[2] STINO, D.P., CAPUTO, A.J., LOWDEN, R.A., Synthesis of fiber-reinforced SiC composites by chemical vapor infiltration, Am. Ceram. Soc., Bulletin, **65** (1986) 347-350.

[3] KOTANI, M., KOHYAMA, A., OKAMURA, K., INOUE, K., Ceramic Engineering and Science Proceeding, **21** (2000) 339.

[4] KATOH, Y., KISHIMOTO H., KOHYAMA, A., J. Nucl. Mater., **307–311** (2002) 1221.

[5] KOHYAMA, A., PARK, J-S., JUNG, H-C., J. Nucl. Mater. **417** (2011) 340.

[6] KOHYAMA, A., KISHIMOTO, H., Nuclear Safety and Simulation, **4** (2013) 72.

[7] KOHYAMA, A., KISHIMOTO, H., PARK, J.S., NAKAZATO, N., HAYASAKA, D., ASAKURA, Y., Irradiation Program of SiC/SiC Fuel Claddings at Halden Reactor", IAEA, Accident Tolerant Fuel Technical Meeting, ORNL, TN, USA, October 13-16, (2014).

IRRADIATION PROGRAMME OF SIC/SIC FUEL CLADDINGS AT HALDEN REACTOR

A. KOHYAMA, H. KISHIMOTO, J. S. PARK,
N. NAKAZATO, D. HAYASAKA, Y. ASAKURA
OASIS, Muroran Institute of Technology Mizumoto-cho
Muroran, Hokkaido
Japan
E-mail: kohyama@mmm.muroran-it.ac.jp

Abstract

This paper introduces on-going Japanese national projects on "Increased Accident Tolerance of Fuel for LWRs", where SiC/SiC R & D is the key activity including reactor irradiation tasks. MEXT fund based project, named as SCARLET (SiC Fuel Cladding/Assembly Research Launching Extra-Safe Technology) and METI fund based projects, named as INSPIRE (Innovative SiC fuel Pin Research) have been launched as 5 year termed projects at OASIS in Muroran Institute of Technology since 2012. INSPIRE is the irradiation project of SiC/SiC fuel claddings aiming to accumulate material, thermal, irradiation effect data of NITE-SiC/SiC in BWR environment. Nuclear fuel inserted SiC/SiC fuel pins are planned to be installed in Halden reactor. The project includes preparing the NITE- SiC/SiC tubes, joining of end caps, preparation of rigs to control the irradiation environment to BWR condition and the instruments to measure the condition of rigs and pins in operation. Also, basic neutron irradiation data will be accumulated by SiC/SiC coupon samples currently under irradiation in BR2. The output from this project presenting the potentiality of NITE-SiC/SiC fuel cladding with the first stage fuel-cladding interaction will become available within three years. SCARLET irradiation test in HBWR under PWR water condition will be started early 2015 providing the environmental stability of SiC/SiC cladding by continuous DEMO NITE process and joint stability with zircaloy endcaps.

1. INTRODUCTION

The East-Japan disaster on March 11, 2011 made big damages all over the systems in East- Japan, which included severe accident of TEPCO Fukushima Daiichi nuclear plants. The disaster made strong impact on European energy policy and the US energy policy. There is a big divergence in two European countries about their responses to the same event. In the UK, policy makers remained firm on their decision to increase nuclear power generation in the near future. Whereas in Germany, the federal government decided to at least temporarily shut down the old generation nuclear reactors. The Japanese government looks like rather close to the UK response and the majority of the Japanese public responds closely to the German [1].

The new Japanese Cabinet Chamber under Prime Minister Abe has approved Strategic Energy Policy on April 11, 2014 [2]. In this new plan, Nuclear Energy is defined one of four base-load power sources and expansion of the Japan-U.S. energy cooperation is emphasized. Commission on Civil Nuclear Cooperation has been launched in order to further enhance cooperative relations between Japan and the U.S. after the TEPCO's Fukushima Daiichi nuclear accident.

Among many government funded programmes on *Increased Accident Tolerance of Fuel for LWRs* the role of advanced high temperature non-metallic materials is becoming more important for the light water reactors to come. As one of the most attractive options for ensuring nuclear reactor safety, SiC fibre reinforced SiC composite has been recognized worldwide. MEXT fund based project, named as SCARLET and METI fund based projects, named as INSPIRE have been launched as 5 year termed projects at OASIS in Muroran Institute of Technology since 2012 [3,4]. These projects aim to replace zircaloy claddings to SiC/SiC based materials.

SiC/SiC R&D for aerospace and nuclear fusion/fission has been accelerated since the Japanese invention of PCS type SiC fibres, by the late Professor S. Yajima of Tohoku University. During these four decades many fabrication processes have been developed.

Among those processes, CVD/CVI based process and NITE process have been recognized to be the potential options for nuclear fusion/fission application [5]. However, SiC/SiC by CVD/CVI process has been recognized to be inherently "leaky" and the necessity of SiC seal coating [6] and the new direction to move to "hybrid" design employing metallic inserts or bladder are being pursued [7].

On the other hand, Nano-powder Infiltration and Transient Eutectic (NITE) process has been intensively developed, starting at Kyoto University [5-8] and now at OASIS, Muroran Institute of Technology. Helium gas permeability of SiC/SiC composite was investigated under the collaboration with Hokkaido University and CEA-Saclay Laboratory, where excellent He gas tightness was reported [9]. Encouraged by these attractive features, SiC/SiC cladding R&D for GFR was carried out from 2002 to 2005, where 200 mm length SiC/SiC cladding with 10 mm inner diameter and 1 mm wall thickness was developed [10] and two years later 0.8 mm wall thickness tube with excellent He gas leak tightness cladding was fabricated and supplied to CEA-Saclay Laboratory. Since the newly establishment of OASIS at Muroran Institute of Technology, March

2009, the original NITE process has been drastically changed from wet aqua slurry system to polymer-based slurry for making green sheets and prepreg sheets as intermediate materials. The advanced SiC/SiC process utilizing those intermediate materials from polymer-based slurry is called as DEMO NITE process [11, 12].

2. INSPIRE PROJECT

INSPIRE project is to establish technological basis and to verify the feasibility of the NITE-method based SiC/SiC fuel claddings and fuelled SiC/SiC fuel pin segment to be used as the replacement of zircaloy fuel pin/assemblies for LWR core component. The goal of the phase 1, 2012 – 2016, is to prepare to go to the next step for Lead Test Rod R&D.

The Important performances of NITE-based SiC/SiC fuel cladding to be confirmed are:

- Compatibility with reactor water and nuclear fuel under PWR condition;
- FP gas leak tightness;
- Stability under Halden reactor irradiation.

Those verifications are using the NITE-based SiC/SiC fuel cladding produced by a large-scale production process at OASIS, Muroran Institute of Technology and Muroran Establishment of IEST Co., Ltd [11].

2.1. INSPIRE Project tasks

2.1.1. Ceramic Fuel Pin Fabrication Modification and Technology Integration

The goal of the fabrication modification is to establish large scale production process of NITE- based SiC/SiC fuel pin with the final goal of 4m length. The verification of the performance should be done with the 1 m length fuel pins. The important technology integration includes design and fabrication of end-cap by zircaloy 2 and welding process establishment with SiC/SiC fuel pin.

2.1.2. Stability of ceramic fuel pin element under BWR condition

To confirm the baseline stability of NITE-based SiC/SiC fuel pin, Halden reactor irradiation in BWR condition water loop with nuclear fuel capsuled fuel pin elements. The current irradiation plan is to finish reactor irradiation by the end of 2015. Based on the results, including PIEs, the modified NITE process and products based on the modified NITE-process will be provided.

2.1.3. Neutron irradiation effects of the NITE-SiC/SiC

To establish engineering database for the design and fabrication of NITE- based SiC/SiC fuel pin, neutron irradiation effect database is essential. This task will provide baseline neutron irradiation effect data from BR2 irradiation and Halden reactor irradiation. Currently, BR2 irradiation had been started and the second irradiation planning is suspended.

The INSPIRE Project was approved as five year termed programme. However the budget situation of METI only allows confirming for the Japanese fiscal year 2013 with the large budget reduction more than 30% from the original plan. The Halden reactor irradiation task is currently under approval only for JFY 2013. Also, under this condition, BR2 irradiation task should be suspended for JFY 2013. The current project plan is shown in Figure 1.

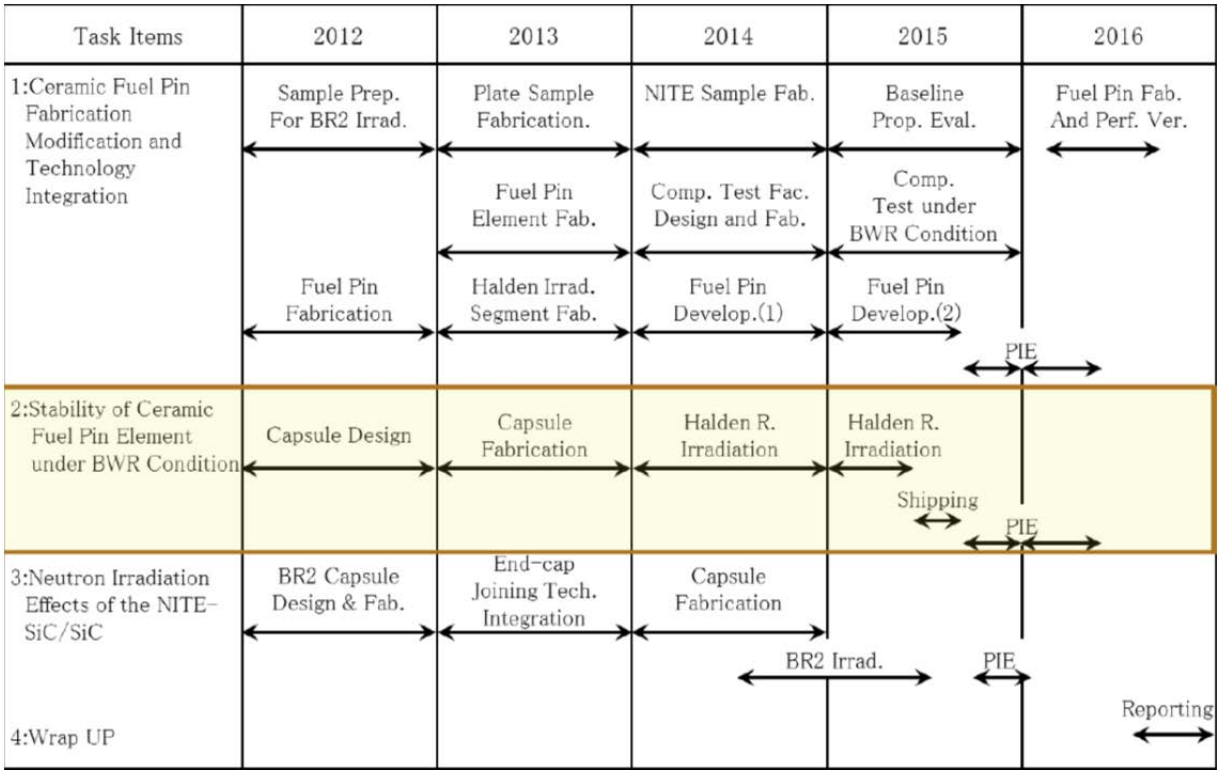

FIG. 1. The current project plan (1 April 2013).

2.2. R&D Target and current status

The INSPIRE project primarily looks for replacing the current zircaloy cladding for LWRs into NITE-SiC/SiC cladding. Thus, the specification is aimed to satisfy ASTM Standard B 353-91, which is for LWR application. Project INSPIRE is targeting to produce 10 mm inner diameter, 1 mm wall thickness and 200 mm long claddings with sufficient gas tightness. The followings are the current targeted value for the NITE-SiC/SiC cladding.

2.2.1. Dimensional accuracy

Diameter: ±0.05mm, Straightness: 1/1200, Wall Thickness: ±10%, Roundness: 1/2000 (accomplished under special machining with order made tool: an example is shown in Fig. 2).

FIG. 2. SiC Cladding with extra-fine machining.

2.2.2. The baseline mechanical properties

Axial Tensile Strength: 300MPa, Hoop Strength: 100 $MPa^{(Comp)}$/300 $MPa^{(Tens.)}$, Fracture at accident: no straight/ crystallographic through thickness fracture (>0.2% Pseudo-plasticity).

2.2.3. Environmental resistance

Out-of-reactor Oxidization test, LOCA simulation test: Better than zircaloy. Neutron Damage Resistance:

- Soundness check up to 10 GWd/t exposure at Halden Reactor under BWR water condition;
- Confirm mechanical property degradation less than 5% at BR2 reactor irradiation.

2.3. The current plan of Halden reactor irradiation

The INSPIRE project primarily looks for replacing the current zircaloy cladding for LWRs into NITE-SiC/SiC. Due to the unclear budget situation of METI toward JFY 2014, Multi-year contract with Halden Reactor Project is suspended and the single year contract is now under final negotiation.

The conceptual planning and design of the irradiation segment and rods has been finished at the end of JFY 2012. The following is the brief summary of the conceptual planning and design activity between INSPIRE project and Halden Reactor Project.

2.3.1. *Test rig to be applied*

The irradiation is to be carried out in a test rig within a pressure flask, cooled by water at BWR thermal- hydraulics and chemical conditions. Some details are shown in Figure 3.

The rig will accommodate 6 test rods, typically 20 cm long, arranged in two clusters, as shown in Figure 4. The rods will be equipped with cladding elongation detector for measuring on-line the amount of pellet-cladding mechanical interaction (PCMI) and cladding permanent growth due to PCMI and neutron irradiation.

2.3.2. *The test rods*

The six rods may contain different variants, such as different cladding. The fuel pellets will be fabricated at the IFE establishment at Kjeller, under agreed specifications. The cladding tube and the end plugs will be provided by the INSPIRE project, which is also to define, in consultation with Halden Reactor Project. The rod inner pressure is atmospheric pressure under current design. The fuel rod assembly, gas filling and end-plug welding will be realized by IFE following further discussions and under agreed specifications. To meet Halden reactor requirements for inserting those test rods into the reactor, preliminary discussions and test fabrication with TIG welding was done by the INSPIRE project. Based on very preliminary investigation, the first conceptual design of the test rod was basically agreed. Figure 4 indicates components to be jointed. For the operation at Halden reactor site for the final insertion of nuclear fuel and shield welding of end cap by EBW facility of Halden, three types of zircaloy elements and a SiC/SiC fuel pin element with fine threading both ends will be fabricated. The element (A) is SiC/SiC fuel pin element with fine threading, element (B) is zircaloy tube with inner threading and elements (C1) and (C2) are zircaloy end cap. The elements (C1) and (C2) are connected by threading to make 6 rods into 3 segments to be inserted irradiation rig, as shown in Figure 3.

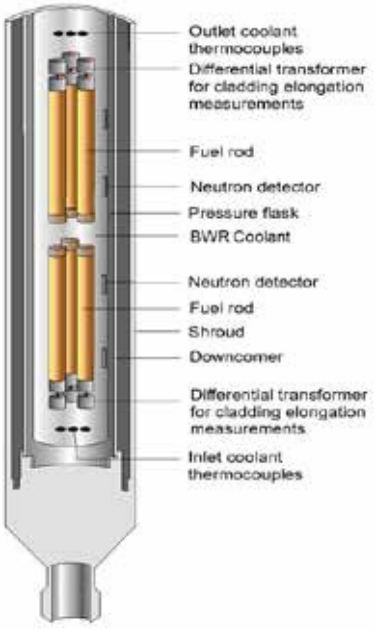

FIG. 3. Conceptual drawing of the test rig.

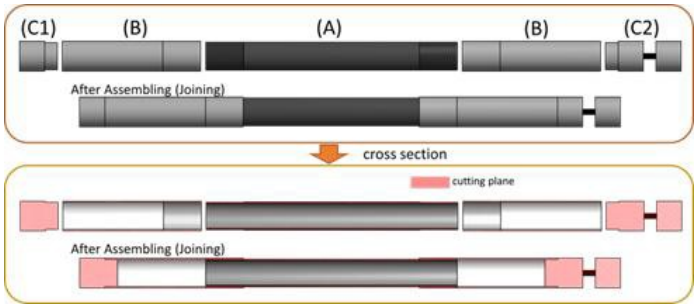

FIG. 4. Concept of the test rod.

2.3.3. In-reactor operation

It is foreseen that the test will be run at power conditions typical for commercial fuel, i.e. 20-25 kW/m at beginning of irradiation and then gradually decreasing. The PCMI and permanent cladding strain will be assessed continuously during the irradiation.

2.4. R&D road map towards the phase-2

Although METI has approved only Phase-1 proposal, the mid-term planning requires the Phase-2 plan with reliable background and supporting R&D structure. Under the preliminary planning with the INSPIRE project members, the Phase-2 road map has been initiated. As is indicated in Figure 5, Phase-1 is to give feasibility of NITE-SiC/SiC fuel cladding contributing the nuclear reactor safety enhancement within a reasonable time scale and with an economical and technological attractiveness.

Phase-1 target is clearly presents the level of the technology *ready to move Lead Test Rod R&D*. For this project, neutron irradiation research activities out of this project, such as MEXT programme for reactor experiment under IMR, Tohoku University and US-Japan Program for Fusion Reactor Materials, should support especially for PIE and database establishment. Fairly a big budget and big industrial support should be required for large scale R & D of fuel cladding to meet power reactor utilization. This should be satisfied for Phase-1 and Phase-2 activities. The aim of Phase-2 is to prepare and complete Lead Test Rod experiments, which will lead to the next step, Lead Test Assembly. By the end of Phase-2, large-scale production industrial infra-structure should be established.

Also the basic concept for reactor safety and efficiency will be adjusted to fully utilize the attractiveness of advanced SiC/SiC fuel cladding and fuel assembly, as well as channel box.

FIG. 5. Phase-2 R&D road map for INSPIRE.

3. SCARLET PROJECT

One of the MEXT funded projects of "Basic Technology Development for Nuclear Safety Innovation" starting from the final quarter of the Japanese fiscal year 2012. Among the Q1 projects, 3 projects are "material oriented", where two projects are on ceramic composite materials. SCARLET project is on "R & D of Basic Fabrication Process Technology of

SiC/SiC Fuel Cladding for Extra- Safe Reactor Core" and is aiming to establish solid-basis of making SiC/SiC Fuel Cladding/Assembly as Japanese Innovation for "Nuclear Safety" and make-a-way to the early realization of the SiC/SiC Fuel Pin Assembly into Nuclear Power Reactors. For this target, the followings are the outputs to be obtained in five years:

- Proof-of-the-reality of SiC/SiC as a replacement of zircaloy Fuel Cladding in a short term;
- Feasibility Demonstration of SiC/SiC Fuel Cladding Sodium Cooling Fast Reactor and GFR;
- Establish large scale production basis of SiC/SiC Fuel Cladding by NITE-Methoda;
- Integrate technologies of making SiC/SiC Fuel Pin and Fabricate Fuel Pin/Reactor Irradiation Capsule with SiC/SiC fuel pin element;
- Evaluate Properties of SiC/SiC Cladding, SiC/SiC Fuel Pin, as long as 1 meter, including environmental tolerance evaluation under light water reactor and LMFBR.

3.1. Task structure

The project task structure and participating organizations are shown in Fig. 6.

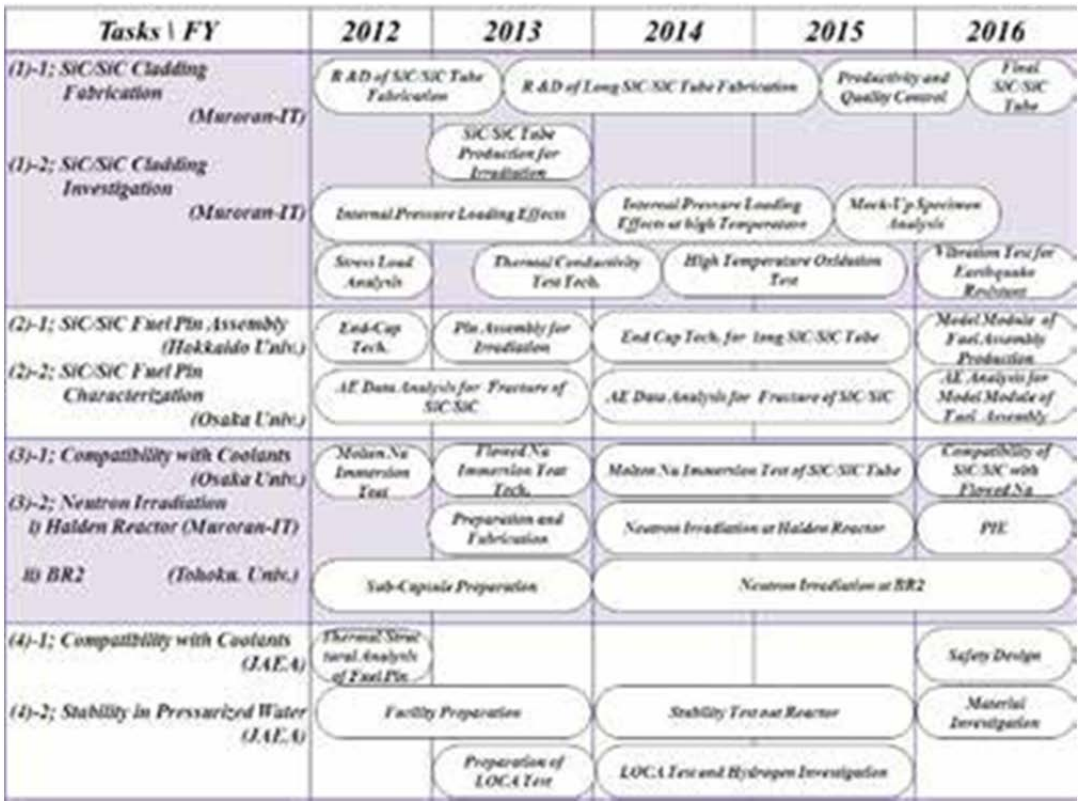

FIG. 6. Schedule and tasks of SCARLET project.

[a] Japan and International patent(PCT/JP01/09365)by A. Kohyama and Y. Katoh

3.1.1. Task 1: SiC/SiC fuel cladding production technology

Task 1 is performed at OASIS in Muroran Institute of Technology. The original NITE method is able to make a good composite, but there were many issues as a mass productive technique. Because the original NITE method was a hand-made technique, the quality control and rapid/mass production of SiC/SiC products were impossible. OASIS in Muroran

Institute of Technology has developed new “Intermediate SiC materials” to solve them. The intermediate SiC materials such as SiC green sheets and SiC/SiC prepreg sheets make the fabrication of composites very easier than before [13]. SiC/SiC preforms are fabricated by these intermediate SiC materials, and sintered in high temperature pressurized environments. For the mass production of SiC/SiC claddings, more special techniques need to be invented. A pre-composite ribbon (PCR) is a kind of a prepreg sheet but having a long and narrow shape as same as a “ribbon”. The other techniques are filament winding and hot roller press forming (HRPF) methods. The outline of recent NITE process is shown in Figure 7. These new techniques are actually special for the making of cladding preforms. The SiC fibres and raw materials of SiC matrix are densely wired and formed to be a tube shape. After the fabrication and densification process, the SiC/SiC preforms are sintered by a hot isostatic pressing (HIP) method. OASIS takes charge of the development of intermediate SiC processing, applying the new technologies for the production of the SiC/SiC claddings and supply materials to the other tasks.

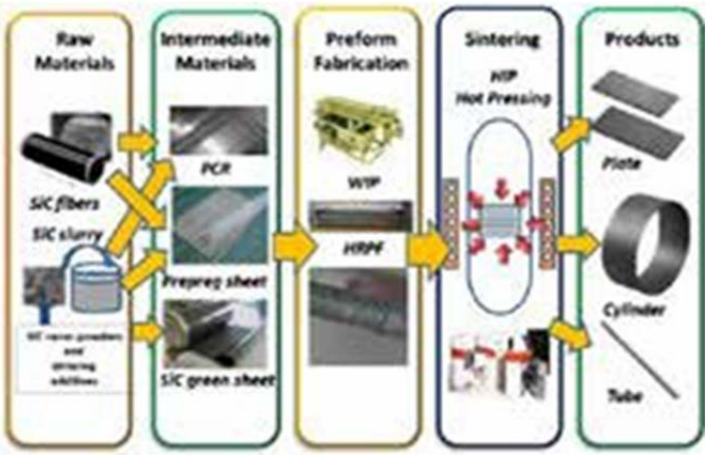

FIG. 7. Outline of NITE process in SCARLET.

3.1.2. Task 2: Assembly technology

Task 2 is for assembly technique developments of SiC/SiC fuel pin. The responsible organization of the task is Hokkaido University. Main subject of the task is to develop the end-plug joint technology. This task includes complex objectives. The highest priority subject is to establish basis of end-plug technologies for long NITE SiC/SiC claddings. Another subject is to assemble mock-up fuel pins as specimens for the neutron irradiation experiments in fission reactors. In this task, basic technology of acoustic emission investigation for NITE SiC/SiC fuel pin assemblies are also developed by Osaka University.

3.1.3. Task 3: Environmental effect evaluation

Task 3 will be performed by two universities, Tohoku University and Osaka University. Tohoku University is in charge of neutron irradiation experiments. The “SCARLET” project is planning to use two fission reactors, Halden reactor in Norway and BR2 in Belgium. In Halden reactor, NITE SiC/SiC tubes without nuclear fuels will be irradiated in a PWR condition. The detail of the experiment will be described later on. Coupon shape NITE SiC/SiC and joint specimens will be irradiated at BR2 to be characterized the irradiation effects on materials. The condition will be 290°C in a helium gas environment. The fluence and dose on SiC in BR2 are estimated to be about 1×10^{24}

n/m^2 and 0.1 dpa, respectively. Task 3 includes coolant and cladding compatibility investigations. The coolant in this task is mainly molten sodium, and this task inspects the capability of NITE SiC/SiC as claddings in LMFBR. The experiments of the subject are performed at Osaka University.

3.1.4. Task 4: Engineering and safety design

Task 4 consists three subjects that applicability investigation of SiC/SiC as cladding for safety design, stability characterization in pressurized high temperature water as same as the PWR conditions, LOCA simulation test. JAEA is in charge of the task 4.

3.1.5. Neutron irradiation test in Halden

The SCARLET project is planning to use fission reactors, both BR2 and Halden reactor. The irradiation of coupon shape materials will be performed at BR2 to investigate irradiation effects for NITE SiC/SiC composite. Additionally, joint specimens aiming to screen the end- cap technique also need to be irradiated because of few irradiation effect data. The irradiation condition will be 290°C in helium gas environment. This environment is convenient to distinguish the irradiation effects because the materialmodification in reactor coolants includes both irradiation and pressurized water effects. The fluence and dose on SiC in BR2 are estimated to be about 1×10^{24} n/m^2 and 0.1 dpa. The first irradiation was finished and the PIE in Japan has been completed in 2013. The second irradiation in BR2 is ready to start and sample insertion into the reactor has been finished. At Halden reactor, the irradiation plan is mainly for NITE SiC/SiC tube and mock-up fuel pin without nuclear fuels. Figure 8 shows schematic image of a rig and rods for the irradiation experiment in Halden reactor. The neutron irradiation will be performed under PWR water condition. 6 rods will be settled in the rig, where 3 rods are standard fuel rod for strengthening neutron flax for the SiC/SiC specimen rods. 3 SiC/SiC cladding rods are segmented with 5 segments in one rod. SiC/SiC tube segments without fuels containing collapsible bellows for failure detection off-line. For this purpose the SiC/SiC segments were attached zircaloy tubes both ends and end caps of zircaloy are used to seal the segments. The rig will be set in the PWR loop of Halden reactor and the irradiation is planned to be performed in two Halden reactor cycles of 80 - 100 full power days. The irradiation environment will be at 290 °C in 15.5 MPa pressurized water. The fluence and dose for SiC/SiC are roughly estimated to be $3.4\text{-}4.3\times10^{24}$ n/m^2 and 0.3-0.4 dpa, respectively. SiC/SiC segments have been delivered to Halden on September 3rd, 2014 and the preparation for the irradiation to be started by March 2015 will be initiated.

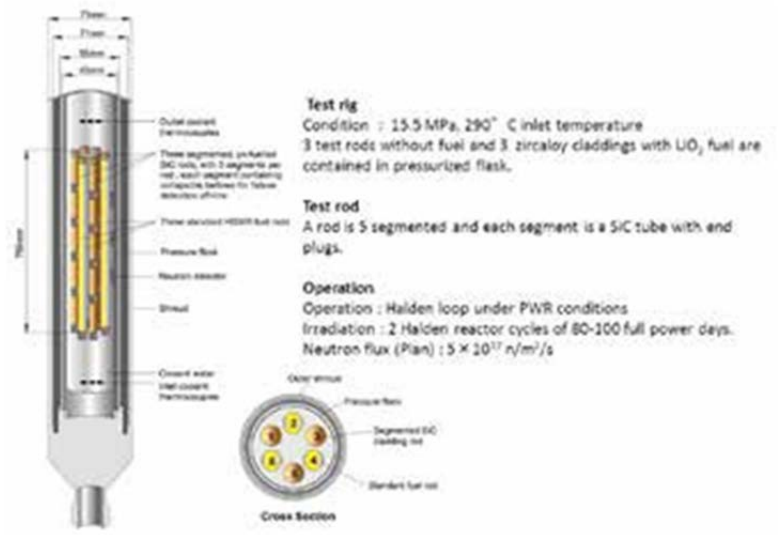

FIG. 8. Neutron irradiation plan at Halden reactor.

4. CONCLUSIONS

The new METI funded project, INSPIRE, where SiC/SiC Fuel cladding R & D for enhancing nuclear energy safety by new NITE method is on-going as five year termed project. Also new MEXT funded project, SCARLET is emphasizing the large scale R & D for early utilization of SIC/SiC fuel cladding as the replacement to zircaloy fuel cladding.

The goal of INSPIRE project is to provide soundness of the SiC/SiC claddings by the current NITE method before and after reactor irradiation in Halden Reactor. The current engineering design activity is provided. To satisfy the design requirements, OASIS is accelerating its effort for making high performance SiC/SiC cladding tubes, as well as integrating joining technologies to fabricate SiC/SiC rods, nuclear fuelled by the end of Japanese fiscal year 2014.

The INSPIRE project may make a way to an early realization of SiC/SiC fuel pin/assembly into LWRs ensuring reactor safe technology in a realistic and economical way.

The MEXT funded SCARLET project is also aiming to replace zircaloy fuel claddings with SiC/SiC based materials by innovative NITE-method under development, where new key process technologies toward industrialized fabrication have been invented. This project includes 1 m length SiC/SiC cladding mock-up fabrication, assembly techniques of fuel pins and characterization including material properties, compatibility with coolants, and neutron irradiation effects in fission reactors. R and D of the SiC/SiC cladding fabrication process technologies. Representing new technologies such as SiC green sheet, SiC prepreg sheet, PCR, WIP and HRPF are applying to the fabrication of the claddings. Current status of the cladding fabrication is that 50 mm SiC/SiC cladding and 50 cm SiC/SiC preform are successfully fabricated.

ACKNOWLEDGEMENT

SCARLET programme is supported by the Ministry of Education, Culture, Sports, Science and Technology of Japan (MEXT) and INSPIRE projects is supported by the Ministry of Economy, Trade and Industry of Japan (METI). Those strong financial supports

and energy strategic and scientific guides are appreciated. The colleagues in OASIS and other institutes and organizations are also acknowledged.

REFERENCES

[1] WITTENBEN, B.B.F., The Impact of the Fukushima Nuclear Accident on European Energy Policy, J. Environmental Sci. Policy, **15** (2012) 1-3.

[2] MINISTRY OF ECONOMY, TRADE AND INDUSTRY OF JAPAN (METI), Strategic Energy Plan, Japan, April, 2014.

[3] KOHYAMA, A., "INSPIRE" Project for R & D of SiC/SiC Fuel Cladding by NITE Method, Ceramic Transactions, **246 (**2014) 99-108.

[4] KOHYAMA, A., KISHIMOTO, H., KOHNO, Y., "SCARLET" Project for R & D of SiC/SiC fuel cladding by NITE method", 10th Pacific Rim Conference on Ceramic and Glass Technology, 1-7 June, (2013).

[5] Advanced SiC/SiC Ceramic Composites, Editors KOHYAMA, A., SINGH, M., LIN, H.T. and KATOH, Y., Ceramics Transactions vol.1**44** American Ceramic Society (2002).

[6] JONES, R. H., "Fusion Reactor Materials", Semi-annual Progress Report for Period Ending September 30, 1991, DOE/ER-0313/11, pp.304-308. (1991).

[7] YANG, J. H. "SiC", Second Meeting of the Expert Group on Accident Tolerant Fuels for Light Water Reactors, OECD/NEA Paris, 23-25 Sept. (2014).

[8] KOHYAMA, A., KOTANI, K., KATOH, Y., NAKAYASU, T., SATO, M., YAMAMURA, Y., OKAMURA, K., J. Nucl. Mater. **565** (2000) 283–287.

[9] HINO, T., HAYASHISHITA, E., YAMAUCHI, Y., HASHIBA, M., HIROHATA, Y, KOHYAMA, A., Fusion Engineering and Design, **73** (2005) 51-56.

[10] KOHYAMA, A., HINOKI, T., PARK, J.S., KISHIMOTO, H., "Advanced GFR utilizing NITE-SiC/SiC Shield Fuel Pin", Proceedings of the 2006 International Congress on Advanced in Nuclear Power Plants – ICAPP06, p. 2149-2156 (2006).

[11] KOHYAMA, A., KOHNO, Y., KISHIMOTO, H., PARK, J. S., JUNG, H. C., "Industrialization of advanced SiC/SiC Composites and SiC Based Composites; Intensive Activities at Muroran Institute of Technology under OASIS", Proceedings of ICC3 (2010).

[12] PARK, J.S., NAKAZATO, N., NISHIMURA, H., HAYASAKA, D., KISHIMOTO, H., KOHYAMA, A., to be presented at NUMAT 2014, Clear Water, U.S.A. (2014).

EFFECT OF CONSTITUENTS OF SILICON CARBIDE COMPOSITES ON OXIDATION BEHAVIOUR

T. HINOKI[*], M-H. LEE[*], F. KANO[**], Y. KAWAHARADA[**]
[*]Institute of Advanced Energy, Kyoto University,
Gokasho, Uji, Kyoto
[**]Power and Industrial Systems Research and Development Centre
Toshiba Corporation, Isogo-ku, Yokohama, Kanagawa
Japan
E-mail: hinoki@iae.kyoto-u.ac.jp

Abstract

Silicon carbide (SiC) composites consist with SiC fibers, SiC matrix and fiber/matrix interphase. SiC composites and monolithic SiC ceramics which are the reference materials for the SiC composite matrices were exposed in air or steam environment up to 1400 °C. Significant degradation was observed for the composites with C interphase after exposure in air or steam. Oxidation behaviour was also affected by impurities in SiC.

1. INTRODUCTION

Silicon carbide (SiC) is very attractive engineering ceramics in particular for high temperature use and nuclear application. Superior stability of SiC under high temperature steam to that of metal is critical motivation for light water reactor application [1]. Silicon carbide composites have pseudo ductile fracture behavior by debonding and sliding at fiber/matrix interphase. However carbon (C) as fiber/matrix interphase is the weakest link for severe environments including oxidation by steam. And SiC composites have pores and impurities depending on fabrication methods and conditions. The objective is to understand effect of constituents of SiC composites on oxidation behavior and to develop the oxidation resistant SiC composites.

2. EXPERIMENTAL

The SiC composites were prepared including chemical vapor infiltration (CVI) composites (Rolls-Royce plc), nano-infiltration and transient eutectic phase (NITE) composites (Institute of Energy Science and Technology) in which matrix was formed based on liquid phase sintering (LPS) [2] and LPS-based porous SiC composites (Kyoto University) [3]. The CVI composites and the NITE composites had C interphases. The NITE composites and the porous composites had remained sintering additives (Al_2O_3 and Y_2O_3). The porous composites had extra pores within matrix. Monolithic SiC ceramics were prepared as reference materials for SiC matrices in SiC composites. The high purity chemical vapor deposition (CVD) SiC (Dow Chemical Company) was prepared as the reference material for CVI composites. The LPS SiC ceramics were fabricated with 3~12 wt% of sintering additives (Al_2O_3 and Y_2O_3) as the reference materials for LPS-based composites.

The materials were exposed in air (1100°C, 10 h) or 100% steam (1200°C or 1400°C, 72 h). Mechanical properties were characterized by tensile test or flexural test. Microstructure was observed by FE-SEM.

3. RESULTS

Microstructures of exposed surfaces of monolithic SiC ceramics following high temperature steam experiments are summarized in Figs. 1 and 2. The SiO_2 scales were formed in all materials following 1200 °C steam exposure and no significant effect of impurities were observed. Complicated changes of microstructure were observed at the surface in LPS SiC

ceramics following 1400°C steam exposure, although no significant change was observed in CVD SiC. It was observed that remained Al_2O_3 and Y_2O_3 close to surface moved to surfaces and concentrated according to EDS analysis. The thickness of the complicated layers including Al_2O_3 and Y_2O_3 depended on the amount of sintering additives used for LPS SiC.

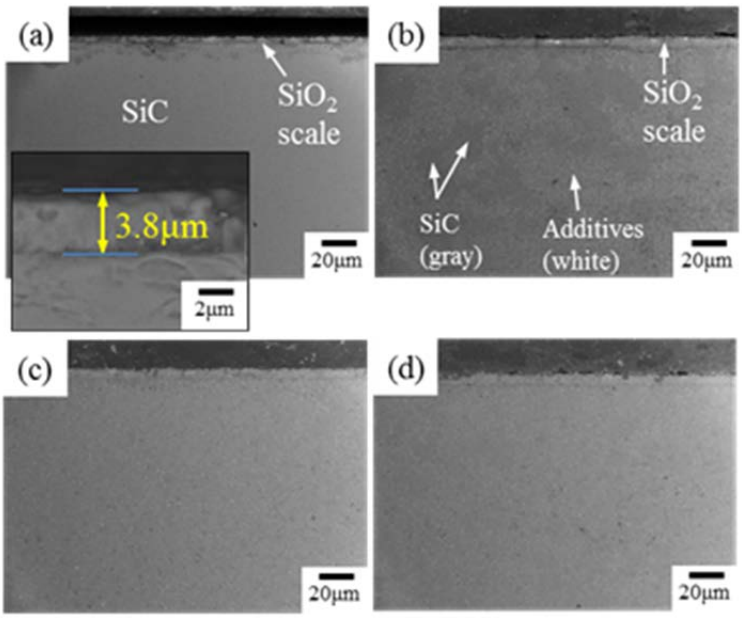

FIG. 1. SEM images of various monolithic SiC ceramics following 1200°C steam exposure ((a) CVD SiC, (b) LPS SiC with 12 w% sintering additives, (c) LPS SiC with 6 w% sintering additives, (d) LPS SiC with 3 w% sintering additives).

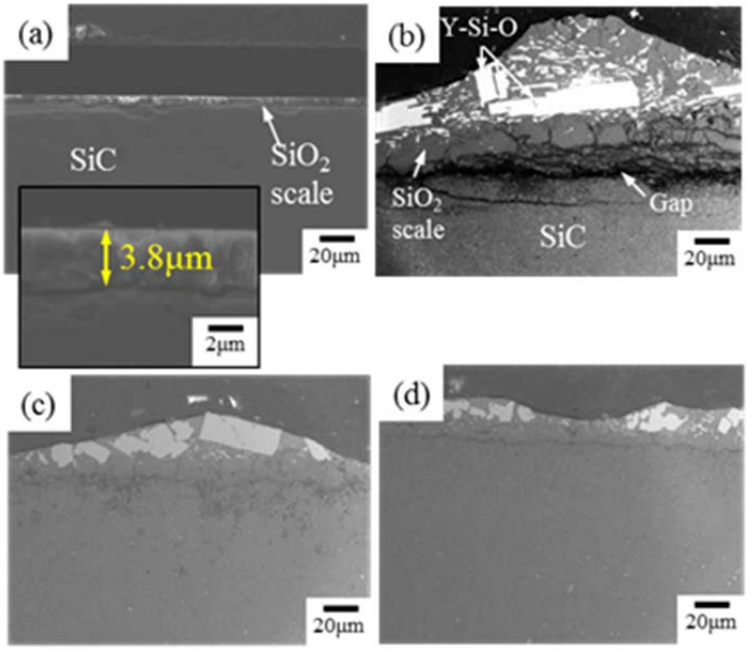

FIG. 2. SEM images of various monolithic SiC ceramics following 1400°C steam exposure ((a) CVD SiC, (b) LPS SiC with 12 w% sintering additives, (c) LPS SiC with 6 w% sintering additives, (d) LPS SiC with 3 w% sintering additives).

The NITE composites and zircaloy-2 as a reference material were also exposed in the high temperature steam. The zircaloy-2 deformed following 1200°C and 1400°C steam exposure. The NITE composites also deformed significantly following 1200 °C steam exposure as shown in Fig. 3, although they kept their shape following 1400°C steam exposure. Significant oxidation was observed within the NITE composites following 1200°C steam exposure, although the significant oxidation within the composites seemed to be prevented by thick surface oxide layer following 1400°C steam exposure as shown in Fig. 4.

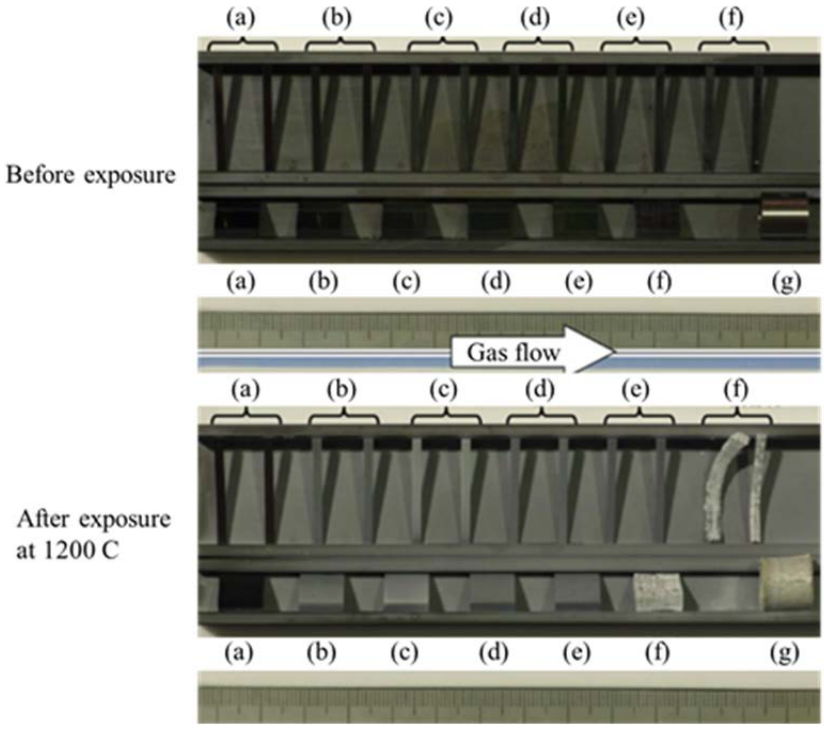

FIG. 3. Appearance of specimens before and after 1200°C steam exposure ((a) CVD SiC, (b) LPS SiC with 6 w% sintering additives, (c) LPS SiC with 12 w% sintering additives, (d) LPS SiC with 6 w% sintering additives, (e) LPS SiC with 3 w% sintering additives, (f) NITE composites, (g) zircaloy-2).

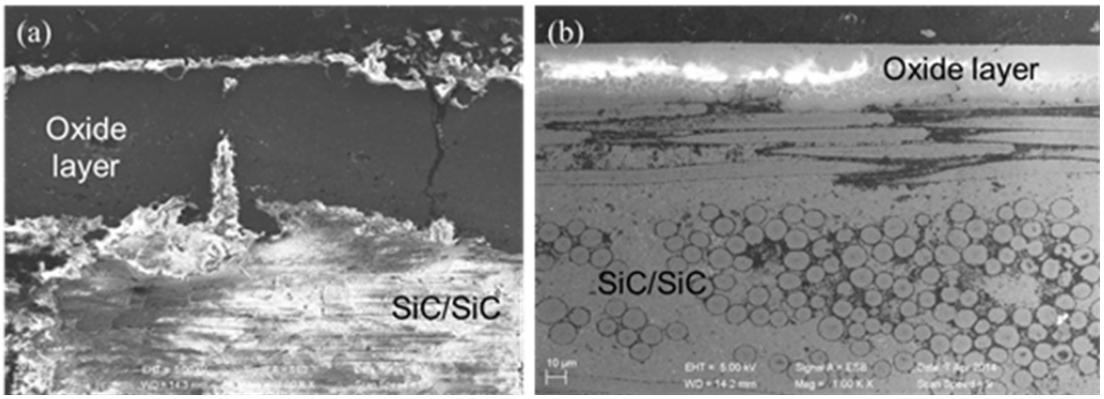

FIG. 4. SEM images of the NITE composites following (a) 1200°C steam exposure and (b) 1400°C steam exposure.

In the case of the CVI composites, approximately 30 % of strength decreased with pseudo-ductile fracture behavior following 1100°C air exposure. No significant change of strength was observed in the case of the LPS-based porous SiC composites following 1100°C air exposure.

4. DISCUSSION

Steam oxidation behavior of monolithic SiC ceramics was affected by the amount of impurities in particular at 1400°C steam exposure. However the monolithic SiC ceramics even with relatively large amount of impurities had still advantage compared with the zircaloy in terms of high temperature steam oxidation.

Silicon carbide composites consist with SiC fibers, SiC matrix and fiber/matrix interphase like the C phase. Oxidation behavior of SiC composites was different from that of monolithic SiC ceramics. Apparently, the C interphase is the weakest link for oxidation. The C interphase and large amount of the impurities in matrix enhanced oxidation within the whole material in the NITE composites following 1200°C steam exposure. Oxidation of SiC matrix with large amount of the impurities occurred rapidly following 1400°C steam exposure in the NITE composites. The rapid oxidation prevented oxidation within the composites. The oxidation rate is the important factor for the composites and the rapid oxidation is preferred to protect the further oxidation. The low temperature in which SiC oxidation rate is low and C is sufficiently oxidized isn't preferred to the high temperature in which SiC oxidation rate is high for the SiC composites with C interphase. The environmental coating including SiC over coating is required for the SiC composites with C interphase. Mechanical properties of the LPS-based porous SiC composites were basically stable following oxidation, as they didn't have the C interphase. However the composites require hermetic coating or metallic liner to keep fission product gas at normal condition.

5. CONCLUSION

The SiO_2 formation was observed for both CVD SiC and LPS SiC following high temperature steam oxidation at 1200°C and 1400°C. Remained Al_2O_3 and Y_2O_3 at grain boundary was the significant link for steam oxidation in LPS SiC.

Oxidation behavior of SiC composites was affected by carbon interphase and the impurities. Significant oxidation was observed in particular at relatively lower temperature in the NITE composites. More strength is retained at higher temperature due to rapid and thick SiO_2 formation on surface. Conventional SiC composites have C interphase and environmental coating is required considering oxidation behavior. Porous SiC composites don't have C interphase and have excellent oxidation resistance, although hermetic coating or metallic liner is required for normal operation.

ACKNOWLEDGEMENT

This work was performed under contract with Toshiba Corporation in "Research and Development of Innovative Technologies for Nuclear Reactor Core Material with Enhanced Safety" entrusted to Toshiba by the Ministry of Education, Culture, Sports, Science and Technology of Japan (MEXT).

REFERENCES

[1] Johnson, S.C., Henry, R.E., Paik, C.Y., Severe Accident Modeling of a PWR Core with Different Cladding Materials, Proceedings of ICAPP '12 (2012) 12175.

[2] Hinoki, T. and Kohyama, A., Current Status of SiC/SiC Composites for Nuclear Applications, Annales de Chimie Science des Matériaux, **30** [6] (2005) 659-71.

[3] Hinoki, T. and Shimoda, K., Proc. TopFuel 2013, Charlotte, North Carolina, September 15-19, 2013, (2013) 1060-62.

MECHANICAL PROPERTY OF TRIPLEX SIC COMPOSITE TUBES AND CORROSION OF CVD SIC IN PWR-SIMULATING WATER

W.-J. KIM, D. KIM, J.Y. PARK
Korea Atomic Energy Research Institute, Daejeon
Republic of Korea
E-mail: weonjkim@kaeri.re.kr

Abstract

Through the development and demonstration of advanced SiC_f/SiC composites with a superior neutron irradiation tolerance, the composites have attracted potential applications for advanced fission and fusion reactors. Recently, there are also growing efforts on applying the SiC_f/SiC composites to the light water reactor (LWR) fuel cladding and a guide tube to increase the accident tolerance of nuclear fuels under severe accident conditions. In this study, we evaluated the corrosion behaviour of CVD SiC under a PWR-simulating water condition and the hoop strength of triplex SiC composite tubes. To simulate the PWR primary water conditions, corrosion tests were carried out in deoxygenated, pressurized water at 360°C with a control of dissolved hydrogen. The dissolved hydrogen dramatically reduced the corrosion rate of SiC compared with the water condition without the dissolved hydrogen. It was revealed that the dissolution of the surface oxide of SiC primarily contributed to the weight loss at the initial stage of corrosion. Further weight loss hardly occurred for up to 120 days because the dissolved hydrogen effectively retarded the formation of SiO_2. The hoop stress of the composite tubes tended to be proportional to the volume fraction of the reinforced fibers. The highest fibre volume fraction was obtained using a Tyranno SA3-0.8k with dense winding patterns such as bamboo-like mosaic patterns, which resulted in the highest hoop stress. The hoop stress increased slightly as the winding angle increased from 45 to 65. The fracture behaviour of the SiC triplex tube was also investigated through observations of the microstructure of the failed samples.

1. INTRODUCTION

Silicon carbide (SiC) ceramics and their composites have been considered as structural materials for high temperature applications such as parts of engines and aerospace vehicles because they have high chemical stability, superior high-temperature strength, a low thermal expansion, high thermal shock resistance, and so on [1, 2]. They also have attractive properties regarding nuclear applications, including a low neutron absorption cross-section, low induced activation, and high resistance to neutron irradiation. Therefore, it has been considered for use as reactor core materials, such as for a constituent coating layer of TRISO fuel particles and control rod sheath as a form of the composite in very high temperature gas-cooled reactors, and blanket structural materials and flow channel inserts in nuclear fusion reactors [3-7].

In recent years, there have been growing efforts to apply SiC ceramics as an accident tolerant nuclear fuel cladding and guide tube for pressurized water reactors (PWRs) [8, 9]. One of the SiC cladding concepts has a form of triplex composite tube, consisting of a chemically vapour deposited (CVD) SiC inner layer, SiC_f/SiC composite layer, and another CVD SiC outer layer for corrosion protection [10, 11]. SiC ceramics show an outstanding oxidation resistance and a low hydrogen liberation rate in hot steam compared with the current Zr alloys, which promise larger safety margins under severe accident conditions of PWRs [12-14]. Moreover, its high temperature strength and stability under high neutron doses also provide high burn-up capability [8].

In order to use SiC as a nuclear fuel cladding, there are some critical issues such as the fabrication of thin-walled long tubes, the hermetic joining of end-cap seals, capability of fission products retention, and corrosion under the normal operating condition of PWRs [11, 15-17]. Several results have been reported with regard to the dissolution phenomena of SiC ceramics in high-temperature and high-pressure water [18-23]. The dissolution phenomena of SiC in hydrothermal water reported in the previous studies are problematic for the application of SiC to PWR fuel claddings. However, one should consider that the PWR coolant water

contains some amounts of dissolved hydrogen about 25 to 50 cc H_2 / kg H_2O. Until now, the effect of dissolved hydrogen on the corrosion behaviour of SiC has not been elucidated. Therefore, in this study, we investigated the effect of dissolved hydrogen on the corrosion behaviour of CVD SiC, analogous to the outermost environmental barrier coating of the triplex composite tube, under simulated PWR primary water condition. In addition, the SiC triplex tubes which consisted of a monolith SiC inner layer, a SiC/PyC/SiC composite intermediate layer and a monolith SiC outer layer were fabricated by the chemical vapour processes such as CVD and CVI. Influences of filament winding methods, type of SiC fibres on hoop stress of the triplex tubes were investigated. The damage process during the hoop tests were examined via microstructure observation.

2. EXPERIMETAL PROCEDURE

2.1. Evaluation of corrosion behaviour of CVD SiC

Commercial CVD β-SiC (99.9995%, Morgan Technical Ceramics, Hudson, NH) was used for the corrosion tests. Plate specimens with a dimension of 10×10×3 mm^3 were machined and mechanically polished using a diamond disk of grit 800. Corrosion tests were carried out for up to 120 days using a simulated PWR water loop in which water was deoxygenated and pressurized at 360°C under 20 MPa. To simulate the PWR primary water chemistry, the dissolved oxygen and the dissolved hydrogen were maintained to be below 5 ppb and at approximately 2.7 ppm (35 cc/kg H_2O), respectively. Deionized water was treated at pH 6.4 with 2.2 ppm LiOH and 1200 ppm H_3BO_3, as listed in Table 1. Our previous experiments performed without the control of dissolved hydrogen had a minor difference in pressure and pH from the water condition in this study as shown in the Table 1. The weight change after each test duration was averaged from three specimens measured using an electronic balance with an accuracy of 0.01 mg.

TABLE 1. CORROSION TEST CONDITIONS OF CVD β-SiC

	Temp. (°C)	Pressure (MPa)	DO (ppb)	DH (ppm)	pH at RT	$LiOH/H_3BO_3$ (ppm)
PWR-simulating loop (without DH control)	360	18.5	< 5	-	6.8	2.2/650
PWR-simulating loop (with DH control)	360	20	< 5	~ 2.7	6.3 – 6.5	2.2/1200

The surface microstructure before and after the corrosion test was analyzed using a scanning electron microscope (SEM). The surface roughness was measured using an atomic force microscope (AFM). Any phase formation on the surface after the corrosion test was characterized using a glancing-angle X-ray diffractometry (GAXRD). The angle of the incident X-ray was fixed at 2 to reduce the penetration depth of the X-ray. The chemical composition of the surface was analyzed using an X-ray photoelectron spectroscopy (XPS) to identify any chemistry change on the surface of the corroded specimens.

2.2. Fabrication and hoop stress test of SiC composite tubes

A monolith SiC inner layer was uniformly deposited with 320.3±6.4 μm by a chemical vapour deposition method using methyltricholorosilane (MTS, CH_3SiCl_3) onto the high purity graphite rods with 8.5 mm in diameter and a length of 100 mm. Then the SiC fibres were applied to a SiC-coated cylindrical mandrel by a filament winding method. SiC fibre bundles (tows) consisting of 500 to 1600 fibres were provided on a spool under a little tension which

was generated only by the friction of the fibre supplying system. Helical layers of 1 – 2 fly covered the mandrel. The properties of SiC fibres are listed in Table 2. The commercial generation III SiC fibres such as Tyranno SA3 and Hi-Nicalon Type S were used in this study. They contain a small amount of impurities and they are crystallized and near-stoichiometric, so called nuclear grade SiC fibers.

TABLE 2. PROPERTIES OF SiC FIBRES USED IN THIS STUDY

SiC fibre	Compositions (wt%)	Filament dia. (μm)	Filaments /yarn	Tensile strength (GPa)	Tensile modulus (GPa)	Ply No.
Tyranno SA3-0.8k	68Si+32C+0.6Al	7.5	800	2.1	395	2
Tyranno SA3-1.6k	68Si+32C+0.6Al	7.5	1600	2.1	395	1
Hi-Nicalon Type S	69Si+31C+0.2O	12	500	2.6	420	1

A fibre volume fraction was controlled by changing the band width of each fibre. For helical winding it is usual to lay fibres side by side, to give complete coverage as the winding progresses. Because of the difference in band width, the reciprocating motions of a transverse carriage for the complete coverage were varied from 12 to 21 times, which results in the change in fibre volume fraction and corresponding thickness of the composite intermediate layer. As the input value of the band width is smaller than the actual value, accordingly the pattern is open which results in the less fibre volume fraction. The winding pattern was controlled by adjusting the position of second fibre trajectory. Figure 1 shows four phase winding patterns wound with the winding angle of ±55° using Tyranno SA3-0.8k. Winding angles were varied to ±45, ±55, and ±65° using Tyranno SA3-0.8k with the 1-return winding pattern.

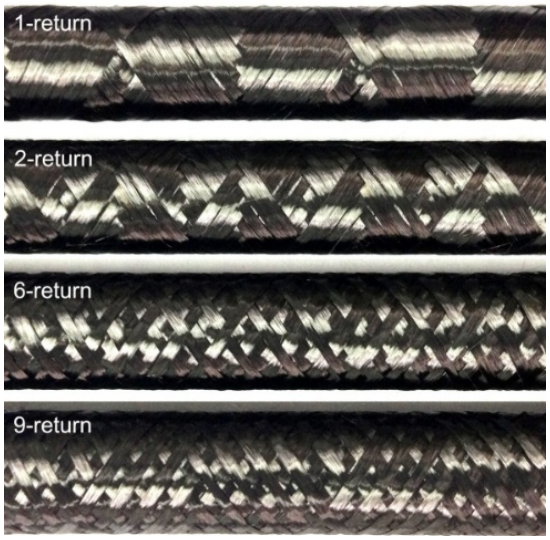

FIG. 1. Four phase winding patterns wound by a helical filament winding method using Tyranno SA3-800 with the winding angle of ±55°.

After the filament winding, PyC was deposited as an interphase of the SiC_f/SiC composite onto SiC fibres by dehydrogenation of CH_4 using by a CVD method. For the infiltration of SiC matrix phase, the isothermal CVI was processed at 1000°C at the low pressure of 3.3 kPa to reduce density gradient to the radial direction of the tubular specimens.

Finally a SiC outer layer was deposited by a CVI method with the same conditions to the matrix infiltration in sequent. The SiC outer layer exhibited the wide thick variation of 39.8±18.6 μm.

After removal of graphite mandrel, the polyurethane plug with 8.45 mm in diameter and a length of 22 mm was inserted into the tubular specimen. Hoop stress of the tubular specimens with dimension of a length of 30 mm, an inner diameter of 8.5 mm, and an outer diameter of 9.6 - 10.1 mm was measured via internal pressurization at room temperature using screw driven universal testing machine (Instron 4465, load cell capacity = 5 kN). Axial pressure was applied with loading rate of 0.01 mm/s to the cylindrical polyurethane plug. A series of hoop tests were carried out at room temperature and each test was repeated 2 to 4 times. Radial displacement measurements were made by attaching four displacement transducers (Kyowa, Co. Ltd) to the central section of the outer tube surface. Hoop stress of tubular SiC composite specimens, σ_θ was calculated by the following equation [24],

$$\sigma_\theta = \frac{r_i^2 P}{r_o^2 - r_i^2}\left(1 + \frac{r_o^2}{r_i^2}\right)$$

where P is the internal pressure, r_i and r_o are the inner and outer radii of the tubular specimens, respectively. Contact stress was typically 50 to 100 N which was determined at the increasing point of radial displacement.

3. RESULTS AND DISCUSSION

3.1. Corrosion behaviour of CVD SiC in PWR-simulating water

Figure 2 shows the weight change of the as-polished CVD SiC after corrosion tests in 360°C deoxygenated water with the dissolved hydrogen content of 2.7 ppm. The corrosion data of CVD SiC obtained without the control of dissolved hydrogen are also included in Fig. 2(a) for the purpose of comparison. Figure 2(b) is a detailed plot on the corrosion data obtained under the dissolved hydrogen-controlled condition in Fig. 2(a).

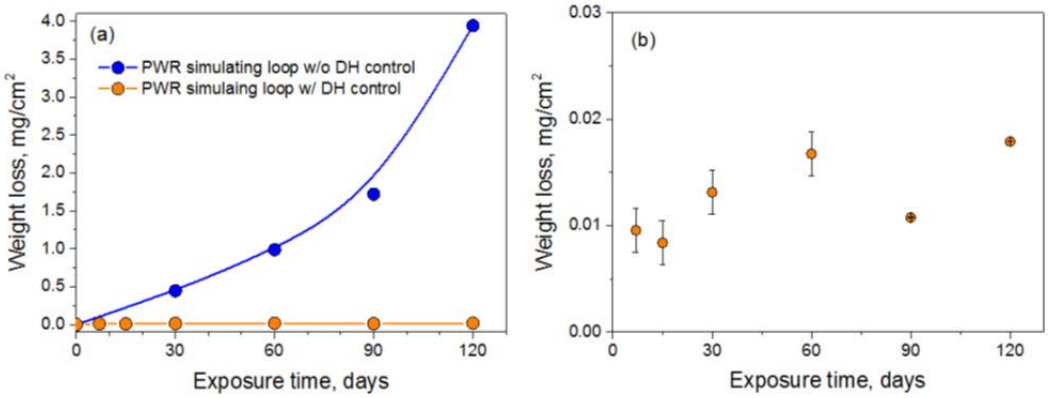

FIG. 2. Corrosion behaviours of the CVD SiC specimens in the 360°C PWR-simulating water loops with and without controlling the dissolved hydrogen.

According to our previous results [22], the corrosion rate was much higher in the static autoclave containing several ppm of dissolved oxygen than in the loop test, in which the dissolved oxygen content was maintained less than 5 ppb. However, there was also a considerable amount of corrosion occurred even in the loop test without controlling the dissolved hydrogen. The grain boundaries of CVD SiC were preferentially attacked at the

early stage of corrosion, and the grains became thinner and some grains were detached from the surface, leading to the acceleration of weight loss after corrosion test for 120 days, as shown in Fig. 2(a). However, the corrosion weight loss is dramatically reduced, less than 2 mg/dm^2 after 120 days of corrosion, in the PWR-simulating water loop test with the control of dissolved hydrogen. At the initial stage of corrosion test for 7 days of the as-polished specimen, a small amount of weight loss about 1 mg/dm^2 can be observed, being due to the dissolution of the native oxide layer. However, after the dissolution of the native oxide layer, the additional weight loss is kept very low, less than 1 mg/dm^2 after corrosion test for 120 days.

Figure 3 shows the SEM micrographs of the CVD SiC specimens before and after the corrosion tests in the simulated PWR water environment with the control of dissolved hydrogen. Although the specimens have rather rough surfaces because we have not applied a fine polishing for the preparation of test specimens, the surface microstructures are hardly changed after corrosion tests for up to 120 days. Compared with the previous corrosion test results [18, 20-23], it is clear that the dissolution of SiC is extremely limited. Moreover, there was no evidence of a preferential corrosion at grain boundaries or a pitting corrosion.

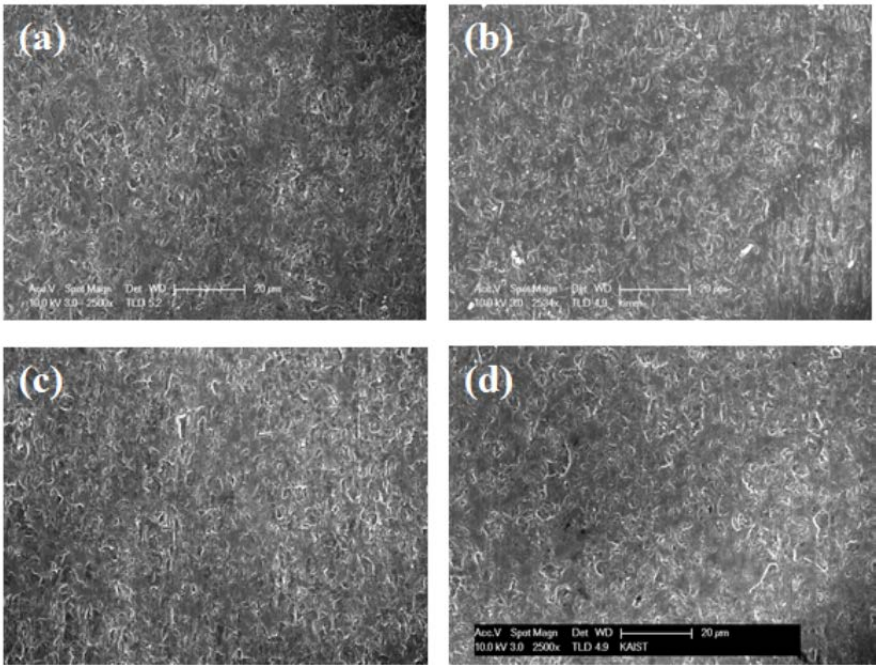

FIG. 3. SEM micrographs of the as-polished (a) and the corroded CVD SiC specimens after the corrosion tests for 7 (b), 30 (c), and 120 days (d) in the PWR-simulating water with controlling the dissolved hydrogen.

Figures 4 and 5 display the AFM surface morphology and roughness of CVD SiC specimens, respectively, before and after corrosion tests. In general, the corrosion of SiC or the formation of SiO_2 causes an increase in surface roughness because of the local corrosion such as pitting or grain boundary attacks and the inhomogeneous growth of SiO_2 [5, 23]. However, we cannot observe any meaningful change in surface morphology and roughness after the corrosion tests from the AFM results in Figs 4 and 5, supporting the absence of a preferential corrosion at grain boundaries or a pitting corrosion.

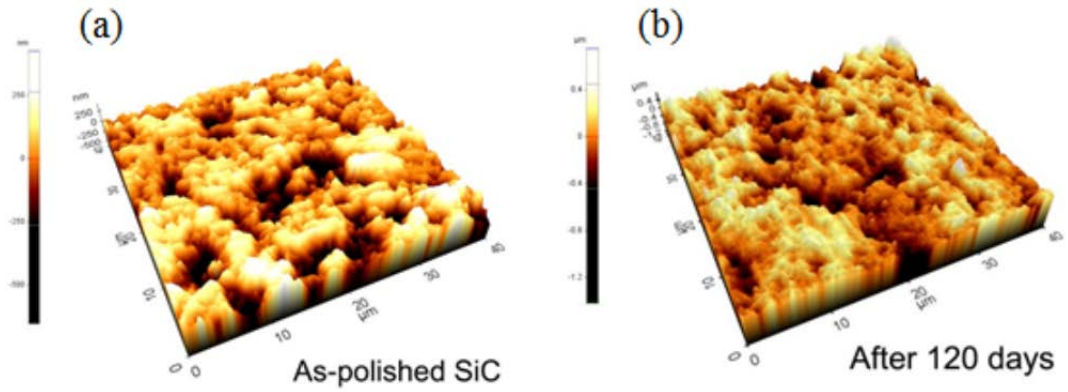

FIG. 4. AFM surface morphologies of the as-polished (a) and the corroded CVD SiC specimens after the corrosion test for 120 days (b).

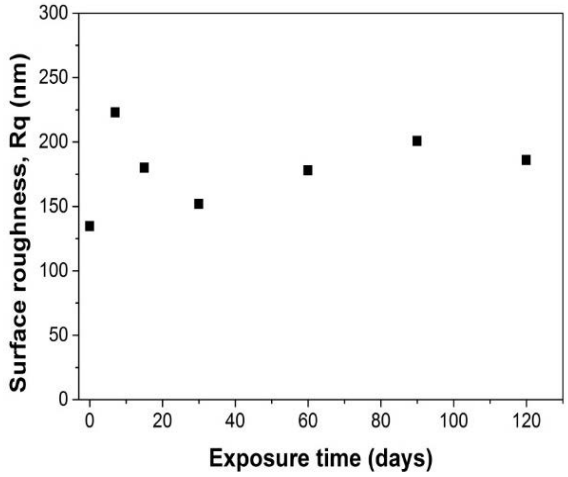

FIG. 5. Changes in the surface roughness determined by AFM analyses as a function of the corrosion time.

Any phase change of the surface of the corroded specimens was analyzed using glancing-angle X-ray diffraction. Figure 6 shows the XRD results of CVD SiC before and after the corrosion tests in the PWR-simulating water with the control of dissolved hydrogen. The as-polished SiC specimen generally contains native oxide consisting of amorphous SiO_2 and SiO_xC_y on the surface as will be shown in the XPS analysis. However, only β-SiC was detected in the as-polished specimen despite the low incident angle of the X-ray beam because the thickness of the native oxide was very thin. In addition, no other phase except for the β-SiC was detected in the XRD patterns of the corroded specimens irrespective of the corrosion time.

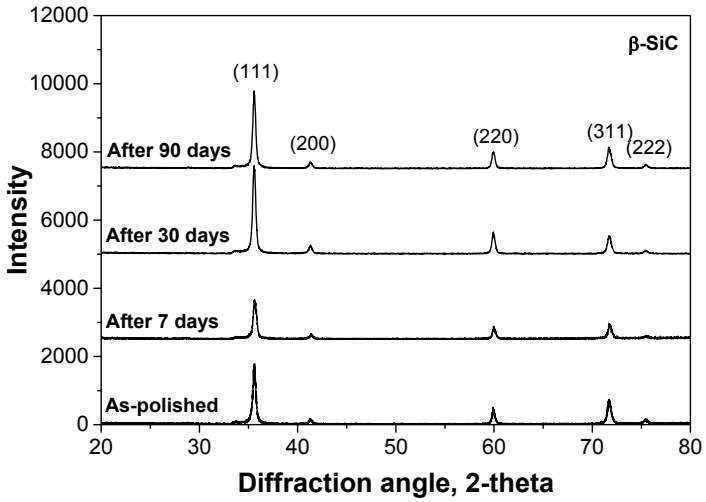

FIG. 6. Glancing-angle XRD patterns of the CVD SiC specimens before and after the corrosion tests in the PWR-simulating water with controlling the dissolved hydrogen.

Figure 7 shows the chemical states on the surface of CVD SiC determined by XPS analysis before and after corrosion tests. The Si $2p_{1/2,3/2}$ peak of the as-polished specimen can be distinguished by three peaks, which are attributed to the very thin native oxide and the SiC bulk beneath the oxide layer, as shown in Fig. 7(a) [5]. The native oxide Si $2p_{1/2,3/2}$ peaks consist of Si-O bonds originating from SiO_2 and SiO_xC_y peaks located at 103.2 and 102.2 eV, respectively. The Si-C peak from the SiC bulk is located at 100.5 eV. After corrosion test for 7 days, the Si $2p_{1/2,3/2}$ peaks correspond to the native oxide completely disappeared, and only a peak for the Si-C bond remained, as shown in Fig. 7(b). The XPS spectra did not show any change with the further increase of corrosion time.

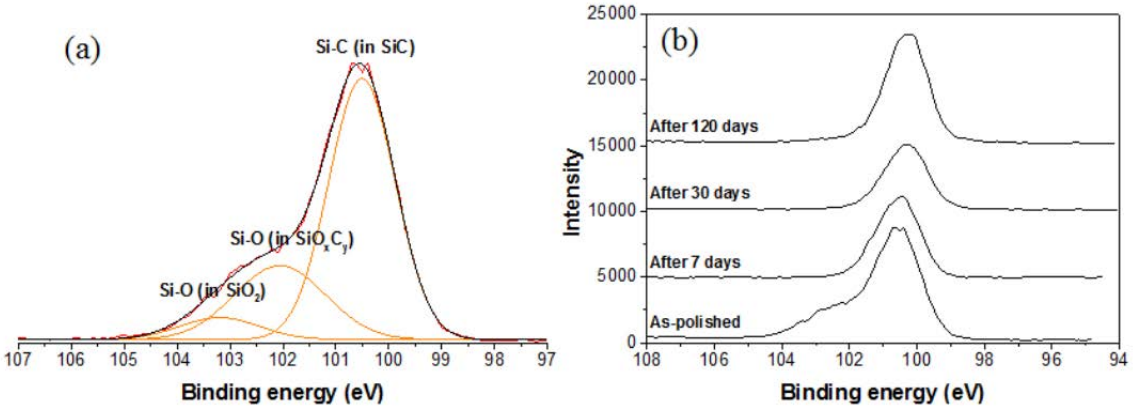

FIG. 7. XPS analysis results of the as-polished (a) and the corroded (b) CVD SiC specimens.

Based on the XPS and weight measurement results in this study, the hydrogen injection is not very effective in preventing the oxide layer from dissolution into the water. On the other hand, the dissolved hydrogen is believed to effectively retard the formation of the oxide or hydroxide layer and thereby significantly reduce the corrosion rate of CVD SiC in the PWR-simulating water.

The corrosion test condition in this study is close to the PWR coolant water chemistry except for the existence of irradiation. Highly corrosive oxygen radicals formed by the radiolysis of water under irradiation can facilitate the corrosion of SiC [25] and irradiated SiC

ceramics can be more susceptible to corrosion [26]. Therefore, the effects of irradiation on the corrosion behaviour of SiC need to be further evaluated for an assessment of the corrosion resistance of SiC in the PWR coolant water while controlling the dissolved hydrogen content.

3.2. Hoop stress of SiC triplex composite tubes

Figure 8(a) shows the applied load-axial displacement curves of the SiC triplex tubes. Load gradually increases until the polyurethane plug contacts with the tubular specimen at the initial stage, and it steeply increased after the contact. Especially some load drops are observed before failure of the tube which might be caused by the formation of crack in the inner monolithic SiC layer. The stress-strain curve displays an initial almost linear up to almost a half of the curve, as shown in Fig. 8(b). The onset of non-linearity could be associated with matrix cracking and manifests itself in degradation in tube stiffness after a significant load drop and an increase in radial displacement.

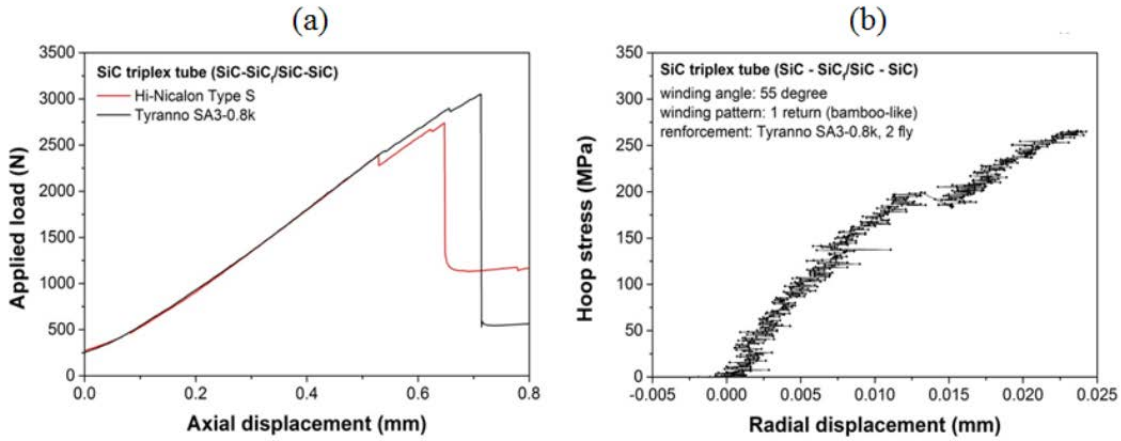

FIG. 8. (a) Typical load-axial displacement and (b) hoop stress-radial displacement curves of the SiC triplex tubes.

Figure 9 shows the microstructure of the triplex tube interrupted just after a first load drop during the hoop test. Failure of the SiC inner layer has been taken place, as shown in Fig. 9(a). However, the crack from the inner layer does not propagate immediately into the composite layer. In the SiC triplex tube, PyC with about 200 nm in thickness exists between the SiC inner and the composite layers, which was formed during the deposition of PyC interphase on SiC fibres. When the crack propagates from inner layer to composite layer, the PyC interphase become the preferred site for crack propagation. It indicates that the existence of a thin PyC layer play a role of an obstacle of crack propagation. In a SiC_f/SiC composite layer, a significant delamination and detachment of the SiC fibre bundles does not take place but a number of intrabundle microcracks are observed primarily at the matrix/fibre interface to the circumferential direction. The microcracks with several tens of micrometers are occasionally observed through the thickness of the composite layer, as shown in Fig. 9(d). Therefore, main damage mechanism of a composite layer is delamination or detachment to the circumferential direction by shear stress at the initial fracture stage. The load drop could be caused by fracture of a SiC inner layer. The quasi-ductile composite layer might suddenly expand after the cracking in a SiC inner layer.

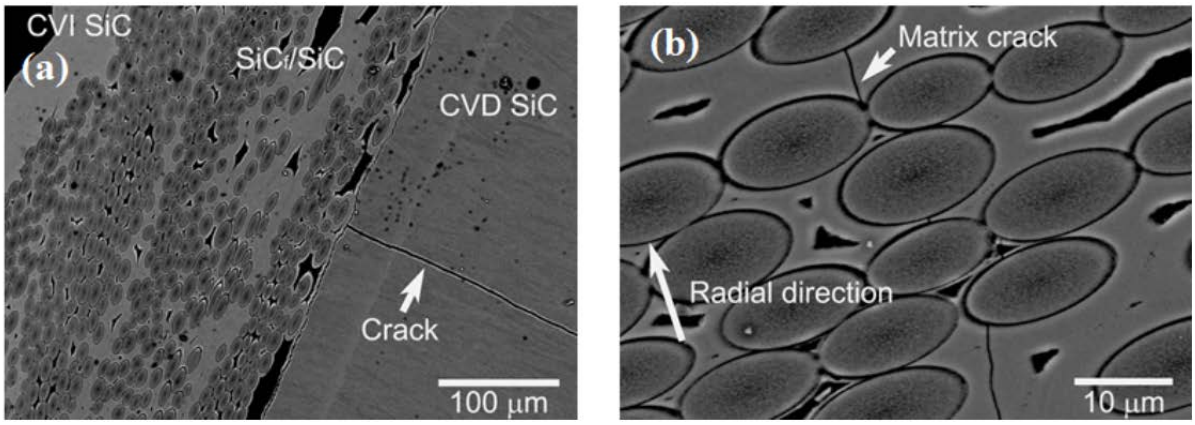

FIG. 9. Microstructure of the SiC triplex tube after a first load drop: (a) a crack in the SiC inner layer and (b) a matrix crack in the SiC_f/SiC composite layer.

The mechanical properties of a composite are usually determined by the properties of matrix and fibre, volumetric ratio, matrix density and orientation of the fibres [27]. When the fibre strength is much higher than that of matrix, the fibre properties and fraction have a significant effect on the composite strength [28]. The volumetric ratio of fibres is mainly determined by the winding method such as lay-up architecture and fibre tension.

Figure 10 shows the hoop stresses of the SiC triplex tubes depending on the fibre volume fraction in the triplex tubes and a type of the reinforcement fibre. Although the SiC triplex tubes have a thick monolith layer, the fibre volume fraction still has a significant effect on the hoop stress. The fibre volume fraction of each tube is in the range of 18 to 25%. The hoop stress of the triplex tube tends to be proportional to the fibre volume fraction regardless of both the reinforcement fibre and fly number. The highest fibre volume fraction was obtained when the Tyranno SA3-0.8k fibre was used so that the Tyranno SA3-0.8k reinforced triplex tube exhibits the highest hoop stress. In the case of the Hi-Nicalon Type S-reinforced triplex tubes, the fibre volume fraction is less than Tyranno SA3 because a diameter of Hi-Nicalon type S is higher than Tyranno SA3 and thus Hi-Nicalon Type S is less flexible. Since Hi-Nicalon Type S has higher tensile strength and tensile modulus (Table 2), the hoop stress of Hi-Nicalon Type S reinforced tubes was slightly higher than the Tyranno SA3-reinforced triplex tube when the fibre volume fraction in the SiC triplex tube is equal.

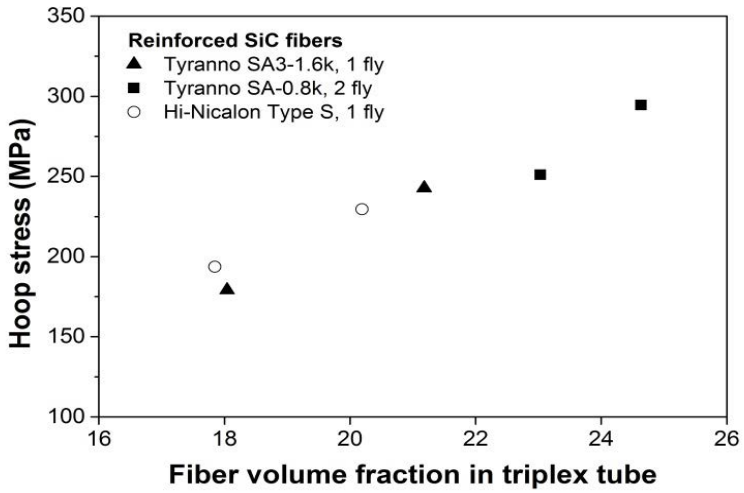

FIG. 10. Hoop stresses of the SiC triplex tubes as a function of the fibre volume fraction.

4. CONCLUSIONS

The dissolved hydrogen of about 2.7 ppm significantly reduced the corrosion rate of SiC at 360°C under 20 MPa. There was no evidence of a preferential corrosion at grain boundaries or a pitting corrosion on microstructure observations. The native oxide layer or the thermally grown SiO_2 formed on the SiC specimens was readily dissolved and the SiC bare surface was exposed at the initial stage of the corrosion test. After the dissolution of the oxide layer, further corrosion occurred in a very sluggish way. This indicates that the dissolved hydrogen significantly increases the corrosion resistance of the CVD SiC by retarding the formation of the surface oxide layer.

The hoop stresses of the SiC triplex tubes tended to be proportional to the fibre volume fraction of the composite layer. The Tyranno SA3-0.8k reinforced SiC triplex tube exhibited the highest hoop strength because the highest fibre volume fraction was achieved by a filament winding method. Quasi-ductile fracture occurred for the triplex composite tubes. Crack initiated in the SiC inner layer which resulted in the load drop and a sudden increase in radial displacement in the stress-displacement curve. Matrix cracking along the fiber-matrix interface led to a decrease in the slope of the stress-radial displacement curve.

ACKNOWLEDGEMENT

This work was supported by the National Research Foundation of Korea (NRF) grant funded by the Korea government (MSIP) (No. 2012M2A8A5009818).

REFERENCES

[1] YAMADA, K., MOHRI, M., "Properties and applications of silicon carbide ceramics", Silicon Carbide Ceramics – Fundamental and Solid Reaction (SOMIYA, S., INOMATA, Y.), Elsevier Applied Science, London and New York (1991) 13-44.

[2] NASLAIN, R., Design, preparation and properties of non-oxide CMCs for application in engines and nuclear reactors: an overview, Compos. Sci. Technol. **64** (2004) 155.

[3] VERFONDERN, K., NABIELEK, H., KENDALL, J.M., Coated particle fuel for high temperature gas cooled reactors, Nucl. Eng. Technol. **39** (1989) 603.

[4] FUKUDA, F., OGAWA, T., HAYASHI, K., SHIOZAWA, S., TSURUTA, H., TANAKA, I., SUZUKI, N., YOSHIMUTA, S., KANEKO, M., Research and development of HTTR coated particle fuel, J. Nucl. Sci. Technol. **28** (1991) 570.

[5] KIM, D., KIM, W.-J., PARK, J.Y., Compatibility of CVD SiC and SiC_f/SiC composites with high temperature helium simulating very high temperature gas-cooled reactor coolant chemistry, Oxid. Met. **80** (2013) 389.

[6] SNEAD, L.L., NOZAWA, T., KATOH, Y., BYUN, T.-S., KONDO, S., PETTI, D.A., Handbook of SiC properties for fuel performance modelling, J. Nucl. Mater. **371** (2007) 329.

[7] KATOH, Y., NOZAWA, T., SNEAD, L.L., OZAWA, K., TANIGAWA, H., Stability of SiC and its composites at high neutron fluence, J. Nucl. Mater. **417** (2011) 400.

[8] YOUINOU, G., SEN, R.S., "Enhanced accident tolerant fuels for LWRs – A preliminary system analysis", INL/EXT-13-30211, Idaho National Laboratory, ID (2013).

[9] YUEH, K., CARPENTER, D., FEINROTH, H., Clad in clay, Nucl. Eng. Intern. **55** (2010) 14.

[10] FEINROTH, H., ALES, M., BARRINGER, E., KOHSE, G., CARPENTER, D., JARAMILLO, R., Mechanical strength of CTP triplex SiC fuel clad tubes after irradiation in MIT research reactor under PWR coolant conditions, Ceram. Eng. Sci.

Proc. **30-10** (2009) 47.
[11] KIM, W.-J., KIM, D., PARK, J.Y., Fabrication and material issues for the application of SiC composites to LWR fuel cladding, Nucl. Eng. Technol. **45** (2013) 565
[12] CHENG, T., KEISER, J.R., BRADY, M.P., TERRANI, K.A., PINT, B.A., Oxidation of fuel cladding candidate materials in steam environments at high temperature and pressure, J. Nucl. Mater. **427** (2012) 396.
[13] MAKHAM, G., HALL, R., FEINROTH, H., Recession of silicon carbide in steam under nuclear plant LOCA conditions up to 1400°C, Ceram. Eng. Sci. Proc. **33** (2013) 101.
[14] TERRANI, K.A., PINT, B.A., PARISH, C.M., SILVA, C.M., SNEAD, L.L., KATOH, Y., Silicon carbide oxidation in steam up to 2 MPa, J. Am. Ceram. Soc. **97** (2014) 2331.
[15] KATOH, Y., SNEAD, L.L., SZLUFARSKA, I., WEBER, W.J., Radiation effects in SiC for nuclear structural applications, Curr. Opin. Solid State Mater. Sci. **16** (2012) 143.
[16] ZINKLE, S.J., TERRANI, K.A., GEHIN, J.C., OTT, L.J., SNEAD, L.L., Accident tolerant fuels for LWRs: a perspective, J. Nucl. Mater. **448** (2014) 374.
[17] BARRETT, K., BRAGG-SITTON, S., GALICKI, D., "Advanced LWR nuclear fuel cladding system development trade-off study", INL/EXT-12-27090, Idaho National Laboratory, ID (2012).
[18] HIRAYAMA, H., KAWAKUBO, T., GOTO, A., Corrosion behaviour of silicon carbide in 290°C water, J. Am. Ceram. Soc. **72** (1989) 2049.
[19] KIM, W.-J., HWANG, H.S., PARK, J.Y., Corrosion behaviour of reaction-bonded silicon carbide ceramics in high-temperature water, J. Mater. Sci. Lett. **21** (2002) 733.
[20] KIM, W.-J., HWANG, H.S., PARK, J.Y., RYU, W.-S., Corrosion behaviours of sintered and chemically vapor deposited silicon carbide ceramics in water at 360°C, J. Mater. Sci. Lett. **22** (2003) 581.
[21] TAN, L., ALLEN, T.R., BARRINGER, E., Effect of microstructure on the corrosion of CVD-SiC exposed to supercritical water, J. Nucl. Mater. **394** (2009) 95.
[22] PARK, J.-Y., KIM, I.-H., JUNG, Y.-I., KIM, H.-G., PARK, D.-J., KIM, W.-J., Long-term corrosion behaviour of CVD SiC in 360°C water and 400°C, J. Nucl. Mater. **433** (2013) 603.
[23] HENAGER, JR., C.H., SHEMER-KIOHRN, A.L., PITMAN, S.G., SENOR, D.J., GEELHOOD, K.J., PAINTER, C.L., Pitting corrosion in CVD SiC at 300°C in deoxygenated high-purity water, J. Nucl. Mater. **378** (2008) 9.
[24] JADAAN, O.M., SHELLEMAN, D.L., CONWAY Jr., J.C., MECHOLSKY Jr., J.J., TRESSLER, R.E., Prediction of the strength of ceramic tubular components: Part I-analysis, J. Test. Eval. **19** (1991) 181.
[25] CARPENTER, D., "An assessment of silicon carbide as a cladding material for light water reactors", Ph. D. Dissertation, Department of Nuclear Science and Engineering, Massachusetts Institute of Technology, MA (2010).
[26] KONDO, S., LEE, M., HINOKI, T., "Hot water corrosion at ion-irradiated surface of SiC". Paper presented at ICACC 2014, Daytona Beach, FL (2014).
[27] JONES, R.M., Mechanics of Composite Materials, Scripta Book Company, Washington, D.C (1975).
[28] COHEN, D., MANTELL, S.C., ZHAO, L., The effect of fibre volume fraction on filament wound composite pressure vessel strength, Composites: Part B **32** (2001) 413.

ACCELERATION OF THE HOT WATER CORROSION OF SIC BY ION 7.7. IRRADIATION

S. KONDO, M-H. LEE, T. HINOKI
Institute of Advanced Energy, Kyoto University
Kyoto
Japan
E-mail: kondo@iae.kyoto-u.ac.jp

Abstract

The corrosion rates are known to be affected significantly by the water conditions such as oxygen content, hydrogen content, and temperature, though the dependency is not clear. Furthermore, the irradiation may modify the corrosion rates significantly because the significant population of the irradiation-induced defects were reported especially under LWR relevant temperatures. In this study, the corrosion behaviour following the ion irradiation was studied for high purity CVD SiC. Specimens were irradiated with Si ions up to 10 dpa at 400°C in DuET facility, Kyoto University. The irradiated surface subjected to 360°C water containing 8 ppm dissolved oxygen was studied by scanning and transmission electron microscopy. Selective corrosion was observed at crystallographic boundaries such as grain boundaries, twin boundaries, and stacking faults for both the irradiated and unirradiated regions for CVD SiC. It is clear that the regions ion-irradiated (~3 μm in depth) were preferentially dissolved compared to the unirradiated regions, implying the operation of the irradiation accelerated corrosion in SiC.

1. INTRODUCTION

SiC and SiC/SiC composites are attracting attention as alternative materials for fuel cladding because of the conceivable better chemical stability and strength under LOCA or beyond design basis conditions [1]. The use of SiC may allow the fuel components to use in a long cycle operation with larger safety margin comparing to Zr based alloys. Although the superior corrosion resistance in a hot water environment has been reported by many researchers for high purity SiC, impurities, such as sintering aids and free Si, were reported to enhance the corrosion rates primarily through the selective corrosion at the grain boundaries as described below [2-7]. Preferential grain boundary attack and an overall loss of Si at the surface have been reported for even pure CVD SiC [6]. The presence of free silicon, or presumably other sintering aids residing at grain boundaries, has been shown to enhance corrosion of SiC for water temperatures as low as 290 °C [2]. The loss of Si was not attributed to the formation of protective silica layer but the formation of soluble silicide such as silicon hydroxides in these conditions. Therefore, understanding of the corrosion rates and the underlying mechanisms is essential to predict the applicability of the SiC cladding.

During reactor operation, SiC specimens are subjected to neutron bombardment, which mostly produce the Frenkel pairs in both the silicon and carbon sub-lattices in addition to few clustered defects and anti-sites through the displacement damage. Although the populations of these defects are saturated at an early stage of the irradiation at low temperature for SiC due primary to the very high sink density of practically immobile vacancies and tiny vacancy clusters, these are known to cause various material property changes such as the dimension and strength [8]. Despite the near surface properties should also be modified by the irradiation, the information of the effects of irradiation damage on the corrosion rates is practically absent. In this work the effects of the irradiation damage on the hot-water corrosion of SiC was studied to predict the corrosion rates under LWR normal operation.

2. EXPERIMENTAL

The material used was polycrystalline 3C-SiC produced by chemical vapour deposition by Dow Chemical Company (Marlborough, Massachusetts, USA). The chemical vapour deposited (CVD) SiC was of very high purity, with typical total metal impurity concentration

less than 5 wppm. The typical grain size was between 5 and 100 μm in the plane parallel to the deposition substrate, with grains elongated in the <111> growth direction perpendicular to the substrate. The material was essentially free of micro-pores, micro-cracks, or other large flaws, but atomic layer stacking faults on the {111} planes were common. The density measured using Archimedes' principle was in good agreement with the theoretical density (3.21 g/cm^3).

Ion irradiation method was employed for simulating the neutron irradiation in this study. A polished surface of each square specimen ($10\times10\times3^t$ mm) was irradiated with 5.1 MeV Si^{2+} ions at 400°C in the DuET facility at Kyoto University as shown in Fig. 1, prior to the hot-water corrosion test. It should be noted that the ion range, and of course the irradiation damage, are limited to approximately 2.5 μm from the irradiated surface as described in elsewhere [9]. The nominal irradiation fluence, which were averaged to a depth of less than 1 μm from the surface, were 1, 3, or 10 dpa (displacement per atom), depending on specimens.

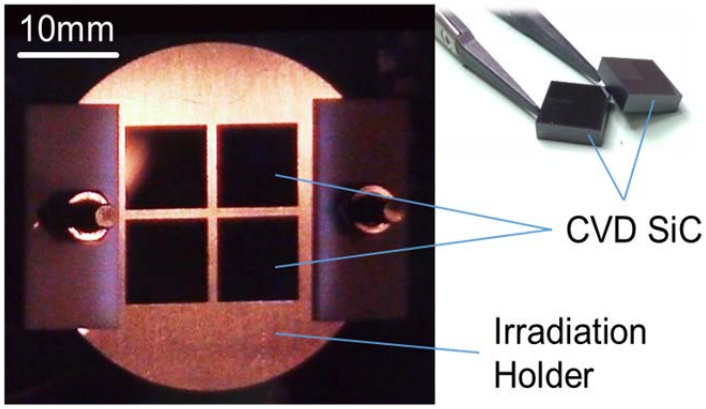

FIG. 1. CVD SiC specimens and fixtures for the ion-irradiation experiment at DuET, Kyoto University.

The irradiated specimens were tested for 176-500 hrs. in an autoclave aqueous corrosion test at 20 MPa pressure and at 360°C. Then, cleaned surfaces were evaluated by optical microscopy (OM), atomic force microscopy (AFM), and scanning electron microscopy (SEM).

3. RESULTS AND DISCUSSION

The typical surface images of the irradiated specimens (10 dpa) before and after the corrosion test at 360 °C were shown in Fig. 2a and b, respectively. Each image contains both unirradiated and irradiated surfaces as indicated by arrows. Although the as-irradiated surface appeared dark in the SEM image (Fig. 2a), indicative of minor hydrocarbon contamination during ion irradiation, no clear differences in the surface smoothness from the unirradiated region was detected by AFM analysis. However, the absolute height of the irradiated region was higher than that of the unirradiated region as summarized in Table 1. This is a common occurrence for the ion-irradiated SiC because the ion range was very limited and the irradiation induced swelling was mostly manifested as the elevation of the free surface. For all the corroded specimens the boundaries between the two regions was very clear as representatively shown in the inset OM image of Fig. 2b for the highest irradiation-damage case. As seen in the SEM image in Fig. 2b, the grain boundaries was preferentially damaged regardless of the irradiation. The damage at the grain boundaries, however, seemed to be significant in the irradiated regions comparing to that in the unirradiated regions. Indeed, the

survived grains in the irradiated regions clearly are finer than those in the unirradiated regions. This indicates that the corrosive attack progressed towards the grain interior from the grain boundaries.

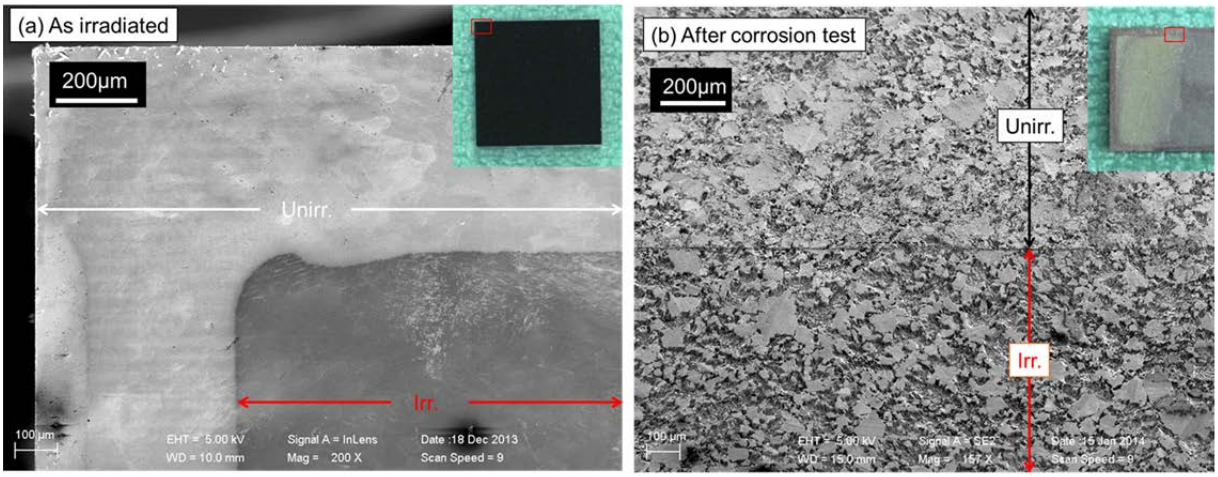

(a) (b)

FIG. 2. SEM images of the irradiated surfaces (a) before and (b) after hot-water corrosion test at 400°C for 500 hours.

A typical SiC grain lying astride the unirradiated and irradiated surfaces was shown in Fig. 3. A steep "cliff" was observed at the boundary as shown in the figure, indicating significant differences in the corrosion rate between the two regions. Many tetrahedral pits composed of 111 crystal planes and preferentially damaged lines mostly parallel to the 110 crystallographic directions were found on the grain interior especially in the irradiated regions as shown in the magnified image in Fig. 3. The step height based on the unirradiated region was listed in Table 1 for both the as-irradiated and corroded specimens. Because the corrosion rates seemed to be dependent on the grain orientation, height of the step formed on each single grain was separately measured by AFM and averaged in the table. All the specimens showed positive step before the corrosion tests because of the irradiation induced swelling in the as-irradiated specimens. Contrary to this, the irradiated regions showed negative step for all the corroded specimens, meaning higher corrosion rates. Therefore, one can conclude that the irradiation accelerate the rate of corrosion even at the SiC grain interior even in a very low dpa condition.

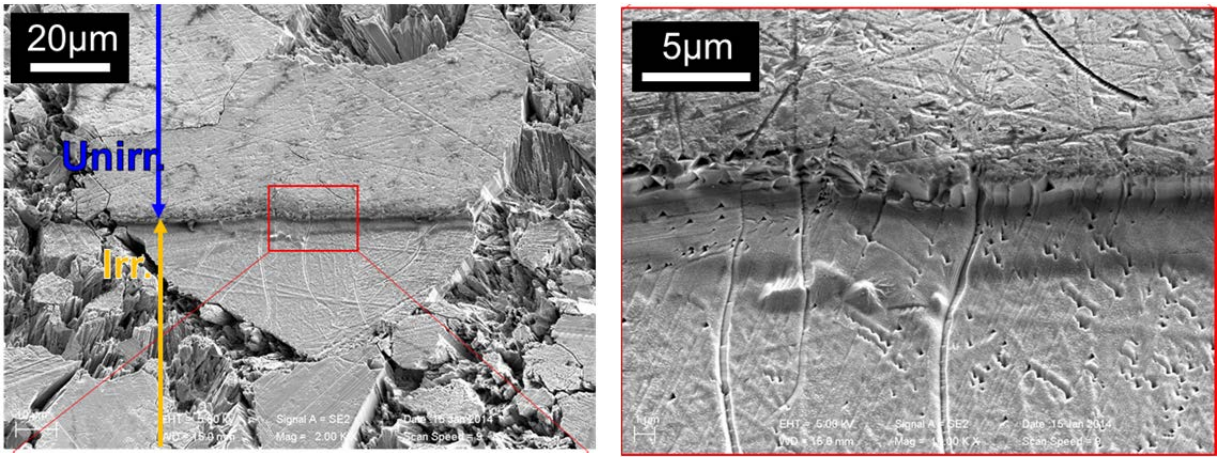

FIG. 3. SEM image of a typical unirradiated-irradiated boundary in a grain after corrosion tests for 500 hrs.

The amount of the loss of surface increased with increasing both in the irradiation fluence and corrosion time. However, it seems that the corrosion rate was practically saturated below few dpa rather than the linear dependence. This is similar to the fluence dependence of the irradiation induced point-defect swelling of SiC [10], which is believed to be caused by the accumulation of point defects such as vacancies, interstitials, antisites, and tiny defect clusters. The point defect swelling reaches the saturation value defined by the irradiation temperature because of the practical saturation of the population of theses defects. Therefore, the saturation of the corrosion rates may refer the saturation of the number of point defects, though further study is required to understand the underlying mechanisms of the irradiation induced acceleration of the corrosion rates.

4. CONCLUSIONS

The corrosion behaviour following the ion irradiation was studied for high purity CVD SiC. Specimens were irradiated with Si ions up to 10 dpa at 400°C in DuET facility, Kyoto University. The irradiated surface subjected to 360°C water containing 8 ppm dissolved oxygen was studied by scanning and transmission electron microscopy. Selective corrosion was observed at crystallographic boundaries such as grain boundaries, twin boundaries, and stacking faults for both the irradiated and unirradiated regions for CVD SiC. It is clear that the regions ion-irradiated (~2.5 μm in depth) were preferentially dissolved compared to the unirradiated regions, implying the operation of the irradiation accelerated corrosion in SiC.

ACKNOWLEDGEMENTS

This work was performed under contract with Toshiba Corporation in “Research and Development of Innovative Technologies for Nuclear Reactor Core Material with Enhanced Safety” entrusted to Toshiba by the Ministry of Education, Culture, Sports, Science and Technology of Japan (MEXT).

REFERENCES

[1] ZINKLE, S.J., TERRANI, K.A., GEHIN, J.C., OTT, L.J., SNEAD, L.L., Accident Tolerant Fuels for LWRs: A Perspective, J. Nucl. Mater., **448** (2014) 374–9.

[2] HIRAYAMA, H., KAWAKUBO, T., GOTO, A., Corrosion Behaviour of Silicon Carbide in 290°C Water, J. Am. Ceram. Soc., **72** (1989) 2049-53.

[3] VERRALL, R.A., VLAJIC, M.D., KRSTIC, V.D., Silicon Carbide As An Inert-Matrix for a Thermal Reactor Fuel, J. Nucl. Mater. **274** (1999) 54-60.

[4] KIM, W.J., HWANG, H.S., PARK, J.Y., RYU, W.S., Corrosion Behaviours of Sintered and Chemically Vapour Deposited Silicon Carbide Ceramics in Water at 360°C. J. Mater. Sci. Let., **22**, (2003) 581-584.

[5] BARRINGER, E., FAIZTOMPKINS, Z., FEINROTH, H., ALLEN, T., LANCE, M., MEYER, H., WALKER, L., CURZIO, E. L., Corrosion of CVD Silicon Carbide in 500°C Supercritical Water, J. Am. Ceram. Soc., **90** (2007) 315–318.

[6] HENAGER, Jr., C.H., SCHEMER-KOHRN, A.L., PITMAN, S.G., SENOR, D.J., GEELHOOD, K.J., PAINTER, C.L. Pitting Corrosion in CVD SiC at 300°C in Deoxygenated High-Purity Water, J. Nucl. Mater., **378**, 9–16 (2008).

[7] PARK, J.Y., KIM, I.H., JUNG, Y.I., KIM, H.G., PARK, D.J., KIM, W.J., Long-term Corrosion Behaviour of CVD SiC in 360°C Water and 400°C Steam, J. Nucl. Mater., **443** (2013) 603-607.

[8] KONDO, S., KATOH, Y., SNEAD, L.L., Microstructural Defects in SiC Neutron Irradiated at Very High Temperatures, J. Nucl. Mater., **382** (2008) 160-169.

[9] KONDO, S., KOYANAGI, T., HINOKI, T., Irradiation Creep of 3C–SiC and

Microstructural Understanding of the Underlying Mechanisms," J. Nucl. Mater., **448** (2014) 487-496.
[10] KATOH, Y., SNEAD, L.L., NOZAWA, T., KONDO, S., BUSBY, J.T., Thermophysical and Mechanical Properties of Near-Stoichiometric Fibre CVI SiC/SiC Composites after Neutron Irradiation at Elevated Temperatures, J. Nucl. Mater. **403**, 48-61 (2010).

SILICON CARBIDE BEHAVIOUR UNDER PROTOTYPIC LWR CHEMISTRY/NEUTRON FLUX AND ACCIDENT CONDITIONS

M.A. PANTANO[*], D.M. CARPENTER[**], T.J. McKRELL[*], G.E. KOHSE[**]
P.B. GUENOUN[*], M.S. KAZIMI[*]
[*]Nuclear Science and Engineering Department, MIT
[**]Nuclear Reactor Laboratory, MIT
United States of America
E-mail: tmckrell@mit.edu

Abstract

The Accident Tolerant Fuels (ATF) programme was started with the goal of finding alternative fuel and cladding materials that perform as well as or better than current materials under normal operating conditions with enhanced performance during accidents. SiC has been a long-time candidate for this programme. Here we will discuss both out-of-core and in-core test results that are incorporated into analytical models developed at MIT. Out-of-core research has subjected un-irradiated SiC ceramic matrix composite (CMC) samples to a series of tests to gauge performance in a loss-of-coolant accident (LOCA). Previous work by the group with monolithic α SiC has exposed samples to steam temperatures up to 1,500°C for 8 to 48 hours at various steam flow rates. Additionally, monolith samples have been quenched from up to 1,300°C into both room temperature and saturated water at atmospheric pressure. Following this testing, burst testing was performed to quantify strength degradation and ceramographic analysis was completed to determine microstructural effects. Using the same techniques as this previous monolithic work, testing of tube samples composed of three integrated layers have been tested. The three layers are an outer environmental barrier, a ceramic matrix composite, and an inner monolith layer; all layers are composed of SiC. These SiC/SiC CMC samples have been exposed to 1,400°C steam at ~6 g/min for 48 hours. Quench testing was performed from 1,200°C into saturated water to simulate the condition of reflood water after a LOCA, and burst and ceramographic analysis performed. Several different architectures of the CMC layer are in the process of being tested. Initial results for one CMC architecture indicate that the CMC samples exhibit the expected low oxidation rate of SiC in steam, and improved burst performance of both quenched and as-received samples. In the future two additional fibre architectures and sealed tubes will be examined, with the results being used to evaluate differences between them and for input into analytical models. In-core research has included irradiation of monolithic and various types of CMC and CMC/monolithic hybrid SiC samples in both tube and plate geometries. Utilizing a pressurized water loop facility in the core of the MIT Research Reactor, samples were exposed to prototypical LWR neutron flux (10^{14} n/cm^2-s), temperature (300°C), and chemistry (H water chemistry, B/Li) conditions. Samples have been exposed in multiple irradiation campaigns for periods of a few months to 1.5 years accumulated residence time, generally with some intermediate post-irradiation examination (PIE). PIE has included weight and dimensional change, as well as burst, ceramographic, and thermal diffusivity studies. Corrosion performance of the SiC has been found to be influenced strongly by both composition/manufacturing and irradiation. High-purity β-phase CVD SiC has been found to have the lowest weight loss, whereas fibre-composite SiC with matrices of elevated oxygen or free silicon and carbon content experience higher rates of loss.

1. INTRODUCTION

Silicon carbide has been a material of interest in the Accident Tolerant Fuels (ATF) programme for years [1, 2]. This material has been of particular interest in other fields due to its oxidation resistance and strength at high temperatures, both of which are a valuable attribute for an ATF cladding. An additional advantage of SiC is its low neutron cross-section. The oxidation of SiC has been studied in a variety of gaseous environments [3, 4]. Of particular interest for the nuclear industry is oxidation resistance in a water/steam environment [5, 6]. As a ceramic, SiC fails by a brittle manner modelled by a statistical treatment. For this reason, repeated strength measurements are necessary. It has been shown that radiation significantly affects important material properties relevant to it as a fuel cladding [1, 7-9]. In this paper, both recent out-of-core and in-core experiments are described.

2. EXPERIMENTAL FACILITIES

The out-of-core experiments have been conducted in three facilities. In simulating a prototypic loss of coolant accident, the order of these would be exposure to steam in the oxidation column, followed by a simulated reflood in the quench apparatus, and ending with a strength measure by burst testing with a load frame.

2.1. Oxidation column

The high temperature steam oxidation facility is designed as a column in which water is brought to a boil under a constant heat source. The rising steam flows through a vertical quartz tube and escapes to the atmosphere. Along this flow path, the steam is subjected to several heating stages. In the final heating stage, where a sample would be placed, the steam temperature is capable of reaching 1550°C. This facility, Figure 1a, has previously been validated against existing data and models for the oxidation of zircaloy-4 [10]. The results presented below for monolith α SiC where conducted at a range of flow rates (2-20 g/min) and steam temperatures (1200°C - 1500°C). Subsequent experiments conducted on CMC SiC were performed at ~6 g/min and 1400°C. Exposure periods on the order of days were chosen to ensure a measurable weight change and to simulate a prolonged loss of coolant scenario.

2.2. Quench apparatus

To simulate the reflood of a reactor core following a severe accident, the quench apparatus, Fig. 1b, is used to heat the sample and then drive it into a pool of water open to the atmosphere. The radiant furnace used to heat the sample is capable of reaching 1550°C. To minimize radiative heat loss, compressed air is used to drive the sample down into the quench pool. A hot plate below the quench pool allows for control of the temperature of the pool. Tests with monolith α SiC have been conducted at sample temperatures up to 1300°C into pools of either room temperature or saturated water. Based on RELAP simulations, quenching into water near saturation is more representative of loss of coolant conditions in pWRs. Because of this, CMC SiC samples have been quenched from 1200°C into a pool near saturation (85°C – 99°C).

2.3. Burst test

Both the monolith SiC and CMC SiC samples tested to date have been tubes open on both ends. To measure the failure hoop stress of these samples, a burst test is used with a load frame expanding a polyurethane plug, as seen in Fig. 1c. For this test, a polyurethane with hardness 80A was selected. The plug size was chosen with a diameter close to the inner diameter of the sample and a plug volume equal to the internal volume of the sample. The load frame moved at a rate of 1 mm/s to compress the plug, thus, the force applied was acquired with time.

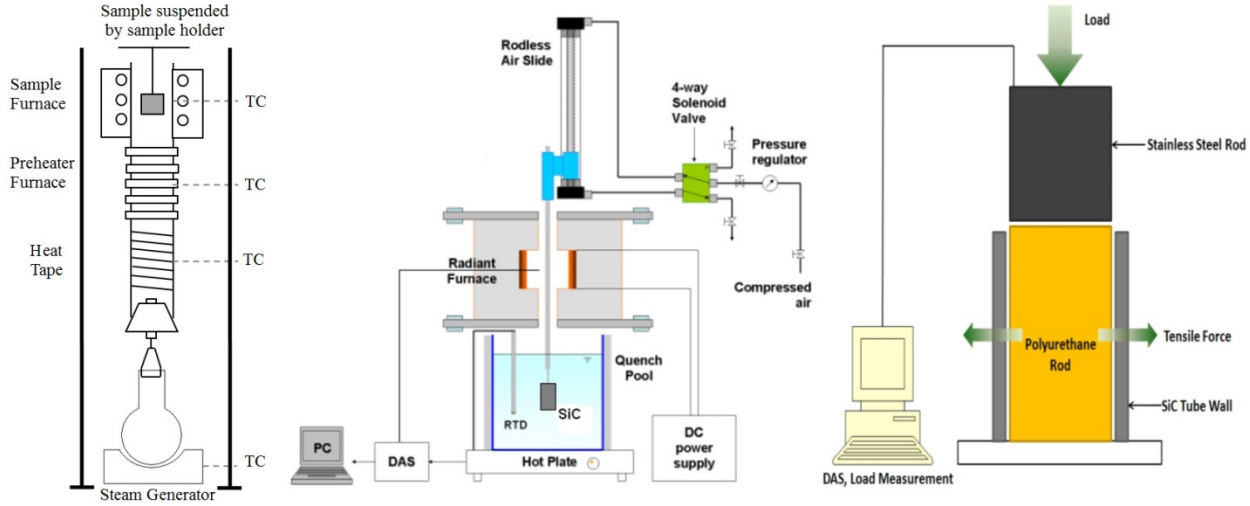

(a) (b) (c)

FIG. 1. Schematics of expermental facilities for out-of-core sample testing (a) Oxidation column (b) Quench apparatus (c) Burst test.

3. PREVIOUS SiC TUBE TESTING

Prior to conducting experiments using CMC SiC, a wide range of tests were performed on monolithic α SiC tubes, Saint-Gobain Hexoloy. The trends witnessed in these tests were used to inform the subsequent and ongoing testing on CMC SiC. In addition, operational experience in proper procedure for running these tests was obtained, and ensured accurate CMC SiC results.

3.1. Steam oxidation

As mentioned, through the use the oxidation column, the weight change of SiC in steam at a wide range of exposure times, steam flow rates, and temperatures has been obtained. At the conditions tested, the SiC weight decreased linearly with time, as expected. Semi-empirical correlations for the normalized weight loss rate have been developed [5]. These correlations are based on non-dimensional conservation equations and a heat and mass transfer analogy. From these correlations, the limiting effects of lower temperature and/or lower flow rate could be observed. At lower temperatures, the oxidation of the SiC to SiO_2 becomes limited. Thus, the SiO_2 layer forms slowly and will rapidly volatize in the flowing steam. When flow is limited the low steam velocity slows the SiO_2 volatilization leading to a thicker oxide layer. Based on the monolithic SiC tube testing results, CMC SiC test conditions were selected to be representative of reactor accidents as well as avoiding conditions that are either temperature or flow limited.

3.2. Quench testing

A number of quench tests were performed using both tubular and bar shaped SiC as well as bar shaped Al_2O_3 [5]. All samples survived as well or better when quenched into water near saturation compared with room temperature water. At larger initial sample temperatures, this discrepancy became quite pronounced. In order to obtain a better understanding, high speed video recordings were taken of the quenching transient. In examining these videos, it was seen that, in the saturated pool, a vapour film quickly forms around the sample, cooling it slowly, whereas, in the room temperature pool, liquid conduction to form the vapour film is prolonged, compared to room temperature water, and this rapidly cools the outer edge of the sample. This creates a large, initial thermal gradient across the ceramic sample that is not experienced when quenched in saturated water. A larger temperature gradient leads to larger thermal stresses experienced by the sample. It is this thermal stress that leads to the sample cracking and breaking more easily when quenched into room temperature water. Extensive thermal stress calculations during the various quenching heat transfer regimes has been conducted [5]. The duration of each heat transfer regime observed via the high speed video is used in these calculations.

3.3. Burst testing

While the sample may remain intact, it is possible that previous testing by oxidation and quenching has damaged the sample, causing it to lose some of its strength. For this reason, the strength of both as received, to establish a baseline, and post testing samples are measured. As seen in Fig. 2, monolith SiC quenched into saturated water survived without a loss of strength for all sample temperatures examined. In comparison, some samples quenched into room temperature water appeared to be unaffected, but when examined by burst testing a noticeable loss in strength is observed at temperatures above 400°C. Similar results were obtained for the bar samples as well. Note that these bar samples could not be examined by a burst test. Instead, a four-point bend test was used.

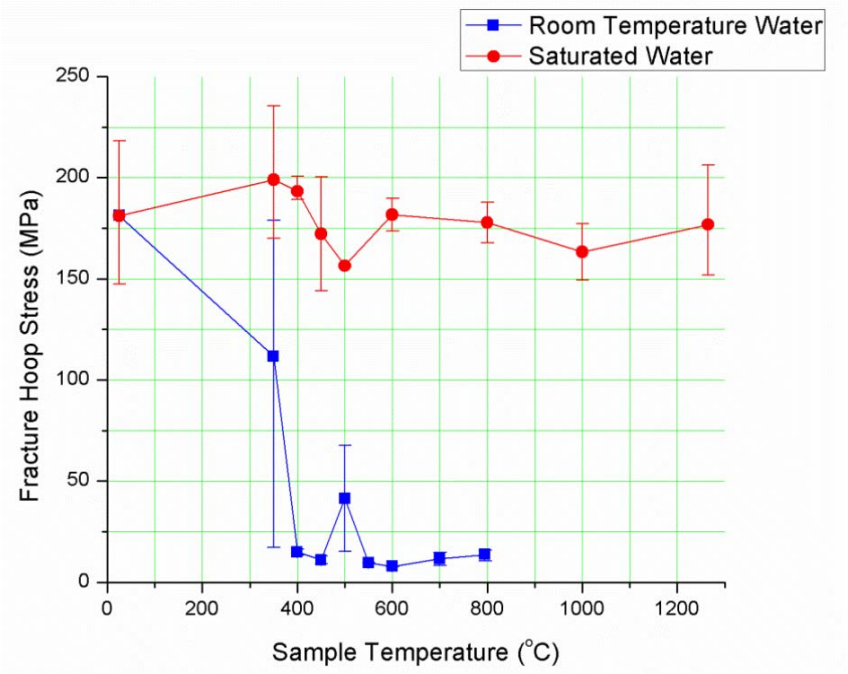

FIG. 2. Fracture hoop stress of monolith SiC as a functon of sample (quenching) temperature and subcooling.

4. CMC SIC TUBE SAMPLE TESTING

As a part of a new project, five different architectures of CMC SiC samples are to be tested, with up to ten samples of each architecture to undergo testing.

4.1. Samples received

The first three architectures, designated as WEC01-xxx, are roughly similar, each differing primarily by how the tows were laid/woven. The other two architectures differ primarily in that one is a tube, open on both ends, while the other has one end (the bottom end, for testing purposes) closed. All CMC SiC tube samples were manufactured by General Atomics.

To date, testing has been completed on the architecture designated as WEC01-196. As can be seen in Fig. 3, the fibres in these samples are laid out in a simple crossing pattern, this the next layer roughly perpendicular to the layer below it. It can also be seen that, while an environmental barrier coating has been applied to the samples, the outer surface still has some contours and roughness.

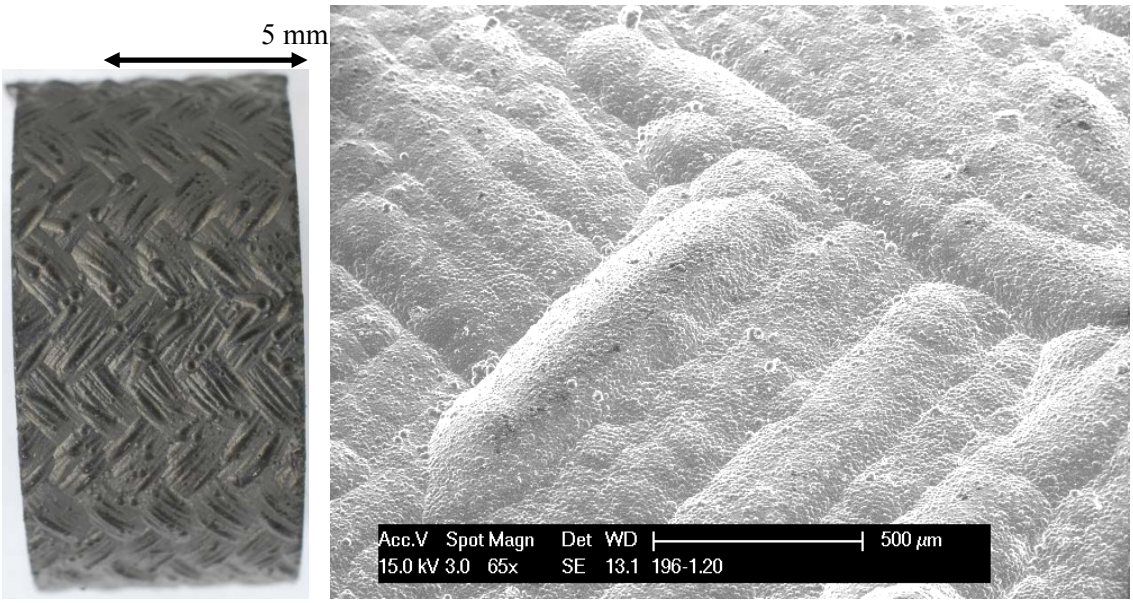

FIG. 3. As-received images of WEC01-196 samples (a) Optical – 196-1.19 (b) ESEM – 196-1.20.

The following table details the size and specifications of the four samples labelled WEC01-196 that have been tested.

TABLE 1. WEC01-196 SAMPLE SIZES, MASS, AND TESTS CONDUCTED

Sample Category	Sample Number	Test(s) Conducted	Avg Height (mm)	Avg Wall Thickness (mm)	Avg Outer Diameter (mm)	Sample Mass (g)
WEC01-196	1.19	High Temp Ox. & Burst	6.62	2.63	13.58	1.4052
WEC01-196	1.20	Quench & Burst	20.24	2.63	13.57	4.2560
WEC01-196	1.26	Quench & Burst	20.78	2.64	13.57	4.3918
WEC01-196	1.27	ARS Burst	20.48	2.65	13.54	4.1907

4.2. Test results

As described above, previous work with monolith SiC and the given properties CMC SiC samples helped to dictate the test conditions for these latest samples.

4.2.1. Oxidation

Based on past testing, it was desirable to test at flow conditions representative of an accident, but such that the oxidation process was neither flow nor temperature limited. For this, CMC SiC samples are oxidized at ~6 g/min at 1400°C. The WEC01 samples, like all CMC SiC samples, have an environmental barrier coating to avoid oxidizing the carbon in the matrix layer. Based on monolith SiC oxidation rate correlations, it was determined that tests could be run for 48 hours at this condition without completely oxidizing the EBC.

After exposing sample WEC0196-1.19 to steam as described, the sample gained 4 mg of mass. As mentioned, a weight gain for SiC at these test conditions should lead to a loss of mass. In order to explain this observation, SEM images were taken and an overall image can be seen in Fig. 4. There is no evidence of an oxide layer on the outer or inner diameter; however, there is an added layer inside the openings between fibre layers. To confirm this, EDS line scans were taken at several locations, as found in Fig. 5.

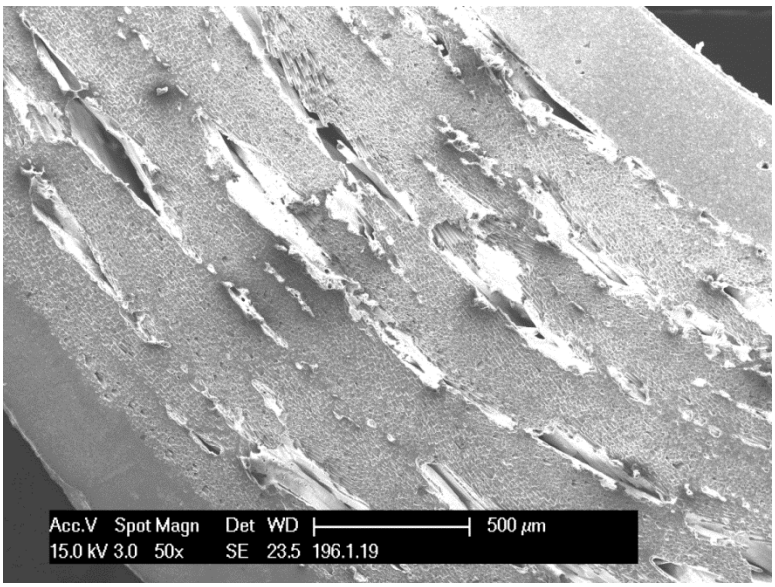

FIG. 4. SEM image of WEC01-196-1.19 after 48 hrs steam oxidation at 1400°C.

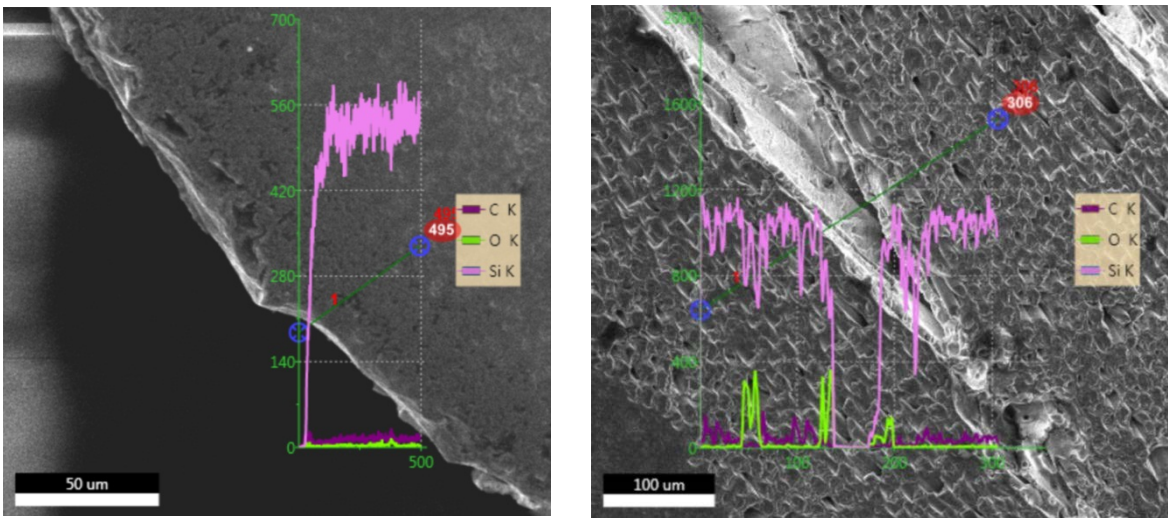

(a) *(b)*

FIG. 5. EDS line scans of (a) exterior and (b) interior of WEC01-196-1.19 after steam oxidation.

From the images taken, it is clear that the volatilization process is retarded, if not completely eliminated, between the fibre layers. For this reason, a relatively thick oxide layer was able to form in the gaps between the fibre layers. With the lack of volatilization on the interior surfaces, mass is gained as oxygen is reacted. The net mass change between the oxidation on the exterior surfaces with volatilization and the interior surfaces with limited volatilization leads to the relatively small mass gain recorded.

4.2.2. Quench

As it is useful to be able to compare CMC SiC data with monolith SiC data from previous tests, the furnace temperature for these was chosen as 1200°C. This is roughly the upper temperature limit at which previous quench data exists. As mentioned, based on RELAP simulation, it was found that quenching into near saturated water is more representative of accident conditions. This is important given the impact of subcooling on quench survivability and loss of strength.

Two samples were quenched as described. Likely due to the increased mass compared with α-SiC samples, the time to complete the quench transient for these WEC01 was several times longer than that for previous tests. Due to memory limitations, the first quench test (196-1.20) high speed video was unable to record the full transient. After adjusting settings, the complete event was recorded for the second quench test (196-1.26), with screenshots included in Fig. 6. The events shown are the sample first entering the water bath at the initial $t = 0$. Next is the sample reaching the lowest point for the driving rod, followed by an image showing a well-developed vapour film surrounding the sample. In the fourth image, a quench front of liquid water coming in contact with the sample instead of water vapour is seen moving up the sample. A large amount of bubbles can be seen outside the film, due to transitioning from film boiling to nucleate boiling. Lastly is an image showing the end of the transient, just as the quench front finishes moving up the sample.

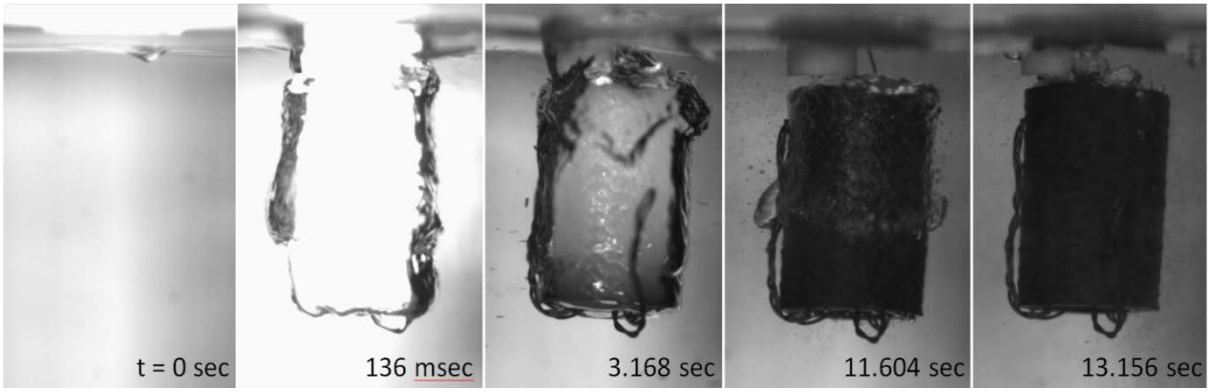

FIG. 6. Time -stamped images from high speed video during quenching testing.

As more samples are tested, an effort to normalize the quench transient times will be made. This will take into account both the mass and size of the samples. Using these normalized values, comparisons between samples tested will be made, to determine relative sample properties such as thermal conductivity.

4.2.3. Burst

For the burst test, no changes were made from previous tests, simply improvements. For the CMC SiC samples, the polyurethane tube was machined down to a diameter within roughly 0.3 mm of the inner diameter of the tube. Small variations in sample size and lack of a perfect right cylinder inner monolith led to variation in this fit tolerance. The polyurethane diameter used was 7.9 mm.

Given that the WEC01 samples are relatively thick-walled and are made of three layers-including a fibre layer, the interpretation of this into a failure stress from the load v.

displacement curve depends on simplifying assumptions. The first crack is in the inner monolith layer. Based upon the assumption that the elasticity in the fibre layer is much larger than that of the inner monolith layer, it can be assumed that all loading from the plug leads to stress in the monolith layer. For this, the monolith layer was taken to be 480 μm. The ultimate crack is a crack that penetrated fully through the sample wall, leading to the load dropping to roughly zero. By this point, cracking within the monolith has been audible repeatedly, leading to the sample's inner monolith being destroyed. From this, it can be assumed that the loading at the time of the final crack is exclusively a stress in the fibre layer. A second perspective on each of these cases is to assume the sample is uniform and calculate an average stress across the entire wall. The results from these tests are detailed in Tables 2-3.

TABLE 2. FIRST CRACK LOADS IN CMC SiC SAMPLES

Sample Category	Sample Number	Test(s) Conducted	Load at First Crack (kN)	Stress at First Crack, Assuming Monolith Only (MPa)	Stress at First Crack, Assuming Entire Wall (MPa)
WEC01-196	1.19	High Temp Ox. & Burst	TBD	TBD	TBD
WEC01-196	1.20	Quench & Burst	2.53	499	123
WEC01-196	1.26	Quench & Burst	2.72	536	133
WEC01-196	1.27	ARS Burst	2.67	524	130

TABLE 3. FINAL CRACK LOADS IN CMC SiC SAMPLES

Sample Category	Sample Number	Test(s) Conducted	Load at Final Crack (kN)	Stress at Final Crack, Assuming Fibre Only (MPa)	Stress at Final Crack, Assuming Entire Wall (MPa)
WEC01-196	1.19	High Temp Ox. & Burst	TBD	TBD	TBD
WEC01-196	1.20	Quench & Burst	5.87	434	286
WEC01-196	1.26	Quench & Burst	5.44	402	265
WEC01-196	1.27	ARS Burst	5.61	414	273

5. IRRADIATION TESTING

Radiation in the core of an LWR may influence material behaviour through several different mechanisms. Cumulative damage to the microstructure including dislocations and transmutations may induce local stresses, swelling, and changes in mechanical properties such as yield strength, toughness, and elastic modulus. There are also effects on a much shorter timescale – for example radiolysis in the reactor coolant will produce chemical species that may attack surfaces and especially crevices, or promote transport or deposition of corrosion products. In order to capture these important effects, integrated irradiation testing is an important tool for evaluating the performance of LWR core cladding and structural materials.

5.1. Irradiation facility

The irradiations described in this paper took place in the water loop facility at the MIT Research Reactor (MITR). The MITR is a 6 MW light-water-cooled, heavy-water-reflected tank-type research reactor located on the MIT campus. The reactor's core configuration provides three dedicated positions for in-core irradiation tests; one of these positions is used for a long-term water loop facility. Because the reactor's primary system operates nominally at 50°C and atmospheric pressure, in order to provide a typical LWR environment it is necessary to operate a self-contained loop. This allows control of the experiment temperature, flow, pressure, and chemistry conditions independent of the reactor while benefitting from the neutron and gamma radiation. Because of the compact size of the MITR core, the neutron flux and spectrum in the water loop position are comparable to those found in commercial power plants (6×10^{12} n/cm^2·s thermal and 8×10^{13} n/cm^2·s >0.1 MeV at 6 MW), making it an excellent proxy for real-time irradiation testing.

The current MITR water loop facility has been used since 2006 for irradiation of SiC specimens under typical PWR and BWR core conditions. The loop, shown schematically in Fig. 7, consists of a primary loop with a titanium autoclave to contain the specimens in-core, electrical heating and pumping to provide flow and thermal control, and a let-down system with chemistry monitoring, cleanup, and pressure control subsystems. The loop normally operates at 296°C at the inlet to the specimen section, with negligible temperature drop across the in-core region. Pressure is maintained at 10.3 MPa to keep the system sub-cooled, i.e. prevent boiling, and the total coolant flow is approximately 0.25 kg/s.

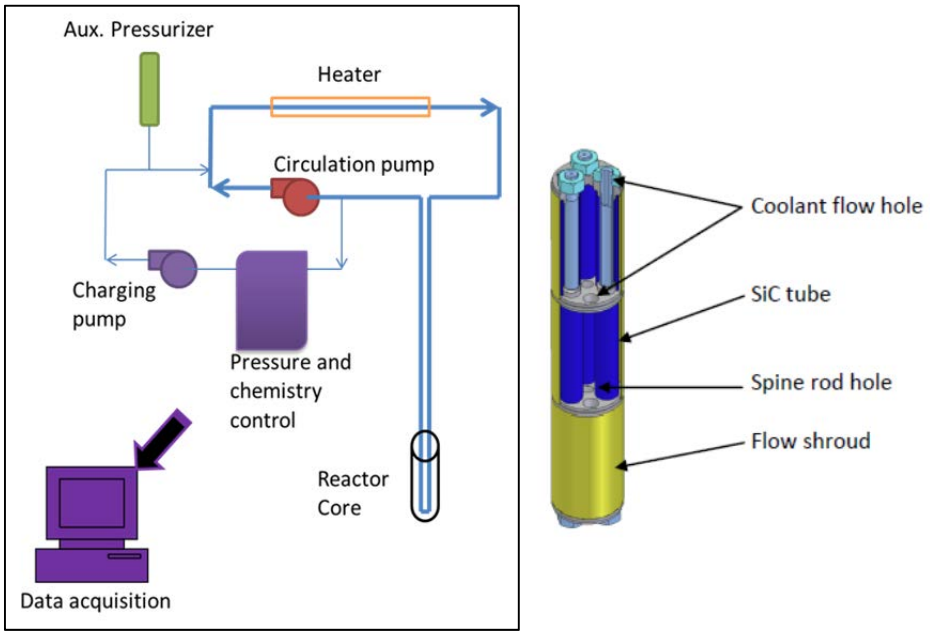

FIG. 7. Schematic of the water loop system (left) and example of a specimen capsule (right).

Two thermocouples in-core and a dozen thermocouples in the out-of-core sections provide real-time feedback and monitoring of the main loop, along with static pressure and circulating pump pressure drop. The letdown system can incorporate a variety of sensors including electrical resistivity, dissolved oxygen and hydrogen, and pH. The water chemistry is normally controlled by applying an overpressure of hydrogen gas and utilizing a catalyst to remove oxygen from the system, in concert with ion-exchange resins and particulate filters. In order to simulate PWR chemistry conditions, boric acid and lithium hydroxide may be added as well after appropriate reconditioning of the ion resins.

The in-core section, approximately 5 cm in diameter, can contain specimens in the 46 cm active length of the core and several meters above it. Flow is directed down the inside diameter of the autoclave tube to the bottom of the core, and then flows upwards over the specimens before exiting the core tank.

5.2. Specimen irradiations

A series of irradiation campaigns have taken place, testing a range of SiC materials. Interest has focused on using SiC to replace traditional zirconium-alloy fuel cladding, requiring a strong and hermetically-sealed structure that would retain fuel and fission products [8]. One such design uses an inner monolithic SiC tube surrounded by an SiC matrix-infiltrated SiC fibre composite. This structure may then be over-coated with additional SiC in order to form an outer barrier coating. The first set of tubes with this "triplex" structure were irradiated under hydrogen water chemistry conditions (<10 ppb O_2) in the MITR loop during a series of irradiations lasting 102, 238, and 240 days.

The specimens, described in Table 3, consisted of α- and β-phase SiC from different manufacturers and formed using different techniques. The tube specimens *A* through *I, M, R7,* and *T* are approximately 5 cm long, 0.5-1 mm wall thickness, and 0.9-1.1 cm outer diameter. The first series of irradiations was primarily a scoping study with small numbers of each type of tube used to identify promising candidates for further testing. A subset of the tube types had specimens located in a region above the core and outside of the appreciable neutron flux, downstream of the in-core section. These specimens would be exposed to coolant conditions and gamma flux very similar to the in-core specimens but without the neutron irradiation. Based on the experience from these initial irradiations, a follow-up set of irradiations (46 and 371 days) focused on a single type of triplex tube "R7" and their monolith-only parts "R7M". The post-irradiation data on this second set (including all "R7M" specimens) is not yet available.

Following these tests, a third set of irradiations for 90 days focused on SiC for use as core structural materials rather than fuel cladding. These specimens were fibre composite rectangular plates "Co" (76×10×1.5 mm) and "Cr" (89×10×1.5 mm) and tubes "RR" (50 mm long, 2 mm thick, and 13.5 mm outer diameter). The water chemistry was altered for this irradiation by replacing the hydrogen cover gas with helium to achieve ~1 ppm dissolved oxygen for conditions more similar to BWR coolant.

TABLE 3. TYPES OF SiC TUBE SPECIMENS IRRADIATED IN TH MITR WATER LOOP

Designation	Monolithic Tube	Composite fibre / Matrix	Barrier Coating
Composite			
A	Trex	Hi-Nicalon-S / CVI	N/A
B	Trex	Hi-Nicalon-S / CVI	HyperTherm CVI
C	Trex	Hi-Nicalon-S / PIP	TA&T CVD
D	Trex	Sylramic iBN / CVI	Trex CVD
E	Trex	Sylramic iBN / CVI	HyperTherm CVI
F	CoorsTek	Hi-Nicalon-S / CVI	HyperTherm CVI
G	CoorsTek	Sylramic iBN / PIP	TA&T CVD
H	CoorsTek	Sylramic iBN / CVI	HyperTherm CVI
I	Trex	Hi-Nicalon-S / CVI	Trex CVD
R7	Trex	Hi-Nicalon-S / CVI	HyperTherm CVI
RR	N/A	HyperTherm	N/A

Designation	Monolithic Tube	Composite fibre / Matrix	Barrier Coating
Monolith Only			
M	Coorstek	N/A	N/A
T	Trex	N/A	N/A
R7M	Trex	N/A	N/A

5.3. Irradiation results

Post-irradiation examinations took place at the MIT Nuclear Reactor Laboratory. The specimens were removed from their irradiation capsules in the MITR main hot cell, and after screening for activity moved to lab spaces for further study.

5.3.1. Post-test inspection

From a handling perspective, SiC is convenient because of its low level of activation compared to zirconium alloys. The predominant activation product, ^{14}C, is a beta emitter that is easily shielded. The primary dose from the SiC extracted from the water loop was due to deposition of corrosion products, primarily ^{60}Co and ^{46}Sc from the piping and capsule structures, onto the specimen surfaces. When zirconium-bearing specimens were present in the loop, ^{95}Nb and ^{95}Zr were also detected. This contamination was most pronounced on the fibre composites with deeply textured surfaces and open porosity. In general, total radioactivity of any SiC specimen was low enough to allow immediate unshielded manual handling.

For most specimens there was no dramatic change in their appearance after irradiation, other than some lightening or darkening of the surfaces. On the poorest performing tubes ("C") cracking occurred during the irradiation (see Fig. 8), and on some "R7" tubes that were over-coated to protect the ends, some of this over-coating chipped or delaminated. During the first round of tests it was noted that there were lighter-coloured regions at the ends of some composite tubes of approximately 20-40 mm. It was hypothesized that this was due to preferential attack on the open porosity and exposed inter-layer and matrix material exposed at the ends of the tube where they had been cut from longer stock. These areas would not normally be exposed to water, and while these ends have no flow directed over them in the experiment, no special provision was given to protect them. After the first two rounds of irradiations, tube specimens were over-coated at the ends to attempt to protect these areas ("R7"). Similar attack was seen at the ends of the plate specimens (see Fig. 9).

FIG. 8. SEM of a crud deposit on a fibre composite surface (left); post-irradiation images of triplex tubes from the first round of irradiation "C" (centre left), "F" (centre right), and "R7" (far right).

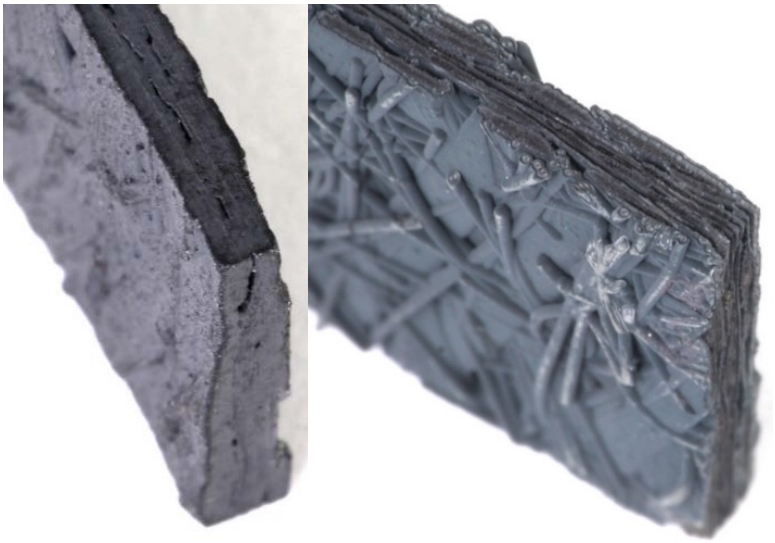

FIG. 9. Macrophotography of "Co" composite plates before and after exposure in the loop showing removal of matrix material.

Dust and debris generation was a persistent issue during handling of the irradiated composites. This material appeared to primarily emanate from the cut ends of the tubes, or in some cases where the outer coatings or composites had cracked, from these fracture surfaces. While in general this material proved to be too small to significantly affect weight change measurements, it does pose a contamination and abrasion hazard.

5.3.2. Corrosion

The initial procedure for measuring weight change involved allowing the specimens to air dry followed by repeated baking at 120°C in air until no additional change was detected. In practice, a single bake-out for 15 minutes was sufficient to remove the additional moisture. As discussed previously, the specimens with fibre composite layers were believed to be experiencing preferential corrosion at the cut surfaces at the ends of the tubes. In an attempt to

reduce this effect and allow for better (though not ideal) comparison for the initial scoping analysis, approximately 0.7 cm was cut from each end of composite tubes with a low-speed saw to allow comparison assuming a constant mass per unit length. Later tube specimens ("R7") were over-coated at the ends to prevent this and were therefore not cut before weighing.

Because there has not yet been a measurement of the effective surface area of the specimens, weight loss is given only in terms of percentages of initial mass. Fig. 10 plots the weight changes for all of the composite specimens. The wide spread of corrosion rates reflects the strong dependence of composition and manufacturing on SiC performance. The specimens with the most weight loss were those without an outer barrier coating ("A") leaving the composite more exposed, and the two composites formed by polymer impregnation ("C" and "G"). Those tubes with the lowest corrosion rates were the monoliths and the "F", "H", and "R7" triplex tubes. When normalized by exposure time as in Fig. 11, it is more apparent that the corrosion rate is remains steady over time and that there is also a substantial increase in corrosion due to the presence of neutron irradiation. Note that the monolith specimens, made from the same material underlying the composite layers of the triplex tubes, are the most resistant to oxidation.

There is a large spread in the "R7" data due in part to delamination of the outer coating applied to prevent preferential attack the cut ends of the tube. Also it is not known whether the high rates of corrosion experienced by the composite-only specimens was due to the presence of unprotected cut surfaces or the higher dissolved oxygen content in those tests.

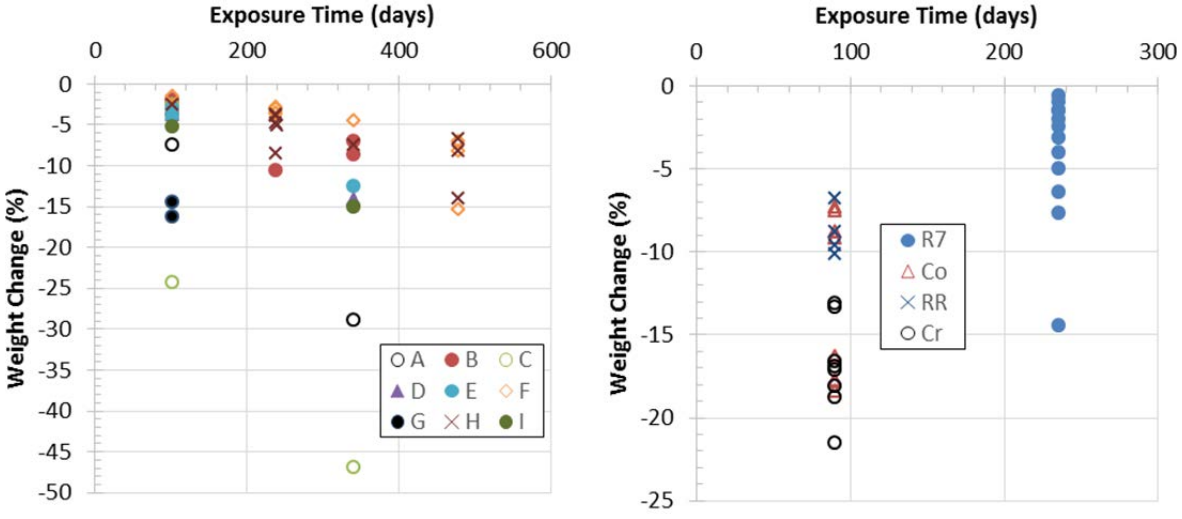

FIG. 10. Weight change results for triplex tubes (left) and R7 and composite-only specimens (right).

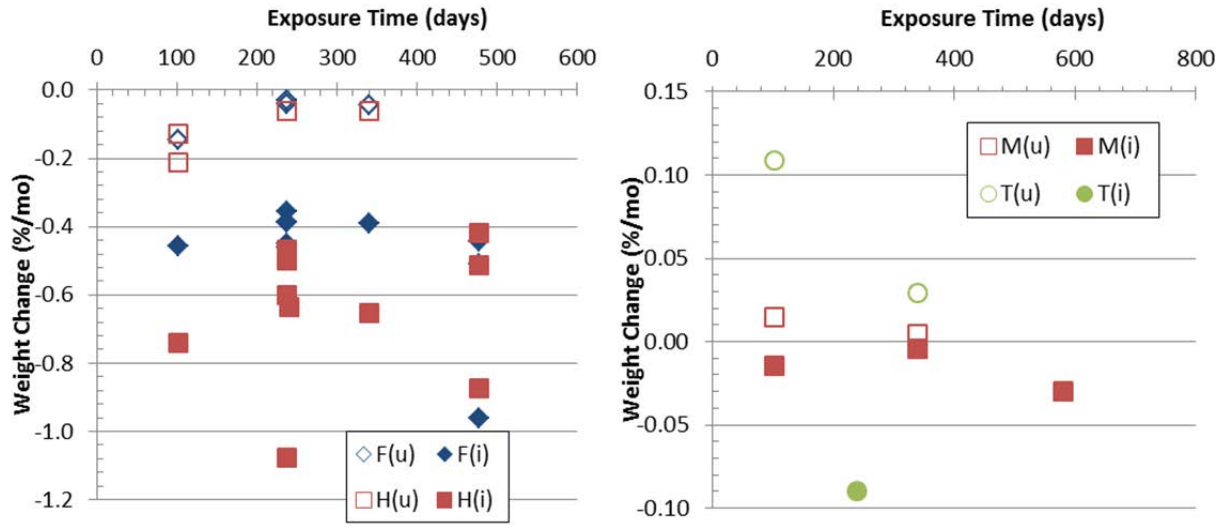

FIG. 11. Rate of weight change data for two types of SiC triplex tubes (left) and monoliths (right) with irradiated (i) and downstream of the core with no neutron flux (u) specimens.

5.3.3. Burst testing of irradiated samples

A primary concern for fuel cladding is the hoop strength – as fuel pellets swell due to fission product accumulation or thermal transients, the pellets may come into physical contact with the cladding. In addition, fission gas release into the fuel rod will gradually increase its internal pressurization. It is important to determine how SiC cladding will resist these forces to prevent release of fuel and fission products and deformation of the rod geometry.

A mechanical expanding plug test machine was constructed by Ceramic Tubular Products and used to test specimens as-received, those that were exposed normally in the water loop, and those that were in the water loop but outside of the core (no neutron irradiation) downstream of the in-core specimens. The machine uses a hydraulic ram to compress an elastomer plug, positioned inside of the tube specimen, against a counter-pin mounted to a force plate. Micrometers allow the travel of the ram head to be measured versus the force applied to elastomer. The elastomer quickly achieves plastic deformation, simulating internal pressurization of the tube.

The results of this testing are shown in Figs 12 and 13 for different sets of specimens. The overall data suggests a reduction in strength for those tubes exposed to neutron irradiation; however it is difficult to draw conclusions for several reasons. First, there are few duplicate specimen types tested due to the limited space in the scoping irradiations and the need to carry some specimens forward intact for other testing. Second, it is expected there will be inherent scatter in the ultimate strength of SiC materials due to the dependence on random flaws as crack initiators. This variation can be described using Weibull statistics; however there is limited data available for these types of composites to create fitting parameters [5]. In addition, while ultimately the hoop strength of the tube is the figure of interest, it is difficult to determine how that should be calculated based on this test, as the stress distribution between the monolith and composite layers of the triplex tubes is not known.

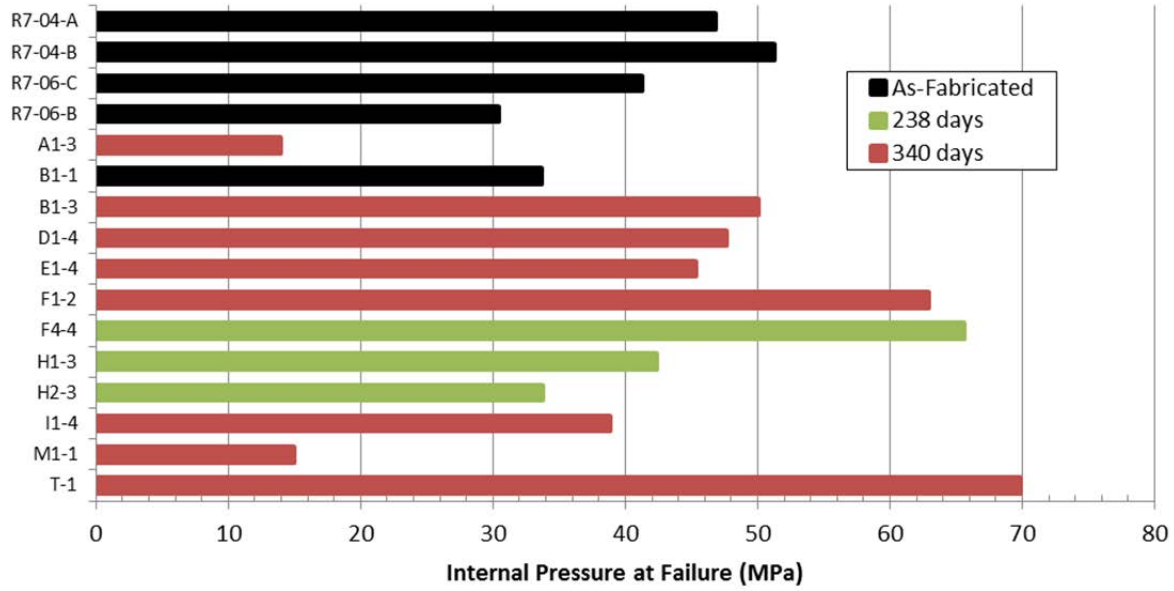

FIG. 12. Results of burst testing of un-irradiated SiC tubes, either in as-received condition or exposed in the water loop but outside of the neutron flux downstream of the in-core specimens (incl. [9]).

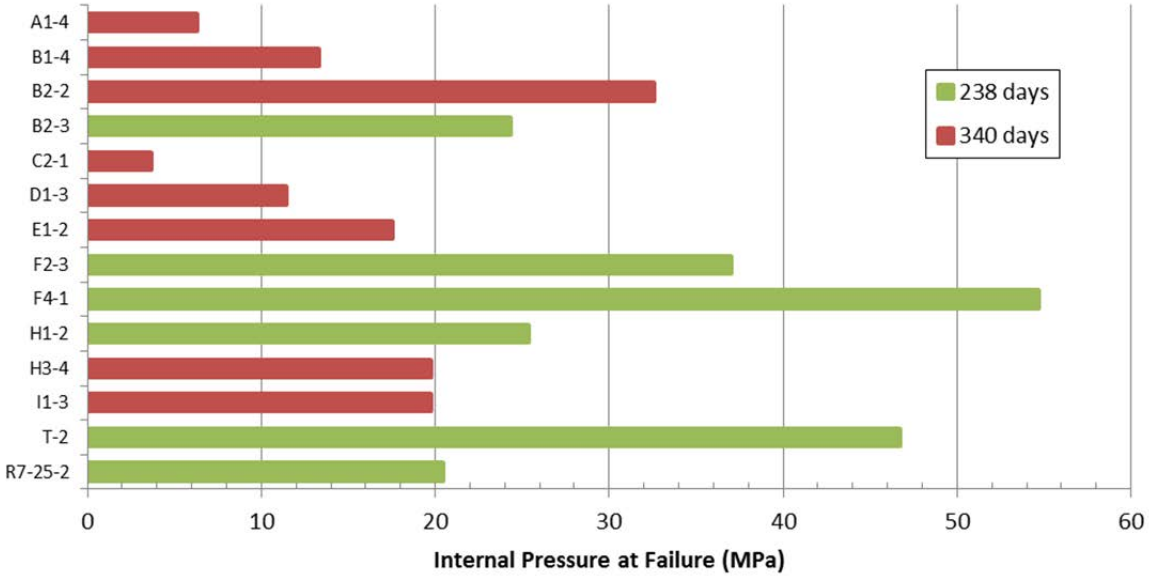

FIG. 13. Results of burst testing irradiated SiC tubes (incl. [9]).

An important finding of the burst testing was the "pseudo-ductility" of triplex tubes after failure. This is a dramatic difference in performance between monolithic tubes and those with an outer fibre composite – the monolithic tubes fracture explosively at the point of through-wall crack propagation, whereas composite tubes fail in a more graceful manner, retaining their general shape and instead growing an axial crack that allows the tube to open from the point of failure. This has important implications for maintaining a cool-able geometry and preventing fuel migration in the event of cladding damage.

5.3.4. Thermal diffusivity

The fuel cladding is part of the primary path of heat conductance from the fuel to the reactor coolant, and therefore fuel temperature is dependent on the cladding conductivity. SiC

thermal conductivity has a strong dependence on irradiation [1], and at 300°C this effect begins to saturate after 0.1 DPA (about 1 month in the MITR).

The thermal diffusivity of the SiC specimens was measured [9] using a xenon-flash technique from 25-300°C. Because the specimens irradiated in the water loop are in a tube geometry, the disk-shaped diffusivity specimens cut from these tubes have a fixed curvature. Measurements were taken with the curvature facing towards and away from the detector, with generally only small differences noted, and the results averaged. As shown in Fig. 14, the diffusivity of SiC decreases both as a function of temperature and irradiation. Monolithic CVD SiC has the highest diffusivity, and composites lower diffusivity due in part to their fibre/matrix anisotropy and matrix voids. It is expected that in a multi-layer cladding design there will be additional thermal resistances introduced at the interfaces between the monolithic and composite layers. In preparing the triplex tubes after irradiation it was found that there was poor adhesion between these layers and this de-bonding may contribute to additional thermal resistance not found in an intact tube.

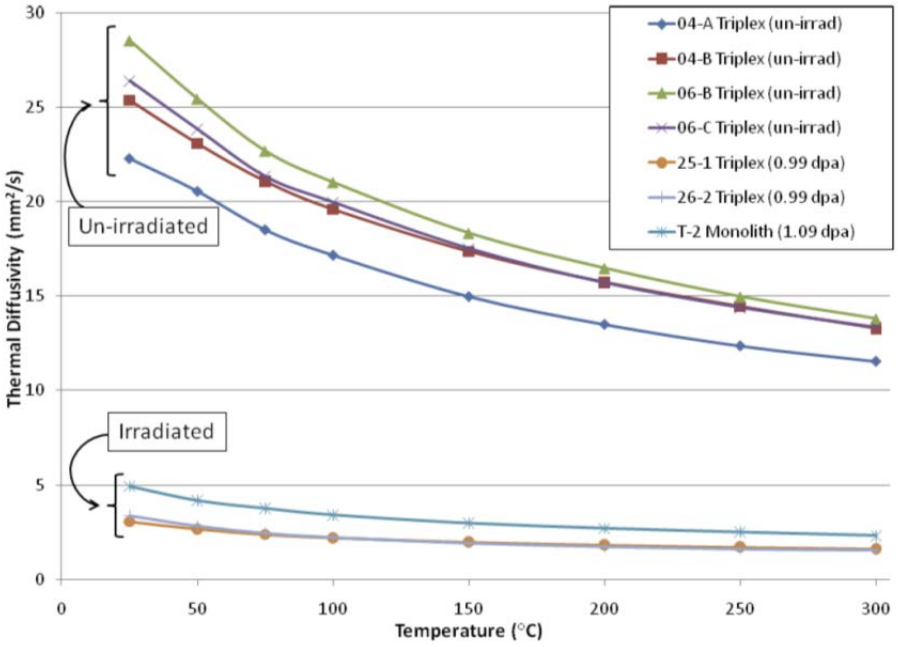

FIG. 14. Thermal diffusivity of R7 SiC tubes and Trex monolith.

6. SUMMARY

Exposure of SiC and SiC fibre composites in the MITR water loop facility has generated data on corrosion rates and property changes as a function of irradiation with some specimens achieving up to 600 days exposure. Monolithic CVD SiC has the lowest corrosion rates, however designs incorporating fibre composites offer better mechanical behaviour. The corrosion of the composite layers is driven strongly by details of their manufacturing and availability of the matrix and open porosity to the coolant; neutron irradiation also has an accelerating effect on this corrosion. Initial investigations into changes in strength indicate a trend due to composition and irradiation, but require large sample sizes due to statistical noise. Thermal diffusivity (and therefore conductivity) is a strong function of irradiation and composition. The composite and composite/monolith interfaces are important sources of thermal resistance and will significantly impact the heat transfer performance of SiC materials.

ACKNOWLEDGEMENTS

The authors are grateful to Westinghouse Electric Corporation for sponsoring the work, DOE NEUP for Michael Pantano's fellowship, and General Atomics and Saint-Gobain for providing SiC tube samples. The irradiation testing was supported by U.S. Department of Energy (SBIR grants and the ATR National Scientific User Facility), Gamma Engineering Corporation, Ceramic Tubular Products, Westinghouse Electric Corporation, and the Electric Power Research Institute, and collaboration with Oak Ridge National Laboratory.

REFERENCES

[1] SNEAD, L.L., et al., Handbook of SiC Properties for Fuel Performance Modelling, J. Nucl Mater. **371** (2007) 329.

[2] CARPENTER, D.M., AHN, K., KAO, S.P., HEJZLAR, P., KAZIMI, M.S., "Assessment of Silicon Carbide Cladding for High Performance Light Water Reactors", Nuclear Fuel Cycle Program. CANES, MIT MIT-NFC-TR-098 (2007).

[3] OPILA, E. J., Variation of the Oxidation Rate of Silicon Carbide with Water-Vapour Pressure, Journal of the American Ceramic Society, **82(3)** (1999) 625-636.

[4] OPILA, E., Volatility of Common Protective Oxides in High-Temperature Water Vapour: Current Understanding and Unanswered Questions, Materials Science Forum, **461** (2004) 765-774.

[5] LEE, Y.H., McKRELL, T., KAZIMI, M.S., "Safety of Light Water Reactor Fuel with Silicon Carbide Cladding", Advanced Nuclear Power Program, CANES, MIT, MIT-ANP-TR-150 (2014).

[6] TERRANI, K.A. et al, Silicon Carbide Oxidation in Steam Up to 2 MPa, J. Am. Ceram. Soc. **97** (2014) 2331-2352.

[7] KATOH, Y., SNEAD, L. L., NOZAWA, T., KONDO, S., BUSBY, J. T., Thermophysical and Mechanical Properties of Near-Stoichiometric Fibre CVI SiC/SiC Composites after Neutron Irradiation at Elevated Temperatures, J. Nucl. Mater, **403** (2010) 48-61.

[8] CARPENTER, D.M., KOHSE, G., KAZIMI, M.S., "An Assessment of Silicon Carbide as a Cladding Material for Light Water Reactors". Advanced Nuclear Power Program, CANES, MIT, MIT-ANP-TR-132 (2010).

[9] STEMPIEN, J.D., CARPENTER, D.M., KOHSE, G., KAZIMI, M.S., "Behaviour of Triplex Silicon Carbide Fuel Cladding Designs Tested under Simulated PWR Conditions", Advanced Nuclear Power Program, CANES, MIT, MIT-ANP-TR-135 (2011).

[10] RAMSEY, A. P., McKRELL, T., KAZIMI, M. S., "Silicon Carbide Oxidation in High Temperature Steam", Advanced Nuclear Power Program, vol. MIT-ANP-TR-139, September (2011).

TECHNICAL AND ECONOMIC VIABILITY OF CERAMIC MULTI-LAYER COMPOSITE SIC CLADDING FOR LWRS

K. SHIRVAN, M.S. KAZIMI
Nuclear Science and Engineering Department, MIT
United States of America
E-mail: kshirvan@mit.edu

Abstract

The Ceramic Multi-layer Composite (CMC) cladding has been under investigation at MIT for many years. Recently, increasing focus has been given to the modelling and performance of the cladding under PWR conditions for traditional and advanced fuel designs. These designs include use of annular pellets to reduce the centreline fuel temperature while including additional free volume to accommodate fission gases. Another option considered is adding a small amount of BeO to improve the thermal conductivity of the fuel. The reactor physics of both of these options were analyzed and found to have similar behaviour to a core with zircaloy cladding. These options often come at the cost of higher enrichment requirements. A third option was the replacement of the helium with liquid lead-bismuth in the fuel-cladding gap to improve its thermal conductivity. If the average fuel temperature and plenum pressure are considered as figures of merit, the BeO fuel was seen as the best option among the three designs. The economic implication of investing in CMC cladding for the current US operating reactors to improve the accident tolerance of nuclear fuel is analyzed. The CMC cladding is the only option among the proposed accident tolerant fuel concepts in the US that could result in a fuel enrichment savings, thus compatible with current enrichment infrastructure. The CMC cladding could also result in additional economic benefit by avoiding the costs that might be incurred following a severe accident. However, due to its long development period and likely higher cost of manufacturing compared to zircaloy, its economics merits are uncertain. The significant role that thermal conductivity degradation and swelling induced irradiation plays in performance of CMC cladding has already been documented. However, the impact of material properties on the performance of the neighbouring layers has been underrated and found recently to be critical for the viability of the concept. The current analysis using finite element software ADINA shows that by considering the existing irradiation data for composite fibres and CVD SiC, a promising design can be achieved with an inner monolith surrounded by a fibre composite that compress the inner monolith layer followed by an environmental CVD barrier coating. A sensitivity study of the thermo-mechanical performance of such three layer cladding and its comparison to a two layer design with an inner composite and thick outer monolith layer are also presented.

1. INTRODUCTION

The goal of achieving higher burnup and extending the fuel residence time in light water reactors has been one of the main areas of focus for nuclear R&D. Such improvements have been achieved through structural changes to the fuel pin as well as reactor operation strategy. The maximum lifetime of the current fuel in the reactor core is mainly limited by the enrichment available in the commercial infrastructure and the fuel's uncertainty in performing beyond the current experienced lifetime and irradiation fluence. The uncertainty in the fuel performance is dominated by the current zircaloy cladding behaviour, which undergoes accelerated corrosion at high burnups. Therefore, nuclear R&D has been focused on how to improve the zirconium based alloy for extended operation.

However, the Fukushima Daiichi accident highlighted serious safety concerns about the long term pursuit of only zirconium based advanced alloys. Zirconium's exothermic reaction with water at high temperature was also the weak fuel feature in the TMI accident. In order for nuclear power to take the next step in its evolution in safety and performance, advanced safety systems, fuels and designs are required. If the increase in accident tolerance of current reactors in the US is targeted, then the new option must not modify the plant systems greatly to be economically competitive. One such approach is to change the fuel and/or cladding. Under the current accident tolerant fuels (ATF) US programme, the options under study include: a ceramic matrix composite silicon-carbide (CMC SiC), multi component molybdenum based cladding and an advanced iron-chromium-aluminium steel alloy (FeCrAl) as top cladding candidates. All the claddings have been considered for current pressurized water reactors that operate with RFA and OFA fuel (smaller cladding diameter than RFA) [1].

The CMC SiC cladding has been the subject of research for about a decade as an option for LWR cladding to be retrofitted in the existing PWR assemblies [2]. The main advantages of CMC SiC over zircaloy are its orders of magnitude slower reaction with steam during accidents, irradiation stability, high strength and lower absorption of neutrons. Since, monolithic CMC SiC is far too brittle for nuclear operation, where the cladding is subject to stress and vibration, it is common to surround the monolith layer with a fibre composite layer, thus boosting the strength and "effective" ductility of the cladding. The composite layer is porous and thus subject to both oxidation and hydrogen diffusion from the coolant side and fission gas leakage from the fuel side. Hence, the composite layer is typically covered by a thin environmental protective CVD SiC layer on the outside and thick monolithic layer on the inside. Such a configuration yields a base material which is more ductile and fails by cracking when subject to high tensile stress as opposed to shattering of the monolith material [3].

The thermal conductivity of the monolith and the composite degrades to values lower than zircaloy after a small amount of radiation damage. The temperature drop across the cladding may reach 150°C for the hot pins, giving rise to thermal stresses. SiC also swells due to irradiation and the amount of swelling is temperature sensitive, thus each layer will exhibit a different mechanical response [4, 5]. This results in a non-monotonic stress distribution within the cladding thickness. The quantification of the stress distribution is very important in prediction of the cladding performance and failure rates. Typically, a ceramic material's failure strength is associated with a probability determined by its Weibull modulus. The Weibull modulus is also dependent on irradiation and on the manufacturing method as well as the volume of the material [4, 5]. Since the tensile stress in the cladding directly results in some probability of "micro-cracking", there is a non-zero probability for larger cracks resulting in release of fission products. This is hypothesized to compromise the main function of the cladding, which is to contain the fission products within a fuel rod. Therefore, it is highly desirable to minimize the stress induced in the cladding during normal operation and transient conditions. Compared to fuel with zircaloy cladding, a higher fuel temperature will be present due to the fuel-cladding remaining open from lack of SiC creep down, its low thermal conductivity and larger thickness due to current fabrication limitations. This results in higher fission gas release and thus higher plenum pressures. Therefore, while the cladding waterside corrosion in a PWR might not be limiting, the fuel residence time will be limited by the magnitude of allowable plenum pressure during steady state and transient operation.

2. NEUTRONICS PERFORMANCE

2.1. SiC cladding

In terms of the thermal absorption, the capture cross sections of the carbon and silicon are about an order of magnitude smaller than zirconium cross-sections yielding to less parasitic absorption in the thermal spectrum of a light water reactor core. Heinisch et al. [6] estimated the damage per displacement (dpa) of SiC at mid-plane of typical LWR to be 3.1 dpa which is lower than for Zirconium (~4-5).

The neutronics performance of CMC SiC cladding has been assessed at MIT [7, 8]. The analysis used the well-known commercial codes CASMO4e/SIMUALTE3 [9, 10] to perform full core PWR reactor physics calculations. Since CMC SiC is not used in LWRs, the implementation of multi-group ENDFVI libraries in CASMO4e was verified through benchmarking against continuous energy Monte-Carlo calculations using MCNP5 with ENDFVII. The verification study revealed that the relative difference in reactivity between Zirc-4 and CMC calculated by CASMO4e was within 50 pcm of the difference calculated by MCNP5 for a reference 4% enriched UO_2 pin. In the neutronics studies, the zircaloy cladding

was replaced with an equally thick or thicker CMC cladding. The motivation behind analyzing the neutronic performance of the fuel with thicker cladding was due to current limitations on manufacturing. The thicker cladding could result in reduction in fuel volume or reduction in coolant/moderator volume. The neutronic analysis aimed to assess the enrichment gain/loss of different CMC designs in the context of an existing PWR. A 3587 MWth Westinghouse reactor with 193 assemblies of 17×17 RFA type [1] was used as the reference design. Additionally, reactivity coefficients were calculated to assure the safety performance of the core with CMC cladding.

2.2. CMC SiC with advanced fuels

The thicker CMC cladding thickness along with its lower thermal conductivity compared to zircaloy result in higher fuel temperatures. Three options were considered to reduce the fuel temperature: using annular fuel pellets, adding some beryllium-oxide (BeO) to the fuel and replacing the helium gap with a conductive liquid metal (lead-bismuth) [11]. The first two options are expected to have a much stronger impact on reactor physics of the core compared to the third option and thus, were neutronically analyzed. The annular pellets were modelled with 10% void volume in order to reduce the fuel maximum temperature and provide additional space for fission gas release. Similarly, 10% by volume of the UO_2 fuel was replaced with BeO to reduce the fuel temperature by enhancing the fuel thermal conductivity. Three cases were analyzed with the annular pellets, one with the same cladding thickness as zircaloy, while the other two with thicker claddings. One thick cladding design had the same clad outer diameter as the zircaloy design while the other had the same pellet diameter as the zircaloy design (noted by RCF). All the fuel designs for this study are listed in Table 1.

TABLE 1. PHYSICAL CHARACTERISTICS OF FUEL RODS

Parameters	Zircaloy solid	Thin CMC annular	Thick CMC annular	Thick CMC RCF annular	Thick CMC w/BeO solid
Clad OD (mm)	9.50	9.50	9.50	10.13	9.50
Clad thick (mm)	0.56	0.56	0.89	0.89	0.89
Pellet OD (mm)	8.18	8.18	7.54	8.18	7.54
Pellet ID (mm)	0.00	2.59	2.59	2.59	0.00
U per rod (kg)	1.779	1.603	1.336	1.603	1.362
U per assy (kg)	469.7	423.1	352.8	423.1	359.4

Before full core physics simulations of advanced fuels could be performed, an average pin power history from the base zircaloy cladding core was used to model the fuel performance of the advanced fuel designs. The analysis would then generate fuel average temperatures as a function of burnup, as shown in Fig. 1a, that will inform the SIMULATE3 core simulator to use cross sections with the correct temperature. The analysis also would generate fuel plenum pressures for each design as shown in Fig. 1b. If the fuel average temperature and pressure are used as the figures of merit for the best design, then the BeO, followed by LBE are considered the best designs for improved performance with CMC SiC cladding [11].

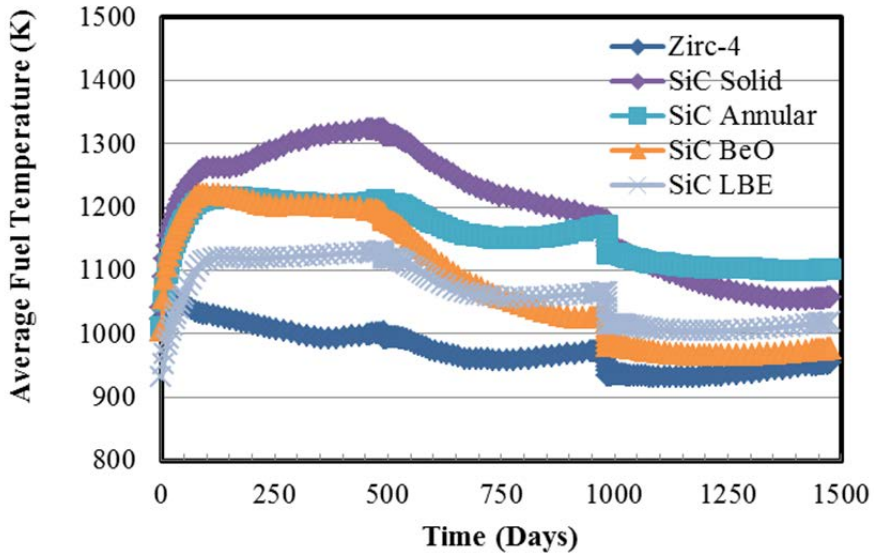

(a)

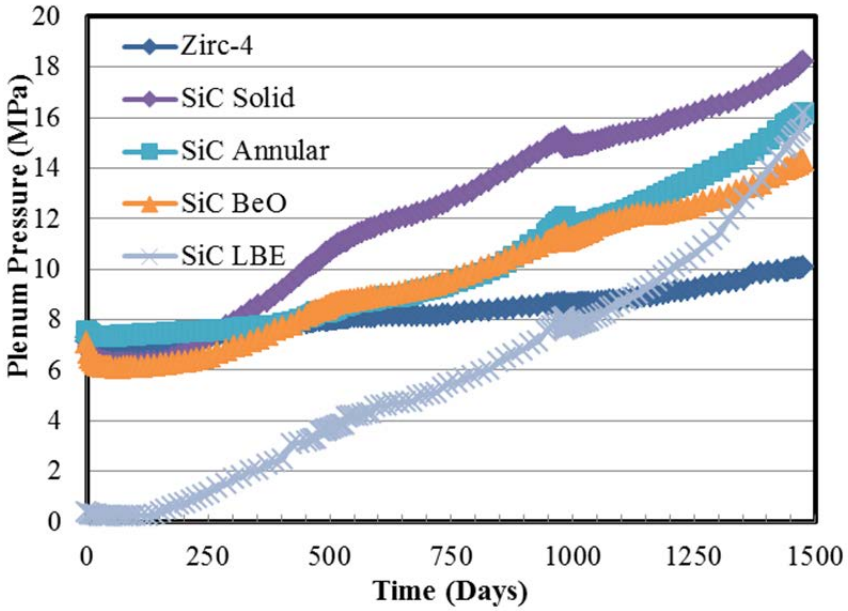

(b)

FIG. 1. The fuel average temperature (a) and plenum pressure (b) of advanced fuel options with CMC SiC cladding vs. zircaloy (Figures from Sukjai et al., [11]).

The enrichment requirements for the designs listed in Table 1 are shown in Table 2. There is about 0.3% enrichment penalty for going from zircaloy cladding with solid pellets to CMC SiC cladding with annular pellets. The annular pellet actually results in a 0.4% penalty as cores using CMC SiC and solid pellet exhibited 0.1% less enrichment requirement compared to zircaloy. The lower absorption and (n,2n) reaction of BeO results in enrichment savings of 0.17% compared to just accommodating an equal void volume in the pellet. The RCF design has about 0.8% enrichment savings over the design that conserves zircaloy outer diameter. The main reason behind improved performance of the RCF design is the conservation of hydrogen-to-heavy metal ratio (H/HM) compared to zircaloy fuel. Through utilizing annular pellets, about 10% HM has been lost and the RCF larger cladding outer diameter both increases the HM and reduces the H/HM level close to the zircaloy fuel. The relative ^{235}U mass is a strong indicator of the fuel cycle cost, implying the RCF design will be the most cost effective design option.

The boron, peaking factor, moderator temperature coefficient and Doppler fuel coefficient evolution during a fuel cycle were calculated and found to have the same sign and shape as the zircaloy cladding core. The RCF design, due to having similar H/HM, had almost identical physics performance as the nominal zircaloy core. However, unlike the other designs, the RCF design impacts the thermal hydraulic performance of the core due to the smaller hydraulic diameter of the assembly. In the past, PWRs have operated with many cladding designs. In the context of 17 × 17 array assemblies, the current PWRs operate with two different main fuel designs: OFA and RFA [1]. The difference between the cross-sectional area that each fuel accommodates is about ~8%, while for thick CMC SiC cladding the difference is about ~13.8%. In the future, it is expected that the CMC SiC would be fabricated even with thinner cladding thickness and therefore, the RCF design approach is most likely the best option for CMC SiC introduction to current US PWRs.

Lastly, the impact of SiC on replacing the BWR channel box was analyzed using CASMO4e. It was found that the lower absorption in CMC SiC is able to reduce the enrichment requirement for a typical BWR assembly by 0.07 w/%. Since the channel box does not interact directly with fuel, this could be the ideal way to introduce CMC SiC to LWRs.

3. ECONOMIC PERFORMANCE

In order to assess the economic performance of CMC SiC against the other two ATF cladding concepts, the enrichment requirement of the multi-component Mo based and FeCrAl cladding are needed.

TABLE 2. ENRICHMENT, BURNUP, AND RELATIVE FISSILE CONTENT [8]

Parameters	Zr Solid	Thin CMC Annular	Thick CMC Annular	Thick CMC RCF Annular	Thick CMC UO_2/ BeO Solid
U-235 w/o	4.475	4.77	5.750	4.966	5.583
Cycle Burnup (MWd/kgU)	19.47	21.60	25.92	21.60	25.44
Burnup at discharge (MWd/kgU)	44.1	49.6	58.7	47.3	57.1
Relative U-235 mass	1.000	0.960	0.965	0.999	0.955

Both cladding thicknesses were assumed to be 0.4 mm, which is smaller than zircaloy (0.57 mm) and consistent with stainless steel claddings in the past. The neutronics analysis was performed with MCNP5 since CASMO4e does not have a complete set of molybdenum cross-sections. Natural Mo gives similar neutronic penalty as stainless steel, however, its performance could be drastically improved if Mo-95 can be separated, which constitutes 15 w/% of Mo. Mo-95 has an order of magnitude greater absorption that iron. For this analysis natural Mo was used with 0.2 mm cladding thickness. The Mo layer is designed with an inner 0.075 mm zircaloy layer and outer 0.125 mm oxidation protective FeCrAl layer [12]. Linear theory of reactivity was utilized to transform the assembly based reactivates to full core enrichment requirements for an 85 fresh loaded assembly PWR similar to the previous analysis. The zircaloy and SiC CMC predicted enrichments are slightly different than the values shown in Table 2 due to use of linear theory of reactivity to have a consistent comparison between the four concepts. The FeCrAl concept has a slightly lower enrichment than the Mo design due to the lower reactivity penalty of FeCrAl compared to natural Mo.

The incremental enrichment increase of FeCrAl compared to zircaloy is also consistent with previous analysis by Terani et al., [13].

The fuel cycle cost can then be estimated using current uranium prices. In order to estimate fuel cycle costs of advanced fuel it is assumed that the uranium fuel cycle cost is composed of the following units: 80 $/kgU for mining, 7.5 $/kgU for conversion and 100 $/SWU for enrichment and 200 $/kgU for fabrication. Then the nuclear fuel cost is multiplied by a factor of 1.3 to accommodate charges of interest rates. The current fuel enrichment infrastructure is licensed to ~5% and it is expected to remain the same for many years due to the large required cost of increasing such limit. However, since in the nuclear reactor there are many parts of assemblies loaded with different enrichment levels, the reload average enrichment should not exceed ~4.75%.

Table 3 lists the enrichment requirement and fuel cost of advanced fuels with the reload per cycle strategy for selected designs. As listed, if the 4.75% constrained is lifted then more economical fuel cycles can be achieved. The CMC SiC design results in the lowest relative cost increase even with annular pellet and thicker cladding. The FeCrAl and Mo based designs result in similar performance. For consistency, only the cases that met the 4.75% enrichment constraint were considered from Table 3 for the rest of the economic analysis.

TABLE 3. ZIRCALOY ENRICHMENT REQUIREMENTS AND FUEL CYCLE COSTS OF LEADING ATF CLADDING CONCEPTS

Fuel	Cladding	# of Reload Per Cycle	Batch Av. E (%)	Discharge B (MWD/KgU)	Fuel Cost (M$)	Cost Diff (%)
Solid	0.57 mm Zirc	85	4.38	45.4	85.93	0
Annular	0.87 mm SiC	85	5.62	59.8	86.06	0.15
Annular	0.87 mm SiC	110	4.75	46.3	92.17	7.26
Solid	0.4 mm FeCrAl	85	4.82	41.9	102.52	19.31
Solid	0.4 mm FeCrAl	88	4.75	40.7	103.73	20.72
Solid	0.4 mm Mo	85	4.89	41.9	104.01	21.04
Solid	0.4 mm Mo	90	4.75	39.8	106.27	23.67

For the next 30 years, before shutdown of old PWRs, one then could calculate the net present value (NPV) of each option, assuming 8% discount rate. The ATF fuel goal is to avoid the potential cost upon a severe accident through avoiding reactor meltdown and containment of fission products. For this work as analysis consistent with recent work by Westinghouse [14] was applied. Considering the severe accidents of Fukushima Daiichi and TMI, two scenarios are considered. First scenario is the cost imposed by losing the reactor but containing the fission products within the containment, thus incurring no cleanup cost. Given the probability of severe accidents, the cost is estimated to be $313 million for the 100 reactors of the US annually. The second scenario is the probable cost imposed by losing the reactor as well as not containing the fission products, which is calculated to be $1020 million based on the Westinghouse analysis. The last assumption in comparing the costs is that CMC SiC requires at least 20 year development time vs. FeCrAl and Mo based cladding that only require 10 years. Fig. 2 shows both the NPV of the additional cost of the new fuel and the NPV of the gain from avoiding the two types of accidents. Considering CMC SiC, it is clear that the potential economic gain, even if the fabrication cost of CMC SiC was increased by

factor of 3 times over that of zircaloy. The cost of CMC SiC after 30 years from now at 600 $/kgU corresponds to the cost of the first scenario after 20 years where CMC SiC is introduced. At that time, the small penalty of the fuel cost is negligible compared to that of avoiding both types of accidents.

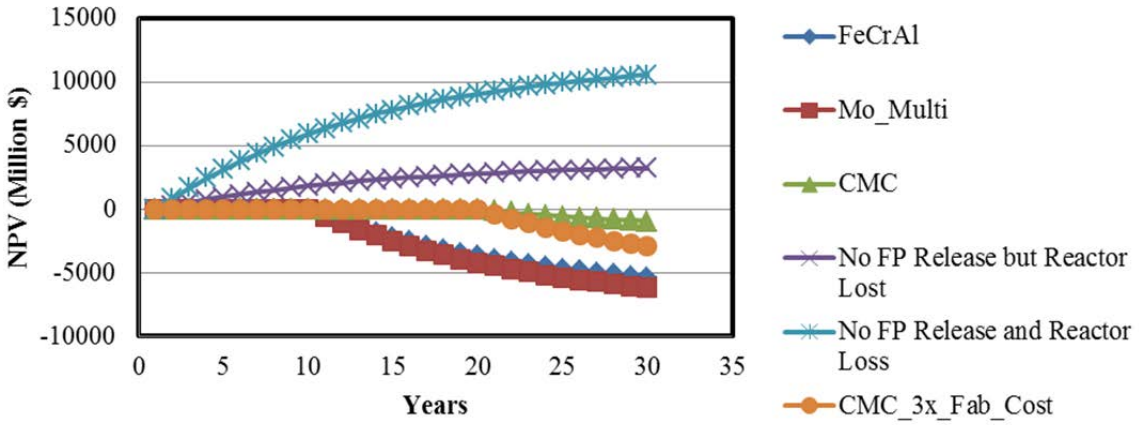

FIG. 2. The fuel cycle cost of ATF leading cladding concepts and the cost of severe accidents.

Since it is not expected for FeCrAl to be able to contain fission products in a severe accident, due to its low melting point [14], then its use does not provide an economic incentive, unless backed with government subsidies. The Mo based cladding has an uncertain potential to confine fission products during the severe accident, as both of its sides can melt at low temperature. But if it does, it can provide a lower cost alternative to CMC SiC if the development of CMC SiC is billions of dollars less than that of the Mo option. A more detailed analysis of the net present value of various options is under assessment at MIT [15].

4. STRUCTURAL PERFORMANCE

The structural performance of CMC cladding under steady and transient conditions has been performed through many modelling approaches at MIT [16-19] and at ORNL [20]. This work focuses on presenting the sensitivity found to be important in its modelling.

4.1. Material properties

The unirradiated material properties for CVD SiC have been well characterized and documented in literature [4]. The composite material properties are highly dependent on fabrication and manufacturing technique as well as the architecture of the fibres with the matrix. The irradiation properties of selected composites were compiled by Katoh et al [5]. In general, the irradiation data at LWR temperature range (270°C-330°C) are scarce. Most notably, the data for irradiation induced swelling at LWR temperature for composites are very few with very large uncertainties. For the current analysis the Hi-Nicalon^{TM} Type-S CVI-SiC composite (HNLS CVI) was chosen as a promising composite candidate for reactor conditions due to its high quality of fabrication. The available data also does not include the integral CVD SiC and composite performance, which is another area of ambiguity.

4.1.1. Thermal conductivity

The thermal conductivity of CVD SiC and CMC has been shown to degrade drastically upon few DPAs. The magnitude of such degradation has shown to be independent of the unirradiated value of thermal conductivity. For a quality CVD SiC samples, the thermal

conductivity was found to saturate at ~9.5 W/(m·K). While for the HNLS CVI composite it was found to saturate at ~1.5 W/(m·K) after 2.0 DPA in 450°C. Therefore, for a material composed of half of each constitute, the expected thermal conductivity is 5.5, which is about one/third of the zircaloy cladding. This value is higher than the ~4.5 W/(m·K) obtained from 3 layer CMC SiC after irradiation at MIT [3]. The MIT irradiations were performed at typical PWR temperature, pressure and chemistry. This reduction in thermal conductivity could be due to oxidation of the sample via water ingress or due to different composite architecture.

4.1.2. Mechanical properties

It has been shown that both the young's modulus and poison ratio of CVD and composites remains relatively the same in the temperature and irradiation fluence range of LWRs. The modulus of 460 GPa and 230 GPa and Poisson's ratio of 0.21 and 0.13 were used for the CVD SiC and CMC layer. As shown by Katoh, the composite material proportional stress limit is much lower than CVD SiC and the fibres could go through micro-cracking and realignment which effectively could act as a visco-elastic or plastic strain deformation of the composite layer. Additionally, the material properties are strong functions of the fabrication technique. For instance, for a filamentary wiring technique the modulus in the radial direction is 78 GPa compared to 248 GPa in hoop and axial directions. The Poisson's ratio is 0.16 in the axial to hoop direction while for a 3D braid CMC the position ratio is 0.085 in such orientation [21].

According Katoh et al., [5], both CVD SiC and composite should experience similar thermal expansion. The following relation was used for thermal expansion which is applicable for LWR temperature range:

$$\alpha = -1.8276 + 0.0178T - 1.5544 \times 10^{-5}T^2 + 4.5246 \times 10^{-9}T^3 \left(\frac{10^{-6}}{K}\right) \quad (1)$$

Another mechanism that affects the volumetric strains in the CMC SiC cladding is the irradiation swelling. Unlike the thermal expansion, due to the different material density, the irradiation induced swelling of SiC CVD could be higher than the composites According to the available data [5], this notion seems to be true, though large uncertainty in the data does not allow for reaching a conclusive position. For this analysis the thermal expansion is added to the temperature dependent isotropic swelling, resulting in the curves shown in Fig. 3.

4.2. Cladding stress distribution in CMC SiC

To perform sensitivity analysis, a three layer CMC cladding has been modelled in the commercial finite element code, ADINA [22], with the discussed material properties. The linear heat rate of 32 kW/m (representing peak pin) and plenum pressure of 13.5 MPa (representing close to EOL) were assumed for the following sensitivity analysis.

The first sensitivity was focused on the effect of the assumed thermal conductivity in the composite (1.5 W/m-k for the base case). It was found that the outer EBC layer is the most sensitive compared to the other 2 layers. Though a factor of 2 increase in thermal conductivity of the composite only resulted in 15% more compressive hoop stress. By introducing the discussed orthotropic property by filamentary wiring, it was found that the hoop stress, which was the limiting stress, was underestimated for the inner monolith and over-estimated for the EBC by 15%. The effect of assuming effective "visco-elastic or plastic behaviour" of the fibres above its proportional limit stress was also were modelled, assuming proportional stress limit of 100 MPa. This resulted in higher axial and hoop stress in the three layers by ~5%.

The effect of thermal conductivity, orthotropy and plasticity were within 15% of the assumed thermo-elastic behaviour for the base analysis. However, slight changes in the thermal expansion coefficient have large effects on the stress distribution. In fact, the change in the total volumetric strain in each layer becomes extremely important when differential swelling between each layer exists. Fig. 4 displays such large sensitivity when the CVD SiC and composite layer total thermal expansion that was shown in Fig. 3 is assumed to be equal or greater/less. Since the CVD SiC layers are stronger than the composite layers, they can push or pull the composite layers and result in very different stress distribution depending on the relative total strain imposed by temperature and irradiation.

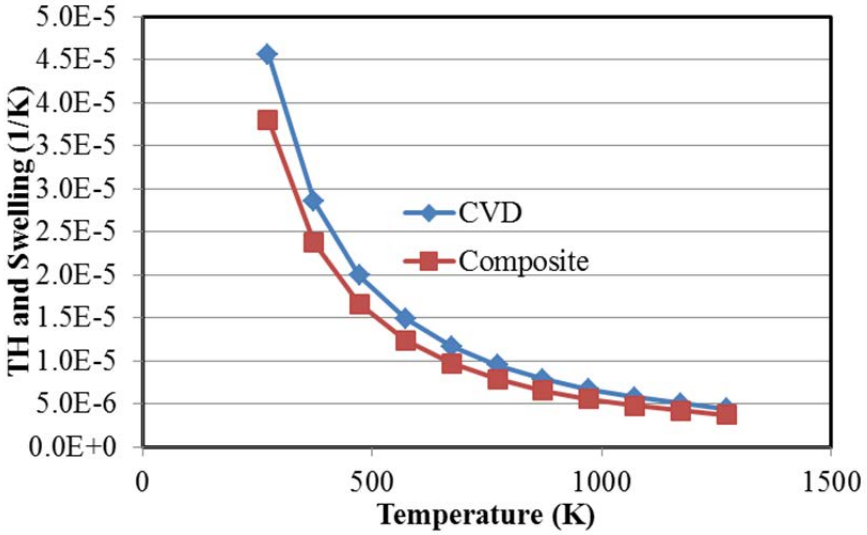

FIG. 3. The total thermal expansion and swelling for CVD and composite [19].

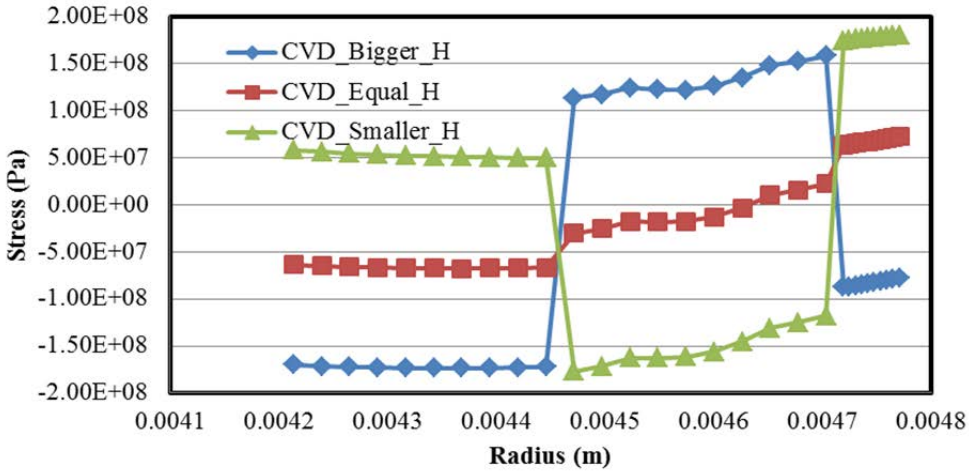

FIG. 4. The sensitivity of assumed total thermal volumetric thermal strain for the three layer CMC SiC design.

The sensitivity for assuming anisotropic swelling was also assessed. The total thermal strain in the radial direction was increased and decreased by a factor of 1.2. The resultant stress distribution almost showed a linear response sensitivity to such assumed anisotropy. While the stresses in the inner monolith and composite layer are relatively insensitive to such anisotropic swelling, a 20% change in the axial/hoop stress of the EBC layer was observed for 20% change in the radial swelling in the same direction.

A “duplex” two layer CMC SiC design could be composed of a composite inner layer followed by a thick CVD SiC layer. The radial stress distribution of the three principal stresses, shown in Fig. 5, implies that for the same material properties, the two concepts behave similarly with similar minimum and maximum stresses.

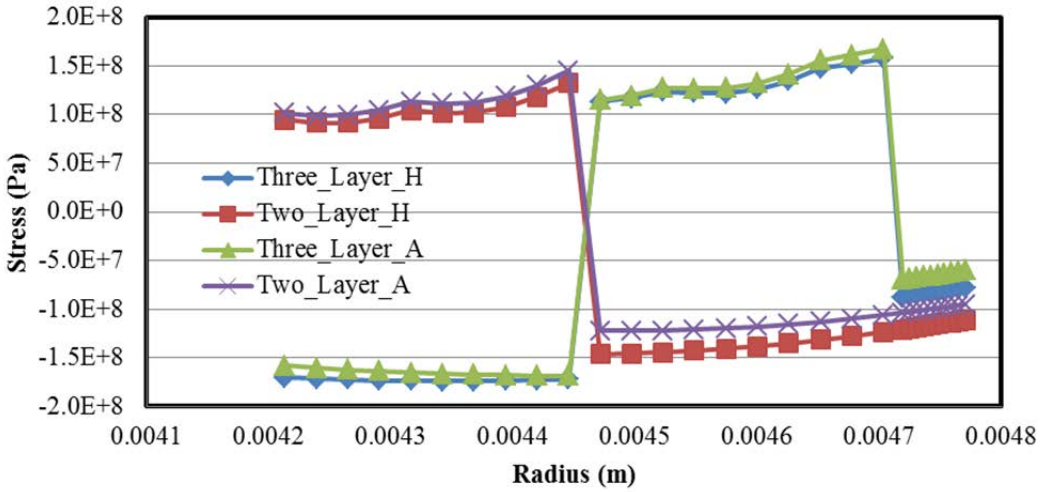

FIG. 5. The comparison of a three layer to a two layer CMC SiC cladding concepts.

In the two layer design, the porous composite layer is exposed to fission gasses that could diffuse through the fibres and result in additional swelling. Alternatively, upon micro-cracking from operating with tensile stress as shown in Fig. 5, the pathways to the fibres could be connected and the fission gases could apply pressure on the outer CVD SiC layer. As an upper limit, all the fission gases were modelled to exert pressure on the outer CVD SiC layer. The radial stress is profile of the two layer and three layer designs in the radial direction is compared in Fig. 6. The pressure on the inner wall of the CVD SiC layer causes tensile stress in the composite fibres but was found to not affect the stress in the other principal directions significantly.

Unlike the two layer design, in the three layer design the fibres could be fabricated with a certain pre-stress level that would put the monolith and/or composite layer under compressive hoop stress. Such pre-stressing can reduce the tensile hoop stress, however it will increase the stress in the axial direction. It was found that a threshold pre-stress of less than 10 MPa is ideal for CMC SiC three layer design to obtain an optimum performance (e.g. minimize tensile stress).

4.3. Failure criterion discussion

The failure criterion for a multilayer CMC is still an unknown due to lack of sufficient data at prototypical conditions and mature simulation tools. The Wiebull statistics is one approach that has been used to model the failure in ceramics. The Wiebull modulus of 7.5 with Weibull characteristic strength of 369 MPa for CVD-SiC has been used in a previous analysis [17]. According to Katoh et al., [5] irradiated samples at 1.9 dpa exhibited a Weibull modulus of 4.4, which worsens the probability of failure. While for the composite layer two different failure criteria were considered, one for the proportional stress limit (105 MPa) and the other for the ultimate stress limit (290 MPa) with Weibull modulus of 5 and 17, respectively [17].

However, no conclusive basis can be reached on the effective Wiebull modulus or failure behaviour of the three or two layer CMC SiC due to lack of sufficient relevant data. Additionally, at certain high compressive stresses, failure could occur in fibres in the composite due to material "buckling" [23]. Therefore, the CMC SiC designs have to consider the magnitude of both the tensile and compressive stress. Regardless of the approach, the failure probability for commercial development of CMC SiC has to be competitive with current zircaloy cladding which implies only a few MPa of tensile stress during the lifetime of the cladding.

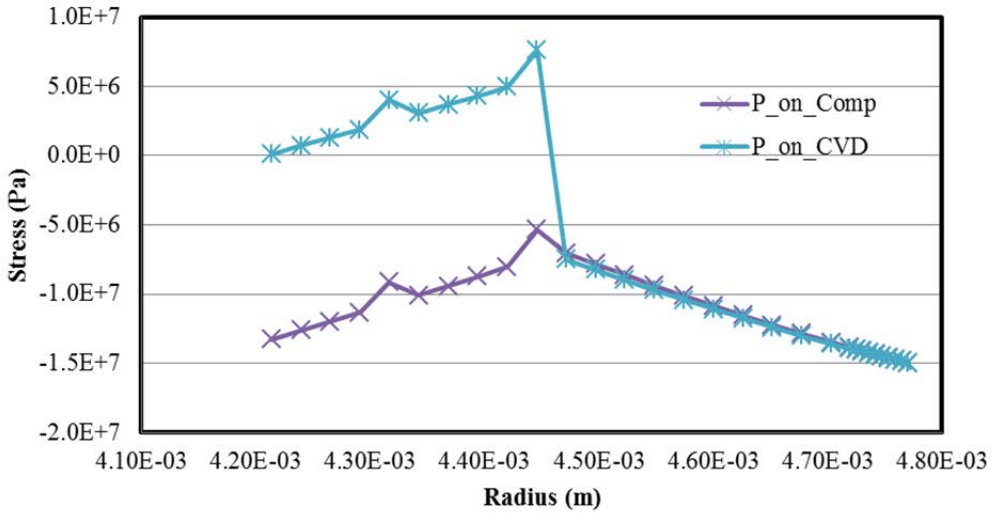

FIG. 6. The radial stress of the three-layer and the two-layer CMC SiC cladding concepts.

5. IMPORTANT GAPS FOR FUTURE STUDY

The following areas are considered important gaps, where experiments and modelling is needed to support the development of CMC SiC concept for LWRs:

- Larger material strength database for both monolith and composite at LWR temperature and irradiation range:
  - Further validation of the advanced fuels performance models to overcome CMC SiC lower thermal conductivity;
- Even for annular pellets, current models result in different predictions in performance [18]:
  - CMC SiC Fuel vibration analysis;
  - Effect of pellet rattling within SiC → becomes more significant at high burnup when the pellet is weaker and the gap is still open;
- Effect of support grid-to-rod wear and fretting:
  - Details of layers design and manufacture and their effects on thermo-mechanical properties as well as corrosion under reactor steady and transient operation for test and commercial reactors;
- End cap design should also be focused through consideration of differential strain rates between the CVD SiC and composite layer at each end of the rods, where irradiation swelling is the highest due to lower operating temperature.

ACKNOWLEDGEMENTS

This work was funded primarily by the Center for Advanced Nuclear Energy Systems (CANES) at MIT. Partial funding for this work was provided by Ceramic Tubular Products, IBC and Consortium for Advanced Simulation of Light Water Reactors and primarily funded by Center for Advanced Nuclear Energy System at MIT.

Significant insights were derived from the work of graduate students David Bloore, Yanin Sukajai and Nathan Andrews respectively on neutronics, FRAPCON fuel performance analysis and economics of the advanced fuels concepts.

REFERENCES

[1] BRADFUTE, J. L., CHAPIN, D. L., REPARAZ, A., QUECEDO GUTIÉRREZ, M., RUIZ, C.M., "Westinghouse Fuel Designs and Performance Overview", Water Reactor Fuel Performance TopFuel, Manchester, UK, (2012).

[2] CARPENTER, D. M., AHN, K., KAO, S.P., HEJZLAR, P., KAZIMI, M. S., "Assessment of Silicon Carbide Cladding for High Performance Light Water Reactors", Nuclear Fuel Cycle Program CANES, MIT MIT-NFC-TR-098 (2007).

[3] STEMPIEN, J.D., CARPENTER, D.M., KOHSE, G., KAZIMI, M.S., Characteristics of Composite Silicon Carbide Fuel Cladding after Irradiation Under Simulated PWR Conditions, Nuclear Technology **183** (2013) 13.

[4] SNEAD, L.L., NOZAWA, T., KATOH, Y., BYUN, T.S., KONDO, S., PETTI, D.A., Handbook of SiC Properties for Fuel Performance Modelling, J. Nucl. Mater. **371** (2007) 329.

[5] KATOH, Y., OZAWA, K., SHIH, C., NOZAWA, T., SHINAVSKI, R.J., Continuous SiC Fiber, CVI SiC Matrix Composites for Nuclear Applications: Properties and Irradiation Effects, J. Nucl. Mater. **448** (2014) 448.

[6] HEINISCH, H.L., GREENWOOD, L.R., WEBER, W.J., WILLIFORD, R.E., Displacement damage in silicon carbide irradiated in fission reactors, J. Nucl. Mater. **327** (2004) 175.

[7] DOBISESKY, J., RICHARD, J., PILAT, E.E., KAZIMI, M.S., CARPENTER, D.M., Fuel Management of PWR Cores with Silicon Carbide Cladding, Nuclear Technology **186** (2014) 353.

[8] BLOORE, D.A., PILAT, E.E., KAZIMI, M.S., "Reactor Physics Assessment of Thick Silicon Carbide Clad PWR Fuels", CANES, MIT, MIT-ANP-TR-148 Massachusetts Inst. of Technology, MA (2013).

[9] STUDSVIK, *CASMO*-4E: "A Fuel Assembly Burnup Program User's Manual", Studsvik SSP-09/443-U Rev 0 proprietary (2011).

[10] STUDSVIK, "Simulate-3: Advanced Three Dimensional Two Group Reactor Analysis Code", SSP-09/447-U Rev 0, proprietary (2011).

[11] SUKJAI, Y., PILAT, E., SHIRVAN, K., KAZIMI, M.S., "Silicon Carbide Performance as Cladding for Advanced Uranium and Thorium Fuels for Light Water Reactors", Advanced Nuclear Power Program, MIT-ANP-TR-149 (2014).

[12] CHENG, B., KIM, Y.J., CHOU, P., DESHON, J., "Development of Mo-alloy for LWR Fuel Cladding to Enhance Fuel Tolerance to Severe Accidents", TopFuel, NC (2013).

[13] TERRANI, K.A, ZINKLE, S.J., SNEAD, L.L., Advanced Oxidation-Resistant Iron-Based Alloys for LWR Fuel Cladding, J. of Nuclear Materials, **448** (2013) 420.

[14] LAHODA, E., HALLSTADIUS, L., BOYLAN, F., RAY, S., What should be the Objective of Accident Tolerant Fuel, Trans. Am. Nuc. Soc. NV (2014).

[15] ANDREWS, N., Ph D thesis, MIT, expected early 2015.

[16] LEE, Y., McKRELL, T., YUE, C., KAZIMI, M.S., Safety Assessment of SiC Cladding Oxidation under Loss of Coolant Accident (LOCA) Conditions in LWRs, Nuclear Technology **183** (2013) 210.
[17] LEE, Y., McKRELL, T., KAZIMI, M.S., "Safety of Light Water Reactor Fuel with Silicon Carbide Cladding", MIT-ANP-TR-150 Massachusetts Inst. of Technology, MA (2014).
[18] SHIRVAN, K., "Assessment of BISON Fuel Performance Code and its Application to Advanced Fuels", ICAPP, NC, (2014).
[19] AVINCOLA, V., SHIRVAN, K., KAZIMI, M., "Stress Analysis Study of Silicon Carbide Cladding under Accident Conditions", Nuclear Fuels and Structural Materials, ANS annual meeting, NV, (2014).
[20] BEN-BELGACEM, M., RICHET, V., TERRANI, K.A., KATOH, Y., SNEAD, L.L., Thermo-Mechanical Analysis of LWR SiC/SiC Composite Cladding, J. Nucl. Mater. **447** (2013) 125.
[21] HUGUET, G.J., "Study of the Thermo-Mechanical Behaviour of an Innovative Multi-Layered Ceramic-Based Nuclear Fuel Cladding", M.S. Thesis, CEA, (2012).
[22] ADINA, "Theory and Modelling Guide", vol. I, Report ARD 00-7, MA, (2000).
[23] FLECK, N.A., Compressive Failure of Fibre Composites, Advances in Applied Mech. **33** (1997) 43.

LIST OF ABBREVIATIONS

AF	as fabricated
AOOs	anticipated operational occurences
ATR	Advanced Test Reactor
BDBA	beyond design basis accident
BNL	Brookhaven Nuclear Laboratory
BO	breakaway oxidation
BSE	back-scattered electron
CARAT	Collaborative Research on Accident Tolerant Fuel
CF	cold-forged
CMC	ceramic matrix or multi-layer composite
CMS	core management system
CP	Cathcart-Pawel
CTE	coefficient of thermfl expansion
CVD	chemical vapour deposited
CVI	chemical vapour infiltration
DBA	design-basis accident (new name is postulated accident)
DBTT	ductile-brittle temperature transition
DEC	design extension conditions
DSC	Differential scanning calorimetry
EATF	enhanced accident tolerant fuel
EB	electron beam
ECCS	emergency core cooling system
ECR	equivalent cladding reacted
EDS	energy-dispersive X-ray spectrometry
EFPD	effective full power days
EPRI / NFIR	Electric Power Research Institute / Nuclear Fuel Industry Research
FCM	fully ceramic microencapsulated (fuel)
FP	fission product

GETR	General Electric Test Reactor
GTAW	gas tungsten arc welding
HBS	high burnup structure
HB or HBU	high burnup
HFETR	High Flux Engineering Test Reactor
HIP	hot isostatic pressing
HRPF	hot roller press form
HVAF	hjgh velocity air fuel
HVOF	high velocity oxygen fuel
HWC	hydrogen water chemistry
IASCC	irradiation-assisted stress-corrosion cracking
IFBA	integrated fuel burnable adsorber
INL	Idaho Nuclear Laboratories
INPRO	in-situ neutron radiography reaction oven
KIT	Karlsruhe Institute of Technology
LANL	Los Alamos National Laboratory
LBLOCA	large break LOCA
LCAC	low carbon arc cast
LFA	lead fuel assembly
LFR	lead fuel rod
LHGR	linear heat generation rate
LIT	LOCA integral testing
LOCA	loss-of-coolant accident
LPS	liquid phase sintering
LTA	lead test assembly
MAX phases	a group of ternary ceramic compounds composed of early transition metals (Sc, Ti, V, Cr, Zr, Cr, Nb, Mo, Hf, and Ta) as M, of elements in the A group (mainly Al, Si, P, S, Ga, Ge, As, In, Cd, Sn, Tl, and Pb) as A, and carbon or nitrogen as X
M:F	moderator to fuel
MITR	Research Reactor of the Massachusettes Instutute of Technology

MTC	moderator temperature coefficient
(NEA) EGATFL	(Nuclear European Agency) Expert Group on Accident Tolerant Fuels for LWRs
NFA	nano ferritic alloy
NFC	Nuclear Fuel Complex (Hyderabad, India)
NITE	nano-infiltration and transient eutectic phase
NPIC	Nuclear Power Instutute of China
NPV	net pressure value
NSRR	Nuclear Safety Research Reactor
ODS	oxide-dispersion strengthed
OM	optical microscopy
PBF	Power burst facility
4-PBT	four-point bend test
PCI/PCMI	pellet-cladding interaction/pellet-cladding mechanical interaction
PCT	peak clad temperature
PCR	pre-composite ribbon
PH	pre-hydrided
PIE	post-irradiation examination
PM	powder metallurgy
POR	parabolic oxidation rate
PQD	post-quench ductility
PVD	physical vapour deposition
RCT	ring compression test
RIA	reactivity-initiated accident
RIS	radiation-induced segregation
RT	room temperature
SA	safety assessment
SATS	Severe Accident Test Station
SBLOCA	small break LOCA
SBO	station blackout

SCC	stress-corrosion cracking
SCWR	supercritical water reactor
SEM	scanning electron microscope
SGTR	steam generator tube rupture
SHE	standard hydrogen electrode
SI	safety injection
SMR	small modular reactor
TC	thermocouple
TGA	thermogravimetry analysis
TREAT	transient reactor test
TRISO	tri-layer coating for fuel particles used in high-temperature reactors
TRL	technological readiness level
UHP	ultra high purity
UV	ultra violet
VHS	volumetric heat capacity
WIP	warm isostatic pressing
XPS	X-ray photoelectron spectroscopy
XRD	X-ray diffraction

LIST OF PARTICIPANTS

Barbosa, R. A.	Indústrias Nucleares do Brasil S.A Brazil Email: rodrigobarbosa@inb.gov.br
Brachet, J.C.	Commissariat à l'Energie Atomique et aux Energies Alternatives France Email: jean-christophe.brachet@cea.fr
Bragg-Sitton, S.	Idaho National Laboratory United States of America Email: shannon.bragg-sitton@inl.gov
Brown, N	Brookhaven National Laboratory United States of America nbrown@bnl.gov
Carmack, J.	Idaho National Laboratory United States of America Email: Jon.Carmack@inl.go
Cheng, B.	Electric Power Research Institute United States of America Email: bcheng@epri.com
Cheng, L. Y.	Brookhaven National Laboratory United States of America Email: cheng@bnl.gov
Chichester, H.	Idaho National Laboratory United States of America Email: heather.chichester@inl.gov
Choi, J.	Westinghouse Electric Company LLC United States of America Email: Choi2j@westinghouse.com
Chou, P.	Electric Power Research Institute United States of America Email: pchou@epri.com
Field, K.	Oak Ridge National Laboratory United States of America Email: fieldkg@ornl.gov
George, N.	University of Tennessee United States of America Email: ngeorge3@vols.utk.edu
Goldner, F.	U.S. Department of Energy United States of America Email: frank.goldner@nuclear.energy.gov
Heuser, B.	University of Illinois

	United States of America Email: bheuser@illinois.edu
Hinoki, T.	Kyoto University\ Japan Email: hinoki@iae.kyoto-u.ac.jp
Hu, H.	China Nuclear Power Technology Research Institute China Email: huhaixiang@cgnpc.com.cn
Katoh, Y.	Oak Ridge National Laboratory United States of America Email: katohy@ornl.gov
Killeen, J.	International Atomic Energy Agency Austria Email: j.c.killeen@iaea.org
Kim, W.J.	Korea Atomic Energy Research Institute Korea, Republic of Email: weonjkim@kaeri.re.kr
Kim, Y. J.	GE Global Research Center United States of America Email: kimyj@ge.com
Kishimoto, A.	Muroran Institute of Technology Japan Email: hkishi@mmm.muroran-it.ac.jp
Kohyama, H.	Muroran Institute of Technology Japan Email: kohyama@mmm.muroran-it.ac.jp
Kondo, S.	Kyoto University Japan Email: kondo@iae.kyoto-u.ac.jp
Li, W.	Nuclear Power Institute of China China Email: lwj280@163.com
Liu, T.	China Nuclear Power Technology Research Institute China Email: liutong@cgnpc.com.cn
Malone, J.	Lightbridge Corporation United States of America Email: jmalone@ltbridge.com
Mathers, D.	National Nuclear Laboratory United Kingdom Email: daniel.p.mathers@nnl.co.uk

Mazzoccoli, J.	Westinghouse Electric Company LLC United States of America Email: MazzocJP@westinghouse.com
McKrell, T.	Massachusetts Institute of Technology United States of America Email: tmckrell@mit.edu
Nelson, A.	Los Alamos National Laboratory United States of America Email: atnelson@lanl.gov
Patel, M.	University of Tennessee United States of America Email: maulik@utk.edu
Ping, C.	Nuclear Power Institute of China China Email: chenping@npic.ac.cn
Powers, J.	Oak Ridge National Laboratory United States of America Email: powersjj@ornl.gov
Reddy, V.V.	Nuclear Fuel Complex India Email: vishnu@nfc.gov.in
Robb, K.	Oak Ridge National Laboratory United States of America Email: robbkr@ornl.gov
Savchenko, A.	A.A. Bochvar Institute of Inorganic Materials Russian Federation Email: sav-alex111@mail.ru
Shirvan, K.	Massachusetts Institute of Technology United States of America Email: kshirvan@mit.edu
Snead, L.	Oak Ridge National Laboratory United States of America Email: sneadll@ornl.gov
Sowder, A.	Electric Power Research Institute United States of America Email: asowder@epri.com
Terrani, K.	Oak Ridge National Laboratory United States of America Email: terranika@ornl.gov
Todosow, M.	Brookhaven National Laboratory United States of America Email: todosowm@bnl.gov

Wirth, B.	University of Tennessee United States of America Email: bdwirth@utk.edu
Yamamoto, Y.	Oak Ridge National Laboratory United States of America Email: yamamotoy@ornl.gov
Yang, J. H.	Korea Atomic Energy Research Institute Korea, Republic of Email: yangjh@kaeri.re.kr
Zhang, Y.X.	China Nuclear Power Technology Research Institute China Email: zhangyixin@cgnpc.com.cn

IAEA
International Atomic Energy Agency

No. 24

ORDERING LOCALLY

In the following countries, IAEA priced publications may be purchased from the sources listed below or from major local booksellers.

Orders for unpriced publications should be made directly to the IAEA. The contact details are given at the end of this list.

BELGIUM
Jean de Lannoy
Avenue du Roi 202, 1190 Brussels, BELGIUM
Telephone: +32 2 5384 308 • Fax: +32 2 5380 841
Email: jean.de.lannoy@euronet.be • Web site: http://www.jean-de-lannoy.be

CANADA
Renouf Publishing Co. Ltd.
22-1010 Polytek Street, Ottawa, ON K1J 9J1, CANADA
Telephone: +1 613 745 2665 • Fax: +1 643 745 7660
Email: order@renoufbooks.com • Web site: http://www.renoufbooks.com

Bernan Associates
4501 Forbes Blvd., Suite 200, Lanham, MD 20706-4391, USA
Telephone: +1 800 865 3457 • Fax: +1 800 865 3450
Email: orders@bernan.com • Web site: http://www.bernan.com

CZECH REPUBLIC
Suweco CZ, s.r.o.
SESTUPNÁ 153/11, 162 00 Prague 6, CZECH REPUBLIC
Telephone: +420 242 459 205 • Fax: +420 284 821 646
Email: nakup@suweco.cz • Web site: http://www.suweco.cz

FRANCE
Form-Edit
5 rue Janssen, PO Box 25, 75921 Paris CEDEX, FRANCE
Telephone: +33 1 42 01 49 49 • Fax: +33 1 42 01 90 90
Email: fabien.boucard@formedit.fr • Web site: http://www.formedit.fr

Lavoisier SAS
14 rue de Provigny, 94236 Cachan CEDEX, FRANCE
Telephone: +33 1 47 40 67 00 • Fax: +33 1 47 40 67 02
Email: livres@lavoisier.fr • Web site: http://www.lavoisier.fr

L'Appel du livre
99 rue de Charonne, 75011 Paris, FRANCE
Telephone: +33 1 43 07 43 43 • Fax: +33 1 43 07 50 80
Email: livres@appeldulivre.fr • Web site: http://www.appeldulivre.fr

GERMANY
Goethe Buchhandlung Teubig GmbH
Schweitzer Fachinformationen
Willstätterstrasse 15, 40549 Düsseldorf, GERMANY
Telephone: +49 (0) 211 49 874 015 • Fax: +49 (0) 211 49 874 28
Email: kundenbetreuung.goethe@schweitzer-online.de • Web site: http://www.goethebuch.de

HUNGARY
Librotrade Ltd., Book Import
Pesti ut 237. 1173 Budapest, HUNGARY
Telephone: +36 1 254-0-269 • Fax: +36 1 254-0-274
Email: books@librotrade.hu • Web site: http://www.librotrade.hu

INDIA
Allied Publishers
1st Floor, Dubash House, 15, J.N. Heredi Marg, Ballard Estate, Mumbai 400001, INDIA
Telephone: +91 22 4212 6930/31/69 • Fax: +91 22 2261 7928
Email: alliedpl@vsnl.com • Web site: http://www.alliedpublishers.com

Bookwell
3/79 Nirankari, Delhi 110009, INDIA
Telephone: +91 11 2760 1283/4536
Email: bkwell@nde.vsnl.net.in • Web site: http://www.bookwellindia.com

ITALY
Libreria Scientifica "AEIOU"
Via Vincenzo Maria Coronelli 6, 20146 Milan, ITALY
Telephone: +39 02 48 95 45 52 • Fax: +39 02 48 95 45 48
Email: info@libreriaaeiou.eu • Web site: http://www.libreriaaeiou.eu

JAPAN
Maruzen-Yushodo Co., Ltd.
10-10, Yotsuyasakamachi, Shinjuku-ku, Tokyo 160-0002, JAPAN
Telephone: +81 3 4335 9312 • Fax: +81 3 4335 9364
Email: bookimport@maruzen.co.jp • Web site: http://maruzen.co.jp

RUSSIAN FEDERATION
Scientific and Engineering Centre for Nuclear and Radiation Safety
107140, Moscow, Malaya Krasnoselskaya st. 2/8, bld. 5, RUSSIAN FEDERATION
Telephone: +7 499 264 00 03 • Fax: +7 499 264 28 59
Email: secnrs@secnrs.ru • Web site: http://www.secnrs.ru

UNITED STATES OF AMERICA
Bernan Associates
4501 Forbes Blvd., Suite 200, Lanham, MD 20706-4391, USA
Telephone: +1 800 865 3457 • Fax: +1 800 865 3450
Email: orders@bernan.com • Web site: http://www.bernan.com

Renouf Publishing Co. Ltd.
812 Proctor Avenue, Ogdensburg, NY 13669-2205, USA
Telephone: +1 888 551 7470 • Fax: +1 888 551 7471
Email: orders@renoufbooks.com • Web site: http://www.renoufbooks.com

Orders for both priced and unpriced publications may be addressed directly to:

IAEA Publishing Section, Marketing and Sales Unit
International Atomic Energy Agency
Vienna International Centre, PO Box 100, 1400 Vienna, Austria
Telephone: +43 1 2600 22529 or 22530 • Fax: +43 1 2600 29302
Email: sales.publications@iaea.org • Web site: http://www.iaea.org/books

International Atomic Energy Agency
Vienna
ISBN 978–92–0–105216–2
ISSN 1011–4289